17

A COMPARATIVE STUDY OF METAMORPHOSED SUPRACRUSTAL ROCKS FROM THE WESTERN NAMAQUALAND METAMORPHIC COMPLEX

by

JOHN MICHAEL MOORE

Thesis submitted in fulfilment of the requirements for the degree of Doctor of Philosophy in the Faculty of Science, University of Cape Town.

Department of Geology

1986

D86/205

ABSTRACT

A regional study of highly metamorphosed supracrustal rocks was undertaken in the western portions of the Namaqualand Metamorphic Complex. The study area was essentially restricted to a north-south section some 50 kilometres wide and 220 kilometres long. Eight east-west-trending belts of supracrustal rocks were examined, together with several smaller paragneiss remnants, in an area dominated by quartzo-feldspathic gneisses of granitic composition.

The supracrustal rocks were classified into seven major lithological groups: quartzitic rocks, metapelitic and metapsammitic rocks, quartzo-feldspathic rocks, metabasites, metacarbonate rocks, magnesium-rich cordierite rocks and iron formations. Further subdivision, based on variations in mineral constituents within each group, also occurred, as well as the presence of lithologies with compositions transitional between certain groups.

The various supracrustal sequences were subdivided into formations containing minor distinctive members on an informal lithostratigraphic basis. Correlation between the major supracrustal belts was then undertaken. Four subgroups were identified across the study area, comprising a quartzo-feldspathic gneiss subgroup and an overlying feldspathic quartzite/garnet-cordierite gneiss subgroup that both predominate in the southern and central part of the area, a glassy quartzite/mica-sillimanite schist subgroup that predominates in the northern part, and a cordierite gneiss/metacarbonate subgroup that is restricted to the Geselskapbank synform. The supracrustal rocks appear to have been emplaced on a basement of augen gneisses. This relationship is, however, complicated by the intrusion of granitic rocks within the contact zone.

The bulk compositions of the metapelitic rocks were used to examine potential modifying effects on composition caused by granulite- and amphibolite-facies metamorphism in the light of previous studies that proposed major amounts of partial melting. Trends displayed by incompatible elements across the amphibolite/granulite facies boundary indicate significant depletion in Rb (20%) and lesser K (5%) in the granulite facies. Residual enrichment in Ba and Sr is also possible. Estimations of potential partial melt loss were undertaken by least-squares approximation using mean compositions of amphibolite- and granulite-facies metapelitic rocks and various minimum melt compositions. Partial melting resulting in the formation of up to 20% minimum-melt granite and 80% restite was estimated for the granulite facies, which is compatible with observed in-situ leucosome formation.

Metapelitic rocks have bulk compositions similar to unmetamorphosed Proterozoic platform shales. Two distinctive groups of metapelitic rocks were

identified. Metapelites in the northern part of the area show depletion in Na_2O, CaO, MgO, FeO, TiO_2, Ba, Sr, Ni, Co, Y, La, Ce and Nd, and enrichment in K_2O and Rb, compared to similar lithologies from the south/central parts. A minor third group of metapelitic rocks is present in the Geselskapbank synform. Principal components analysis and least-squares approximation were employed to estimate premetamorphic mineral constituents. Both major groups contained significant amounts of quartz and illite, lesser chlorite and minor ilmenite, with the northern rocks containing additional K-feldspar and kaolinite, and the south/central rocks increased plagioclase. A highly acidic igneous source and warmer climate are proposed for the northern lithologies.

Leucogneisses and biotite gneisses are the dominant lithologies in the supracrustal assemblages and have bulk compositions compatible with origins as K-rich rhyolitic to rhyodacitic extrusive acid volcanic rocks. The leucogneisses have extremely high SiO_2 and K_2O contents indicating derivation from highly fractionated magmatic sources. Biotite-hornblende rocks having intermediate dacitic to andesitic compositions are extremely rare components of the supracrustal sequences.

Metabasites, either amphibolites or basic granulites, are present as a widespread minor lithology. The majority of these mafic rocks represent metamorphosed equivalents of typical tholeiites, somewhat depleted in alkali elements, derived by fractional crystallisation from normal mantle peridotite sources. Distinctive Si-, Mg-rich, Ti-poor amphibolites with high Ni and Cr contents are present in the northern portions of the area. These metabasites appear to have been derived from more primitive magmas, possibly from a depleted peridotite source.

A suite of uncommon cordierite-hypersthene/anthophyllite-phlogopite rocks occurs in association with the metabasic and metapelitic rocks. Their bulk compositions are highly variable but generally show enrichment in MgO, FeO and Al_2O_3 and sometimes K_2O whilst depleted in CaO and Na_2O. Genetic models for these rocks involving partial melting are rejected due to their presence in both amphibolite and granulite facies zones. The cordierite-hypersthene/anthophyllite rocks are taken to represent metamorphosed chlorite-rich weathering products of mafic volcanic rocks with the cordierite-phlogopite lithologies containing an additional K-rich component due to mixing with pelitic material.

A diverse group of metacarbonate rocks is present with the majority having their chemical compositions considerably modified in decarbonation reactions. Forsterite marbles and calcite-wollastonite rocks represent relatively pure dolomites and limestones respectively, with massive diopside rocks and plagioclase-garnet rocks representing similar, more siliceous, precursor lithologies. Plagioclase-diopside calc-silicate rocks have bulk compositions indicating origins either as pelite-limestone mixtures or as calcite-bearing degraded mafic volcanic rocks. Precursor constituent modelling reveals that the metacarbonate rocks in the study area are depleted in potassic components compared to typical carbonate rocks and, in the calc-silicate varieties, enriched in chlorite and kaolinite. Low Na_2O and Sr contents imply an absence of strongly evaporitic, saline conditions. Certain

diopside-bearing rocks are anomalously enriched in P_2O_5 (up to 4.5%) and indicate restricted shallow-water conditions.

Two distinctive types of quartzite are present in the area. Feldspathic quartzites with minor K_2O and Al_2O_3 contents predominate in the south/central parts and are interpreted as metamorphosed feldspathic sandstones derived from weathering of quartzo-feldspathic source material. Glassy quartzites of extreme purity dominate the northern supracrustal sequences. They contain minor ferruginous units and thin intercalated metapelitic bands. Most of these latter quartzitic rocks are thought to have formed by siliceous chemical sedimentation - i.e. chert formation - associated with acid volcanism.

Iron formations are present as an uncommon, close associate of the glassy quartzites in the northern part of the area. Outside the Aggeneys-Gamsberg area, they show low concentration levels of metals such as Pb, Zn, Cr, V and Ni, similar to Lake Superior-type iron formations of sedimentary origin. Additional low concentration levels of Y, Zr and light rare earth elements, high SiO_2 contents and low Co/Zn ratios are, however, similar to hydrothermal deposits. The iron formations are distinctly enriched in MnO (6.6% mean) and Al_2O_3 (6.1% mean) relative to typical iron formations and can be compared to ancient manganese deposits associated with acid volcanism.

Metavolcanic rocks in the supracrustal sequences of the study area represent a bimodal, acid-dominated suite formed during an extensional tectonic regime, in marked contrast to the preceding calc-alkaline, andesite-dominated volcanic suite of the Orange River Group to the north. They represent the products of subaerial volcanism, deposited as a relatively thin cover sequence in a shallow continental basin. Many of the associated sedimentary lithologies such as the northern metapelites, the glassy quartzites, iron formations, magnesium-rich cordierite gneisses and plagioclase-diopside calc-silicate rocks apparently formed by weathering and degradation of similar volcanic rocks. A continental-collision model is proposed to explain the nature of the supracrustal sequences observed in the western Namaqualand Metamorphic Complex.

CONTENTS

Chapter 1

INTRODUCTION

1.1 General comment

The majority of studies within the Namaqualand Metamorphic Complex have been primarily concerned with the destructive dynamic processes that were operative during the formation of the mobile belt itself. Attempts at looking through the structural/metamorphic imprint to the original formative geological processes of the pretectonic lithologies have been few, and then mainly in areas of less intense deformation (e.g. Reid,1977). The reasons for this state of affairs are obvious as the metamorphic imprint has obliterated much of the crucial mineralogical and textural evidence required in sedimentological and volcanological studies that can be so important for regional basin reconstruction and palaeoenvironmental interpretation.

One tool, however, remains that has not been utilised to any large extent in earlier studies and this is whole-rock geochemistry. Although it too has its limitations, whole-rock geochemistry can point in a general, and sometimes more specific, way to the premetamorphic lithologies (volcanic or sedimentary, mature or immature, greywacke or shale, etc.) that have been transformed during the formation of the Namaqualand Metamorphic Complex, and so indicate various pre-existing environments of deposition. Studies such as these can play an important role in the understanding of the initial formative processes of ancient mobile belt terranes, and more specifically, can also assist in defining the environmental controls of such phenomena as volcanicity, chemical sedimentation and ore deposition within the pretectonic lithologies.

Whole-rock geochemistry can also be of assistance in stratigraphic studies, providing additional confirmatory evidence or otherwise, of regional and local correlations of various lithologies, particularly across metamorphic facies boundaries where the physical appearance of rocks of similar origin may be totally dissimilar.

It is basically with the two above goals in mind - regional correlation and palaeoenvironmental interpretation of the supracrustal lithologies of the western Namaqualand Metamorphic Complex - that this thesis is concerned.

1.2 Locality and regional setting

The portions of Namaqualand and Bushmanland covered by this study are roughly bounded by latitudes 29° and 31° south and longitudes 18° and 18° 30' east, representing a north-south section through Mokolian basement rocks from their first appearance beneath late Precambrian Nama Group cover rocks north of Vanrhynsdorp to the southern approaches of the Orange River in the north (Fig 1-1).

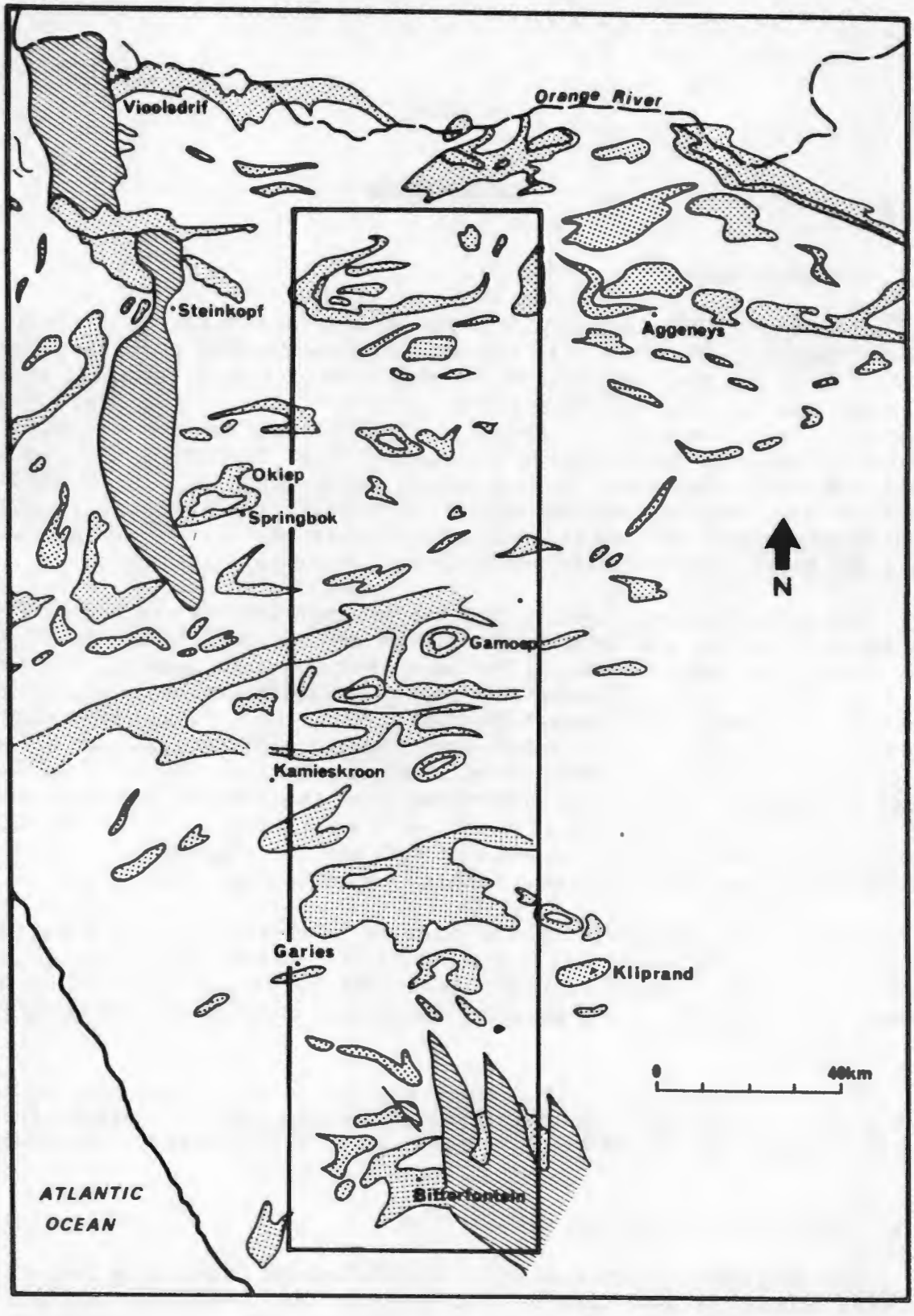

Fig. 1.1 Locality map showing the approximate boundaries of the study section in the western portions of the Namaqualand Metamorphic Complex. Major outcrop belts of pretectonic supracrustal rocks of the Complex are outlined (stipple) together with cover rocks of the Nama Group (solid line).

The basement rocks in the defined area belong to the Namaqualand Metamorphic Complex (NMC) and are currently divided into three pretectonic metasedimentary and metavolcanic groups of rocks that are intruded by six different syntectonic rock suites (SACS,1980). Ages deduced from isotopic studies place all these lithologies within the mid-Proterozoic timespan of 2000 to 1000 Ma (Nicolaysen and Burger,1965; Clifford et al., 1975a, 1981; Reid,1979,1982; Koeppel,1980; Reid and Barton,1983) (Table 1-1).

The regional geological setting of the NMC has been reviewed by Joubert (in Hunter,1981) and Jackson (in Tankard et al., 1982) who summarise the current geological knowledge of the area and highlight many of the outstanding problems and paradoxes. Basically both Joubert and Jackson (op.cit.) divide the area into three-to-four major subdivisions based on contrasting tectonic, metamorphic and/or lithological characteristics and distinctive radiometric age signatures. The subdivisions include an eastern zone in the Upington-Prieska area, a broad central zone from Kenhardt to the west coast and up through Grunau to Luderitz in southern Namibia, and a smaller western zone centred around the Orange River from Goodhouse westwards. It is with rock units of the southern portions of the central zone and their relationship to lithologies in the western zone that this study is primarily concerned.

Of particular pertinence are the three metasedimentary/metavolcanic groups defined from south to north as the Okiep Group, Bushmanland Group and Orange River Group respectively, which are described as representing "geographical domains between which stratigraphic correlation at the present state of knowledge is conjectural" (SACS,1980). It is partially towards the resolution of this particular problem that this study is aimed.

1.3 Previous work

The study area has been essentially covered in three regional geological studies by Jansen (1960), Joubert (1971) and Strydom (in progress) from south to north, and their mapping has provided a basis for the location and examination of the various paragneiss belts. Further regional studies of certain adjacent areas by Albat (1984), Jack (1980), Joubert (1974a) and Blignault et al. (1983) provide the basic framework for a regional map of the entire Namaqualand/Bushmanland area.

Although there are no previous major geochemical studies within the study area that predate this one, geochemical examination of various rocks in Namaqualand and Bushmanland was initiated in the early 1940's by Coetzee (1940,1941,1942a,b,1958) who recognised the sedimentary parentage of many of the paragneisses, and by Mathias (1940a,b). Since then, geochemical reports and studies have tended to concentrate on the sillimanite-corundum rocks in the Pofadder district (de Jager,1963; de Jager and von Backstrom,1961; Frick and Coetzee,1974; Moore,1977), the quartzo-feldspathic gneisses (Kroner,1968; McCarthy,1978; Lipson and McCarthy,1977; Lipson,1980), the mafic rocks (Moore,1977; Zelt,1980; Clifford et al., 1981) and the banded iron formations (Rozendaal,1982). The only comparable regional geochemical study undertaken to

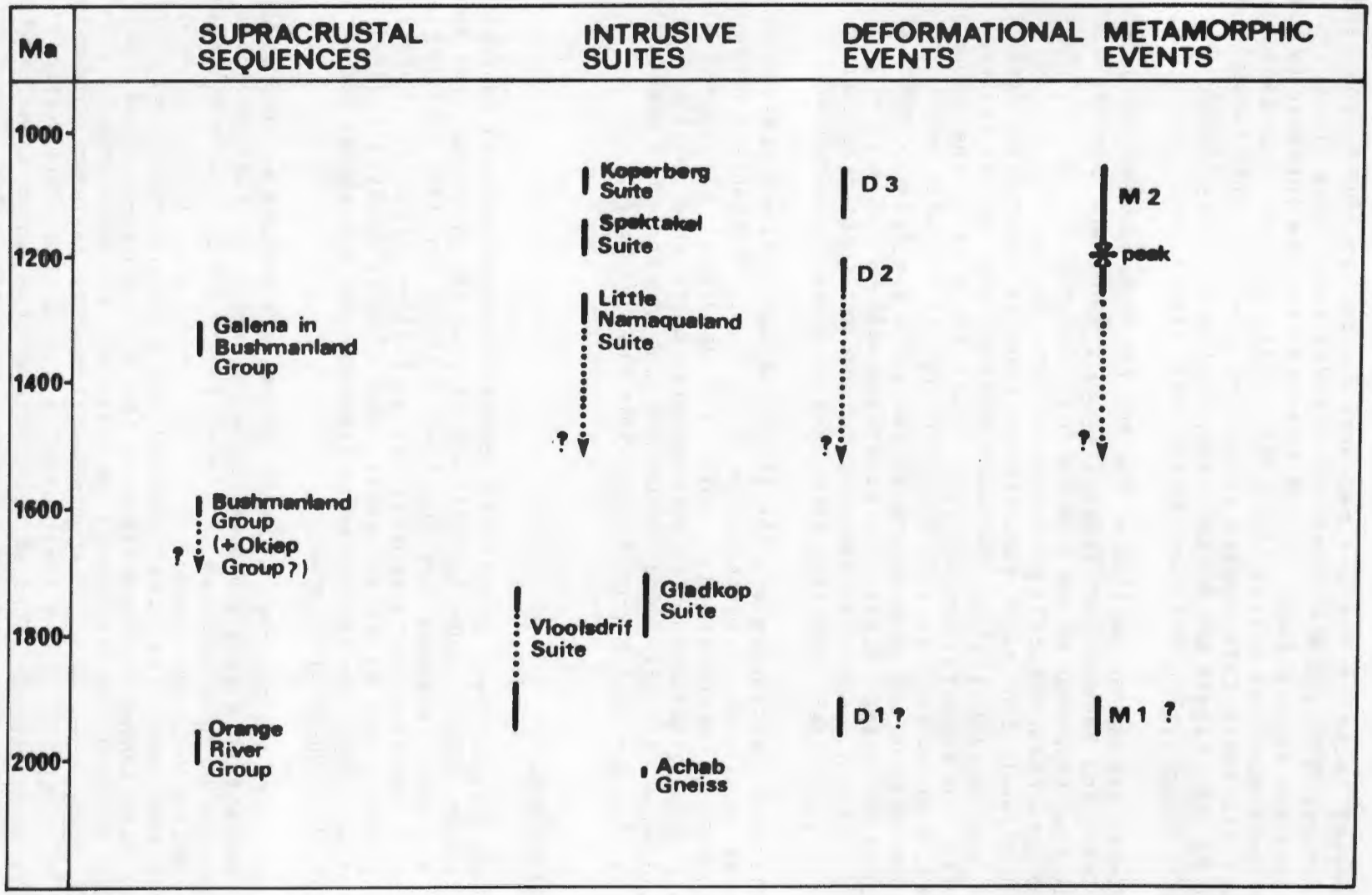

Table 1.1 A summary of ages obtained in a number of isotopic studies of the supracrustal rocks, intrusive episodes, deformational and metamorphic events in the western Namaqualand Metamorphic Complex. The sources of the data are referred to in the text in Chapter 2.

date in the western NMC is that by Reid (1977) of the metavolcanic and intrusive rocks in the Orange River area to the north of this project.

Brief geochemical examinations of metapelitic rocks (besides the sillimanite-corundum rocks) in the NMC are few and widespread, being those of the eastern kinzigites (von Backstrom,1964; Geringer,1973; Beukes,1973) and of the more unusual cordierite-rich and sapphirine-bearing metapelites (Mathias,1952; Clifford et al., 1975b, 1981). A few metapelitic gneisses from the Buffels River area were also analysed during a geothermometric study by Zelt (1980).

1.4 Present investigation

The present study concerns the regional distribution and geochemistry of various paragneiss/schist belt lithologies, and the aims of the study are both broad and more specific :-

1. to separate and/or correlate the various groups of metasedimentary and metavolcanic rocks;

2. to use the bulk compositions of the metamorphic rocks to present models for precursor lithologies and palaeoenvironmental settings;

3. to isolate certain associations and/or palaeoenvironments most suitable for the formation of base metal sulphide concentrations;

4. to indicate the sources, both compositional and geographical, of the paragneiss material and the enclosed metal sulphides;

5. to determine whether the three major groups of supracrustal rocks (Orange River, Bushmanland and Okiep Groups) are coeval as suggested by Bertrand (1975) or whether the Orange River Group represents an older volcanic pile as inferred by the contrasting geochronological data of Reid (1977) and Koeppel (1980).

1.5 Method

The initial approach employed in this study was to identify prominent paragneiss/schist belt outcrops from the previous regional mapping, and then to remap on air photos and 1:50,000 topocadastral maps relevant portions of these belts, selecting at the same time suitable geochemical sampling sites for the different lithologies. Once a particular paragneiss belt had been covered in this manner, representative lithologies were then sampled for both microscopic and geochemical analysis. By this process, some 12 man-months were spent between September 1979 and July 1982, sampling eight major and a few minor paragneiss belts between Bitterfontein in the south and Geselskapbank in the north.

Standard X-ray fluorescence analytical procedures, as adopted by the

During the fieldwork phase of this study, the writer was received, without exception, in a most friendly and hospitable way by the farming community of Namaqualand and Bushmanland. Special thanks are due to Mr Ben Rhoode of Bitterfontein, Mr Visser of the farm Witwater, the de Vries family of the farm Vaalkoei, the Roussouw family of the farm Gamoep and Mr and Mrs Dirk van Niekerk of the farm Kangnas for their hospitality and the provision of camping facilities. The writer is also indebted to the mine personnel of Black Mountain Mineral Development Company for providing access to borehole core for analytical purposes.

Chapter 2

REGIONAL GEOLOGY

2.1 Lithology

The study area contains a variety of metamorphic lithologies which under current SACS (1980) lithostratigraphic subdivision have been classified into three pretectonic metasedimentary/metavolcanic rock units, namely the Orange River Group, the Bushmanland Group and the Okiep Group, and some six to seven syntectonic intrusive rock suites.

2.1.1 The pretectonic units

The Orange River Group is subdivided into two subgroups and nine formations (SACS,1980) consisting of leucocratic (rhyolitic) to andesitic meta-lavas, quartz-feldspar porphyries, volcaniclastics, tuffs and metasediments (including quartzites, iron formations and schists) which stretch along the Orange River from the Richtersveld to Goodhouse in the east. Regional studies of the lithologies were conducted by de Villiers and Sohnge (1959), von Backstrom and de Villiers (1972), Blignault (1977), Ritter (1980) and Blignault et al., (1983), and the geochemistry of the volcanic rocks was examined by Reid (1977). Rb-Sr and U-Th-Pb isotopic studies indicated radiometric ages of 2000 to 1950 Ma for the Orange River Group (Reid,1979). No units of this group per se, extend into the study area.

The Bushmanland Group is subdivided into four subgroups and two formations (SACS,1980) and comprises various mica-sillimanite schist and quartzite associations (Pella and Aggeneys Subgroups), biotite/hornblende schists and gneisses (Guadom Subgroup) and leucogneisses with interbanded metasediments (Hom Subgroup). Studies of these lithologies in the Aggeneys-Gamsberg-Namiesberg area include those of Rozendaal (1975), Moore (1977), Lipson (1978) and Stedman (1980). Amphibolites from near the top of the Bushmanland Group succession at Gamsberg and Aggeneys yielded Nd isochron ages of 1600 Ma (Betton,1984). Pb-Pb isotopic studies of galena from sulphide deposits within the Bushmanland Group yielded model ages of 1350 to 1300 Ma (Koeppel,1980; Welke and Smith,1984), considerably younger than the ages obtained for the Orange River Group. Lateral equivalents of some of these subgroups extend into the northern portions of the study area.

The Okiep Group is subdivided into five subgroups comprising various schist/quartzite associations (Eenriet, Khurisberg and Aardvark Subgroups) in the north, a mixed central subgroup of biotite gneisses with lenses of metacarbonate rocks, quartzites and metapelitic rocks (Garies Subgroup) and a southern feldspathic quartzite/cordierite gneiss-dominated sequence (Bitterfontein Subgroup). Regional studies of these supracrustal rocks include those of Jansen (1960), Joubert (1971), Jack (1980) and Albat (1984). No radiometric studies have been undertaken of these lithologies and their age is

Department of Geochemistry, University of Cape Town, were employed in the whole-rock chemical analysis of the metamorphic rocks. 3 to 5 kilogram samples were crushed and reduced to 160 gm samples before grinding to -200 mesh. 5 gm samples of this powder were then pressed to form briquettes for trace element and Na analysis. For major element analyses, the Norrish fusion method was applied (Norrish and Hutton,1969). 2 gm powder samples were heated to 110 ^{o}C and ashed at 1000 ^{o}C to measure H_2O- and loss on ignition respectively. Duplicate weighed mixtures of ashed sample (0.28 gm), flux (Johnson Mathey Spectroflux 105) and sodium nitrate were then fused in 5%Au-95%Pt crucibles at 980 ^{o}C and cast as discs in a graphite dish at 230 ^{o}C. These discs were then used for all major element analyses aside for Na.

A Philips PW1400 and a Siemens SRS-1 automatic wavelength-dispersive sequential X-ray fluorescence spectrometer were utilized as the analytical intruments for major and trace element analysis. Instrumental conditions adopted for the XRF spectrometers are listed in Table A.1. Raw data capture and reduction was undertaken on a HP-1000 minicomputer using software compiled by staff of the Department of Geochemistry, University of Cape Town. Samples were run together with blanks, interference standards and calibration standards. The calibration standards include sets of USGS standards (G-1, W-1, G-2, GSP-1, AGV-1, BCR-1, PCC-1, DTS-1) and South African NIMROC standards (NIM-G, NIM-N, NIM-P, NIM-S). The detection limits and precision obtained for major element oxides are given in Table A.2 and the detection limits and counting errors for trace elements in Table A.3. Various graphical and statistical computer programs were used to display and examine the processed data. Relevant statistical procedures are explained at appropriate places in the text.

1.6 Acknowledgements

This study was made possible thanks to a Chamber of Mines Precambrian Research Unit bursary sponsored by Gold Fields of South Africa Limited to whom the writer expresses his gratitude. The Director of the Precambrian Research Unit, Geology Department, University of Cape Town, Prof. P. Joubert and Prof. A. J. Erlank, Head of the Geochemistry Department, University of Cape Town, jointly supervised this study and their assistance and constructive reviews of the thesis manuscript were much appreciated.

Many colleagues in the Precambrian Research Unit and the Geology and Geochemistry Departments assisted in various direct and indirect ways. The writer would particularly like to thank Assoc. Prof. A. R. Duncan, Assoc. Prof. J. P. Willis, Dr D. L. Reid, Dr D. J. Waters, Dr C. J. Hartnady, Dr C. W. Stowe, Dr. H-M Albat and Dr. M. K. Watkeys in this regard. Technical and laboratory support was ably provided by Mr R. S. Rickard, Mr S. B. Lawrence, Mr C. W. Steyl, Mr P. Meyer, Mr H. C. F. Hendricks and Mr R. J. Oliver, to whom the writer is indebted. The drafting of maps, diagrams and figures by Mrs R. Kovats, Ms S. Mostert and Mrs. M. Brandstatter was most appreciated, as was the typing of tables and editing of drafts of the manuscript by Mrs. A. Bateman.

thus poorly constrained. U-Pb isotopic studies of zircon fractions from cordierite-orthopyroxene gneisses within the Khurisberg Subgroup at the northern limit of its distribution in the Okiep Copper District, indicated inherited ages of greater than 1700 Ma and a 1200 Ma age for the subsequent high-grade metamorphic event (Clifford et al., 1981). Most of these subgroups are extensively covered in this study.

The various lithologies occurring within these pretectonic supracrustal groups in the study area are described in more detail in Chapter 3, and regional correlations are proposed in Chapter 5.

2.1.2 The intrusive suites

The intrusive rock suites in the Namaqualand/Bushmanland area can be subdivided into pretectonic, early syntectonic and late syntectonic/post-tectonic categories depending on their relationship to the major structural event (D2, Joubert,1971).

Pretectonic banded biotite gneisses have been identified in the Okiep Copper District (Brandewynsbank Formation, Marais et al., 1975) and in the Pofadder district (Achab gneiss, Moore,1977) where they have been proposed as a basement to the supracrustal successions. The Brandewynsbank gneisses have not yielded satisfactory model ages due to lack of variation in Rb-Sr data and Pb-isotopic composition (Barton,1983). If a close temporal relation is assumed with associated Steinkopf gneisses (both are members of the Gladkop Suite), however, emplacement ages in the region of 1800 Ma are predicted for the Brandewynsbank gneiss (Barton, op.cit.). A slightly older Pb-isochron age (2020 Ma) has been obtained from the Achab gneiss (Welke and Smith,1984).

The early syntectonic granitoids of the Little Namaqualand Suite (SACS,1980) are dominated by augen gneisses of granitic composition that were emplaced syntectonically during the early stages of the major D2 structural event. The Nababeep and Modderfontein augen gneisses have Rb-Sr ages of 1150 Ma with a relatively high initial Sr ratio of 0.725 (Reid and Barton,1983). A poorly constrained Pb-Pb age of 1500 Ma (Barton,1983) and the high initial Sr ratio are consistent with the emplacement of these gneisses between 1600 and 1500 Ma and their subsequent resetting during high-grade metamorphic events between 1200 and 1150 Ma.

The late syntectonic granitoids of the Spektakel Suite (SACS,1980) are typified by a variety of leucogranites (Concordia-type) and phenocrystic granites (Rietberg-type) that were emplaced in the later stages of the major D2 structural event or during the subsequent structural event (D3, Joubert,1971). The Concordia and Rietberg granites yield Rb-Sr ages in the region of 1200 Ma with relatively low initial Sr ratios (0.705), indicating that this represents an emplacement age that coincides with the peak of thermal metamorphism (Clifford et al., 1981).

Rocks of all three intrusive categories are present in the study area, generally in large east-west-trending belts separating the narrower paragneiss

enclaves from one another. They are often intricately interfolded and roughly concordant with the supracrustal rocks. Large-scale, transgressive, intrusive relationships are also apparent in certain areas (e.g. Bitterfontein and Buffels River areas).

Mafic granulites and amphibolites are commonest in the central and northern portions of the western NMC. Whilst some appear to be components of the supracrustal successions (i.e. they have formed from the metamorphism of extrusive volcanic rocks), the majority appear to be early syntectonic intrusive rocks. These lithologies have been studied in the Buffels River area (Zelt,1980), in the Copper District (Clifford et al., 1981) and Namiesberge (Moore,1977). The mafic rocks commonly occur as very thin bands within the supracrustal sequences, some with obliquely cross-cutting attitudes, or as large rafts and xenoliths within the other syntectonic intrusives, indicating an early temporal position within the intrusive suites.

Charnockitic gneisses comprise an important component of the syntectonic suite in the central portions of the western NMC, from the Kliprand area in the south (Albat,1984) to the Gamoep - Buffels River area further north (hornblende-hypersthene gneisses described by Joubert, 1971). These are mostly early syntectonic rocks, commonly closely associated with the mafic intrusives which they enclose as large, xenolithic bodies. Late syntectonic enderbitic types are, however, also present (Albat,1980,1984).

The intrusive rocks have been specifically excluded from this study and receive only superficial treatment in subsequent sections. Their relationships to the supracrustal rocks, however, either as part of a pretectonic basement complex or as disruptive intrusive masses, are of indirect importance and are referred to in several sections.

2.2 Structure

The regional reference framework for the subdivision of the structural events in Namaqualand/Bushmanland has been that of Joubert (1971), who identified four significant structural events, each with its own unique deformational style, orientation, intensity and associated metamorphism :-

1. D1. The first deformational event is poorly defined and its significance in the structural history of the study area is not apparent. Although many authors recognise the event (Joubert,1971; Halbich,1978; Jack,1980; Theart,1980), little is known as to its intensity, orientation, and associated metamorphism, and major structures related to this event have yet to be convincingly demonstrated. Generally, D1 characteristics are identified by recognition of a pre-D2 tectonic banding and tight minor folds (usually only on the cm scale).

A major early deformational episode is recognized in the metavolcanic rocks of the Orange River Group to the north of the study area, involving isoclinal folding with planar and linear fabrics (Blignault et al., 1983). This event predates the intrusion of Vioolsdrif granitoids and therefore must

be at least older than 1750 Ma. An early fabric is also identified in the pretectonic gneisses of the Steinkopf domain (including the Brandewynsbank gneiss) (Blignault et al., op.cit.) and in the Achab biotite gneiss at Namiesberg (Moore,1977).

2. D2. The second deformational event is widely recognised as resulting in the highest intensity of structural modification of the study area, with the creation of major isoclinal folds and thrust planes and large-scale re-orientation of the primary fabric of the pre-existing rocks by recrystallisation to high grade regional metamorphic mineral fabrics. Gneisses such as the Nababeep and Modderfontein gneisses, belonging to the early syntectonic Little Namaqualand Suite, contain the D2 penetrative foliation and regional lineation (Joubert,1971; Blignault et al.,1983), indicating that this deformational event is younger than their estimated emplacement age (1500-1600 Ma). Granites of the Spektakel Suite do not, however, contain the D2 fabrics, implying that the event is also older than 1200 Ma.

The orientations of linear and planar fabrics related to the D2 event have been highly modified by the succeeding D3 event, but both Joubert (1971) and Jackson (in Tankard et al., 1982) have interpreted the planar elements as originally having northerly dips of varying steepness in the study area. The linear fabrics show a wide degree of variability throughout the study strip and adjacent areas, commonly having either north-westerly, northerly or north-easterly plunges. This variability may be due to rotation during the D3 event, and it is quite possible that D2 structures in fact had more of a north-south attitude for both linear and planar fabrics prior to the D3 event.

3. D3. Major open folds and associated shear zones have greatly modified the attitudes of the isoclinal D2 structures and created the mosaic of closed structures (basins and domes) and interference patterns (mushroom and Christmas-tree shapes) that typifies the present-day attitudes of the NMC lithologies. These D3 structures are generally asymmetric with steep north-dipping axial planes, east-west trends, shallow plunges and variable intensities ranging from large open structures such as the Geselskapbank synform, to tighter nearly isoclinal structures in central and southern Namaqualand where associated linear fabrics become more noticeable.

In certain areas such as Dabenoris on the Orange River (Blignault et al., 1983), the Aggeneys-Gamsberg area and on Tweefontein in the Buffels River area, the major structures are distinctly non-cylindrical, varying from boat-shaped to sheathlike in appearance. Non-cylindrical folding is generally associated with episodes of shearing (Quinquis et al., 1978; Cobbold and Quinquis,1980) and east-west-trending shear zones are invariably associated with major F3 folds in the western NMC. Major shear zones were identified by Joubert (1971) in the Platbakkies-Witwater area, the Buffels River area and on the farm Silverfontein in the study area. Many of these shear zones appear to be closely associated with contacts between the paragneiss belts and the intrusive suite, and are suspected of representing re-activation of major early structures (D2) such as thrust zones. Both the open folding and the shearing affect rocks of the Spektakel Suite indicating that this phase of deformation is younger than 1200 Ma.

4. D4. Deformation of the open D3 structures by succeeding events varies in intensity, style and trend in different areas. North-east trending upright open folds deform the major F3 synforms in the Aggeneys, Gamsberg and Namiesberg area (Rozendaal,1975; Moore,1977; Lipson,1978), and north-west trending folds have been reported from the Kliprand area (Albat,1984). Superimposed on these structures are later upright north-south folds (either monoclinal or symmetric), commonly associated with prominent fracturing and some mylonitisation.

2.3 Metamorphism

The metamorphic history of the western NMC is complex due to its polyphase nature combined with the variability in P-T conditions of the different metamorphic events across the area. Attempts have been made to relate the various metamorphic imprints to the structural events, and it is generally accepted that the major metamorphic imprint (M2) is coincident with the major structural episode (D2, Joubert,1971). Resolution of the metamorphic episodes that pre- and post-date the M2 imprint, however, is considerably less satisfactory:-

1. Metamorphism associated with the D1 structural event in the western NMC has not been convincingly identified and remains speculative. A general assumption is that this metamorphic event, if it existed, was of lower grade than the succeeding major D2-related metamorphism. Upper greenschist facies mineral assemblages (Reid,1977) are present in the axial planar foliation of the early pre-Vioolsdrif-Suite structures in the Orange River Group metavolcanic rocks (Blignault et al., 1983). Ritter (1980) has identified a relatively high-grade migmatite complex of pre-Namaqua age at Helskloof in the eastern Richtersveld.

In the core of the Geselskapbank synform, metapelitic rocks have been subjected to two high-grade metamorphic imprints (see Sections 3.3 and 6.6), the first of granulite grade (K-feldspar-quartz-garnet-cordierite-sillimanite) and the second of upper amphibolite grade (biotite-sillimanite). This is in contrast to the surrounding metapelitic schists which only bear the imprint of the amphibolite-facies event. A similar two-phase metamorphic imprint (granulite facies succeeded by amphibolite facies) is observed in metapelitic rocks to the east of the Kenhardt-Kakamas road on the farms Melkboom and Hugo's Puts (R.Harris,pers. comm.), but only a single metamorphic imprint occurs in similar rocks from the southern and central portions of the western NMC (Albat,1984). The former metapelitic rocks were apparently subjected to a high-grade metamorphic event prior to the main Namaqua event which occurred at approximately 1200 Ma (Clifford et al., 1981).

2. Metamorphism with which the D2 structural event is closely associated, has resulted in the major regional metamorphic imprint observed in the western NMC, and varies from low grade in the northern Orange River Group domain through intermediate medium grades in the Bushmanland Group domain to high grades in the southern areas of the Okiep Group domain (Fig. 3.4). The

major portion of the study area has undergone M2 metamorphism from upper amphibolite to granulite grades involving temperatures in the region of 600 °C to 800 °C and pressures in the 4 to 6 kbar range (Jack,1980, Albat,1984; Moore,1977; Zelt,1980).

3. Metamorphism associated with the D3 structural event is widely regarded as retrogressive and less pervasive, generally being restricted to lower grade assemblages within the F3 shear zones. In the study strip, retrogressive metamorphic features were most obvious in the northernmost (Geselskapbank) and southernmost (Bitterfontein) major F3 structures. The absence of obvious evidence of retrogression within major F3 structures in the intervening area may be due to two possibilities - either that the granulites were too dry for large-scale retrogression to take place outside of narrow shear zones, or that the P-T conditions in this region were of similar high grade to M2. The regional zonation of the imprint associated with the D3 event is very poorly understood at present. Metamorphic signatures associated with the D2 and D3 deformations are regarded as part of a single thermal event with the D2 deformation occurring at the thermal maximum and the D3 deformation at some later time under lower P-T conditions (Albat,1984).

4. Metamorphism associated with the post-D3 events is invariably low grade and highly localised within F4 structural zones. Chlorite and epidote typify these metamorphic imprints which are insignificant in the regional context. Partial chloritization of biotite in the metapelitic schists and leucogneisses of the northern amphibolite-facies domain is a widespread, if somewhat erratic, phenomenon that appears to be related to post-D3 processes. High grades of metamorphism related to this event by Joubert (1971,1981) were not observed in the study area, and wollastonite occurrences examined in the Garies-Platbakkies area belonged to the earlier metamorphic assemblages associated with the D2 or D3 deformational events.

High-grade regional metamorphism such as occurs within the study area, can and does have a major modifying effect on the geochemistries of the supracrustal lithologies examined. These effects are discussed in Chapter 3 and Chapter 6 along with the important mineral reactions that form the typical upper-amphibolite- and granulite-facies assemblages.

Chapter 3

LITHOLOGICAL CLASSIFICATION

3.1 Introduction

Metamorphic rocks are often difficult to correlate on a regional basis due primarily to the extreme mineralogical and textural variability that rocks of similar origin can show under differing metamorphic conditions, even down to the scale of their appearance on fold limbs and in fold hinges. Classification of metamorphic rocks is also made more complex by the lack of an internationally accepted nomenclature scheme of any sort that has gained widespread acceptance. The result is that many authors use the loosely defined terms gneiss, schist or simply rock, prefixed by the suite of major or significant metamorphic minerals present (e.g. garnet-cordierite gneiss, cordierite-anthophyllite rock), to describe individual lithologies. This can be an extremely cumbersome procedure when dealing with many multi-component lithologies such as metapelitic or calc-silicate rocks. Widespread general usage has resulted in the loose grouping of common metamorphic rocks into various categories such as quartzo-feldspathic gneisses, calc-silicate rocks, amphibolites, etc..

For a study such as this, covering a large area across varying metamorphic facies zones, a well-defined lithological classification scheme is an essential prerequisite to allow for consistent observation and thus to assist correlation. The scheme must be both practical (i.e. easy to apply to field mapping) and discriminatory (i.e. easy to subdivide with subsequent petrological and geochemical examination). Such a scheme has been devised by the Geological Survey of New South Wales (Stevens and Willis,1983) during detailed lithological mapping of the Willyama Complex - a metamorphic complex of similar age to the NMC hosting the famous Broken Hill Pb-Zn ore deposit which is comparable in many aspects to the Aggeneys/Gamsberg ore deposits of the NMC. The rock types in this classification scheme are subdivided into seven major divisions - metasediments (essentially clastic rocks), quartzo-feldspathic gneisses, leucocratic quartzo-feldspathic gneisses, amphibole- and/or pyroxene-bearing rocks (including calc-silicate rocks), Fe-, Mn-, Zn-rich rocks, and various minor rock units (including quartz-rich rocks, chlorite-rich rocks and tourmaline-rich rocks). Composite gneisses (with 10-50% neosome formation) and migmatites (with greater than 50% neosome formation) are also distinguished in this classification.

Whilst the Willyama Complex classification can be used as a broad basis on which to develop a scheme for the classification of the supracrustal rocks of the western NMC, several major adaptations have to be made, particularly due to the wider variety of lithologies encountered within the study area when compared to the Willyama Complex. This classification scheme is also limited solely to the lithologies belonging to the pretectonic supracrustal sequences

and specifically excludes the intrusive suites of gneisses, charnockites and granulites.

3.2 A general classification scheme

The term "metasediment" used by Stevens and Willis (1983) is misleading as it pertains only to certain metasediments of clastic origin in their scheme and does not include quartzitic, conglomeratic or chemogenic metasediments. It has therefore not been used in the classification scheme devised for this study. Willis et al. (1983) have further subdivided the "metasedimentary rock types" into psammite, psammopelite and pelite based on the (quartz + feldspar) vs (sillimanite/andalusite + mica) contents of the rocks, presumably with the assumption that the quartz and feldspar contents of the rocks represented original detrital material, and were not subsequently formed by diagenetic or metamorphic reaction.

Such subdivisions could perhaps be applied to the upper-amphibolite-facies quartz-mica-sillimanite schists of the northern portion of the study area, but not to the cordierite gneisses of the south/central portion which formed under granulite-facies conditions with the breakdown of micas and sillimanite and the formation of cordierite, garnet and, more importantly, K-feldspar (for reactions see Section 3.3). The result is an increase in the amount of "psammitic" constituents and a decrease in the amount of "pelitic" constituents with the potential for misclassifying original pelitic rocks as psammites.

For the western NMC, therefore, the following subdivisions are proposed for broad field classification of the clastic metasediments excluding the highly siliceous rocks:

(1) in the granulite-facies terrane :

(a) metapsammitic gneisses: those in which the "pelitic" constituents cordierite + sillimanite + garnet + biotite + hercynite make up <15% of the rock.

(b) metapelitic gneisses: those in which the "pelitic" constituents cordierite + sillimanite + garnet + biotite + hercynite make up >15% of the rock.

(2) in the upper-amphibolite-facies terrane :

(a) metapsammitic gneisses/schists: those in which the "pelitic" constituents biotite, muscovite, sillimanite and garnet make up <20% of the rock.

(b) metapelitic schists: those in which the "pelitic" constituents biotite, muscovite, sillimanite and garnet make up >20% of the rock.

The metapelitic rocks of western NMC, therefore, by definition, incorporate both the pelitic and psammopelitic subdivisions of the Willyama Complex classification (Willis et al., 1983).

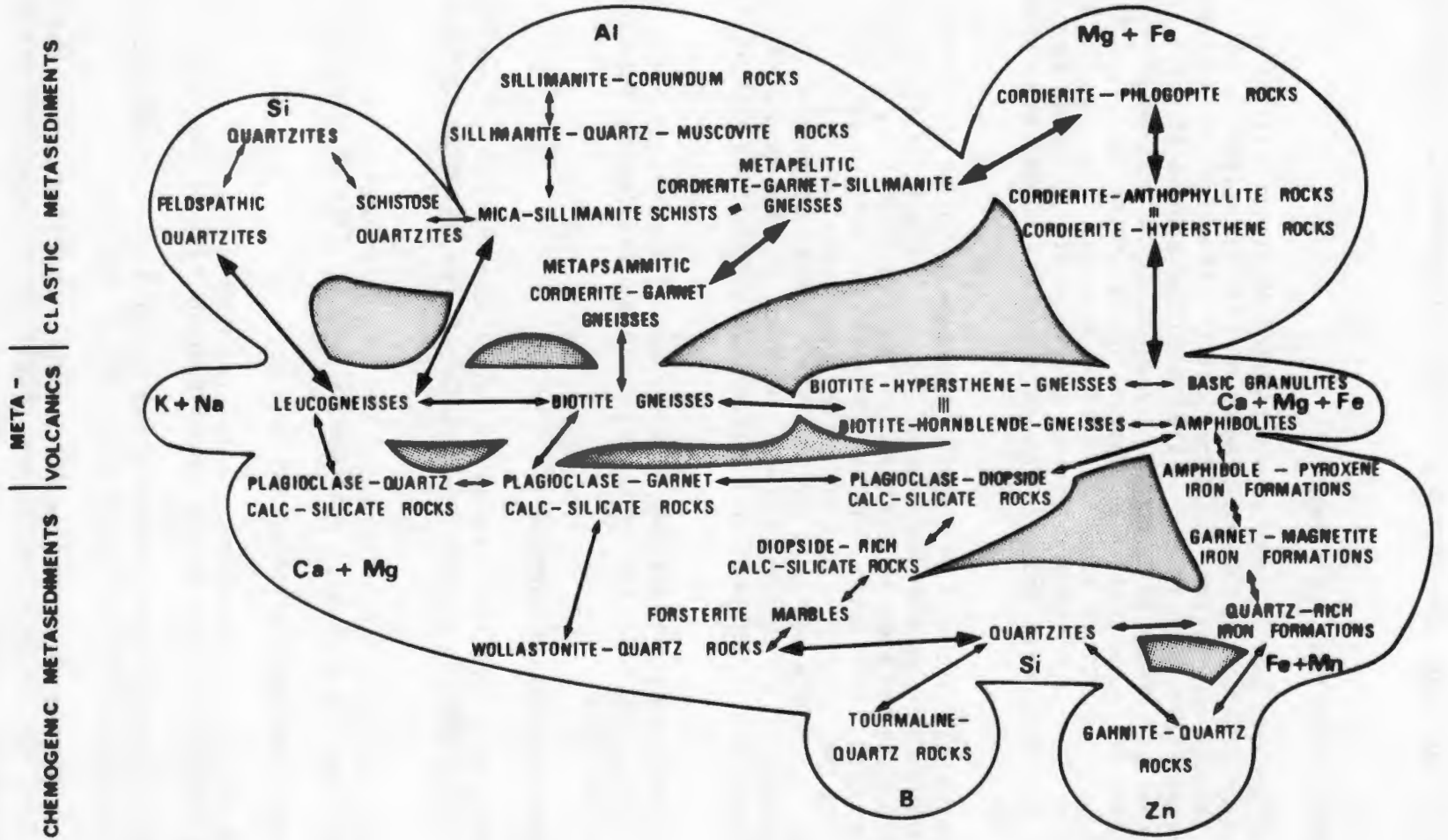

Table 3.1 Classification "tree" showing the various types of supracrustal rocks in the western NMC and their complex inter-relationships.

The paragneisses of the Willyama Complex do not contain major units of quartzitic rocks, and these rock types have thus been omitted from the classification scheme. In the western NMC, several types of quartzite are present that are essentially defined as lithologies having quartz contents of greater than 80%. The common varieties include feldspathic quartzites (where K-feldspar makes up the bulk of the minor constituents) which represent the common variety in the southern portions of the study area; glassy quartzites (with quartz content of approximately 99%) which predominate in the northern part of the study area; micaceous quartzites (where muscovite and, less commonly, biotite are the minor constituents) which again are commonly found in the northern portions of the study area; and ferruginous quartzites (where iron oxides, iron sulphides and/or garnet make up the bulk of the minor constituents). These varieties of quartzite show gradational relationships with leucogneisses, metapelitic schists and iron formations respectively.

Due to the paucity or absence of metacarbonate rocks that lacked amphibole or clinopyroxene, the calc-silicate rocks of the Willyama Complex were incorporated into a large suite of amphibole- and pyroxene-bearing lithologies which also included amphibolites and basic granulites of probable igneous parentage (Stevens and Willis,1983). This is not a satisfactory classification for the western NMC metacarbonate rocks which include marbles, wollastonite-quartz rocks and garnet-plagioclase-quartz lithologies - all essentially devoid of amphibole and pyroxene. The metacarbonate rock types, therefore, have been separated into their own grouping, showing gradations towards amphibolites (amphibole-pyroxene-rich rocks), quartzites (quartz-diopside rocks) and quartzo-feldspathic gneisses (plagioclase-quartz rocks).

A suite of lithologies incorporating a variety of magnesium-rich cordierite gneisses such as cordierite-phlogopite rocks and cordierite-hypersthene/anthophyllite rocks is present in the supracrustal sequences of the western NMC whereas these rock types or their equivalents are apparently absent within the Willyama Complex sequences. They are classified as an additional group and show gradations to both metapelitic cordierite gneisses and basic granulites.

Most of the gneissic lithologies are very similar in both the Willyama Complex and the western NMC. Biotite-hornblende schists and gneisses of transitional composition between biotite-rich quartzo-feldspathic gneiss and amphibolite are also present in the northern portions of the western NMC. Nomenclature pertaining to quartzo-feldspathic gneisses is abbreviated to leucogneiss instead of leucocratic quartzo-feldspathic gneiss and biotite gneiss instead of biotite-rich quartzo-feldspathic gneiss.

In general, then, the supracrustal rocks of the western portions of the NMC can also be divided into seven major groups: those whose mineralogy is essentially controlled by Si - i.e. quartzitic rocks; those whose mineralogy is controlled by Al - i.e. metapelitic and metapsammitic rocks; those whose mineralogy is controlled by Ca and lesser Mg - i.e. metacarbonate rocks; those whose mineralogy is controlled by Mg and to a lesser extent by Fe and Al -i.e. magnesium-rich cordierite rocks; those whose mineralogy is controlled by Fe

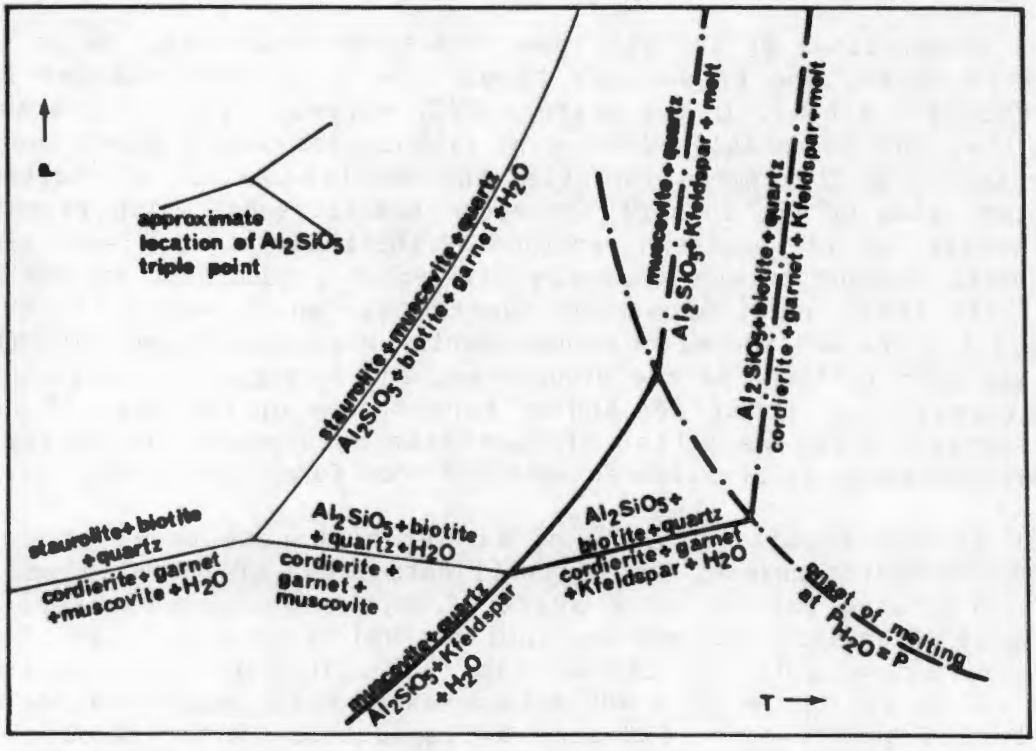

Fig. 3.1 A schematic P-T diagram (after Ashworth and Chinner, 1978) showing the significant reactions that occur during metamorphism of pelitic rocks. Reactions of particular significance to this study are emphasized by heavy lining.

and lesser Mn and Zn - i.e. iron formations; those whose mineralogy is controlled by K, Na and Ca - i.e. quartzo-feldspathic gneisses; and those whose mineralogy is controlled by the association of Ca, Mg and Fe - i.e. amphibolites and basic granulites. Many of these groups show gradations towards each other and certain transitional lithologies are difficult to classify into one specific group. The classification scheme is presented in Table 3.1.

3.3 Metapelitic and metapsammitic rocks

Rocks from these two groups form a major portion of the lithologies examined in this study. Some 150 samples have been petrologically examined and chemically analysed.

The division between the two groups - metapelitic and metapsammitic - is an arbitrary boundary (see Section 3.2) and gradations exist between them. It is essentially provided as a field standard to segregate rocks of dominant psammitic origin from those with a more prominent pelitic component. There are in outcrop and in petrological examination, however, other more prominent subdivisions within this rock group. The most obvious of these is the presence of schistose rocks in the northern portions of the study area and of gneisses in the southern and central portions. These divisions appear to be controlled by metamorphic grade which in general increases from north to south in the study area (Joubert,1971; Albat, 1984).

The gneissic rocks are typified by the mineral paragenesis quartz + K-feldspar + cordierite + plagioclase + garnet + sillimanite + ore/hercynite with small quantities of biotite usually present (Table 3.2) and the schistose rocks by the mineral paragenesis quartz + biotite + sillimanite + muscovite with varying amounts of K-feldspar and garnet and, more rarely, plagioclase (Table 3.3). The differences in mineralogy between these two groups of rocks can be explained by the prograde metamorphic reactions:

muscovite + quartz → sillimanite + K-feldspar + (either melt or H_2O) ...(1)

sillimanite + biotite + quartz → cordierite + garnet + K-feldspar + (either melt or H_2O) ...(2)

(Holdaway and Lee,1977; Ashworth and Chinner,1978). These two reactions represent the breakdown of the hydrous phases muscovite and biotite, and the formation of anhydrous phases garnet and K-feldspar together with relatively H_2O-poor cordierite. The muscovite-melting reaction (1) occurs at temperatures approximately 50 °C lower than reaction (2), with both reactions occurring in the region of 700 °C at 3 kbars pressure (Holdaway and Lee, op.cit.), and together representing the transition from upper-amphibolite-facies parageneses to granulite-facies parageneses in metapelitic rocks (Fig. 3.1). Texturally the rock is transformed from a schistose mica-rich lithology to a gneissic quartzo-feldspathic rock with markedly different field appearance, although of common premetamorphic origin. The classification scheme presented in Table 3.4, therefore, is dependant on correct textural and mineral assemblage

Table 3.2 Estimated modal analyses of metapelitic gneisses from the granulite facies domain in the study area. Trace constituents such as zircon and apatite are excluded (m = <1% concentration)

sample number	quartz	K-feldspar	plagioclase	cordierite	biotite	sillimanite	garnet	iron oxide/ hercynite
LC-2	19	22	12	40	2	m		5
WG-1	22	34	6	29	1	3		5
BA-1	22	37	8	23		4		6
WP-2	35	5	13	21	6	15		5
BI-23	34	22	6	29	2	3		4
BI-5	35	22	6	15	9	6	6	1
BP-8	27	46	8	2	4	3	9	1
KB-4	21	29	4	21		7	15	3
BI-11	25	24	10	19	5	3	12	2
RP-1	24	24	1	44	5	1	m	1
ZR-1	24	29	13		18	8		8
BP-5	39	15	8	12	2	4	19	1
ZR-4	28	24	7	27	1	1	10	2
BI-13	13	30	7	29	1	6	10	4
KB-1	22	1	35	18	22		2	
BI-2	24	36	4	22	7	1	5	1
BI-6	48	20	17		8		6	1
BI-4	35	22	15	18	1	4		5
LC-5	22	29	11	29		3		6
ZR-2	30	26	4	25	1	7		7
KB-3	35	12	12	24	1	9		7
BP-4	25	34	7	18	3	m	13	m
HY-2	35	1	5	25	20		14	m
HY-3	30	23	32		6	1	7	1
TW-4	65	11			2	22		m

Table 3.2 (continued) Estimated modal analyses of metapelitic gneisses from the granulite facies domain in the study area. Trace constituents such as zircon and apatite are excluded (m = <1% concentration).

sample number	quartz	K-feldspar	plagioclase	cordierite	biotite	sillimanite	garnet	Fe oxide/ hercynite
DM-3	51	19		22		2		6
DM-9	37	21		25	1	3	8	5
SK-1	44	21	16	14	m	1		4
SK-4	25	21	m	1	3	19	29	2
SK-7	35	27	12	2	1	m	20	3
HY-20	22	56	1	12	m	7		4
VK-4	27	32	23	1	2	m	14	1
SK-6	49	12	16	17	1	m		5
TW-10	35	38	2	8	1	7	7	2
BPT-3	30	18	24	11	1	2	10	4
ROF-7	44	4	8	16	3	2	20	3
KGV-1	41	18	15	7	2		12	5
PH-1	46	19	5	18	5	m		7
RW-3	42	15		25		8	2	8
WW-3	33	24	12	13	8		8	2
WW-4	44	19	15	10	4	2		6
WW-8	52	18	10	10	1	m	4	5
WW-10	28	34	8	21	1	1	1	6
WW-13	44	27	13	6	1	1	3	5
9-PEL	29	14	29	22	2	m		4
HK-1	18	36	12	11	5		17	1
TW-4	34	18	19	m	5	2	21	1
ROF-12	46	7	23	7	2	14	1	2
ROF-3	39	18	21	3	12	4	1	2
TW-13	28	24	32		13		2	1

Table 3.3 Mineral compositions of metapelitic schists from the amphibolite facies domain of the study area. (M = major constituent <5%; m = minor constituent 5-1%; vm = minor constituent <1%). Accessory minerals such as zircon, apatite and tourmaline are not included.

sample number	quartz	K-feldspar	plagioclase	biotite	muscovite	sillimanite	garnet	cordierite	Fe oxide	graphite
BH156-1	M		m	M	m	M				
BH156-2	M		m	M	vm	M			vm	
BH156-3	M			M	m	M			vm	
BH156-4	M			M	m	M			m	
BH156-5	M			M	m	M			m	
BH156-7	M			M	M	M	m			
HS4-55	M	M	m	M	m	m	m		m	
BH126	M	M	m	M	m	m			m	m
BH114	M	M	m	M	m	m	m		m	
EK2-85	M	m		M	m	M			m	
EK2-130	M	m		M	m	M			m	
EK2-210	M			M	m	M			m	
AG51-215	M			m	M	M		m	m	
AG56-115	M			M	m	m			vm	
AG80	M		vm	M	m	M	M			
SW22-155	M	m	vm	M	M	M			m(sulphide)	vm
SKF-1	M			m	M	M			vm	m
SKF-2	M			M	m	M				m
SKF-4	M	M	m	M		M		M	m	
SKF-9	M	M		M		M		M	m	
SKF-10	m					M		M	m	
NB-3	M		m	M		M		M	vm	
NB-5	M		m	M		M		M	vm	
NB-6	M		m	M		vm	m	M	vm	
SS-2	M			M	m	m				
SS-5	M			M		M		m		
SS-8	M			M		M			vm	
SS-9	M			M		M			vm	
KN-9	M			vm		m			m	
KN-10	M	M		M		m		M		
KN-11	M			M		M			m	
LB-1	M	M		m		M	vm		m	
KO-5	M			M		M			vm	
BB-1	M	vm	m	M	m	M			vm	
BB-6	M	m	vm	M	m	m			vm	
BB-8	M			M	m	m				
BB-9	M			m	M	M			vm	

identification in the field.

The petrology and field characteristics of the cordierite-bearing metapelitic and metapsammitic gneisses from the southern and central portions of western NMC are well described by Brink (1950), Joubert (1971), Jack (1980) and Albat (1984). The gneisses are either massive, crudely banded or well banded and have a distinctive red-brown appearance in the field. Where banding occurs, this is generally due to alternating quartz-feldspar-rich and aluminous-mineral-rich bands. On the farm Zout Rivier in the Bitterfontein area, features interpreted as indicative of graded bedding (Glen and Laing,1975) were observed. Fine-grained quartz-feldspar bands (psammitic base) grade systematically into much coarser grained garnet-biotite bands (pelitic top). Elsewhere within the more massive varieties, quartz-feldspar-garnet and quartz-feldspar-biotite leucosomes are present in varying amounts, indicating a certain degree of in-situ melting of the gneisses. Migmatitic rocks of this nature were most common to the south of the Platbakkies-Witwater paragneiss belt and extend into the Kliprand area (Albat, op.cit.).

The gneisses consist of xenoblastic quartz, K-feldspar (either orthoclase, perthite or microperthite) and plagioclase together with xenoblastic or poikiloblastic cordierite, coarse garnets of various habits (skeletal, subhedral, symplectic with hercynite/iron oxides, helicitic with sillimanite), coarse, euhedral sillimanite which also occurs as fine needles in quartz, cordierite and garnet, and complex intergrowths of iron oxides and hercynite. Corona features involving growth rims of cordierite, sillimanite, garnet or even plagioclase surrounding hercynite/iron oxide or garnet grains are fairly common. Symplectic quartz-cordierite intergrowths were observed in a few samples, and a quartz-cordierite-K-feldspar-hypersthene symplectite-rich rock (sample BA-3) on the farm Banke in the Bitterfontein area (Brink,1950) possibly represents the breakdown products of an original osumilite-bearing lithology (W. Schreyer, pers. comm.).

The cordierite gneisses have mineral parageneses that are ideally suited for garnet-cordierite geothermometry and geobarometry (Holdaway and Lee,1977). Various studies of the mineral chemistries of these gneisses from western NMC (Jack, 1980; Albat, 1984; Waters and Moore, in press) have obtained P-T estimates for the major prograde metamorphic event from these lithologies. Temperatures in the region of 750 - 800 ^{o}C and pressures of 5-6 kbars have been obtained by Albat (op. cit.) in the most comprehensive study to date, yielding geothermal gradients marginally less than 40 ^{o}C per km. P-T conditions obtained by Jack (op.cit.), from metapelitic gneisses in the extreme western NMC yield variable lower temperatures and pressures indicating either lower Namaqua metamorphic conditions or the effects of later Pan-African metamorphism in this area. Estimates by Zelt (1980) using less precise methods proposed by Green (1976,1977) and Currie (1971) gave temperatures (780-860 ^{o}C) and pressures (in the region of 7 kbars) of a somewhat higher nature from metapelitic rocks in the Buffels River paragneiss belt. Low-pressure granulite-facies P-T conditions are thus assumed to have existed over a large area of south/central western NMC.

The mica-sillimanite schists from the northern portions of the western

TEXTURE	PELITIC COMPONENTS	%	CLASSIFICATION
schistose	biotite sillimanite muscovite (garnet)	>20%	metapelite
		<20%	metapsammite
gneissic	cordierite garnet sillimanite hercynite (biotite)	>15%	metapelite
		<15%	metapsammite

Table 3.4 A basic classification for metapelitic and metapsammitic rocks in the western NMC.

NMC are well-banded rocks, also of distinctive red-brown appearance in the field. They are commonly highly weathered, soft, friable rocks of poor exposure, being masked by scree-cover from adjacent lithologies, usually overlying glassy quartzites. Sampling of these rocks for geochemical analysis is problematical due to their highly weathered state and as many samples as possible were collected from borehole core samples during this study.

Petrological descriptions of these lithologies are given in Rozendaal (1975), Moore (1977) and Lipson (1978). The schists consist of elongate, highly strained, anhedral quartz with oriented brown-to-red/brown biotite laths and lenticular "wispy" clusters of fibrolitic sillimanite. Coarse muscovite is commonly either intergrown with biotite or mantles the sillimanite clusters. K-feldspar occurs as dusty, xenoblastic grains of microcline, and garnet, when present, invariably occurs as round, subhedral grains. In many samples there is a certain degree of chloritic alteration of biotite. Graphite is also present in several samples, particularly from the Geselskapbank area.

Metapsammitic varieties of the mica-sillimanite schists are rare, and the common transition observed is one between schists and quartzites, resulting in a schistose mica-sillimanite quartzite. Where the mica-sillimanite schists are underlain by a prominent leucogneiss unit (such as the Aggeneys/Gamsberg/Namiesberg area; Rozendaal,1975; Moore,1977), the schists become increasingly K-feldspar-rich towards their lower contact with these gneisses.

Two minor subgroups of schistose rocks are associated with the mica-sillimanite schists. Quartz-muscovite schists are present locally in the Aggeneys/Gamsberg area towards the top of the supracrustal sequence and are also located in the Geselskapbank area. These schists are relatively common in the Goodhouse/Hom area along the Orange River to the north of the study area where they form part of the Hom Subgroup (SACS,1980). Quartz-sillimanite(-muscovite) schists are more widespread, but uncommon, minor constituents of the metapelitic schists. The latter rocks are closely associated with massive sillimanite and sillimanite-corundum rocks in the Aggeneys-Pofadder area (Coetzee,1940; de Jager,1963; Frick and Coetzee,1974; Moore,1977) to the north-east of the present study area.

The mica-sillimanite schists of the western NMC have not been utilised in geothermometric or geobarometric studies although they are well suited to such studies using the garnet-biotite geothermometer (Ferry and Spear,1978) and perhaps the garnet-plagioclase-quartz-sillimanite geobarometer (Ghent,1976). P-T approximations using the FeO/(MgO + FeO) ratios of schists containing the assemblage cordierite + almandine + sillimanite + quartz (Hensen and Green,1971; Currie,1971), and the presence of quartz-feldspar metatects indicating onset of anatexis, indicate temperatures in the region of 650 - 700 ^{o}C and pressures between 4.5 and 6 kbars (Moore,1977). The mica-sillimanite schists therefore, appear to represent lower temperature (and possibly slightly lower pressure) equivalents of the cordierite gneisses at P-T conditions within the upper amphibolite-facies range.

minor minerals	quartz < 80 %	80 % < quartz < 90 %	quartz > 90 %
biotite	metapelitic schist	schistose quartzite	glassy quartzite
k-feldspar	leucogneiss	feldspathic quartzite	
garnet magnetite pyrite	iron formation	ferruginous quartzite	
diopside amphibole	calc - silicate rock		
tourmaline	tourmalinite		

Table 3.5 A basic classification scheme for quartzitic rocks in the western NMC.

3.4 Metaquartzites

Quartzitic rocks are common components of the paragneiss belts of the western NMC, particularly in the southern portions around Bitterfontein and again in the north in a broad belt from the Okiep Copper District eastwards to Pofadder. Their distribution is similar to that of the metapelitic rocks, being commonest where these are most prolific, and also consisting of two major types, one dominant in the south, the other in the north. Quartzites in the western NMC are arbitrarily defined as paragneisses containing >80% quartz, and they show gradations into leucogneisses (increasing quantities of feldspars), metapsammitic gneisses (increasing feldspars with cordierite, garnet), mica-sillimanite schists (increasing micas, sillimanite), iron formations (increasing iron oxides, sulphides or garnet) and, more rarely, calc-silicate rocks (increasing diopside, plagioclase).

As a broad generalisation, the quartzites of the western NMC can be divided into two major types. A feldspathic quartzite in which evenly-distributed K-feldspar dominates as the minor constituent, is the common variety encountered in the southern portions of the western NMC. A glassy quartzite, virtually entirely composed of quartz (>99% SiO_2) with a variety of minor-to-trace constituents comprises one of the major lithological units in the northern paragneiss belts. The trace minerals include garnet, biotite, iron oxides, iron sulphides, tourmaline and diopside - either as fine, disseminated grains or as thin, impersistent bands within massive, transparent to translucent quartz, as well as widely-spaced, interlaminated, muscovite-rich schistose bands (generally <1cm thick) with lesser biotite and sillimanite. Rarely these micaceous quartzites are green in colour and have been identified as "fuchsitic quartzites" although fuchsite has yet to be positively identified. The classification scheme for quartzitic rocks is presented in Table 3.5.

3.5 Quartzo-feldspathic gneisses

Quartzo-feldspathic gneisses are by far the dominant rock types in the paragneiss belts of the western NMC, particularly the central and far western portions (Joubert,1971; Jack,1980; Theart,1980). They are usually fairly easily distinguishable from the intrusive or "basement" rocks of similar mineral composition due to their relatively fine, equigranular texture (as opposed to the coarser-grained augen-to-megacrystic texture of the intrusive gneisses) and by their finely banded nature (as opposed to a more massive, irregular banding in the intrusive gneisses), most prominent on weathered surfaces.

In the field they can be subdivided into two distinct groups, a virtually biotite-free leucocratic "pink" gneiss (hereafter termed leucogneiss), and a relatively biotite-rich "grey" gneiss (hereafter termed biotite gneiss). The distinction between these two varieties is based on their mafic mineral content - the leucogneisses containing <5% (commonly <2%) biotite or, more rarely, hornblende, and the biotite gneisses >5% biotite sometimes together

Table 3.6 Estimated modal analyses of metapsammitic and biotite gneisses from the study area. Accessory constituents such as apatite and zircon are excluded. (epi = epidote; hb = hornblende; opx = orthopyroxene).

sample number	quartz	K-feldspar	plagioclase	biotite	garnet	cordierite	iron oxide	sillimanite	mafic minerals
BI-20	36		37	24			3		
BI-24	33	5	28	26			2		6 epi
BI-1	60	10	13	2		14	1		
BI-19	40	12	26	20			2		
BP-3	32	29	20	15		4	m		
WG-2	72		22	5			1		
BI-9	38	28	18	9		4	3		
BI-14	45	31	9	9		2	2	2	
BI-15	44	28	13	4	1	9	1		
KB-2	49	29	7	4	m	5	4	2	
VK-11	40	23	21	15			1		
TW-1	40	20	30	7			1		2 hb
PH-6	43	25	21	2		7	2	m	
PH-11	39		44	7			2		8 opx
PH-16	33	38	25	m			4		
BPT-2	38	8	26	5			3		
ROF-1	28	36	25	8			3		
ROF-2	57	10	23	5	1		4		
ROF-6	29	23	37	5			6		
ROF-10	27	20	41	10			2		
PH-2	28	30	31	6			2		3 opx
GHP-1	42	20	33	1		2	1	1	
WW-1	36	32	26	5			1		
WW-5	38	32	18	1		8	3		
RFN-6	32	29	30	7			2		m opx
RFN-7	34	32	29	4			1		
RFN-8	27	27	34	10			2		
ROF-11	40	2	38	18			2		
BB-4	58	2	35	4					1 rutile
HY-5	49	25	8	7		10	1		

with lesser hornblende or hypersthene.

The quartzo-feldspathic gneisses have a granoblastic texture with xenoblastic quartz, perthite and/or microcline-microperthite dominating the mineral assemblages, with lesser plagioclase, sometimes showing peripheral myrmekitic intergrowth with quartz, strongly aligned biotite flakes (in the biotite gneisses), and opaque iron oxides, together with traces of hercynite in the granulite-facies domain (Table 3.6). Biotite in the leucogneisses commonly shows partial alteration to chlorite in both the granulite- and amphibolite-facies domains. Muscovite, garnet and idioblastic sillimanite are occasional minor constituents in the leucogneisses, and garnet, hornblende, epidote and hypersthene in the biotite gneisses. Traces of fluorite are observed in certain leucogneiss samples and sphene and apatite in the biotite gneisses.

The leucogneisses occasionally contain zones with prominent nodules or more irregular lenses of sillimanite and quartz (± muscovite) (Theart,1980; Moore,1977), and the biotite gneisses occasional clusters or knots of hypersthene or hornblende. Certain lithologies containing >20% biotite are classified as biotite schists, and in the Geselskapbank area a suite of biotite-hornblende schists and gneisses are present in which hornblende becomes a major constituent. Similar schists and gneisses are relatively widespread along the Orange River from Goodhouse to Klein Pella where they form part of the Guadom Subgroup (SACS,1980). In the central portions of the western NMC, particularly in the Anegas-Dounabees-Boesmanplaat paragneiss belt, but also in the Rooifontein and Buffels River areas further north, a plagioclase-rich, K-feldspar-poor biotite gneiss occurs, containing prominent quartz "pebbles" or augen, which by their randomly scattered distribution may indicate that the original lithology was a porphyritic volcanic rock (sample ROF-11). A classification scheme for leucogneisses, biotite gneisses and schists, biotite-hornblende gneisses and schists is presented in Table 3.7.

The quartzo-feldspathic gneisses commonly contain metatects as the result of anatexis. Within the leucogneisses, this is commonly represented by coarse, almost pegmatitic, concordant to discordant quartz-feldspar leucosome bands, and within the biotite gneisses by either coarse "blotchy" quartz-feldspar-biotite segregates (common in the Bitterfontein and Rietfontein areas) or by quartz-feldspar-garnet or quartz-feldspar-hypersthene leucosome veins (common in the Witwater and Buffels River areas).

3.6 Calc-silicate rocks and marbles

Metamorphic rocks derived from carbonate-rich precursor sediments represent some of the most variable lithologies in the western NMC (see also Jackson,1976), a feature which complicates their classification into any relatively simple, field-applicable scheme. Common minerals observed in these lithologies are calcite, dolomite, diopside, plagioclase, garnet, quartz, scapolite, wollastonite, forsterite, chondrodite, phlogopite, hornblende, tremolite, vesuvianite/sphene and epidote, and it is this wide variety of minerals which makes classification difficult. As an initial generalisation,

	biotite < 5%	5% < biotite < 20%	biotite > 20%
hornblende < 5%	leucogneiss	biotite gneiss	biotite schist
5% < hornblende <20%	hornblende gneiss	biotite - hornblende gneiss	biotite-hornblende schist
hornblende >20%	amphibolite		

Table 3.7 A basic classification scheme for cordierite-free quartzo-feldspathic rocks in the western NMC. This scheme is for lithologies of amphibolite-facies grade. At granulite grades, hornblende is replaced by orthopyroxene and amphibolite by basic granulite.

however, the metacarbonate rocks can be subdivided into five groups - a broad group of plagioclase-diopside-quartz-dominated lithologies; a similar group of plagioclase-garnet-quartz (± diopside) lithologies; a group of almost monomineralic diopside-rich rocks with lesser scapolite and/or plagioclase; a diverse group of rocks containing wollastonite - generally either wollastonite-quartz or calcite-wollastonite (± garnet) rocks; and a marble group whose mineralogy is dominated by dolomite and forsterite (commonly altered to serpentine) or chondrodite (Table 3.8).

The plagioclase-diopside-quartz rocks are the most widespread metacarbonate lithologies, occurring from the Bitterfontein area in the south to the Aggeneys area in the north (Namiesberg, Moore,1977). In the northern portion of the study area, they generally contain a prominent hornblende constituent, and appear to grade via certain banded hornblende-plagioclase-quartz rocks (samples ER-2, GB-12 and KBB-1) into true amphibolites. Elsewhere they contain minor orthopyroxene (samples MF-1 and DM-6) and show transitions towards basic granulites. The textures of the calc-silicate rocks are typically granoblastic with xenoblastic plagioclase and quartz and skeletal, sometimes poikiloblastic, diopside. Hornblende is commonly xenoblastic. Iron oxides and biotite are common minor constituents, and these lithologies were probably some of the least pure metacarbonate rocks prior to metamorphism. The more diopside-rich varieties generally have sphene and rarely scapolite as minor constituents. Where calcite is present, it is generally of a secondary nature (alteration).

The plagioclase-garnet-quartz calc-silicate rocks have virtually as great a distribution in the western NMC as the plagioclase-diopside-quartz rocks, and are only absent (or were overlooked) in the southern Bitterfontein area. They were sampled from the Witwater-Platbakkies paragneiss belt to the Smorgen Schaduwe-Kangnas belt, and also occur further north in the Namiesberg (Moore,1977) and Pella (Coetzee,1941) areas where retrograde epidote is a common minor constituent. Gradations to plagioclase-diopside-quartz and plagioclase-quartz calc-silicate rocks occur. Sphene and, more rarely, scapolite are minor constituents. Sample SS-4 from the farm Smorgen Schaduwe contains 20-15% allanite in a rock which otherwise resembles the others in this group. The plagioclase-garnet-quartz calc-silicate rocks have a granoblastic texture and commonly occur as one of two different types, either as a finer network of garnet and diopside (the former partially rimming the latter) enclosing coarser xenoblastic plagioclase and quartz, or as large skeletal poikiloblasts of garnet together with xenoblastic plagioclase and quartz.

The "monomineralic" diopside-rich subgroup comprises relatively massive to poorly banded rocks whose mineralogy is dominated by coarse, xenoblastic diopside with lesser plagioclase and/or scapolite and minor quartz, calcite, sphene/vesuvianite, pyrite and spinel (the latter two constituents being present in sample VK-10) and opaque oxides (in sample KO-6). Sample GB-1, a massive tremolite rock, represents a chemically similar lithology of lower metamorphic grade. The diopside-rich calc-silicate rocks generally show close association with the dolomitic marbles and are thus concentrated in the central paragneiss belts between Garies-Platbakkies and the Buffels River.

Table 3.8 Mineral compositions of metacarbonate and calc-silicate rocks from the study area. (M = major constituent >5%; m = minor constituent 5-1%; vm = minor constituent <1%). Accessory minerals such as apatite and zircon are omitted. (phl = phlogopite; opx = orthopyroxene).

sample number	carbonate	forsterite	wollastonite	clinopyroxene	hornblende	garnet	plagioclase	quartz	scapolite	biotite	sphene	iron oxide	other
DM-1				M			M	m			m	m	
MF-2				m			M	M				m	vm (opx)
BA-2				m			M	M				m	
BI-7				m			M	M		m		m	vm (opx)
BI-10				M			M	M		vm		m	
BI-16				M			M	M		vm		m	
RFN-10				m	m		M	M			vm	m	
ZR-7				M			M	M			m	m	
RFN-11				m		vm	M	M			m	m	
VK-5	m			M			M	M			m	vm	
PH-10				m			M	M		m		m	
PH-13	m			m			M	M			vm		
GHP-4				m			M	M			m	m	
TW-3				M			M	m			m	m	
RW-2				M			M	M			m	m	
DM-6				M			M	M		vm		m	vm (opx)
RFN-5				m			M	M			m	m	
RFN-1				m			M	m			vm	m	
DM-5				m			M	M	m		m		
HY-6				m			M	M			vm	m	
9-CS				m			M	M			m	M	M (opx)
KGV-3	m			M			M	M	m	vm	m	vm	
SS-3				M	m		M	m			vm		
DM-7	vm			M			M	m			m		m (phl)
ROF-4				m		m	M	M			vm		
PH-4				m		m	M	M	m		m		
KO-7				M		M	M	M					
ND-1				M		M	M	M					
TW-2				m		m	M	M	m		m		

Table 3.8 (continued) Mineral compositions of metacarbonate and calc-silicate rocks from the study area. (M= major constituent 75%; m = minor constituent 5-1%; vm = minor constituent <1%). Accessory minerals such as apatite and zircon are omitted. (all = allanite; sp = spinel; tr = tremolite; opx = orthopyroxene; phl = phlogopite; gr = graphite; chd = chondrodite).

sample number	carbonate	forsterite	wollastonite	clinopyroxene	hornblende	garnet	plagioclase	quartz	scapolite	biotite	sphene	iron oxide	other
SS-4				m		M	M	m	vm		m		M (all)
WW-6				M			M				vm		
WW-14				M			m				vm		
SK-8				M			m						
HY-19				M			m				m		
KO-6				M			M				m	M	
TW-15				M			m	m	M	m	m		
VK-10	m			M					vm			m	m (sp,tr)
ROF-15				M					M		vm		
GN-4				M				M					m (opx)
RFN-2						M	M	m					
VK-6						M	M	m					
GB-2	vm		M			m		M					
PH-15	m		M	m			m	M			vm		m (phl)
RW-1	m		M	m		m		M	m				
WF-2	M		M	m		m							
SYN-1	M		m	m		M							m (tr)
PH-14	M			m				m	m		vm		
NB-1	M	m											m (tr)
NB-2	M	m											m (phl)
VK-9	M	M				vm							m (gr)
DM-4	M	M				vm						vm	m (phl)
SK-9	M	M	(chd)			vm						m	
VK-1	M	M											m (phl)
DM-8	M	M											m (gr)
HY-18	M	M											M (tr)
ER-2					M		M	M				M	
GB-12					M		M	M				m	
KBB-1					M		M	M				M	

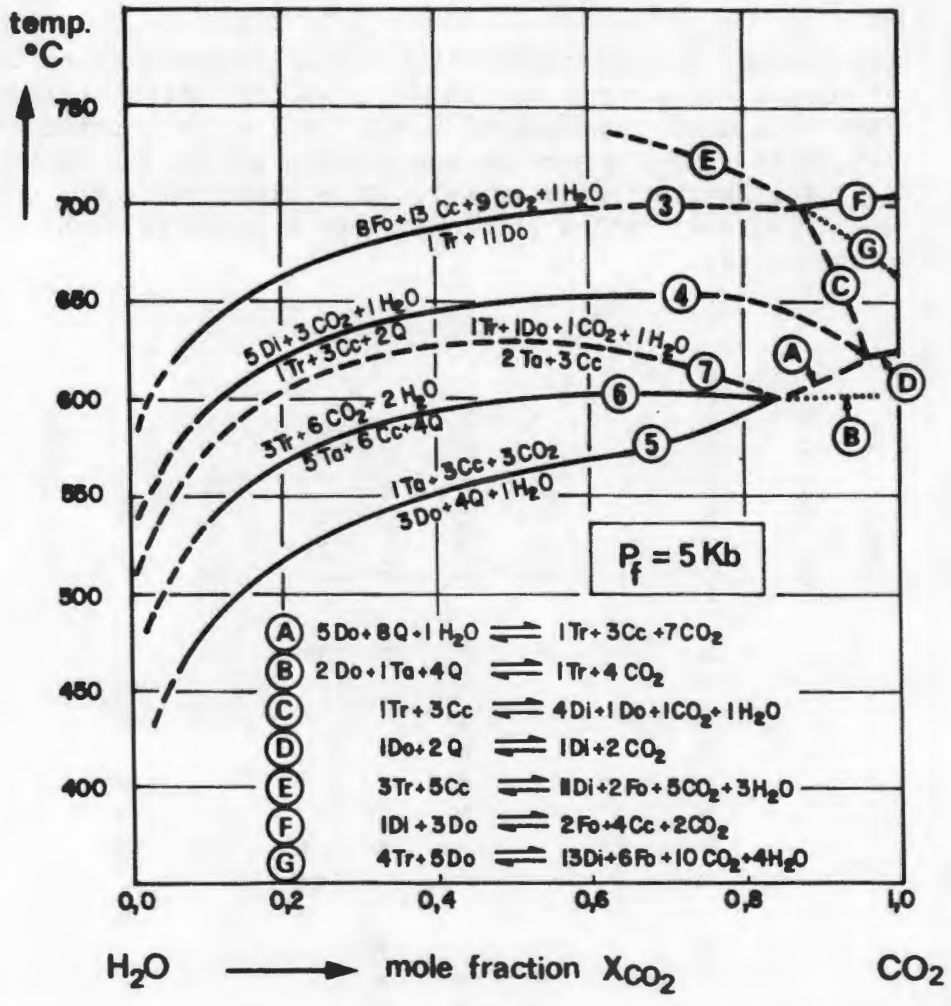

Fig. 3.2 An isobaric diagram (at 5 kbar) of temperature vs mole fraction XCO_2 (after Winkler, 1976) showing various common metamorphic reactions that take place in siliceous dolomites.
(Di = diopside; Q = quartz; Do = dolomite; Cc = calcite; Tr = tremolite; Fo = forsterite; Ta = talc).

Sample GB-1 is associated with wollastonite-quartz rocks and marbles in the Geselskapbank area.

The wollastonite-bearing calc-silicate rocks and marbles comprise two different lithologies, wollastonite-quartz rocks and calcite-rich carbonate rocks which contain wollastonite as a common minor constituent together with garnet and, less commonly, diopside. They are generally coarsely banded rocks with wollastonite displaying negative weathering and thus having been overlooked in previous surveys with the exception of the prominent occurrence on the farm Wilgenhoutfontein, north of Garies (de Jager and Simpson,1962; Joubert,1971). The wollastonite-bearing calc-silicate rocks have a restricted distribution, being commonest within the Garies-Platbakkies paragneiss belt and further east near Kliprand (Albat, 1984) in the central portions of the western NMC. They are also present in the northern portions of the western NMC and were located at Heiorigas in the Geselskapbank area, the Aggeneysberge (Lipson,1978; sample SYN-1) and Gamsberg (Rozendaal,1975,1978).

The forsterite-dolomite marbles are generally thick, crudely banded rocks, outcropping as impersistent, relatively thin lenses and pods (<5 metres thick) in association with the other calc-silicate rocks. They have the most restricted distribution of all the metacarbonate rocks, outcropping at Rooifontein in the northern part of the Leliefontein Reserve, in the Stofkraal-Dikmatje and Buffels River paragneiss belts, and on the farm Naab in the Geselskapbank area. Joubert (1971) reports marbles from the farm Anegas to the south-west of Rooifontein, and Theart (1980) metacarbonate rocks from the Groothoek area to the west of the Geselskapbank and Eenriet paragneiss belts. Metacarbonate lenses located in the Garies-Platbakkies belt during this survey all belong to the wollastonite-calcite group. The marbles are commonly granoblastic rocks comprising rounded, highly serpentinized forsterite grains and slightly coarser grained xenoblastic calcite/dolomite. Phlogopite and rarer garnet are present as minor constituents, and in sample SK-9 the magnesium silicate mineral is chondrodite and not forsterite. Sample VK-9 contains minor pyrite and small amounts of graphite were observed in a few samples. Marble samples NB-1 and NB-2 from the Geselskapbank area contain minor tremolite and rare spinel.

The metamorphism of quartz-bearing carbonate rocks and alumino-silicate-bearing marls involves reactions during which minerals such as talc, tremolite, forsterite, diopside, wollastonite, zoisite, anorthite, scapolite and grossularite are formed and CO_2 and lesser H_2O are liberated. At moderate pressures ($\pm$5 kbars) as pertain to the western NMC, dolomite-quartz carbonate rocks (i.e. dolomites) are involved in a series of metamorphic reactions (where the mole fraction XCO_2 lies between 0 and 0.8) in the temperature range 500 to 700 ^{o}C, forming progressively talc, tremolite, diopside and forsterite plus calcite. In rocks with excess dolomite over quartz, the resultant mineral assemblage is essentially forsterite + calcite + dolomite, forming as a result of the reaction

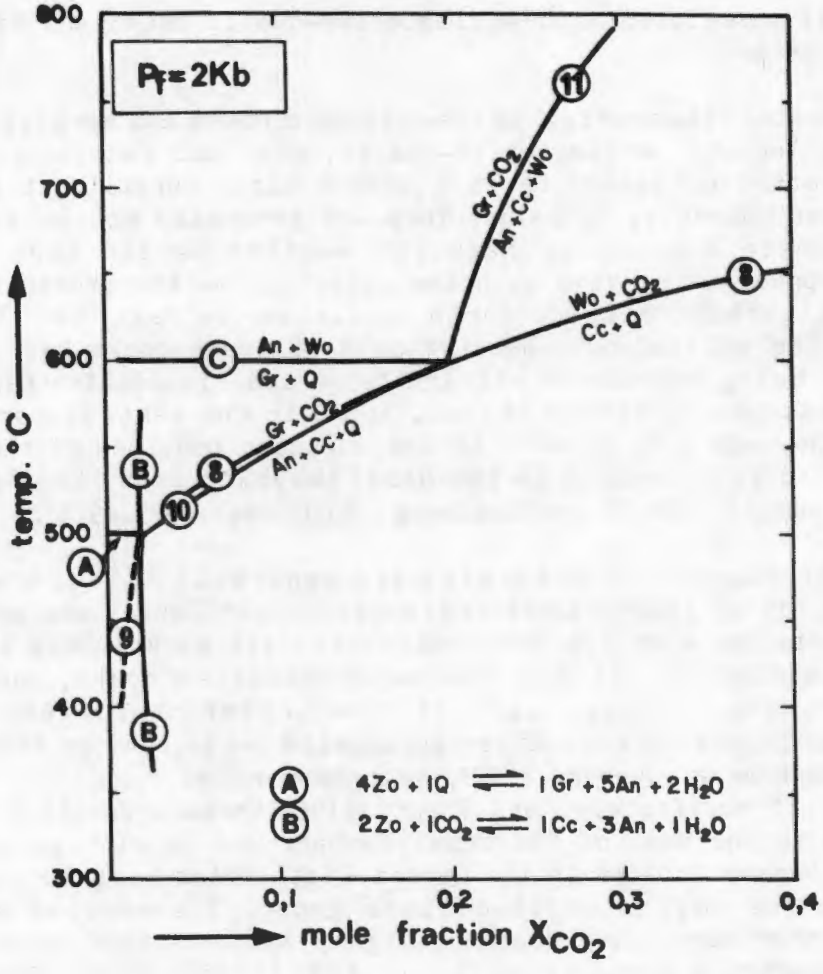

Fig. 3.3 An isobaric diagram (at 2 kbar) of temperature vs mole fraction XCO_2 (after Winkler, 1976) showing various common metamorphic reactions that take place in calcite-rich impure carbonate rocks.
(An = anorthite; Wo = wollastonite; Gr = grossular garnet; Q = quartz; Cc = calcite; Zo = zoisite).

1 tremolite + 11 dolomite → 8 forsterite + 13 calcite + 9 CO_2 + 1H_2O ... (3)

(Winkler,1976), whereas those rocks with excess quartz over dolomite form massive diopside-rich rocks as a result of the reaction

1 tremolite + 3 calcite + 2 quartz → 5 diopside + 3 CO_2 + 1 H_2O ... (4)

the tremolite and calcite having formed by lower-temperature prograde reactions such as

3 dolomite + 4 quartz + 1 H_2O → 1 talc + 3 calcite + 3 CO_2 ... (5)

5 talc + 6 calcite + 4 quartz → 3 tremolite + 6 CO_2 + 2 H_2O ... (6) and

2 talc + 3 calcite → 1 tremolite + 1 dolomite + 1 CO_2 + 1 H_2O. ... (7)

All these reactions are from Winkler (1976). At XCO_2 mole fractions in excess of 0.80, the situation is more complex (Fig. 3.2), but again tremolite, diopside and forsterite are formed during progressive metamorphism between temperatures ranging from 600 to 700 °C at 5 kbar pressure.

In calcite-quartz carbonate rocks (i.e. limestones), little mineralogical change is anticipated as the association calcite + quartz is stable to considerably higher temperatures than dolomite + quartz. However, when the fluid phase is enriched in H_2O relative to CO_2 or at low CO_2-rich fluid pressure, such as in contact metamorphism, the reaction

1 calcite + 1 quartz → 1 wollastonite + 1 CO_2 ... (8)

takes place with loss of CO_2 in the vapour phase (Winkler, 1976). This reaction takes place at temperatures in excess of 650 °C at pressures of 5 kbars and XCO_2 between 0.25 and 1.0. Small amounts of grossularite and diopside, present in the wollastonite-bearing rocks of the western NMC, are due to small amounts of alumino-silicates (clays) and dolomite respectively in the original carbonate rock.

The plagioclase-garnet and plagioclase-diopside calc-silicate rocks are derived from carbonate - alumino-silicate mixtures (i.e. marls) in metamorphic reactions occurring in a far more complex chemical system which besides the major components CaO, MgO, SiO_2, CO_2 and H_2O, also includes Al_2O_3, FeO, Na_2O and small amounts of K_2O as the result of the addition of alumino-silicate minerals to the system. The garnet-plagioclase calc-silicate rocks have low MgO, Na_2O and K_2O contents and could be described as forming in the system $CaO-Al_2O_3-SiO_2(-FeO)-CO_2-H_2O$ which has been studied experimentally by Gordon and Greenwood (1971) at 2 kbar pressures. Grossular garnet was found to be stable only at relatively low XCO_2 values although this stability field does expand with increasing temperature and, more markedly, with increasing pressure (Greenwood,1967). The garnet formed in decarbonation reactions involving calcite and a variety of other reactants including zoisite (epidote), quartz, anorthite and wollastonite:

Table 3.9 Mineral compositions of metabasic rocks from the study area. (M = major constituent >5%; m = minor constituent 5-1%; vm = minor constituent <1%). Accessory minerals such as apatite and zircon are omitted. (her = hercynite; chl = chlorite; ser = sericite; act = actinolite; rut = rutile).

sample number	plagioclase	orthopyroxene	clinopyroxene	hornblende	biotite	iron oxide	quartz	epidote	other
BP-I	M	M	M		m	m	m		
ZB-I	M	M	M		m	m	m		
BI-8	M	M	M		m	m			
TW-5	M	M	M		m	m	vm		
DM-2	M	m	M		vm	m			
HY-14	M		M		vm	m			m (her)
PH-17	M	m	M		vm	m	M	vm	
RW-6	M		M		vm	m	m		m (her)
GHP-2	M	M	M		m	m	m		
WW-2	M	m	M		m	m	m	vm	
SK-5	M	m	M	m	vm	m	m	vm	
HY-23	M	M	M	m		m			
ROF-8	M	M	M	m	vm	m	m		
BP-2	M	M	M	M		m			
WP-1	M	m	M	M	m	m			
HK-2	M	M	M	M	m	m			
BP-7	M	M	M	M	m	m			
HY-8	M	M	M	M	m	m	m		
HY-16	M		M	M		m			m (her)
GHP-3	M	M	M	M		m			
VK-7	M	M		M		m			
RFN-3	M	M		M		m	vm	vm	
GN-3	M	m		(M)		m	m	m	M (chl)
SKF-5	M			M	m	m	m	m	
NB-4	(M)			M		m	m	M	M (ser)
GB-11				M (act)		m (rut)			
SKF-11	M			M (act)		m (rut)			

5 calcite + 2 zoisite + 3 quartz = 3 grossularite + 5 CO_2 + 1 H_2O ... (9)

1 calcite + 1 anorthite + 1 quartz = 1 grossularite + 1 CO_2 ... (10)

1 calcite + 1 anorthite + 1 wollastonite = 1 grossularite + 1 CO_2 ... (11)

with increasing temperature (Gordon and Greenwood, op.cit.) (Fig. 3.3). Addition of Na_2O to the system markedly increases the amount of plagioclase present at the expense of grossularite (Greenwood, op.cit.) and the further addition of MgO as dolomite in the place of calcite results in the disappearance of grossular garnet and the appearance of diopside and, in some instances, hornblende or hypersthene.

3.7 Basic granulites and amphibolites

Mafic rocks are relatively uncommon within the paragneiss belts of the western portions of the NMC and consist of a group of lithologies whose mineralogy is dominated by plagioclase (>40%) and either hornblende or orthopyroxene, commonly with associated clinopyroxene, opaque oxides and lesser quartz, biotite, epidote, actinolite and/or spinel (mafic minerals totalling >40%)(Table 3.9). Rarer olivine-bearing mafic rocks have been recorded from the western portion of the NMC (Joubert,1971; Albat,1984) but were not located or sampled within the paragneiss belts themselves during this study. Other larger mafic bodies are present in the study strip, most notably to the immediate north of the Platbakkies-Witwater paragneiss belt, to the north of the Boesmanplaat-Dounabees-Anegas belt, to the north of the Dikmatje-Stofkraal belt and within the Geselskapbank synform. These mafic units show close relationships with a suite of intrusive charnockitic and megacrystic granitic rocks and are excluded from this study as their relationship to the supracrustal rocks is obscure - probably an intrusive one.

Only mafic rocks obviously interbanded within (or slightly transgressive to) the paragneisses were sampled during this study, and they generally consist of narrow bands or lenses no wider than a few metres. Mafic rocks are most common within the Dikmatje-Stofkraal and Buffels River paragneiss belts; in the Geselskapbank area in the extreme north, and in the Bitterputs portion of the Bitterfontein paragneiss belt in the south. All the mafic rocks examined display typical metamorphic (not igneous) textures; the granulites being gneissic rocks with xenoblastic grains showing 120° triple contacts (plagioclase, hornblende, pyroxenes) or poikiloblastic grains (pyroxenes) enclosing plagioclase, and the amphibolites containing strongly oriented amphiboles and rarer micas with xenoblastic plagioclase and quartz.

Mineralogically the mafic rocks can be divided into four subgroups based on the specific mafic minerals present which are apparently related to the grade of metamorphism. These subgroups are amphibole-free plagioclase-orthopyroxene rocks with lesser clinopyroxene or spinel and iron oxides; plagioclase-orthopyroxene-clinopyroxene-hornblende rocks; plagioclase-hornblende rocks sometimes with lesser clinopyroxene; and plagioclase-

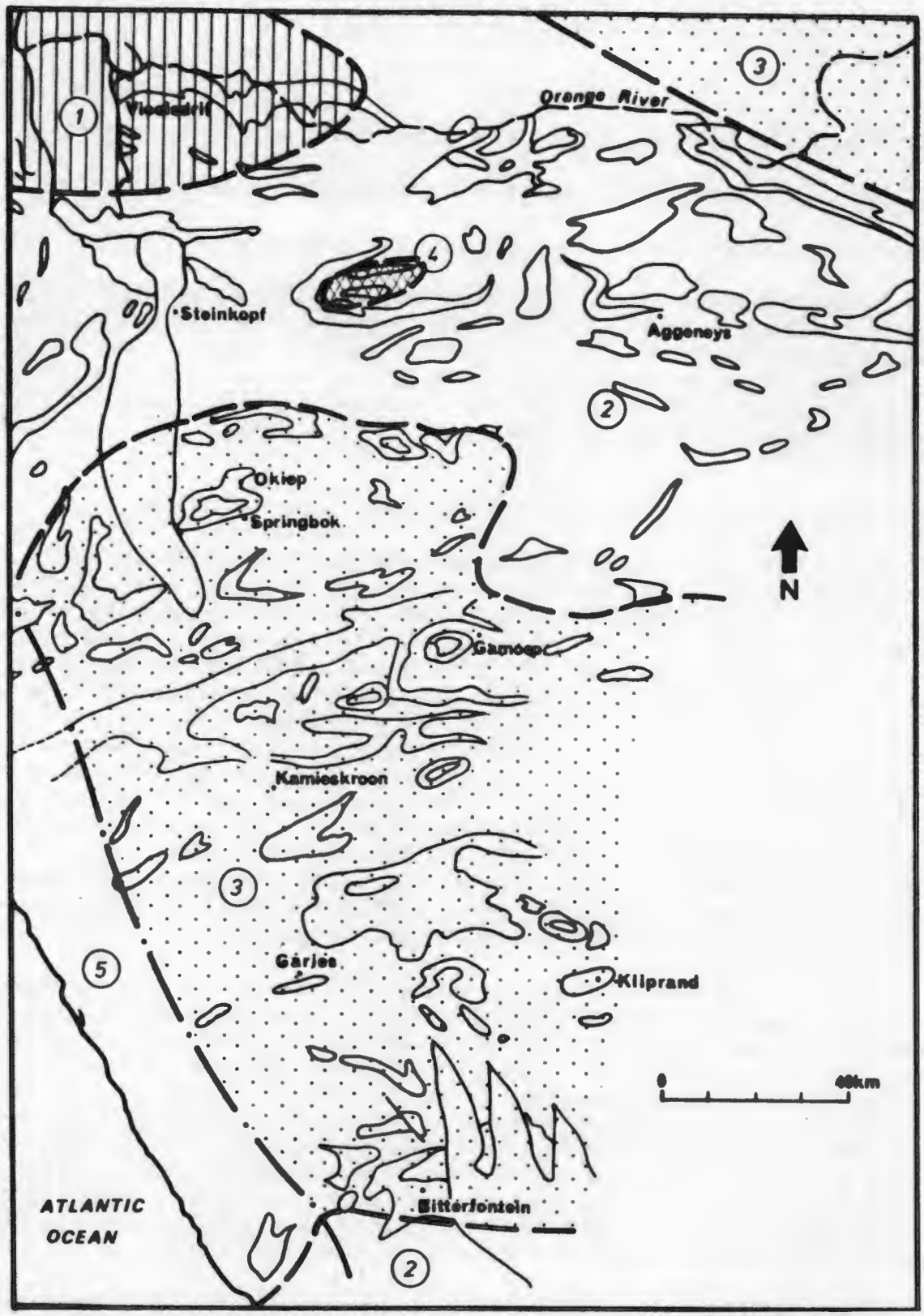

Fig. 3.4 A summary of regional metamorphic zonation within the western NMC. Zone (1) represents greenschist/lower amphibolite facies with the upper boundary defined by the transition from andalusite to sillimanite; Zone (2) represents amphibolite facies with the upper boundary defined by the appearance of orthopyroxene; Zone (3) represents granulite facies; Zone (4) represents the polyphase high-grade metamorphism in the Geselskapbank area; and Zone (5) represents the superimposed Pan-African imprint along the west coast. Data from a variety of sources, principally Blignault et al., 1980; Albat, 1984; Beukes, 1973; Waters et al., 1984; Joubert, 1971.

pargasite/actinolite rocks (Table 3.9).

The amphibole-free and hornblende-bearing orthopyroxene granulites have identical distributions, being present from the Bitterfontein belt in the south through to the Smorgen Schaduwe-Kangnas paragneiss belt in the north. From this belt northwards, only orthopyroxene-free hornblende-rich mafic rocks were observed, and this latter belt could mark the transition between the granulite facies and upper amphibolite facies using the presence or absence of orthopyroxene as the discriminant phase (de Waard,1965). Whilst most of these plagioclase-hornblende rocks are crudely banded and compositionally uniform in appearance, some banded varieties containing clinopyroxene and quartz are indistinguishable in the field from the plagioclase-diopside-hornblende-quartz calc-silicate rocks (see Section 3.6). Actinolitic/pargasitic amphiboles are present in two samples (GB-11 and SKF-11) in the extreme north of the study strip within the Geselskapbank area. Similar lithologies were described from the Namiesberg by Moore (1977). Sample GB-11 is a massive actinolitic rock of similar texture, but darker colour to the tremolite-rich calc-silicate sample GB-1. These amphiboles could indicate even lower metamorphic grades in the extreme north of the study strip.

The presence or absence of orthopyroxene in mafic rocks, as stated above, is commonly regarded as defining the boundary between the amphibolite and granulite facies of metamorphism. The orthopyroxene-clinopyroxene geothermometer, based on the distribution of Mg and Fe^{2+} between co-existing pyroxenes in basic granulites is well established (Wood and Banno,1973; Saxena,1976; Wells,1977) and widely used in granulite-facies terranes including the western NMC (Zelt,1980; Jack,1980; Clifford et al.,1981; Albat,1984). Temperatures obtained by Zelt (op.cit.) from the Buffels River belt range from 800 to 860 °C; by Jack (op.cit.) from the extreme western NMC between 795 and 921 °C; by Clifford et al. (op.cit.) for the Okiep Copper District from 787 to 875 °C; and by Albat (op.cit.) for the Kliprand area from 795 to 910 °C . These temperatures are somewhat higher than those obtained for the metapelitic rocks (see Section 3.3) from the same area, indicating slight discrepancies between the various geothermometers. Pressure estimates were obtained from the two-pyroxene granulites by Clifford et al. (op.cit.), using the methods of Irving (1974) and Wood (1977,1979), in the broad region from 4.5 to 8.5 kbars. These P-T conditions place the metamorphic grades under which the basic granulites of the western NMC formed as low-to-medium pressure granulite facies with approximate thermal gradients of 40 to 45 °C per km. The facies boundary between the granulite and amphibolite facies is shown in Fig. 3.4. There is a relatively close association of the granulite facies with the presence of charnockitic rocks (hornblende-hypersthene gneisses of Joubert,1971) in the study area. The amphibolites from the northern portion of the study area are not constrained by any geothermometric or geobarometric studies.

3.8 Magnesium-rich cordierite rocks

Cordierite-phlogopite-hypersthene/anthophyllite lithologies are rare minor components of the supracrustal sequences of the western NMC. Although

Table 3.10 Mineral compositions of magnesium-rich cordierite gneisses from the study area (M = major constituent >5%; m = minor constituent 1-5%; vm = minor constituent <1%). Accessory minerals such as apatite and zircon omitted. (trm = tourmaline; kfs = K-feldspar; cpy = chalcopyrite; rut = rutile; gar = garnet).

sample number	sillimanite	quartz	cordierite	phlogopite/ biotite	hypersthene	anthophyllite/ gedrite	iron oxide	hercynite	sapphirine	kornerupine	plagioclase	other
7-S1	M		M	M			m	vm			m	
HY-7	M		M	M			m	vm	m	m	m	vm (trm)
HY-17	M	vm	M	M			vm					vm (kfs)
SKF-10	M	vm	M				m					vm (cpy)
DRL169			M	M								
9-CD			M	M								
7-CD			M	M				m	m		m	
7-S			M	M				m	m		m	
7-K			m	M				m	m	m		
HY-9			M	M					M	m		vm (rut)
K3-K			M	M		vm						
HY-21		M	M	M			m	vm				
HY-10		M	M	M								vm (kfs)
HY-22		M	M	M	m							
HY-15		M	M	M	m		m					
HY-4		m	M	M	m		vm					
HY-12			M	m	M		m					
K3-S			M	M	M			m	m			
9-GG			M	m	M		M	m			m	m (gar)
RW-4		m	M	M	M		m	m			M	M (kfs)
RW-5			M	M	M		m				m	
GN-1		m	M	m	M	m	m					
ND-4		M	M	M	M		m					
HY-13			M	m	M	M	m	M				
9-ANT			M	m	M	M	m	M	vm			
ND-2			M	m	m	M						m (rut)
ND-3			m	M	M	M	m	m	m			
ND-6			m	m	M	M	M	m	m			
9-SG			m	m		M			M			m (rut)
ER-1		m	M	M		M	M					m (gar)
DRL168		m	M	M		M	m					

they are extremely uncommon, their distribution is fairly widespread, occurring from the Witwater-Platbakkies paragneiss belt (on the farm Roodewal) northwards to the Orange River. These lithologies appear to be absent from the Bitterfontein paragneiss belt in the south . They were also located and sampled on the farms Dabeeb, Rietfontein, Hytkoras and Nuwedam in the Buffels River paragneiss belt; on the farm Goinoep in the Oranjefontein paragneiss belt; at Geselskapbank and in the Eenriet paragneisses and on the farm Houniams near the Orange River during this study. Further occurrences are recorded from the Okiep Copper District (Clifford et al., 1975b,1981); the Steinkopf area (Blignault et al., 1980; Theart,1980) and from extreme western Namaqualand (Jack,1980). They are also found in southern Namibia (Beukes,1973) and cordierite-hypersthene rocks were recorded by Albat (1984) to the immediate east of the study area.

These rather unusual rocks comprise a wide variety of lithologies that can be broadly grouped into two main types, each containing three subgroups (Table 3.10). Many of these varieties show transitional compositions between each other, making classification complex and somewhat arbitrary. The first group consists of lithologies whose mineral parageneses are dominated by cordierite and phlogopite with hypersthene and/or anthophyllite/gedrite being either absent or present only in very minor amounts. They comprise three subgroups, those in which quartz is also a major component, those in which sillimanite (sometimes with corundum) is a major component, and those where cordierite and phlogopite alone predominate. Iron oxides and hercynite are relatively uncommon minor constituents and, with the exception of the quartz-rich subgroup, sapphirine, kornerupine, tourmaline and plagioclase occur as minor components, most commonly in the gneisses from the Buffels River paragneiss belt. Many of these lithologies are coarsely to more finely banded rocks and are commonly associated with the garnet-cordierite-sillimanite metapelitic gneisses.

The second group consists of lithologies whose mineral parageneses are dominated by hypersthene and/or anthophyllite/gedrite together with cordierite and phlogopite either as major or minor constituents. They can be divided into three subgroups depending on whether only hypersthene, hypersthene and gedrite, or only anthophyllite are present. The first two subgroups appear to co-exist and have the same distribution in the western NMC, but the cordierite-anthophyllite rocks appear to be restricted to the northern portion of the study area within the amphibolite facies metamorphic zone where hypersthene is no longer a stable component. Opaque oxides and hercynite are common minor constituents together with either quartz or sapphirine. Garnet and plagioclase are also occasionally present. These rocks generally occur as dark, massive, coarse-grained outcrops in the field, and are commonly associated with basic granulites in the granulite-facies paragneiss belts as well as with the cordierite-phlogopite rocks.

3.9 Iron-, manganese- and zinc-rich rocks

Iron-, manganese- and zinc-rich rocks are rare lithologies within the paragneiss belts of the western NMC, occurring locally as lenses and irregular

Table 3.11 Mineral compositions of iron formations from the study area. (M = major constituent >5%; m = minor constituent 1-5%; vm = minor constituent <1%). (kfs = K-feldspar; apa = apatite; epi = epidote; ga = galena; zcn = zircon; mnz = monazite).

sample number	quartz	magnetite/ hematite	garnet	pyroxene	grunerite/ anthophyllite	iron sulphides	ilmenite	biotite	muscovite	gahnite/ hercynite	other
OF-1		vm	M							vm	
SS-6	M	vm	M					vm			
KN-7	M	M	M					vm	(chl)		
KN-12	M	M	M								
SK-3	M	vm	M								
TW-12	M	m	M								
TW-11	M	vm	M								
WW-15	vm	M	M							vm	vm (kfs)
WW-11	M	M	M								vm (apa)
WW-7	M	M	M								
AG51/145	M	vm	M			vm		vm			
AG56/240	M	m	m		m					vm	
BHU 424	M	M	vm		vm					vm	
BHU 302	M	M		vm		vm				vm	
VK-8	M	vm	M	m	vm						M (epi)
TW-8	M		M	(M)							
TW-6	vm	vm	M	M	m						
DBD-1	vm	m	M	M							
BHU 213	m	M	M	M	m	m					m (ga)
AG56/195	m	M		M	m						
BHU 148	vm	M		M	M	m					
ER-3	vm						M	M	m		vm (zcn)
ER-4	M						M	m	m		vm (zcn)
GA-BIF	vm	M					M		vm		vm (mnz, zcn)
ROF-9	M						M				vm (zcn)

bands, commonly comprising iron oxides, quartz and almandine-spessartine garnet. Less commonly, iron/manganese amphiboles (such as grunerite), pyroxenes (such as ferro-augite and orthoferrosalite), pyroxenoids (such as pyroxmangite), fayalite, iron sulphides, rhodonite and the zinc minerals gahnite or sphalerite together with galena and chalcopyrite are present, particularly in the Aggeneys-Gamsberg area (Rozendaal,1980, 1982; Ryan et al., 1982).

These lithologies can be classified broadly into three major and several minor groups (Table 3.11). The commonest variety is represented by garnet-quartz rocks whose parageneses are dominated by these two minerals with minor iron oxides (commonly magnetite), iron sulphides (pyrite or pyrrhotite), iron-rich amphiboles (grunerite) or pyroxenes, biotite and/or apatite. A second relatively widespread lithology is a banded iron oxide-quartz iron formation which, in certain areas, shows gradations to a third type comprising iron oxide-quartz-iron-rich amphibole/pyroxene/olivine (± garnet) rocks. Both these groups contain minor apatite and, less commonly, iron sulphides, sphalerite, galena, chalcopyrite and gahnite. Rarer rocks are the iron sulphide-quartz lithologies, with associated garnet, sphalerite, galena, chalcopyrite and gahnite (Aggeneys, Ryan et al., 1982), iron sulphide-muscovite-quartz schists, with associated sphalerite at Gamsberg (Rozendaal,1980) and Aggeneys (Ryan et al., op.cit.) and coarse-grained banded iron oxide-barite rocks also at Gamsberg (Coetzee,1958) and Aggeneys (Mathias,1940a). Quartz-gahnite rocks, with associated garnet and galena are a rare local lithology at Oranjefontein in the Smorgen Schaduwe-Kangnas paragneiss belt (Hicks, 1983).

With the exception of the Aggeneys-Gamsberg area, the iron-, manganese- and zinc-rich lithologies are restricted in their distribution and variety, generally comprising garnet-quartz or iron oxide-quartz rocks, and were sampled from the Garies-Platbakkies paragneiss belt and successive belts northwards, but were not found in any of the southern supracrustal sequences in the Bitterfontein area.

A distinctive iron oxide-quartz rock with a prominent minor zircon component and with ilmenite as a major component of the iron oxides was sampled at Hosabees in the Anegas-Boesmanplaat paragneiss belt and in the Eenriet paragneisses to the west of the Geselskapbank area. Similar rocks are described by Joubert (1971) as iron-rich pods and lenses in the Garies-Buffelsfontein area.

3.10 Tourmaline-rich rocks

Tourmaline-rich rocks (>15% tourmaline) are an extremely rare minor component of the supracrustal rocks of the western NMC. They appear to be restricted to the northern parts of the study area where they occur as several different varieties. Tourmaline-bearing glassy quartzites are present at Smorgen Schaduwe and in the Oranjefontein paragneisses where local tourmaline concentrations in irregular bands reach 1cm thickness. Tourmaline-plagioclase rocks and tourmaline-muscovite-quartz schists were sampled on the farm Heiorigas in the Geselskapbank area. Tourmaline-quartz-sillimanite and

tourmaline-sillimanite-corundum rocks occur as minor constituents of the aluminous-rich rocks (Moore,1977) in the Aggeneys-Gamsberg-Namiesberg area. These latter rocks were not sampled during this study.

1.11 Summary

The metamorphic lithologies of the western portions of the NMC can be classified into seven main groups, each containing several subgroups. Many lithologies of transitional composition between the various groups and subgroups make sharp definition or classification of the NMC supracrustal rocks impractical.

Clastic metasedimentary rocks are classified into groups comprising metapelitic/metapsammitic rocks, magnesium-rich cordierite rocks and quartzitic rocks. The chemistries of these three groups are essentially controlled by Al, Mg ($\pm$Fe) and Si respectively. The chemogenic metasedimentary rocks are classified in the groups calc-silicate/metacarbonate rocks, iron-, manganese-, zinc-rich rocks and again quartzitic rocks, whose chemistries are controlled by Ca ($\pm$Mg), Fe ($\pm$Mn $\pm$Zn) and Si respectively. The metavolcanic rocks are classified in the groups quartzo-feldspathic rocks and basic granulites/amphibolites whose chemistries are basically controlled by K + Na and Ca + Mg + Fe respectively. A minor eighth group of rocks are the B-rich tourmalinites which are apparently of chemogenic origin.

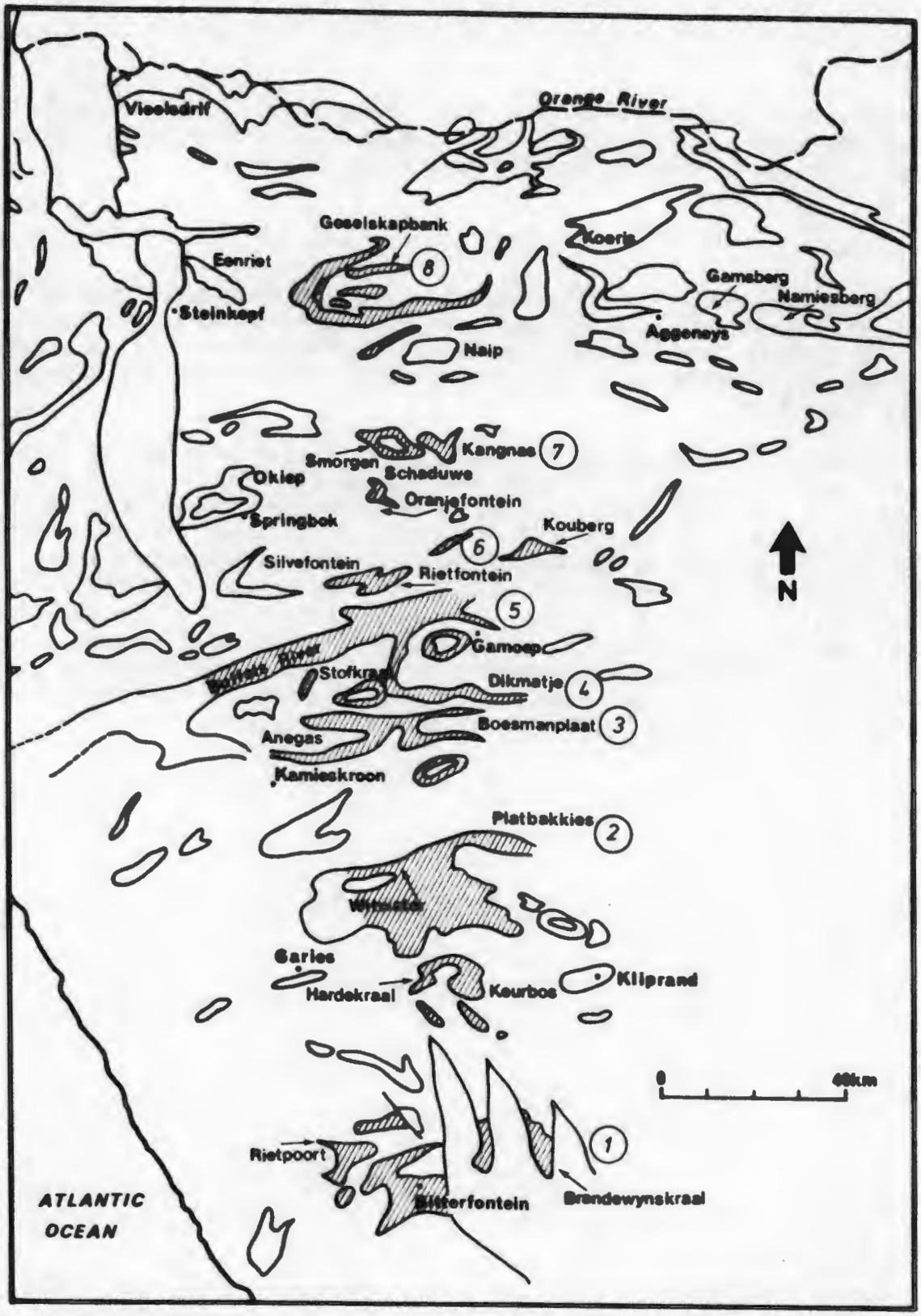

Fig. 4.1 Locality map of the eight major paragneiss belts examined in this study (shaded area). Numbers 1 to 8 as in text (Section 4.1).

Chapter 4

GENERAL GEOLOGY OF THE PARAGNEISS BELTS

4.1 Introduction

Eight major paragneiss belts stretching some 240 km from Bitterfontein in the south to Geselskapbank in the north were examined, partially mapped and sampled for geochemical analysis during this study (Fig. 4-1). The paragneiss belts are, respectively from south to north :

1. Rietpoort - Bitterfontein - Brandewynskraal belt
2. Garies - Witwater - Platbakkies belt
3. Anegas - Hosabees - Boesmanplaat belt
4. Stofkraal - Kammassies - Dikmatje belt
5. Buffels River belt (Nuwedam - Hytkoras - Tweefontein)
6. Silverfontein - Rietfontein belt
7. Smorgen Schaduwe - Kangnas belt
8. Geselskapbank belt (Heiorigas - Naab - Kabib - Beenbreek).

A suite of samples was also collected in the Aggeneys area where borehole core, provided by Black Mountain Mineral Development Corporation was used to supplement weathered samples of schist and quartzite collected from the northern paragneiss localities.

Certain smaller outcrop areas of supracrustal rocks, such as the Keurbos - Hardekraal area south of the Witwater - Platbakkies belt, the Oranjefontein - Goinoep area south of the Smorgen Schaduwe - Kangnas belt, Kouberg and Luisberg to the east of the Buffels River belt and Eendop se Kop and Eenriet, to the south and west of the Geselskapbank belt, were also sampled. Other paragneiss localities such as Potkley in the extreme south, the Rondefontein area to the north of the Bitterfontein belt, and Naip se Berg south of the Geselskapbank belt were omitted from this study due partly to their similarity to adjacent belts, and also due to the necessity to limit the number of samples in the study.

Brief descriptions of the various paragneiss belts, their lithological components, structural-stratigraphic configurations and degree of metamorphism follow.

4.2 The Bitterfontein paragneiss belt

4.2.1 The supracrustal sequence

In southern Namaqualand, a relatively thick sequence of supracrustal rocks is well preserved in a number of basinal-to-synformal structures of F3 age (Joubert,1971) stretching from Rietpoort in the west via Bitterfontein to Brandewynskraal in the east (Fig. 4-2). The sequence appears to be best

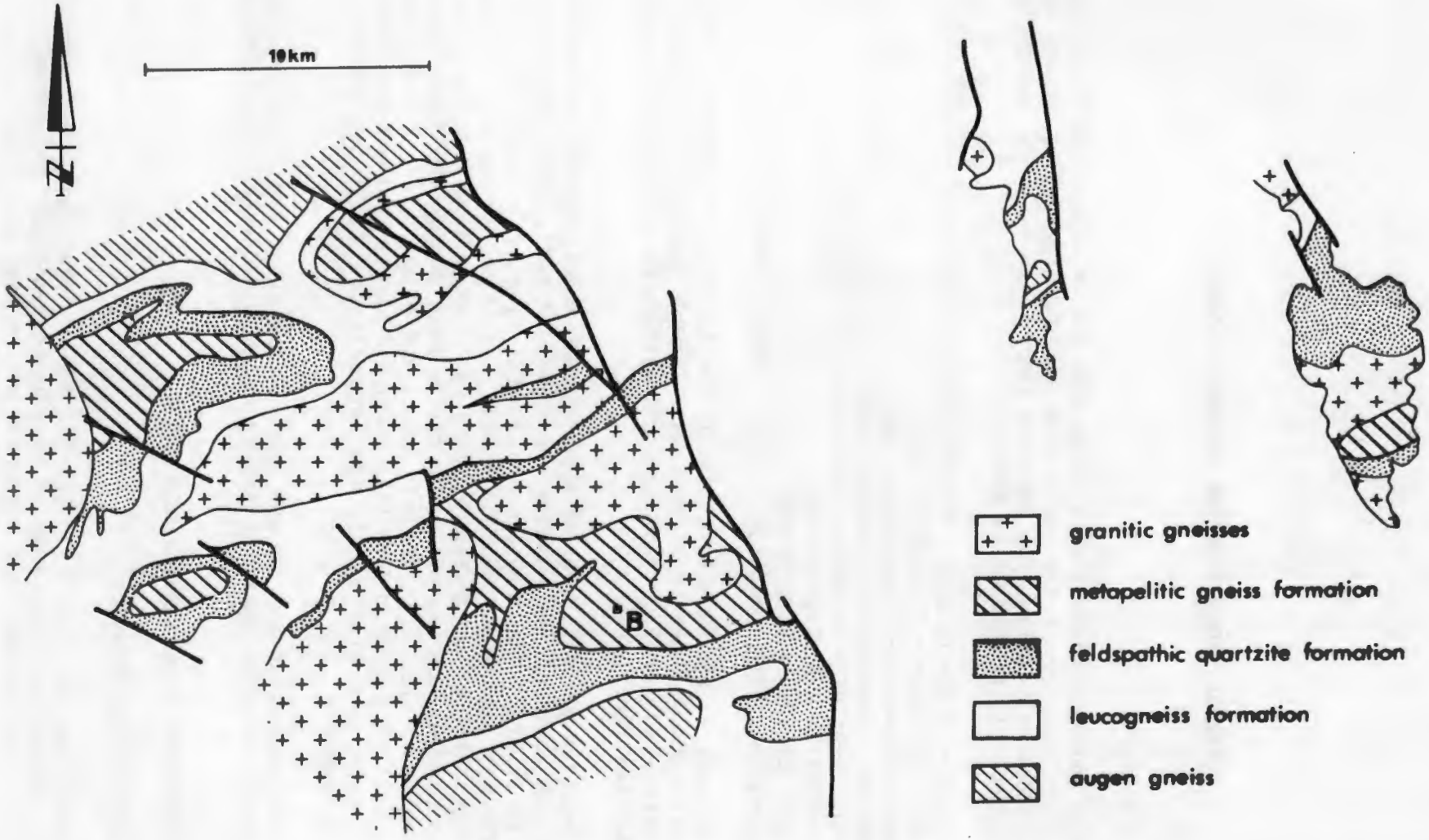

Fig. 4.2 Simplified geological map of the Bitterfontein paragneiss belt showing the distribution of the major lithological units. (B = Bitterfontein).

represented within the Bitterfontein and Rietpoort synforms. Brief descriptions of the various lithologies are as follows:-

Leucogneiss. A medium-grained banded K-feldspar-rich, biotite-poor gneiss, similar to many of the so-called "pink" gneisses of the NMC (Kroner,1968; Lipson,1980). In places it contains flattened discs of altered sillimanite and grades through progressively more siliceous varieties into overlying feldspathic quartzites. Lenses of calc-silicate rock occur in the upper portions of the unit on the farms Zout Rivier and Louws Cyfer. An amphibolite/basic granulite band was also observed within this unit on the southern portions of Zout Rivier and more prominently in the Brakputs synform in the north. The contact with underlying augen gneiss appears conformable and abrupt, with calc-silicate lenses present at the contact on the farm Mierhoofd Kasteel.

Lower feldspathic quartzite. The feldspathic quartzites have a flaggy appearance in the field and consist of quartz and altered K-feldspar (usually microcline) with trace amounts of iron oxides, sillimanite and muscovite. The quartzite is coarse-grained in places and grades upwards into progressively more siliceous varieties. Thin lenses of strongly sheared quartz-iron oxide-sillimanite rock, intercalated within the quartzites, were located on the farms Louws Cyfer, Bitterfontein and Zout Rivier. Fine bands of iron oxides are present throughout the unit.

Biotite gneiss and schist. Varieties of medium-grained biotite-rich schist and banded gneiss overlie the feldspathic quartzite and contain intercalated bands of coarse-grained, massive cordierite-rich metapelitic gneiss. These schists and banded gneisses are repeated higher in the sequence above the overlying banded hornblende-epidote rock.

Hornblende-epidote rock. A prominent, distinctly banded, green-coloured unit crops out, enclosed in biotite gneisses and schists on the farms Bitterfontein and Krantz Kraal. The mineral assemblage comprises hornblende-epidote-plagioclase-quartz with minor iron oxides, sphene and calcite.

Metapelitic cordierite gneiss. A coarse-grained, massive to crudely banded cordierite-rich gneiss is intercalated with and overlies the biotite gneisses, generally consisting of cordierite, quartz, K-feldspar, iron oxides with lesser plagioclase, sillimanite, biotite, hercynite and rarely garnet.

Upper feldspathic quartzite. This unit is similar to the lower feldspathic quartzite, also grading upwards into progressively more siliceous varieties and containing scattered fine iron oxide bands.

Metapsammitic cordierite gneiss. A coarse-grained, relatively coarsely banded and invariably highly folded unit overlies the upper feldspathic quartzite, consisting of quartz, K-feldspar, plagioclase and biotite with darker lenses or bands containing cordierite and garnet. Bands of the following three lithologies, varying from a few cm to several metres, are intimately interbanded with these gneisses.

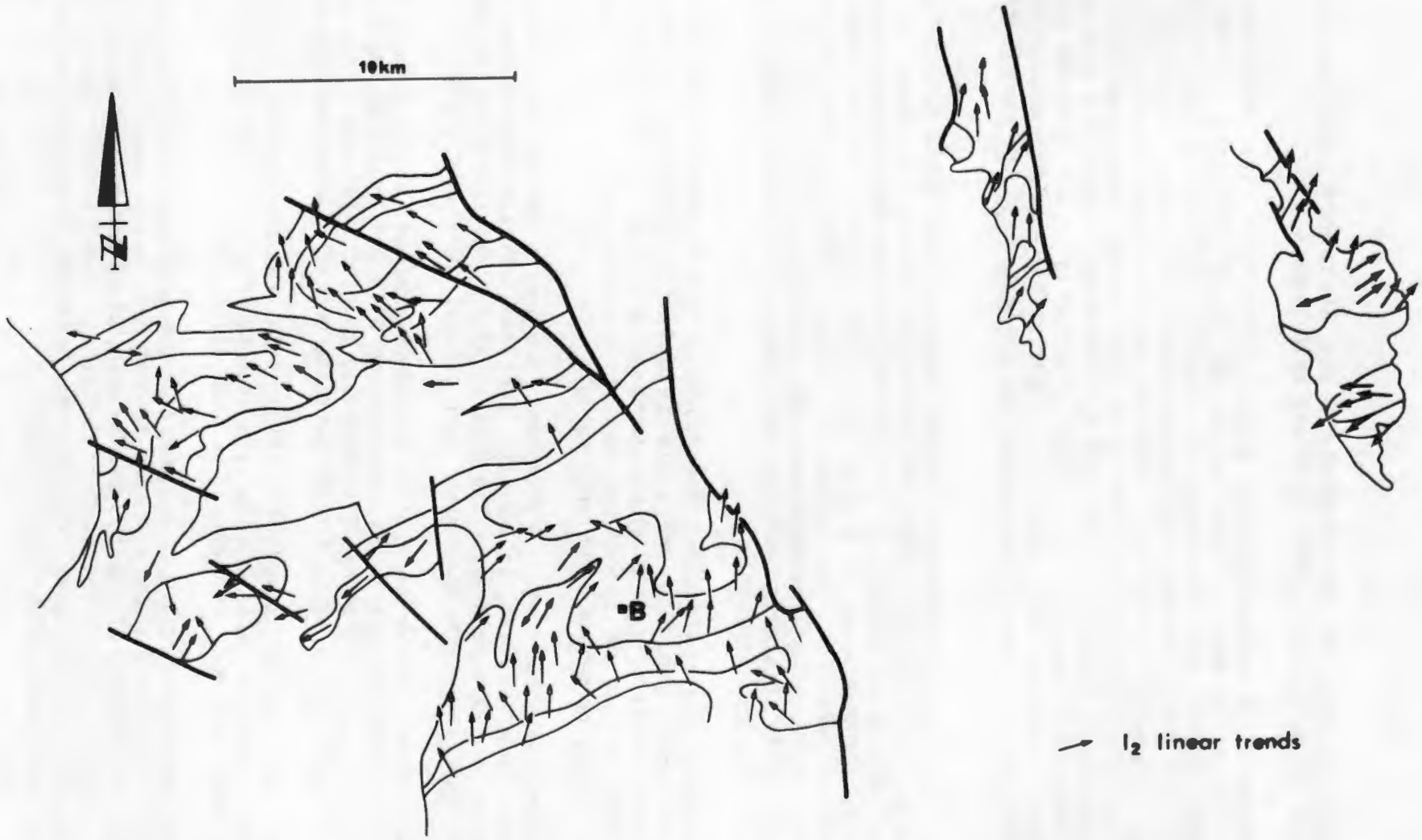

Fig. 4.3 Structural map of the Bitterfontein paragneiss belt showing the regional trend of the dominant L2 lineation.

Metapelitic cordierite-garnet-sillimanite gneiss. A very coarse-grained, massive to crudely banded gneiss which occurs interbanded with the previous gneiss, becoming more common higher in the sequence, particularly in the Rietpoort and Bitterfontein synforms. The mineral assemblage comprises quartz, K-feldspar, plagioclase, cordierite, sillimanite, garnet, biotite, iron oxides, spinel and corundum. In the Bitterfontein synform the spinels are brown in colour, but elsewhere dark green hercynite varieties are present.

Calc-silicate rock. A medium- to coarse-grained, moderately to poorly banded rock, consisting of quartz, plagioclase, clinopyroxene, biotite, opaques (commonly pyrite) with rare K-feldspar and occasional amphibole and epidote as alteration products of clinopyroxene and calcic plagioclase, occurs as thin bands and lenses with the two previous lithologies, also increasing in frequency higher in the sequence. This unit appears to be commonest in the Bitterfontein synform.

Basic granulite. Associated with the cordierite gneisses in the Bitterfontein and Brakputs synforms are thin lenses of a dark granulite consisting of orthopyroxene, clinopyroxene, plagioclase with minor brown hornblende, quartz, biotite and opaques (including pyrite).

4.2.2 Intrusive rocks

The supracrustal sequence is intruded by a variety of syntectonic to post-tectonic granitoids which vary from medium-grained late syntectonic "Concordia-type" granites within the Bitterfontein synform and on the farms Menschlief and Banke in the east, to coarser more biotite-rich syntectonic varieties on the farm Brakputs, to coarse post-tectonic megacrystic granites on Mierhoofd Kasteel, Wolwegat and Bitterfontein farms, and more mafic (amphibole-bearing) varieties in the south-eastern corner of the Brakputs farm. An even younger post-tectonic granite (Biesiesfontein granite, Jack,1980) truncates the Rietpoort synform at the western extremity of the area examined.

The leucogneisses at the base of the supracrustal succession are apparently conformably underlain by augen gneisses at the southern and northern extremities of the area. These augen gneisses are pretectonic granitoids possibly representing a basement complex.

4.2.3 Structure

The planar attitudes of the rocks in the Bitterfontein area are principally controlled by large-scale F3 structures, with the supracrustal sequences concentrated in four major F3 synforms. All structural events (F1,F2,F3,F4) refer to Joubert's (1971) classification. The following is a brief summary of structural events observed in the area.

No major structures related to the F1 deformational event were positively identified in the area. Major isoclinal structures of the F2 event were only

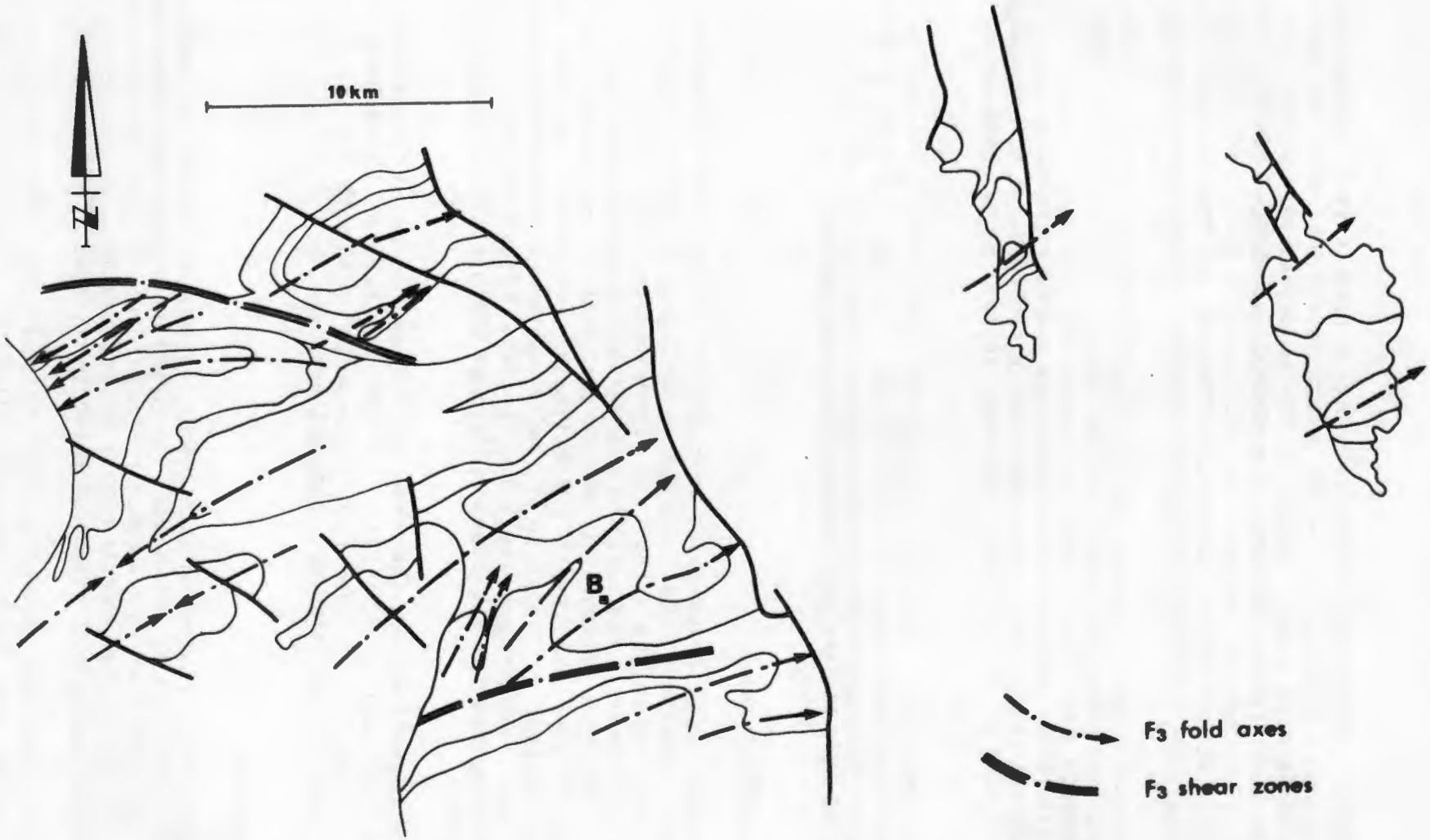

Fig. 4.4 Structural map of the Bitterfontein paragneiss belt showing the major F3 structures.

positively identified in the Menschlief area. In the Rietpoort-Bitterfontein-Brandewynskraal area no major F2 isoclinal folds were observed, although microscopic and mesoscopic folds were common. The duplication of the feldspathic quartzites in these areas may be due to a major F2 thrust fault, although this was not conclusively proven. Linear elements related to the F2 event were commonly oriented north-east in the east, to north-south in the central area, to north-west in the west (Fig. 4-3). Lineations measured in the cores of the major F3 structures were parallel to the axial trend of these folds and represent either L3 lineations or L2 lineations rotated into the axial direction of the F3 folds. Unequivocal L3 lineations were generally rare in the Bitterfontein area.

The F3 event is well represented in the area, typically by east-west trending, asymmetric synformal structures with distinctly overfolded northern limbs. Major antiformal structures are less common but are also present such as the structure on the farms Krantz Kraal and Nieuwoudts Naauwte. The plunge of the major F3 structures varies considerably throughout the area (Fig. 4-4). The Rietpoort synform, Zout Rivier basin and associated structures generally plunge westwards, whereas the Brakputs and Bitterfontein synforms and their associated antiforms plunge eastwards. In the east, the synform on Extensie and Klein Banke plunges eastwards whereas the Brandewynskraal synform plunges westwards. These changes in plunge direction appear to be related to the intrusion of late syntectonic to post-tectonic F3-age granites in these areas.

Two major east-west zones of tectonic sliding appear within the area along which F3 fold structures are replaced by zones of translative movement and appear to die out abruptly. One of these occurs to the north of the northern limb of the Rietpoort synform and the second to the south of the southern limb of the Bitterfontein synform.

Structures belonging to the F4 event are not prominent in the area, probably being masked by a series of younger north-south and north-west trending faults and shear zones. Several of these latter faults post-date the deposition of the Nama Group of sediments. In the Brakputs synform, a swarm of narrow diabase dykes has intruded along these north-south fractures.

4.2.4 Metamorphism

There appears to be a general prograde increase in metamorphic grade from the south-west to the north-east in the area (see also Waters *et al.*, 1984). The area south of the Bitterfontein synform is dominated by biotite schists and gneisses showing green-brown to brown biotite and also by hornblende-epidote assemblages, indicative of amphibolite facies grades of metamorphism. From the Bitterfontein synform northwards, the area is dominated by cordierite gneisses with red-brown biotite and also orthopyroxene/clinopyroxene-bearing mafic rocks, indicative of granulite facies grades of metamorphism (see Section 3.7).

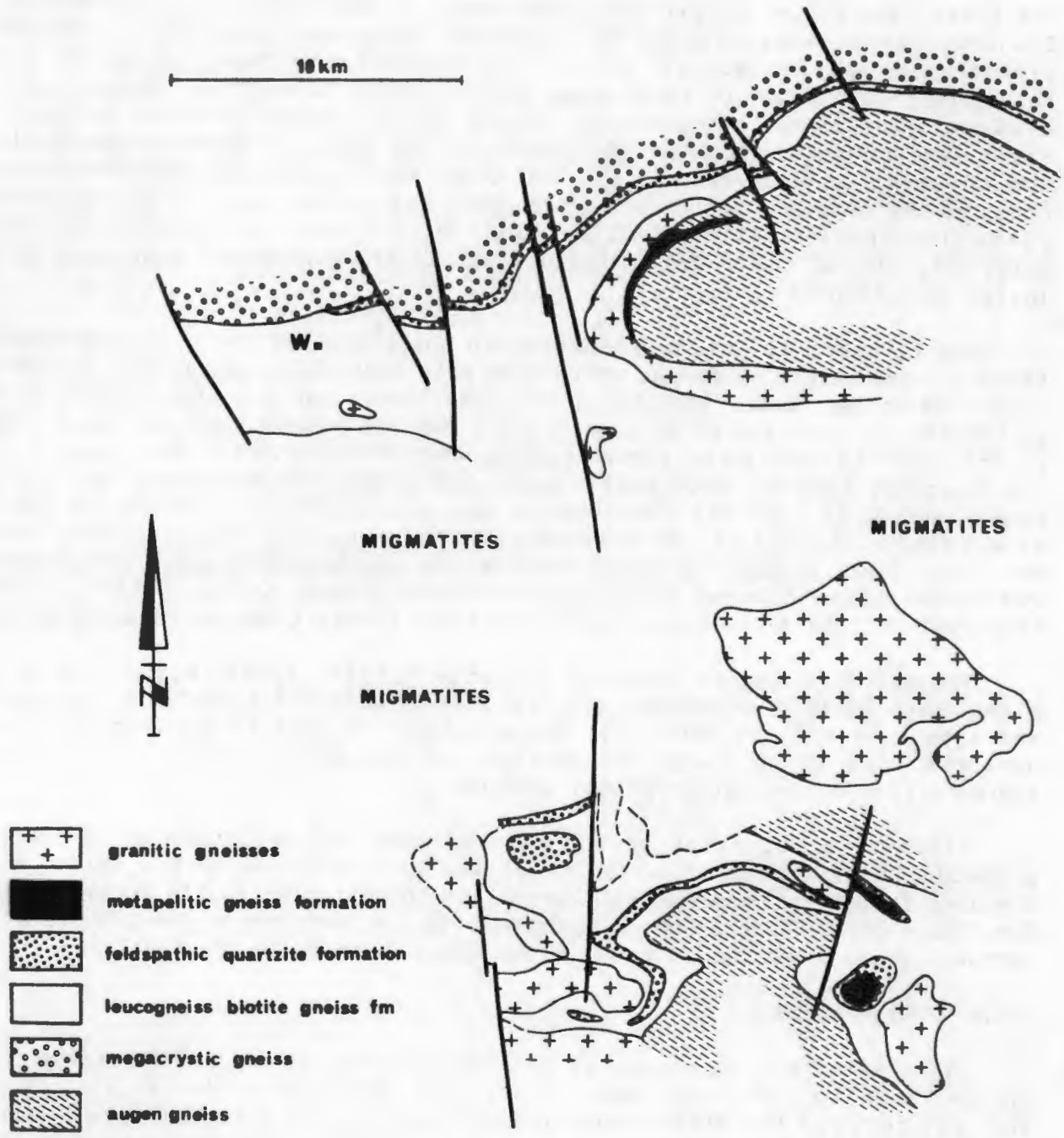

Fig. 4.5 Simplified geological map of the Witwater-Platbakkies paragneiss belt and the Hardekraal-Keurbos area to the south, showing the distribution of the major lithological units. (W = Witwater).

4.3 The Witwater-Platbakkies paragneiss belt

4.3.1 The supracrustal sequence

A broad belt of supracrustal rocks, commonly highly migmatitic in appearance, stretches across the Namaqua mountainland from Garies to Platbakkies and Kliprand (Fig. 4-5). At the southern and northern extremities of this belt, in the Doornkraal/Keurbos/Bokkraal and Eselfontein/Witwater/Platbakkies areas respectively, the paragneisses are less migmatitic and thus more amenable to stratigraphic and geochemical study. The supracrustal rocks in this belt are preserved in major F2-age synformal and thrust structures that are complicated by subsequent F3 and F4 overprints, producing complex basins and mushroom-shaped domes, features which are best observed in the Keurbos area.

The following lithologies were recorded in the supracrustal sequences:-

Leucogneiss. Biotite-poor, K-feldspar-rich leucogneisses form the basal portions of the supracrustal sequence at Keurbos as they do in the Bitterfontein area. Occasional basic granulite bands and lenses are found within the unit and a distinctive metapsammitic biotite-cordierite gneiss separates the leucogneisses from the feldspathic quartzite. In the Witwater area, leucogneisses are not present as the extreme basal unit, but occur as several (at least three) prominent bands in the basal portions of the sequence underlying the feldspathic quartzite. Here they contain occasional lenses of calc-silicate and metacarbonate rocks, garnet-rich iron formations and basic granulites. The central leucogneiss band also contains zones of irregularly-shaped flattened sillimanite-quartz nodules.

Metapsammitic biotite/cordierite gneisses. Banded medium-grained quartzo-feldspathic gneisses containing relatively low and variable amounts of biotite and/or cordierite with occasional garnets, and commonly having a migmatitic appearance, are located between the leucogneisses and feldspathic quartzite at Keurbos, and are interbanded with leucogneisses in the Witwater area. The cordierite gneisses generally appear more massive and lighter coloured than the biotite gneiss bands, and certain units show similarities to the metapsammitic cordierite gneisses of the Bitterfontein area.

Metapelitic garnet-cordierite gneisses. Poorly banded darker coarse-grained gneisses containing quartz, K-feldspar, plagioclase, garnet and cordierite with lesser biotite, iron oxides and rare sillimanite occur interbanded in the biotite/cordierite gneisses at both localities but are more common in the Witwater area, particularly at the base of the sequence. One band on the farm Witwater was noticeably pyritic.

Metapelitic cordierite-garnet-sillimanite gneisses. Massive to poorly banded gneisses containing quartz, K-feldspar, cordierite, sillimanite, garnet, plagioclase and occasionally biotite, with lesser iron oxides and hercynite are present at Witwater and on Keurbos farm at the extreme top of

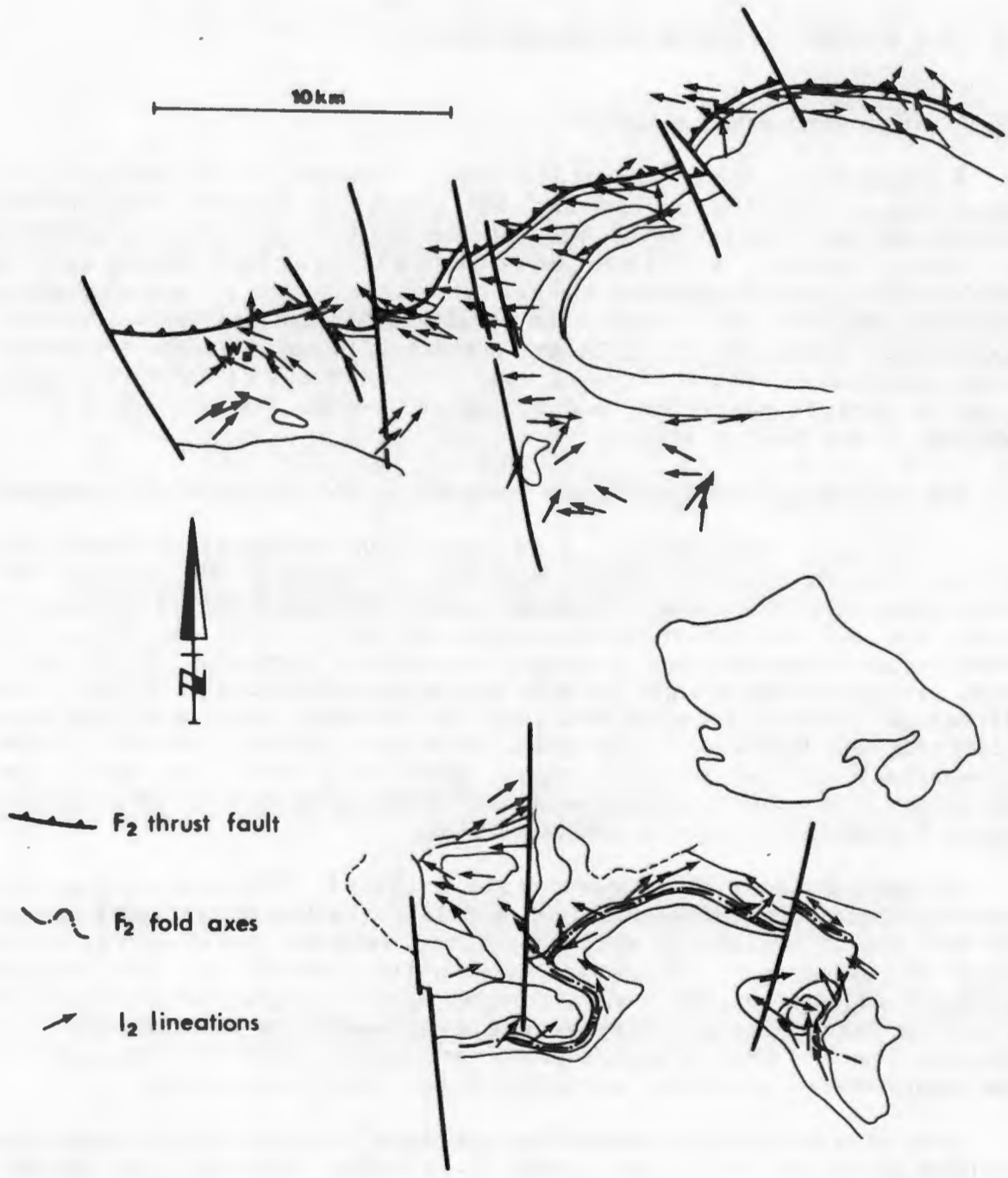

Fig. 4.6 Structural map of the Witwater-Platbakkies paragneiss belt showing the major F2 structures.

the observable sequence, directly overlying the feldspathic quartzite. These gneisses are similar to those located above the upper feldspathic quartzite in the Bitterfontein area. In the Witwater area the supracrustal sequence is terminated along a major thrust fault at the upper contact (?) of the feldspathic quartzite and so this unit is not represented.

Feldspathic quartzite. A single band of feldspathic quartzite, identical in composition to those of the Bitterfontein area is present at both localities towards the top of the sequence. Although isoclinal folding in the Keurbos area and thrust faulting in the Witwater area make estimations of the unit's thickness extremely difficult, the quartzite appears to be considerably thinner than those in the Bitterfontein area, having thicknesses in the 10 to 20 metre range as opposed to the 100 metre range around Bitterfontein.

Calc-silicate and metacarbonate rocks. Metacalcareous rocks are poorly developed as thin lenses and pods within the sequence below the feldspathic quartzite in the Witwater area and they are virtually completely absent in the Keurbos area. Garnet-clinopyroxene-quartz-plagioclase assemblages are the most common, occurring at various levels within the sequence. Massive diopside-rich rocks are present on the farm Witwater in association with iron formations in the central part of the sequence. Wollastonite-rich and calcite-rich rocks are located immediately beneath the feldspathic quartzite at Paulshoek and Brakfontein in the Leliefontein Reserve and also on the farm Rooiwal.

Iron formation (BIF). Small irregular pods and lenses of poorly banded garnet-magnetite-quartz BIF were observed on the farms Kougoedvlakte and Witwater. On the latter farm the BIF occurs in association with a massive diopside-rich calc-silicate band and most occurrences are located in the central part of the stratigraphic sequence. No BIF bands were observed in the Keurbos area.

Basic granulite. Massive, dark, medium-grained orthopyroxene-clinopyroxene-plagioclase gneisses are present in two distinctive geological situations in the area. Firstly they occur as large irregular rafts and lenses within or adjacent to syntectonically intruded leucogranitic gneisses (in the Keurbos area) and megacrystic granitic gneisses (in the Witwater area), and secondly as thin lenses and occasional larger bands, such as on the farm Bruinkop, within the lower portions of the supracrustal sequence.

Biotite-hypersthene gneiss. Thin bands and lenses of a biotite-quartz-plagioclase-hypersthene gneiss were located in the upper portions of the sequence together with thin calc-silicate lenses in the Witwater area. A similar rock was also found in association with the cordierite-hypersthene gneiss.

Cordierite-hypersthene gneiss. A large lens-shaped body of cordierite-biotite-hypersthene gneiss was observed on the farm Rooiwal in association with basic granulites and cordierite-garnet-sillimanite gneisses. The precise stratigraphic position of these paragneisses, however, could not be ascertained.

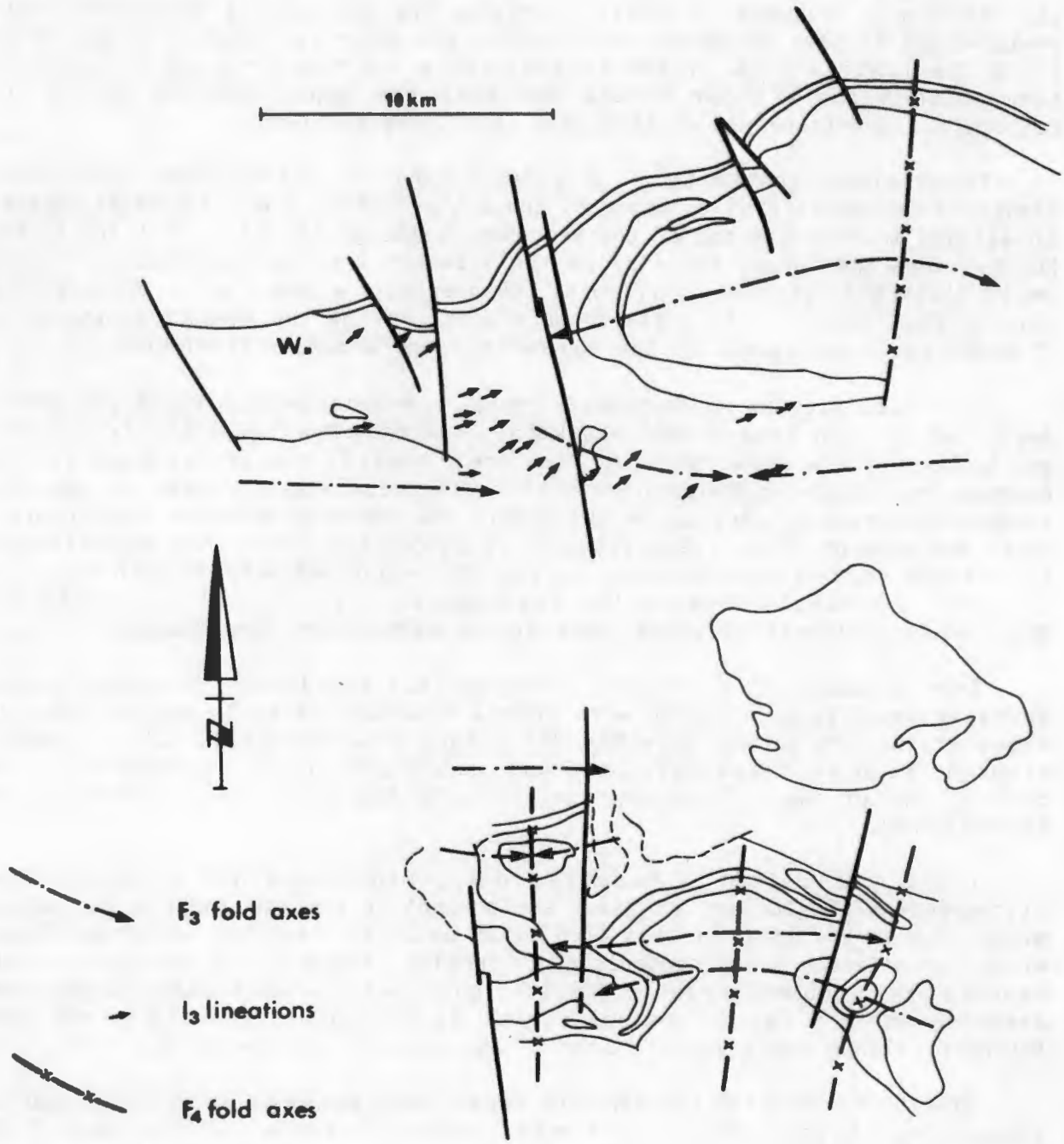

Fig. 4.7 · Structural map of the Witwater-Platbakkies paragneiss belt showing the major F3 and F4 structures.

4.3.2 Intrusive rocks

As in the Bitterfontein area, several syntectonic granitoids disrupt the supracrustal sequence, varying in composition from "Concordia-type" leucogranitic gneisses to charnockitic varieties. Associated with these granitoids, in contrast to the Bitterfontein area, however, are mafic granulite bodies which appear to predate the granitoids and are included within these granitic gneisses, particularly those of "Concordia-type" in the Keurbos area, on all scales from large rafts or pendants to small xenoliths.

To the north of the Witwater area, the supracrustal rocks are structurally overlain by a thick megacrystic biotite granite gneiss body with very coarse K-feldspar phenocrysts, which also encloses large lenticular bodies of basic granulite. The contact between the supracrustal rocks and the megacrystic granite gneiss is interpreted as a major F2-thrust plane and not as an intrusive contact.

In the western closure of the Kougoedvlakte antiform, a prominent, red-weathering, coarse-grained, leucogranitic gneiss has intruded the basal portions of the supracrustal sequence, and partially transgresses through these supracrustal rocks into the basal augen gneisses further east.

In both the Keurbos and Witwater areas, as in the Bitterfontein area, a pretectonic streaky augen gneiss underlies the supracrustal sequences with sharp lithological contact, and may represent a suite of basement rocks.

4.3.3 Structure

Large-scale structures related to the F2 event are more dominant in the Garies-Platbakkies-Kliprand area than in the Bitterfontein area and play a major controlling role in the distribution of the supracrustal sequences (Fig. 4-6). The F2 structures were subsequently considerably deformed by large-scale structures of the F3 and F4 events, resulting in complex basin and dome interference patterns. No significant structures related to the F1 event could be positively identified.

In the Keurbos area, the supracrustal sequence is preserved in a tight, east-west trending, isoclinal F2-age synformal fold that has been considerably deformed by a co-axial east-west trending F3-age synform and then by a succession of north-south trending F4-age synforms and antiforms. The resultant interference pattern is an alternating succession of east-west elongate closed basins and mushroom-shaped domes. Much rotation of the early L2 lineation is apparent.

In contrast to this, the supracrustal rocks in the Witwater area are preserved along an east-west-striking linear belt that is interpreted as a major pre-F3 thrust fault that can be traced from north of Garies in the west to the area between Platbakkies and Kliprand in the east where it disappears

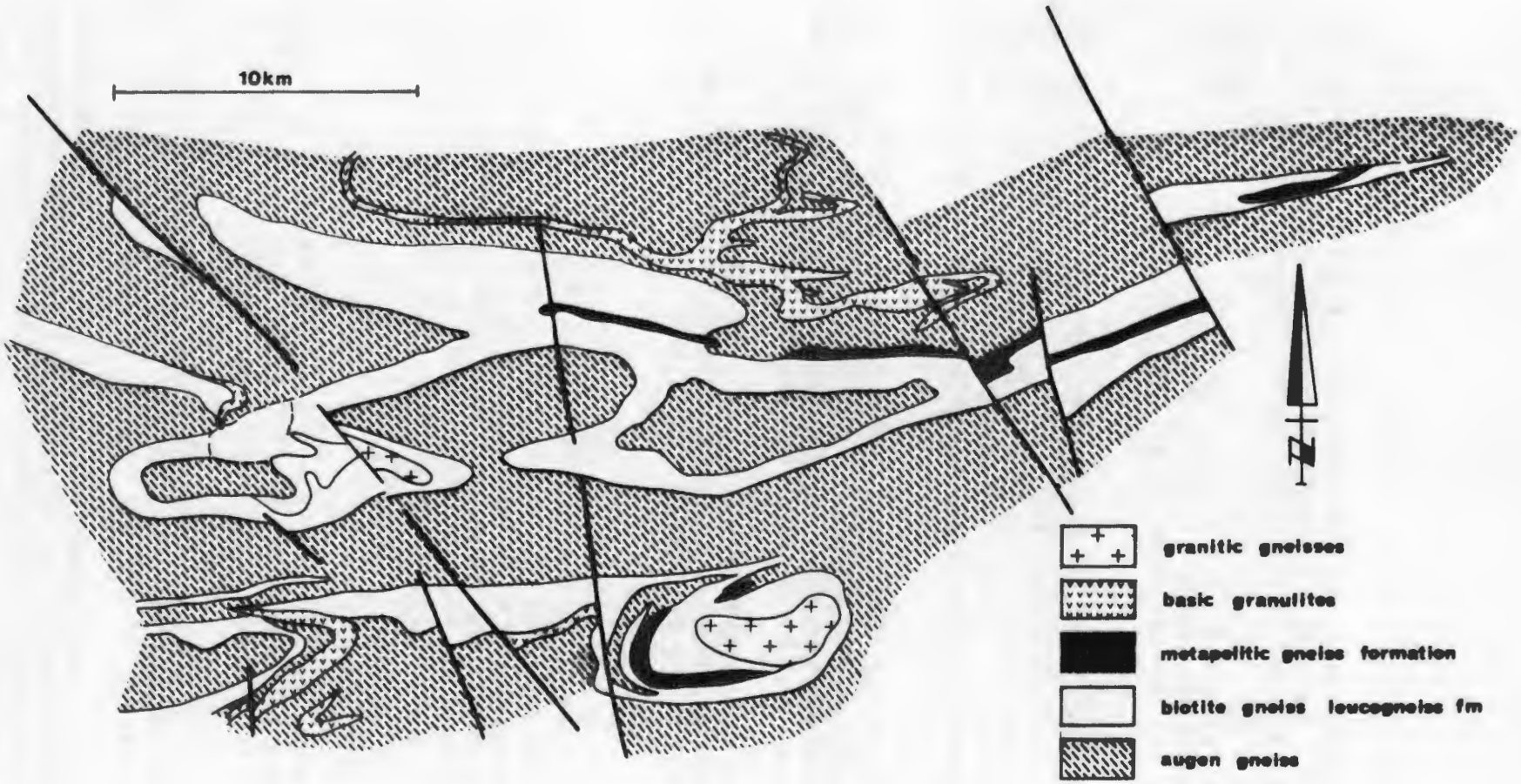

Fig. 4.8 Simplified geological map of the Anegas-Boesmanplaat paragneiss belt and the Couragiefontein area to the south, showing the distribution of the major lithological units.

beneath younger cover rocks (Albat,1984). Here a thick succession of megacrystic granitic gneisses, augen and leucogranitic gneisses and basic granulites appear to have overthrust an essentially unfolded (not duplicated) supracrustal sequence during the F2 event. To the south of this linear belt, in a similar fashion to the Keurbos area, the supracrustal rocks are preserved in complex basin and dome structures, and diverse linear L2 trends are again observed with the added complexity of the presence of L3 lineations in several places (Fig. 4-7). Joubert (1971) has observed some major F3-age shear zones in the Platbakkies-Witwater area which were not obvious within the supracrustal sequence. The majority of these shears may, however, lie just to the north of the area mapped in this study.

4.3.4 Metamorphism

Uniform granulite grades of metamorphism dominate across the entire area, typified by the two-pyroxene granulite assemblages in the mafic rocks and quartz-K-feldspar-cordierite-garnet assemblages in the metapelitic rocks, and are related to the major D2 deformational event (Joubert,1971; Albat,1984). Evidence of later retrogression associated with either D3 or D4 deformational events in the area, was essentially restricted to localised zones of epidotisation mostly in the Keurbos area where its common association with the lenticular bodies of syntectonic granitic gneiss was noted.

4.4 The Anegas-Boesmanplaat paragneiss belt

4.4.1 The supracrustal sequence

A fairly narrow linear east-west trending belt of supracrustal rocks stretches from Arakoep farm south of Kamieskroon, eastwards through the Namaqua mountainland via Anegas, Pedroskloof and Hosabees in the Leliefontein Reserve to Boesmanplaat where it disappears beneath Recent sand and calcrete cover (Fig. 4-8). In similar fashion to the Witwater and Keurbos belts, this paragneiss belt generally shows a highly linear northern contact with overlying augen gneisses, and a more complex southern boundary with basinal and domal structures. To the south of this belt, in the Bakleikraal-Nourivier portion of the Leliefontein Reserve and on the farm Couragiefontein further east, remnants of a second paragneiss belt of similar structural pattern are also patchily preserved. The following lithologies were recorded from these belts:-

Leucogneiss. Red-weathering, well-banded, biotite-poor leucogneisses were observed at various levels in the sequence, although most commonly at the base where they are very coarse-grained at some localities. Bands of a distinctive white-weathering leucogneiss with characteristic "ghost" nebulitic banding on weathered surfaces were also relatively common in both the Anegas-Boesmanplaat and Couragiefontein sequences, and may be related to the cordierite-bearing metapsammitic gneisses of the Witwater area. As in this latter sequence, one of the central leucogneiss bands contains streaks, lenses

and nodules of sillimanite-quartz which are clearly aligned in the axial planes of minor folds, cross-cutting the regional foliation. Sporadic garnets are also present in this leucogneiss which displays ferruginous coatings along weathering fractures giving the rock a distinctive, slightly gossanous appearance.

Biotite gneiss. Fine-grained banded biotite gneisses are the other common component of the Anegas-Boesmanplaat sequence, being interbanded with the leucogneisses. In certain more restricted bands, the biotite is largely substituted by magnetite, and elsewhere a distinctive biotite gneiss with prominent quartz eyes (porphyritic ?) was observed. This latter gneiss was noted for its lack of K-feldspar and dominance of plagioclase and was most prominent as a massive broad band on the farm Anegas.

Metapelitic garnet-biotite gneiss. Sporadic bands of banded garnet-biotite-rich gneiss are present in association with the biotite gneisses. Cordierite is occasionally present in these gneisses which were recorded chiefly in the Couragiefontein sequence, but also on the farm Pedroskloof.

Metapelitic cordierite-garnet-sillimanite gneiss. Coarse-grained, poorly banded, quartz-K-feldspar-garnet-cordierite gneisses with lesser plagioclase, sillimanite, biotite, iron oxides and hercynite occur as sporadic, disrupted lenses and bands at the extreme top of the sequence in the eastern portions of the Anegas-Boesmanplaat sequence. Similar lithologies were recorded in the Bitterfontein and Keurbos sequences.

Basic granulite. As in the Witwater and Keurbos areas, these orthopyroxene-clinopyroxene-plagioclase gneisses occur as thin lenses and bands throughout the supracrustal sequence, and as larger, more prominent bands together with the overlying intrusive rock suite, most notably at Klein Nourivier and De Kuilen.

Calc-silicate rock. Thin lenses and pods of garnet-clinopyroxene-plagioclase-quartz calc-silicate rocks were sporadically observed in the central portions of the sequence in association with nodular leucogneiss and lenses of BIF. This association was also observed in the Witwater sequence. The calc-silicate rocks were most apparent in the Hosabees area and further east. Joubert (1971) recorded a marble band on the farm Anegas, but this was not located in the present study.

Iron formation. Sporadic lenses of a coarse-grained massive to poorly banded iron oxide-quartz-bearing BIF with noticeable amounts of accessory zircon were located in close proximity to the calc-silicate lenses in the Hosabees area, and were also poorly developed in the Pedroskloof-Anegas area.

Feldspathic quartzite. A thin (one to five metre) band of feldspathic quartzite occurs at the top of the sequence in the Couragiefontein supracrustal rocks, but was not observed in the Hosabees sequence or any other sequences further north. This appears to be the most northerly extension of the "Bitterfontein-type" feldspathic quartzites.

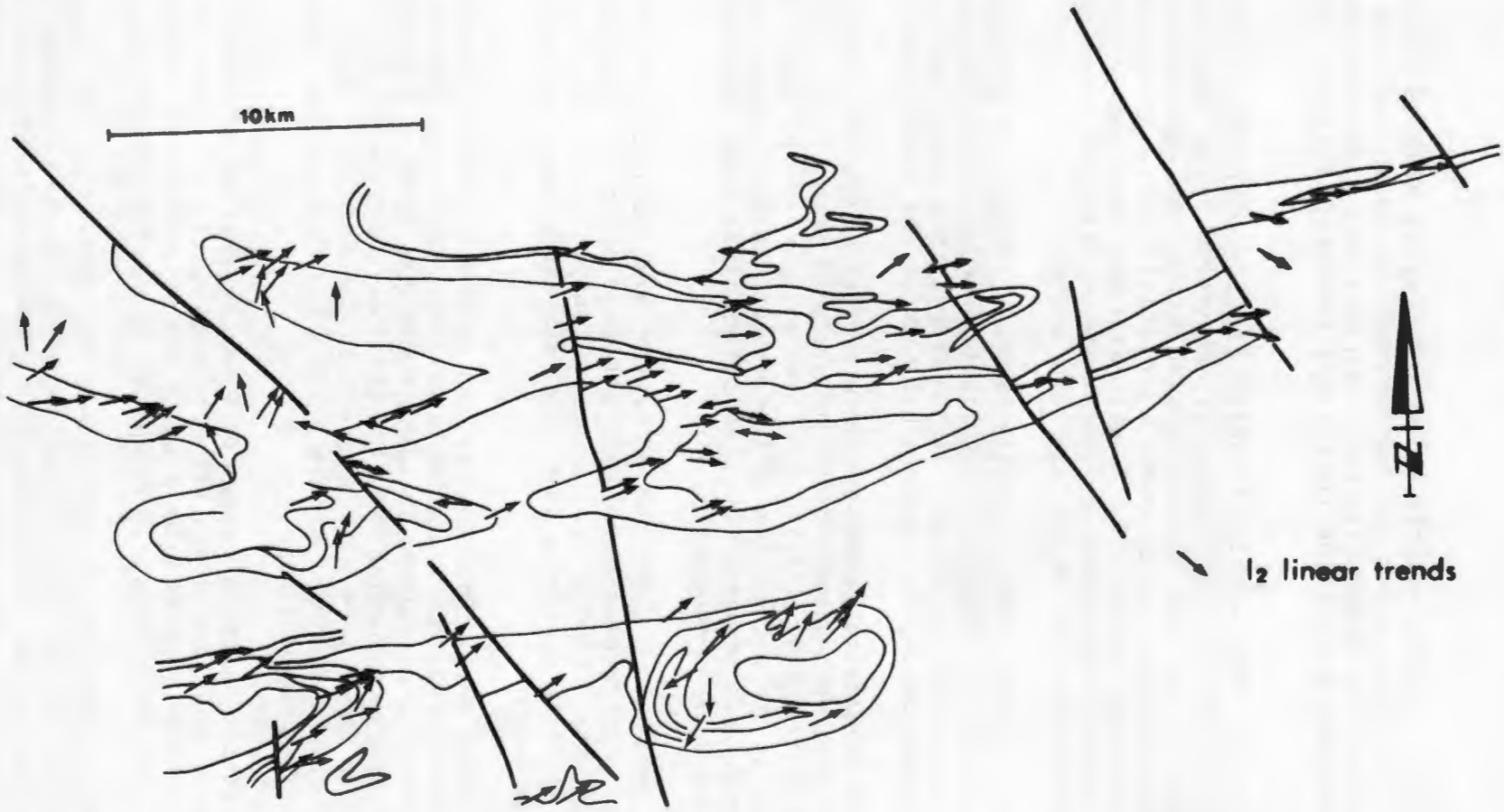

Fig. 4.9 Structural map of the Anegas-Boesmanplaat paragneiss belt showing the regional trend of the dominant L2 lineation.

4.4.2 Intrusive Rocks

The Couragiefontein paragneiss belt consists of impersistent lenses and bands of supracrustal rocks alternating with similar bands of an augen gneiss. This pretectonic gneiss also forms the major overlying unit between the Couragiefontein and Anegas-Boesmanplaat paragneiss belts as well as the major unit underlying the Couragiefontein supracrustal sequence. In a few places these field relationships appear to represent a lit-par-lit intrusive contact, but the persistence of this characteristic along such a linear belt indicates that this duplication could be due primarily to tectonic processes such as imbrication during the major thrust fault event.

In the core of the Couragiefontein domal structure, the supracrustal rocks are underlain by a very coarse-grained red-weathering biotite-free granitic gneiss similar to that observed in the basal portions of the Kougoedvlakte dome in the Witwater area. Major bands of basic granulite are associated with the upper contact between the supracrustal rocks and the augen gneisses, particularly in the Klein Nourivier area.

The Anegas-Boesmanplaat paragneiss belt contains few obvious syntectonic intrusive rocks, and is generally conformably overlain and underlain by typical augen gneisses. In the Pedroskloof-De Kuilen area and in the area south of Rooifontein (Leliefontein Reserve), however, the sequence is overlain and at the former locality, partially intruded by leucogranitic and charnockitic gneisses containing large rafts and prominent bands of basic granulite.

4.4.3 Structure

The structure of the Anegas-Boesmanplaat and Couragiefontein paragneiss belts is complex, but in many respects similar to that of the Witwater area. The Couragiefontein belt appears to represent a pre-F3 thrust with underlying supracrustal rocks that has been folded into several major north-east trending F3-age synformal and domal structures to the immediate south of an east-west striking F3-age linear belt. The domal structures appear to have resulted from non-cylindrical folding associated with shearing along the linear belt to the north (see Section 2-2), although it is possible that they formed as the result of interference patterns caused by later north-west striking F4 folding.

The Anegas-Boesmanplaat paragneiss belt is more complex, and probably represents two paragneiss belts that have been sheared together in the Hosabees area and again in the Boesmanplaat area. The southern portion of this composite belt is very similar to the Couragiefontein belt and is also represented by a pre-F3 thrust with underlying supracrustal rocks that has likewise been folded into F3-age east-west-trending synformal and antiformal structures along a shear plane that links the two portions of the composite belt. Subsequent north-west trending F4 folding has resulted in mushroom-shaped basinal and domal structures in the De Kuilen and Hosabees areas

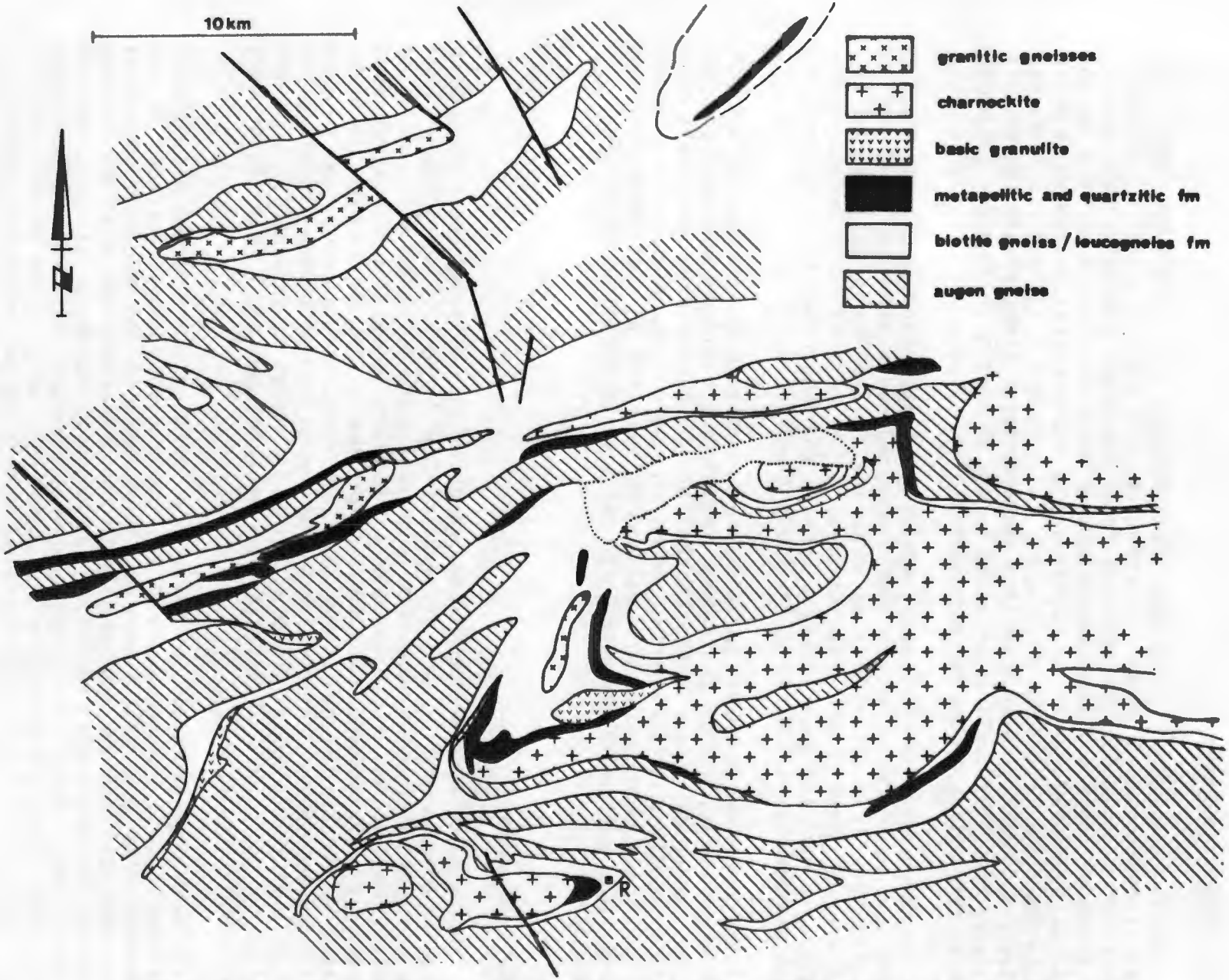

Fig. 4.10 Simplified geological map of the Silverfontein-Rietfontein, Buffels River and Stofkraal-Dikmatje paragneiss belts, showing the distribution of the major lithological units. (R = Rooifontein).

respectively. Earlier L2 linear trends are predominantly east-north-east although they also show rotation within certain F3 structures (Fig. 4-9).

The northern portion of the composite Anegas-Boesmanplaat paragneiss belt is preserved within a major F3 synformal structure which ultimately closes in the west at the boundary between the farms Inkruip and Stofkraal, The southern limb of the fold in the supracrustal rocks comes into the intervening F3 shear zone in the Swartklaasriet-Hosabees area, and again on the farm Boesmanplaat. The northern limb of the fold is subsequently deformed by F4-age folding in the area where it cuts the Buffels River south of Rooifontein (Leliefontein Reserve). In the west, both portions of the composite belt swing northwards into what appears to be a very major north-east trending upright F4 synformal structure, related to the major Buffels River linear zone to the north.

4.4.4 Metamorphism

As in the Keurbos and Witwater areas to the south, pervasive granulite grade metamorphism dominates in the two supracrustal sequences. The only evidence of a possible significant retrogressive post-D2 metamorphic imprint in the area was the presence of amphibolite instead of basic granulite as the dominant mafic band overlying the supracrustal sequence on the northern side of the Couragiefontein domal structure.

4.5 The Buffels River paragneiss belts

4.5.1 The supracrustal sequence

Supracrustal sequences in the Kamieskroon to Gamoep area are preserved in three fairly narrow, east-west trending belts displaying considerable structural complexity that has resulted in their fragmentation in places and the shearing out of certain portions of the sequence in other areas (Fig. 4-10). The southern belt is located in the Stofkraal-Kammassies-Dikmatje area, on the southern portions of the farm Hytkoras, and in a closed basinal structure in the Rooifontein (Leliefontein Reserve) area. The central belt is located on the farms Gamoep (Velskoen), Dabeeb, Tweefontein, Rietfontein, Hytkoras and Nuwedam and is considerably disrupted and duplicated within the prominent Buffels River linear zone. Rocks of this paragneiss belt also crop out to the south of the linear zone in two domal structures on the southern portions of the farm Tweefontein. The northern belt is the least persistent and stretches from the farm Silverfontein in the west across Rietfontein and Brakputs to the Kouberg hills in the east. The supracrustal sequences in these belts contain several previously unrecorded lithologies such as dolomitic marble and glassy quartzite and comprise the following rock types:-

Leucogneiss. As in most of the preceding supracrustal sequences, banded biotite-poor leucogneisses predominate in the basal portions of the Buffels River sequence where they generally occur as broad bands, interbanded with

more biotite-rich gneisses. Sillimanite-quartz nodules/streaks occur in certain localised zones at a few places (e.g. at Rooifontein and Kouberg) and the banding in the gneiss becomes distinctively disrupted (in places best described as pseudo-crossbedding) in the central Dabeeb-Hytkoras zone. On the farms Rietfontein and Hytkoras unusual corundum-K-feldspar-rich, quartz-free leucogneisses are locally present.

Biotite gneiss. Banded biotite gneisses are also common in the lower portions of the sequence where they are, in places, either magnetite-, hornblende- or hypersthene-bearing. In the central zone, particularly on the farm Nuwedam, migmatised garnetiferous varieties predominate. Just to the north of Rooifontein, bands of a distinctive "conglomeratic" variety were observed, containing distinctive quartz and lesser feldspar "pebbles", up to 2 cm in diameter. This biotite gneiss is thought to be related to the porphyritic variety observed in the Hosabees belt to the south, and is also plagioclase-rich. The biotite gneisses commonly contain thin bands of basic granulite and garnetiferous calc-silicate rocks.

Calc-silicate rocks. As in the Witwater belt, several varieties of calc-silicate rock are present in the Buffels River area. Massive to poorly banded garnetiferous varieties (with diopside, plagioclase and quartz) together with banded diopside-plagioclase varieties (with magnetite and quartz) are located within the basal portions of the sequence in the biotite gneiss/leucogneiss association, most prominently in the northern Silverfontein belt. Massive coarse-grained diopside-rich varieties (with minor plagioclase, scapolite, pyrite and spinel) are generally associated with dolomitic marble bands and more banded, less diopside-rich, siliceous varieties at or near the contact between the basal biotite gneiss/leucogneiss zone with the overlying metapelitic rocks.

Dolomitic marble. Poorly banded coarse-grained dolomitic marbles containing dolomite, lesser calcite, forsterite and/or chondrodite, both altering to serpentine, and phlogopite crop out as sporadic but widespread lenses and pips together with massive diopside-rich calc-silicate rocks at or near the contact between the metapsammitic gneisses and overlying metapelitic rocks. Marbles were common in the Dikmatje and Hytkoras belts but were not observed in the Kouberg sequence.

Basic granulite. Thin bands and lenses of basic granulite are very common throughout the supracrustal sequence - more so than in any previous paragneiss belt. In the Nuwedam-Hytkoras area, certain granulites are associated with the following sequence of unusual lithologies:

hypersthene-cordierite-spinel-plagioclase
hypersthene-cordierite-biotite-spinel ($\pm$ sapphirine, $\pm$ kornerupine)
cordierite-sillimanite-plagioclase-spinel.

These rock types appear to represent transitional lithologies between basic granulite and the metapelitic assemblage described below.

Metapelitic cordierite-garnet-sillimanite gneiss. Coarse-grained banded

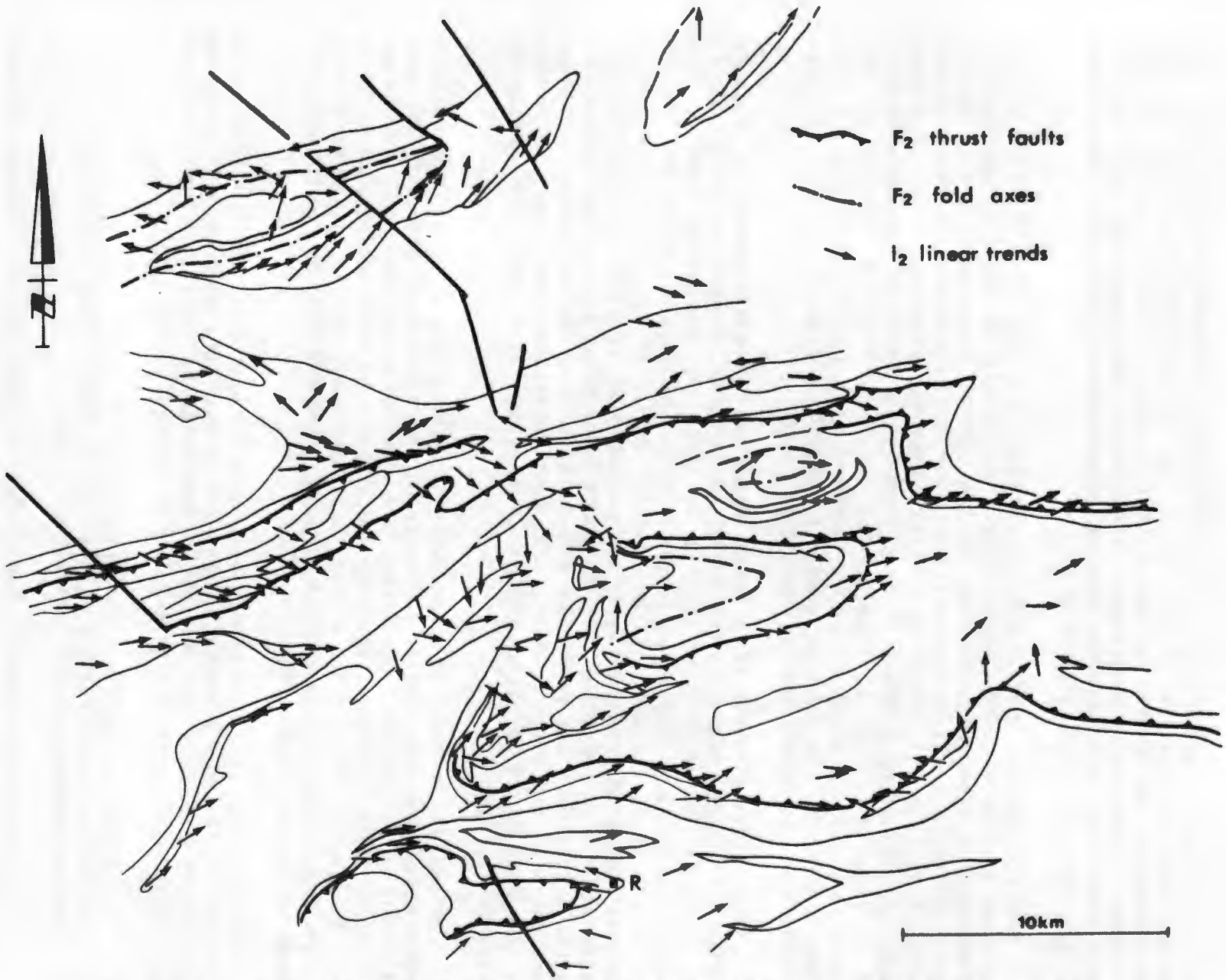

Fig. 4.11 Structural map of the Silverfontein-Rietfontein, Buffels River and Stofkraal-Dikmatje paragneiss belts showing the major F2 structures.

metapelitic gneisses in the Dikmatje and Hytkoras belts can be broadly divided into two types, a lower cordierite-rich, sillimanite-poor variety and an upper cordierite-poor, sillimanite-rich variety that is closely associated with the glassy quartzite unit which it both overlies and underlies. This subdivision is best observed in a large F3-age closure on the farm Stofkraal and also more locally on the farms Tweefontein and Hytkoras. Mica-sillimanite schists are present in the place of the metapelitic gneisses in the Kouberg sequence.

Cordierite-hypersthene gneisses. Finely banded to massive coarse-grained varieties of these cordierite-hypersthene-biotite-rich gneisses are present in the Hytkoras belt in association with the metapelitic and basic granulite bands. Occasionally they contain local concentrations of the rare magnesium-aluminium silicates sapphirine and kornerupine.

Glassy quartzite. Thin bands and lenses of a massive to poorly banded quartzite, comprising essentially quartz with a few darker bands containing biotite or magnetite, overlie the metapelitic gneisses and schists in all three belts, being very thin and localised in the southernmost Dikmatje belt and most prominent, up to 50 m thick, in the Kouberg sequence in the extreme north-east.

Iron formation. Lenses and pods of a well-banded to massive garnet-quartz-magnetite($\pm$ orthopyroxene) BIF were located in association with glassy quartzite on Tweefontein, where it appears to overlie the quartzite, Stofkraal and Gamoep (Velskoen). A small pod of apatite-rich rock was found at one locality on Tweefontein in association with the BIF. In the Kouberg area, a thin BIF lens is associated with Cu-mineralisation, calcite, garnet and sillimanite-nodule development within the biotite gneisses of the lower portions of the sequence.

4.5.2 Intrusive rocks

Unlike the preceding Hosabees paragneiss belt, the paragneiss belts of the Buffels River area, particularly the Dikmatje and Hytkoras belts, are highly disrupted by granitic gneisses of the various intrusive suites. In general the intrusive rocks show a crude stratigraphy, also noticed in the preceding belts, namely that augen gneisses generally underlie the supracrustal sequences whereas the charnockitic, leucogranitic and megacrystic granitic gneisses together with basic granulites, generally overlie the supracrustal sequences and partially intrude the upper portions of these latter rocks.

The Dikmatje belt is severely disrupted, particularly in the upper portions of the sequence, by overlying syntectonic charnockitic gneisses which also contain large rafts of basic granulites and leucogranitic gneisses, both of which are most prevalent in the large F3-age synformal closure on the farm Stofkraal. The basal portions of the sequence show much interbanding between supracrustal rocks and augen gneisses which also underlie the sequence. This latter interbanding may represent tectonic duplication or syntectonic intrusion.

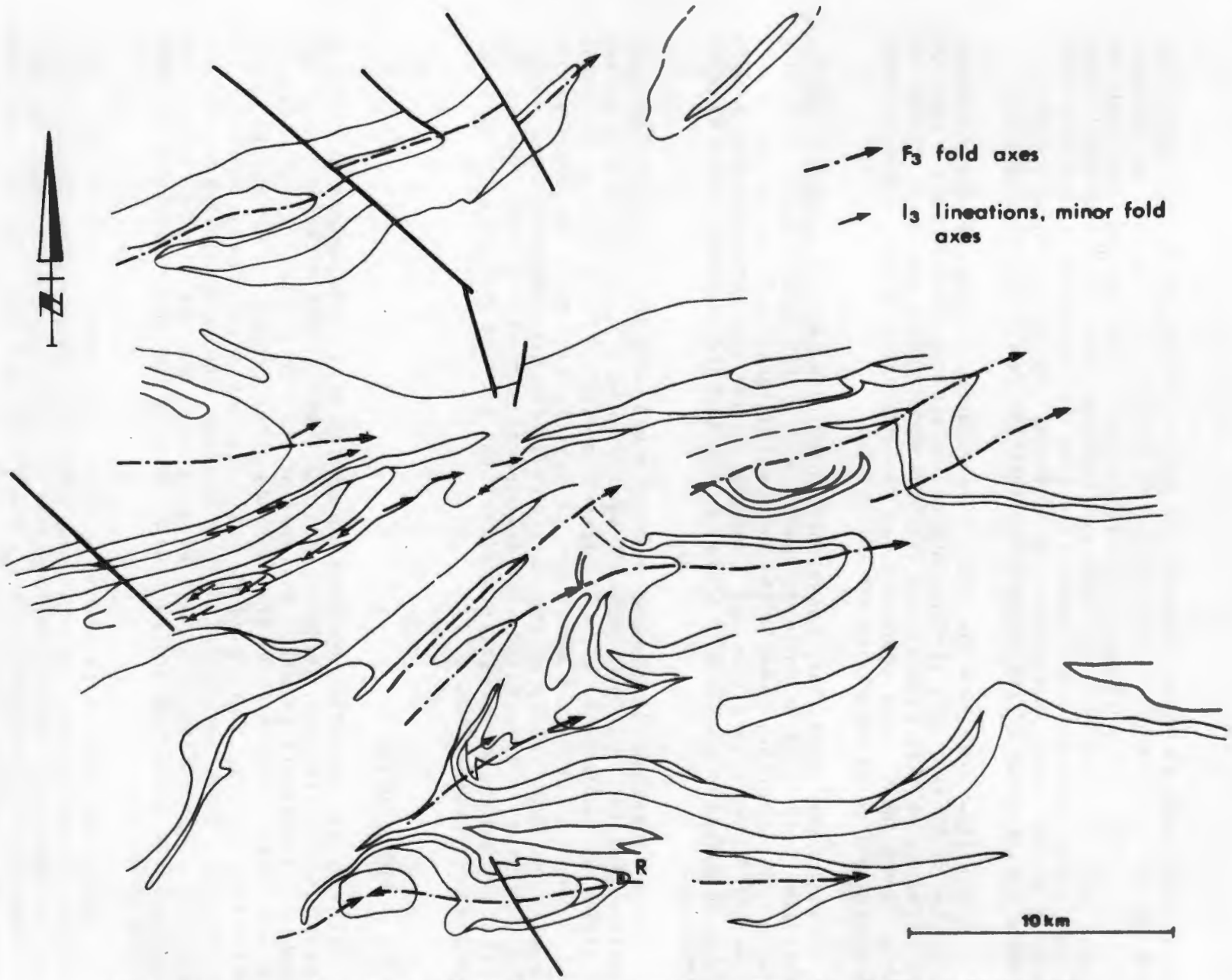

Fig. 4.12 Structural map of the Silverfontein-Rietfontein, Buffels River and Stofkraal-Dikmatje paragneiss belts showing the major F3 structures.

In the Hytkoras belt, the supracrustal rocks are likewise strongly disrupted by interbanded charnockitic and/or leucogranitic gneisses and are underlain by augen gneisses. Larger basic granulite bodies are not present as they are in the Dikmatje belt, but smaller bands and lenses are very common throughout the supracrustal sequence. In places they can be seen to be transgressive, but elsewhere apparently conformable. The Silverfontein-Kouberg supracrustal sequences show very little evidence of intrusive rocks aside from one leucogranitic body and occasional basic granulite/amphibolite bands. In the Silverfontein and Rietfontein area the supracrustal rocks are conformably underlain by augen gneisses.

4.5.3 Structure

Although the distibution of the supracrustal sequences is primarily controlled by phenomena such as thrusting and isoclinal folding during the F2 deformational event (Fig. 4-11), their present configuration is largely governed by major F3-age structures which include a large-scale linear "shear" zone in the central belt on the farms Nuwedam, Hytkoras, Rietfontein and Dabeeb, and adjacent large-scale fold structures to the north and south (Fig. 4-12).

The supracrustal rocks of the Dikmatje belt, as in several preceding belts, represent a major east-west striking, north-dipping F2-age thrust plane along which these rocks have been overthrust and syntectonically intruded by a large mass of charnockitic gneiss. The belt has subsequently been folded by a major east-west striking, east-plunging F3-age synform and antiform on the farms Stofkraal and Hytkoras respectively. To the south in the Rooifontein area (Leliefontein Reserve), supracrustal rocks reappear, preserved within a basinal structure resulting from the coincidence of an east-west striking F3-age synform and a north-north-west striking F4-age synform.

The supracrustal rocks of the Hytkoras belt are generally highly disrupted within the F3-age linear belt, but to the south and east of this belt on the farms Gamoep (Velskoen), Dabeeb and Tweefontein, it is possible to observe that the distribution of the supracrustal sequence is again initially controlled by pre-F3-age structures, either isoclinal folding or thrust faulting. These early structures are subsequently caught up in the major F3-age Buffels River linear belt which is a steeply south-dipping east-west striking zone some five km wide, stretching across the area from Nuwedam in the west to Dabeeb, Driegat and Kouberg in the east. To the south of the linear belt, the supracrustal rocks reappear in two shallow-plunging sheath-like domal structures on the southern portions of the farm Tweefontein, resulting from non-cylindrical folding associated with the major shear zone.

The distribution of supracrustal rocks in the Silverfontein, Brakputs and Kouberg areas is largely controlled by major F3-age folds immediately to the north of the Buffels River linear belt. They crop out in east-north-east striking structures of varying plunge, due to the influence of later gentle

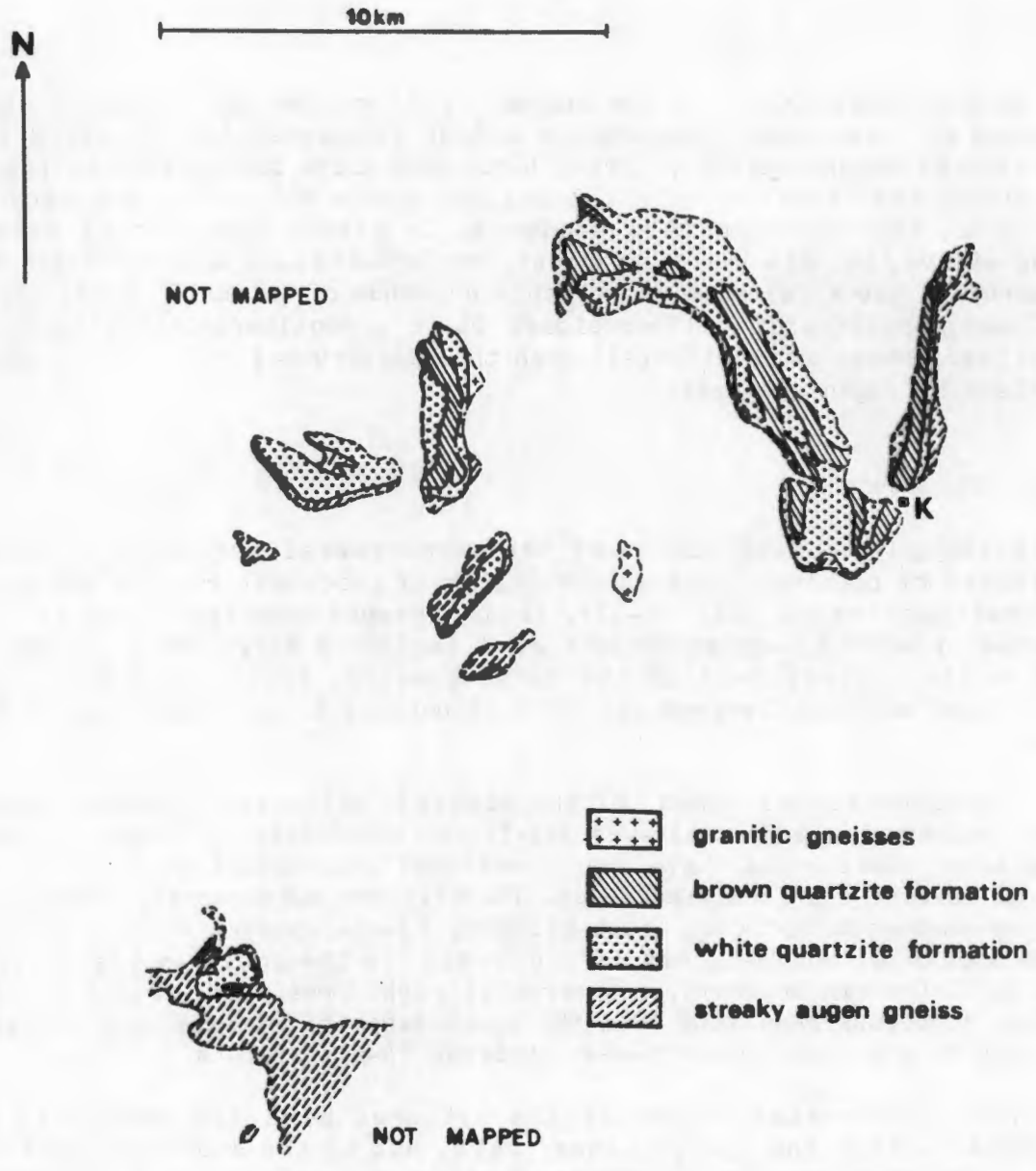

Fig. 4.13 Simplified geological map of the Smorgen Schaduwe-Kangnas paragneiss belt, showing the distribution of the major lithological units. (K = Kangnas).

north-south striking F4-age folds.

Late-stage vertical tectonics, typified by north-south striking fractures and faults, are widespread throughout the area, but not as prevalent as in the Bitterfontein to Witwater areas.

4.5.4 Metamorphism

Once again, granulite-facies grades of metamorphism predominate throughout the area, even within the major later structural zones such as the Buffels River linear belt. In the Silverfontein supracrustal sequence, certain mafic bands are represented by amphibolite and not basic granulite, and this may represent a lower metamorphic grade in the north, although compositional variation may also be responsible for this feature. The schistose biotite-sillimanite-rich metapelitic rocks in the Kouberg area indicate that lower metamorphic grades are probably present in this area (see also Albat,1984).

4.6 The Smorgen Schaduwe-Kangnas paragneiss belt

4.6.1 The supracrustal sequence

The volume and quality of rock exposure is considerably reduced between the Buffels River and the close approaches to the Orange River with Recent sand cover encroaching from the Bushmanland plateau to the east. Due to the resistance of the glassy quartzites to erosion and their dominance in the northern supracrustal sequences, however, the paragneiss belts tend to be the least affected by this feature and the biotite and augen gneisses the most. Supracrustal rocks crop out in one major belt (Smorgen Schaduwe-Kangnas) and one minor, isolated remnant further south, and the sequences are notable for their marked reduction in thickness, combined with the virtual absence of several units including the entire lower leucogneiss-biotite gneiss unit, carbonate and calc-silicate rocks, cordierite-dominated metapelitic rocks and mafic rocks, with a dominant role now played by glassy quartzites (Fig. 4-13).

Leucogneiss. Thin impersistent lenses of leucogneiss, some containing sillimanite nodules, are present at the base of the sequence at Vioolskraalberg, overlying "basement" biotite gneisses. Elsewhere leucogneisses are absent from the sequence.

Calc-silicate rocks. Thin lenses of calc-silicate rocks are present at Vioolskraalberg and Kangnas (clinopyroxene-quartz and garnet-plagioclase) and at Smorgen Schaduwe (garnet, diopside, plagioclase and allanite). These generally occur within the extreme basal portions of the metapelitic schists.

Metapelitic biotite-sillimanite schists. Biotite-sillimanite-quartz schists make up the lowermost major unit of the supracrustal sequence in both belts, between the underlying gneisses and the overlying glassy quartzites. Garnet, cordierite, K-feldspar and less commonly muscovite and graphite are

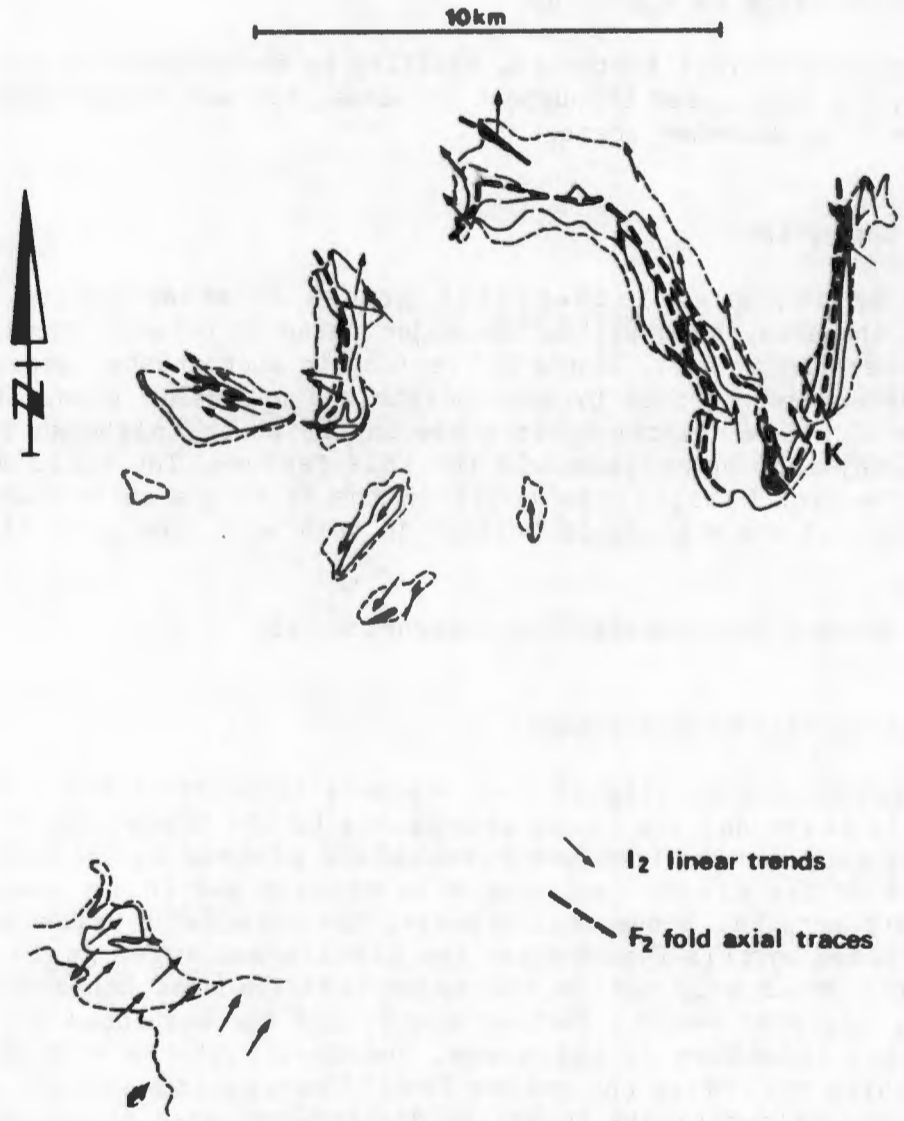

Fig. 4.14 Structural map of the Smorgen Schaduwe-Kangnas paragneiss belt, showing the major F2 structures.

also present in varying amounts in certain bands, commonly towards the base of the unit. Localised lenses of muscovite-sillimanite schists occur in the Smorgen Schaduwe-Kangnas belt. On Kangnas, biotite-sillimanite-quartz schists also crop out above the white glassy quartzite, between it and the uppermost brown quartzites and as thin intercalations within this upper quartzite.

White glassy quartzite. A massive, white glassy quartzite containing minor amounts of biotite and muscovite overlies the metapelitic schists. At Vioolskraalberg on the farm Goinoep, the basal portions of the quartzite are commonly amphibole-bearing, giving the rock a very dark green appearance and on the farm Oranjefontein in the same belt, the lowermost portions of the quartzite contain bands of garnet, gahnite and, more rarely, disseminated galena (Hicks,1983). Higher up in the quartzite formation, at Vioolskraalberg and to a lesser extent on the farm Smorgen Schaduwe, disseminations and occasional thicker bands of tourmaline occur within certain stratigraphic zones.

Brown glassy quartzite. A massive, slightly more schistose and generally thicker glassy quartzite with noticeably more biotite, muscovite, and/or iron oxides is present as the uppermost unit in the supracrustal sequence. This quartzite immediately overlies the white glassy quartzite in the Vioolskraalberg belt, but is separated from it by metapelitic schists and BIFs in the Smorgen Schaduwe-Kangnas belt. At Kangnas, the quartzite also contains many thin (less than one m thick), intercalated biotite-sillimanite-quartz schist bands.

Iron formation. Thin lenses of BIF are present in both paragneiss belts. At Vioolskraalberg, a banded garnet-rich rock occurs in close association with the gahnite-rich quartzites immediately below the white glassy quartzite. In the Smorgen Schaduwe-Kangnas belt, various BIF lenses crop out in pelitic schists between the two glassy quartzite units. Typically they immediately overlie the white quartzite formation, the uppermost unit of which is generally a dark grey ferruginous quartzite comprising disseminated hematite in a quartz matrix. On Smorgen Schaduwe, the BIF is a quartz-garnet rock. On Karas, increasing amounts of iron oxide are present, and at Kangnas near the farmhouse, an iron-rich pyroxene is apparently present (surface samples of BIF are silicified). These mineralogical changes coincide with an increasing thickness of the sequence from west to east and might imply primary facies/compositional changes in the BIF.

Basic granulite/amphibolite. Mafic rocks are extremely rare in the Smorgen Schaduwe-Kangnas area and appear to be absent from the major paragneiss belt. Small amounts of two-pyroxene granulite and a coarse-grained hornblende-rich amphibolite crop out within the metapelitic schists on the Goinoep portion of Vioolskraalberg.

Cordierite-hypersthene gneiss. A small outcrop of cordierite-hypersthene-biotite gneiss is present in the metapelitic schists in the Vioolskraalberg belt on the farm Goinoep and another on the Areb portion of the Kangnas hills. The rocks are very coarse-grained and massive and are associated with basic granulite. A similar rock is described from Smorgen Schaduwe by Clifford

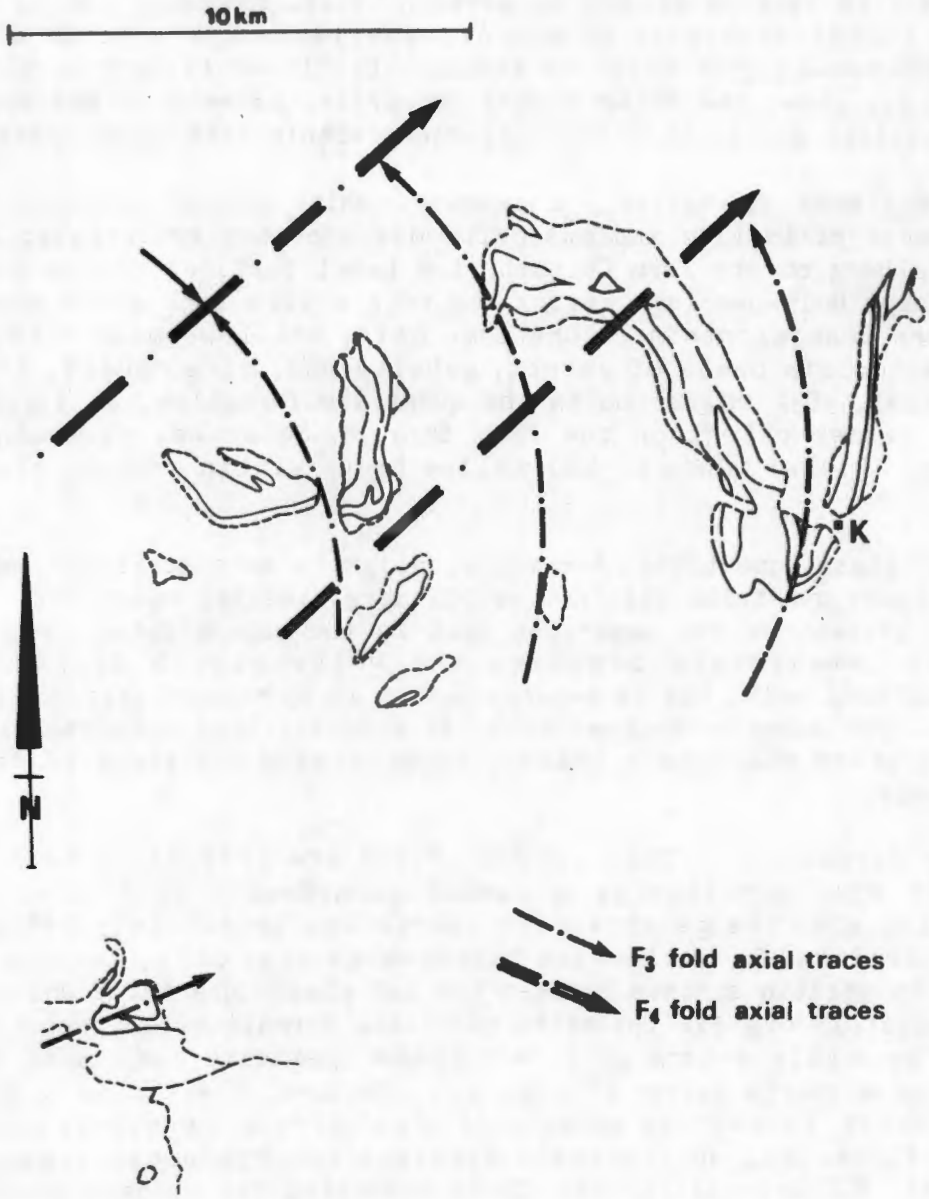

Fig. 4.15 Structural map of the Smorgen Schaduwe-Kangnas paragneiss belt, showing the major F3 and F4 structures.

et al. (1981). This outcrop actually occurs on the farm Kaitob to the north of the area studied.

4.6.2 Intrusive rocks

Very few intrusive rocks are present within the Smorgen Schaduwe-Kangnas paragneiss belt. The supracrustal rocks are underlain by various "streaky" augen gneisses that, judging by their extensive structural history, particularly on the farm Oranjefontein, are pretectonic in origin. Calc-silicate remnants (xenoliths?) were observed within these gneisses on the farm Kangnas.

Within the streaky augen gneisses on the farm Smorgen Schaduwe, isolated outcrops of a probably more continuous, larger, syntectonic leucogranitic gneiss body were observed. Other leucogranitic bodies outcrop on the farm Areb to the immediate north of Smorgen Schaduwe.

4.6.3 Structure

The structural configurations of the supracrustal rocks in the Smorgen Schaduwe-Kangnas belt can be interpreted in terms of early (F2) isoclinal, now recumbent, synformal structures, folded by a series of more upright, generally northerly plunging synforms and antiforms of F3-age (Fig. 4-15). These have, in turn, been distorted by large-scale north-east-trending F4 structures that appear to plunge to the north-east. Coincidence of synforms of F3- and F4-age has resulted in the prominent basinal structure on Areb and Smorgen Schaduwe, partly north of the area examined.

Early F2 isoclinal synforms are best displayed on the farm Kangnas and to a lesser extent on Karas and Smorgen Schaduwe, with the brown quartzites forming the central, uppermost units of the narrow elongate synforms. One of these synforms can be seen to be refolded by a major F3 synform just to the south-west of the Kangnas farmhouse.

The L2 lineations show marked rotation from north-east-trending plunges at Vioolskraalberg and in the southern part of Smorgen Schaduwe, through northerly plunges on Kangnas and Karas, to north-west plunges on the northern portions of Smorgen Schaduwe, indicating the extent of the effect of the later folding on the orientation of the F2 isoclinal folds (Fig. 4-14).

The Vioolskraalberg supracrustal rocks appear to be an outlier of this belt, preserved within a north-east-trending F3 synform with a virtually horizontal fold axis.

4.6.4 Metamorphism

At Vioolskraalberg, two-pyroxene granulites and garnet-cordierite-bearing metapelitic rocks indicate that granulite facies conditions are still present.

Amphibolites and epidote-rich calc-silicate rocks observed along the southern limb of the F3 synform there are most probably due to a D3-related retrograde metamorphic imprint associated with this folding.

In the Smorgen Schaduwe-Kangnas area, however, biotite-sillimanite-quartz schists predominate as the typical metapelitic lithology although certain garnet-cordierite varieties are locally present at the base of the sequence at Kangnas and at Kaitob to the immediate north-west of the area examined. Unfortunately, mafic rocks appeared to be absent from these critical sequences although hypersthene-cordierite-spinel rocks are present at Kaitob and in the Kangnas hills. It would appear that the Smorgen Schaduwe-Kangnas belt represents the transitional zone between granulite and upper amphibolite facies in the northern part of the study area as demonstrated by the change from garnet-cordierite-K-feldspar-bearing lithologies to biotite-sillimanite-quartz assemblages in the metapelitic rocks.

4.7 The Aggeneys-Gamsberg paragneiss belt

The lithological, structural and metamorphic aspects of the geology of the Aggeneys-Gamsberg-Namiesberg area are extensively covered in a number of publications (Joubert,1974a; Rozendaal,1975,1978,1982; Moore,1977,1983; Lipson,1978; Stedman,1980; and Ryan et al.,1982). As no mapping was undertaken in this specific area during the present study (only sampling for geochemical analysis), it was felt unnecessary or inappropriate to discuss the geological features of this area in any detail here. The following brief descriptions, for comparison with the previous paragneiss belts, have been summarized from the above-mentioned publications.

4.7.1 The supracrustal sequence

Leucogneisses, quartz-biotite-muscovite-sillimanite schists, quartzites, iron formations, calc-silicate and metacarbonate rocks, amphibolites and metaconglomerates are all present within the supracrustal sequence in the Aggeneys-Gamsberg area and are adequately described in several previous publications listed in Section 4-7 above. They are therefore not discussed in any detail here. Throughout the area, the supracrustal sequence is underlain by streaky augen gneisses that have been described as basement lithologies in certain areas (Paizes,1975; Moore,1977).

4.7.2 Intrusive rocks

Intrusive rocks are generally absent from the major supracrustal sequence in the Aggeneys-Gamsberg area as in the previous Smorgen Schaduwe-Kangnas belt. In certain areas, namely within the footwall metapelitic schists of the Broken Hill ore deposit at Aggeneys and along the southern margin of the Namiesberg (Moore,1977), large pegmatitic bodies are present - a lithology not recorded on this scale within the granulite-facies terrane to the south. Thin amphibolite bands are also present within the metapelitic schists and show

transgressive relationships, cutting through the iron formation, at Black Mountain, Aggeneys (Stedman,1980). Other thicker amphibolite units at Aggeneys East and Gamsberg have conformable attitudes within the enclosing supracrustal rocks and appear to represent metamorphosed extrusive mafic volcanic rocks (Rozendaal,1978).

Leucogranitic gneisses are intrusive into the augen gneisses that underlie the supracrustal sequence and occasionally into the basal portions of the supracrustal sequence where they superficially resemble the leucogneisses (Moore,1977). These leucogranitic rocks are, however, highly restricted in size and distribution and are generally small, lenticular bodies that follow the regional foliation. The basal leucogneisses that have been included in the supracrustal sequence in this study, have been described as leucogranitic intrusive rocks in previous studies (Mathias,1940b; Lipson and McCarthy,1977; Lipson,1980) and are included in the Hoogoor Suite by SACS (1980). Discussion of these lithologies and the various models proposed for their origins is presented in Chapter 8.

4.7.3 Structure

As observed in the previous Smorgen Schaduwe-Kangnas belt, the structural aspects of the area are dominated by major early (F2) recumbent, isoclinal synforms of east-west trend, that have been refolded by later (F3) synformal structures with steep, northerly-dipping axial planes and shallow easterly plunges, in contrast to northerly plunges observed in the previous belt. These latter synforms are themselves distorted by north-east-trending upright F4 structures, most notably the Aggeneysberge and Gamsberg synforms (Moore,1977; Lipson,1978). Thrust faulting on a relatively minor scale is associated with the early F2 folding, and tectonic slides or shear zones with the F3 structures (Lipson,*op. cit.*; Moore,*op. cit.*).

Certain more complex structural interpretations have been made for the Aggeneysberge (Lipson,1978) and Gamsberg (Odling,1983) incorporating postulated major F1 synformal structures. In both instances these major F1 structures have been invoked to explain certain symmetry observations and cannot be convincingly demonstrated in the field. As such, they remain disputed and somewhat controversial.

4.7.4 Metamorphism

The Aggeneys-Gamsberg area contains the first metamorphic mineral parageneses that unequivocally belong to the amphibolite facies as opposed to all the previous paragneiss belts to the south which contain parageneses partially or entirely belonging to the granulite facies. The metapelitic rocks are commonly schistose (as opposed to gneissic) lithologies consisting of quartz-biotite-muscovite-sillimanite ($\pm$ garnet, $\pm$ K-feldspar) parageneses and the mafic rocks comprise plagioclase-hornblende-quartz ($\pm$ diopside) parageneses which lack hypersthene. Both these parageneses indicate that the major dehydration and/or melting reactions which typify the granulite

facies/amphibolite facies transition (see Sections 3.3 and 3.7) have not taken place in these lithologies.

Although thin quartz-K-feldspar metatects are present sporadically throughout the metapelitic schists and leucogneisses (at <5% concentration), true migmatitic rocks appear to be absent. P-T estimates in the Aggeneys-Gamsberg area vary in the range 650 - 750 ^{o}C and 3 - 6 kbars (Rozendaal,1975; Moore,1977).

4.8 The Geselskapbank paragneiss belts

As in the case of the Aggeneys-Gamsberg area, the geological aspects of this area will only be treated superficially because the Geselskapbank area is the subject of a major current study (D.Strydom, Ph.D thesis, U.O.F.S., in progress) and to avoid unneccessary duplication, no detailed mapping was undertaken during this study.

4.8.1 The supracrustal sequences

The supracrustal rocks in the Geselskapbank area crop out in at least three, possibly four, closely-spaced paragneiss belts that contain a considerable variety of different lithologies. The paragneiss belts can be subdivided into two outer belts, comprising schist-quartzite lithologies similar to those of the Smorgen Schaduwe-Kangnas and Aggeneys-Gamsberg belts, that define the periphery of the major Geselskapbank synform, and a second group of supracrustal rocks within the northern limb, along the southern boundary of the farm Heiorigas, and in the core of the structure on the farms Naab and Geselskapbank, consisting of a variety of markedly different lithologies.

Leucogneiss. Biotite-poor, K-feldspar-rich leucogneisses are not common within the various supracrustal sequences, but, when present, are generally located in the basal portions of these sequences. Sillimanite-quartz and muscovite-rich knots are commonly observed in these rocks. The muscovite-bearing varieties are restricted to the Heiorigas supracrustal sequence where they occur in association with biotite-hornblende schists.

Biotite gneiss. Quartz-rich biotite gneisses with lesser microcline, plagioclase and minor rutile and muscovite are present in the basal portions of the supracrustal sequences in the Beenbreek-Kabib area where they are interbanded with metapelitic schists and schistose quartzites. Certain bands within these gneisses contain sillimanite-quartz knots, a feature more typical of leucogneisses and not recorded in biotite gneisses in other paragneiss belts.

Biotite-hornblende gneiss and schist. Fine-grained, almost hornfelsic, quartz-plagioclase-biotite-hornblende gneisses with minor iron oxides crop out in association with metapelitic cordierite-bearing gneisses in the "core" supracrustal rocks at the western closure of the Geselskapbank synform on the

Steinkopf Reserve at Slaphaaksteenkop. The mafic mineral content of these rocks is relatively high (>25%) making it difficult to classify as either gneiss, schist or amphibolite. A similar, more schistose lithology comprising quartz, K-feldspar, biotite, plagioclase, hornblende, sphene and minor iron oxides is present in the supracrustal sequence on the southern boundary of Heiorogas. These rock types show distinct low-grade retrograde metamorphic effects with the formation of chlorite, epidote and calcite from the breakdown of biotite and hornblende.

Metapelitic quartz-biotite-muscovite-sillimanite schist. Two distinctly different metapelitic rock types are present in the Geselskapbank area. Within the two outer paragneiss belts, quartz-biotite-muscovite-sillimanite schists, similar to the metapelitic schists of the Aggeneys-Gamsberg area, are a common lithology in association with biotite gneisses and glassy quartzites. Microcline and rarer plagioclase are present in certain schists and graphite-bearing bands are common throughout the two outer belts from Heiorigas in the north to Kabib in the south. Many of these metapelitic schists, particularly those along the northern limb of the Geselskapbank synform, show varying degrees of low-grade retrogressive metamorphism with the breakdown and partial replacement of biotite by chlorite (together with distinctive fine rutile needles) being most obvious. Quartz and K-feldspar grains are also commonly cracked, crushed and/or highly strained or distorted.

Metapelitic quartz-plagioclase-biotite-sillimanite-cordierite gneiss. The second metapelitic rock type is a fine-grained, banded gneiss consisting of quartz, plagioclase, biotite, sillimanite, cordierite, minor iron oxides and occasional microcline. These gneisses crop out as the dominant paragneiss lithology in the core of the Geselskapbank synform. Sample NB-6 is less aluminous in character, lacking sillimanite and containing garnet in symplectic intergrowth with iron oxide. The metamorphic history of these rocks appears to be complex, and four different modes of sillimanite were observed in sample SKF-9 - an early, coarser grained tabular type was cross-cut by later "kinked" fibrolite; short, stubby sillimanite grains rim xenomorphic microcline; and a biotite-sillimanite intergrowth replaces cordierite. These mineral relationships indicate the presence of an early high-grade (granulite facies ?) quartz-K-feldspar-cordierite-sillimanite assemblage and a later slightly lower grade (upper amphibolite facies ?) quartz-biotite-sillimanite assemblage. Muscovite is absent from both assemblages.

Cordierite-sillimanite gneiss. Lenses of a banded cordierite-sillimanite gneiss are located within metapelitic schists of the inner schist-quartzite belt in the Steinkopf Reserve. Chalcopyrite and pyrite are present as minor constituents in this lithology which is chemically related to the cordierite-anthophyllite suite of rocks (see Chapter 10).

Quartz-muscovite schist. Coarse-grained quartz-muscovite schists directly overlie the calc-silicate-bearing quartzites in the supracrustal sequence along the southern boundary of Heiorigas. They contain occasional thin (one cm scale) tourmaline-bearing bands.

Glassy quartzite. Extremely pure quartzitic rocks similar to those of the

Smorgen Schaduwe-Kangnas and Aggeneys-Gamsberg areas are prominent members of the two outer paragneiss belts of the Geselskapbank area. In the lower portions of these sequences on the farm Beenbreek, schistose varieties of quartzite are relatively common, interbanded with biotite gneiss and metapelitic schists. More massive pure quartzites generally occur towards the top of the supracrustal sequence where they contain minor muscovite and, in the lower part, pyrite and/or graphite. Thinner, pale green quartzite bands, containing disseminated diopside and occasional massive tremolite and wollastonite-garnet lenses, are present in the supracrustal sequence along the southern Heiorigas boundary, but elsewhere within the "core" paragneisses, quartzitic rocks are apparently absent.

Amphibolite. Mafic rocks are relatively uncommon in the Geselskapbank supracrustal sequences, particularly in the two outer belts. Where present in the "core" sequences, they commonly comprise relatively fine-grained hornblende-plagioclase rocks with varying amounts of quartz and minor iron oxides. The more quartzitic varieties are generally also the more banded rocks. Biotite is present in some samples as well as epidote and sphene, the latter sometimes rimming iron oxide. Plagioclase shows varying degrees of sericitization - most obvious in sample NB-4. A massive actinolite rock (with trace amounts of rutile) occurs within the southern Heiorigas sequence, and an actinolite-plagioclase amphibolite with minor rutile and quartz crops out in the inner schist-quartzite belt in the Steinkopf Reserve. These latter two lithologies are similar to amphibolites observed in the Namiesberg portion of the Aggeneys-Gamsberg area (Moore,1977).

Calc-silicate rocks and marble. Dolomitic marbles are present as a distinctive minor unit associated with the cordierite-bearing metapelitic rocks of the "core" supracrustal sequence. They typically comprise serpentinized forsterite, tremolite and phlogopite with rare spinel and pyrite in a coarse carbonate groundmass. Lenses and thin bands of a massive tremolite rock and a quartz-wollastonite-garnet rock crop out within the quartzites on the southern Heiorigas boundary. Calc-silicate rocks are rare within the outer two schist-quartzite belts and are generally represented by hornblende-plagioclase-quartz lithologies described above.

4.8.2 Intrusive rocks

A variety of intrusive rocks is present in the area, with each paragneiss belt apparently associated with a different type of intrusive rock. The outermost schist-quartzite paragneiss belt is underlain by a distinctive megacrystic leucogranitic rock throughout the area from Heiorigas in the north to Beenbreek in the south. Although its upper contact with the supracrustal rocks appears locally transgressive and intrusive, the regional conformity displayed by this rock with the overlying lithologies suggests that it might represent a basement lithology to these rocks, or else that it had a remarkably conformable, tabular, syntectonic emplacement during isoclinal folding/thrusting related to the early F2 event. Superficially, this megacrystic leucogranite is similar to those observed intruding the base of the supracrustal sequences in the Witwater-Platbakkies and Couragiefontein

paragneiss belts.

The inner schist-quartzite belt is underlain by a highly-deformed streaky augen gneiss, similar in field character to the Achab gneiss of the Namiesberg (Moore,1977) that has been proposed as a basement lithology to the supracrustal rocks. Similar augen gneisses underlie the megacrystic granitic gneiss in the northern part of the Steinkopf Reserve. Slightly more granitic, less deformed, but otherwise similar biotite gneisses underlie and overlie the supracrustal sequence along the southern Heiorigas boundary.

The "core" supracrustal rocks are structurally overlain by coarse-grained, more mafic, granodioritic to dioritic intrusive rocks that contain large plug-like bodies of mafic intrusive rocks. Some of these mafic bodies apparently also intrude the supracrustal rocks themselves on the farm Naab.

In general, the Geselskapbank area is similar to many of the other paragneiss belts to the south (e.g. the Buffels River area, the Witwater-Platbakkies belt), being underlain by augen gneisses and, more locally, by megacrystic leucogranitic rocks, and overlain by more melanocratic intrusives (further south these are commonly charnockitic rocks) containing large bodies of mafic intrusive rocks.

4.8.3 Structure

The structure of the Geselskapbank area is dominated by a major east-west-trending, easterly-plunging F3 synform that affects all the paragneiss belts, whose configurations were initially controlled by earlier F2-age structures. The major F3 synform has an accompanying tighter antiform to the north on the farm Heiorigas.

The earlier F2-age structures, along which the three paragneiss belts are located, are, from structural top to bottom, (1) the "core" supracrustal sequence, including the lithologies along the southern boundary of Heiorigas, and associated intrusive rocks that have been thrust over (2) the innermost schist-quartzite sequence, and (3) the outermost schist-quartzite belt which represents either another thrust duplication (i.e. the inner schist-quartzite belt has been thrust southwards over the outer belt), or a tight isoclinal synform of F2-age. Paragneiss belts to the immediate south of the Geselskapbank area at Eendop and Naip (not examined in this study) are similar isoclinal F2 synforms that have been refolded by an F3 synform (Eendop) and antiform (Naip). In previous paragneiss belts to the south, the more mafic intrusive rocks are commonly thrust over the supracrustal rocks from the north, and it is possible that such a relationship exists between the "core" supracrustal rocks and the overlying granodioritic intrusive rocks.

The structural configuration of the Geselskapbank area is thus similar to previous belts to the south with F2-age thrust faulting from north to south dominating the northernmost supracrustal outcrops, and tight isoclinal F2-age folding and F3-age refolding constraining the more southerly outcrops.

4.8.4 Metamorphism

The prevailing metamorphic grade in the Geselskapbank area is amphibolite facies with hornblende-plagioclase parageneses dominating in the mafic assemblages and quartz-biotite-muscovite-sillimanite parageneses in the metapelitic rocks in an identical manner to assemblages observed in the Aggeneys-Gamsberg area. The finer-grained metapelitic rocks of the "core" paragneisses are somewhat different, containing quartz-K-feldspar-cordierite-sillimanite assemblages that lack muscovite. There is additional textural evidence in these rocks of cordierite breakdown to form biotite + sillimanite, indicating the presence of two relatively high-grade metamorphic imprints. Associated mafic rocks (both amphibolites and biotite-hornblende gneisses) lack any orthopyroxene, implying that granulite grades were not attained. Major thrust faulting as proposed above, may explain why these rocks of slightly higher metamorphic grade overlie others of lower grade. The metamorphic complexity of the "core" metapelitic rocks is discussed further in Chapters 6 and 14.

Retrograde metamorphic effects are noticeable throughout the area, most commonly along the northern limb of the major synform. Biotite breaks down to form chlorite and rutile, hornblende is replaced by chlorite, epidote and calcite, and feldspars are strongly sericitized.

Chapter 5

CORRELATION AND SUBDIVISION OF THE SUPRACRUSTAL ROCKS

5.1 General comment

An initial lithostratigraphic subdivision of the Namaqualand Metamorphic Complex has been undertaken by SACS (1980) in which the "pretectonic" rocks of the western portion of the NMC, including all the paragneiss belts examined in this study, have been divided into three groups - the Orange River Group, the Bushmanland Group and the Okiep Group. These three groups are not very rigidly defined and are described as representing "geographical domains between which correlation at the present state of knowledge is conjectural" (SACS, op.cit.).

Lithostratigraphic subdivision is based on the classification of rock units at the level of the formation which is the fundamental formal unit used to divide the entire stratigraphic column into named units. The formation can be defined as "a mappable lithologic entity characterized by a particular rock type or types" (Davis,1983). Once various formations within a rock sequence have been defined they are then successively combined into larger assemblages of formations defined as subgroups, groups and supergroups, or subdivided into smaller units such as members and beds.

The subdivision of the pretectonic rocks of the western NMC by SACS (1980), however, is not based on this fundamental classification of formations, as the Okiep Group contains no formally defined formations and the Bushmanland Group only two defined formations - one of which, the Gams Formation, is an extremely rare and localised unit. The subgroup is generally the smallest unit defined by SACS for these two groups, and whilst the three groups are described as "geographical domains", it would appear from the maps provided (Figs. 5.1.5 and 5.1.6, SACS, op. cit.) that the subgroups commonly represent geographical "subdomains" between which, presumably, correlation is also conjectural. This is particularly apparent in the Okiep Group with all the subgroups showing minimal geographical overlap.

The "geographical domains" selected for division of the pretectonic units into the three groups by SACS (1980) have resulted in confusing groupings which cut across the distinctive lithological pattern of the western NMC. The various pretectonic units of the western NMC vary systematically and uniformly from north to south, ocurring as broad east-west-striking zones that incorporate several paragneiss belts. As reported in regional reviews of the supracrustal lithologies of the western NMC (Viljoen et al.,1975; Paizes,1975; Moore,1980a), a predominantly metavolcanic association in a northern zone along the Orange River is replaced southwards by a schist/quartzite association stretching from east of Pofadder via Aggeneys and the Okiep Copper District to Komaggas and the west coast. This schist/quartzite association is replaced further south in the Buffels River region by the biotite gneiss and cordierite gneiss dominated associations of the Namaqua mountainland, with

Table 5.1 A suggested reclassification of the various subgroups wit supracrustal rocks of the western NMC.

SACS (1980) classification		Classification this study
Bushmanland Group	Hom Subgroup	"Goodhouse"
	Guadom Subgroup	
	Pella Subgroup	"Bushmanland" Group
	Aggeneys Subgroup	
Okiep Group	Eenriet Subgroup	
	Aardvark Subgroup	
	Khurisberg Subgroup	
	Garies Subgroup	"Khamiesberg" Group
	Bitterfontein Subgroup	

feldspathic quartzites becoming conspicuous in the southern Bitterfontein region. The boundaries between these broad divisions appear gradational and ill-defined, possibly indicating that they represent facies-type transitions between one another (Moore,op. cit.).

Two major problems arose when attempting to use the SACS (1980) nomenclature in this specific regional study. These involved, firstly, the separation of the schist/quartzite supracrustal sequences into two different groups - the Okiep Group and the Bushmanland Group - as opposed to their incorporation into a single group; and secondly the incorporation of a variety of very different supracrustal sequences into the Okiep Group - i.e. schist/quartzite paragneisses (Eenriet, Aardvark and Khurisberg Subgroups) in the north, biotite gneiss-dominated supracrustal rocks (Garies Subgroup) in the central Namaqua mountainland, and feldspathic quartzite/cordierite gneiss sequences (Bitterfontein Subgroup) in the south - instead of their division into separate groups. The basic differences between the SACS (op. cit.) subdivision and the one proposed in this study involve how the various subgroups should be assembled to form the various major groups. These differences are shown in Table 5.1.

Further points of difference between this study and the SACS (1980) lithostratigraphy centre around two assumptions in the latter correlation - namely that the "ubiquitous pink gneiss (is) not considered part of the pretectonic volcano-sedimentary succession" and that "the succession ... has been pieced together by ignoring the intersheeted intrusives".

All the (pink) leucogneisses in the western NMC have been included in an intrusive suite of granitic rocks, the Hoogoor Suite, by SACS (1980). This represents an acceptance of the models proposed by McCarthy (1978), Lipson and McCarthy (1977) and Lipson (1980) that the leucogneisses in the Okiep Copper District and the Aggeneys area represent highly differententiated intrusive equivalents of underlying syntectonic augen gneisses (such as the Nababeep Gneiss), and a rejection of the proposals of Kroner (1968), Moore (1977) and Jack (1980) that they instead commonly represent units of the pretectonic supracrustal sequences, probably of an arkosic origin. Arguments for the retention of major units of leucogneisses within the pretectonic supracrustal rocks, probably representing either extrusive rhyolitic rocks or their reworked equivalents are presented in Chapter 8. This has a major impact on correlations regarding the various subgroups of the Bushmanland Group and on the identification of a biotite gneiss/leucogneiss-dominated subgroup in the southern and central portions of the study area.

The device of simply removing the "intersheeted intrusives" when constructing the geological column for western NMC as applied by SACS (1980), is also questionable. As can be seen from the previous section, many major syntectonic intrusive suites overlie the pretectonic supracrustal rocks in apparent thrust contact, and therefore simple removal of the intrusive packages will merely pile thrust-duplicated supracrustal sequences on top of one another. Furthermore, portions of the intrusive rocks appear to be part of a pre-paragneiss basement sequence (Paizes,1975; Moore,1977), and their presence, interbanded within their cover sequences, must also be explained by

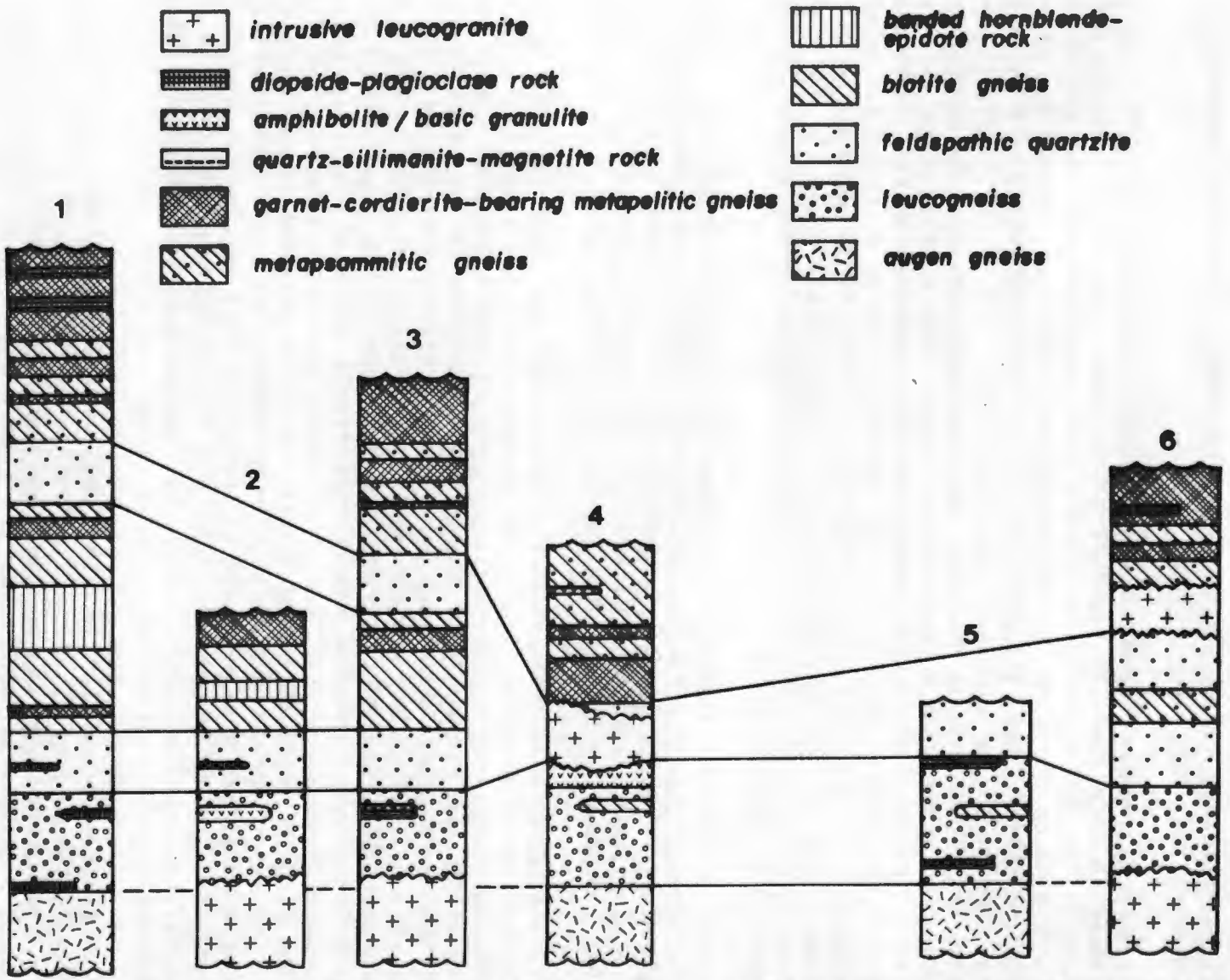

Fig. 5.1 Structural-stratigraphic sections through the supracrustal sequence in the Bitterfontein paragneiss belt. Stratigraphic columns are from Bitterfontein (1), Zout Rivier (2), Louw's Cyfer (3), Brakputs (4), Menschlief (5) and Banke-Brandewynskraal (6).

either isoclinal folding or thrust faulting. Recognition of basement augen gneisses to the supracrustal sequences is of critical importance to lithostratigraphic subdivision in the western NMC, as it will help to distinguish thin cover sequences, duplicated by thrusting or folding, from thicker sequences duplicated by cyclic sedimentation and volcanism.

It should be apparent from the above discussion that major differences exist between the philosophies and approach employed by SACS (1980) and this study. Bearing these in mind, the following represents an alternative regional correlation for the pretectonic supracrustal sequences of the western NMC.

5.2 Correlation within individual paragneiss belts

As an initial step within the correlation process, cross-sections were constructed across the various paragneiss belts at different localities and the persistence of various units within individual paragneiss belts investigated. Schematic geological columns of these cross-sections have been constructed for correlation purposes and for the definition of various formations. The columns show approximate relative thicknesses, although many minor units are exaggerated in thickness and intercalated relationships are highly simplified. As this is an informal subdivision of the supracrustal sequences into subgroups, formations and members, it was not felt appropriate to give these units specific names.

5.2.1 The Bitterfontein belt

The basal unit of the supracrustal sequence throughout the belt was represented by a leucogneiss with intercalated thin biotite gneiss bands, calc-silicate rock lenses and amphibolite/basic granulite (Fig. 5-1). The leucogneiss grades into a feldspathic quartzite which contains thin lenses of quartz-sillimanite-magnetite rock. Overlying the feldspathic quartzite in the southern parts of the area (notably at Bitterfontein, Zout Rivier and Louws Cyfer) is a biotite gneiss/schist unit which contains a prominent central band of hornblende-epidote rock and interbanded minor metapelitic cordierite gneiss. This unit is overlain by another feldspathic quartzite at Bitterfontein, Louws Cyfer and Brandewynskraal. Both these latter two units (biotite gneiss and quartzite) appear to be absent from the northern Bitterputs section. Overlying the feldspathic quartzites at Bitterfontein, Louws Cyfer, Bitterputs and Brandewynskraal is a sequence of interbanded metapsammitic and metapelitic cordierite-garnet gneisses with local thin intercalated calc-silicate bands. This represents the top of the supracrustal sequence preserved within the belt.

Although the base of the sequence is disrupted by late syntectonic granitic rocks in many places, the supracrustal rocks are underlain by a streaky pretectonic-to-early-syntectonic augen gneiss at Bitterfontein, Bitterputs and Menschlief.

The supracrustal rocks of the Bitterfontein belt can be subdivided into

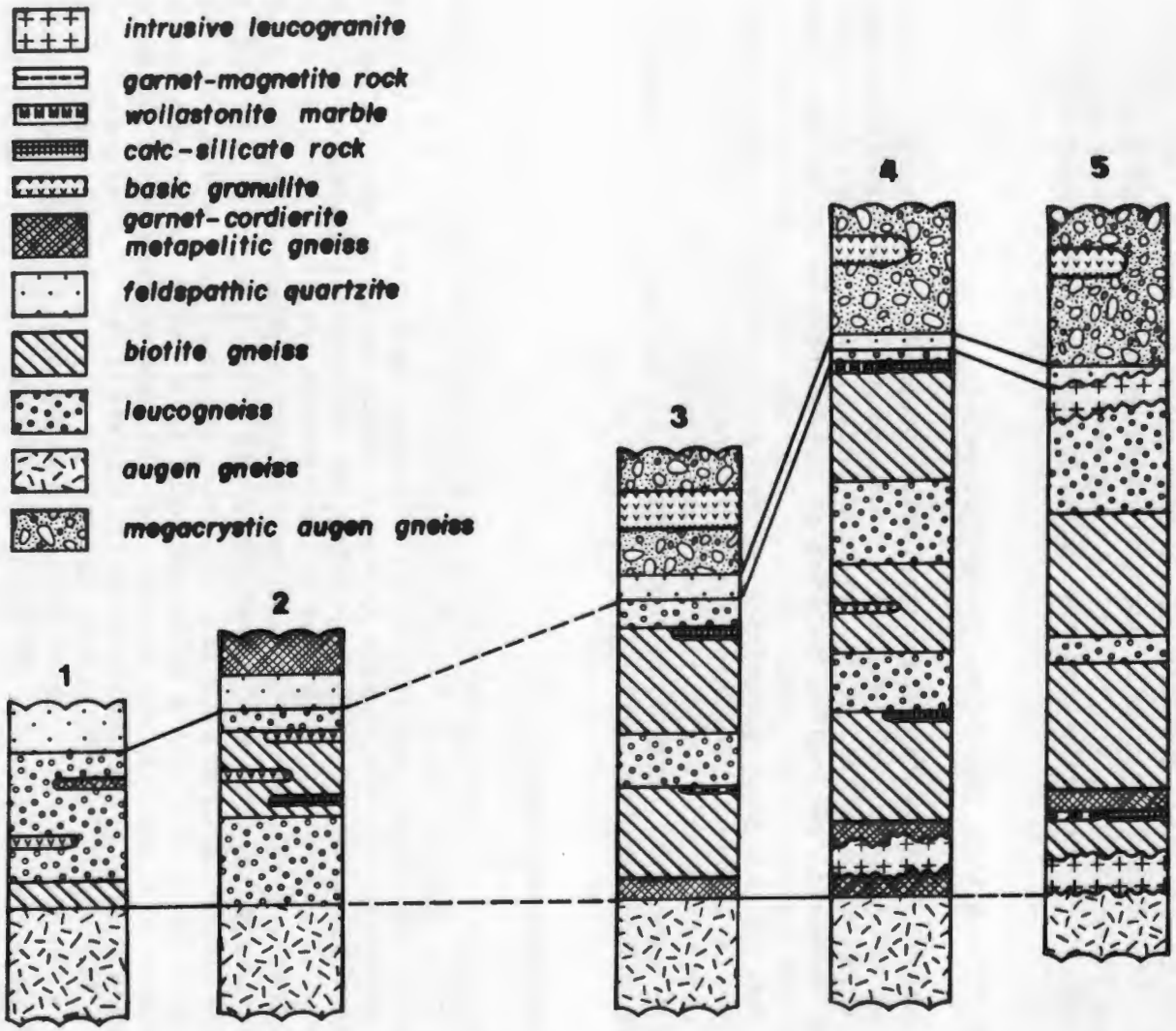

Fig. 5.2 Structural-stratigraphic sections through the supracrustal sequence in the Witwater-Platbakkies paragneiss belt. Stratigraphic columns are from Hardekraal (1), Keurbos (2), Kougoedvlakte (3), Paulshoek (4) and Witwater (5).

five distinct formations and one prominent member:

1. basal leucogneiss

2. lower feldspathic quartzite

3. biotite schist/gneiss

3a. hornblende-epidote rock

4. upper feldspathic quartzite

5. garnet-cordierite metapelitic and metapsammitic gneisses.

5.2.2 The Witwater-Platbakkies belt

Two distinct areas were examined in this belt - the Keurbos-Hardekraal sector in the south and the Witwater-Paulshoek-Kougoedvlakte sector in the north. In both areas, the basal unit consisted of interbanded leucogneisses and biotite gneisses with minor intercalations of amphibolite/basic granulite, garnet-cordierite gneiss and calc-silicate rock (together with iron formation and wollastonite-bearing marble in the north) (Fig. 5-2). In the Witwater-Paulshoek-Kougoedvlakte sector, however, this basal unit was considerably thicker with a greater biotite gneiss component, and cordierite-garnet gneiss was present as the lowermost member. A distinctive leucogneiss with prominent sillimanite-quartz lenses appears in the centre of the Paulshoek section together with garnet-plagioclase calc-silicate lenses. These members are important in establishing correlations with paragneiss belts to the north. The topmost member of this basal unit is invariably a leucogneiss which grades into an overlying feldspathic quartzite, similar to that of the Bitterfontein belt but considerably thinner. The quartzite appears to be thinner too, in the northern sections compared to the southern Keurbos-Hardekraal sector. In the Keurbos section in the south, the feldspathic quartzite is overlain by a sequence of cordierite-garnet gneisses that represent the topmost unit observed in the Witwater-Platbakkies paragneiss belt.

The supracrustal rocks are underlain throughout the area by pretectonic-to-early-syntectonic augen gneisses, and overlain in the northern sector by megacrystic syntectonic augen gneisses containing large basic granulite masses.

The supracrustal rocks of the Witwater-Platbakkies belt can be divided into three distinct formations:

1. basal leucogneiss/biotite gneiss

2. feldspathic quartzite

3. garnet-cordierite gneiss (local in the south).

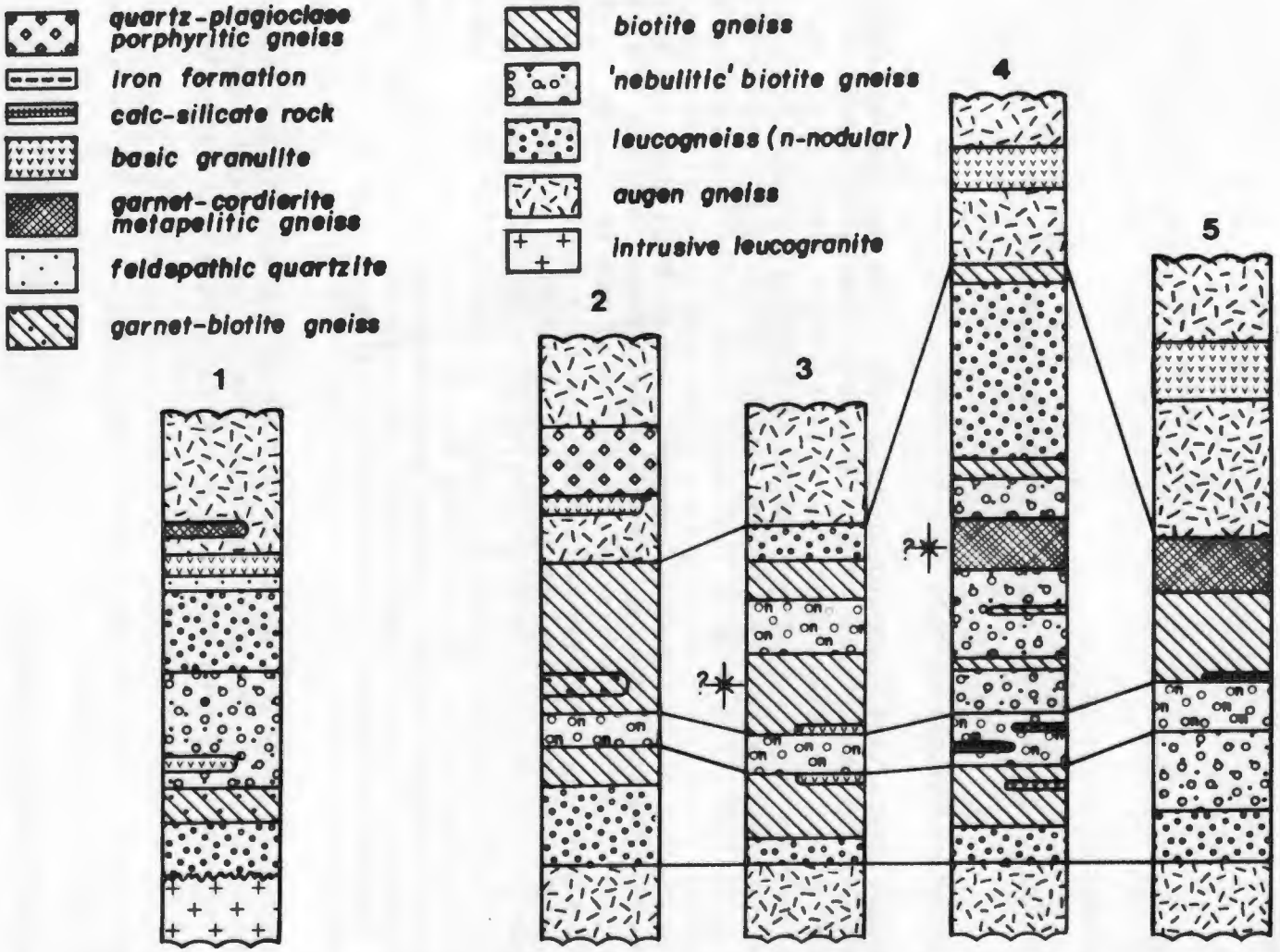

Fig. 5.3 Structural-stratigraphic sections through the supracrustal sequence in the Anegas-Boesmanplaat paragneiss belt. Stratigraphic columns are from Couragiefontein (1), Anegas (2), Pedros Kloof (3), Hosabees (4) and Boesmanplaat (5).

5.2.3 The Anegas-Boesmanplaat belt

Cross-sections of this paragneiss belt are complicated by possible duplication due to isoclinal folding, particularly in the Pedros Kloof and Hosabees sections. The supracrustal rocks are dominated by a thick sequence of biotite gneisses and leucogneisses that overlie an augen gneiss "basement", similar to the previous belt (Fig. 5-3). The unit includes a characteristic leucogneiss member containing sillimanite-quartz knots as well as minor basic granulite, garnet-biotite gneisses, garnet-rich calc-silicate lenses and, more rarely, iron formation. Another characteristic quartzo-feldspathic member of this unit is the "nebulitic" gneiss - a white-weathering biotite-poor gneiss (termed leptynite by Joubert,1971) with distinctive wavy banding. No quartzitic rocks were observed in this paragneiss belt, but in the western portions of the belt (as seen in the Hosabees and Dounabees sections), the topmost unit of the sequence is represented by metapelitic cordierite-garnet gneisses. Similar augen gneisses to those that underlie the paragneiss belt also overlie the sequence, commonly containing large bodies of basic granulite and, on Anegas, a thick porphyritic quartz-plagioclase gneiss body.

To the south of the Anegas-Boesmanplaat paragneiss belt, on the farm Couragiefontein, a similar sequence of supracrustal rocks is exposed within a domal structure. Here leucogneisses, "nebulitic" biotite gneisses with lesser bands of garnet-biotite gneiss and basic granulite make up the major basal unit whose lowermost members are obscured by a syntectonic granitic gneiss in the central portion of the dome. Overlying this basal unit is a very thin feldspathic quartzite (only a metre or two thick), amphibolites, and remnants of cordierite-garnet gneisses within an upper augen gneiss mass. This represents the northernmost outcrop observed of the feldspathic quartzite unit.

Within the Anegas-Boesmanplaat belt, therefore, only two distinctive formations can be recognised:

1. a thick lower biotite gneiss/leucogneiss assemblage

2. a thinner upper garnet-cordierite gneiss.

5.2.4 The Stofkraal-Dikmatje belt

Cross-sections of this belt contain several previously unrecorded lithologies and formations. The basal unit of the supracrustal sequence, however, is similar to those of the previous belts, being dominated by quartzo-feldspathic gneisses, although in this case leucogneisses predominate over biotite gneisses in contrast to the preceding belt (Fig. 5-4). Minor thin bands within this unit include basic granulites and garnet-biotite gneisses. A prominent, relatively thin metacarbonate member is present near the top of the unit, comprising forsterite marble lenses, massive diopside rocks and banded diopside-plagioclase calc-silicate rocks. In the Kammassies cross-section, two augen gneiss bands occur within the unit, representing either syntectonic

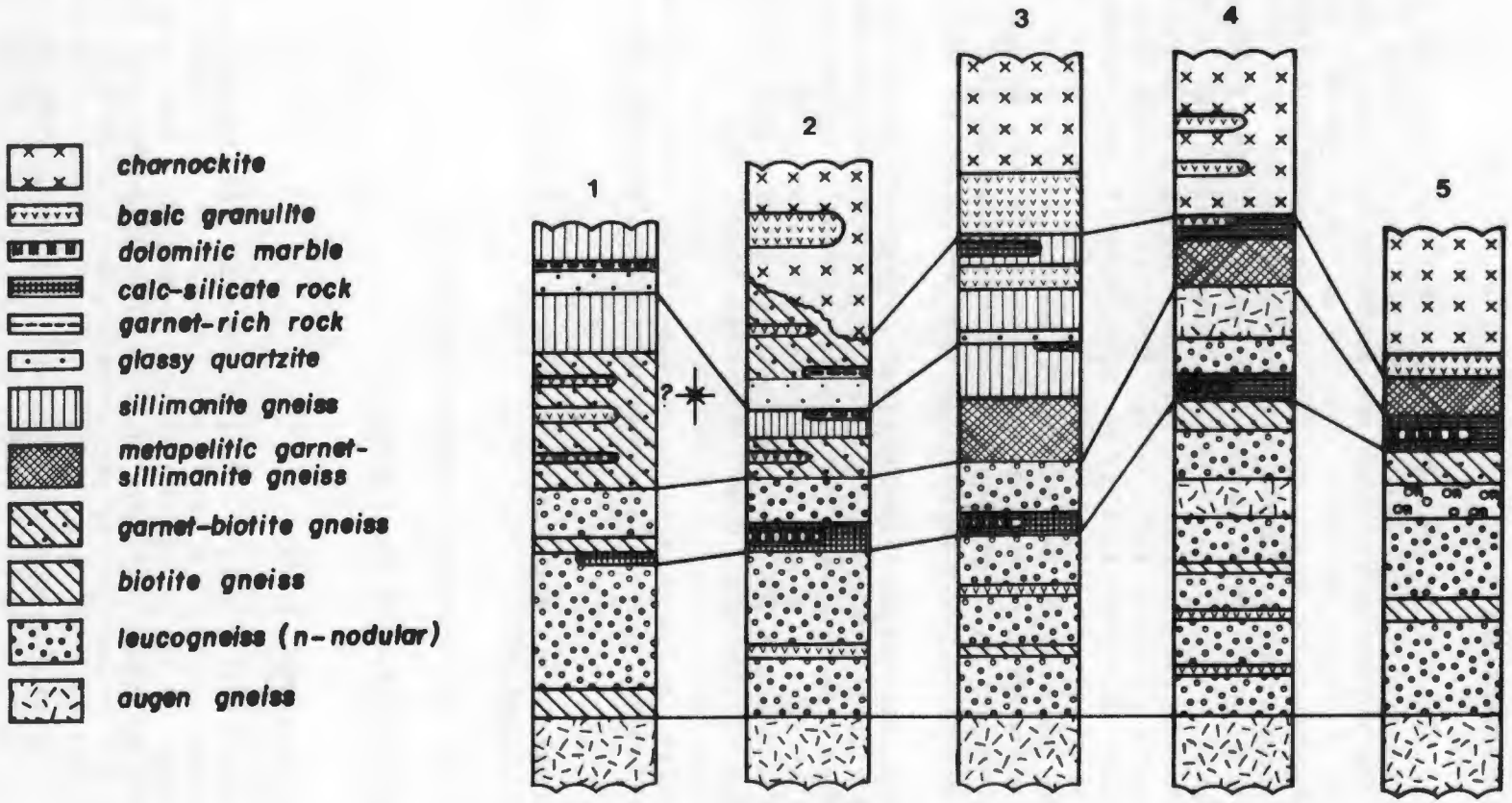

Fig. 5.4 Structural-stratigraphic sections through the supracrustal sequence in the Stofkraal-Dikmatje paragneiss belt. Stratigraphic columns are from Tweefontein-Hytkoras boundary (1), Tweefontein (2), Stofkraal (3), Kammassies (4) and Dikmatje (5).

intrusive rocks or thrust slices of a basement gneiss. Similar augen gneisses underlie the supracrustal sequence across the entire belt.

Overlying the basal quartzo-feldspathic unit are a variety of metapelitic and metapsammitic garnet-cordierite and garnet-biotite gneisses containing many minor basic granulite lenses and bands. These are succeeded in the western sections (at Stofkraal and Tweefontein) by further sillimanite-dominated metapelitic gneisses with associated glassy quartzites and thin iron formation lenses. This latter suite of sillimanite gneisses/schists, quartzites and iron formations is very thin in the Stofkraal-Dikmatje belt (seldom >50 metres) but becomes thicker and more dominant in the paragneiss belts further north. The iron formations and sillimanite gneisses both underlie and overlie the glassy quartzite unit, possibly as the result of isoclinal folding. Basic granulite and calc-silicate rock lenses are present locally within the sillimanite gneisses. The supracrustal sequence is transgressively overlain by syntectonic charnockitic rocks containing both large and small bodies or xenoliths of basic granulite.

At least four distinctive formations and one prominent minor member can be discriminated in the Stofkraal-Dikmatje belt:

1. basal leucogneiss-dominated assemblage

1a. forsterite marble/diopside calc-silicate rock member

2. garnet-cordierite and garnet-biotite gneisses

3. sillimanite gneiss

4. glassy quartzite.

5.2.5 The Buffels River belt

The cross-sections in the Buffels River belt are perhaps the most complex and difficult to construct due to several causes - namely isoclinal folding, regional southerly dips requiring certain sections to be constructed from south-to-north and others north-to-south, and disruption by syntectonic leucogranitic rocks, augen gneisses and charnockites (Fig. 5.5).

The basal units of the supracrustal sequence in the belt are again similar to the previous belts, being dominated by quartzo-feldspathic gneisses - more specifically by leucogneisses in the lower portions and biotite gneisses (in the east) or migmatitic garnet-biotite gneisses (in the west) in the upper portions. Minor basic granulite bands are widespread, and a distinctive member containing cordierite-hypersthene-phlogopite gneisses occurs at the top of the unit in most cross-sections. The forsterite marble/calc-silicate rock member from the previous Stofkraal-Dikmatje belt is also present in the Velskoen and Hytkoras sections at a similar (slightly higher) stratigraphic position to the magnesium-rich cordierite gneisses, immediately underlying the metapelitic rocks.

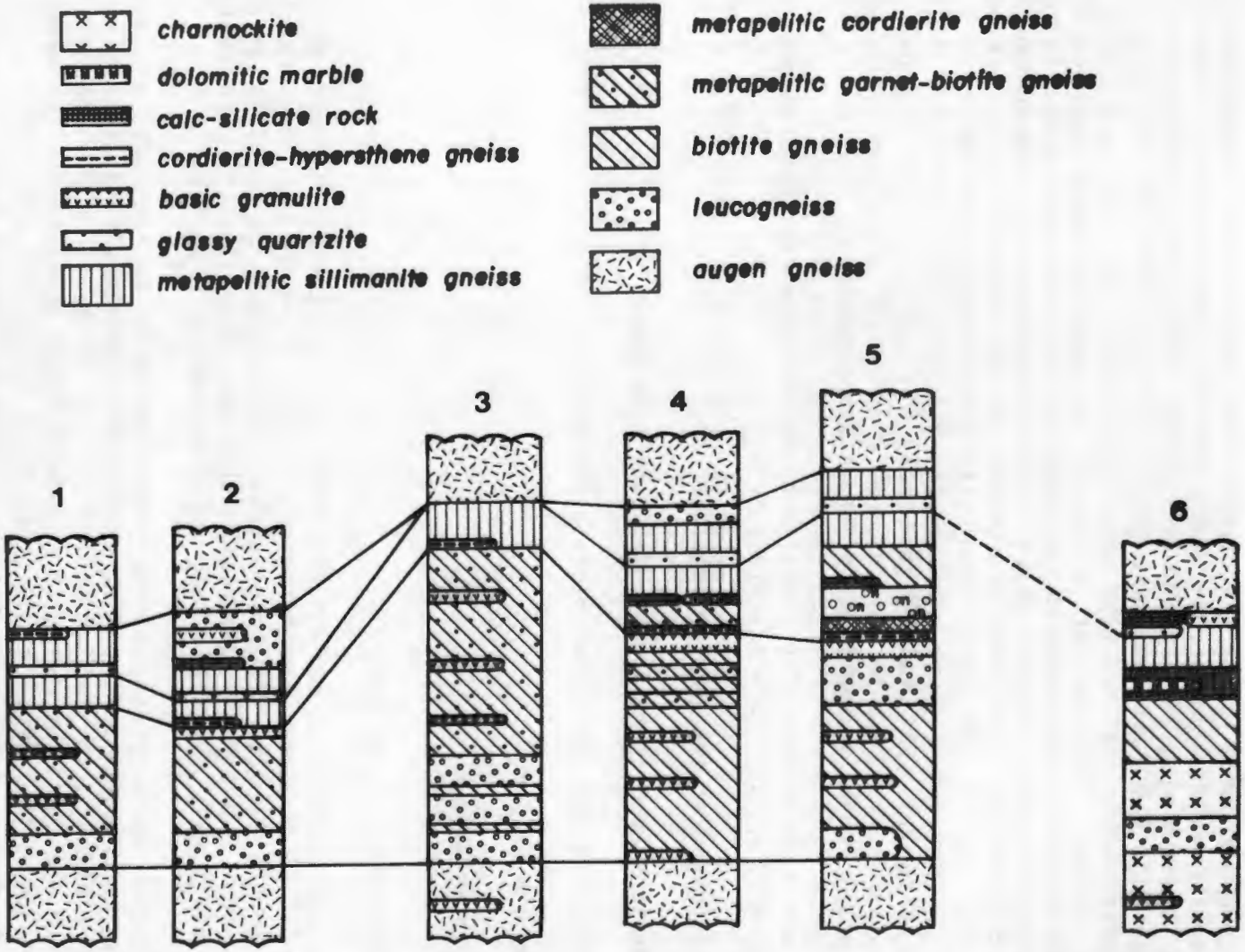

Fig. 5.5 Structural-stratigraphic sections through the supracrustal sequence in the Buffels River paragneiss belt. Stratigraphic columns are from Nuwedam (1) and (2), Nuwedam-Hytkoras boundary (3), Hytkoras (4), Hytkoras-Dabeeb boundary (5) and Velskoen (6).

Thin remnants of the cordierite-garnet gneisses are present in the Hytkoras sections. The overlying metapelitic rocks, however, are now chiefly sillimanite-dominated metapelitic gneisses which occur in association with a thin glassy quartzite unit that persists across the entire belt from west to east. As in the previous belt, sillimanite gneiss duplication about the glassy quartzite unit may be due to isoclinal folding.

The supracrustal sequence is both overlain and underlain by large bodies of relatively inclusion-free augen gneiss (i.e. only a few thin basic granulite lenses are present). In the eastern Velskoen area, charnockitic rocks syntectonically intrude the basal portions of the sequence.

The supracrustal sequence in the Buffels River belt can be subdivided into three distinctive formations and two minor members:

1. basal leucogneiss/(garnet-) biotite gneiss assemblage

1a. cordierite-hypersthene-phlogopite gneiss member

1b. forsterite marble/diopside calc-silicate rock member

2. sillimanite gneiss

3. glassy quartzite.

5.2.6 The Silverfontein-Rietfontein belt

This paragneiss belt contains one of the least complete geological sections within a tightly refolded synformal structure. The sequence is almost entirely made up of quartzo-feldspathic gneisses, predominantly biotite gneisses with minor leucogneiss bands (Fig. 5.6). A rare corundum-bearing gneiss crops out at the base of the section on Rietfontein, and minor calc-silicate bands (both diopside-plagioclase and garnet-plagioclase rocks) and mafic bands (basic granulite and amphibolite) are present. This sequence is again similar to many of the basal units observed in the other paragneiss belts to the south and is both underlain and overlain by augen gneisses. No metapelitic or quartzitic rocks, which generally form the upper units of the supracrustal sequences, were observed in this belt, although small remnants of these paragneiss units are present on the farms Kourkamma and Brakdam to the east of the belt.

The Silverfontein-Rietfontein belt thus comprises a single distinctive supracrustal formation:

1. biotite gneiss/leucogneiss assemblage.

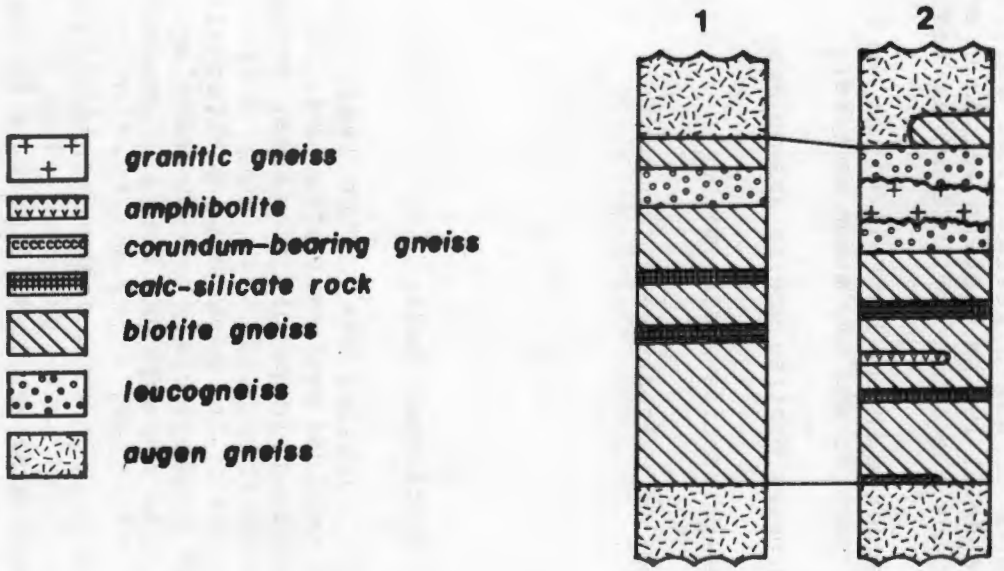

Fig. 5.6 Structural-stratigraphic sections through the supracrustal sequence in the Silverfontein-Rietfontein paragneiss belt. Stratigraphic columns are from Silverfontein (1) and Rietfontein (2).

.2.7 The Smorgen Schaduwe-Kangnas belt

The supracrustal sequence in this belt is markedly different to those further south, with the major basal quartzo-feldspathic unit virtually absent (only represented by thin lenses of leucogneiss in the Vioolskraalberg outlier) (Fig. 5.7). Metapelitic schist/quartzite upper units now form the dominant component to the sequence. The major basal unit is a metapelitic schist, commonly quartz-K-feldspar-sillimanite-garnet with biotite and cordierite, in places similar to the sillimanite gneiss of the Stofkraal-Dikmatje and Buffels River belts. This unit contains lenses of calc-silicate rocks near the basal contact with the augen gneisses, as well as cordierite-hypersthene gneisses at Vioolskraalberg and on the northern side of the Kangnas mountains. A garnet-rich iron formation also occurs within the upper portions of the unit at Vioolskraalberg.

The basal schist unit is overlain by a prominent white glassy quartzite unit which contains bands and disseminations of tourmaline at Vioolskraalberg and Smorgen Schaduwe. The upper portions of this unit are commonly dark grey in colour, containing disseminated iron oxides (hematite), and a distinctive garnet-bearing iron formation is present as the topmost member in the major belt. Bands of gahnite-garnet-bearing quartzite occur as the lowermost part of this unit on the Oranjefontein portion of Vioolskraalberg.

Overlying the white quartzite is a relatively thin quartz-biotite-sillimanite schist unit which separates the two major quartzite units and is persistent throughout the belt. The uppermost unit in the belt is a red-weathering glassy quartzite with regular thin (<1 metre) intercalations of similar quartz-biotite-sillimanite schist.

The supracrustal sequence is underlain by augen gneisses throughout the belt. These augen gneisses contain lenses of a leucogranitic gneiss at Smorgen Schaduwe, but otherwise syntectonic intrusive rocks were absent from the belt.

The Smorgen Schaduwe-Kangnas paragneiss belt contains four distinctive formations, one prominent member, and remnants of an additional basal formation:

1. leucogneiss (very minor at Vioolskraalberg)

2. quartz-K-feldspar-sillimanite-garnet schist

3. white glassy quartzite

3a. garnet-bearing iron formation

4. quartz-biotite-sillimanite schist

5. brown glassy quartzite with schist bands.

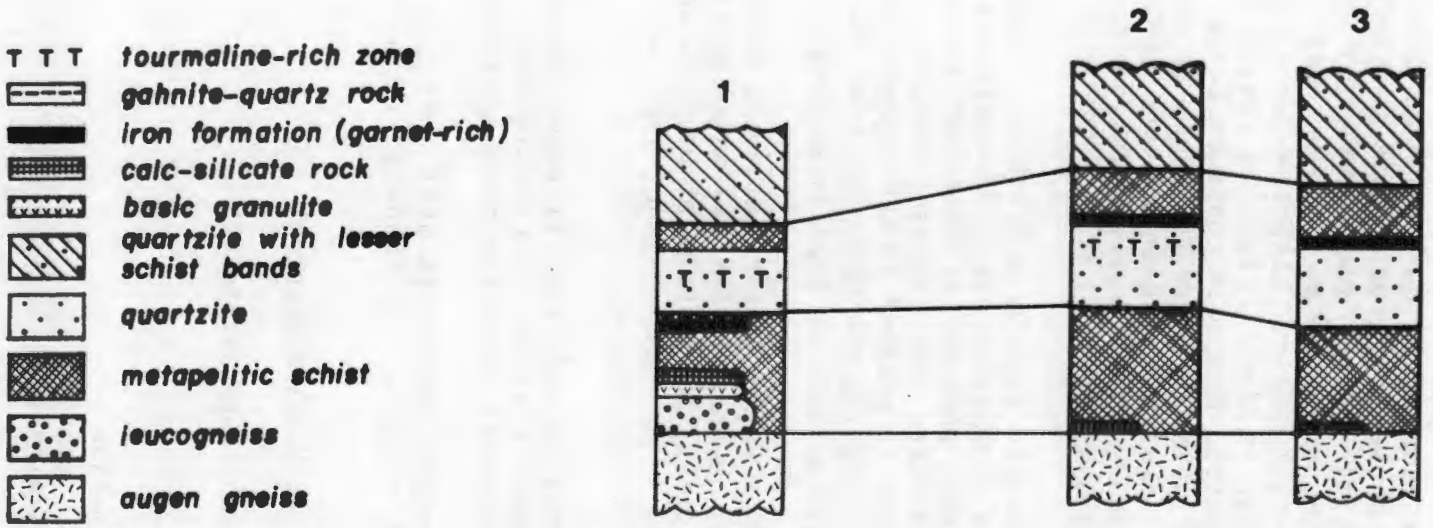

Fig. 5.7 Structural-stratigraphic sections through the supracrustal sequence in the Smorgen Schaduwe-Kangnas paragneiss belt. Stratigraphic columns are from Vioolskraalberg (Oranjefontein) (1), Smorgen Schaduwe (2) and Kangnas (3).

5.2.8 The Aggeneys-Gamsberg-Namiesberg area

The supracrustal sequence in this area bears certain similarities to that of the previous belt. The lower portions of this sequence could be regarded as representing an expanded, thicker version of the Smorgen Schaduwe-Kangnas sequence. The following represents a summary of stratigraphies presented by Lipson (1978) for the western Aggeneysberge, Rozendaal (1975) for Gamsberg and Moore (1977) for the Namiesberg range (Fig. 5.8).

Throughout the area, augen gneisses, regarded as representing a basement complex in the Namiesberg area (Moore,1977) underlie the supracrustal sequence which has as its basal unit a thick uniform leucogneiss formation. The leucogneiss is succeeded by metapelitic quartz-biotite-muscovite-sillimanite schists, termed the Namies Schist Formation (SACS,1980), that are feldspathic in the basal portions, becoming increasingly siliceous towards the top. Distinctive minor units within the schist include a variety of sillimanite-rich lithologies (Frick and Coetzee,1974; Moore,op. cit.), banded diopside-hornblende calc-silicate rocks and thin amphibolite bands.

The metapelitic schists are overlain by a prominent, thick, white quartzite with rare thin intercalated schist bands. The uppermost portions of this unit are represented by darker ferruginous quartzites at Gamsberg (Rozendaal,1975) and in the northern Aggeneysberge (Lipson,1978) in a similar manner to the Smorgen Schaduwe-Kangnas belt. The quartzite unit is succeeded by a variety of iron formations and calc-silicate/metacarbonate rocks of highly variable mineralogy together with intercalated metapelitic schist bands. Sulphide-rich and baritic members are also present and this iron-rich unit has been termed the Gams Formation (SACS,1980).

In the western Aggeneysberge (Lipson,1978), the iron formation unit is overlain by a varied succession of quartz-muscovite-sillimanite schists, schistose quartzites and quartzites containing, in places, pyrrhotite, pyrite and sphalerite. Likewise at Gamsberg (Rozendaal,1975), the iron formations are succeeded by quartz-muscovite schists with interbedded quartzitic rocks.

Up to this point, the sequence is similar to that observed in the Smorgen Schaduwe-Kangnas belt, with most of the units being somewhat thicker and perhaps deposited in slightly deeper water conditions, indicated by the appearance of carbonate and sulphidic rocks. At Gamsberg and in the eastern portions of the Aggeneysberge, quartz-pebble metaconglomerates and diamictites, followed by amphibolites and amphibole gneisses with intercalated pebble bands and siliceous calc-silicate rocks, make up the topmost units of the supracrustal sequence (Rozendaal,1975). In the Namiesberge to the east (Moore,1977), the sequence terminates at the white quartzite unit.

The supracrustal sequence in the Aggeneys-Gamsberg-Namiesberg area can be subdivided into at least seven formations in the following manner:

1. basal leucogneiss (Hoogoor Suite - SACS,1980)

2. quartz-biotite-muscovite-sillimanite schist (Namies Schist

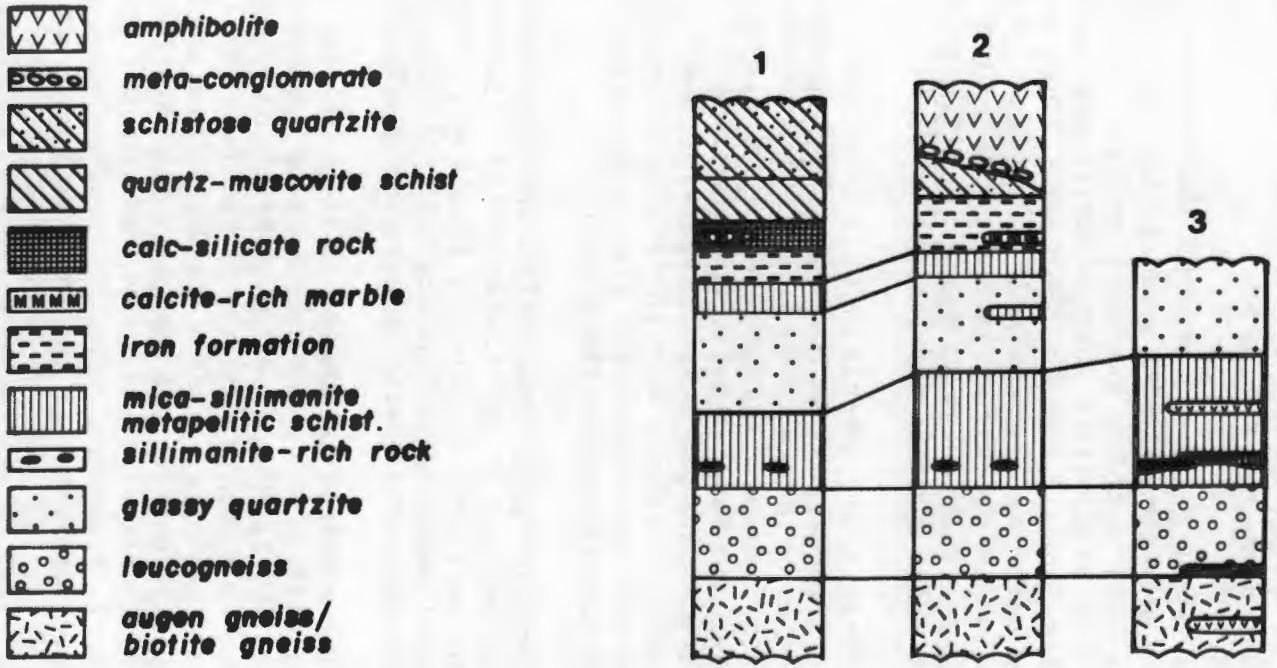

Fig. 5.8 Structural-stratigraphic sections through the supracrustal sequence in the Aggeneys-Gamsberg area. Stratigraphic columns are from the Aggeneysberge (1) (after Lipson, 1979), Gamsberg (2) (after Rozendaal, 1975) and Namiesberg (3) (after Moore, 1977).

Formation - SACS, 1980)

3. white quartzite

4. iron formation (Gams Formation - SACS,1980)

5. quartz-muscovite schist and quartzite

6. quartz-pebble metaconglomerate and diamictite

7. amphibolite and amphibole gneiss.

The precise stratigraphic position of the Broken Hill iron formations and base metal sulphide deposits to the south of the Aggeneysberge is uncertain. Lipson (1978) and Ryan et al. (1982) maintain that the iron formations are the equivalents of the Gams Formation and stratigraphically overlie the white quartzite unit although they structurally underlie this quartzite in outcrop. This would make the quartz-biotite-muscovite-sillimanite schists that structurally underlie the iron formations at Broken Hill, the equivalents of the quartz-muscovite schists and quartzites that overlie the Gams Formation in the Aggeneysberge and at Gamsberg.

Data from boreholes intersecting the footwall rocks of the Broken Hill deposit indicate that a leucogneiss/biotite gneiss (which is not exposed at surface due to extensive sand cover) underlies these metapelitic schists (Black Mountain mine personnel, pers.comm.). Samples of metapelitic schist from these boreholes examined in this study (the BH156 series) indicate an increasingly feldspathic character to the metapelitic schists, both petrographically and geochemically, with increasing depth. These features are more in keeping with the typical basal gneiss/schist units of the supracrustal sequences in the area than with the siliceous, muscovite-rich lithologies that overlie the Gams Formation, and it is felt that the Broken Hill iron formations are the right way up in outcrop. They probably represent localised iron formation units that stratigraphically underlie the white quartzite, and are not, therefore, equivalents of the Gams Formation. The Broken Hill iron formations would have a similar stratigraphic position to the garnet-rich iron formation lenses and gahnite-galena-quartz rocks at Vioolskraalberg in the Smorgen Schaduwe-Kangnas paragneiss belt.

5.2.9 The Geselskapbank area

As mentioned in Section 4-8, the Geselskapbank area is the subject of a major current study which includes a detailed stratigraphic subdivision of the various supracrustal lithologies (D. Strydom, in prep.). No detailed stratigraphic examination of the area was thus undertaken in this study, and the following represents a generalised summary of the supracrustal sequences for comparative purposes with the preceding supracrustal assemblages.

The stratigraphy of the supracrustal rocks in the Geselskapbank area is complicated because the area consists of several closely-spaced, parallel

paragneiss belts - probably major early thrust slices or isoclinal folds (F2, Joubert,1971) - whose lithologies vary considerably from one belt to the next. The two outermost paragneiss belts that enclose and define the major Geselskapbank synform, contain an alternating basal unit of biotite gneisses, leucogneisses with muscovite-sillimanite knots, quartz-muscovite-biotite-sillimanite schists and quartzites. The outermost belt overlies a coarse-grained to megacrystic leucogranitic gneiss across the entire area and the inner belt is underlain by a streaky augen gneiss. The basal unit is well exposed at Groot Nooisabesberg in the east, where it can be seen to comprise three gneiss-schist-quartzite cycles with the more gneissic rocks tending to dominate the succession.

The varied basal unit is overlain by a metapelitic quartz-muscovite-biotite-sillimanite schist followed by a prominent white glassy quartzite that is commonly pyritic in the basal portions. These two lithologies are similar to the schist-white quartzite associations observed in the previous two areas. From the farm Naab westwards, the basal unit becomes less dominant, and the metapelitic schists, and to a lesser extent some of the quartzitic rocks, contain distinctive graphite-rich zones. Minor amphibolites, banded calc-silicate rocks and iron formations are present in these two outer paragneiss belts.

A supracrustal sequence comprising several markedly different lithologies to those of the outer paragneiss belts is observed within the northern limb of the Geselskapbank synform along the boundary between the farms Heiorigas and Naab. A cross-section through the central part of this belt revealed a sequence comprising basal leucogneisses (with muscovite-sillimanite knots) interbanded with biotite-hornblende schists, a central green-coloured quartzite with minor diopside-, tremolite- and wollastonite-rich bands, and an upper unit of muscovite-quartz schists with sporadic tourmaline-rich bands, actinolite/hornblende calc-silicate rocks and rare marbles. The sequence is underlain by a granitic biotite gneiss. The biotite-hornblende and muscovite-quartz schists are similar in appearance to lithologies belonging to the Guadom and Hom Subgroups of the Bushmanland Group (SACS,1980) whose major areas of outcrop are to the north and north-east of the Geselskapbank area, chiefly along the Orange River.

Within the central and southern portions of the major synform, a somewhat different supracrustal sequence is present, dominated by quartz-K-feldspar-cordierite-sillimanite-biotite gneisses with interbanded amphibolites, biotite-hornblende gneisses and dolomitic marble bands. This sequence structurally overlies the gneiss-schist-quartzite supracrustal rocks at the western end of the major synform in the Steinkopf Reserve, and surrounds or mantles a megacrystic dioritic/granitic body on the farms Naab and Geselskapbank.

These two latter sequences are distinctly different to those observed in the peripheral belts of the Geselskapbank structure and also those to the south, east and west. This may indicate that a major lithological or early structural (F2,Joubert,1971) boundary exists within the Geselskapbank synform. Whilst the northern sequence can be tentatively correlated with lithologies to

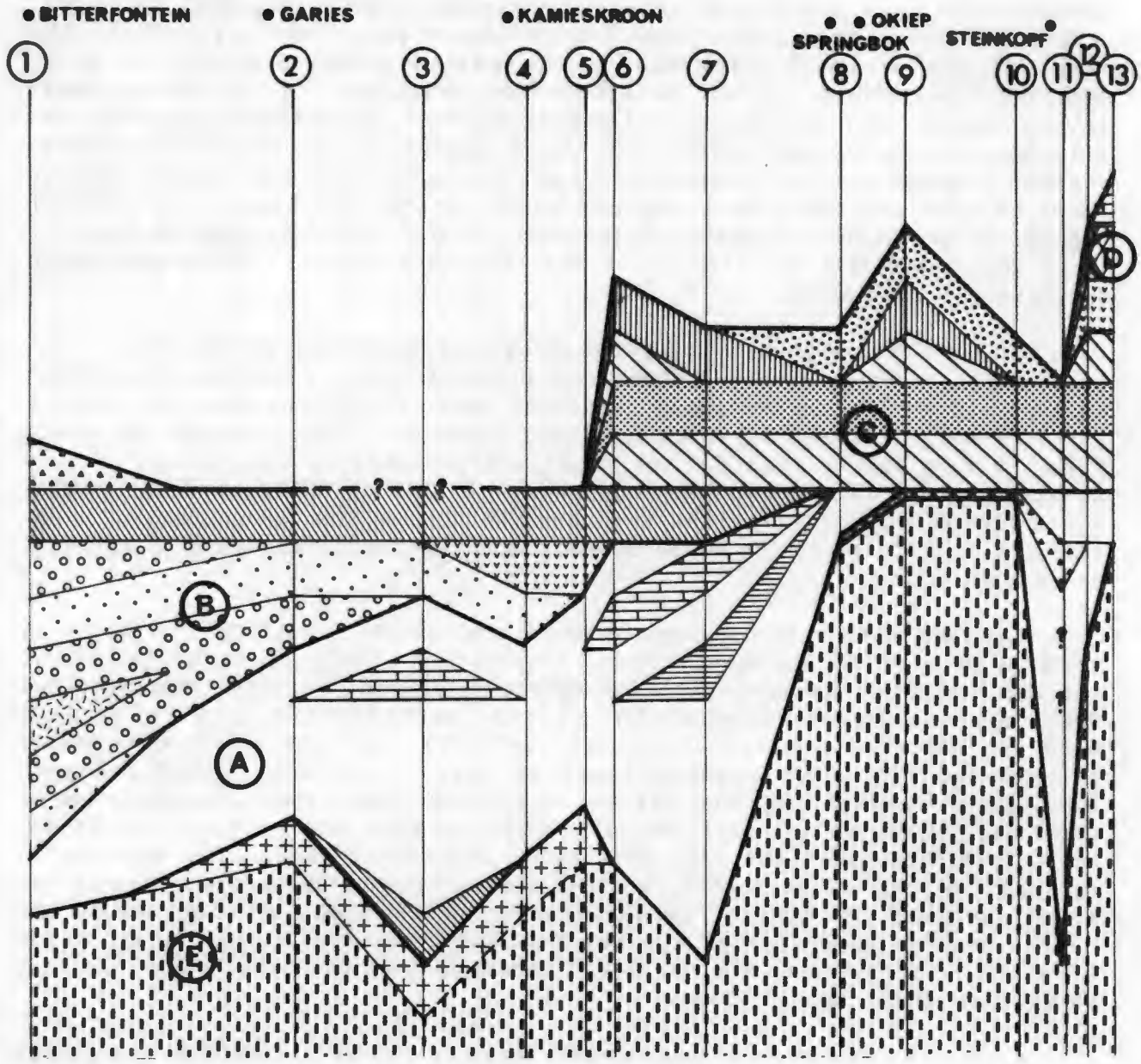

Fig. 5.9 Schematic cross-section through the supracrustal sequences of the western NMC, showing the observed variation between the different paragneiss belts. Potential subgroups are delineated by heavy lining and are: (A) a quartzo-feldspathic gneiss subgroup; (B) a feldspathic quartzite/garnet-cordierite-sillimanite gneiss subgroup; (C) a glassy quartzite/mica-sillimanite schist subgroup; (D) a cordierite gneiss/metacarbonate subgroup; and (E) an augen-gneiss-dominated basement complex. The various section lines represent Bitterfontein (1), Keurbos (2), Witwater-Platbakkies (3), Couragiefontein (4), Anegas-Boesmanplaat (5), Stofkraal-Dikmatje (6), Buffels River (7), Oranjefontein (8), Smorgen Schaduwe-Kangas (9), Naip (10), Beenbreek (11), Geselskapbank (Steinkopf Reserve) (12) and Geselskapbank (Naab) (13). For geological column see overleaf.

the north and north-east, the metapelite-dominated group bears little resemblance to other supracrustal sequences in the immediate vicinity and may be regarded at this stage as an "exotic block". Speculations as to its stratigraphic position will be discussed subsequent to the sections on geochemistry (Chapter 14).

5.3 Correlations between the various paragneiss belts.

It can be seen from the previous section that certain formations that have been identified within individual paragneiss belts, are also commonly repeated in adjacent belts, making correlation between the various belts possible. This repetition even occurs at the level of thin, distinctive members such as the cordierite-hypersthene-phlogopite gneisses and dolomitic marble bands, indicating that the relative tectonic displacement along the thrust faults that separate the various paragneiss belts is not necessarily very extensive.

The cross-section displayed in Fig. 5-9 represents a simplified, schematic breakdown of the various formations and members across the entire Namaqua mountainland from Bitterfontein in the south to Geselskapbank in the north with gross vertical exaggeration. The following discussion refers almost exclusively to this diagram.

Firstly it is apparent that across the entire area, the supracrustal sequences are underlain by prominent masses of augen gneisses of various types - some very streaky and almost banded, and others more granitic in texture. In certain belts such as the Witwater-Platbakkies belt, the Couragiefontein dome and the Geselskapbank area, fairly coarse-grained leucogranitic gneisses are also present at the base of the supracrustal rocks, sometimes with fairly obvious intrusive relationships.

Above this "floor" of granitic/granodioritic rocks, the lowermost portions of the supracrustal sequences are invariably made up of banded and interbanded leucogneisses and biotite gneisses. These units vary in proportion from belt to belt, and it is not possible to correlate individual gneissic bands across the area. Certain minor distinctive members such as marble bands, cordierite-hypersthene-phlogopite gneisses and leucogneiss bands with sillimanite nodules could, however, be correlated across belts. These basal gneisses are most prominently developed in the central Namaqualand paragneiss belts from Witwater-Platbakkies to Silverfontein-Rietfontein. Between the latter belt and the Smorgen Schaduwe-Kangnas belt to the north, this basal assemblage thins dramatically and suddenly, and in succeeding paragneiss belts to the north is almost entirely represented by leucogneisses. In the southern Bitterfontein belt, leucogneisses likewise predominate as the basal supracrustal unit. In a formal lithostratigraphic subdivision of the study area, the basal leucogneisses and biotite gneisses would conveniently form a natural subgroup (A in Fig. 5-9).

Overlying the leucogneiss/biotite gneiss units in the southern portions of the study area are feldspathic quartzites that have gradational contacts

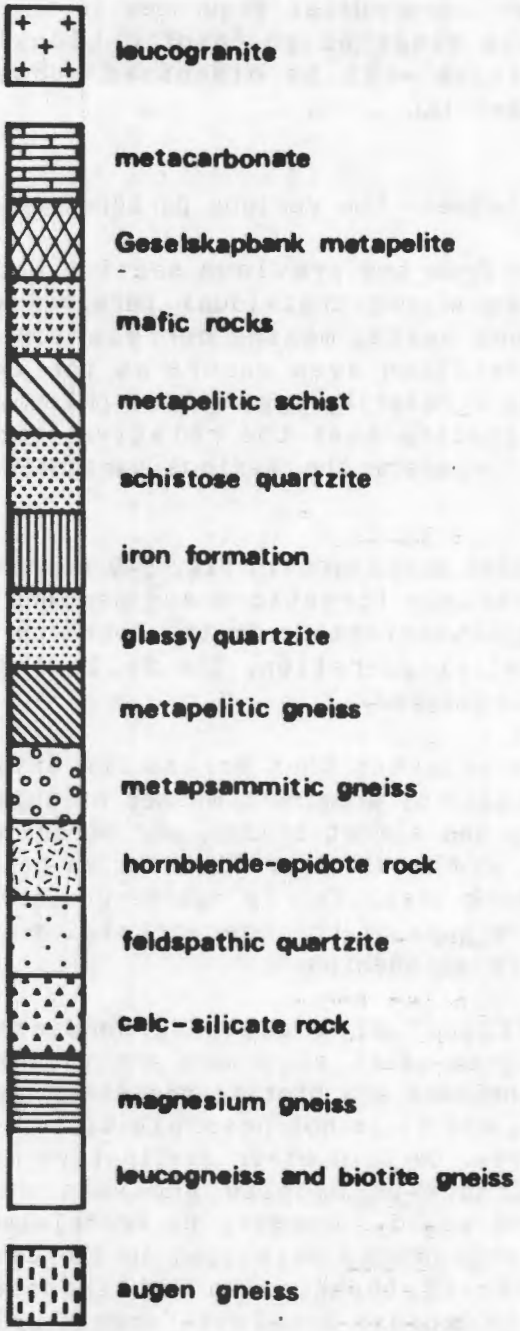

Fig. 5.9 (continued).

with the underlying gneisses and become progressively more siliceous towards the top of the unit. The quartzites are thickest in the southernmost Bitterfontein belt where they occur as two distinct bands separated by biotite gneiss/schist and banded hornblende-epidote rocks, and become progressively thinner in the Hardekraal-Keurbos area, the Witwater-Platbakkies belt and the Couragiefontein dome. They are absent from paragneiss belts further north and appear to be specifically restricted to the southern regions of the western NMC.

The feldspathic quartzite formations are succeeded by an assemblage of metapelitic garnet-cordierite gneisses in the Bitterfontein belt, in the Hardekraal-Keurbos area and in the Couragiefontein dome. They are thickest in the Bitterfontein belt, as were the feldspathic quartzites, where they have associated metapsammitic garnet-cordierite gneisses and calc-silicate rocks. The metapelitic gneisses appear to overlap the feldspathic quartzites and occur above the leucogneiss/biotite gneiss basal unit in the Anegas-Boesmanplaat belt to the north and also as thinner units in the succeeding Stofkraal-Dikmatje and Buffels River belts. The absence of this assemblage from the Witwater-Platbakkies belt is attributed to tectonic processes (see Section 4-3-3). The metapelitic garnet-cordierite gneisses represent the uppermost units observed in the southern and central paragneiss belts from Bitterfontein to Anegas-Boesmanplaat. The feldspathic quartzites, metapsammitic and metapelitic gneisses of the south/central portions of the study area also fall naturally into a convenient subgroup (B in Fig. 5-9).

The Stofkraal-Dikmatje and Buffels River paragneiss belts are important for regional correlation purposes because only they contain formations from both the southern and northern parts of the western NMC in a single structural/stratigraphic sequence. In these two belts, basal leucogneisses and biotite gneisses together with metapelitic garnet-cordierite gneisses - the topmost stratigraphic unit of the southern paragneiss belts - underlie thin units of sillimanite gneiss and glassy quartzite - the two lithologies that dominate the northern supracrustal sequences. This relationship is best observed at the Stofkraal-Leliefontein Reserve boundary and at the Buffels River on the farm Hytkoras, and indicates that the northern supracrustal sequences may be somewhat younger in age than their southern counterparts.

The lowermost leucogneiss/biotite gneiss formations that dominate the southern paragneiss belts are either absent or only poorly developed in the northern belts (north of the Silverfontein-Rietfontein belt), where they chiefly consist of leucogneisses that are best developed in the Aggeneys-Gamsberg area. In the Beenbreek portion of the Geselskapbank area, the basal unit comprises an alternating sequence of metapsammitic biotite and biotite-sillimanite gneisses and thin quartzites.

Overlying these basal units is a more persistent metapelitic quartz-mica-sillimanite schist (in the amphibolite facies) or quartz-K-feldspar-sillimanite gneiss (in the granulite facies). The southernmost outcrops of this unit can be observed in the Stofkraal-Dikmatje belt and it extends throughout the northern portions of the study area to the paragneiss belts in the outer periphery of the Geselskapbank synform. In all these belts it is

invariably intimately associated with an overlying glassy quartzite band. Both the metapelitic and quartzitic rocks are very thin in the southern Stofkraal-Dikmatje and Buffels River belts (tens of metres) but thicken considerably in the northern Smorgen Schaduwe-Kangnas, Aggeneys-Gamsberg and Geselskapbank supracrustal sequences, particularly the quartzites.

The quartzites are commonly ferruginous in their uppermost portions - most noticeably in the Smorgen Schaduwe-Kangnas and Aggeneys-Gamsberg belts, and are succeeded by iron formation units which, although thin and impersistent, appear to be as widespread as the metapelitic and quartzitic rocks, occurring from the Stofkraal-Dikmatje belt in the south, through the Smorgen Schaduwe-Kangnas and Aggeneys-Gamsberg paragneiss belts where they attain their maximium thickness, to the Geselskapbank area where they again occur as thin lenses.

A second cycle of schists and quartzites overlies the iron formations, consisting of a relatively thin metapelitic quartz-biotite-sillimanite schist unit overlain by glassy quartzites that contain interbanded thin metapelitic schists of similar composition to the underlying unit. The latter two lithologies are essentially located within the Smorgen Schaduwe-Kangnas belt (and also the Naip plateau to the immediate north of this belt) and the Aggeneys-Gamsberg area where the schists and quartzites appear to be more muscovite-rich (Rozendaal,1975; Lipson,1978). The topmost units of the northern supracrustal sequences are restricted to the Aggeneys-Gamsberg-Koeris area and consist of metaconglomerates and a variety of mafic rocks and calc-silicate rocks that have not been examined in any detail in this study.

All the northern supracrustal units (formations and members) can be conveniently included in a single subgroup (C in Fig. 5-9) during lithostratigraphic subdivision. This would greatly simplify their current classification into three subgroups belonging to the Okiep Group (Aardvark, Eenriet and Khurisberg Subgroups) and two subgroups of the Bushmanland Group (Aggeneys and Pella Subgroups) (SACS,1980).

In the central and northern portions of the Geselskapbank area, in the extreme north of the study area, two supracrustal sequences occur that differ markedly from those to the immediate south. The one sequence which comprises biotite/hornblende schists, leucogneisses, muscovite schists and quartzites, bears similarities to lithologies observed to the north-east at Abbasas, Dabenoris and Pella. The supracrustal rocks in these areas are classified as belonging to the Hom and Guadom Subgroups of the Bushmanland Group (SACS,1980). There are certain similarities between the metapelitic and quartzitic units in these areas, particularly at Dabenoris and Pella, and the metapelitic and quartzitic units of the Aggeneys-Gamsberg and Smorgen Schaduwe-Kangnas areas, and it is not inconceivable, although speculative, that the Hom muscovite schists and leucogneisses and Guadom hornblende/biotite schists represent metavolcanic lithologies intercalated with the metasedimentary rocks, and that a facies change from a sedimentary to a more volcanic domain accounts for the rapid lithological changes in the extreme north of the study area. Alternatively, these may be entirely unrelated supracrustal sequences, brought into close geographical proximity by tectonic

processes such as thrust faulting.

The second supracrustal sequence, which is essentially restricted to the core of the Geselskapbank synform, having no obvious correlates in the surrounding areas, consists of cordierite-sillimanite gneisses, dolomitic marbles and mafic gneisses that bear a resemblance to lithologies found in the upper portions of the supracrustal sequences in the central Namaqua mountainland. They are also similar to lithologies recorded within the Grunau Sequence of supracrustal rocks from southern Namibia (Blignault et al.,1983; Beukes,1973). It is distinctly possible, therefore, that the exotic supracrustal rocks in the core of the Geselskapbank synform represent a thrust slice of these lithologies overlying more typical western NMC supracrustal rocks of lower metamorphic grade. The precise stratigraphic position of this sequence is thus extremely uncertain and for this reason the sequence should be accorded separate status during formal lithostratigraphic subdivision.

5.4 The effects of subsequent structural events

Although detailed structural examinations were not undertaken during this study, the regional distribution of the supracrustal rocks in relation to the juxtaposed intrusive suites of gneisses and basic granulites, places certain constraints on the tectonic models that can be applied to the western portion of the NMC. The major structural events that control the observed configurations of the various paragneiss belts involve primarily the F2, F3 and, to a lesser extent, F4 phases as defined by Joubert (1971).

5.4.1 The F2 phase of deformation

This phase of deformation has resulted in considerable shortening and thickening in a north-south direction in the study area, by a mechanism involving east-west-striking thrust faulting and associated elongate, recumbent, cylindrical isoclinal folding. The thrust faults have resulted in "basement" augen gneisses, megacrystic gneisses, charnockites and basic granulites overriding the supracrustal sequences from the north, resulting in the preservation of the latter in the footwall of the major thrust faults and in associated synformal folds to the south of these faults. Many of the "granitic" gneisses in the hanging-wall of the major faults may represent tabular, syntectonic intrusive bodies that were emplaced during the tectonic event.

The dominant linear fabrics - mineral lineation, quartz rodding, boudins, hinges of minor isoclinal folds - observed in the supracrustal rocks are also related to this event. In the Bitterfontein and Witwater-Platbakkies belts, small-scale structures are rare and the linear fabrics do not appear to be aligned parallel to the axes of the major structures, but instead have a more north-south orientation. This could indicate that they represent stretching lineations associated with thrusting. In the amphibolite facies domain to the north, however, mineral lineations, intersection lineations and rodding, parallel to large-scale and small-scale isoclinal folds predominate, commonly

trending east-north-east and plunging shallowly eastwards (Rozendaal,1975; Moore,1977; Lipson,1978).

5.4.2 The F3 phase of deformation

The second major observed phase of deformation is associated with a distinct component of lateral displacement that is best exemplified by steeply-dipping, east-west-striking shear zones (Joubert,1974b). The most prominent shear zones are commonly located in regions where F2-age thrusting has occurred (e.g. the Buffels River and Witwater-Platbakkies areas), suggesting that re-activation of major earlier fault structures has probably taken place.

Associated with the shear zones are large-scale fold structures, predominantly synformal or closed structures (basins and domes) resulting from non-cylindrical folding. These closed structures are most prominent in the area between the Buffels River belt and the Witwater-Platbakkies belt and also in the adjacent Kliprand area (Albat,1979,1984). Some of these structures are sheath-like in appearance, particularly on the farm Tweefontein to the immediate south of the Buffels River belt. Similar doubly-plunging structures are present in the Aggeneys-Gamsberg area and others are associated with the major Pofadder lineament although these apparently belong to a younger structural event (Toogood,1976).

Folds that are strongly non-cylindrical or sheath-like in appearance, with fold axes curved within the axial planes of the folds and linear elements parallel to the extension direction are typical of systems in which the bulk deformation is a progressive shear (Cobbold and Quinquis,1980). The association of shear zones and non-cylindrical folds in the F3 phase of deformation is thus quite logical. Shear deformation results in considerable rotation of earlier linear and planar fabrics and the diverse directions of orientation of L2 fabrics in the study area is supportive evidence of this style of deformation.

The lateral displacement that occurred along these linear east-west structures is not thought to have been very great due to their relatively minor extent (generally less than 50 km). The major Buffels River linear belt dies out in the Gamoep area and appears to be at least an order of magnitude smaller than the Pofadder Lineament, the major shear zone of the western NMC. Minimum displacement in the order of 85 km was estimated within the latter shear zone (Toogood,1976) which is at least 200 km long. Displacements of less than 10 km can thus be anticipated for the larger shear zones in the study area. Lateral displacement of this magnitude would not have a great effect on the regional distribution of the various supracrustal subgroups that might result in the juxtaposition of unrelated supracrustal sequences.

Chapter 6

EFFECTS OF METAMORPHISM ON BULK COMPOSITION

6.1 General comments

There are three major mechanisms in the prograde metamorphic process by which the composition of the pre-existing rocks can be modified. Two of these, dehydration and anatexis or partial melting, are important at the relatively high temperature (and pressure) conditions existing in the study area. A third mechanism is that of interaction (local metasomatism) between two lithologies of markedly different composition. This type of chemical modification is particularly appropriate to thin bands or lenses of lithologies such as calc-silicate rocks and amphibolites enclosed within quartzo-feldspathic or metapelitic rocks (Thompson, 1975; Smithson et al., 1971), and is commonly restricted to the immediate contact zone of the two lithologies (centimetre scale). Its effects can be largely avoided by selective sampling procedures.

Retrograde metamorphic events can also modify the compositions of pre-existing prograde lithologies as they are commonly associated with the influx of a fluid phase that brings with it certain chemical species and removes others (i.e. open system conditions prevail). Retrograde metamorphism is, however, generally non-pervasive and more focussed in its occurrence (e.g. within shear zones), and its effects can also be minimized by careful sampling.

In the following section, the potential effects of dehydration and partial melting on the bulk compositions of the western NMC supracrustal rocks are estimated, using the metapelitic rocks. These lithologies are considered to have the most appropriate chemical compositions with which to examine these effects. The quartzo-feldspathic gneisses have compositions too similar to the anatectic melts themselves to be used to estimate amounts of partial melting, and the mafic, metacarbonate and quartzitic rocks, on the other hand, have too minor a granitic component to be considered.

6.2 Dehydration

With increasing temperature and pressure during prograde metamorphism, new metamorphic mineral assemblages are formed in reactions which progressively expel a fluid or vapour phase (i.e. by dehydration). In pelitic rocks, for example, the following reactions release H_2O with increasing temperature and, to a lesser extent, pressure:

staurolite + muscovite + quartz = biotite + Al_2SiO_5 + garnet + H_2O .. (1)

muscovite + quartz = Al_2SiO_5 + K-feldspar + H_2O .. (2)

biotite + Al_2SiO_5 + quartz = cordierite + garnet + K-feldspar + H_2O ..(3)

biotite + garnet = cordierite + orthopyroxene + K-feldspar + H_2O .. (4)

(Kerrick, 1972; Holdaway and Lee, 1977; Grant, 1973).

Reaction (3) has been shown to be pressure sensitive, taking place between 640 °C at 2 kbar and 710 °C at 2.7 kbar (Holdaway and Lee, 1977). At higher pressures and temperatures, reactions (2) and (3) become more temperature sensitive and involve a melt phase of granitic composition into which the released H_2O is incorporated. These two reactions, essentially involving the breakdown of hydrous micas to form less hydrous cordierite and anhydrous garnet and K-feldspar, therefore, are extremely important in studying the chemical changes in pelitic rocks across the amphibolite-facies - granulite-facies boundary.

During these dehydrating, fluid-dispersing reactions, certain incompatible elements that are released by the breakdown of the micas and cannot be incorporated in the newly-formed phases at the same level of concentration, migrate with the fluid phase into higher crustal domains of lower P-T conditions, generally as ionic complexes (Drury, 1973). Elements most likely to behave in this manner include K, Rb, Pb, U, Th, Y, Nb, the light rare earth elements La, Ce, Nd and possibly Si, Al and Na (Drury, op.cit.). The bulk composition of the original pelitic rock is thus modified without the production of a melt phase, by diffusion subsequent to dehydration reactions.

In the western NMC, metapelitic rocks in the granulite-facies domain are characterised by K-feldspar-garnet-cordierite-bearing gneisses which may have formed by dehydration (+ melt?) reactions involving the breakdown of biotite and muscovite. These gneisses in the study area contain, on average, 1.13% H_2O compared to the 3.96% H_2O content of the amphibolite-facies metapelitic schists and approximately 5% for unmetamorphosed pelites, indicating considerable H_2O loss during metamorphism and the possibility of associated incompatible element migration.

6.3 Anatexis or partial melting

Anatexis is essentially the formation of a melt of granite composition during high grades of metamorphism. Granitoid melts are the minimum melts in any system that contains feldspars and quartz, and are formed at temperatures above 750 °C in systems containing geologically reasonable amounts of water (2-5%) (Tuttle and Bowen, 1958; White and Chappell, 1977). The degree of partial melting depends on temperature, volatile content and source rock composition and in practice ranges from a few percent up to 50% of the original mass (White and Chappell, op.cit.). Granitic liquids have been experimentally produced by partial melting of pelitic rocks at temperatures in excess of 750 °C (Green, 1976) and these liquids were found to co-exist with residual cordierite-biotite-sillimanite-plagioclase-quartz at 4 kbars,

cordierite-garnet-biotite-sillimanite-plagioclase-quartz at 7 kbars and garnet-biotite-sillimanite-plagioclase-quartz at 10 kbars. Some of these assemblages are similar to those of the metapelitic rocks in the NMC study area.

When partial melting takes place, the melt and residue phases initially co-exist in equilibrium (Green, 1976) and with cooling this system could recrystallise *in situ* forming migmatites. The leucosome phase of a migmatite represents the recrystallised melt fraction and the melanosome the residue or restite. The bulk composition of these leucosome-melanosome mixtures should approximate the bulk composition of the original rock prior to anatexis (Mehnert, 1968).

Within the NMC metapelitic rocks, evidence of partial melting or migmatisation is observed in varying degrees throughout the area. In the mica-sillimanite schists of the northern Bushmanland sector, sporadic small quartz-K-feldspar veinlets with minor biotite, muscovite and sillimanite are observed, and in the garnet-cordierite-sillimanite gneisses of south/central Namaqualand, quartz-feldspar-garnet leucosomes are commonly present, reaching up to 30% of the rock unit in certain restricted areas (e.g. in a broad belt from Kliprand to Garies, south of the Witwater-Platbakkies area). In the Bitterfontein area, quartz-feldspar-biotite±cordierite leucosomes were also observed. These observations are in rough agreement with the conclusions of Flood and Shaw (1975) and Green (1976) who showed that cordierite- and/or biotite-bearing granitic rocks, derived from partial melting of pelitic rocks, formed under lower P-T conditions than their garnet-bearing equivalents.

If recrystallisation of the melt-residue mixtures does not take place *in situ*, the entire mass could start moving diapirically upward with progressive separation of residue and melt, and in this fashion S-type granites of batholithic proportions, derived from partial melting of paragneisses, can be emplaced (White and Chappell, 1977). Many of the granitic gneisses within the NMC are garnetiferous, indicating that they could have been derived by this process from crustal melting at greater depths.

It has been pointed out by Grant (1973) and Ashworth and Chinner (1978) that the P-T slope of the reaction curve for

Al_2SiO_5 + biotite + quartz = cordierite + garnet + K-feldspar + melt

is considerably steeper than the reaction curve for

Al_2SiO_5 + biotite + quartz = cordierite + garnet + K-feldspar + H_2O

and at reasonable geothermal gradients, the formation of cordierite-garnet assemblages is probably associated with a certain degree of partial melting or migmatisation. In the NMC, therefore, partial melting and perhaps bulk granite component loss, can be anticipated for the granulite-facies cordierite-garnet-sillimanite metapelites.

6.4 Previous models for the NMC

In the NMC, P-T conditions within the granulite facies of metamorphism are widespread and cover a large portion of the study area (Joubert, 1971; Albat, 1984) and so large-scale dehydration and partial melting can be expected. Models invoking major amounts of partial melting within the western portions of the NMC have been proposed by Clifford *et al.* (1975b, 1981) from cordierite-orthopyroxene assemblages and McCarthy (1976) for the major suite of augen gneisses. They (*op.cit.*) both estimate that some 75% of partial melt of either minimum melt or alkali granite composition has been extracted from the pre-existing lithologies. Mechanisms of this magnitude would have a drastic effect on the bulk compositions of the supracrustal rocks and so must be examined closely.

McCarthy (1976), in a study of the geochemistry of augen gneisses and acid granulites in the Okiep Copper District, deduced that there was only a single augen gneiss suite and a corresponding single acid granulite suite, findings supported by the structural interpretation of Clifford *et al.* (1975a). Assuming that "Nababeep District gneisses", containing 32% quartz, 25% sodic plagioclase, and 43% K-feldspar, represented the parental material, and using established model fractionation trends for the trace elements Rb, Sr and Ba, McCarthy (*op.cit.*) showed that the augen gneisses defined a trend similar to predicted residue trends and that the granulites followed trends of crystallised partial melts. Certain augen gneisses (e.g. Brandberg Gneiss) were estimated to have lost up to 74% of their bulk as melt.

It was noted by McCarthy (1976) that other residual granulite terranes have considerably less acidic bulk compositions, much higher K/Rb ratios and lower K/Ba and Rb/Sr ratios than the Namaqualand augen gneisses. These features he attributed in the first case to the composition of his assumed parental material being closer to the composition of melt material than that found in other granulite terranes, with the result that the overall change in bulk composition during melting would be small, and in the second case to the maintenance of low K/Rb ratios in the residual material by the presence of biotite.

Much of McCarthy's (1976) argument rests on his identification firstly of the "Nababeep District gneisses" as parental material for partial melting, and secondly of the acid granulites as crystallised partial melts. Both these assumptions are debatable. Reid and Barton (1983) have challenged McCarthy's (1976) restite model for the augen gneisses, proposing instead that they are themselves the products of partial melting deeper in the crust of a more intermediate suite of parental rocks similar in composition to the Vioolsdrif and Gladkop granitoids to the north. This would explain the acidic nature of the augen gneisses and their low/normal K/Rb ratios. The acid granulites (or leucogneisses) have a close stratigraphic association with the supracrustal rocks to which they have been related by a number of authors (Kroner, 1968; Moore, 1977; Paizes, 1975; Jack, 1980) either as meta-arkosic rocks or extrusive metarhyolitic rocks, (see Section 8.5.1), and an origin as crystallised partial melt material related to the augen gneisses is

TABLE 6.1. Mean major element contents of metapelitic rocks from the study area and for Canadian Proterozoic platform shales (from Cameron and Garrels, 1980).

	NMC granulite facies		NMC amphibolite facies		Geselskapbank		Aphebian shales Canada
no. of samples	52		34		5		396
SiO_2	64.86	(4.19)+	66.14	(6,46)	61.86	(6.15)	65.00
TiO_2	0.95	(0.15)	0.73	(0.15)	0.94	(0.08)	0.76
Al_2O_3	17.47	(2.60)	17.54	(3.74)	18.66	(4.65)	16.22
FeO*	6.85	(1.33)	5.11	(2.35)	8.26	(0.77)	5.73
MgO	2.11	(0.63)	1.10	(0.40)	2.57	(0.33)	2.51
CaO	1.01	(0.60)	0.14	(0.15)	1.09	(1.06)	0.52
Na_2O	1.38	(0.58)	0.17	(0.15)	1.19	(0.44)	1.44
K_2O	3.52	(0.96)	3.85	(1.49)	3.44	(1.81)	4.83
H_2O	1.13	(0.74)	3.96	(1.55)	1.09	(0.21)	3.6

+ standard deviation
* total Fe as FeO

questionable.

In studies of cordierite-orthopyroxene (±sapphirine) rock assemblages in the Okiep Copper District, Clifford et al. (1975b, 1981) used their findings of high temperatures (800-900 °C) at moderate pressures (6-7 kbar) and the unusual chemical composition of the rocks themselves (Al-Fe-Mg-rich) to propose an origin by partial melting whereby a 75% melt of alkali granite composition was removed from an original sedimentary rock of sandy argillite composition. The proposed parental material had a relatively high MgO content (5.49%) and low K_2O content (2.91%), and was enclosed in a suite of garnet-cordierite-sillimanite schistose gneisses whose bulk composition is not known from the Nababeep area, but which elsewhere in Namaqualand closely resembles normal (anhydrous) shale compositions with lower MgO contents (2.5 - 1.5%) and higher K_2O contents (3.5 - 4.0%) (see Section 7.4).

To the immediate north of the Okiep Copper District in the Eenriet mountains, where lower P-T conditions prevail in an amphibolite grade domain (Blignault et al., 1980), cordierite-anthophyllite rocks of similar bulk composition to the cordierite-orthopyroxene rocks are present in association with pelitic schists and quartzites in a similar sequence to the supracrustal rocks near Nababeep. Here it is less likely that such marked partial melting has taken place and a restite model for the formation of these cordierite-anthophyllite rocks is improbable. Alternative explanations for the origins of the thin, uncommon lenses of magnesium-rich cordierite rocks of the NMC are thus more plausible and these genetic models do not invoke such large amounts of partial melting (see Section 10.2).

It would seem from the above arguments that the evidence for major amounts of partial melting within the NMC, creating paragneisses of extreme residual composition as proposed by Clifford et al. (1975b, 1981) and McCarthy (1976), is still debatable. Bearing this in mind, the geochemical data from the present study will be used to test for supporting or contrary evidence for this model.

6.5 General trends in incompatible elements in granulite terranes

Geochemical studies in several granulite terranes show that distinctive trends of depletion in certain large ion lithophile (LIL) elements including K, Rb, Cs, Pb and U, and enrichment in others such as Ba, Sr, Zr, and Ce are commonly encountered (Lambert and Heier, 1968; Sighinolfi, 1971; Lewis and Spooner, 1973; Drury, 1973; Collerson, 1975; Rollinson and Windley, 1980; Barbey and Cuney, 1982). These depletions are, however, not observed in metamorphic zones of lower grade than medium- to high-pressure granulite facies metamorphism (Sighinolfi, op.cit., Collerson, op.cit.) and, even then, not all high grade metamorphic terranes are depleted in incompatible elements (Gray, 1977; Rollinson and Windley, op.cit.). A general assumption has been that processes involving the removal of a fluid phase, rich in certain incompatible elements, during dehydration (involving the breakdown of micas and amphiboles) and/or partial melting accompanying high grades of metamorphism, could be responsible for the observed depletion and enrichment

trends.

One of the most useful and widely used relationships examined in these studies is that between K and Rb. Up to the inception of granulite-facies grades of metamorphism, the K/Rb ratio within metapelitic rocks is essentially controlled by the K/Rb ratios of biotite and muscovite (Barbey and Cuney, 1982). At higher grades, these micas are replaced in dehydration reactions by K-feldspar which has a higher K/Rb ratio and a certain amount of Rb must be lost to the expelled fluid phase. This characteristic is somewhat complicated by the fact that both K and Rb are mobilized at different rates within granulite terranes and the observation is frequently made that there is a general decrease in K/Rb ratio with increasing K content of the granulites themselves (Gray, 1977; Rollinson and Windley, 1980).

Mafic metavolcanic rocks with low initial K contents display extremely high K/Rb ratios (as do some unmetamorphosed mafic volcanics, e.g. Aleutian volcanics, Gray, 1977; and Sarmiento ophiolites, Rollinson and Windley, 1980). In general, however, rocks in medium- to high-pressure granulite facies terranes display higher K/Rb ratios than their unmetamorphosed or moderately metamorphosed equivalents.

Other ratios which have been used in various granulite terranes to support the evidence of the K/Rb ratio are Ba/Rb, Th/U and Ca/Y (enrichment trends) and K/Ba, Rb/Sr and Rb/Ce (depletion trends). These trends relate to the depletion of K, Rb, U and Y and the residual enrichment of Ba, Sr and Ce in the granulites. Th is reported as being depleted in certain granulite-facies lithologies (Lambert and Heier, 1967; Drury, 1973) and not in others (Barbey and Cuney, 1982) whilst U is reported as significantly depleted in most granulite-facies rocks.

6.6 Incompatible element trends in the NMC supracrustal rocks

The metapelitic rocks of the NMC study area can be divided on metamorphic grade into a quartz-mica-sillimanite schist group in a northern amphibolite-facies domain and a K-feldspar-garnet-cordierite-sillimanite gneiss group in a south-central granulite-facies domain (see Section 3.3). A specific small group of cordierite gneisses in the Geselskapbank area, well within the amphibolite-facies domain, possibly represents a local granulite-facies "island" (either structural or basement) within the lower grade metamorphic suite, and has thus been segregated in this section of the study.

The actual concentration of the incompatible elements in the NMC metapelitic rocks can be compared directly to those of unmetamorphosed Aphebian shales of similar age from the Canadian Shield (Cameron and Garrels, 1980) (Table 6.1). This represents one of the most comprehensive composite geochemical data sets of mid-Proterozoic pelitic rocks published (396 samples) and is used as a comparative "standard" for the NMC metapelitic rocks in the absence of unmetamorphosed pelitic rocks in the western NMC.

The mean K contents of both the NMC granulite-facies and amphibolite-

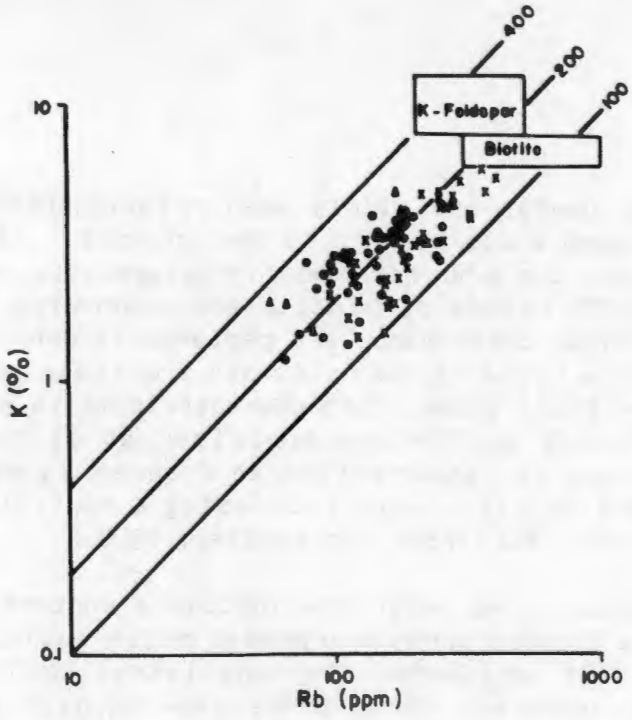

Fig. 6.1a Logarithmic plot of K (%) : Rb (ppm) showing data for metapelitic rocks from the amphibolite-facies (x) and granulite-facies (•) parts of the study area as well as from the Geselskapbank area (▲). The fields for K-feldspar and biotite are shown together with regression lines for certain selected K/Rb ratios (after Barbey and Cuney, 1982).

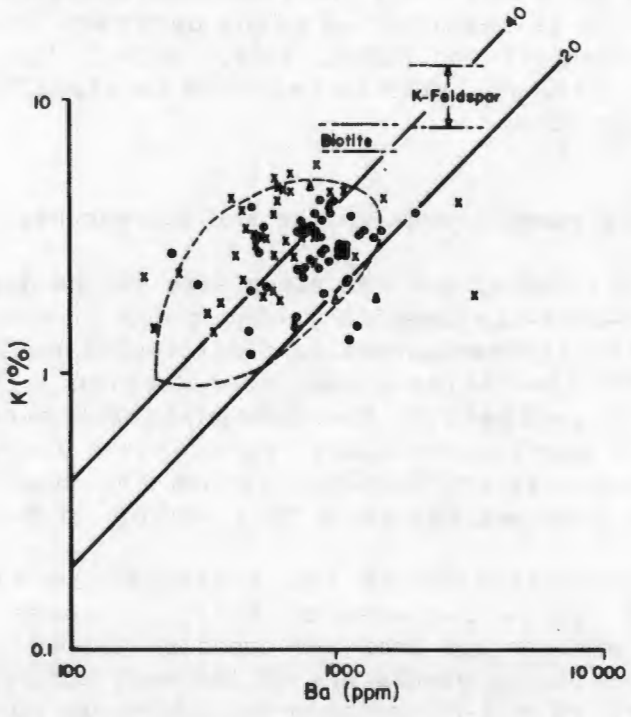

Fig. 6.1b Similar logarithmic plot of K (%) : Ba (ppm) for the same data set. Dashed line represents the compositional field of sediments, low-grade and amphibolite-facies metasediments (after Barbey and Cuney, 1982).

facies rocks (approx. 3%) are lower than those of the Aphebian shales (approx. 4%), but similar to Phanerozoic shales (Cameron and Garrels, 1980). The mean Rb content of the NMC amphibolite-facies rocks (223 ppm) shows relative enrichment compared to shales in general (160-200 ppm) (Barbey and Cuney, 1982) and Aphebian shales in particular (174 ppm), whereas the granulite-facies rocks show a slight depletion (149 ppm). The mean Ba contents of the NMC metapelitic rocks are consistently higher than those of the Aphebian shales (492 ppm) particularly in the granulite facies (872 ppm). Mean Sr contents show the reverse trend to Rb being enriched in the granulite-facies metapelitic rocks (122 ppm) relative to Aphebian shales (69 ppm) and depleted (28 ppm) in the amphibolite-facies metapelites.

These mean element contents are dependent on a number of factors, the majority of which are probably unrelated to metamorphism (e.g. source material, mode and distance of transport, diagenesis) and could thus be unrelated to the regional metamorphic event. It is, therefore, more pertinent to examine interelement ratios when looking for depletion or enrichment trends of incompatible elements. The metapelitic rocks from the amphibolite facies have lower K/Rb ratios (mean 143) than their granulite-facies equivalents (mean 204). These mean ratios are similar to those for biotite/muscovite and K-feldspar respectively (Barbey and Cuney, 1982) (Fig. 6.1a). An explanation of this relative increase in K/Rb ratio at relatively constant K, is that there has been Rb loss relative to K within the metapelitic rocks of the granulite facies in the NMC across the reaction boundary:

muscovite + biotite + sillimanite → cordierite + garnet + K-feldspar.

The range of K contents in the granulite-facies rocks is slightly more restricted (1.2% to 4.6%, mean 2.9%) than that for the amphibolite-facies metapelites (1.1% to 5.7%, mean 3.2%) with a lower mean value, indicating that K might also have been lost to a melt or fluid phase during the granulite transition reactions. The K and Rb data, therefore, could be interpreted as supporting theories of incompatible element loss during transition from amphibolite grades of metamorphism to granulite grades of metamorphism. Mean K and Rb values for the two groupings indicate a 5% loss of K and a 20% loss of Rb from the system, assuming that the K and Rb lost from the granulite-facies rocks have been taken up by the amphibolite-facies rocks. There is, however, no evidence for the K/Rb ratios of the granulite-facies metapelites decreasing with increasing K content as reported from other areas (Rollinson and Windley, 1980) (Fig. 6.2).

The metapelitic paragneisses from Geselskapbank plot mostly within the field of higher granulite-facies K/Rb ratios, and this could be interpreted as evidence that they represent a high-grade "window" within the lower grade schists of the northern amphibolite-facies zone.

The elements Ba and Sr are regarded as being sensitive residual elements, remaining relatively immobile during incompatible element loss. In plots of K/Ba vs K (Fig. 6.3) and Rb/Sr vs K (Fig. 6.5) for the NMC metapelites, the amphibolite-facies schists show markedly higher ratios than their granulite-facies counterparts. The K/Ba ratios of the amphibolite-facies rocks are

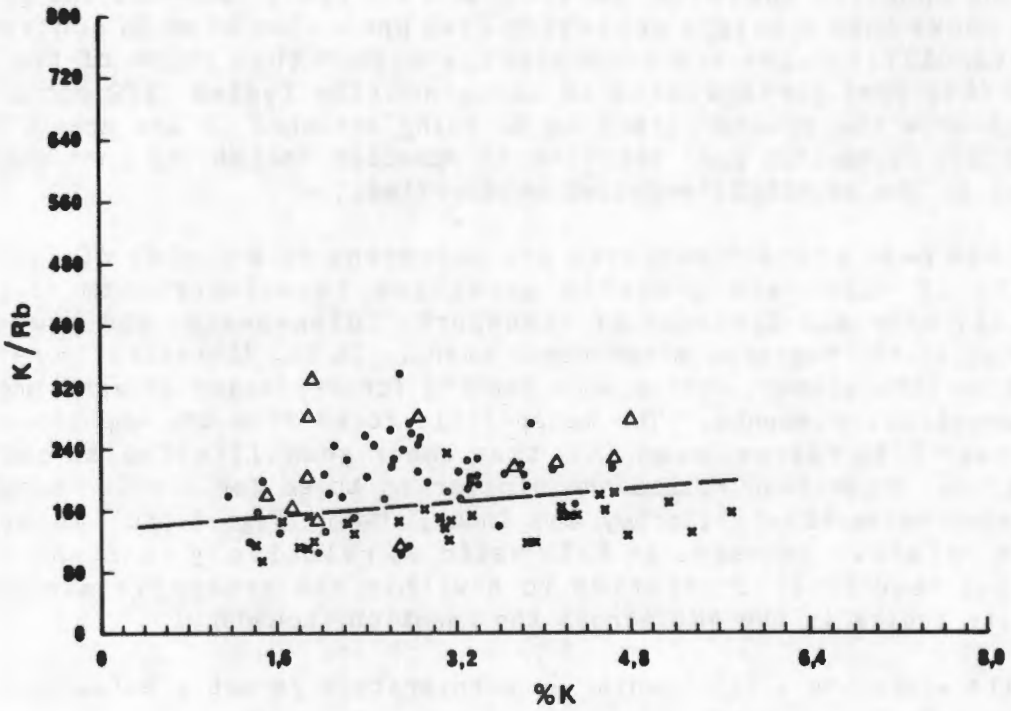

Fig. 6.2 Bivariate plot of K/Rb : K (%) showing data for metapelitic rocks from the amphibolite-facies (x) and granulite-facies (•) parts of the study area as well as for metapelitic rocks and hornblende-biotite schists and gneisses from the Geselskapbank area (△). Dashed line represents the boundary separating the majority of samples from the two major facies groups.

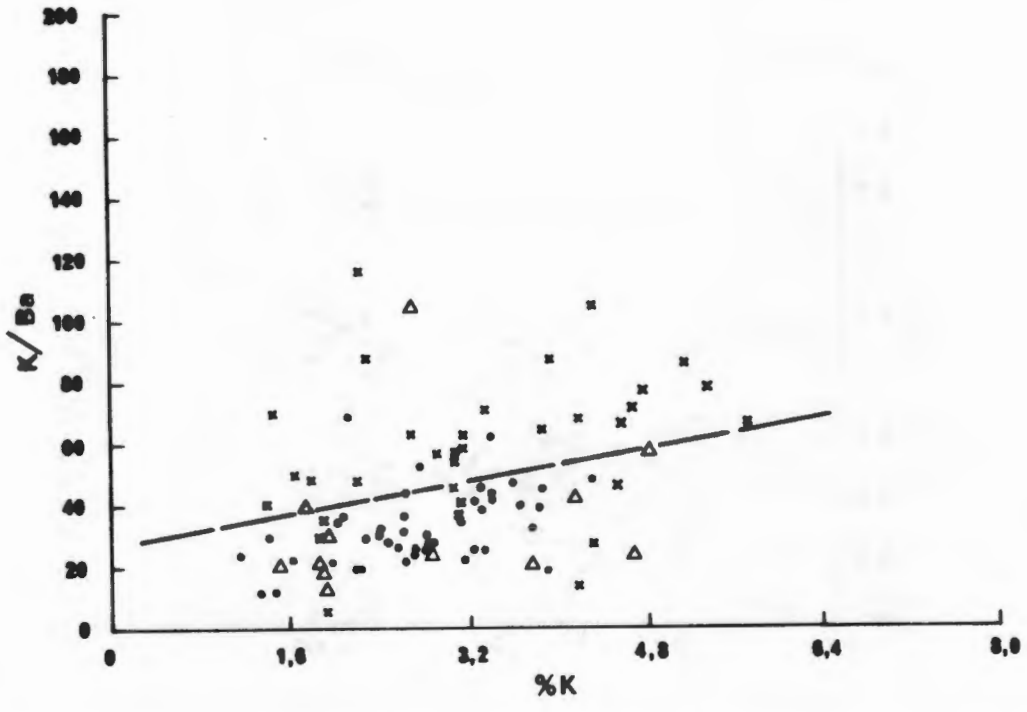

Fig. 6.3 Bivariate plot of K/Ba : K (%) showing data for metapelitic rocks for the amphibolite-facies (x) and granulite-facies (•) parts of the study area as well as for metapelitic rocks and hornblende-biotite schists and gneisses from the Geselskapbank area (△). Dashed line represents the boundary separating the majority of samples from the two major facies groups.

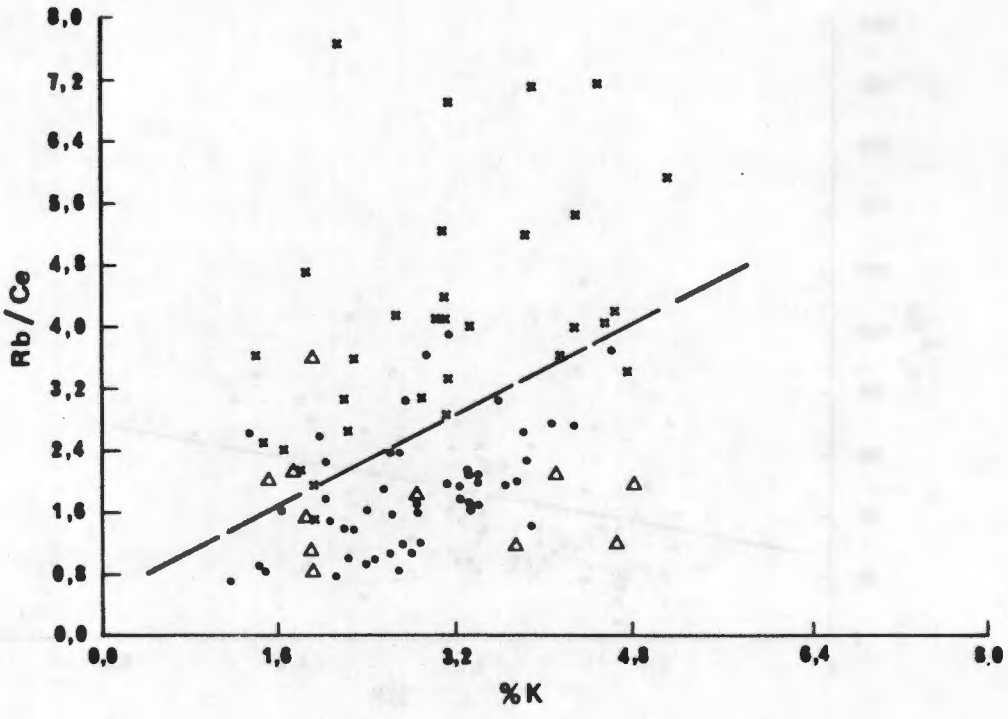

Fig. 6.4 Bivariate plot of Rb/Ce : K (%) showing data for metapelitic rocks from the amphibolite-facies (x) and granulite-facies (•) portions of the study area as well as for metapelitic rocks and hornblende-biotite schists and gneisses from the Geselskapbank area (△). Dashed line represents the boundary separating the majority of samples from the two major facies groups.

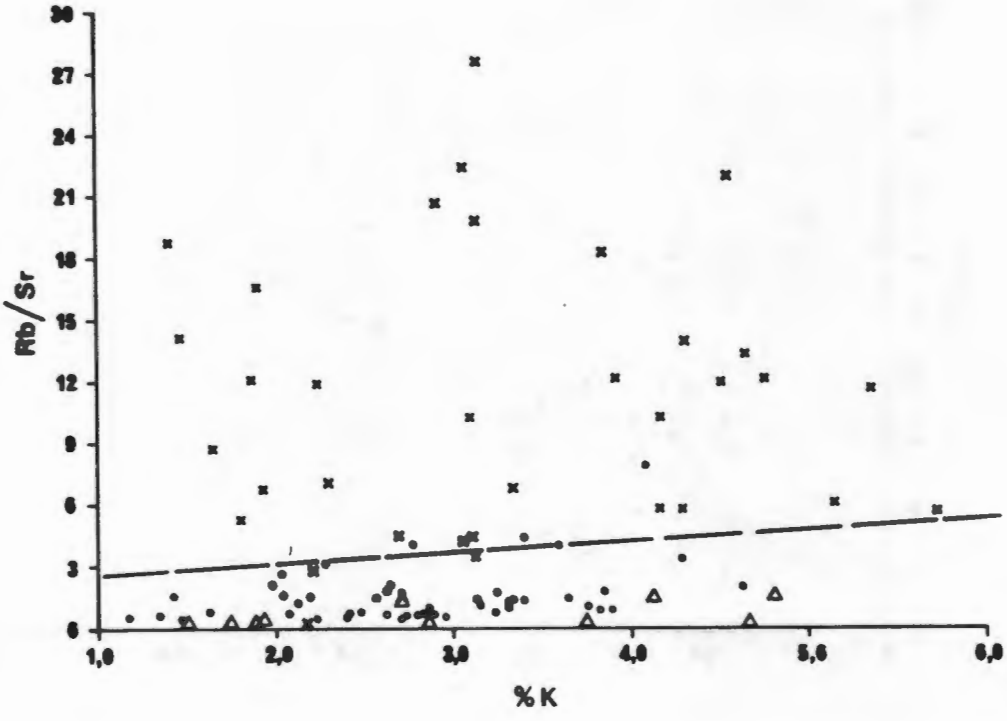

Fig. 6.5 Bivariate plot of Rb/Sr : K (%) showing data for metapelitic rocks from the amphibolite-facies (x) and granulite-facies (•) portions of the study area as well as for metapelitic rocks and hornblende-biotite schists and gneisses from the Geselskapbank area (△). Dashed line represents the boundary separating the majority of samples from the two major facies groups.

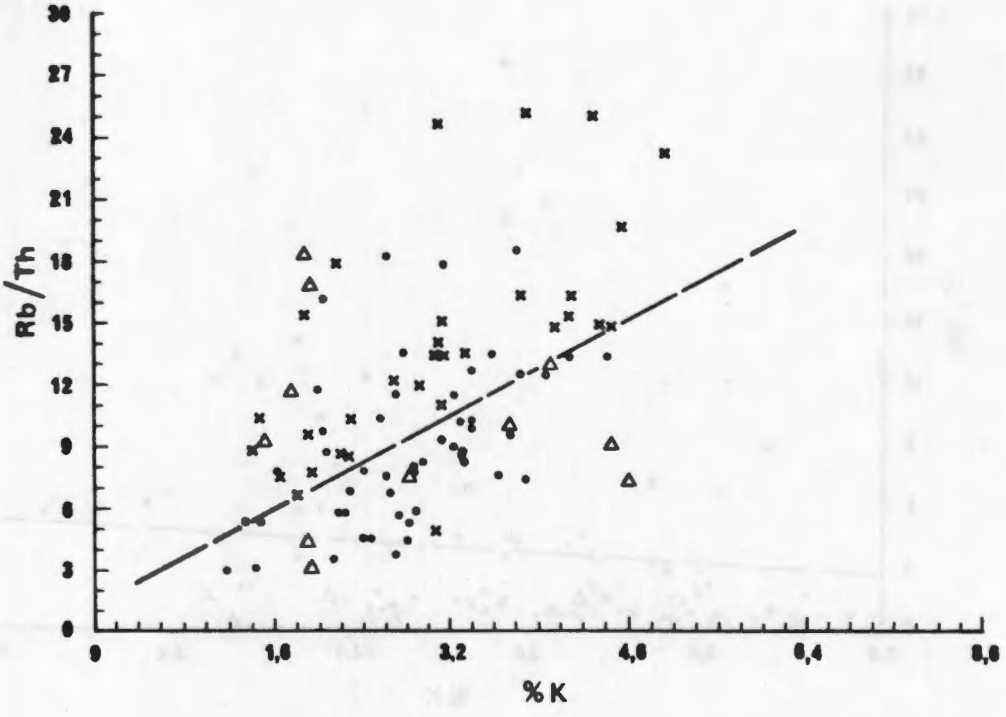

Fig. 6.6 Bivariate plot of Rb/Th : K (%) showing data for metapelitic rocks from the amphibolite-facies (x) and granulite-facies (•) portions of the study area as well as for metapelitic rocks and hornblende-biotite schists and gneisses from the Geselskapbank area (△). Dashed line represents the boundary separating the majority of samples from the two major facies groups.

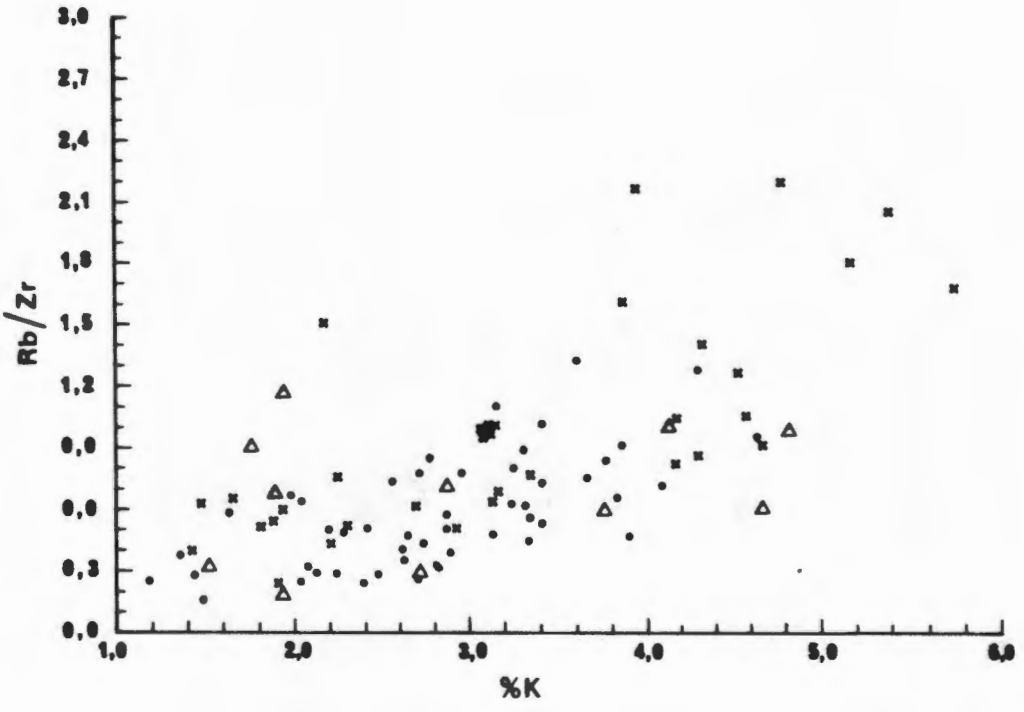

Fig. 6.7 Bivariate plot of Rb/Zr : K (%) showing data for metapelitic rocks from the amphibolite-facies (x) and granulite-facies (•) portions of the study area as well as for metapelitic rocks and hornblende-biotite schists and gneisses from the Geselskapbank area (△).

TABLE 6.2 Mean incompatible element contents and element ratios for metapelitic rocks from the study area and for Canadian Proterozoic platform shales (from Cameron and Garrels, 1980).

	NMC granulite facies		NMC amphibolite facies		Geselskapbank		Aphebian shales Canada
no. of samples	52		34		5		396
K^+	2.93	(0.80)*	3.19	(1.24)	2.86	(1.50)	4.01
Rb	149	(50)	223	(80)	113	(60)	174
Ba	872	(307)	572	(249)	986	(276)	492
Sr	122	(54)	28	(17)	146	(37)	69
Ce	83	(17)	58	(18)	68	(19)	-
Th	17	(4)	18	(7)	16	(5)	-
Zr	275	(65)	266	(74)	242	(61)	-
K/Rb	204		143		260		230
K/Ba	37		58		31		82
Rb/Sr	1.8		11		0.9		2.5
Rb/Ce	2.0		3.9		1.6		-
Rb/Th	9.4		13		7.5		-
Rb/Zr	0.6		0.9		0.6		-

* standard deviation
\+ expressed as percent for K; all other elements as ppm.

generally >45 (mean 58) and those of the granulite facies <45 (mean 37)(Fig. 6.1b). Two samples of amphibolite-facies schists with exceptionally low ratios (<20) come from close proximity to the Aggeneys ore deposits and may have contained trace amounts of barite. The K/Ba ratios show slight increase with increasing K content the granulite/amphibolite transition occurs at ratios of approx. 40 for 1.5% K and approx. 60 for 5% K (Fig. 6.3). The Geselskapbank suite again shows similarities to the granulite-facies rocks from south/central NMC.

Zr, Ce and, in certain instances, Th are also perceived to be relatively immobile during metamorphic processes (Winchester and Floyd, 1976; Rollinson and Windley, 1980; Barbey and Cuney, 1982). The Zr and Th contents of the amphibolite-facies and granulite-facies metapelitic rocks are virtually identical (Table 6.2) whereas Ce is relatively enriched in the granulite-facies lithologies (83 ppm) compared to the amphibolite-facies rocks (58 ppm). Rb/Ce ratios behave in a similar manner to the K/Ba ratios with the granulite-facies rocks having ratios <2.0 for 1.5% K and <3.2 for 5% K and the amphibolite facies metapelites having ratios >2.0 and >3.2 respectively (Fig. 6.4). Rb/Sr ratios are also similar, although increasing K content appears to exert little influence, and an Rb/Sr ratio of 3.0 to 4.0 separates granulite facies from amphibolite facies (Fig. 6.5). The Geselskapbank rocks once again show granulite-facies values for both these ratios.

Rb/Th ratios of the metapelites show a similar, although less well defined relationship. The amphibolite-facies schists have ratios >5 at 1% K and >15 at 5% K and the granulite-facies gneisses generally show ratios less than these values (Fig. 6.6). There is, however, considerable overlap of granulite-facies Rb/Th ratios into the higher amphibolite-facies field, not observed with the K/Ba, Rb/Ce and Rb/Sr ratios. Rb/Zr ratios show an even poorer segregation with vague transition from amphibolite to granulite facies around ratios of 0.3 at 1.5% K and 0.8 at 5% K (Fig. 6.7). The poorer discrimination displayed by Rb/Th and Rb/Zr ratios is probably related to the similar Th and Zr contents of the metapelitic rocks of both metamorphic grades, compared to the enrichments in Ce, Sr and Ba observed in the granulite-facies metapelitic rocks.

The observations above can be interpreted as evidence of loss of incompatible elements during reactions across the amphibolite- and granulite-facies reaction boundary. This is, however, not the only interpretation of the above data. It has been noted previously, and will be expanded on later, that two geochemically-distinct suites of metapelitic rocks are present in the NMC study area. These two suites of rocks merge together in the Gamoep area, slightly to the south of the region where the amphibolite/granulite facies transition occurs (Fig. 7.9). Genetic models, proposed later, indicate that the south/central suite of metapelitic rocks was derived from erosion of a granite/granodiorite basement sequence, whereas the northern metapelites were derived from the erosion of acidic-to-intermediate lavas and tuffs, essentially rhyolites. The latter acidic volcanics represent the highly fractionated upper portion of a major magmatic province, and as such, can be expected to be relatively enriched in K and Rb and depleted in Ba, Ce and Sr when compared to granites and granodiorites. The distinctions observed above,

TABLE 6.3 Results of least-squares mixing exercises involving the mean NMC amphibolite-facies and granulite-facies metapelitic compositions and the Witwater leucosome sample and a minimum-melt granite composition (White and Chappell, 1977).

	1.	2.	3.	4.	5.		6.	
SiO_2	74.98	75.07	64.86	66.14	66.65	(0.51)+	66.35	(0.21)+
TiO_2	0.10	0.28	0.95	0.73	0.80	(0.07)	0.85	(0.12)
Al_2O_3	14.23	12.85	17.47	17.54	16.90	(-0.64)	16.80	(-0.74)
FeO*	0.64	1.52	6.85	5.11	5.75	(0.64)	6.07	(0.96)
MgO	0.48	0.31	2.11	1.10	1.82	(0.72)	1.85	(0.75)
CaO	1.04	1.11	1.01	0.14	1.02	(0.88)	1.02	(0.88)
Na_2O	2.33	3.08	1.38	0.17	1.55	(1.38)	1.63	(1.46)
K_2O	6.58	4.81	3.52	3.85	4.06	(0.21)	3.71	(-0.14)
			Sum of squares of differences		4.32		5.03	

1. Witwater leucosome, WW-9.
2. Minimum-melt granite (after White and Chappell, 1977).
3. Mean granulite-facies metapelite, NMC.
4. Mean amphibolite-facies metapelite, NMC.
5. Best-fit mixture comprising 17.7% Witwater leucosome and 82.3% granulite-facies metapelite.
6. Best-fit mixture comprising 14.6% minimum-melt granite and 85.4% granulite-facies metapelite.

* total Fe as FeO
\+ difference between calculated compositions (5) and (6) and observed composition (4).

therefore, could be partly due to a reflection of the differing source materials.

6.7 Estimation of partial melt loss

If significant partial melting has occurred during the formation of the NMC granulite-facies metapelitic gneisses, then compositional differences between these rocks, their amphibolite-facies equivalents and unmetamorphosed Proterozoic pelite composites (Nanz, 1953; Cameron and Garrels, 1980) should be quantifiable. The factor which discriminates the bulk composition of the granulite-facies rocks from that of the amphibolite-facies rocks will be the granite composition of the newly-formed minimum melt (White and Chappell, 1977). A sample of garnet-bearing leucosome (WW-9) from within the supracrustal sequence in the Witwater-Platbakkies belt, where migmatisation was the most prevalent in the entire study area, was analysed as being representative of the minimum melt composition in the western NMC.

In mass balance calculations using average shale and minimum melt granite compositions, Nesbitt (1980) and MacRae and Nesbitt (1980) have shown the extent to which refractory elements such as Ti, Al, Fe and Mg become enriched in the restite during partial melting, and Si, K and Na depleted. When the mean composition of granulite-facies metapelites from the study area is compared with average Precambrian shale and slate compositions (Nanz, 1953; Cameron and Garrels, 1980), however, there is no evidence of Si, K or Na depletion or Mg enrichment. Only Ti, Al and Fe are slightly enriched (Table 6.1). Inferences that could be made from this comparison are that no (or very little) melting has taken place and that the original sediments are slightly enriched in Ti, Al and Fe compared to average shales, or that partial melting has occurred of a pelitic suite that originally had greater Si, K and Na contents than average shales.

The mean major element compositions of the metapelitic rocks from the amphibolite facies and granulite facies in the study area can be compared in Table 6.1. The granulite-facies metapelites show depletions in SiO_2, K_2O and H_2O and enrichments in TiO_2, FeO, MgO, CaO and Na_2O relative to their amphibolite-facies equivalents. The Al_2O_3 contents of both groups are virtually identical. The majority of these compositional variations between the amphibolite and granulite facies could be explained by removal of a granitic melt component, which would result in SiO_2, K_2O and H_2O losses and TiO_2, FeO, MgO and CaO gains in the resultant granulite-facies restites. The marked gain in Na_2O content (instead of a marked loss) and the unchanged Al_2O_3 content (instead of a discernible gain) in the granulite-facies rocks, however, cannot be explained by removal of a typical partial melt from the amphibolite-facies rocks.

The Na_2O and CaO values for the amphibolite-facies rocks are exceptionally low (less than 0.2%) and much higher values (approximately 2.0% for Na_2O and 1.0% for CaO) are required to balance melt-forming reactions. MgO is also markedly depleted in the amphibolite-facies metapelites in this regard. These anomalous element contents in the amphibolite-facies rocks

TABLE 6.4 Results of least-squares mixing exercises involving the mean NMC amphibolite-facies metapelitic composition, a subset of 8 low-Na granulite-facies metapelitic compositions, the Witwater leucosome sample and a minimum-melt granite composition (White and Chappell, 1977).

	1.	2.	3.		4.	5.		6.	
SiO_2	74.98	75.07	64.17	(4.41) †	66.14	66.72	(0.58)+	66.61	(0.47)+
TiO_2	0.10	0.28	0.97	(0.17)	0.73	0.76	(0.03)	0.82	(0.09)
Al_2O_3	14.23	12.85	18.90	(3.11)	17.54	17.80	(0.26)	17.55	(0.01)
FeO*	0.64	1.52	6.72	(1.14)	5.11	5.29	(0.18)	5.56	(0.45)
MgO	0.48	0.31	2.00	(0.55)	1.10	1.64	(0.54)	1.62	(0.52)
CaO	1.04	1.11	0.39	(0.31)	0.14	0.54	(0.40)	0.55	(0.41)
Na_2O	2.33	3.08	0.53	(0.27)	0.17	0.95	(0.78)	1.10	(0.93)
K_2O	6.58	4.81	3.61	(1.25)	3.85	4.31	(0.46)	3.88	(0.03)
			Sum of squares of differences				1.72		1.73

1. Witwater leucosome, WW-9
2. Minimum-melt granite (after White and Chappell, 1977).
3. Mean low-Na granulite-facies metapelitic subset, NMC (8 samples).
4. Mean amphibolite-facies metapelite, NMC.
5. Best-fit mixture comprising 23.6% Witwater leucosome and 76.4% low-Na granulite-facies metapelite.
6. Best-fit mixture comprising 22.4% minimum-melt granite and 77.6% low-Na granulite-facies metapelite.

* total Fe as FeO
† standard deviation
\+ difference between calculated compositions (5) and (6) and observed composition (4).

would appear to be unrelated to dehydration or melt-forming processes of compositional modification and thus probably represent pre-metamorphic compositional differences, with the bulk of the amphibolite-facies metapelites having a significantly different sedimentary history to those of the granulite facies. These differences are examined in more detail in Section 7.5.

Least-squares mixing (see Section 7.6) of the granulite-facies mean composition (model restite) with the Witwater leucosome (model minimum melt) to re-establish the amphibolite-facies mean composition (model pre-melt pelite), indicates that approximately 18% of the bulk composition of the original pelite has been lost as a partial melt during granulite-facies metamorphic transformation from quartz-mica-sillimanite schists to K-feldspar-garnet-cordierite-sillimanite gneisses (Table 6.3). Calculations using White and Chappell's (1977) minimum melt composition yield similar results (approximately 15%). This mixing model is far from ideal, however, with relatively large differences in Al_2O_3, FeO, MgO, CaO and Na_2O contents for reasons outlined in the previous paragraph. This results in a relatively large sum of squares of differences ($\pm$4-5, instead of ideally <1).

A small subset of low-Na metapelitic rocks (8 samples) from the northern portion of the granulite-facies domain was selected for a separate least-squares mixing exercise (Table 6.4) to try to minimise the pre-metamorphic compositional differences. When modelled against the amphibolite-facies set, this subset gave more realistic mixes using both the Witwater leucosome and minimum melt compositions. Very similar results were obtained in both exercises, and approximately 22% partial melt was indicated with the sum of squares of differences being <2 in both cases.

These partial melt estimates compare well with the field observations of coarse-grained quartz-feldspar-garnet leucosomes within the metapelitic rocks, which vary between 5% and 25% throughout the granulite-facies portion of the study area. The implications of these observations are that partial melting in the NMC metapelites has not resulted in the formation of large granitic bodies of batholithic proportions, but instead in widespread low-order migmatisation of the rocks.

The Geselskapbank metapelitic rocks have major element compositions that are more depleted in SiO_2, Na_2O, K_2O and H_2O, and more enriched in TiO_2, Al_2O_3, FeO, MgO and CaO than the mean granulite-facies metapelite composition (Table 6.5). Least-squares mixing of these two lithologies with the minimum melt composition (White and Chappell, 1977) indicates that the Geselskapbank metapelitic rocks could have formed by 20% partial melting of the granulite-facies metapelites. In this exercise the mix is nearly perfect with the sum of squares of differences totalling <0.2 (Table 6.5). This model supports the arguments, based on the high K/Rb and low K/Ba, Rb/Sr, Rb/Ce and Rb/Th ratios, that these metapelites represent more extreme restite compositions than the other metapelitic lithologies of the study area.

The estimates by Clifford *et al.* (1975b, 1981) of 75-80% granite melt during the formation of the cordierite-orthopyroxene rocks within the supracrustal sequence were obtained from similar least-squares mixing

TABLE 6.5 Results of least-squares mixing exercises involving the mean NMC granulite-facies metapelitic composition, the mean Geselskapbank metapelite composition, the Witwater leucosome sample and a minimum-melt granite composition (White and Chappell, 1977).

	1.	2.	3.	4.	5.		6.	
SiO_2	74.98	75.07	61.86	64.86	64.56	(-0.30)+	64.61	(-0.25)+
TiO_2	0.10	0.28	0.94	0.95	0.77	(-0.18)	0.80	(-0.15)
Al_2O_3	14.23	12.85	18.66	17.47	17.75	(0.28)	17.45	(-0.02)
FeO*	0.64	1.52	8.26	6.85	6.69	(-0.16)	6.85	(0.00)
MgO	0.48	0.31	2.57	2.11	2.14	(0.03)	2.10	(-0.01)
CaO	1.04	1.11	1.09	1.01	1.08	(0.07)	1.09	(0.08)
Na_2O	2.33	3.08	1.19	1.38	1.42	(0.04)	1.58	(0.20)
K_2O	6.58	4.81	3.44	3.52	4.09	(0.57)	3.73	(0.21)
			Sum of squares of differences			0.56		0.17

1. Witwater leucosome, WW-9
2. Minimum-melt granite (after White and Chappell, 1977).
3. Mean Geselskapbank metapelite
4. Mean granulite-facies metapelite, NMC.
5. Best-fit mixture comprising 20.5% Witwater leucosome and 79.5% Geselskapbank metapelite.
6. Best-fit mixture comprising 20.8% minimum-melt granite and 79.2% Geselskapbank metapelite.

* total Fe as FeO
\+ difference between calculated compositions (5) and (6) and observed composition (4).

TABLE 6.6 Major element compositions of cordierite-anthophyllite rock from Eenriet and cordierite-hypersthene-gedrite-quartz rock from the Okiep Copper District as well as the results of least-squares mixing exercises involving the latter rock, an average alkali granite composition and a sandy argillite composition.

	1.	2.	3.	4.	5.		6.	
SiO_2	45.81	46.13	74.20	67.51	67.08	(-0.43)+	46.13	
TiO_2	0.66	2.18	0.20	0.50	0.75	(0.25)	2.19	(0.01)Δ
Al_2O_3	15.34	15.89	13.81	12.53	14.51	(1.98)	15.89	
FeO*	17.58	16.14	1.84	5.74	5.77	(0.06)	16.14	
MgO	10.90	16.24	0.26	5.49	4.69	(-0.80)	16.24	
CaO	0.56	0.61	0.72	0.76	0.70	(-0.06)	0.06	(-0.55)
Na_2O	0.29	0.29	3.53	2.56	2.66	(0.10)	0.03	(-0.26)
K_2O	3.09	0.01	5.15	2.91	3.77	(0.86)	0.04	(0.03)
		Sum of squares of differences			5.57		0.37	

1. Cordierite-anthophyllite rock, ER-1, Eenriet area.
2. Cordierite-hypersthene-gedrite rock, 39, Goinoep (Clifford et al., 1981).
3. Average alkali granite (Nockolds, 1954).
4. Sandy argillite, Lomagundi, Zimbabwe, recalculated anhydrous (Clifford et al., 1975b).
5. Best-fit mixture comprising 72.9% alkali granite and 27.1% of sample 39.
6. Best-fit mixture of 22% quartz, 66% chlorite, 8% kaolinite and 4% ilmenite for comparison with sample 39.

* total Fe as FeO.
\+ difference between calculated composition (5) and observed composition (4).
Δ difference between calculated composition (6) and observed composition (2).

TABLE 6.7 The effect of the addition of 10% increments of minimum-melt granite on the major element composition of the granulite-facies metapelitic rocks of the study area.

	1.	2.	3.	4.	5.	6.
SiO_2	75.07	64.86	65.88	66.90	67.92	68.94
TiO_2	0.28	0.95	0.88	0.82	0.75	0.68
Al_2O_3	12.85	17.47	17.01	16.55	16.08	15.62
FeO*	1.52	6.85	6.32	5.78	5.25	4.72
MgO	0.31	2.11	1.93	1.75	1.57	1.39
CaO	1.11	1.01	1.02	1.03	1.04	1.05
Na_2O	3.08	1.38	1.55	1.72	1.89	2.06
K_2O	4.81	3.52	3.64	3.78	3.91	4.04
H_2O	5.5	1.13	1.57	2.00	2.44	2.88

* total Fe as FeO

1. Minimum-melt granite (after White and Chappell, 1977).
2. Mean granulite-facies metapelitic rock, NMC.
3. Original composition of granulite-facies metapelite assuming 10% minimum-melt granite loss.
4. Original composition of granulite-facies metapelite assuming 20% minimum-melt granite loss.
5. Original composition of granulite-facies metapelite assuming 30% minimum-melt granite loss.
6. Original composition of granulite-facies metapelite assuming 40% minimum-melt granite loss.

exercises using a magnesium-rich sandy argillite as the pre-metamorphic starting material. Although this initial composition is only poorly approximated in mixtures of granitic melts and the cordierite-orthopyroxene rocks (the sum of squares of differences exceeds 5 in this exercise, Table 6.6), the broad variations in sediment geochemistry result in the calculated mixed compositions falling within the field of possible argillite compositions. The weakness in this partial melt model is that it is entirely dependent on the assumed precursor composition. The bulk composition of Clifford et al.'s (1981) cordierite-hypersthene-gedrite-quartz rock can be reproduced by a mixture of quartz (22%), chlorite (66%), kaolinite (8%) and ilmenite (4%) - i.e. a quartz-chlorite shale (see Section 10.4). If the assumption is made that this particular chloritic shale was the starting material in the partial melt calculations, then the conclusion that no melting took place, must result (Table 6.6). In a similar fashion, the bulk compositions of Clifford et al.'s (1981) cordierite-hypersthene gneiss and Clifford et al.'s (1975b) cordierite-sapphirine-bronzite-phlogopite rock can be reproduced by quartz-chlorite-magnetite-ilmenite and illite-chlorite mixtures respectively. Estimations of the amount of partial melting that has taken place which make use of assumed parental material compositions are thus highly questionable.

A more satisfactory estimate of the amount of partial melting involved in the formation of the cordierite-orthopyroxene gneisses can be obtained from a comparison of their bulk composition with that of cordierite-anthophyllite rocks from localities in the Eenriet mountains, some 35 km to the north of the Okiep Copper District - the locality of Clifford et al.'s (1975b, 1981) cordierite-orthopyroxene gneisses. These cordierite-anthophyllite rocks crop out within a supracrustal sequence of metapelitic schists and glassy quartzites similar to the sequence enclosing the cordierite-orthopyroxene gneisses, with the exception that the level of metamorphism is only of amphibolite-facies grade in the Eenriet area (Blignault et al., 1980). If partial melting has occurred during the prograde metamorphic formation of cordierite-orthopyroxene parageneses from cordierite-anthophyllite parageneses, it should be evident in differences in bulk composition between these two lithologies. A comparison of the bulk compositions of the two types, however, shows that they are essentially identical (Table 6.6), with the exception of some K_2O depletion in the granulite-facies rock. This indicates that little or no partial melting has taken place in these lithologies across the granulite/amphibolite facies transition. The K_2O difference may be attributable to incompatible element loss by diffusion during dehydration-related reactions (amphibole breakdown) or perhaps to a slight original lithological difference.

6.8 Summary

In summary, it would appear that partial melting models for the NMC granulite-facies metapelitic rocks involving the removal of major quantities of alkali granite as melt (75% - 80% of the original rock) are untenable. Partial melting seldom exceeds 50% of the original starting material (White and Chappell, 1977) due to a number of factors, including the large amounts of

H_2O required, at levels not normally found in typical pelitic rocks. Comparisons between the K and Rb contents and bulk compositions of amphibolite-facies and granulite-facies metapelites indicate that partial melting of the order of 0% to 20% is more realistic and can be related to field evidence provided by limited migmatization. The removal of up to 20% minimum melt granite from a rock of pelitic composition will not radically alter the bulk composition in any significant way that is greater than the normal variation within a suite of typical pelitic rock samples (Table 6.7).

With the possible exception of the trace element Rb, the compositions of the metapelites can be assumed to represent the somewhat dehydrated equivalents of the original pelitic sediments, and their classification and discrimination based on their chemical composition can be attempted. The marked variations observed in the Na_2O and CaO contents and, to a lesser extent in the MgO and FeO contents, between the northern (mostly amphibolite-facies) and south/central (mostly granulite-facies) metapelites, probably represent premetamorphic sedimentary differences that can be investigated further.

Chapter 7

GEOCHEMISTRY OF THE METAPELITIC ROCKS

7.1 Introduction

In the previous section, metamorphic modification of the bulk compositions of the metapelitic rocks was discussed and generally found to be minimal. It is thus possible to compare the compositions of these paragneisses directly with the compositions of unmetamorphosed sediments and volcanic rocks in order to derive precursor lithologies and palaeoenvironmental conditions that existed prior to metamorphism. This can be done in a number of steps and by a variety of processes. Firstly, an estimate as to the broad classification of the paragneiss precursors can be made by direct comparison of chemical analyses with mean compositions of various sedimentary and volcanic rock types and by the use of relatively basic triangular and bivariate plots of major chemical constituents. Then by use of more sensitive plots (generally of minor or trace elements) and various statistical methods involving correlation coefficients, histograms and discriminant canonical variables, the metapelites can be subdivided into more subtle "facies" groupings. Finally with the use of principal components analysis and least-squares approximation, the sedimentary components of, and their approximate concentrations in, the various metapelite groups can be derived and statements concerning source materials, depositional environment, climate and diagenetic effects can be made.

7.2 Direct chemical comparisons with unmetamorphosed rocks

The two major suites of sedimentary rocks with bulk compositions most similar to the metapelitic rocks of the western NMC are greywackes and shales. Greywackes commonly form by rapid deposition in tectonically active "eugeosynclinal" environments, closely associated with volcanism, and thus contain considerable amounts of detrital feldspar and lithic fragments (Pettijohn,1975). They generally have relatively restricted compositional ranges similar to their source material which is commonly of andesitic-to-dacitic composition. Shales, on the other hand, form in a variety of environments from deep basins to shallow platforms as the result of the selective hydraulic sorting and concentration of clay particles, and can display a wide variety of chemical compositions related to the chemistry of common clay minerals such as illite, chlorite, montmorillonite and kaolinite, diluted with varying amounts of quartz.

Chemically, greywackes and shales may be distinguished by their Al_2O_3:SiO_2 and K_2O:Na_2O ratios which are both greater in shales due to increased Al_2O_3 and K_2O and reduced SiO_2 and Na_2O within common clays (Garrels and Mackenzie, 1971). Shales generally have K_2O:Na_2O ratios considerably greater than 1, whereas greywackes commonly have ratios less than 1.

TABLE 7.1 Comparison of the mean composition of metapelitic rocks from the study area with an average greywacke composition and several mean compositions of Proterozoic and South African shales, siltstones and slates.

	1.	2.	3.	4.	5.	6.	7.
SiO_2	64.51	58.42	57.65	62.6	60.64	64.3	66.7
TiO_2	0.88	0.79	0.86	0.73	0.73	0.7	0.6
Al_2O_3	17.79	16.63	17.04	15.6	17.32	16.7	13.5
FeO^*	6.49	8.81	6.97	5.4	5.69	4.6	4.9
MnO	0.10	0.15	0.11	0.06		0.06	
MgO	1.84	4.12	2.38	2.42	2.60	1.6	2.1
CaO	0.76	2.34	1.20	0.50	1.54	1.2	2.5
Na_2O	0.98	1.57	0.93	1.4	1.19		2.9
K_2O	3.62	3.08	4.18	4.65	3.69	3.8	2.0
P_2O_5	0.07	0.09	0.09	0.13			
H_2O^+	2.19	2.85	6.19	3.6	3.51		1.5

* total Fe as FeO

1. Average western NMC metapelite (93 samples, this study).
2. Early Proterozoic shales and slates from the Russian Platform (460 samples, Ronov and Migdisov, 1971).
3. Late Proterozoic shales and slates from the Russian Platform (1226 samples, Ronov and Migdisov, 1971).
4. Proterozoic Aphebian shales, Canada (326 samples, Cameron and Garrels, 1980)
5. Precambrian slates (33 analyses, Nanz, 1953).
6. Beaufort Group siltstones, Karroo Supergroup (550 samples, Beeson, 1980)
7. Mean greywacke (61 analyses, Pettijohn, 1975).

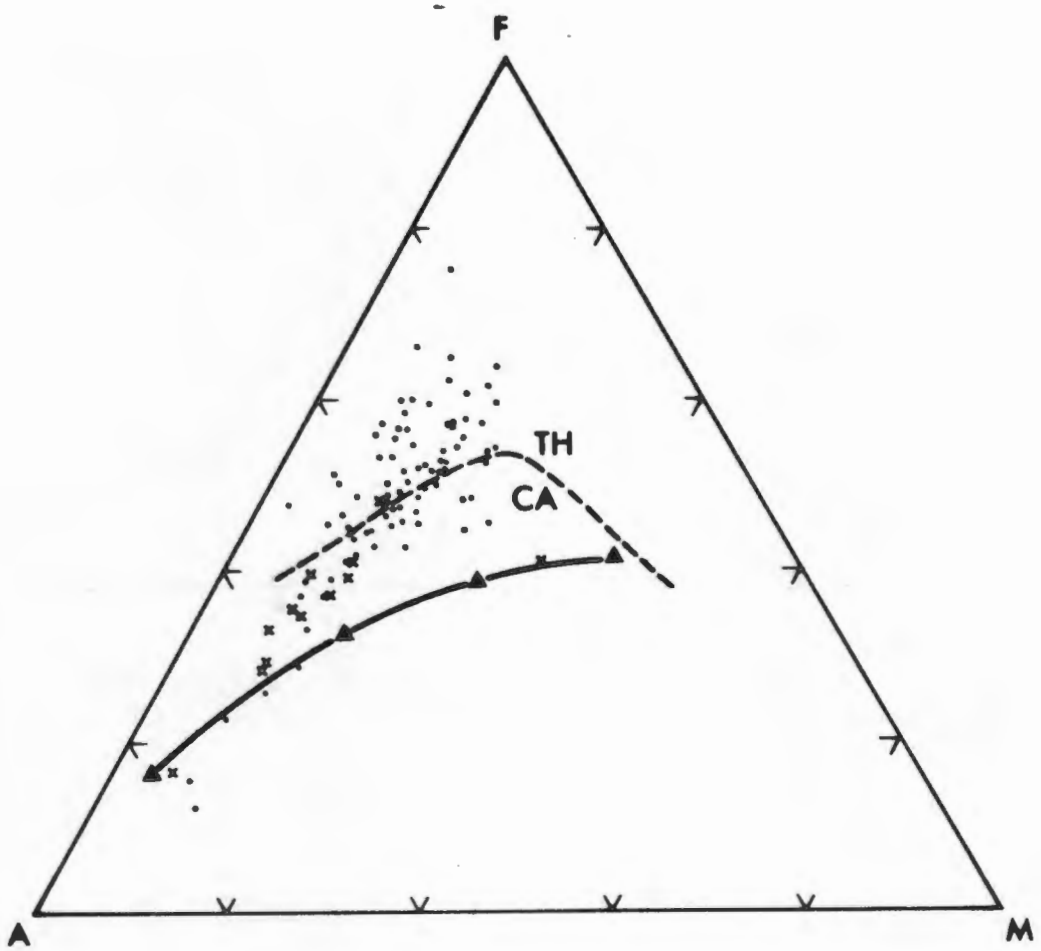

Fig. 7.1 AFM diagram showing the distribution of metapelitic rocks (dots) and cordierite-bearing metapsammitic rocks (crosses) from the study area compared to the general fields of tholeiitic (TH) and calc-alkaline (CA) volcanic rocks. The calc-alkaline trend of the Orange River Group metavolcanic rocks (triangles) from Reid (1977) is also plotted for comparison.

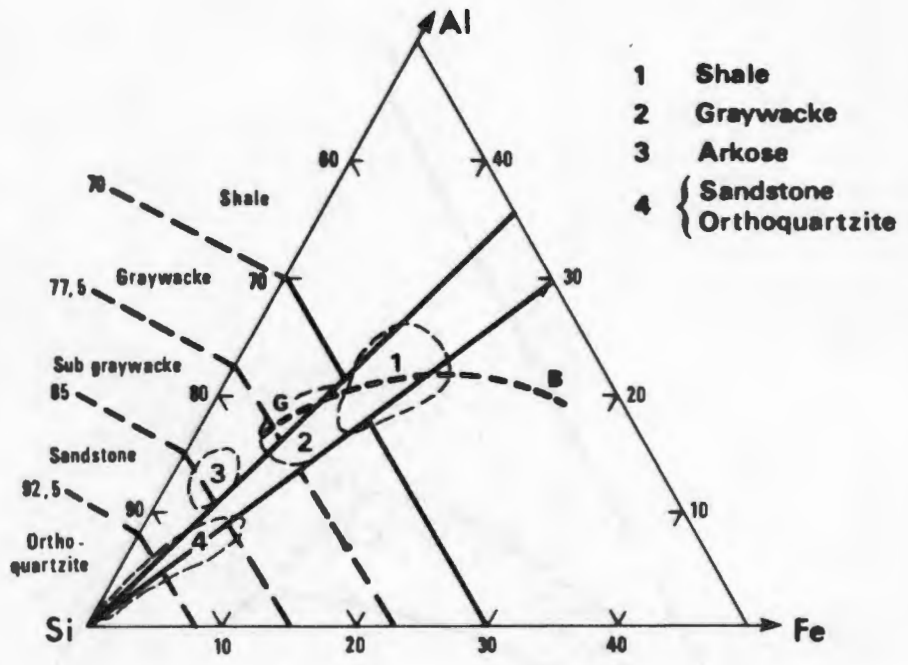

Fig. 7.2a Si-Al-Fe diagram of Moore and Dennen (1970) showing the different fields of various sedimentary rocks together with the igneous trend from granites (G) to basalts (B).

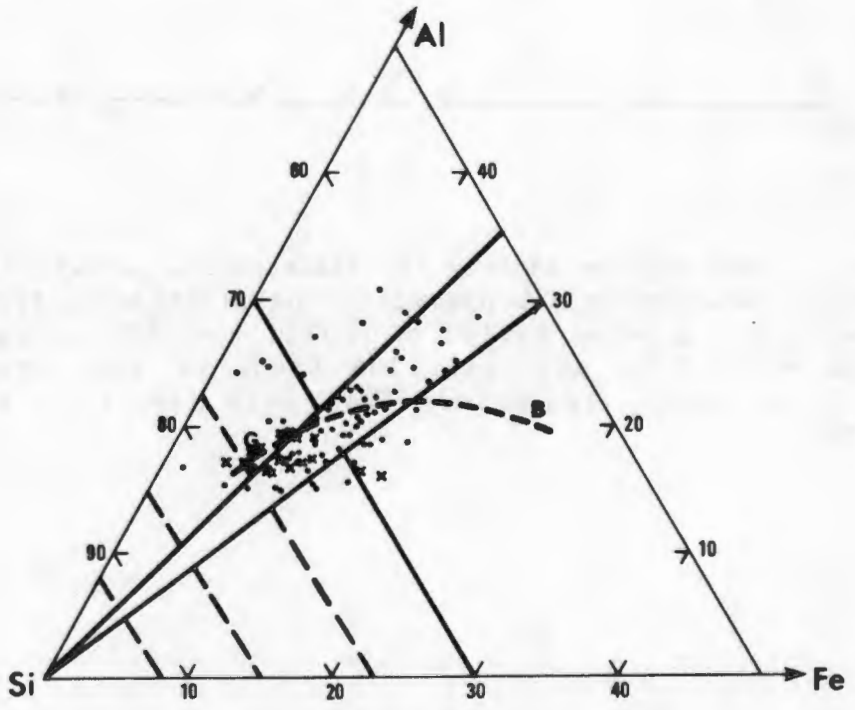

Fig. 7.2b Si-Al-Fe diagram showing the distribution of metapelitic rocks (dots) and cordierite-bearing metapsammitic rocks (crosses) from the study area.

In Table 7.1, the mean value of the metapelitic rocks from the western NMC is compared to an average greywacke composition (Pettijohn,1975) and several age-equivalent unmetamorphosed Proterozoic shales and slates, as well as a more recent South African example from the Beaufort siltstones of the Karroo Supergroup (Beeson, 1980). In this direct comparison, it is apparent that the bulk composition of the NMC metapelitic rocks shows closer resemblance to shale compositions than greywacke compositions, particularly in their Al_2O_3, Na_2O and K_2O contents. The NMC metapelitic rocks, like typical shales, have considerably higher Al_2O_3:SiO_2 and K_2O:Na_2O ratios than typical greywackes.

7.3 Comparison with general sedimentary and igneous trends

The AFM diagram, with apices weights percent (Na_2O + K_2O), total Fe as FeO, and MgO, is widely used in studies of igneous rocks to display the distinctive enrichment trends (iron or alkali) of tholeiitic, alkaline and/or calc-alkaline suites. It has been shown by Robinson and Leake (1975) that sedimentary rocks have trends which mimic the alkali enrichment trends of the various igneous suites, making the AFM diagram a relatively unsatisfactory tool to discriminate between metavolcanic and metasedimentary rocks in high-grade metamorphic terranes such as the study area. The linear trends displayed by sedimentary and metasedimentary rocks are generally attributable to variations in the relative amounts of alkali feldspar and clay minerals (predominantly chlorite) in the sediments, coupled with a narrow range of Fe:Mg ratios in the clays (Robinson and Leake, op.cit.).

Comparison of the NMC metapelitic and metapsammitic gneisses from the study area with typical tholeiitic and calc-alkaline trends on the AFM diagram, reveals that the NMC paragneisses have trends similar to those of tholeiitic rocks rather than calc-alkaline rocks, although they lack the marked iron enrichment trend of typical tholeiitic suites (Fig. 7.1). The NMC metapelitic rocks are also significantly different in their AFM trend to the Haib metavolcanic rocks from the Orange River which follow a calc-alkaline trend (Reid,1977). It can thus be deduced from the AFM diagram that the NMC metapelitic rocks are not necessarily related to (i.e. derived from or distal equivalents of) the Haib metavolcanics in the north or other rocks of calc-alkaline affinity, and that they display relatively constant Fe:Mg ratios, more typical of tholeiitic trends or, more likely, of sedimentary clay minerals.

Moore and Dennen (1970) have shown that the chemical composition of clastic sediments is apparently defined by a near-constant Al:Fe ratio associated with a variable Si content. This they (op.cit.) attribute to the hydraulic sorting of sediments with the coarser "resistate" fraction (essentially quartz) concentrating progressively towards orthoquartzite and the finer "hydrolysate" fraction (clays) concentrating towards shale with Al:Fe ratios between 1.5 and 2.5. The result of this characteristic is that the various sedimentary groups (orthoquartzite, sandstone, greywacke, arkose, shale, etc.) can be segregated on a Si-Al-Fe triangular diagram, with the entire sedimentary suite falling within a narrow "corridor" of Al:Fe ratios,

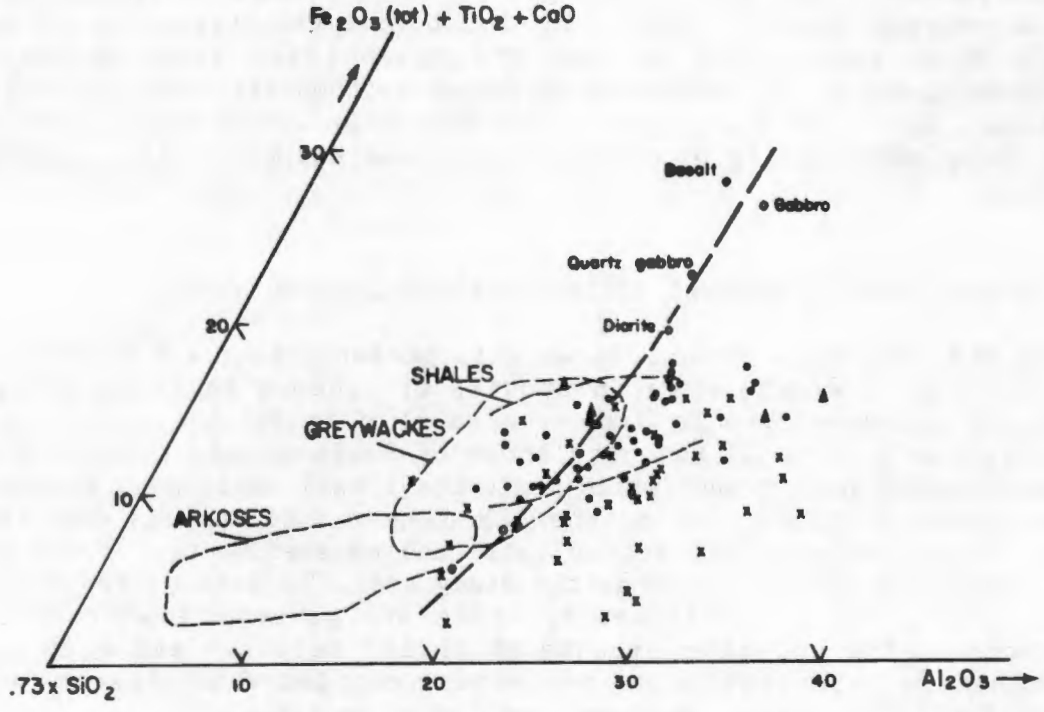

Fig. 7.3 Triangular plot of (SiO_2 x 0.73), Al_2O_3 and (total Fe as Fe_2O_3 + TiO_2 + CaO) showing the fields of various sedimentary rocks together with the typical igneous trend (after de la Roche, 1966). Included on the diagram are metapelitic rocks from the northern (crosses) and south/central (dots) portions of the study area, as well as samples from the Geselskapbank area (triangles). The igneous trend of the Haib metavolcanic rocks (Reid, 1977) is virtually identical to that of the general igneous trend shown.

each with its own distinct Si range. Igneous rocks lie on a curve which cross-cuts this clastic sedimentary field obliquely in the region of greywackes and shales.

Under metamorphic conditions with no or minimal partial melting, the relative Si, Al and Fe contents of metamorphosed sediments will remain essentially constant and thus the diagram can be applied to metasedimentary rocks in order to demonstrate firstly their sedimentary parentage (as opposed to an igneous origin) and secondly their likely sedimentary-group precursor. When this exercise is applied to the metapelitic and metapsammitic rocks from the study area (Fig. 7.2), three main features are apparent. Firstly, the metapelitic rocks fall predominantly within the narrow range of defined Al:Fe ratios; secondly, they follow a sedimentary trend towards the Si apex and do not follow the cross-cutting igneous trend, indicating a sedimentary parentage; and thirdly, they are essentially restricted to the fields of shales and greywackes as defined by Moore and Dennen (1970).

De la Roche (1966) noted that within sedimentary rocks, Si is distributed within free quartz and alumino-silicate fractions, while Al, Na, K and Mg are restricted to alumino-silicate minerals and Ca, Ti and Fe are distributed within the alumino-silicate or other "subordinate" oxide/carbonate phases. When plotted on a $\%(Al_2O_3 + Fe_2O_3$ total $+ TiO_2 + CaO)$ vs $\%SiO_2$ binary plot, common alumino-silicate rock-forming minerals, sedimentary clays and typical igneous rocks of the rhyolite-basalt trend, all plot close to a line of negative slope with x-axis intercept at 100% SiO_2 (i.e. quartz) and y-axis intercept at 73% (de la Roche,1966, Fig.2), indicating that

$$Al_2O_3 + Fe_2O_3 \text{ total} + TiO_2 + CaO = k/100\ (100 - SiO_2) \text{ where } k = 73,$$

is a common natural equation for igneous and sedimentary rocks and rock-forming minerals. Assuming Na, K and Mg to be "satellites" of Al restricted to alumino-silicate minerals, de la Roche (op.cit.) devised a triangular plot with apices $(SiO_2 \times 0.73)$, Al_2O_3 and $(Fe_2O_3$ total $+ TiO_2 + CaO)$ which defines sedimentary rocks on their amounts of free quartz, alumino-silicate minerals (mostly clays) and oxide/carbonate components respectively. On the triangular plot, the fields of quartzites, arkoses, greywackes, shales and also the igneous trend are outlined. The igneous trend cuts obliquely through the fields of greywackes and shales which coincide with the fields of granites, granodiorites and quartz diorites. In many ways, this diagram could be described as a slightly more complex version of Moore and Dennen's (1970) Si-Al-Fe plot, and in similar fashion, the NMC metapelitic rocks generally fall within the field of shales and, to a lesser extent, greywackes, noticeably cross-cutting the igneous trend (Fig. 7.3). The igneous trend followed by the Haib metavolcanics (Reid,1977) is also cross-cut by the sedimentary trend of the NMC paragneisses.

In the three triangular diagrams described above, the differences between sedimentary and igneous trends are small and relatively subtle, and the areas of overlap are considerable, taking place in the fields of relatively common and important rock groups, namely shales, greywackes, diorites and granodiorites. The ability of these diagrams to discriminate between volcanic

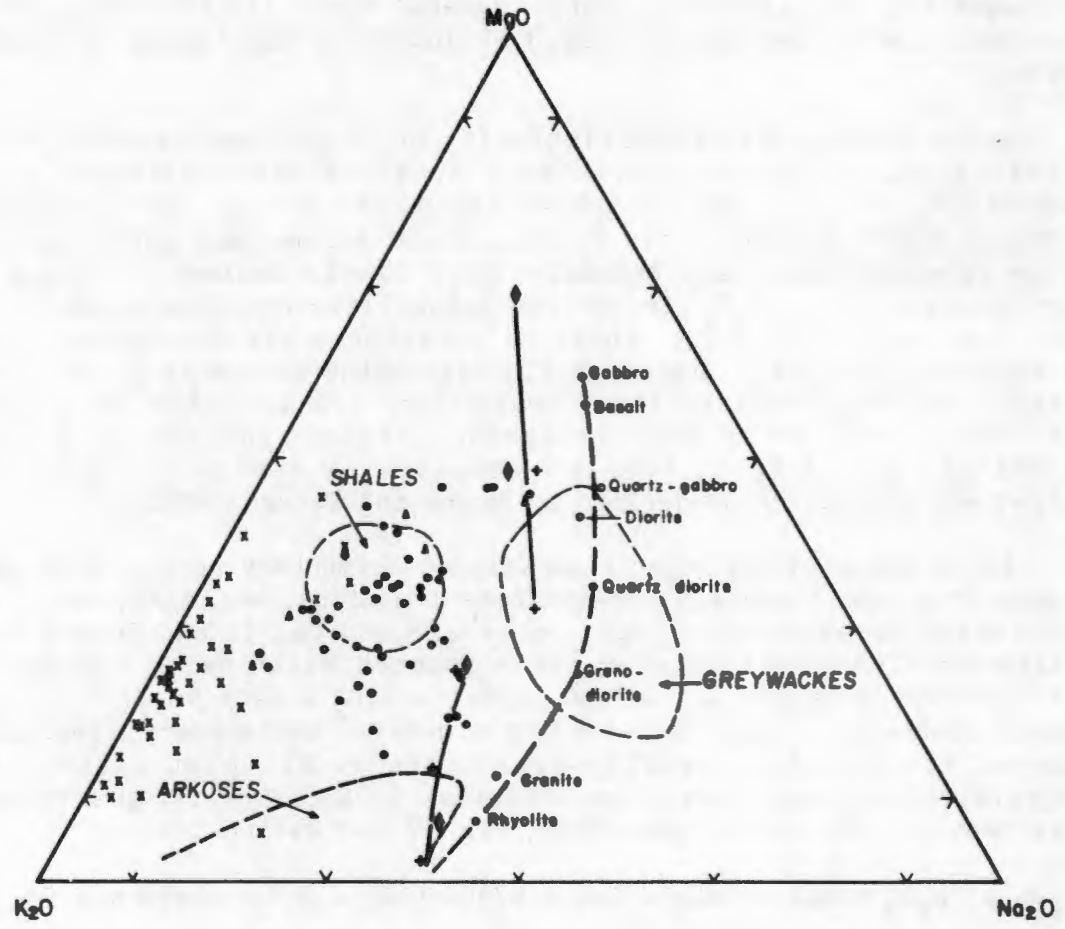

Fig. 7.4 K_2O-Na_2O-MgO triangular diagram showing the fields of arkoses, greywackes and shales together with the normal igneous trend (after de la Roche, 1966). Plotted on the diagram are the metapelitic rocks from the northern (crosses) and south/central (dots) portions of the study area, as well as samples from the Geselskapbank area (triangles). The ingeous trend of the Haib-Vioolsdrif metavolcanic and intrusive suites (+ and ◊) (Reid, 1977) is also plotted for comparative purposes.

and sedimentary precursors, and between the various groups of sedimentary rocks in high-grade metamorphic terranes is thus limited and highly generalised. Nevertheless, the trends displayed by the metapelitic rocks of the study area on these triangular diagrams are not inconsistent with those of typical sedimentary rocks with compositions in the shale-to-greywacke range. It can also be observed that the NMC metapelites show trends markedly different to those of the Haib metavolcanic rocks of the Orange River Group to the immediate north. A close association between these two groups of rocks, with the Haib volcanics either representing source material for, or a lateral volcanic equivalent of, the metapelitic rocks is therefore considered unlikely.

7.4 Comparison with shale and greywacke precursors .

In a second triangular plot, de la Roche (1966) utilized the three major element oxides, K_2O, Na_2O and MgO, that are essentially restricted to the alumino-silicate minerals in sediments, and in this diagram greater separation and discrimination between igneous and sedimentary rocks, based predominantly on their K_2O:Na_2O ratios, is obtained. Whilst there is still considerable overlap between the fields of greywackes and the igneous trend in the region of granodiorites and diorites, more mature sediments such as shales, siltstones and arkoses are distinguished from igneous rocks by higher K_2O:Na_2O ratios and from each other by progressively increasing MgO:K_2O ratios from arkose to shale (i.e. with increasing clay content). The K_2O:Na_2O:MgO diagram can therefore be used to good effect to discriminate between various sedimentary and/or igneous precursors of supracrustal rocks in high-grade metamorphic terranes, provided there has not been considerable modification of the bulk compositions of the rocks by partial melting.

The metapelitic rocks from the NMC study area plot broadly within the field of shales, showing high to extremely high K_2O:Na_2O ratios, well away from the igneous trend and the field of greywackes (Fig. 7.4). The igneous trend defined by the Haib metavolcanics is K-rich relative to normal igneous trends (Reid,1977), but not sufficiently so to overlap with the field of NMC metapelitic rocks to any extent.

The metapelitic rocks from the study area cluster in two distinct groups on the K_2O-Na_2O-MgO plot (Fig. 7.4). One group, dominated by samples from the southern and central, predominantly granulite-facies, portions of the area are concentrated in the area of common shales on the diagram. A second group made up virtually entirely of samples from the northern amphibolite-facies area lies close to the K_2O-MgO tie-line indicating low Na_2O contents and relatively high K_2O contents compared to common shales. As was pointed out in the previous section, these differences were not caused by metamorphic processes, but represent significant premetamorphic differences that indicate the presence of two distinct pelitic types in the western NMC.

The ACF diagram, developed by Eskola (see Winkler, 1976) is a triangular plot designed for the representation and comparison of mineral parageneses and major elementcomposition of metamorphic rocks containing excess silica (as

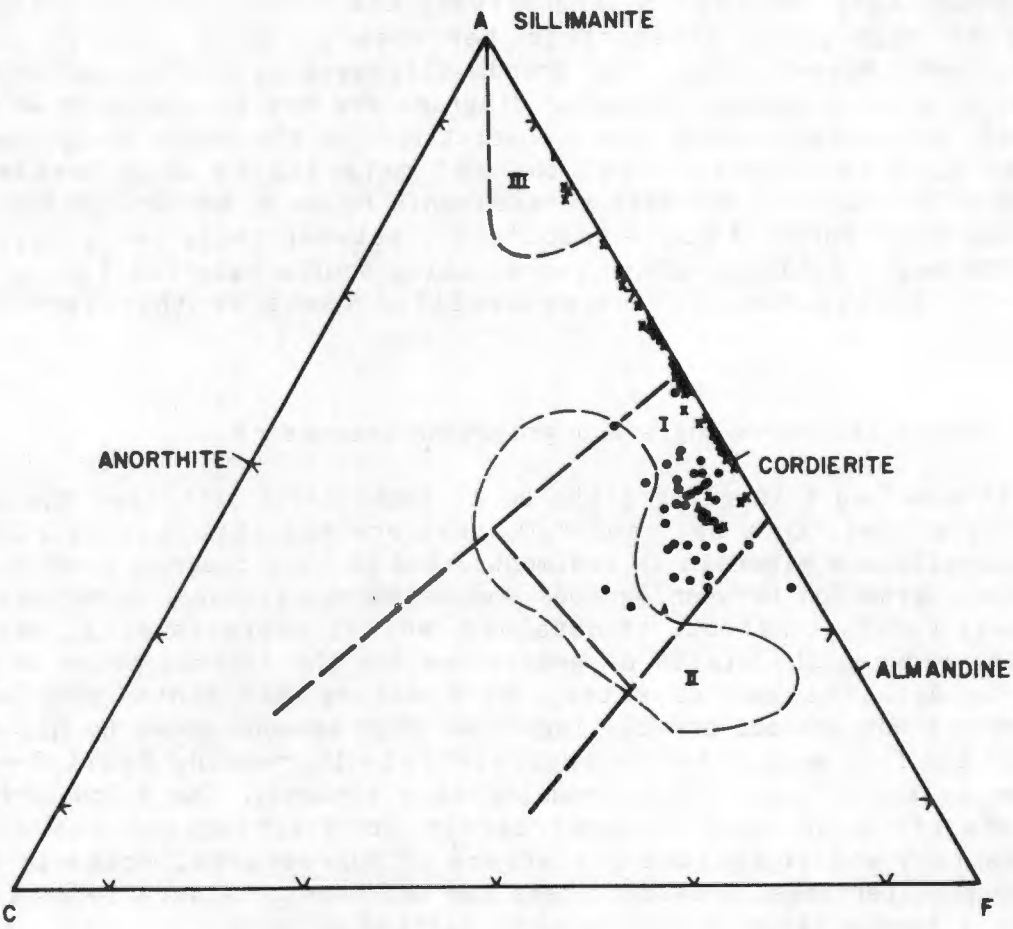

Fig. 7.5 ACF diagram showing the fields of clays and shales containing up to 35% carbonate (I), greywackes (II) and Al-rich clays and shales (III) (after Winkler, 1976), together with metapelitic rocks from the northern (crosses) and south/central (dots) portions of the study area, as well as samples from the Geselskapbank area (triangles).

quartz). The apices of the triangular diagram are represented by the molecular proportions :

$A = [Al_2O_3] + [Fe_2O_3] - [Na_2O] - [K_2O]$

$C = [CaO] - 3.3\,[P_2O_5]$

$F = [MgO] + [MnO] + [FeO]$

after correction for accessory components such as magnetite, ilmenite and sphene. Together with quartz, the potassic and sodic components are excluded from the diagram, removing some of the major mineral phases of pelitic rocks and resulting in the concentration of these lithologies close to the A-F tie-line on the diagram. Winkler (op.cit.) has plotted the fields occupied by various magmatic and sedimentary rocks onto the ACF diagram without applying any special corrections (i.e. for accessory opaques, biotite or muscovite) for comparison with their metamorphosed equivalents.

The metapelitic rocks of the western NMC plot within the field of clays and shales as defined by Winkler (1976) and along the A-F tie-line into the field of Al-rich clays and shales (Fig. 7.5). Their highly depleted C contents exclude them from the field of typical greywackes. In this exercise an Fe_2O_3:FeO ratio of 1:3 was used for the metapelitic rocks, based on the approximate mean of three samples from the Namiesberg (Moore,1977). The samples collected from the southern and central portions of the study area have noticeably greater C and F contents than those from the northern portion which are decidedly A-rich compared to the typical clay/shale field. This may indicate that the south/central metapelites originally contained a significant minor Ca-rich component (plagioclase, calcite ?) whereas the northern metapelites are essentially Ca-free and originally contained a prominent minor Al-rich (or K-Al-rich) component (kaolinite, K-feldspar ?) in varying quantities as demonstated by their spread along the A-F tie-line. As in the case of the K_2O-Na_2O-MgO plot, the ACF diagram reveals significant premetamorphic differences between the two metapelitic types, based in this instance on their Ca and Al components.

Garrels and Mackenzie (1971) have demonstrated that the binary plot $\log[SiO_2/Al_2O_3]$ vs $\log[(CaO + Na_2O)/K_2O]$ is an effective method of distinguishing compositionally between major sediment types and igneous rocks, with the SiO_2:Al_2O_3 factor discriminating between quartz-rich and clay-rich sediments and the $(CaO + Na_2O)$:K_2O factor between carbonate and clastic sediments. Applications to metasediments again carry the assumption of no major bulk loss of Si, Al, K and Na during partial melting.

As in the case of de la Roche's (1966) K_2O:Na_2O:MgO plot, the alkali ratios effectively place the NMC metapelitic rocks outside the range of normal igneous rocks and greywackes, and within the general field of shales and slates. The separation of the south/central and northern metapelitic groups is most pronounced on this diagram (Fig. 7.6) which is the one that was chosen to define which samples belong to each group. The south/central metapelitic rocks cluster within and around the fields of common Palaeozoic shales and

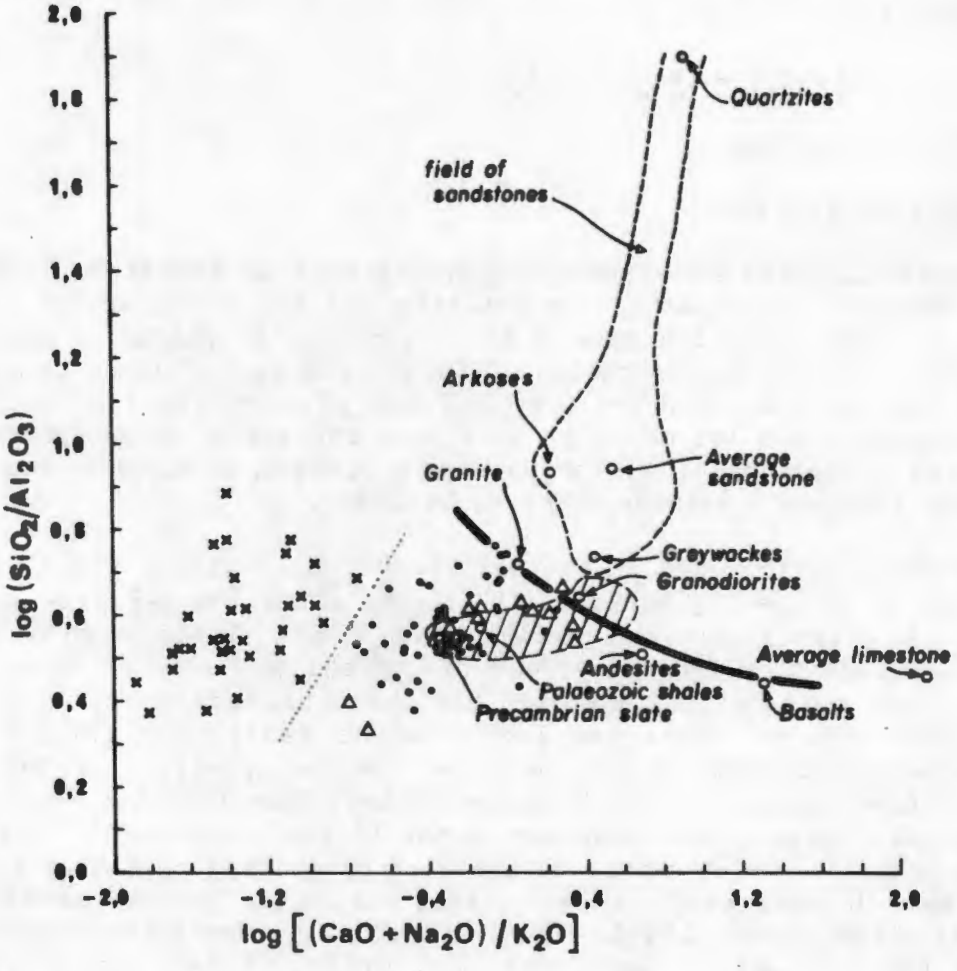

Fig. 7.6 Bivariate plot of log [SiO_2/Al_2O_3] against log [$(CaO + Na_2O)/K_2O$] showing the fields of various sedimentary rocks together with the igneous trend (after Garrels and Mackenzie, 1971). The shaded area represents the field of shales. Also plotted are metapelitic rocks from the northern (crosses) and south/central (dots) portions of the study area as well as the metapelitic rocks and biotite/hornblende schists of the Geselskapbank area (triangles). The dotted line that separates the northern group of metapelitic rocks from those of the south/central group is regarded as the definitive subdivision of these two groups in this study.

TABLE 7.2 Comparison of the major element oxide (%) and trace element (ppm) contents of the two main groups of metapelitic rocks from the study area.

	south/central metapelitic rocks		northern metapelitic rocks	
SiO_2	64.14	(5.52)+	65.40	(6.03)+
TiO_2	0.95	(0.16)	0.76	(0.17)
Al_2O_3	17.68	(2.90)	17.91	(3.52)
FeO*	7.08	(1.60)	5.33	(2.30)
MnO	0.11	(0.09)	0.10	(0.14)
MgO	2.15	(0.70)	1.21	(0.45)
CaO	1.06	(0.63)	0.18	(0.19)
Na_2O	1.42	(0.54)	0.18	(0.16)
K_2O	3.56	(1.30)	3.91	(1.44)
P_2O_5	0.09	(0.05)	0.05	(0.03)
Rb	154	(60)	218	(87)
Ba	914	(343)	728	(651)
Sr	128	(52)	27	(16)
Th	18	(4)	17	(6)
Zr	276	(63)	267	(77)
Nb	16	(3)	16	(3)
Cr	95	(30)	92	(29)
V	105	(23)	93	(48)
Sc	18	(4)	16	(4)
Ni	40	(14)	23	(15)
Co	21	(5)	13	(8)
Pb	23	(8)	21	(19)
Zn	102	(26)	127	(160)
Y	41	(12)	27	(8)
La	41	(9)	26	(10)
Ce	83	(16)	55	(17)
Nd	38	(10)	27	(11)
no. of samples	50		35	

* total Fe as FeO
\+ standard deviation

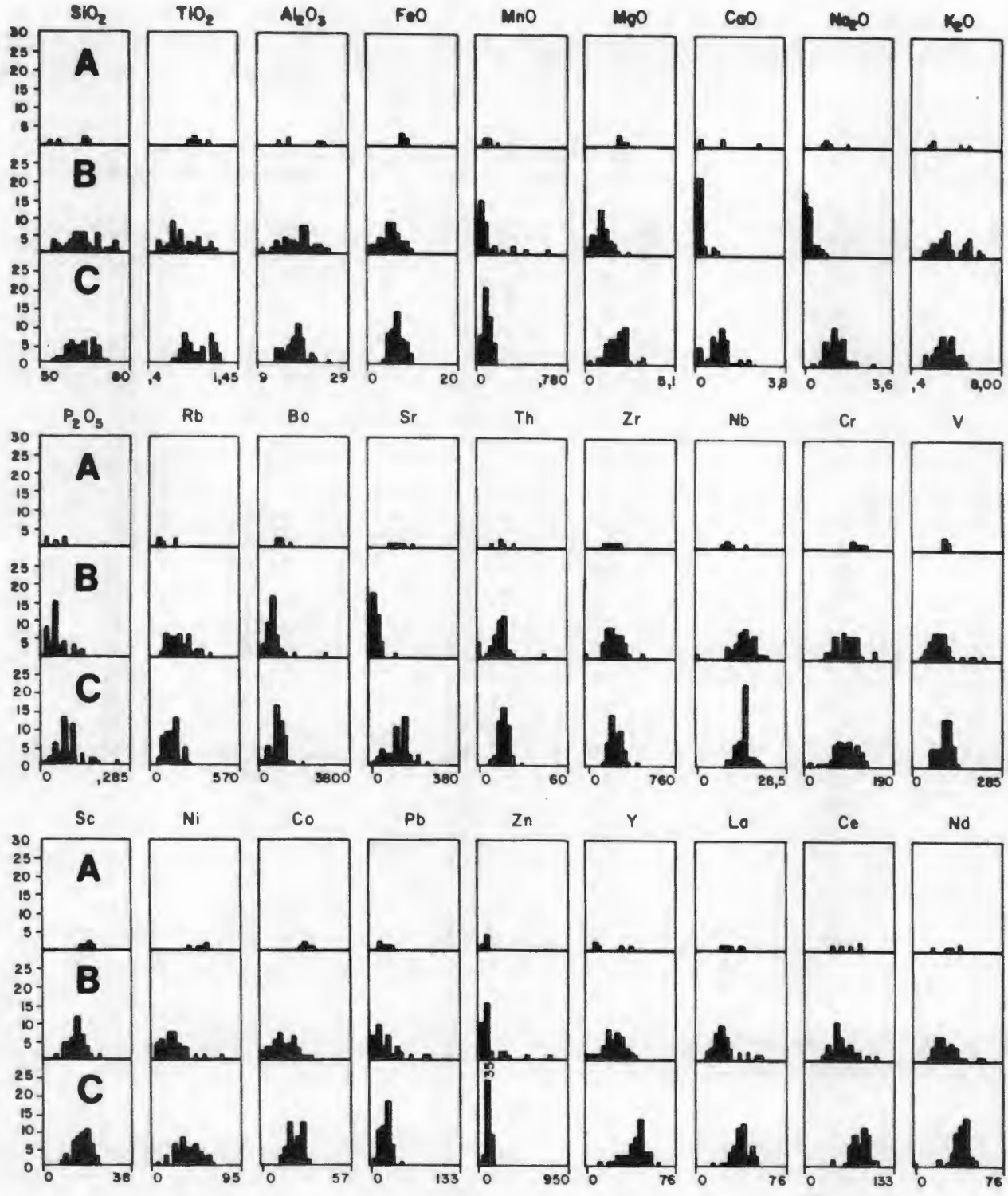

Fig. 7.7 Histograms showing the distribution and range of major element oxides (%) and trace elements (ppm) plotted against number of samples for the Geselskapbank metapelitic rocks (A) and the two major metapelitic groups from the northern (B) and south/central (C) portions of the study area.

Precambrian slates, whereas the northern metapelites reveal their marked (CaO + Na_2O) depletion. Both groups have relatively similar SiO_2:Al_2O_3 ratios.

These latter three plots, making critical use of the ratios of alkali elements within the NMC metapelitic rocks, demonstrate the bulk chemical characteristics which place these rocks within the field of shales and outside the expected range of greywackes and intermediate metavolcanic rocks. It can thus be concluded within this section that the metapelitic rocks of the western NMC, consisting of mica-sillimanite schists and garnet-cordierite gneisses, represent rocks of original mature shale composition, well removed in their composition from igneous rocks and immature sediments such as greywackes and arkoses. The three diagrams also demonstrate the presence of two distinct pelite types, one with chemical compositions identical to common shales, and the other distinguished by a depletion in CaO and Na_2O.

7.5 Comparisons between the two different metapelitic suites

Based primarily on the log plot of Garrels and Mackenzie (1971), the two groups of metapelitic rocks were separated for further statistical analysis. The mean compositions of the two groups are noticeably different (Table 7.2), particularly the major oxides Na_2O, CaO, MgO, FeO and TiO_2 (depleted in the northern metapelites) and K_2O (enriched in the northern metapelites), and the trace elements Ba, Sr, Ni, Co, Y, La, Ce and Nd (depleted in the northern metapelites) and Rb (enriched in the northern metapelites). Certain other elements and oxides, noticeably SiO_2, Zr, Nb, Cr and Pb show no apparent differences between the two groups. All these differences and similarities as well as the ranges of the various elements are displayed on a set of histograms in Fig. 7.7, in which the few Geselskapbank samples can also be compared with the two major populations.

The compositional differences between the two major metapelite groups are also well displayed on various bivariate scatter diagrams, comparing the relative concentrations of two elements or comparing element ratios (Fig. 7.8). Almost complete separation of the two groups is obtained when the trace elements Ce, Y and Sc are plotted against CaO, Na_2O or Sr, indicating that these six elements and oxides are particularly sensitive indicators of changes in the sedimentary environment that existed during deposition of the pelitic rocks of the western NMC. Only minor range overlap occurred in plots using P_2O_5, MgO, Ni, La and Nd, showing that these elements and oxides were also affected by environmental changes in the NMC.

The two groups were separated purely on geochemical grounds, but show obvious differences in their geographical distribution (Fig. 7.9). Only minor overlap occurs within the Buffels River and Stofkraal-Dikmatje paragneiss belts. The geographical and geochemical differences between the two major groups are well-defined and imply significant differences in the source materials from which the original sediments were derived. The northern metapelites could be interpreted as having been derived from source materials depleted in plagioclase (Na_2O and CaO) and mafic minerals (MgO, FeO, TiO_2, Ni, Co) and enriched in K-feldspar (K_2O, Rb) compared to the source materials for

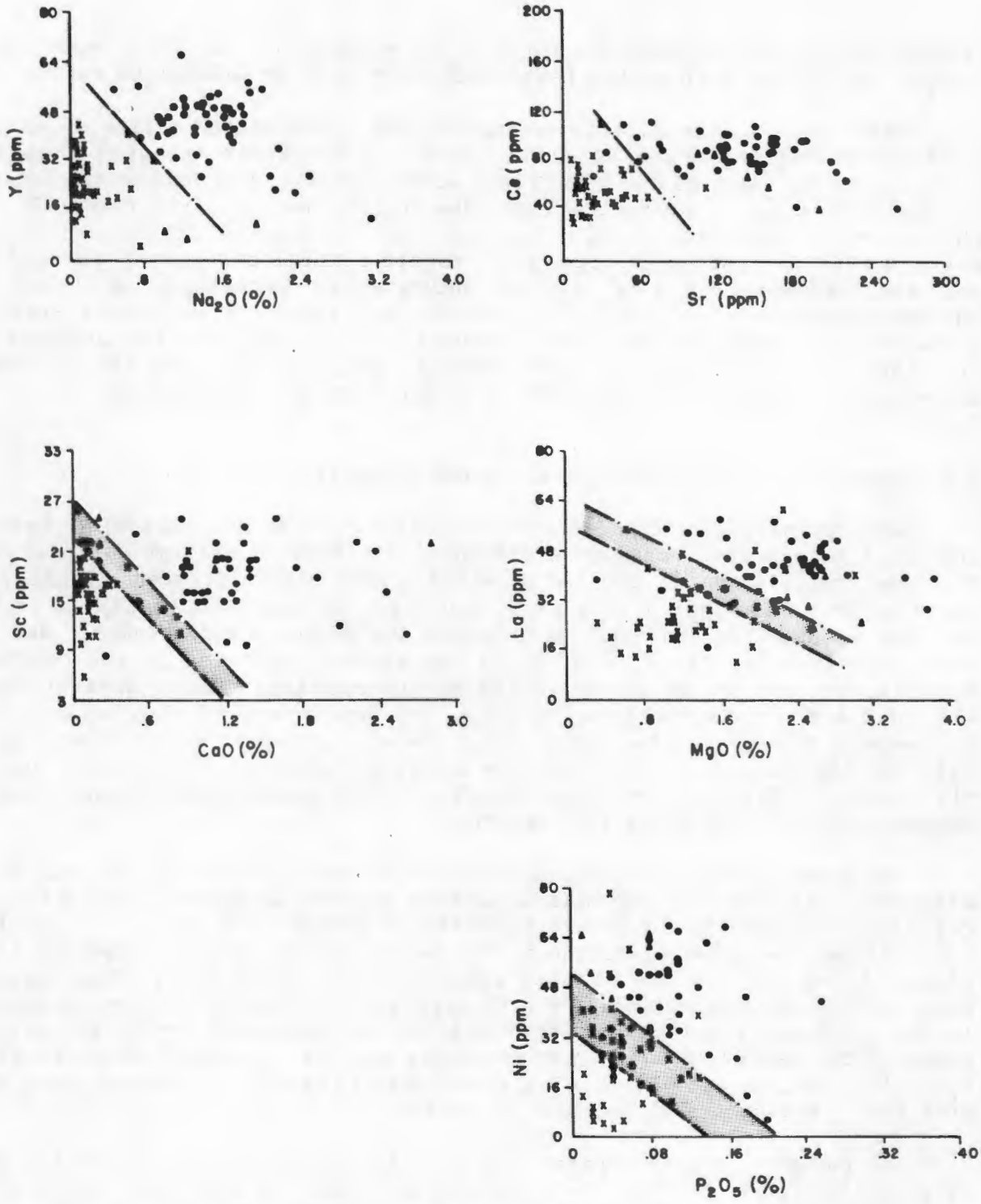

Fig. 7.8 Bivariate scatter plots of major element oxides (Na_2O, CaO, MgO and P_2O_5) and trace elements (Y, Ce, Sr, Sc, La and Ni) showing the relative distributions of the two major groups of metapelites from the northern (crosses) and south/central (dots) portions of the study area as well as samples from Geselskapbank (triangles). The shaded areas on the diagrams represent the areas of overlap of the fields of the two major groups.

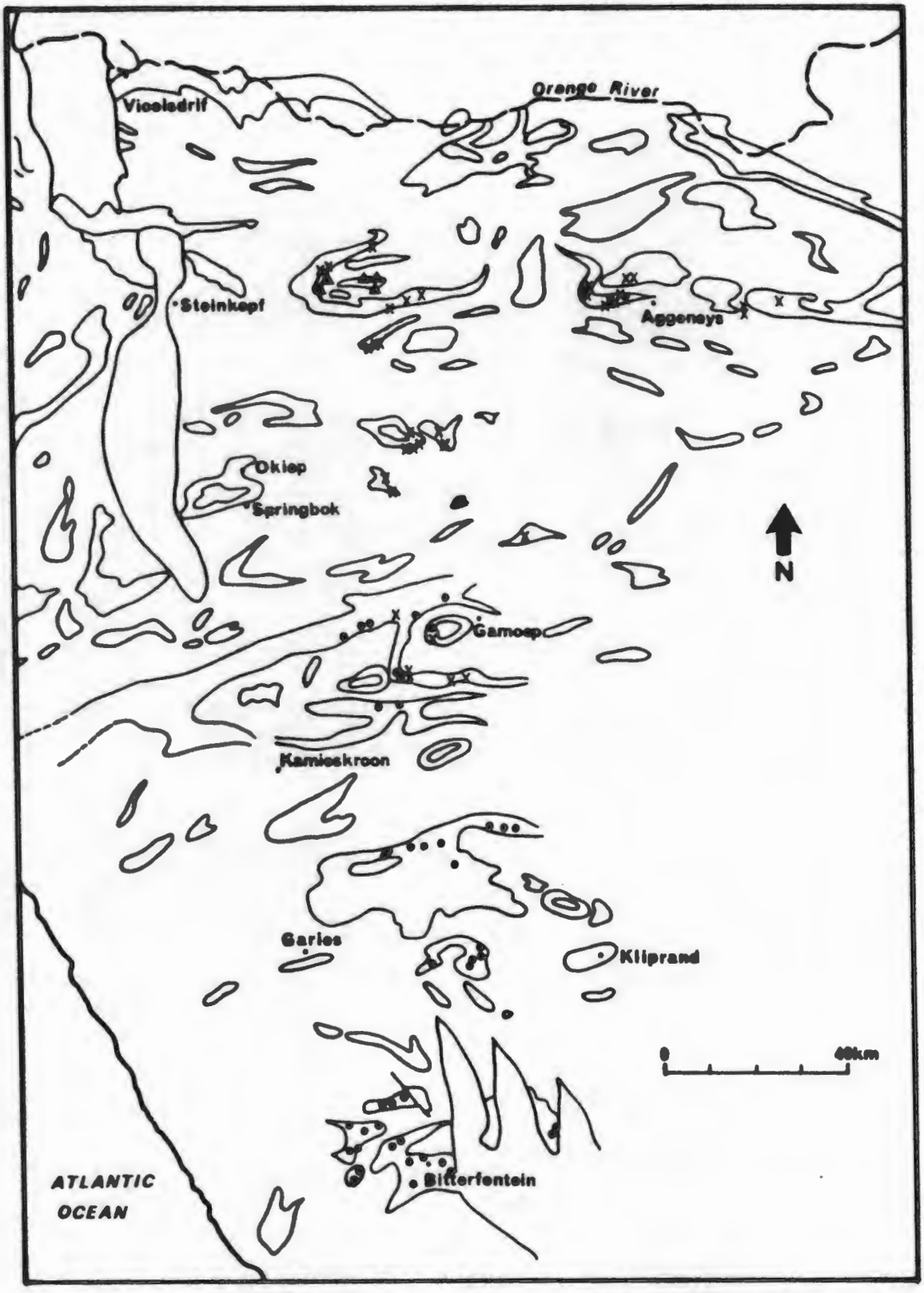

Fig. 7.9 Regional map showing the distribution of the northern (crosses) and south/central (dots) groups of metapelitic rocks. Note the overlap in their distribution in the Gamoep area. The five Geselskapbank samples (triangles) are also shown on the map. Outcrops of major paragneiss belts are outlined.

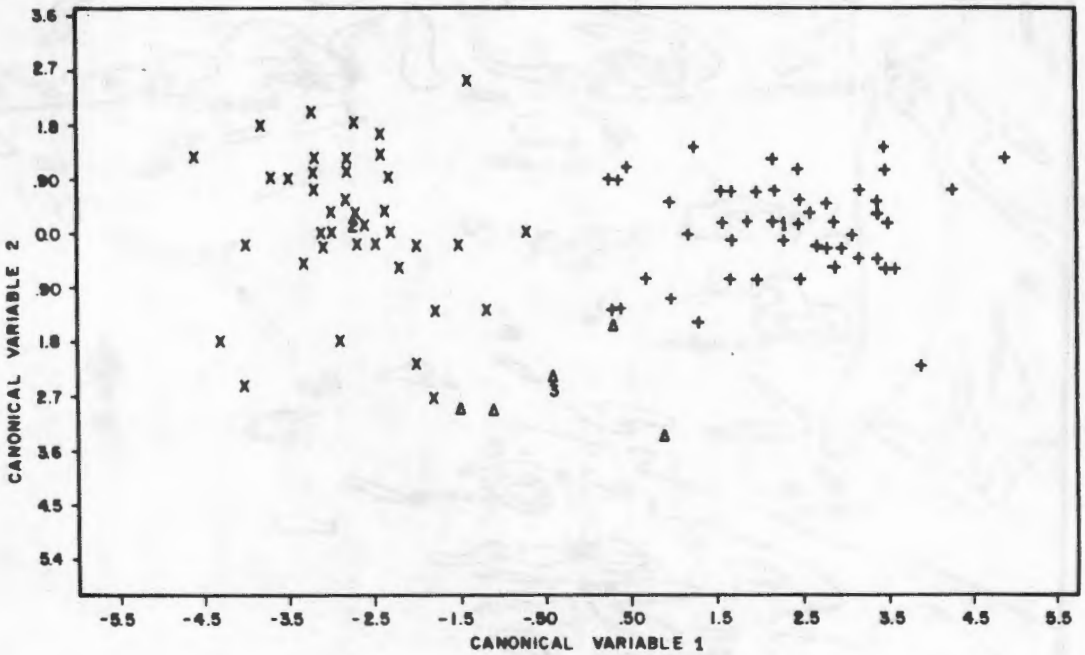

Fig. 7.10 Plot of the two canonical variables calculated in the stepwise discriminant analysis to separate the northern metapelites (x with mean value at 2), the south/central metapelites (+ with mean value at 1) and the Geselskapbank metapelites (Δ with mean value at 3).

the south/central metapelites.

Geochemical studies of metasediments from the Moinian and Dalradian supergroups of Scotland and Ireland (Senior and Leake,1978; Lambert et al., 1981,1982; Winchester et al., 1981; Hickman and Wright,1983) discriminated between metapelitic units in the various groups and subgroups of these divisions using bivariate scatter plots, histograms and factor analysis. Certain elements proved to be most effective in separating the pelitic units, including CaO, P_2O_5, Rb, Sr, Zr, Nb, Ni and Y (and to a lesser extent, Al_2O_3 and Na_2O), whilst other elements including SiO_2, FeO, MgO and K_2O, showed little or no systematic variation between the different units. Similarities are apparent with the NMC metapelites, in which CaO, P_2O_5, Rb, Sr, Ni and Y are significant discriminants between different metapelitic groups, and SiO_2 and K_2O are also generally ineffective. It would appear that, in general, the quartz and K-feldspar/muscovite/illite contents of pelites are relatively insensitive indicators of minor environmental changes whereas lesser constituents such as plagioclase, chlorite, apatite, zircon and perhaps carbonates are more sensitive.

Based on the three observed geochemical divisions within the NMC metapelitic rocks - namely those from the south/central and northern parts of the study area and the Geselskapbank samples - stepwise discriminant analysis was undertaken using computer programme BMDP7M (Dixon, 1981) to calculate canonical discriminant functions which would assist in the classification of these three groups. The total number of cases (metapelite samples) was 92 and the number of variables (major element oxides and trace elements) was 27. The discriminant analysis selected six variables - Na_2O, K_2O, Sr, Co, Y and La - for which coefficients were calculated for two canonical variables (Table 7.3). These two canonical variables successfully segregated the south/central metapelites from the northern metapelites and the northern metapelites from the Geselskapbank samples (Fig. 7.10). One Geselskapbank sample (representing 20% of the sample population) was misclassified with the south/central metapelites.

The two canonical variables can thus be used with confidence to separate samples from the two major metapelitic groups in the study area. They do not, however, convincingly discriminate between the south/central and Geselskapbank samples, due partly to the small sample population of the latter, and the precise interrelationship of these two groups remains an open question.

7.6 Estimations of the precursor mineral assemblages

The major mineral reactions that have taken place in transforming unmetamorphosed pelitic rocks to upper-amphibolite-facies mica-sillimanite schists and granulite-facies garnet-cordierite gneisses in the western NMC have resulted in the chemical redistribution of various elements within these rocks. This makes prediction of the composition of mineral phases that existed in the precursor lithologies extremely difficult. One statistical technique that can be applied to the compositions of the metamorphic rocks (assuming minimal chemical modification during metamorphism) in an attempt to

TABLE 7.3 Coefficients for canonical variables 1 and 2 and the U-statistic from the stepwise discriminant analysis of metapelitic rocks from the western NMC.

Variable	Coefficient for canonical variable 1	Coefficient for canonical variable 2	U-statistic (Wilks' Lambda)
Na_2O	2.165	0.463	0.293
Y	0.079	0.070	0.148
Co	-0.010	-0.124	0.113
K_2O	-0.310	-0.135	0.096
La	0.036	0.007	0.087
Sr	0.007	-0.012	0.078
Constant	-5.384	0.837	

reconstruct the premetamorphic distribution of the elements is principal components analysis.

Principal components analysis "involves no assumption about the original variables" (Marriott, 1974) and therefore, in the following exercises, the calculated factors are unconstrained by the metamorphic petrology of the rocks and can thus be interpreted as element associations related to the original precursor mineral constituents (Lambert et al., 1981, 1982) assuming isochemical metamorphism. Principal components analysis transforms the original set of variables into a new set of variables described as principal components co-ordinates that are uncorrelated with each other and each of which accounts for a certain amount of the variance within the data set (le Maitre, 1982). In practice, only a few sets of principal components co-ordinates generally account for a large proportion of the variance, thus limiting the number of relevant "factors" that need to be considered.

For this exercise, computer programme BMDP4M (Dixon, 1981) was used. The metapelitic rocks of the study area were separated into the two major groups comprising 47 samples of south/central rocks and 41 samples of northern metapelites. The number of variables comprised the same 27 major element oxides and trace elements used in the discriminant function analysis. The computer programme established a correlation matrix on which initial factor extraction was performed by principal components analysis. Eigenvalues were calculated and a varimax orthogonal transformation of the principal factor matrix was performed using Kaiser's (1958) normalization method. Factor loadings between 0.30 and -0.30 were omitted in order to simplify the factors to variables with significant factor loadings. Factors accounting for less than 4% of the variance were also ignored.

One property of chemical analyses which has a considerable effect on statistical techniques such as principal components analysis, is that of constant-sum closure. Because the major element oxides in a whole rock analysis must sum to 100%, one of these oxides cannot increase without others decreasing. Closure thus invalidates the use of the null hypothesis and results in correlation coefficients being considerably more negative than obtained for ordinary data (le Maitre, 1982). The most marked effect of closure on statistical techniques applied to the chemical compositions of rocks in this study involves SiO_2. As a result of closure, most other major element oxides show negative correlations with SiO_2, the dominant variable in the data set. This must be borne in mind when examining the various factors below. Fortunately, a large amount of the SiO_2 in sedimentary rocks commonly indicates the presence of detrital quartz which will also dominate within the mineralogical constituents, and to which the other constituents will show negative correlations.

In the case of the data set for the south/central metapelites, six varimax rotated factors were calculated which cumulatively accounted for 76.5% of the variance (Fig. 7.11). In the case of the data set for the northern metapelites, seven varimax rotated factors were calculated which cumulatively accounted for 81.7% of the variance (Fig. 7.12). A successful factor analysis explains a large proportion of variance with a very few factors (Dixon, 1981).

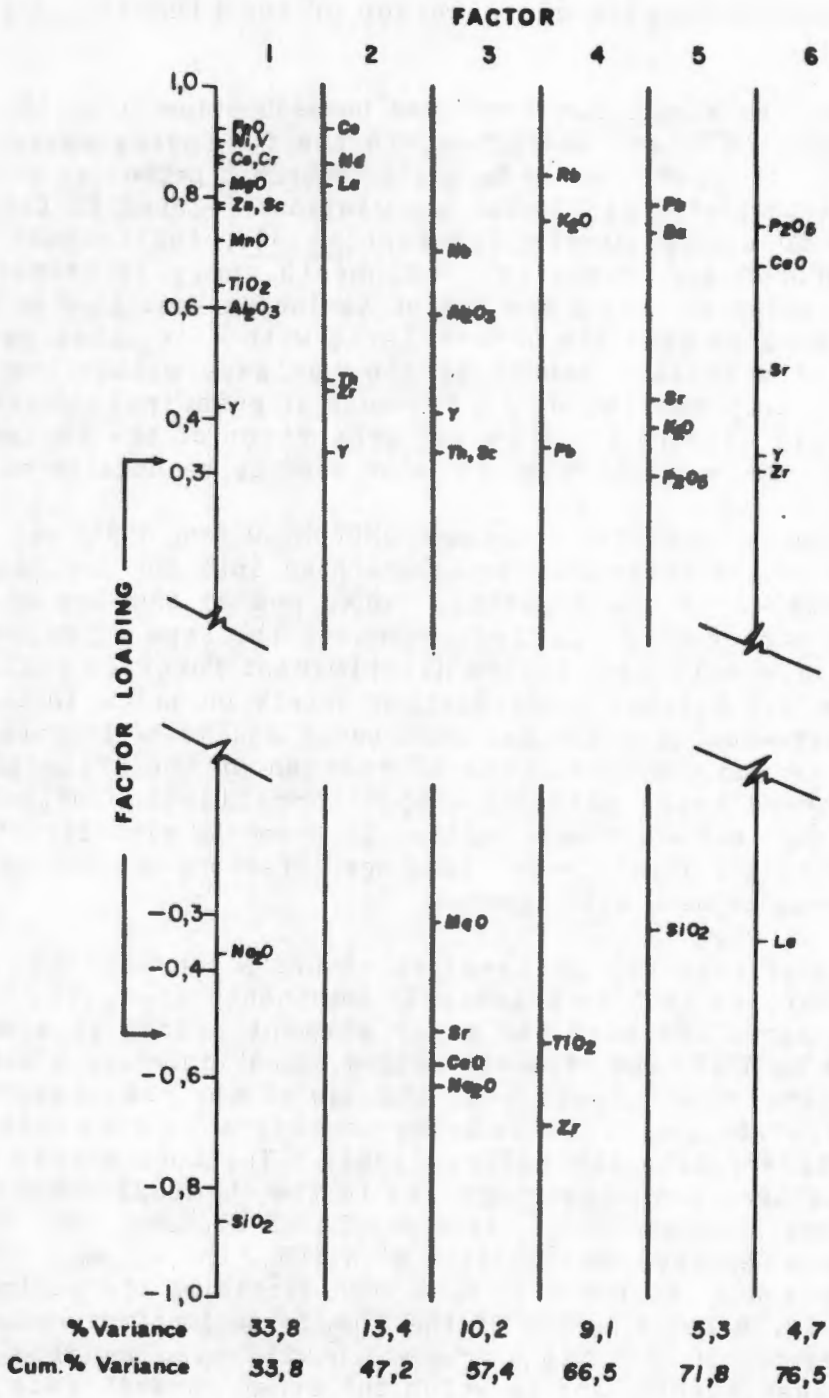

Fig. 7.11 The six major factors together with the factor loadings of the variables and their cumulative variance obtained in the principal components analysis of the metapelitic rocks from the south/central portions of the study area.

Pelitic rocks, however, can contain a variety of mineral constituents. The number of factors obtained in these two analyses (6 and 7) covering ± 80% of the variance, is, therefore, not unacceptably high.

Considering initially the south/central metapelites (Fig. 7.11), factor 1 has high positive loadings for FeO, MgO, MnO, TiO_2 and Al_2O_3 and the trace elements Ni, V, Co, Cr, Zn and Sc, and a high negative loading for SiO_2. This is the "closure factor" and in the sedimentary environment is interpreted as an inverse relationship between a fine-grained chlorite/clay component and detrital quartz. This factor accounts for just under half of the variance contained in the six factors. Factor 2 incorporates Ce, La, Nd, Th and Zr, and represents a heavy-mineral component comprising zircon and perhaps monazite. Factor 3 has high positive loadings for Al_2O_3 and Nb, and high negative loadings for Na_2O, CaO and Sr with significant negative MgO. The inverse relationship between Al_2O_3 and (Na_2O + CaO) appears at first to rule out the presence of plagioclase in this factor which might be interpreted as an antithetic relationship between clay minerals and carbonate/evaporite minerals. The close association of Na_2O and CaO, however, makes an alternative explanation - that there is an inverse relationship between fine-grained kaolinite clay (with Al_2O_3 content of 40%) and coarser-grained detrital plagioclase (with Al_2O_3 content of 25%) equally plausible. Factor 4 has high positive loadings for K_2O and Rb and negative loadings for TiO_2 and Zr, and is interpreted as a fine-grained illite/sericite clay opposed to a coarser heavy-mineral detrital component of ilmenite/rutile and zircon. Factor 5 is a possible sulphate/sulphide factor (Ba,Pb) and factor 6 represents apatite (P_2O_5, CaO, Sr).

This interpretation of element interrelationships within the south/central metapelites suggests that these rocks comprised mixtures of quartz, chlorite, kaolinite, plagioclase (or calcite plus analcite), illite, zircon, ilmenite/rutile, possible barite and galena, and apatite. The principal components analysis has proved to be an extremely sensitive technique, and has identified very minor constituents of the pelitic rocks such as zircon and apatite.

The seven factors identified for the northern metapelites show both similarities and differences in comparison to the six factors obtained for the south/central metapelites (Fig. 7.12). Factor 1 has high positive factor loadings for CaO, Na_2O, MgO, FeO and TiO_2 as well as the trace elements Sr, Ni, Co, Cr and Sc, and a high negative loading for SiO_2. This factor accounts for about a third of the cumulative variance of the seven factors. The presence of CaO and Na_2O and the relatively minor factor loading (0.25) of Al_2O_3 compared to factor 1 of the south/central metapelites, indicate that chlorite may not be the major mafic constituent of these pelitic rocks, but rather that a "basaltic" detrital component, perhaps plagioclase and pyroxene or hornblende, is present.

Factor 2 incorporates Ce, Nd, La, Th and Sc, but lacks the presence of Zr, indicating that the rare earth mineral present is likely to have been monazite and/or allanite rather than zircon. Factor 3 is totally different to any factor observed in the south/central metapelites and can be described as

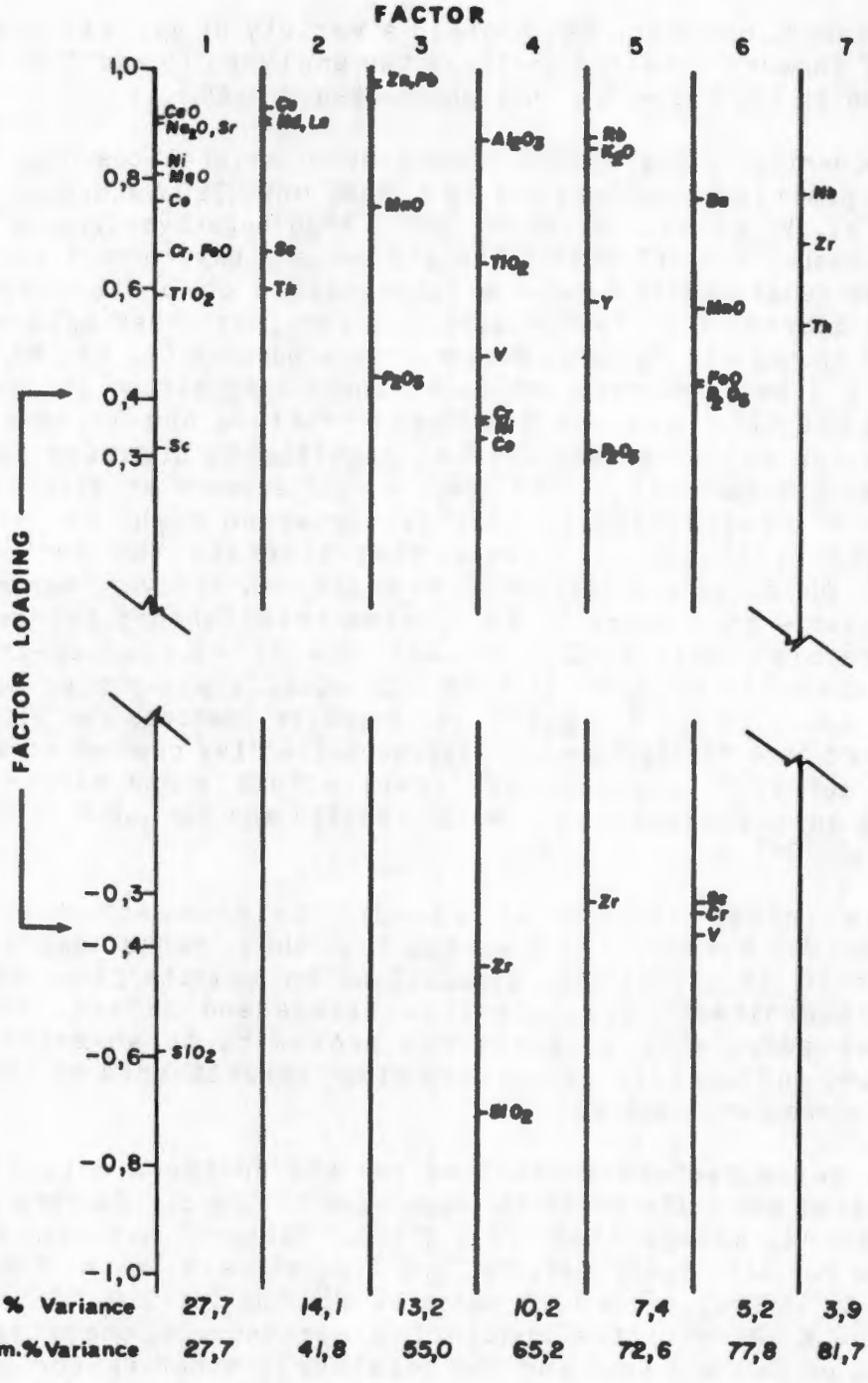

Fig. 7.12 The seven major factors together with the factor loadings of the variables and their cumulative variance obtained in the principal components analysis of the metapelitic rocks from the northern portions of the study area.

the "Aggeneys" factor, incorporating Zn, Pb, MnO and P_2O_5 which are major constituents of the sulphide deposits at Aggeneys and Gamsberg (Rozendaal,1980; Ryan et al., 1982). Factor 4 in the northern metapelites has high positive factor loadings for Al_2O_3 and TiO_2 and a high negative loading for SiO_2. This factor can be interpreted as an inverse relationship between kaolinite plus ilmenite/rutile (the "Swartkoppies" component - after the sillimanite-ilmenite-rutile rocks located at the Swartkoppies mine and elsewhere in the Pofadder area, Frick and Coetzee,1974) and detrital quartz (plus minor zircon). This factor is partially similar to factor 3 of the south/central metapelites which showed an inverse relationship between Al_2O_3 and a plagioclase component.

Factor 5, like factor 4 of the south/central metapelites, is dominated by high positive factor loadings for K_2O and Rb, and suggests an inverse relationship between a K-feldspar/muscovite/illite component and detrital zircon. Factor 6, like factor 5 of the south/central rocks, is dominated by Ba. The association of Ba, FeO, MnO and P_2O_5 in this factor is comparable with the magnetite-barite deposits at Aggeneys and Gamsberg (Mathias,1940a; Coetzee,1958). Factor 7 of the northern metapelites represents detrital zircon.

An interpretation of the premetamorphic mineral constituents of the northern metapelites based on the principal components analysis is: quartz, detrital plagioclase/pyroxene/hornblende (or chlorite), kaolinite, K-feldspar/muscovite/illite, Pb- and Zn-sulphides with Fe- and Mn-oxides, barite, apatite, ilmenite/rutile, monazite/allanite and zircon. The principal components analysis suggests further that there are certain specific groups of elements within the northern metapelites which come from a common source. Of particular interest are the factors related to sulphide (Zn, Pb, Mn, P) and sulphate (Ba, Fe, Mn, P) mineralization and the Al-Ti factor, which are similar to the base metal/barite deposits and sillimanite-rich rocks that occur as distinct units in their own right within the northern metapelitic rocks. The presence of these factors in the northern metapelites, but not in the principal components analysis of the south/central metapelites, adds strength to the credibility of the principal components analysis, and suggests that the processes which formed these sulphide/sulphate and Al-rich rocks were also operative during the deposition of the enclosing metapelitic rocks themselves.

Factor analysis undertaken by Lambert et al., (1981,1982) of Moinian and Dalradian metasediments, reveals similar relationships to those found in the NMC metapelites. These include a factor containing inverse relationships between a biotite/chlorite phase (with positive factor loadings for Fe, Mg, Ni, Zn, Ti and Al) and SiO_2; a factor containing opposite factor loadings for Al and SiO_2; a factor with positive loadings for K, Rb, Ba and Al that is interpreted as representing illite; and factors interpreted as representing zircon, apatite and sulphides. Lambert et al., (1981) state that "factor analysis can prove a useful means for unravelling the present and past mineralogy of metasediments, even to the extent of picking out accessory minerals which are only present in trivial amounts".

TABLE 7.4 List of model mineral compositions used in the least-squares mixing exercise.

	1.	2.	3.	4.	5.	6.	7.	8.
SiO_2	0.11	51.22	45.87	51.14	45.77	22.66	58.16	63.66
TiO_2	48.90	0.01	0.01	0.01	0.01	0.01	0.01	0.01
Al_2O_3	0.54	25.91	38.69	19.76	39.07	17.64	26.57	19.54
FeO*	49.02	5.83	0.01	0.74	0.31	37.85	0.01	0.09
MgO	0.56	2.84	0.10	3.22	0.08	9.96	0.01	0.01
CaO	0.65	0.16	0.01	1.62	0.26	0.01	8.35	0.50
Na_2O	0.01	0.17	0.64	0.11	0.17	0.01	6.92	0.80
K_2O	0.01	6.09	10.08	0.04	0.31	0.01	0.01	15.60

* total Fe as FeO

1. ilmenite 2. illite 3. muscovite 4. montmorillonite 5. kaolinite

6. chlorite 7. plagioclase 8. K-feldspar

All analyses from Deer et al., (1971) except 6. and 7. which were estimated from mean Mg:Fe and Ca:Na ratios of the NMC metapelitic rocks respectively.
Quartz and dolomite were assumed to be pure phases.

Using the major mineral constituents predicted by the principal components analysis to have been present in the metapelites of the study area, namely quartz, chlorite, K-feldspar/muscovite/illite, kaolinite, plagioclase (or calcite plus analcite) and ilmenite, a mixing exercise was undertaken to ascertain the amounts in which they would have occurred in the original sediments. The computer program MIXER (compiled by A.R. Duncan, Geochemistry Department, U.C.T.) which employs a least-squares approximation technique (after Bryan et al., 1969), was used to obtain the closest approximations to the major element compositions of the individual metapelitic rocks by mixtures of these mineral phases. The components comprised 8 major element oxides - SiO_2, TiO_2, Al_2O_3, total Fe as FeO, MgO, CaO, Na_2O and K_2O, and the metapelite sample suite was once again split into the two south/central and northern groups for comparative purposes.

The compositions used for quartz, montmorillonite, K-feldspar, calcite, analcite and dolomite were those of the pure phases, whereas kaolinite and illite compositions were taken from Deer et al., (1971). Due to the near constant Fe:Mg ratio within the metapelites, a chlorite composition with a similar Fe:Mg ratio was used in the exercise. In instances where an excess of Fe or Mg was present, a more Fe-rich or Mg-rich chlorite was used with compositions taken from Deer et al., (op.cit.). A calculated plagioclase component was deduced from the mean Na:Ca ratio of the metapelites. The various mineral compositions employed are listed in Table 7.4.

For the south/central metapelites, solutions with the least sums of squares of differences (i.e. the closest approximations) comprised quartz, illite, chlorite, ilmenite and plagioclase or analcite plus calcite (Table 7.5). Relatively few samples required kaolinite and/or K-feldspar components and three samples appeared to contain a significant minor dolomite component ($\pm$10%). The compositions of the northern metapelites were best approximated using quartz, illite, K-feldspar, kaolinite, chlorite and ilmenite (Table 7.5). Relatively few samples contained a minor plagioclase component. Whilst the average quartz, chlorite and potassic mineral contents of the two groups of metapelites were similar, marked differences occurred in the contents of kaolinite which predominated in the northern metapelites (3% vs 17%), and plagioclase which predominated in the south/central rocks (13% vs 1%). K-feldspar (or perhaps a more K-rich illite) was also commoner in the northern metapelites (5% vs 14%) and illite in the south/central group (38% vs 26%).

The presence of K-feldspar and kaolinite in model premetamorphic mineral phases of the northern metapelites could indicate a near-shore environment with detrital K-feldspar and kaolinite derived from continental/terrestrial weathering. Detrital pyroxene or hornblende may also be present in small amounts as mentioned above in the principal components analysis section. The source material of the northern rocks, however, must have been extremely plagioclase-poor. Likely source materials appear to have been either highly potassic granites or rhyolites.

The south/central metapelites, unlike their northern equivalents, appear to have been more mature, consisting of mixtures of illite (dominant) and chlorite (minor) with quartz. A relatively strong plagioclase component

TABLE 7.5 Estimated proportions of premetamorphic constituents in the two major groups of metapelitic rocks, based on least-squares approximations.

Mineral constituent	South/central metapelites (n = 48)		Northern metapelites (n = 40)	
	%		%	
	mean	range	mean	range
quartz	29	17 - 44	32	12 - 57
K-feldspar	6	0 - 30	14	0 - 42
illite	36.5	0 - 66	26	0 - 68
kaolinite	3	0 - 22	17	0 - 42
plagioclase	13.5	5 - 32	1	0 - 10
chlorite	9	4 - 18	8	0 - 20
ilmenite	2	1 - 2	2	1 - 2
dolomite	1	0 - 10	0	0
Sum of squares of differences	0.17	0.02 - 0.57	0.13	0.00 - 0.42

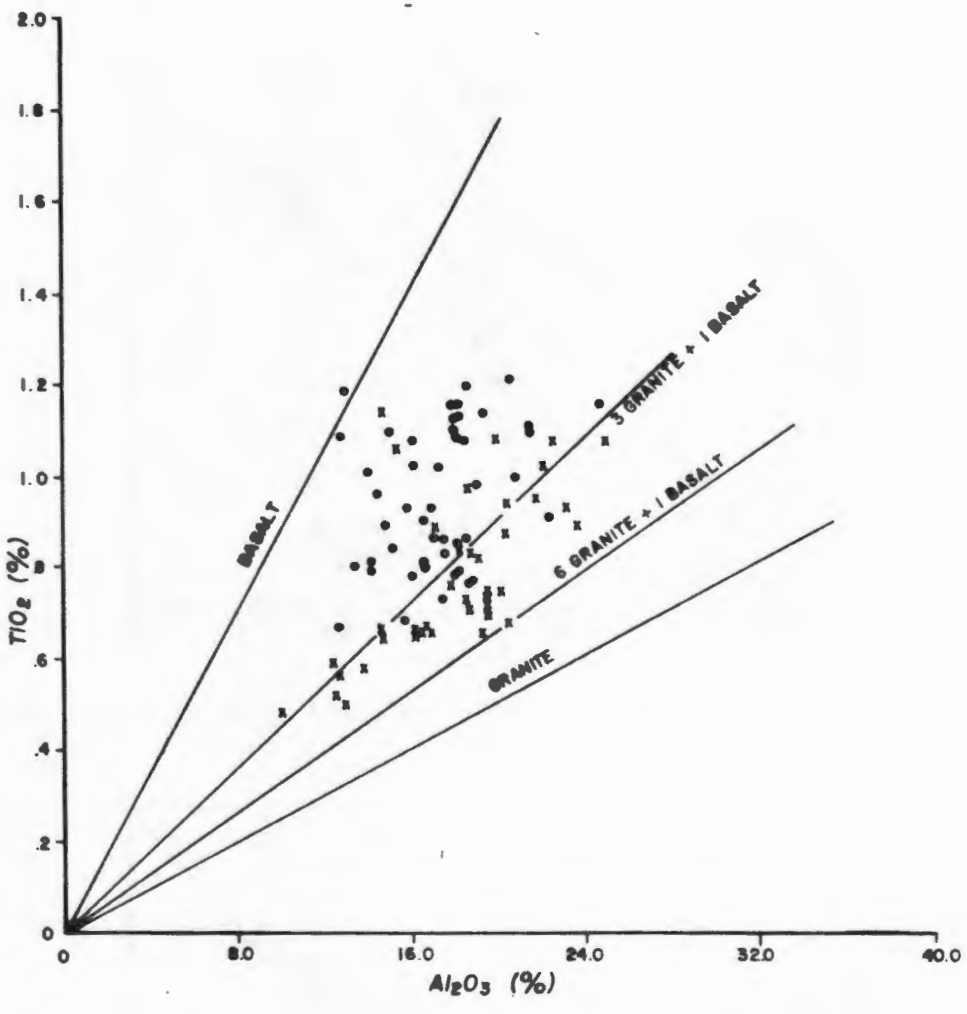

Fig. 7.13 TiO_2:Al_2O_3 plot of metapelitic rocks from the south/central (dots) and northern (crosses) portions of the study area in comparison to the approximate ratios for basalt, granite and certain selected basalt/granite mixtures.

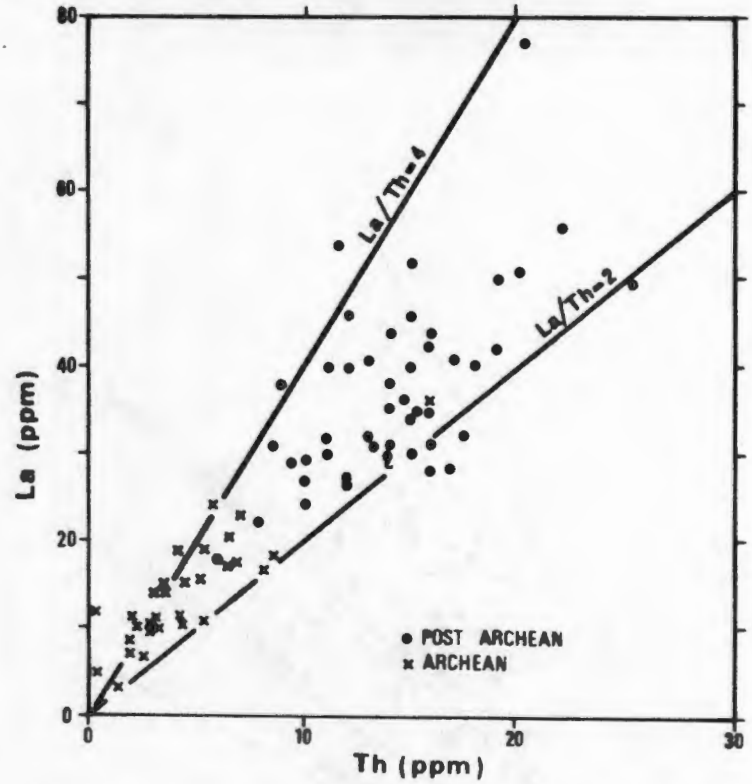

Fig. 7.14a La:Th plot for Archaean and post-Archaean shales (after McLennan et al., 1980).

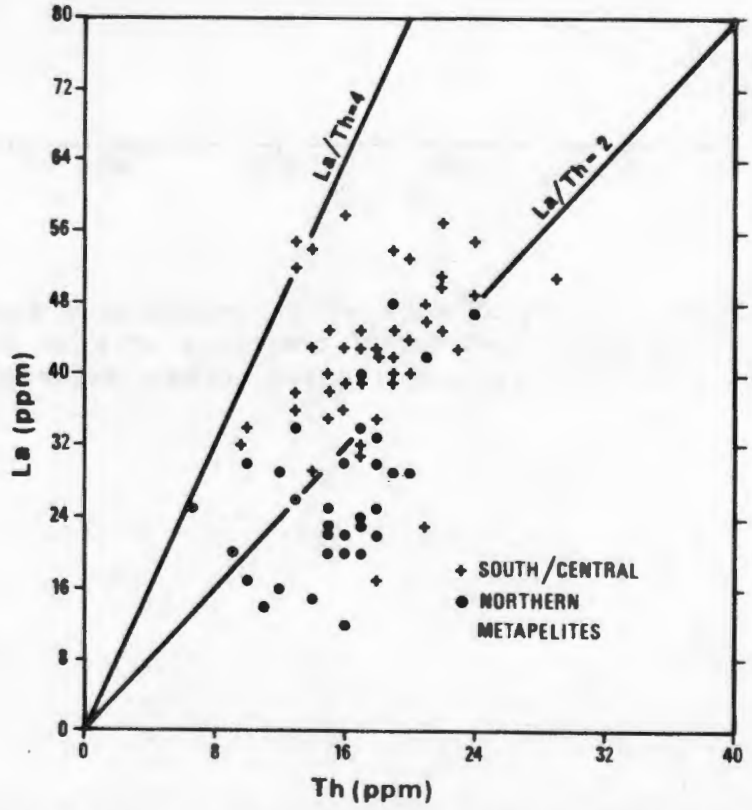

Fig. 7.14b A similar La:Th plot for the metapelitic rocks of the study area.

implies a different source material, perhaps of more granodioritic composition or a mixture of granitic and more basic rocks. A few samples appeared to contain a dolomite constituent, indicating deposition in a marine environment. Certain metapelitic rocks in the Gamoep/Kangnas area showed transitional compositions between the two groups, i.e. mixtures containing both plagioclase and kaolinite, indicating that mixing of the two pelitic types could have occurred in this region.

7.7 Evidence of source materials for the metapelitic rocks

The TiO_2:Al_2O_3 ratios of basaltic rocks are considerably higher than those of granites, and this characteristic can be used to estimate the amounts of end-member components basalt and granite required to derive various sedimentary rocks with intermediate TiO_2:Al_2O_3 ratios. When comparing the TiO_2:Al_2O_3 ratios of the two metapelitic groups from the study area (Fig. 7.13), it is apparent that the bulk of the northern metapelites have considerably lower ratios than the south/central metapelites, implying that they were derived from a more granite-dominated source. The northern metapelites have, on average, ratios similar to a 4:1 mixture of granite and basalt, whereas the south/central metapelites have a mean TiO_2:Al_2O_3 ratio similar to a 2:1 granite-to-basalt mixture. Significantly this diagram does not make use of the alkali elements in coming to these conclusions, as have many of the previous plots, but instead relies on two of the most immobile of the major element oxides. These findings are supported by the other major element oxides which showed relative enrichment in K-feldspar components in the northern metapelites and plagioclase and mafic mineral components in the south/central metapelites as discussed in Section 7.6.

Virtually no thorium or rare earth element loss takes place during the erosional and depositional cycles of detrital sediments. Common sedimentary processes (including diagenesis) and metamorphism (with the exception of granulite-facies grades involving considerable partial melting; Heier,1978) appear to have little effect on the distribution of these elements (McLennan *et al.*, 1980). The La/Th ratios of sedimentary and metasedimentary rocks, therefore, broadly reflect the La/Th ratios of the source material from which they were derived. In igneous rocks, there is a progressive increase in the La/Th ratios from granites and granodiorites (La/Th = 2) to basalts (La/Th = 8) and peridotites (La/Th = 15) (McLennan *et al., op.cit.*). Most common fine-grained sedimentary rocks from the Archaean to the Phanerozoic have La/Th ratios between 2 and 4, indicating the predominance of a felsic component in their source material (Fig. 7.14a).

The La/Th ratios of the NMC metapelites reveal significant differences between the northern and south/central metapelite groups (Fig. 7.14b). The south/central rocks have La/Th ratios (mean 2.5) typical of post-Archaean fine-grained sediments derived from felsic (i.e. granitic-granodioritc) sources. The northern metapelites, however, have anomalously low La/Th ratios (mean 1.8) indicating that they were probably derived from highly fractionated felsic sources such as potassic granites or rhyolites. The evidence of the low La/Th ratios in these latter rocks supports the conclusions derived from the

TABLE 7.6 Comparison of La and Th contents of the NMC metapelites with greywackes from active and passive continental margins (after Bhatia and Taylor, 1981).

Rock type		Abundance (ppm)		La/Th
		La	Th	
Arc-derived greywackes	andesitic source rocks	9.2 ± 1.7	1.4 ± 0.6	6.6
Continental-margin greywackes	granitic and sedimentary source rocks	39 ± 9.9	16 ± 0.6	2.4
NMC northern metapelites		26 ± 13	14.5 ± 7.7	1.8
NMC south/central metapelites		42 ± 8.4	18 ± 3.8	2.5

CaO-Na_2O-depleted, K_2O-enriched bulk compositions of these metapelites and their low TiO_2:Al_2O_3 ratios.

The abundances of Th, U and rare earth elements (REE) in mudrocks and greywackes increases from active continental margins (i.e. calc-alkaline volcanic arcs) to inter-arc basins and passive continental margins (Bhatia and Taylor, 1981). This characteristic is related to the composition of the source rocks with the former sedimentary environment containing a dominant andesitic source component with low Th, U and REE abundances, and the latter containing a prominent felsic volcanic (inter-arc basin) or granitic (passive margin) component with considerably higher abundances (Table 7.6). Within the NMC, the northern metapelites have considerably lower abundances of Th and REE's than the south/central metapelites, but not sufficiently low to imply a source from andesitic volcanics. The northern metapelites have Th and La abundances intermediate between greywackes from active and passive continental margins and similar to the inter-arc basin deposits of Bhatia and Taylor (op.cit.). The south/central metapelites have abundances similar to passive continental margins (Table 7.6). There is thus no evidence to suggest that the NMC paragneisses in the north are sedimentary equivalents of the andesitic volcanism within the Orange River Group, but rather that the metapelitic rocks were derived from the erosion of acidic volcanics in the north and granitic rocks in the south.

7.8 Estimations of the palaeoclimate during deposition

The metapelitic rocks of the western NMC have been derived from parental material dominated by components of granitic composition, and thus dominated by feldspars and quartz. The weathering processes concerned in forming the pelitic precursors of these rocks, therefore, essentially involve the breakdown of feldspars and the formation of clays such as illite and kaolinite. A measure of the degree of weathering, termed the chemical index of alteration (CIA) has been used by Nesbitt and Young (1982) as an estimate of climatic conditions existing during the formation of pelitic rocks. The chemical index of alteration is calculated from the formula :

$$CIA = [Al_2O_3/(Al_2O_3 + CaO^* + Na_2O + K_2O)] \times 100$$

using molecular proportions, where CaO* represents the amount of CaO in silicate form (i.e. correction is made for carbonate and apatite content). Granites and granodiorites have CIA values of the order of 45 to 55 whereas shales and residual clays have much higher values (70 to 90). Glacial tills and clays are formed primarily by mechanical processes at low temperatures and thus have low CIA values similar to their source material (Fig. 7.15). Nesbitt and Young (op.cit.) propose that the CIA can thus be used as an indicator of the palaeoclimate during the formation of ancient pelitic rocks (lutites) with low CIA values indicating cold climates and high CIA values hot, humid ones.

Metamorphism of the western NMC metapelites is not expected to have changed the CIA value significantly, and therefore the index has been applied

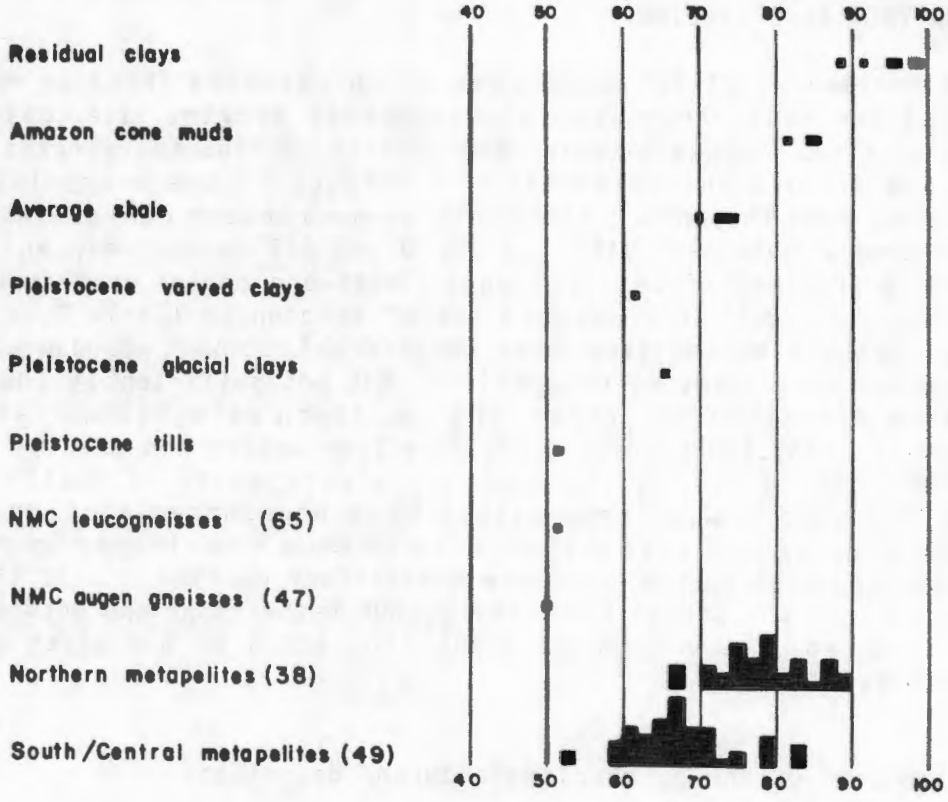

Fig. 7.15 Estimations of the chemical index of alteration (CIA) for the metapelitic rocks of the study area compared to potential source materials (NMC leucogneisses and augen gneisses) and various recent pelitic sediments (after Nesbitt and Young, 1982). Number of samples in brackets.

to these rocks. Comparisons of the CIA values of the metapelitic rocks of the northern and south/central portions of the western NMC with various pelitic rocks from cold to hot climates, and with their potential source material (augen gneisses and leucogneisses from the western NMC) are made in Fig. 7.15. It can be seen that the metapelitic rocks from the two areas have different CIA distributions with the northern metapelites having a mean value of 78.5 and the south/central metapelites a mean value of 68. An interpretation of the data following Nesbitt and Young (1982) would be that the two pelitic suites formed under somewhat different climatic conditions. The south/central metapelites would appear to have formed under relatively cold climatic conditions, slightly colder than those of average shales, and the northern metapelites under considerably hotter conditions, slightly warmer than the temperate climates preferred by common shales. Extreme temperatures - either very cold, glacial (with CIA values < 57) or very hot, humid (with CIA values > 90) - do not appear to be represented in the metapelitic suites of the western NMC.

Chapter 8

GEOCHEMISTRY OF THE QUARTZO-FELDSPATHIC GNEISSES

8.1 Introduction

Associated with the metapelitic rocks in virtually all of the major paragneiss belts of the western NMC, commonly in considerably greater proportions than the metapelites themselves, are various units of biotite-bearing quartzo-feldspathic gneiss and biotite-free leucogneiss. These lithologies have been described respectively as grey and pink gneisses in early literature (von Backstrom,1964; Kroner,1968) and have mineral parageneses that are dominated by quartz and feldspars. For classification of the various quartzo-feldspathic gneisses see Sections 3-3 and 3-5.

The biotite-bearing quartzo-feldspathic gneisses, particularly the cordierite-free varieties, are commonest in the central and extreme western portions of the western NMC (Joubert,1971) and also occur interbanded with the metapelitic gneisses (generally the cordierite-bearing varieties) in the southern Bitterfontein region. They are relatively rare in the northern portions of the study area although they do occur within the Geselskapbank area, notably at Beenbreek. The leucogneisses are commonest in the extreme southern (Bitterfontein, Kroner,1968) and northern (Aggeneys, Joubert,1974a) portions of the western NMC, but are also found interbanded with biotite gneisses in the central parts of the study area.

A total of 12 cordierite-bearing metapsammitic gneisses, 19 cordierite-free biotite gneisses and 14 leucogneisses (the latter chiefly from the central portions of the study area) were sampled and analysed during this study (Fig. 8-1). Four samples of biotite-hornblende schists and gneisses from the Geselskapbank area and five samples of banded hornblende-epidote-plagioclase rocks from the Bitterfontein paragneiss belt are also included in this section. All of these groups represent relatively small sample populations compared to the number of metapelitic, quartzitic and calc-silicate rock samples analysed, and compared to the dominance of these quartzo-feldspathic rock types within the majority of paragneiss belts. It has, however, not been the intention of this particular study to examine the chemistries of the quartzo-feldspathic rocks in any detail. The cordierite-bearing metapsammitic gneisses were sampled as extensions to the range of metapelitic rocks and the biotite gneisses and leucogneisses were sampled in the central parts of the study area to complement other studies in the southern and northern parts (Kroner,1968; McCarthy,1978; Paizes,1975; Lipson,1978,1980).

The origins of the quartzo-feldspathic gneisses, particularly those of the biotite gneisses and leucogneisses, are extremely important in proposing regional models for the supracrustal rocks of the western NMC and in resolving

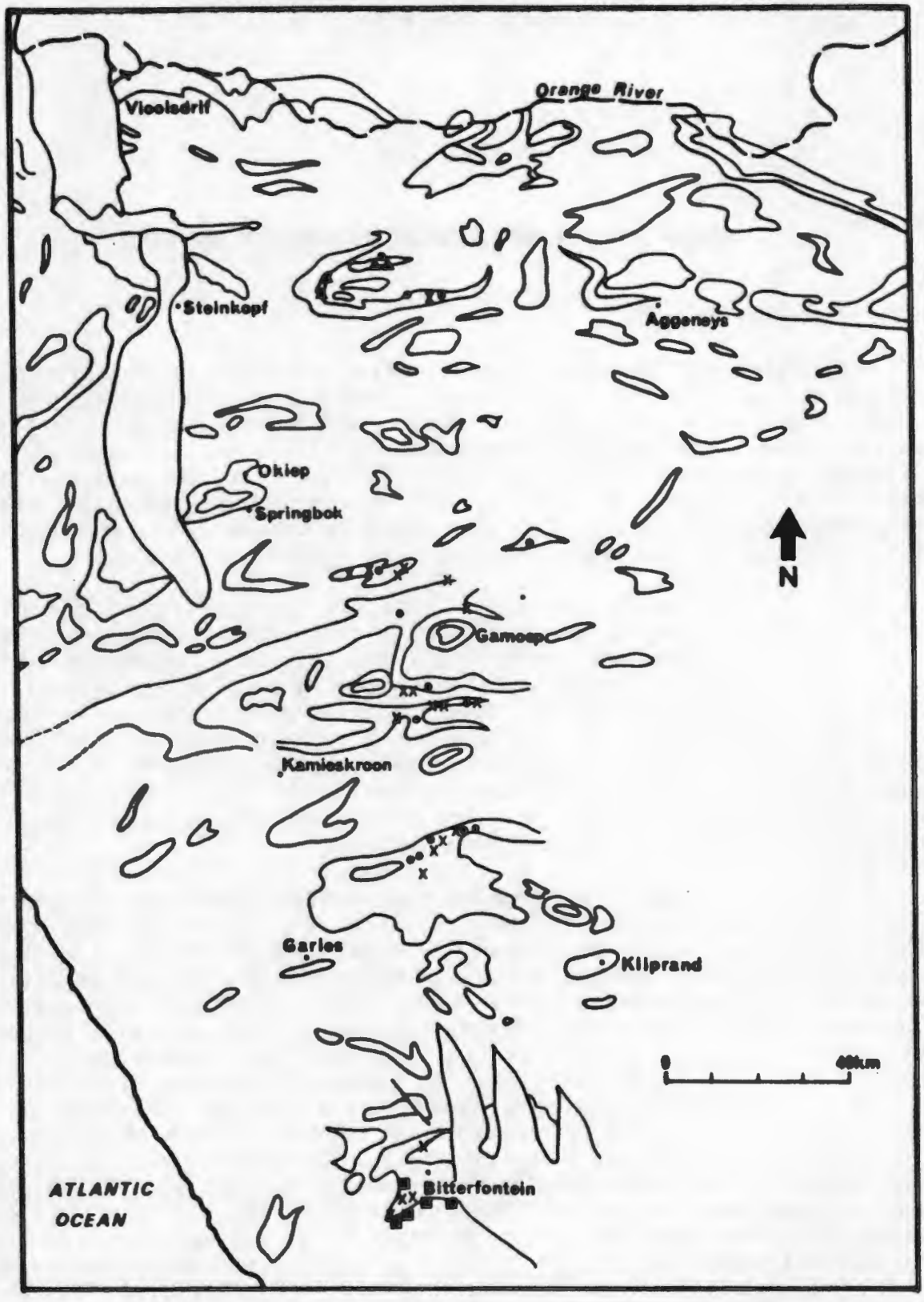

Fig. 8.1 Regional distribution of analysed samples of leucogneisses (dots), biotite gneisses (crosses), biotite-hornblende schists and gneisses (triangles) and hornblende-epidote rocks (squares) from the western NMC.

precursors and source materials for the closely associated metapelitic and quartzitic lithologies. The bulk compositions of this fairly diverse group of quartzo-feldspathic rocks are examined initially with the purpose of discriminating metasedimentary and metavolcanic populations, and then, more specifically, to designate more precise premetamorphic precursors. Due to the relatively small sample populations, statistical techniques employing the variance within and between groups were not deemed appropriate and so have not been utilized as in the case of the majority of other lithologies. Instead the compositions of the quartzo-feldspathic rocks are compared directly to metamorphosed and unmetamorphosed equivalents taken from the literature, and also are compared by means of relatively standard bivariate and triangular plots.

8.2 Previous studies

The quartzo-feldspathic gneisses of the western NMC have attracted considerable attention and created some controversy as to their exact status and origins. Opinions are divided into two broad camps - those favouring a sedimentary, generally arkosic, origin for the biotite gneisses and leucogneisses (von Backstrom,1964; Kroner,1968; Paizes,1975; Moore,1977; Jack,1980) and those favouring an intrusive, igneous origin (McCarthy,1976; Lipson and McCarthy,1977; Lipson,1980; SACS,1980). Both genetic models have their advantages and disadvantages and, given the widespread occurrence of these rocks in the NMC, it is probable that both types are present in certain areas.

In support of the sedimentary model are the field relationships observed in many of the well-exposed paragneiss belts between the quartzo-feldspathic gneisses and other paragneisses. These characteristics have been listed by Moore (1980b) and include maintenance of stratigraphic position within the supracrustal sequence, gradational contacts with metapelitic schists, lack of intrusive relationships with adjacent lithologies and lack of enclosed xenoliths. In the northern portions of the NMC, particularly in the Aggeneys and Okiep areas, the quartzo-feldspathic gneisses are dominated by a single, major leucogneiss unit which separates "basement" augen gneisses from the metapelitic rocks, whilst in the central portions of the western NMC, quartzo-feldspathic gneisses comprise several thinner, conformably interbanded units of biotite gneiss and leucogneiss together with the metapelitic gneisses. An intrusive origin for the quartzo-feldspathic gneisses of the latter area is particularly difficult to envisage, based on the complex, but nevertheless conformable stratigraphic relationships. Although the quartzo-feldspathic gneisses show stratiform relationships with other less equivocal metasedimentary rock types such as metapelitic rocks and quartzites, they do themselves generally lack evidence of obvious sedimentary features such as pebble horizons, cross-bedded units or graded bedding.

An igneous origin for the quartzo-feldspathic gneisses is supported by the geochemical evidence which reveals that the biotite gneisses and, more particularly, the leucogneisses have extremely uniform compositions with relatively narrow ranges of SiO_2:Al_2O_3 ratios. This is unlike the expected

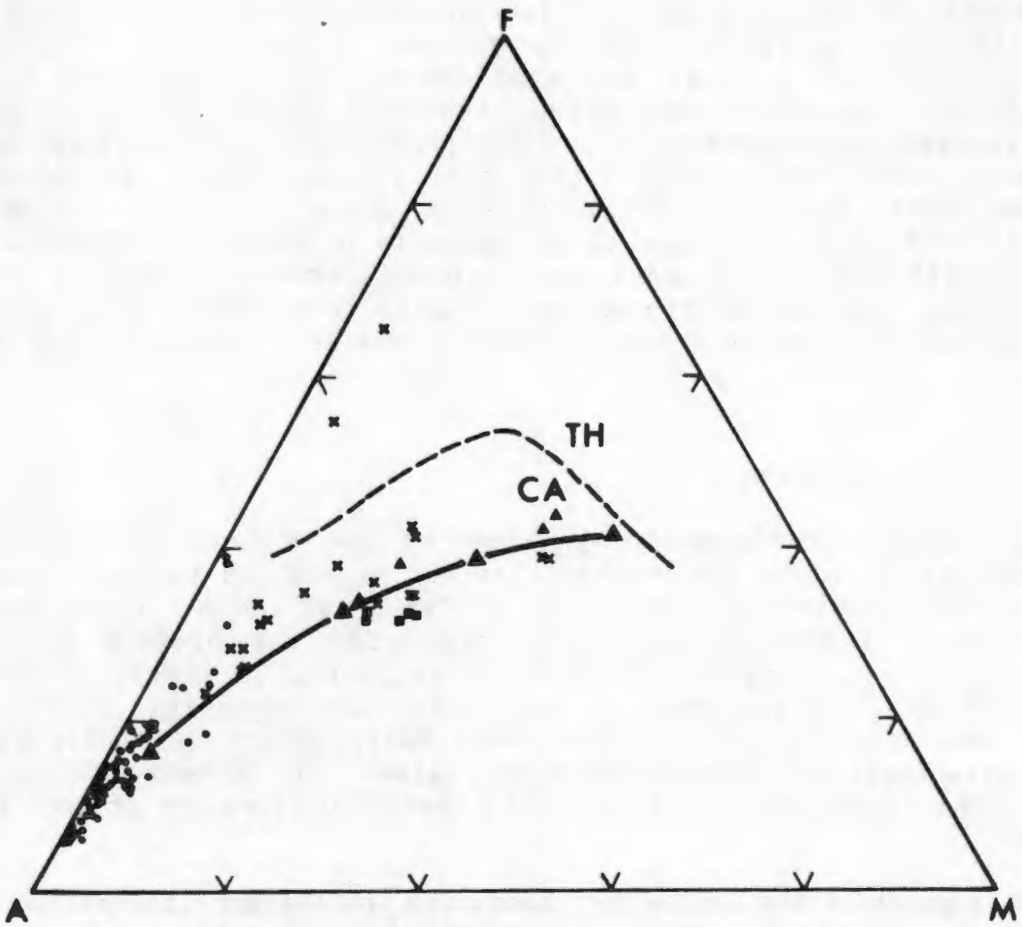

Fig. 8.2 AFM diagram of leucogneisses (dots), biotite gneisses (crosses), biotite-hornblende schists and gneisses from Geselskapbank (small triangles) and hornblende-epidote-plagioclase rocks from Bitterfontein (squares) compared to the fields for tholeiitic (TH) and calc-alkaline (CA) igneous rocks, and the calc-alkaline trend defined by metavolcanic rocks of the Orange River Group (Reid, 1977) (large triangles). The leucogneiss data are from this study, von Backstrom (1964); Kroner (1968); Beukes (1973); Geringer (1973); McCarthy (1976); Paizes (1975); Mathias (1940b); Lamont (1947); Moore (1977) and Lipson (1980). All other analyses are from the present study.

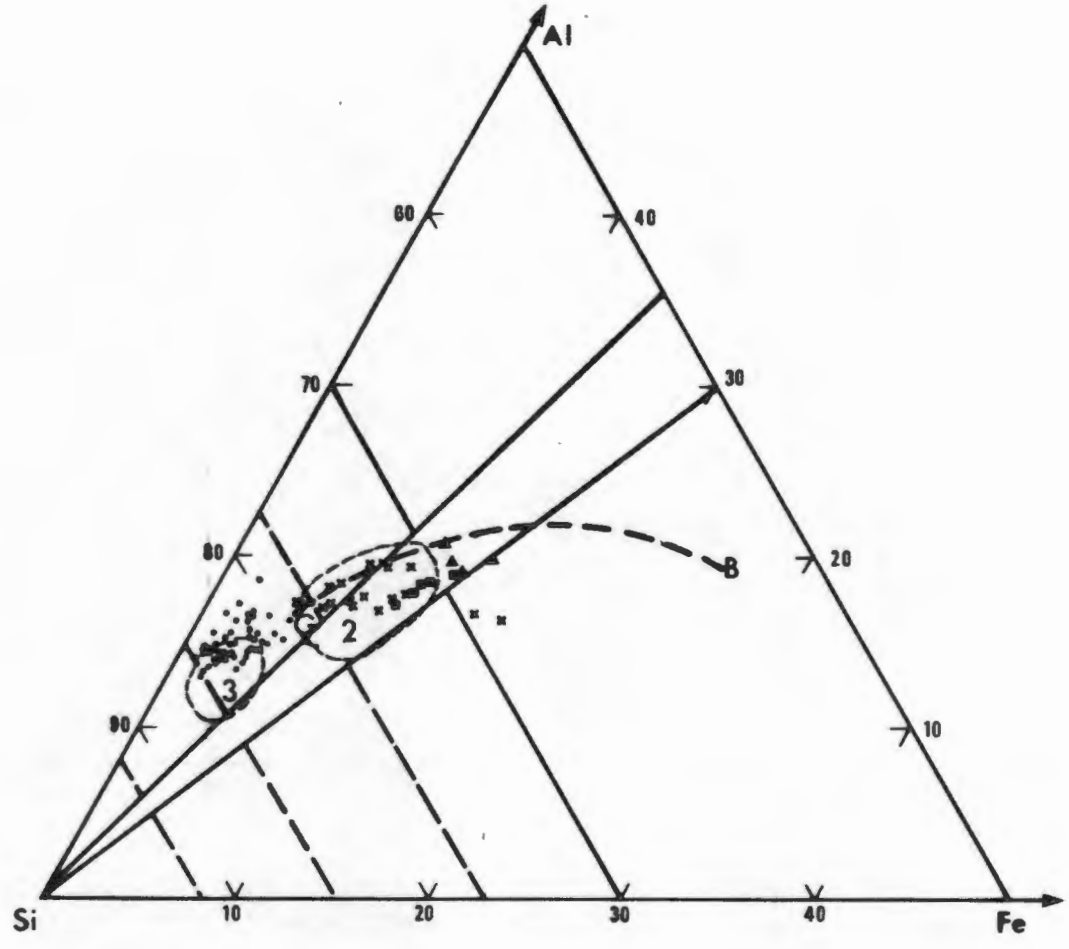

Fig. 8.3 Si-Al-Fe triangular plot showing the positions of leucogneisses (dots), biotite gneisses (crosses), biotite-hornblende schists and gneisses from Geselskapbank (small triangles) and hornblende-epidote-plagioclase rocks from Bitterfontein (squares), compared to the igneous trend (G-B) and the fields of greywackes (2) and arkoses (3) as defined by Moore and Dennen (1970). Data as for Fig. 8.2.

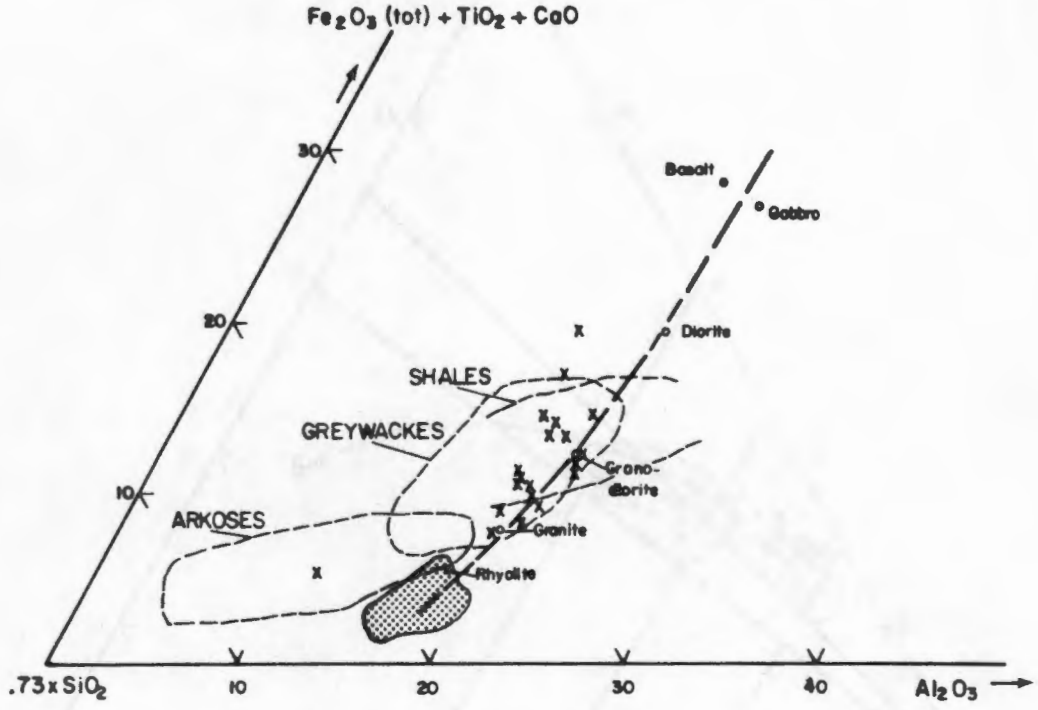

Fig. 8.4 Triangular plot of (SiO_2 x 0.73):Al_2O_3:(FeO + TiO_2 + CaO) showing the igneous trend line and the fields of various sedimentary rocks (after de la Roche, 1966). The distributions of leucogneisses (stipple) and biotite gneisses (crosses) are displayed. Leucogneiss data are as for Fig. 8.2.

ranges of arkosic rocks but more typical of igneous rocks. The geochemical trends displayed by various major and trace elements in the leucogneisses are not inconsistent with interpretations that they represent acid differentiates (Lipson,1980) or granulite-facies partial melts (McCarthy,1976) of the augen gneisses.

An obvious compromise to these two models, which appears to have been overlooked in previous studies, is that of extrusive acid volcanic rocks - i.e. tuffs or ignimbrites. An origin of this nature would satisfy both the conformable, apparently stratiform field relationships and the apparent igneous chemistries of the quartzo-feldspathic gneisses of the western NMC.

8.3 Relationship to general igneous trends

When plotted on the AFM diagram, the biotite gneisses of the western NMC, together with the smaller groups of hornblende-biotite schists and gneisses of the Geselskapbank area and the hornblende-epidote rocks from the Bitterfontein area define an arcuate trend within the calc-alkaline field, similar to that obtained by Reid (1977) for the Orange River Group metavolcanics (Fig. 8.2). This trend contrasts with that of the metapelitic and metapsammitic rocks which define a more linear "tholeiitic" or "sedimentary" trend. The leucogneisses plot near the A apex of the AFM diagram where it is not possible to discriminate between tholeiitic or calc-alkaline volcanic suites. The cordierite-bearing metapsammitic gneisses plot as an extension of the metapelitic rocks towards the A (Na_2O + K_2O) apex (Fig. 7.1), also lying within the relatively narrow linear FeO:MgO field occupied by the metapelites and thus suggesting their derivation by a similar sedimentary process.

In the Si-Al-Fe triangular plot of Moore and Dennen (1970), the distinctions between the various lithologies are less obvious, with the leucogneisses, biotite gneisses and hornblende/epidote/biotite rocks following the igneous curve, but also lying within the fields of arkoses (leucogneisses) and greywackes (biotite gneisses) (Fig. 8.3). There is also considerable overlap between the fields of the biotite gneisses and the cordierite-bearing metapsammitic gneisses. The latter gneisses lie on the Si apex side of the field of metapelitic rocks with the majority of samples falling within the restricted field of Al:Fe ratios of clastic sedimentary rocks (Fig. 7.2).

On the two de la Roche (1966) triangular diagrams, two important chemical features of the leucogneisses are prominently displayed. The tight cluster of leucogneiss samples on the Si:Al:Fe+Ti+Ca plot (Fig. 8.4) is indicative of the remarkably constant Si:Al ratios that characterize these lithologies. The leucogneisses plot along the igneous trend at the extreme end defining acid-rich volcanic rocks and outside the field of arkosic rocks (as defined by de la Roche, op.cit.) which have relatively higher Si:Al ratios. The biotite gneisses also plot along the igneous curve, although they are almost entirely contained within the field of greywackes.

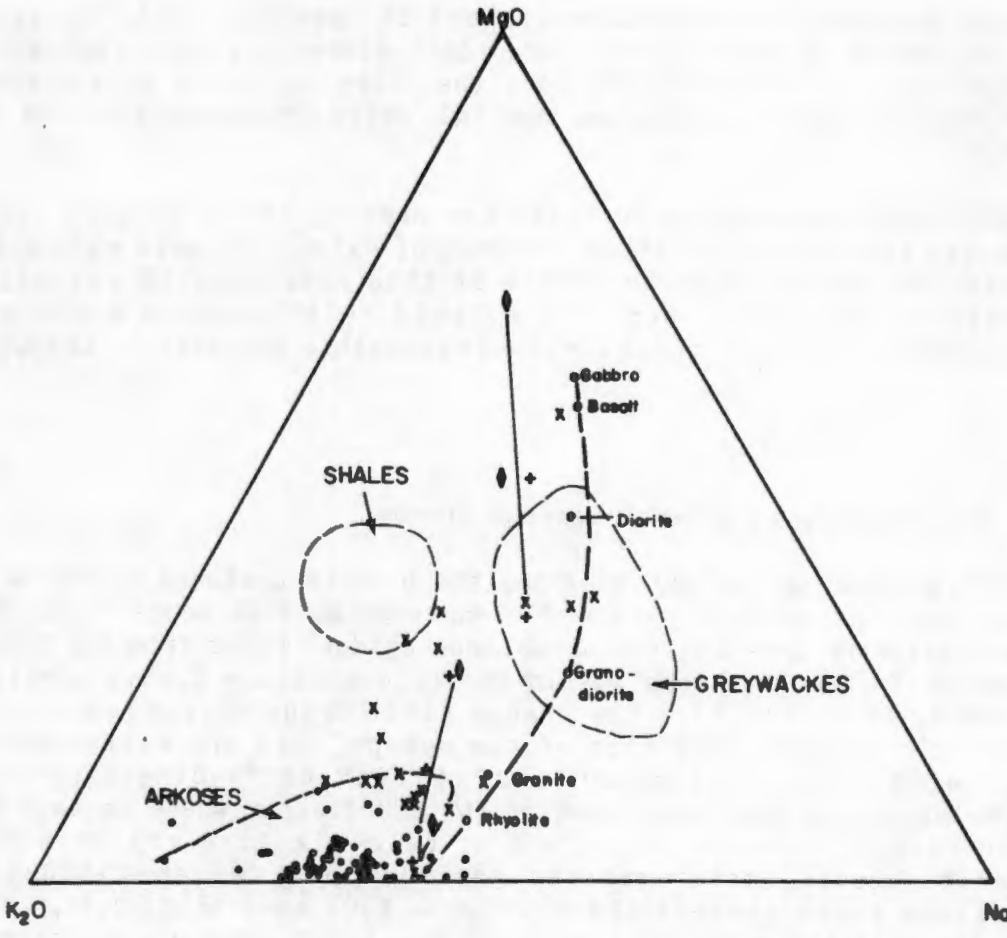

Fig. 8.5 K_2O:Na_2O:MgO triangular diagram showing the igneous trend, a similar trend for the Haib-Vioolsdrif metavolcanic (+) and intrusive (♦) suites (after Reid, 1977), and the fields of various sedimentary rocks. Plotted on the diagram are leucogneisses (dots, data as for Fig. 8.2) and biotite gneisses (crosses).

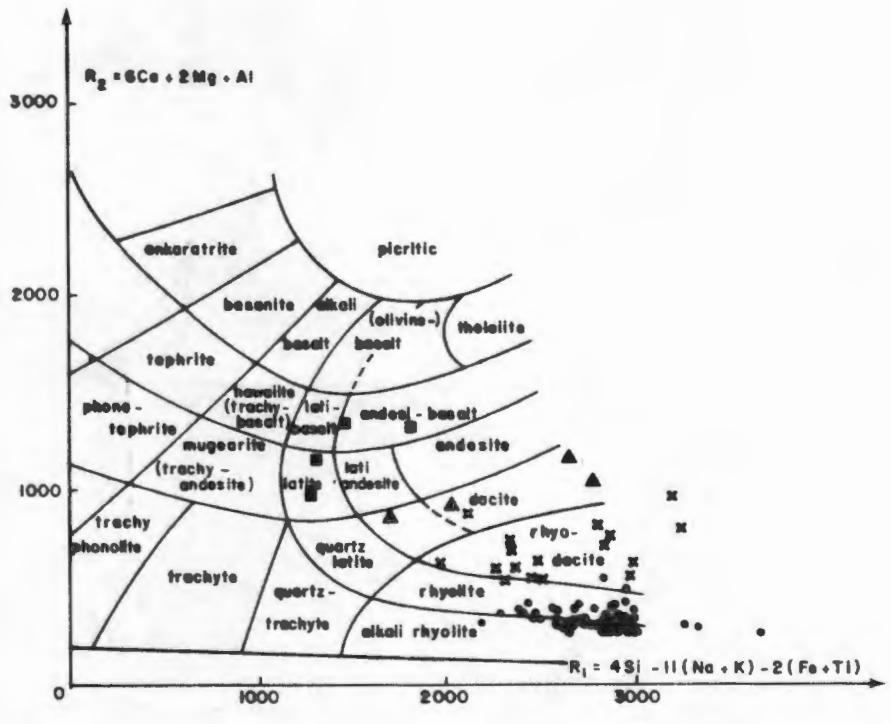

Fig. 8.6 The classification of leucogneisses (dots), biotite gneisses (crosses), biotite-hornblende schists and gneisses (triangles) and hornblende-epidote rocks (squares) on the R1-R2 diagram (after de la Roche et al., 1980). Data as for Fig. 8.2.

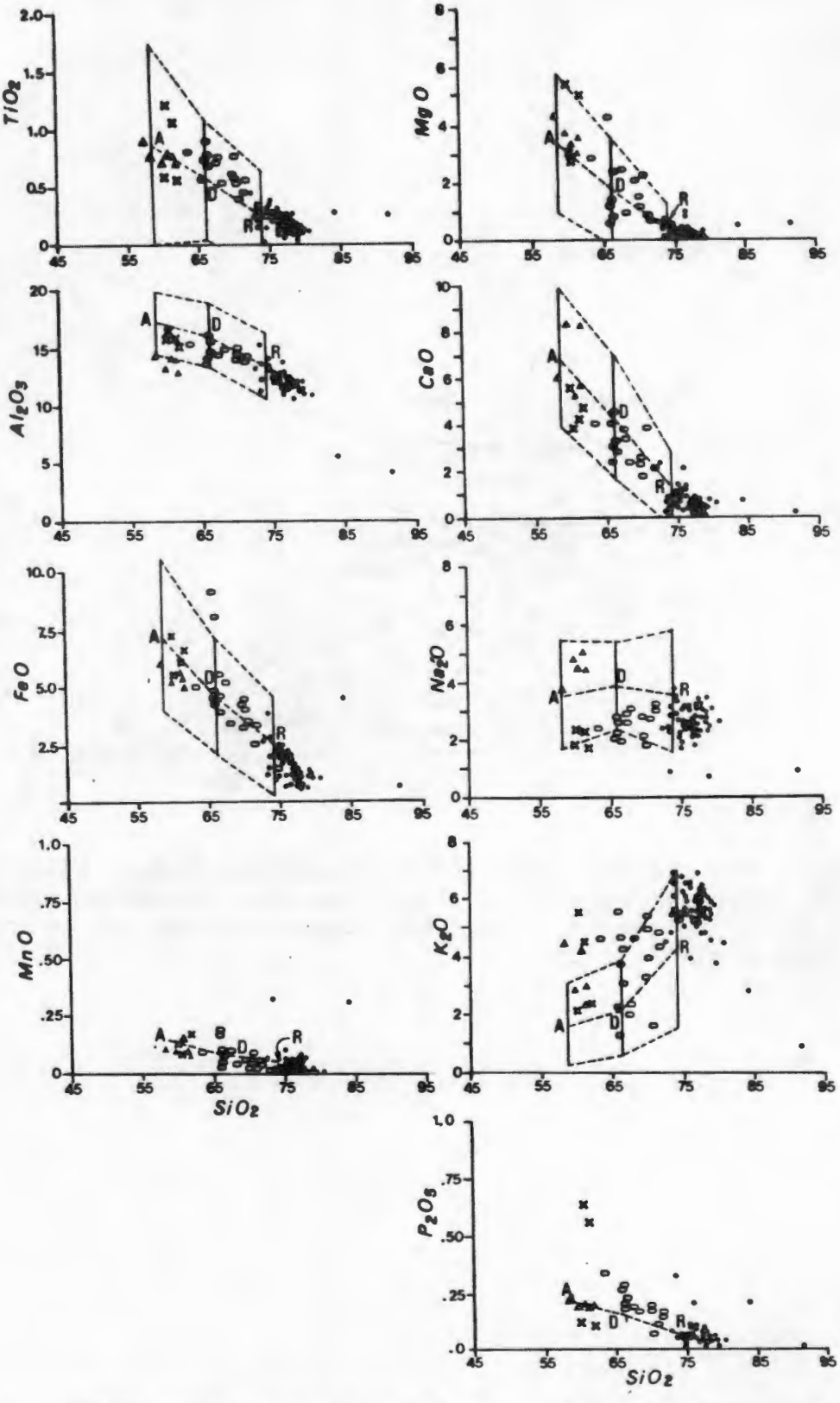

Fig. 8.7 Harker diagrams of major element oxides for leucogneisses (dots), biotite gneisses (ovals), biotite-hornblende schists and gneisses (crosses) and hornblende-epidote rocks (triangles). Data as for Fig. 8.2. The mean values for andesites (A), dacites (D) and rhyolites (R) are also plotted, together with the fields within which 93% of all volcanic rocks between andesite and rhyolite composition are expected to plot (after Brown et al., 1983).

On the K_2O:Na_2O:MgO triangular diagram (Fig. 8.5), however, the majority of leucogneisses show relative enrichment in K over Na compared to common acid igneous rocks, resulting in their plotting within the field of arkosic rocks (as defined by de la Roche, 1966) on the K_2O side of the igneous trend. This feature is also shown by the majority of biotite gneisses and is interpreted as an indication of K-enrichment within a suite of igneous rocks rather than implication of an arkosic origin for the leucogneisses. The majority of biotite gneisses plot well outside the field of typical greywackes on this diagram due to their high K:Na ratios (generally >1). The leucogneisses can be interpreted from these diagrams as extreme acid differentiates of a K-enriched magma, and the biotite gneisses as representing a variety of igneous compositions ranging from granitic to quartz dioritic from a similar source.

8.4 Comparison with specific igneous precursors

De la Roche *et al.* (1980) have devised a bivariate chemical variation diagram using the major cations present in common igneous rocks (as millicationic numbers calculated from the major element oxide percentages). The two selected parameters R1 [= 4Si - 11(Na + K) - 2(Fe + Ti)] and R2 [= 6Ca + 2Mg + Al] have been calculated with the following classical igneous variations in mind: the degree of silica saturation, the variation in the An content of plagioclase, the successive occurrence of clinopyroxene, hornblende and biotite, and the change in the alkali feldspar/plagioclase ratio. Using the geochemical data files of Chayes (1972), le Maitre (1976) and Mutschler *et al.* (1976), de la Roche *et al.* (*op.cit.*) have devised two classification grids using the R1-R2 plot, into which the volcanic and plutonic rock families are subdivided. Whilst the R1-R2 diagrams are primarily designed for the classification of igneous rocks, their use in interpreting the premetamorphic origins of metavolcanic and metaplutonic rocks is considerable.

The R1-R2 diagram has been used to classify the potential metavolcanic precursors of the leucogneisses, biotite gneisses and hornblende/epidote/biotite gneisses and schists of the western NMC. The leucogneisses (including data from various sources, see Section 8.5.1.) straddle the fields of rhyolites and alkali rhyolites, the biotite gneisses fall within the field of rhyodacites, and the hornblende/epidote/biotite gneisses and schists lie within the fields of latites and andesites (Fig. 8.6).

Plots of the major element oxides vs silica for the leucogneisses, biotite gneisses and hornblende/epidote/biotite gneisses and schists from the western NMC are displayed on Harker variation diagrams in Fig. 8.7. For comparative purposes, the mean values for andesite (A), dacite (D) and rhyolite (R) (le Maitre, 1976) are also plotted, together the boundary lines of the fields within which the chemistries of approximately 95% of all andesites, dacites and rhyolites should fall (after Brown *et al.*, 1983).

In comparison with the mean SiO_2 values for andesite, dacite and rhyolite (le Maitre, 1976), it can be seen from the Harker diagrams that the majority of hornblende/epidote/biotite rocks, biotite gneisses and leucogneisses from the western NMC have slightly higher SiO_2 compositions. They also have lower than

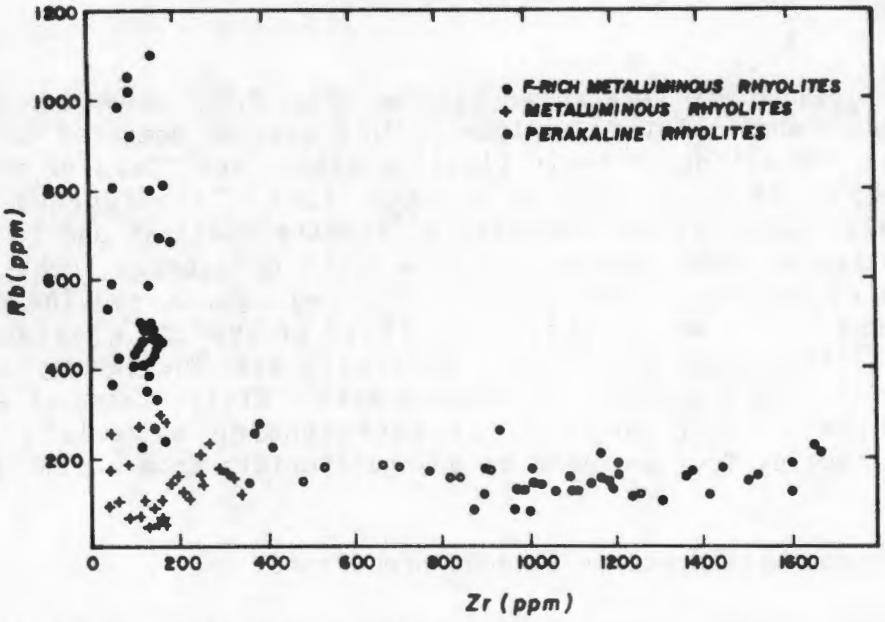

Fig. 8.8a Bivariate plot of Rb : Zr comparing the compositional fields of various rhyolite types (from Christiansen et al., 1983).

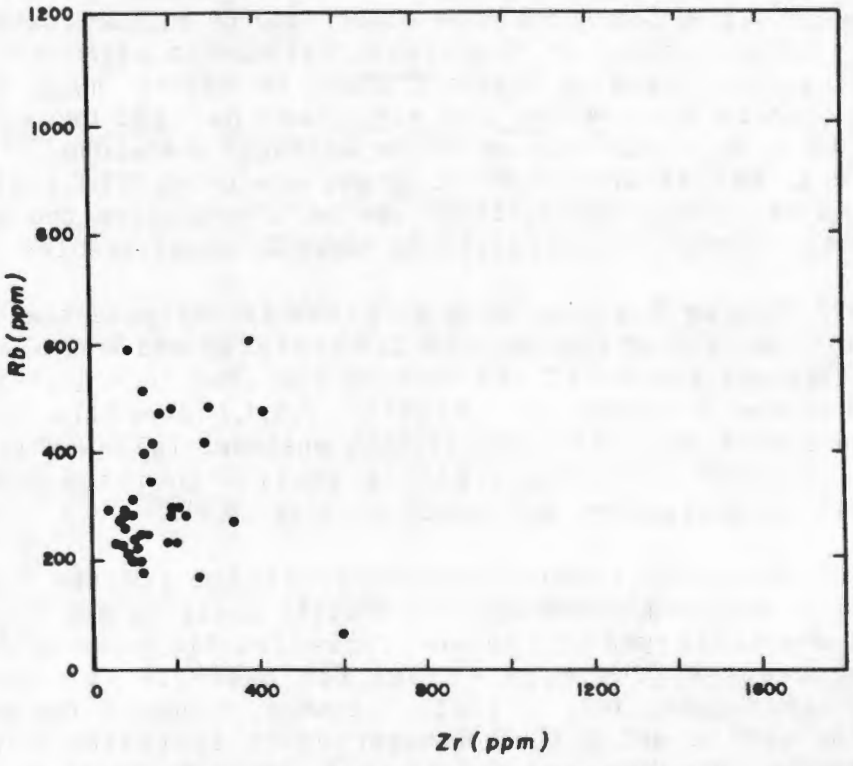

Fig. 8.8b Similar Rb : Zr plot for leucogneisses from the western part of the NMC. Data from this study; Paizes, 1975; McCarthy, 1976; Moore, 1977.

average Al_2O_3, Na_2O (with the exception of the Bitterfontein hornblende-epidote rocks) and CaO, and higher than average K_2O and TiO_2 although the vast majority of analyses plot within the anticipated fields for all the major element oxides or, in the case of the leucogneisses, within expected projections of these fields to the high-SiO_2 side of the rhyolite field. These deviations from typical volcanic rocks cannot be easily explained by high-grade metamorphic processes, as depletions in SiO_2 and K_2O, and enrichments in Al_2O_3 and CaO would be anticipated during metamorphic modifications such as anatexis.

The similarities in the depletion and enrichment trends displayed by these different gneisses could indicate that they are derived from a common magmatic source which also showed these characteristics. A magmatic source relatively enriched in SiO_2, K_2O and TiO_2, and depleted in Al_2O_3, Na_2O and CaO, implies melting of relatively siliceous, potassic material - i.e. a crustal rather than a mantle magma source. The metavolcanic rocks of the Orange River Group (Reid,1977) are likewise enriched in potassium and a common crustal magmatic source for the majority of metavolcanic rocks in the western NMC could be implied.

Christiansen et al. (1983) have demonstrated that the Rb vs Zr plot is a suitable discriminant between the various types of rhyolitic rocks, with F-rich metaluminous rhyolites (such as topaz rhyolites) showing enrichment in Rb at constant Zr, normal metaluminous rhyolites showing relatively constant, restricted Rb and Zr ranges, and peralkaline rhyolites showing enrichment in Zr at constant low levels of Rb (Fig. 8.8.a). Enrichment in Zr (and other highly charged cations such as Ce, Y and Nb) is also reported from peralkaline, anorogenic "A-type" granites from south-eastern Australia (Collins et al., 1982) compared to the more common "I-type" and "S-type" granites derived from igneous and sedimentary sources respectively (Chappell and White, 1974).

Plots of Rb vs Zr for leucogneisses from the western NMC indicate that peralkaline trends are absent and that moderate Rb enrichment (from 200 to 600 ppm) at relatively low Zr contents occurs (Fig. 8.8.b). The western NMC leucogneisses could be said to show trends similar to metaluminous and F-rich metaluminous rhyolites (Fig. 8.8.a).The observation of trace amounts of fluorite in certain leucogneiss samples (see Section 8.5.1) is supportive evidence for this conclusion which is significant because F-rich metaluminous rhyolites in the western USA are related to specific processes, namely evolution by partial melting of "residual granulitic sources in the lower crust" and specific extensional tectonic settings (Christiansen et al., 1983).

8.5 Direct chemical comparisons

8.5.1 Leucogneisses

The leucogneisses associated with the supracrustal sequences of the western NMC are generally well-banded, equigranular, granoblastic gneisses devoid of obvious megacrysts or augen. They are commonest in the basal

TABLE 8.1 Mean compositions of certain leucogneisses and rhyolitic rocks from the western portions of the Namaqualand Metamorphic Complex.

	1.	2.	3.	4.	5.	6.	7.	8.
SiO_2	76.30	77.72	76.46	76.84	75.85	76.36	73.77	75.33
TiO_2	0.15	0.18	0.27	0.19	0.26	0.07	0.36	0.18
Al_2O_3	12.55	11.97	12.37	12.09	12.00	12.04	13.75	13.05
FeO*	1.37	1.12	1.62	1.11	1.73	1.56	1.84	0.98
MnO	0.06	0.03	0.05	0.01	0.03	0.01	0.04	0.08
MgO	0.22	0.14	0.17	0.11	0.25	0.24	0.60	0.37
CaO	0.49	0.72	0.90	0.37	0.72	0.31	1.31	0.43
Na_2O	2.35	2.74	2.37	2.62	2.18	2.85	3.33	3.03
K_2O	6.04	5.38	5.81	5,94	6.27	5.35	4.83	5.66
P_2O_5	0.05	0.06	0.07	0.05	0.04	0.00	0.07	0.03
number of samples	11	14	8	9	4	1	14	1

* total Fe as FeO

1. leucogneiss, central portions of western NMC (this study).
2. "granulite" (leucogneiss), Okiep Copper District (McCarthy, 1976).
3. pink granoblastic gneiss, Aggeneys (Lipson, 1980).
4. selected "pink" gneisses (mostly equigranular), southern portions of western NMC (Kroner, 1968; Lamont, 1947).
5. leucogneiss, Namies area, (Paizes, 1975; Moore, 1977).
6. Haib rhyolite, Orange River Group (Beukes, 1973).
7. rhyolite, Orange River Group (Reid, 1977).
8. leucocratic welded tuff, Orange River Group (Ritter, 1980).

portions of the supracrustal sequences and are thus found in close association with megacrystic and augen gneisses (both "pink" and "grey") with the result that previous studies have commonly incorporated all these quartzo-feldspathic rocks into a single suite and assumed a common mode of origin (e.g. Kroner,1968; McCarthy,1976; Lipson,1980). The relationship between the leucogneisses and the augen gneisses is, however, not necessarily this direct, as certain augen gneisses have been demonstrated as representing part of a basement complex to supracrustal sequences that include leucogneiss units (Moore,1977) whilst many other augen gneisses have been shown to be intrusive into the supracrustal rocks (SACS,1980). The extraction of pertinent geochemical data from previous studies has, therefore, been undertaken with caution and many analyses discarded where the distinction between equigranular and augen "pink" gneisses is not made with clarity.

When geochemical comparison is restricted to the equigranular, biotite-free leucogneisses, remarkable chemical uniformity is apparent over the entire western NMC - from the extreme southern portions (Lamont,1947; Kroner,1968), central Namaqualand (this study), the Okiep Copper District (McCarthy,1976), the Aggeneys-Pofadder area (Mathias,1940b; Paizes,1975; Moore,1977; Lipson,1980), the Warmbad District of southern Namibia (Beukes,1973) and the Augrabies-Kakamas-Kenhardt area (von Backstrom,1964; Geringer,1973) (Table 8.1).

This narrow range of chemical composition, particularly the constancy of the SiO_2:Al_2O_3 ratio, as pointed out by Lipson (1980), and the persistently high K_2O values (commonly 5 to 7%), is somewhat unusual for arkosic rocks which, due to their intimate associations with more siliceous sandstones and conglomerates, would be expected to show a greater spread of SiO_2:Al_2O_3 ratios and K_2O contents. Only in the southern paragneiss belts from Bitterfontein to Witwater, do leucogneisses show close associations (gradational contacts) with quartzitic rocks, and nowhere has an association with conglomeratic rocks been observed.

If a sedimentary origin is to be assumed for these rocks, models invoking widespread remobilisation of minimum-melt granitic melts which "granitise" the arkosic precursors would probably be required to obtain the constancy of chemistry observed. Arkosic model precursors would have had bulk compositions similar to the minimum melt composition prior to metamorphism, and therefore they could be expected to melt during upper-amphibolite- and granulite-facies metamorphism - conditions that existed over most of the area where the leucogneisses are now found. Chemical equilibration on a large scale within the leucogneisses is, however, difficult to envisage given the finely-banded, equigranular nature of rocks which theoretically have undergone major amounts of partial melting, and given the widespread presence of coarse, almost pegmatitic, leucosomes - themselves the products of anatexis - within these lithologies.

Comparison of the chemical data with those of typical igneous rocks, indicates that only highly differentiated acidic rocks - both granitic and rhyolitic - have similar SiO_2-, K_2O-enriched, CaO-, Al_2O_3-depleted compositions (Table 8.2). In the northern portions of the western NMC, certain

TABLE 8.2 Comparison of the mean leucogneiss composition from the western NMC with various rhyolitic rock compositions and similar leucogneisses from the Willyama Complex, New South Wales.

	1.	2.	3.	4.	5.	6.	7.	8.
SiO_2	76.83	72.82	77.4	76.0	74.84	75.11	74.63	74.40
TiO_2	0.20	0.28	0.07	0.6	0.21	0.17	0.45	0.26
Al_2O_3	12.20	13.27	12.3	13.0	12.09	12.29	11.00	13.90
FeO*	1.32	2.44	0.7	0.9	2.17	2.11	2.72	1.78
MnO	0.04	0.06	0.04	0.6	0.04	0.10	0.01	0.03
MgO	0.17	0.39	0.01	0.08	0.35	0.16	0.43	0.37
CaO	0.63	1.14	0.45	0.6	0.39	0.43	0.14	0.60
Na_2O	2.51	3.55	3.9	4.0	1.04	3.62	0.15	2.79
K_2O	5.80	4.30	4.8	4.8	8.00	5.02	9.15	5.30
P_2O_5	0.06		0.01	0.00		0.04	0.09	0.16
F				0.3				
number of samples	46	670		89	100	11	3	13

* total Fe as FeO

1. leucogneiss from the western NMC (this study; McCarthy, 1976; Lipson, 1980; Kroner, 1968; Lamont, 1947; Paizes, 1975; Moore, 1977).
2. average rhyolite (le Maitre, 1976).
3. Bishop tuff, western United States (Hildreth, 1979).
4. topaz rhyolite (Christiansen et al., 1983).
5. ultrapotassic rhyolite (Fromberg, 1980).
6. Precambrian rhyolites, Wisconsin (Smith, 1978).
7. Centaur Bore rhyolite, Queensland (Bultitude and Wyborn, 1982)

metarhyolites and leucogranites in the Orange River area (Beukes,1973; Reid,1977; Ritter,1980) have similar whole-rock compositions to the leucogneisses, whilst meta-igneous acid intrusives from the rest of the western NMC (e.g. Concordia granite; McCarthy,1976) generally have more "normal" granitic compositions (i.e. lower SiO_2, K_2O, Na_2O and higher Al_2O_3, CaO).

The composition of the leucogneisses is comparable with major recent acid ash-flow tuffs such as the Bishop Tuff (Hildreth,1979) and other high-silica rhyolites such as topaz rhyolites of the western USA (Burt et al., 1982; Christiansen et al., 1983) and "ongonites" or ultrapotassic rhyolites of the USSR (Fromberg,1980). These rhyolites are formed when the water- and halogen-rich roof zones of large, highly differentiated magma chambers are erupted during caldera-collapse of the magma-chamber roof. Major volumes of rhyolitic magma (greater than 3000 cu. km per single eruption, Smith,1979) can be extruded in this manner, creating vast ignimbritic and co-ignimbritic air-fall deposits (Sparks and Walker,1977). This could explain the widespread nature of chemically-uniform leucogneisses within the supracrustal sequences of the western NMC. Fluorite is not uncommonly observed in trace amounts in the equigranular leucogneisses (see also Lipson,1980), reaching almost one modal percent in sample RFN-9. Enrichment in fluorine, either as topaz or fluorite, is a characteristic feature of all these high-silica, high-potassium rhyolites (Christiansen et al. op.cit.; Fromberg, op.cit.).

A suite of rhyolites and potassic granites of comparable mid-Proterozoic age (1760 Ma) from the Lake Superior region of Wisconsin (Smith,1978; Anderson et al., 1980) show very similar compositions to the leucogneisses of the western NMC (Table. 8.2). These are high-level intrusives and their extrusive ignimbritic equivalents that are interpreted as having been emplaced in rift-related environments, erupting immediately after a major calc-alkaline cycle. The potassic granites and rhyolites are regarded as the products of fusion of relatively thick crustal material (Anderson et al., op. cit.).

Acid volcanic rocks are also common within the mid-Proterozoic Carpentarian sequences of north-western Queensland, Australia (Wilson,1978b; Bultitude and Wyborn,1982). They have been related to Andean continental-margin calc-alkaline volcanism (Wilson,op.cit.) or continental bimodal volcanism within an extensional crustal environment (Bultitude and Wyborn, op.cit.). The older acid volcanics (Leichhardt volcanics, Argylla formation) are more silica-poor and calcium-enriched when compared to the younger rhyolite suite (Carters Bore rhyolite) which is Si- and K-rich and Al-, Ca- and Na-poor - similar in its composition to the leucogneisses of the western NMC. The acid volcanics of north-western Queensland represent evolution from calc-alkaline conditions to continental bimodal volcanism represented by high-silica, high-potassium rhyolites and associated tholeiitic basalts.

Leucocratic quartzo-feldspathic gneisses from the Willyama Complex, Broken Hill Block, New South Wales are associated with pelitic and psammitic metasediments, banded plagioclase-quartz (Na-rich) gneisses, augen gneisses and iron formation-associated base metal mineralisation in a sequence with considerable similarities to the western NMC supracrustal rocks. These

TABLE 8.3 Comparison of the composition of biotite gneisses, biotite-hornblende rocks and hornblende-epidote-plagioclase rocks from the western NMC with the average compositions of various volcanic and plutonic rock types

	1.	2.	3.	4.	5.	6.	7.	8.
SiO_2	68.61	65.55	68.65	65.95	65.01	60.93	60.44	57.94
TiO_2	0.65	0.60	0.54	0.59	0.58	0.87	0.76	0.87
Al_2O_3	14.61	15.04	14.55	13.43	15.91	15.67	13.71	17.02
FeO*	4.19	3.92	3.79	4.79	4.46	6.36	5.46	6.95
MnO	0.06	0.09	0.08	0.10	0.09	0.13	0.11	0.14
MgO	1.37	2.09	1.14	4.23	1.78	4.07	3.67	3.33
CaO	2.65	3.62	2.68	4.60	4.32	4.66	6.78	6.79
Na_2O	2.68	3.67	3.47	2.11	3.79	2.02	4.51	3.48
K_2O	4.45	3.00	4.00	1.25	2.17	3.65	3.41	1.62
P_2O_5	0.19	0.25	0.19	0.19	0.15	0.36	0.20	0.21

* total Fe as FeO

1. biotite gneiss from the western NMC (15 samples, this study).
2. average rhyodacite (100 analyses, le Maitre, 1976).
3. average adamellite (135 analyses, le Maitre, 1976).
4. biotite-hypersthene gneiss, PH-11 (this study).
5. average dacite (651 analyses, le Maitre, 1976).
6. biotite-hornblende schist and gneiss, Geselskapbank area (4 samples, this study).
7. banded hornblende-epidote-plagioclase rocks, Bitterfontein paragneiss belt (5 samples, this study).
8. average andesite (2600 analyses, le Maitre, 1976).

leucogneisses are interpreted as metamorphosed rhyolitic volcanics, some of which are "unusually potassium rich" (Brown et al., 1983) and many of which, due to their thin but extensive distribution, are interpreted as metamorphosed airfall tuffs (Willis,1982). The composition of these leucocratic quartzo-feldspathic gneisses is again comparable to the western NMC leucogneisses.

8.5.2. Biotite gneisses

The cordierite-free biotite gneisses which occasionally contain minor amounts of hornblende, epidote or hypersthene, have compositions comparable to slightly less acidic igneous rocks such as adamellites and rhyodacites (le Maitre,1976) with noticeable increases in the contents of TiO_2, total Fe as FeO, MgO and CaO, and depletions in SiO_2 compared to the leucogneisses (Table 8.3). A few samples (PH-11, ROF-2 and ROF-11) have compositions more in the dacite or monzonite range. Certain other minor units such as the banded hornblende-epidote rocks from the Bitterfontein area and the hornblende-biotite schists and gneisses of the Geselskapbank area have compositions within the fields of tonalites and andesites (Table 8.3). The more widespread amphibolites and pyroxene granulites have basaltic to tholeiitic compositional ranges (Moore,1977; Zelt,1980) (see Section 9.2). It would appear that a range of rocks of potential volcanic origin, but dominated by rhyolitic to rhyodacitic components forms a major portion of the supracrustal rocks of the western NMC. All these various potential metavolcanic units, with the exception of the amphibolites and basic granulites, show enrichment in K_2O relative to normal "average" volcanic rock suites. This potassic enrichment is also a feature of the calc-alkaline metavolcanic rocks of the Orange River Group to the north (Reid,1977), and may indicate some common, somewhat anomalous, K-enriched magma source for most of the metavolcanic rocks of the western NMC.

The biotite gneisses of the western NMC are chemically similar to the fine-grained quartzo-feldspathic gneisses of the Willyama Complex, New South Wales (Brown et al., 1983). These latter gneisses have been interpreted as original dacitic ash-flows or mud-flows which underwent subsequent minor chemical alteration, either by diagenetic or metamorphic processes (Brown et al., op.cit.).

8.5.3 Cordierite-bearing metapsammitic gneisses

The cordierite-bearing metapsammitic gneisses have compositions which are generally incompatible with their direct derivation from igneous rocks. Relatively high SiO_2 and K_2O values suggest granitic/rhyolitic compositions, but their total Fe as FeO, TiO_2 and MgO contents are too high and Na_2O too depleted for such lithologies. Their compositions are comparable to the NMC metapelitic rocks to which greater quartz and K-feldspar components have been added, thus diluting the Ti, Al, Fe and Mg components. They may thus be classified as psammo-pelitic to psammitic metasediments. Similar mid-Proterozoic metasediments with comparable compositions have been described from the Willyama Complex, Broken Hill Block, New South Wales (Willis et al., 1983).

TABLE 8.4 Comparison of the effects of K-feldspar authigenesis in the Wagon Bed Formation, Wyoming (Boles and Surdam, 1979) with the major element composition of leucogneisses from the Aggeneys-Namiesberg area.

	1.	2.	3.	4.
SiO_2	73.6	74.2	73.77	76.42
TiO_2			0.36	0.25
Al_2O_3	14.9	13.3	13.75	12.32
FeO*	2.52	2.34	1.84	1.59
MgO	1.2	1.1	0.60	0.18
CaO	2.1	1.3	1.31	0.86
Na_2O	2.2	1.5	3.33	2.46
K_2O	3.2	6.0	4.83	5.70

* total Fe as FeO

1. fresh glass-smectite tuffs, Wagon Bed Formation (5 samples, Boles and Surdam, 1979).
2. K-feldspar tuffs, Wagon Bed Formation (3 samples, Boles and Surdam, 1979).
3. Mean metarhyolite, Orange River Group (14 samples, Reid, 1977).
4. Mean leucogneiss, Aggeneys-Namiesberg area (11 samples, Paizes, 1975; Moore, 1977; Lipson, 1980).

8.6 Comparison with diagenetically-altered volcanic rocks

Although the compositions of the various gneisses described in this chapter compare favourably with those of certain volcanic rocks, their field relations indicate that they were generally conformably deposited within a volcano-sedimentary sequence. Thus, in all probability some of them represent distal tuffaceous rocks - either air-fall, ash-flow or mud-flow deposits and not massive lava flows. Tuffaceous rocks are highly susceptible to diagenetic alteration after deposition, and it is possible that the depletions in Na_2O and CaO and enrichments in K_2O are the result of either mild weathering processes (dissolution of plagioclase) during sedimentary reworking, or diagenetic alteration (breakdown of plagioclase/analcite and formation of authigenic K-feldspar).

Fresh glass-smectite tuffs from the Wagon Bed Formation, Wind River, Wyoming have such K-feldspar-rich rocks as their end-products during diagenesis under moderately saline pore fluid conditions (Boles and Surdam, 1979) and show chemical transformations of this nature. The leucogneisses of the northern parts of the study area show similar chemical variations (i.e. relative increases in K_2O and SiO_2 content and decreases in Al_2O_3, total Fe as FeO, MgO, CaO and Na_2O contents) when compared to the proximal metarhyolitic volcanic rocks of the Orange River Group (Reid,1977) to the north (Table 8.4). These differences could be interpreted as resulting from authigenic processes subsequent to the deposition of the leucogneiss precursors as tuffaceous rocks in a sedimentary basin. Certain thin, highly potassic, tuffaceous bands located in the Urquhardt shales at Mount Isa - a mid-Proterozoic sedimentary/volcanic succession of similar age to the western NMC supracrustal rocks - have been interpreted as forming in this manner (Croxford,1964). Similar enrichment in K_2O (together with MnO) and depletion in Na_2O and CaO compared to calc-alkaline trends was noted for the fine-grained quartzo-feldspathic gneisses of the Willyama Complex, New South Wales (Brown *et al.*, 1983) and also attributed to some form of premetamorphic alteration of distal volcanic rocks.

8.7 Potential as source material for the metapelitic rocks

In Section 7.7, it was pointed out that the two different groups of metapelitic rocks from the northern and south/central portions of the western NMC had markedly different La/Th ratios, indicating their formation from different source materials. More specifically, the La/Th ratios of the northern metapelities implied a source material that had a highly differentiated acidic composition, whereas the south/central metapelites displayed La/Th ratios more typical of normal post-Archaean pelitic rocks (Fig. 7.14). The mica-sillimanite schists of the northern portions of the western NMC commonly show close associations with underlying leucogneisses including gradational contacts (Moore,1977, 1980b), and their derivation by sedimentary reworking of rhyolitic material is quite feasible. The northern metapelites are typified by extremely high K:Na ratios and very low Na_2O, CaO and MgO contents which would support such an argument. Unfortunately,

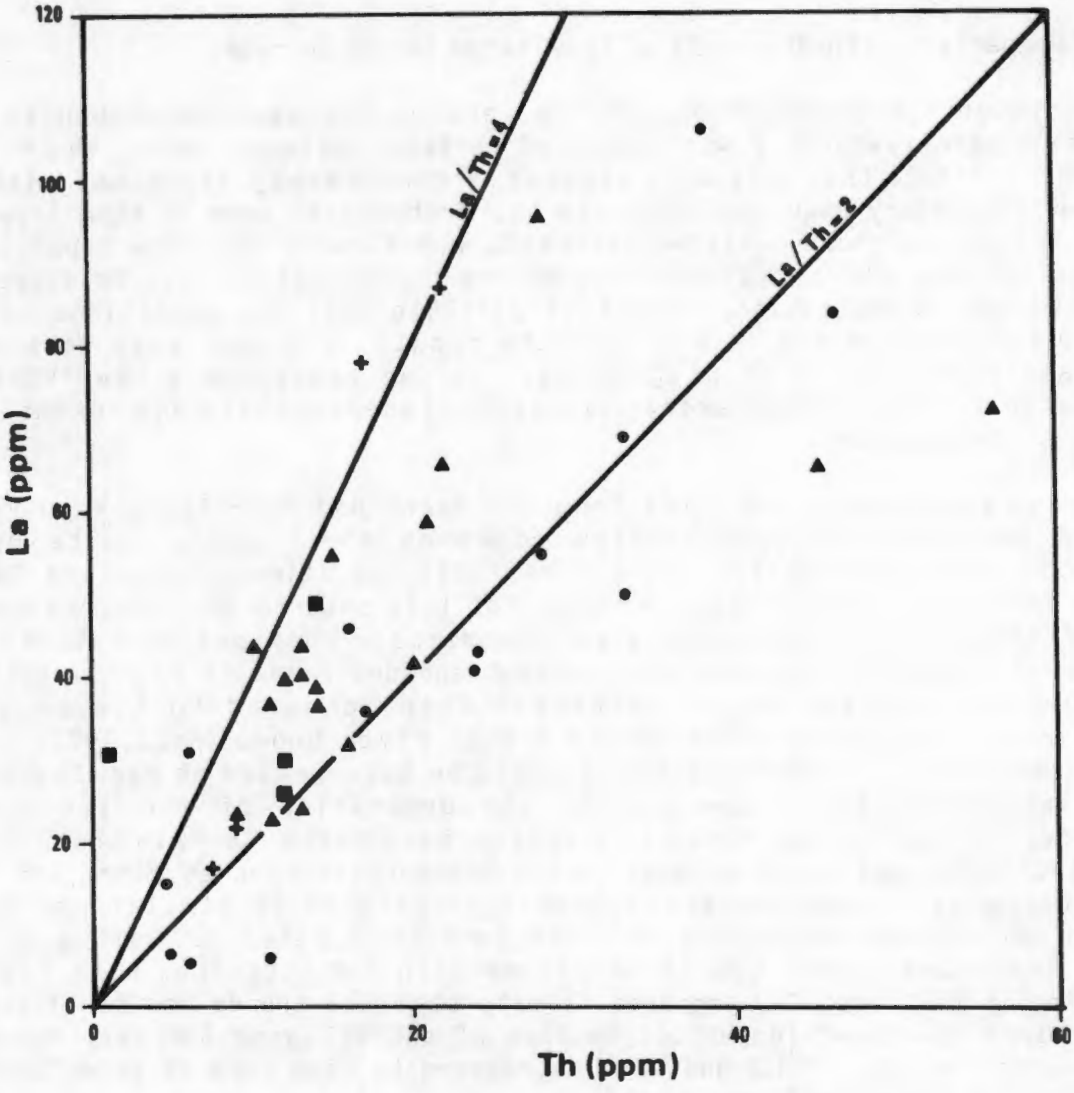

Fig. 8.9 Bivariate plot of La : Th of leucogneisses (dots), biotite gneisses (triangles), biotite-hornblende schists and gneisses (crosses) and hornblende-epidote rocks (squares). All data are from the present study.

although major element data are available for leucogneisses from this portion of the NMC (McCarthy,1978; Paizes,1975; Lipson,1980), there are no analyses for La and Th for direct comparison with the metapelites.

Thirteen samples of leucogneisses collected during the present study - all essentially from the central portions of the western NMC - have La and Th values plotted in Fig. 8.9 together with those for the biotite gneisses and hornblende/epidote/biotite rocks. The majority of leucogneiss samples have La:Th ratios of 2 or less, whereas the other gneisses have ratios in the region of 2 to 4. By analogy, therefore, the leucogneisses of the northern portion of the western NMC could well have similar La:Th ratios to the associated overlying mica-sillimanite schists (commonly <2). This similarity of La:Th ratio between the two lithologies indicates that the leucogneisses could well have provided the source material for the northern metapelitic rocks.

The La:Th ratios of the biotite gneisses and hornblende/epidote/biotite rocks appear to be slightly higher (commonly 3 to 4) than those of the south/central metapelitic gneisses (commonly 2 to 3), and, therefore, the formation of the latter entirely by degradation or weathering of the former is less likely.

8.8 Estimation of precursor mineral assemblages

The cordierite-bearing metapsammitic gneisses are of probable metasedimentary origin and so their chemistries were modelled in a similar manner to the metapelitic rocks. The sample population (11 analyses) was regarded as too small for meaningful principal components analysis, and so the mineral phases used for the metapelites (with identical mineral chemistries) were also employed in a least-squares approximation exercise (see Section 7.6).

Relatively consistent results were obtained for the metapsammitic gneisses (Table 8.5), indicating that they comprised on average, approximately 40% quartz, 20% K-feldspar, 20% plagioclase, 15% illite, 5% chlorite and minor ilmenite with traces of calcite possibly present in a few samples. Relative to the south/central metapelitic gneisses, the cordierite-bearing metapsammitic gneisses contain increased K-feldspar (18% compared to 6%), plagioclase (19% compared to 13.5%) and quartz (40% compared to 29%) and reduced amounts of illite (16% compared to 36.5%) and chlorite (6% compared to 9%). This decrease in clay constituents, including the total absence of a kaolinite phase, and increase in detrital feldspar and quartz constituents is compatible with the classification of these gneisses as metamorphosed psammitic sediments.

8.9 Summary

The compositions and stratigraphic relationships of the leucogneisses and biotite gneisses are compatible with models that propose their premetamorphic origins as rhyolitic to rhyodacitic extrusive acid volcanic rocks. Many of the

TABLE 8.5 Estimated proportions of premetamorphic constituents in the cordierite-bearing metapsammitic gneisses, based on least-squares approximations, compared to the metapelites from the southern and central portions of the study area.

Mineral constituent	cordierite-bearing metapsammitic gneisses (n = 12) %		south/central metapelites (n = 48) %
	mean	range	mean
quartz	40	32-58	29
K-feldspar	18	0-32	6
illite	16	0-30	36.5
kaolinite	0	0	3
plagioclase	19	3-27	13.5
chlorite	6	2-11	9
ilmenite	1	1-2	2
dolomite	0	0	1
Sum of squares of differences	0.13	0.01 - 0.50	0.17

leucogneisses have high SiO_2 and K_2O contents and contain minor fluorite, indicating their possible formation from highly fractionated magmas that are commonly found in high-level magma chambers susceptible to major eruptive phases during caldera-collapse. The quartzo-feldspathic gneisses contain associated minor bands of mafic granulite/amphibolite of tholeiitic composition in most paragneiss belts (see Section 9.2), indicating that bimodal, acid-dominated volcanism predominated during the formation of the metasedimentary/metavolcanic sequences. Rocks of dacitic-to-andesitic composition are rare and occur primarily in the extreme southern (Bitterfontein) and northern (Geselskapbank) areas.

The type of volcanism described above is commonly restricted to certain continental regions where extensional tectonics predominate and with which certain distinctive types of mineralisation are associated. Peralkaline acid volcanism with asssociated Sn, W, Mo, Ta, Be, Li mineralisation is apparently excluded, as indicated by the low Zr concentrations of the quartzo-feldspathic gneisses. Instead, the acid extrusives have resulted from I- or S-type magmatism with associated Zn, Pb, Cu, Ag and lesser W, F mineralisation. These aspects are dealt with in more detail in Chapter 14.

The cordierite-bearing metapsammitic gneisses have chemical and stratigraphic similarities to the metapelitic gneisses in the southern and central portions of the study area and represent psammitic associates of these former pelites.

Chapter 9

GEOCHEMISTRY OF THE METABASIC ROCKS

9.1 Introduction

The vast majority of amphibolites and basic granulites in the western NMC derive their origin from the metamorphism of mafic igneous rocks - more specifically rocks of basaltic to tholeiitic composition (Moore,1977; Zelt,1980; Clifford et al., 1981). Their outcrop characteristics and mineral assemblages are generally sufficiently distinct from those of calc-silicate rocks for discrimination to be made in hand specimen or thin section (see Section 3.7) with the exception of certain banded amphibolites (hornblende + diopside) in the northern portions of the study area. Field relationships (this study; Joubert,1971; Zelt, op.cit.) indicate that some of the western NMC metabasites represent cross-cutting dykes and sills (i.e. they are orthogneisses) whilst others represent conformable lavas or tuffs (i.e. they are paragneisses). Some of the latter type appear to have undergone local chemical modification subsequent to deposition, possibly due to weathering (Moore,1977 and Section 10.6), complicating attempts to define the specific origins of these lithologies. In this study, sampling of metabasites was restricted to those mafic rocks which were intimately interbanded with other supracrustal rocks. Both mafic orthogneisses and paragneisses were probably sampled due to the difficulty in distinguishing between these two types in the majority of outcrops. Larger mafic bodies which occurred in association with the charnockites and augen gneisses were not examined as their relationship to the supracrustal rocks was obscure, although apparently of an intrusive nature similar to the charnockites and augen gneisses themselves. For this reason, the specific basic granulites studied by Clifford et al. (op.cit.) have been omitted from the comparative part of this study.

Within the basaltic suite of volcanic rocks, there is an important relationship between the major and trace element composition of the rocks and their specific tectonic settings. Discriminatory studies of basalts from various tectonic environments - ocean floor basalts, low-potassium tholeiites from island arcs, calc-alkali basalts, ocean island and continental basalts and tholeiites - have been made using major element distributions (Pearce,1976; Pearce et al., 1975,1977; de la Roche et al., 1980; de la Roche,1981) and incompatible and transition trace element contents (Pearce and Cann,1973; Floyd and Winchester,1975; Winchester and Floyd,1976; Wood et al., 1979; Nicollet and Andriambololona,1980) and have been applied to amphibolites and granulites in various metamorphic terranes (e.g. Clark,1979; Garrison,1981). The metamorphosed mafic rocks of the paragneiss belts of the western NMC are examined using these techniques to demonstrate initially their specific igneous parentage, and secondly to attempt to classify their tectonic setting by means of their compositions.

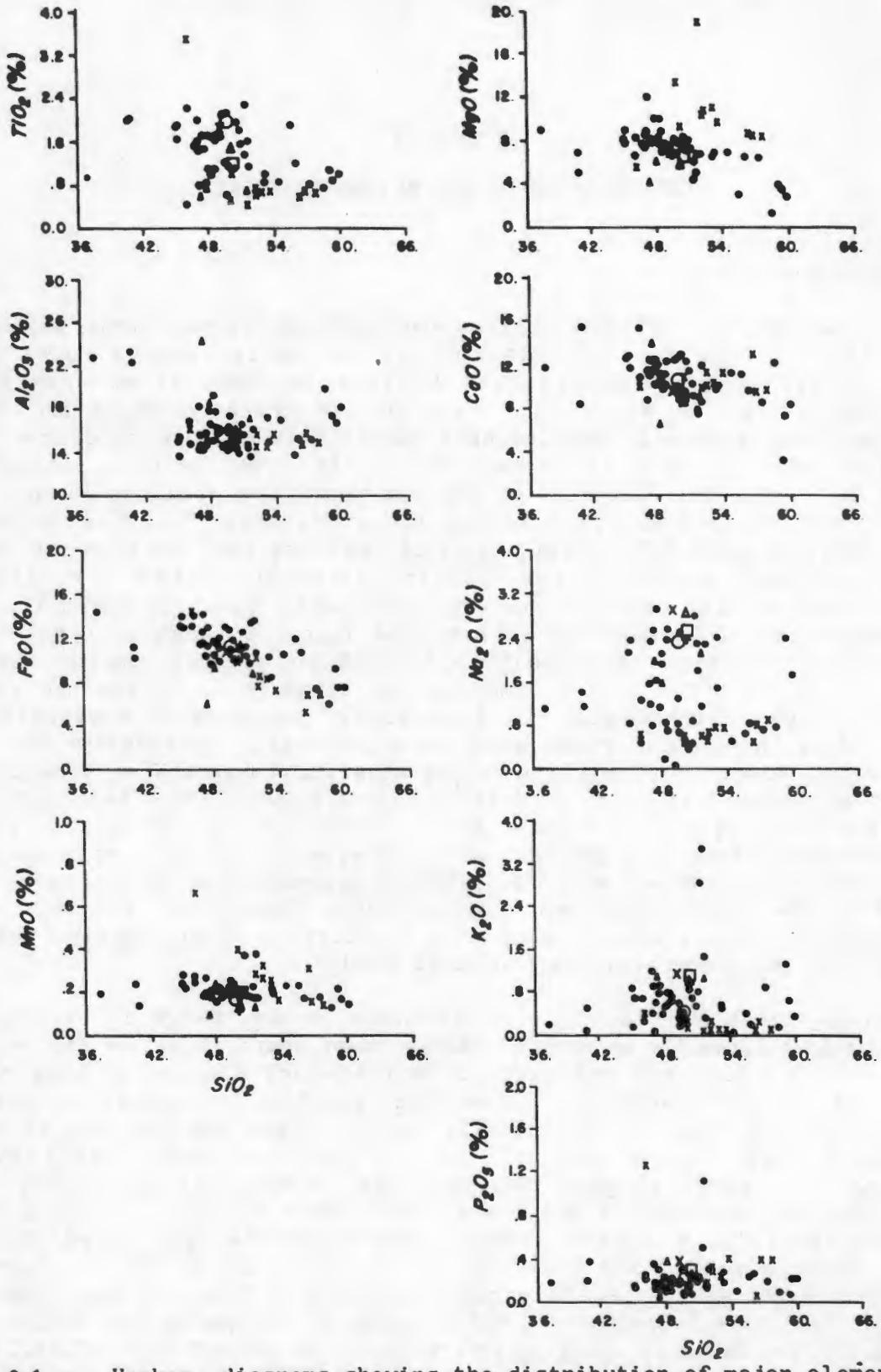

Fig. 9.1 Harker diagrams showing the distribution of major element oxides within the metabasic rocks of the study area. Namiesberg-type amphibolites (small crosses) are distinguished from the bulk of the metabasites (dots). Mean compositions for dolerite (0), diabase (large cross), gabbro (Δ) and basalt (□), taken from le Maitre (1976), are also shown for comparison.

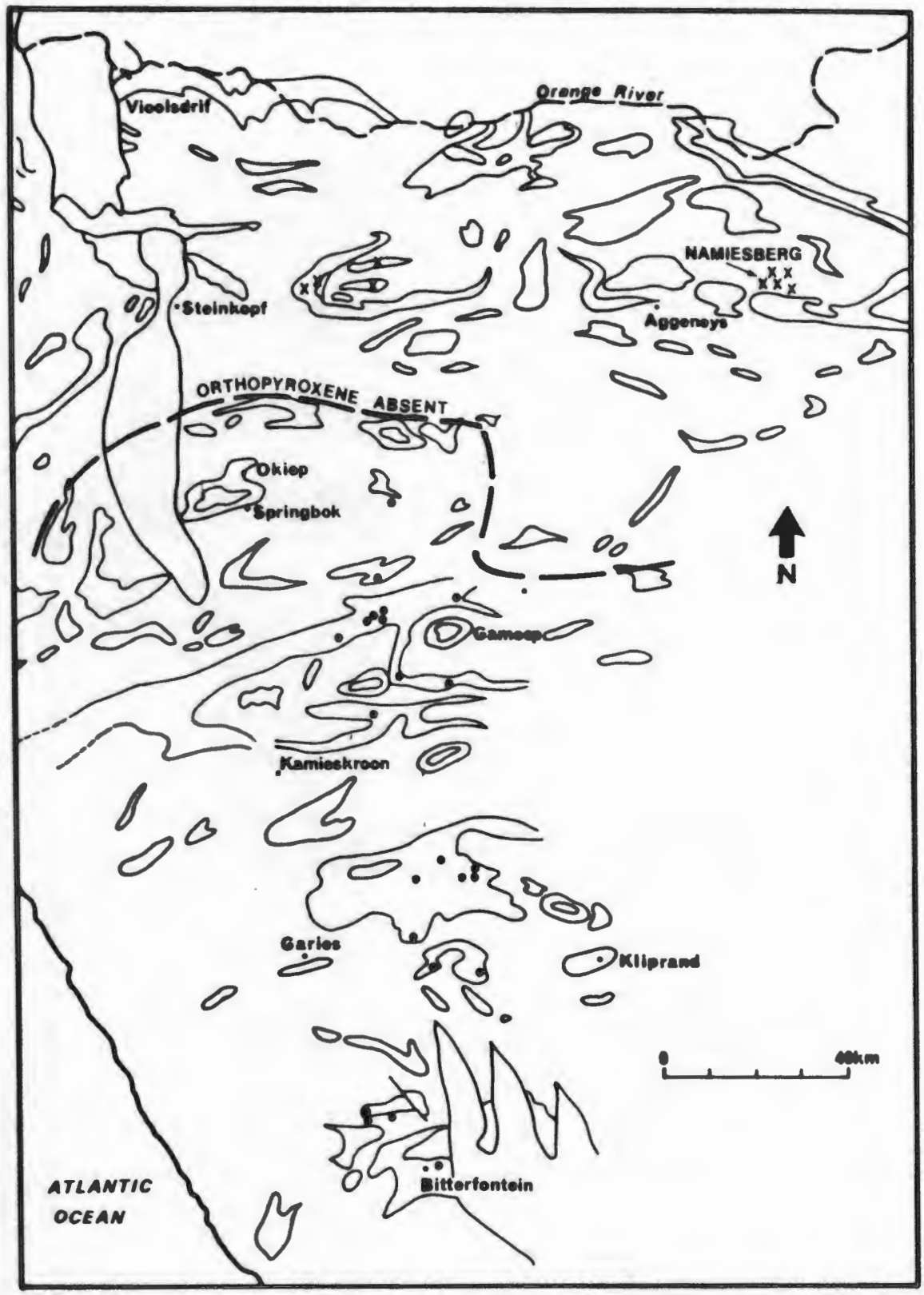

Fig. 9.2 Regional map of the western portions of the NMC showing the localities of the metabasite samples within the various supracrustal sequences. Namiesberg-type amphibolites (crosses) are distinguished from the bulk of the metabasites (dots). The metamorphic boundary defining the transition between orthopyroxene-bearing and orthopyroxene-free mafic rocks is also displayed.

TABLE 9.1 Comparison of the major element contents of amphibolites and basic granulites from the study area with average values for gabbro, basalt and tholeiite as well as boninites from Bonin Island.

	1.		2.	3.	4.		5.
SiO_2	49.48	(5.56)+	49.58	49.20	53.71	(2.47)+	58.04
TiO_2	1.46	(0.43)	1.98	1.84	0.61	(0.10)	0.12
Al_2O_3	16.93	(2.71)	14.79	15.74	14.11	(2.70)	11.78
FeO*	11.20	(2.07)	11.07	10.54	8.10	(1.74)	8.55
MnO	0.21	(0.05)	0.18	0.20	0.23	(0.07)	0.04
MgO	6.82	(1.85)	7.30	6.73	10.57	(3.43)	11.02
CaO	10.25	(1.84)	10.36	9.47	10.28	(1.13)	8.52
Na_2O	1.49	(0.69)	2.37	2.91	0.84	(0.57)	1.40
K_2O	0.65	(0.56)	0.43	1.10	0.19	(0.14)	0.51
P_2O_5	0.21	(0.10)	0.24	0.35	0.27	(0.11)	-
no. of samples	25		202	3594	10		3

* total Fe as FeO
\+ standard deviation

1. amphibolites, basic granulites of major group (analyses from present study).
2. average tholeiite (le Maitre, 1976).
3. average basalt (le Maitre, 1976).
4. amphibolites of "Namiesberg-type" group (analyses from present study; Moore, 1977).
5. boninite (mean of 3 samples, Bonin Island, Japan; Hickey and Frey, 1982).

9.2 General comparisons with mafic volcanic rocks

Chemical comparisons of 32 metabasites from the study area, together with additional data from the Buffels River area (17 samples; Zelt,1980) and the Namiesberg (9 samples; Moore,1977) and mean values for gabbro, dolerite, diabase, basalt and tholeiite (le Maitre,1976) are presented on Harker diagrams in Fig. 9.1. The pargasitic/actinolitic amphibolites from the Geselskapbank and Namiesberg areas in the extreme north of the study area (Fig. 9.2) have sufficiently different compositions to the bulk of the metabasites to warrant their own symbol on the diagrams. This is particularly apparent on the TiO_2:SiO_2, MgO:SiO_2 and K_2O:SiO_2 plots.

The major group of amphibolites and basic granulites have a relatively broad spread of SiO_2 values from 40% to 60%, although the bulk of the samples are concentrated between 45% and 55% SiO_2, and in general compare well with the mean values for the various basaltic types as quoted by le Maitre (1976) (Table 9.1). Only Na_2O and possibly K_2O appear to be slightly depleted in the metamorphosed rocks compared to the mean values. The Namiesberg-type amphibolites, however, show relative depletions in TiO_2, FeO, Na_2O and K_2O, and enrichments in SiO_2, MnO and MgO compared to the mean values of basalts and the major group of western NMC mafic rocks.

The scatter displayed by certain samples at the extremes of the ranges may be due to post-depositional/emplacement processes. A high-TiO_2-MnO-P_2O_5 garnet amphibolite from the Namiesberg suite has been explained as resulting from lateritic weathering processes (Moore,1977). Three high-Al_2O_3, low-SiO_2 samples from the major group of metabasites (HY-14, HY-16, RFN-3) may also have resulted from weathering or leaching, particularly as the HY samples are closely associated with cordierite-hypersthene gneisses (see Section 10.6). The small cluster of high-SiO_2 ($\pm$60%) "feldspathic" basic granulites in the major group do not appear to be significantly depleted in any specific major elements except perhaps MgO, and may have resulted from partial silicification of these rocks prior to metamorphism. Certain samples from the Witwater-Platbakkies paragneiss belt are enriched in K_2O (RW-6, GHP-2; at the 3-4% level) and P_2O_5 (GHP-2; at the 1% level) and are also suspected of having been subjected to post-emplacement modification, either by diagenesis or weathering.

Stepwise discriminant analysis was conducted to calculate a canonical variable that would successfully separate the two groups of western NMC metabasites. A similar method was used to that employed for the metapelitic rocks (see Section 7.6). The elements selected in the calculation of the canonical variable were TiO_2, Ba, Cr, Pb and Zn (Fig. 9.3 and Table 9.3). The mean values for the two groups (Tables 9.1 and 9.2) indicate significant depletions in the Namiesberg-type amphibolites in TiO_2, Al_2O_3, total Fe as FeO, Na_2O, K_2O, Rb, Ba, Sr, Zr, V, Cu and Y compared to the major group and enrichments in SiO_2, MgO, Cr, Ni, Pb and Zn, with close similarities in MnO, CaO, P_2O_5 and Co contents.

On the AFM diagram, the western NMC metabasites plot within the field

TABLE 9.2 Comparison of trace element contents of amphibolites and basic granulites from the study area with values for Karroo basalts and boninites from Bonin Island.

Rb	28	(34)*	12	5	(5)*	10
Ba	159	(204)	177	49	(74)	26
Sr	372	(281)	192	284	(246)	75
Zr	124	(61)	94	82	(21)	18
Nb	6	(5)	5	4	(4)	
Cr	197	(129)	283	714	(366)	753
V	248	(73)	240	158	(48)	161
Ni	93	(50)	94	311	(151)	152
Co	49	(12)	48	46	(14)	42
Pb	10	(7)	3	24	(21)	
Zn	100	(34)	86	131	(51)	
Cu	14	(25)	87	9	(19)	
Y	32	(9)	24	17	(6)	4
no. of samples	25		49	10		3

* standard deviation

1. amphibolites and basic granulites of major group (analyses from present study).

2. Karroo basalts from Lesotho Formation (analyses from Duncan et al., in press).

3. amphibolites of Namiesberg group (analyses from present study; Moore, 1977).

4. boninite (mean of 3 samples, Bonin Island, Japan; Hickey and Frey, 1982).

TABLE 9.3 Coefficients for the canonical variable and the U-statistic from the stepwise discriminant analysis of metabasic rocks from the study area.

Variable	Coefficients for canonical variable	U-statistic (Wilks' Lambda)
TiO_2	1.973	0.439
Ba	0.003	0.098
Cr	-0.006	0.146
Pb	-0.066	0.135
Zn	-0.024	0.269
Constant	2.722	

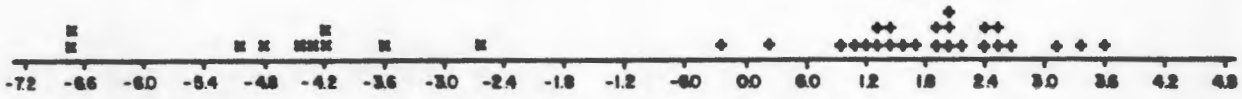

Fig. 9.3 Separation of the Namiesberg-type amphibolites (x) from the major group of metabasites (+) using the canonical variable listed in Table 9.3.

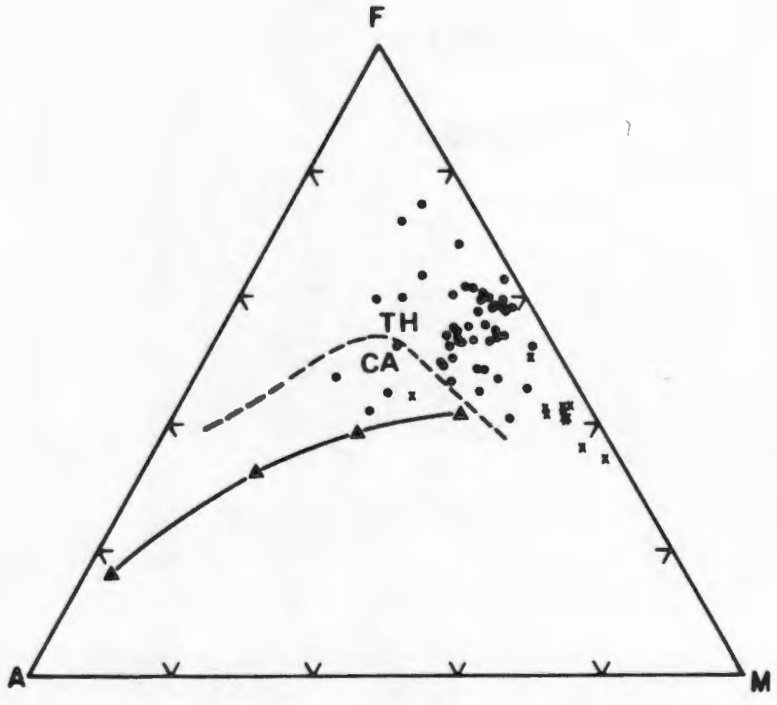

Fig. 9.4 AFM diagram showing the positions of Namiesberg-type amphibolites (crosses) and other metabasites (dots) from the western NMC compared to the fields of tholeiitic (TH) and calc-alkaline (CA) igneous rocks, and the calc-alkaline trend (triangles) defined by metavolcanic rocks of the Orange River Group (Reid, 1977). Data are from this study, Moore (1977) and Zelt (1980).

predicted for mafic rocks belonging to a tholeiitic rather than a calc-alkaline volcanic suite (Fig. 9.4). The major group of amphibolites and basic granulites show relative enrichments in Fe compared to the calc-alkaline trend of the Orange River Group metavolcanics (Reid,1977), but the Namiesberg-type amphibolites plot on an extension of this calc-alkaline trend into the tholeiite field, being distinctly more magnesian in character. As the Namiesberg-type amphibolites are located in relatively close geographical proximity to the Orange River Group metavolcanics, this may imply some common genetic association.

On the ACF diagram (Fig. 11.5) the metabasites plot predominantly within the anticipated field for basaltic and andesitic rocks (Winkler,1976) with a few samples, depleted in the C component, falling within the adjacent greywacke field. When plotted on the Si-Al-Fe diagram (Fig. 11.6) they lie along the predicted igneous trend towards the basaltic end, and generally well outside the narrow Al:Fe range of common sedimentary rock types (Moore and Dennen, 1970). On the plot of Niggli values c vs mg (Fig. 11.3a) the western NMC metabasites cluster on the igneous trend defined by Karroo basalts (Leake,1964). All of the above plots, together with the comparisons on the Harker diagrams with typical volcanic rocks demonstrate the mafic volcanic ancestry of the amphibolites and basic granulites of the western NMC and their close chemical similarity to basaltic and tholeiitic rocks as opposed to greywackes and shales (van de Kamp,1970).

9.3 Comparison with specific categories of basalts and tholeiites

As in the case of the leucogneisses and biotite gneisses (see Section 8.4), the R1-R2 diagram of de la Roche *et al.* (1980) can be applied to predict potential premetamorphic volcanic precursors for the amphibolites and basic granulites of the western NMC. Two discriminant functions were calculated, using the eight major cations Si, Ti, Al, Fe, Mg, Ca, Na and K, and are plotted against a classification grid, devised from a large geochemical database of volcanic rocks. When plotted on the R1-R2 diagram, the western NMC metabasites show a relatively wide degree of scatter, unlike the leucogneisses, plotting within the fields of andesi-basalt, basalt, tholeiite and picrite and also in positions showing anomalously high R1 values for typical volcanic/plutonic rocks (Fig. 9.5). When compared to the "critical line of silica saturation" and the field of the basaltic family from the CLAIR file of le Maitre (1976), it can be seen that the majority of western NMC metabasites represent silica-saturated basaltic-to-tholeiitic rocks. The samples which plot outside the field of normal basaltic rocks due to high R1 (= 4Si - 11(Na + K) - 2(Fe + Ti)) values are most probably due to high Si and complementary low Fe values, and include all the Namiesberg-type amphibolites. High Si values could be the result of post-emplacement processes such as silicification.

9.3.1 The F-E-D-A tetrahedron and related discriminants

De la Roche (1981) has converted a mineralogical tetrahedron with

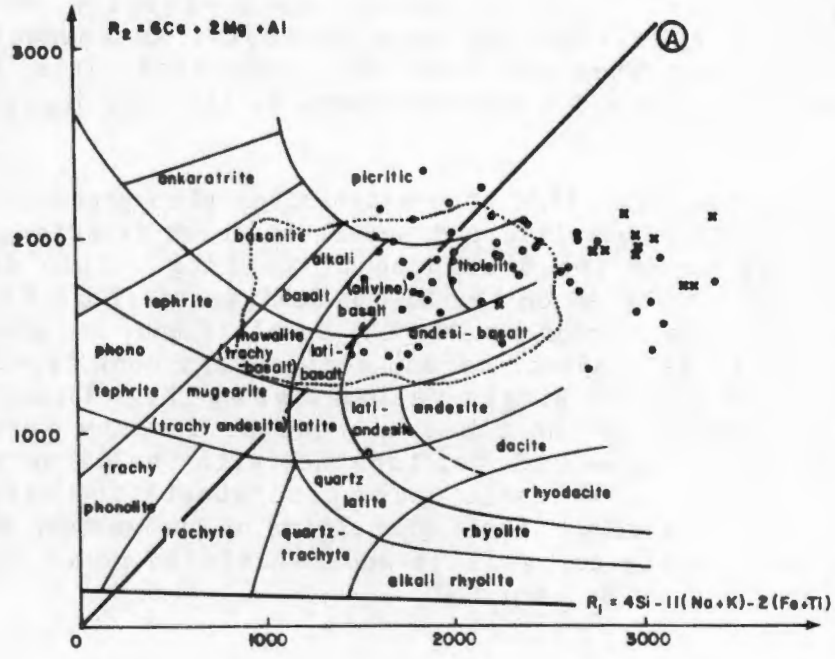

Fig. 9.5 The distribution of Namiesberg-type amphibolites (crosses) and other metabasites (dots) on the R1-R2 diagram (after de la Roche et al, 1980). The range of basaltic compositions contained in the CLAIR data file of le Maitre (1976) is also demarcated (stippled line).

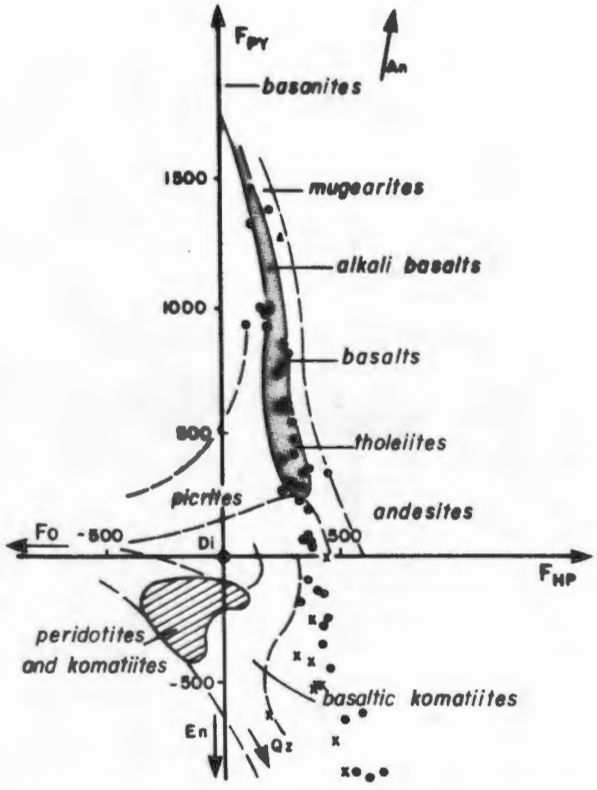

Fig. 9.6a Fpy vs Fhp diagram (after de la Roche, 1981) showing the positions of metabasic rocks from the western NMC relative to the fields of various mafic volcanic rocks. Namiesberg-type amphibolites (crosses) are distinguished from the other metabasites (dots). Data as for Figure 9.4. An - anorthite , Di - diopside, En - enstatite, Fo - forsterite, Qz - quartz. Basaltic field (shaded) and field of peridotites and komatiites (lined) are emphasized.

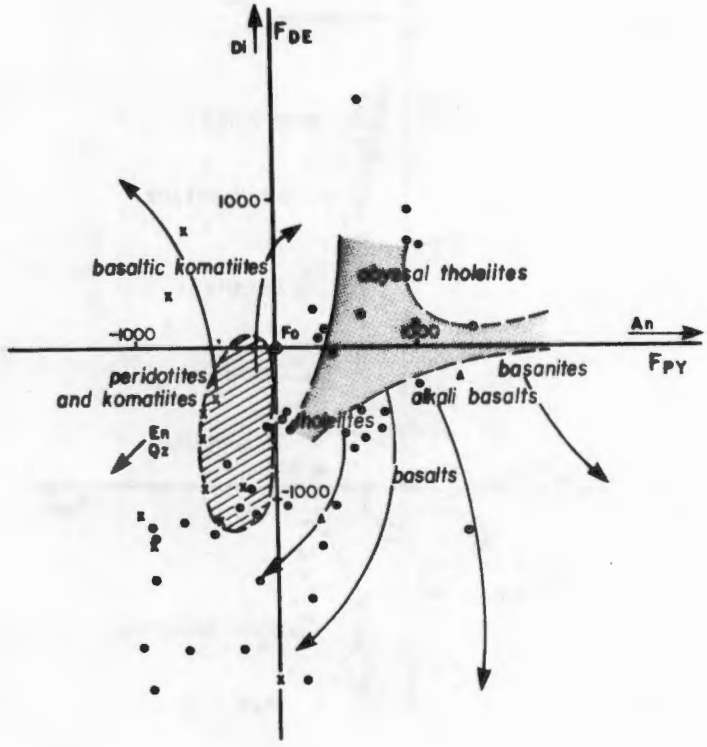

Fig. 9.6b Fde vs Fpy diagram (after de la Roche, 1981) showing the positions of metabasic rocks from the western NMC relative to the fields of various mafic volcanic rocks. For explanation see Figure 9.6a. Lines of increasing differentiation (arrowed) are included.

forsterite (F), enstatite (E), diopside (D) and anorthite (A) at the four apices, into a chemical tetrahedron consisting of four multicationic variables expressed as terms of the major elements present, and from this tetrahedron has calculated chemical discriminant functions which define dividing planes of petrological interest within the tetrahedron that are applicable to ultramafic and mafic rocks. The discriminant functions calculated by de la Roche (op.cit.) are plotted as cross-sections and the broad fields of various basaltic and ultramafic rock types are defined on these diagrams from analyses taken from the literature.

The most significant discriminant function is Fpy which separates plagioclase-dominated rocks (positive values) from orthopyroxene-dominated rocks (negative values). This function thus successfully discriminates the basalt family from peridotites and komatiites. High SiO_2 values also have a negative influence on Fpy and thus spread the basalt family from SiO_2-poor basanites to SiO_2-rich andesites. When plotted against discriminant function Fhp, an olivine-dominated function, the division is more pronounced, and picrites are segregated within the basaltic family (Fig. 9.6a). When Fpy is plotted against function Fde, a clinopyroxene-dominated function, further separation of abyssal tholeiites (relatively clinopyroxene-rich) from common tholeiites is possible (Fig. 9.6b).

The metabasites of the western NMC are compared to typical ultramafic and mafic suites in the two diagrams (Figs. 9.6a and b). On the Fpy:Fhp plot, they are situated along the elongate line of the basaltic series with the majority of samples plotting within the broad range of basalts and tholeiites. A relatively large number of samples, however, including all the Namiesberg-type amphibolites, plot on an extension of this line into the field of negative Fpy values, indicating enrichments in SiO_2 and/or orthopyroxene, or conversely depletions in plagioclase, relative to typical basaltic rocks. This is similar to the trends observed on the R1-R2 diagram.

Fpy (= -4Si + 4Ti + 3Al + Fe + 2Mg + 6Ca + 13Na + 15K as millicationic numbers calculated from oxide percentages) is relatively sensitive to variations in SiO_2 content. Slight enrichments in SiO_2 may explain the negative distributions observed on the plot, particularly in the case of the "feldspathic" basic granulites from the Bitterfontein and Platbakkies areas which have the most negative Fpy values. The Namiesberg-type amphibolites are relatively SiO_2-rich, but also have high MgO values, and their distribution may be related to orthopyroxene enrichment, or conversely to plagioclase depletion, in the original rock.

On the Fpy:Fde plot, the bulk of the metabasites have negative Fde values and thus bear no apparent relationship to abyssal tholeiites (Fig. 9.6b). The majority of samples fall either within the expected ranges of common tholeiites or along lines of differentiation for these latter rocks. Once again the effects of SiO_2 and/or orthopyroxene enrichment in the Fpy factor can be observed. This results in the majority of Namiesberg-type amphibolites falling within the field of peridotites and komatiites on this diagram, although it can be seen on the previous Fpy:Fhp plot that they lack the presence of the olivine component of these latter rock types.

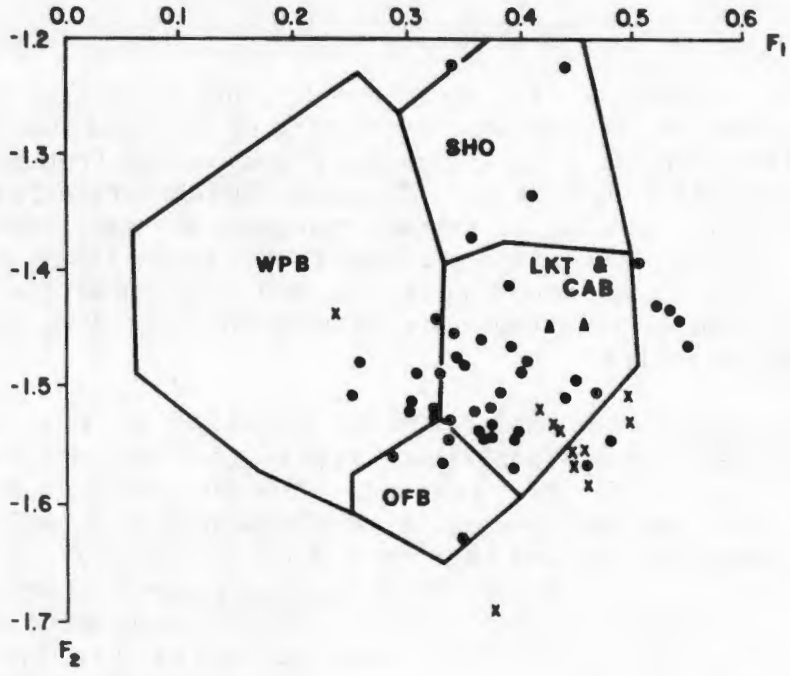

Fig. 9.7a F1-F2 diagram (after Pearce, 1976) for major elements, showing the relative positions of Namiesberg-type amphibolites (crosses) and other metabasites (dots) from the western NMC relative to the fields of within-plate basalts (WPB), shoshonites (SHO), low-K tholeiites (LKT), calc-alkali basalts (CAB) and ocean-floor basalts (OFB). Data as for Figure 9.4.

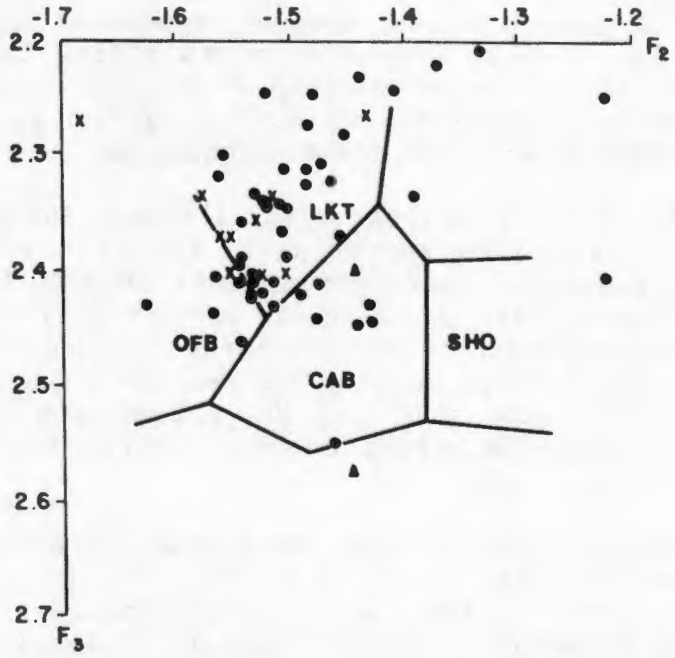

Fig. 9.7b F2-F3 diagram (after Pearce, 1976) showing similar relationships to Figure 9.7a using the same data set.

It can thus be interpreted from the F-E-D-A tetrahedron and its associated discriminant functions that the western NMC metabasites represent basaltic to tholeiitic rocks (excluding oceanic tholeiites), some of which show relative SiO_2 enrichment, possibly coupled with enrichment in orthopyroxene and depletion in plagioclase, particularly in the case of the Namiesberg-type amphibolites.

9.3.2 Major cation discriminant analysis

Pearce (1976) employed discriminant functional analysis to separate six tectonically-defined basaltic magma types using the eight major element oxides - SiO_2, TiO_2, Al_2O_3, total Fe as FeO, MgO, CaO, Na_2O and K_2O to calculate three factors F1, F2 and F3. On Pearce's (op.cit.) F1-F2 diagram, "within-plate" basalts incorporating both continental and ocean-island basalts could be segregated from shoshonites, ocean floor basalts and a field incorporating both low-K tholeiites of island arc environments and calc-alkali basalts. The F2-F3 diagram further segregated low-K tholeiites from calc-alkali basalts, shoshonites and ocean-floor basalts.

Application of these factors to the western NMC metabasites results in the majority of samples plotting within the low-K tholeiite/calc-alkali basalt field in the F1-F2 diagram (Fig. 9.7a) and in the field of low-K tholeiites in the F2-F3 diagram (Fig. 9.7b). In both diagrams, the western NMC metabasites plot relatively close to the boundary line between low-K tholeiites and ocean floor basalts, and generally away from the relatively K-enriched shoshonites. F1 is particularly sensitive to TiO_2, F2 to K_2O and F3 to Al_2O_3 (Garrison,1981), and it is the contents of these three major element oxides which essentially classify the western NMC metabasites as medium-to-low-K tholeiites that have similarities to tholeiitic basalts associated with island-arc environments. The low K_2O contents of the metabasites (see also Fig. 9.1) may, however, be partly related to metamorphic processes and therefore this classification should be treated with caution.

9.3.3 The K_2O-TiO_2-P_2O_5 plot

Pearce et al. (1975) demonstrated that the K_2O-TiO_2-P_2O_5 plot successfully discriminates between abyssal oceanic basalts and continental basalts at the 93% certainty level. Garrison (1981), however, has demonstrated that low-K island arc tholeiites from the Pacific plot in a field which straddles the dividing line between the two fields of Pearce et al. (op.cit.), and extends parallel to the K_2O-TiO_2 tie-line indicating that fluctuations exist in the relative amounts of these two element oxides in island-arc tholeiites.

The western NMC metabasites plot in a similar extended field parallel to the K_2O-TiO_2 tie-line, cross-cutting the two fields of Pearce et al. (1975) (Fig. 9.8). Part of this extension, particularly the extreme K_2O-enriched and K_2O-depleted samples, may be due to high-grade metamorphic processes involving

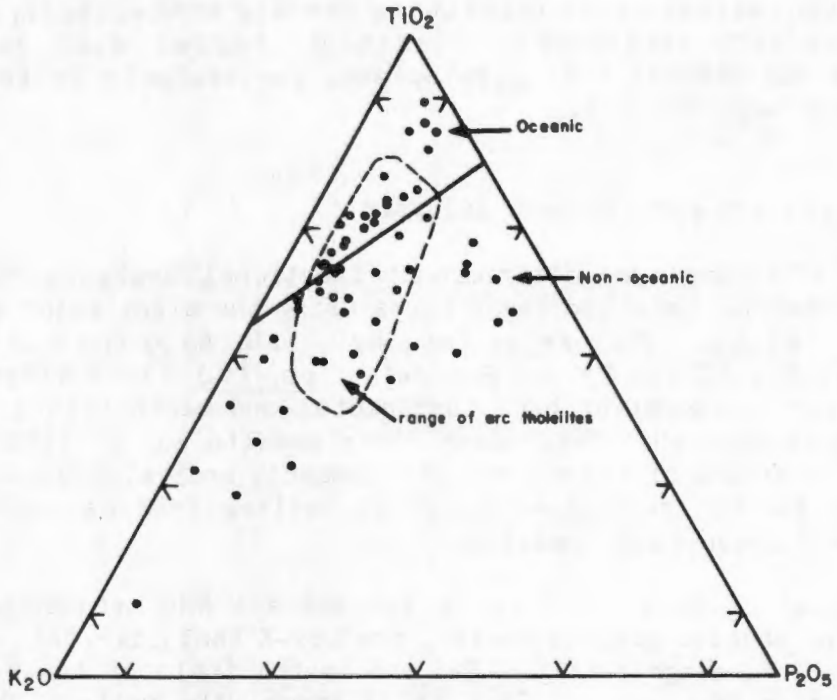

Fig.9.8 K_2O:TiO_2:P_2O_5 triangular diagram showing the position of metabasic rocks from the western NMC (undivided) relative to the fields of oceanic and continental basalts (as defined by Pearce et al, 1975) and of island arc tholeiites (as defined by Garrison, 1981).

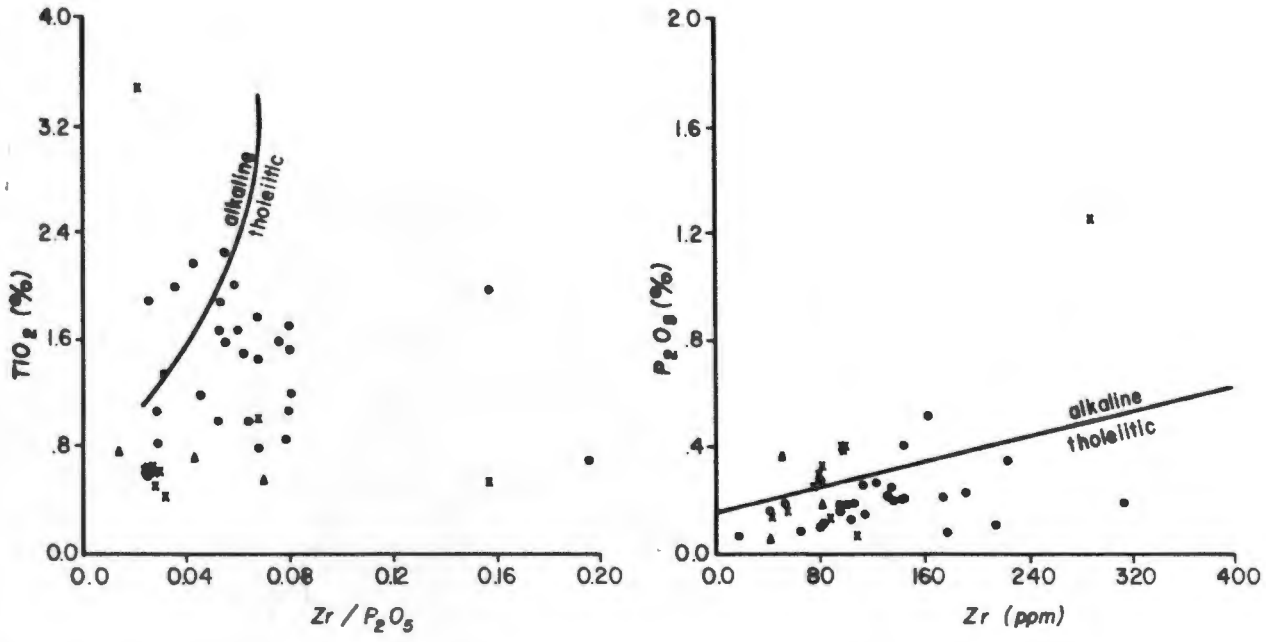

Fig. 9.9a Plot of TiO_2 vs Zr/P_2O_5 showing the positions of Namiesberg-type amphibolites (crosses) and other metabasites from the western NMC (dots) relative to the fields occupied by alkaline and tholeiitic basalts (after Winchester and Floyd, 1976). Data from this study and Moore (1977).

Fig. 9.9b Similar plot of P_2O_5 vs Zr using the same data set.

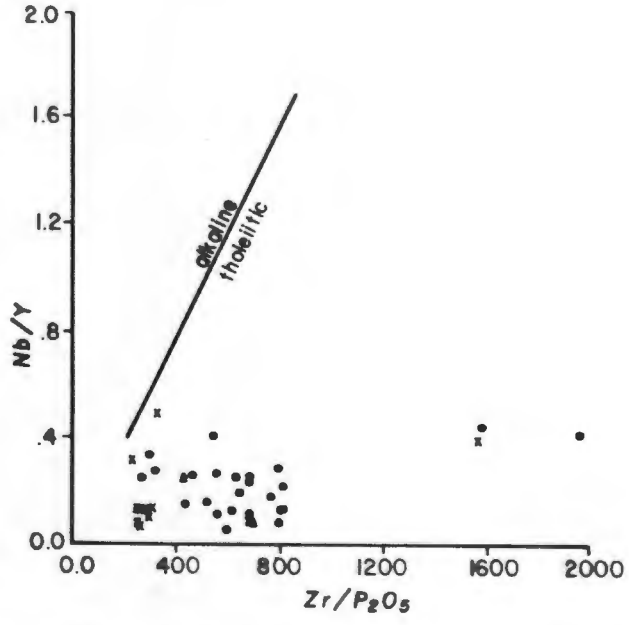

Fig. 9.9c Similar plot of Nb/y vs Zr/P_2O_5 using the same data set.

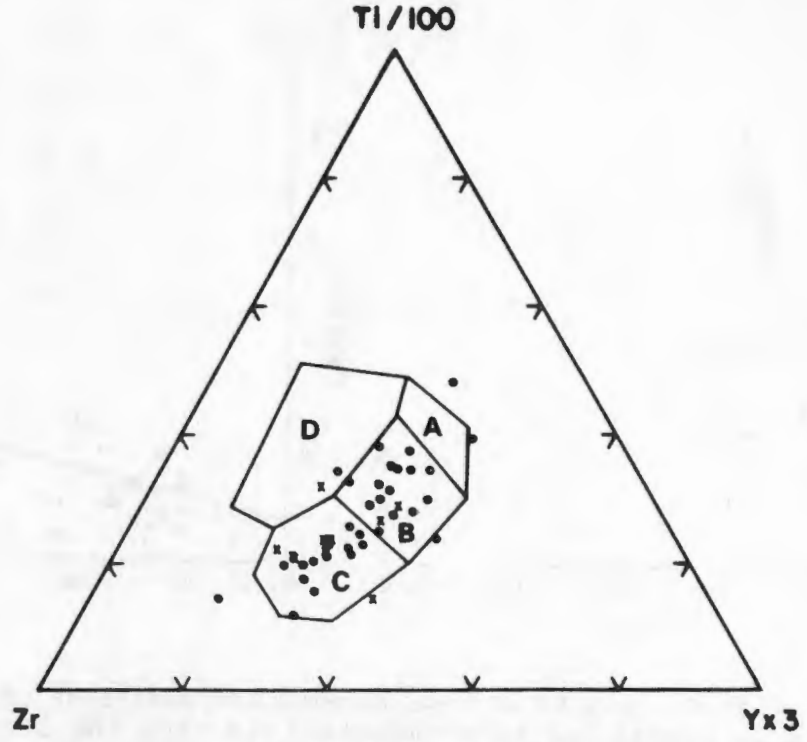

Fig. 9.10a Ti-Y-Zr triangular diagram showing the position of Namiesberg-type amphibolites (crosses) and other metabasites (dots) from the western NMC relative to fields defined by Pearce and Cann (1973) for low-K tholeiites (A), ocean-floor basalts (B), calc-alkali basalts (C) and within-plate basalts (D). Data from this study and Moore (1977).

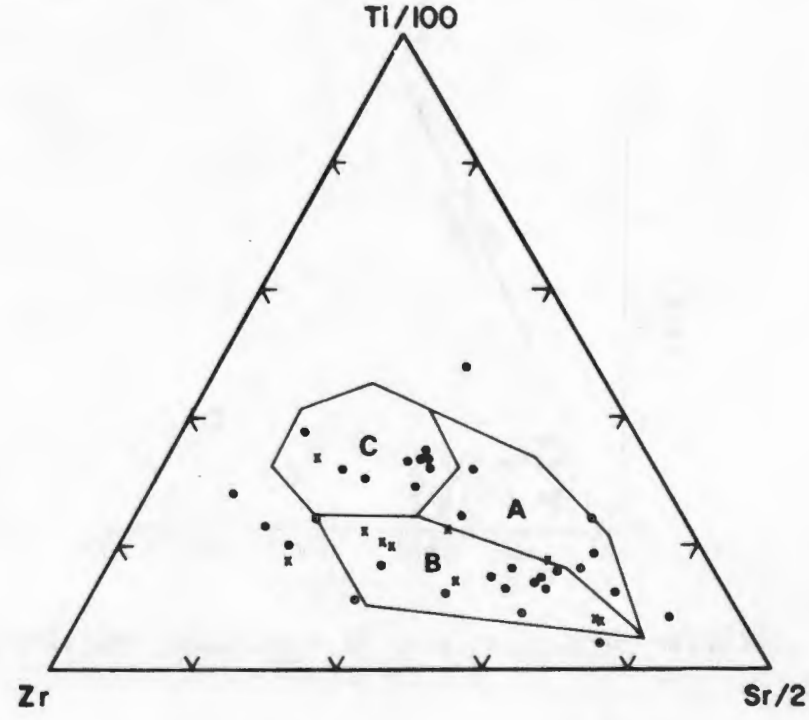

Fig. 9.10b Similar triangular diagram of Ti-Sr-Zr using the same data set.

the limited mobility of lithophile light elements including K (see Section 6.6). The bulk of the samples, however, fall within the range of island arc tholeiites as defined by Garrison (1981). Although the metabasites may have been affected by K_2O mobility during metamorphism, it can be observed on the Harker diagrams (Fig. 9.1) that the Namiesberg-type amphibolites have lower K_2O contents than the higher grade basic granulites from south/central Namaqualand. This is the opposite trend to that expected from metamorphic processes and is therefore in all probability a premetamorphic characteristic of the rocks.

9.3.4 Incompatible trace elements

Much use has been made of the incompatible elements Ti, P, Zr, Y and Nb in the chemical classification of basalts. These elements are regarded as relatively immobile during post-emplacement alteration processes such as diagenesis and metamorphism. Winchester and Floyd (1976), in a series of bivariate plots, have shown that distinctions between alkaline and tholeiitic trends in basalts and their altered and metamorphosed equivalents can be made using the elements Ti, P, Zr and Nb. Application of their plots to the western NMC metabasites reveals dominant tholeiitic trends, which are most apparent in the Nb/Y vs Zr/P_2O_5 diagram (Fig. 9.9).

Pearce and Cann (1973) used the elements Ti, Zr, Y and Sr in a series of triangular and bivariate diagrams to segregate basalts from the various tectonic settings outlined in Section 9.3.2 above. Discrepancies in this classification due to poor representation of continental tholeiites within their sample suite, have been pointed out by Holm (1982). Continental tholeiites are shown by Holm (op.cit.) to extend substantially into field B and to a lesser extent into field C in the Ti-Y-Zr diagram of Pearce and Cann (op.cit.) (Fig. 9.10a). This makes field B a highly ambiguous area containing basalts of low-K tholeiitic, ocean floor, calc-alkaline and continental tholeiitic affinity. Approximately 50% of the western NMC metabasites plot within field B on the Ti-Y-Zr diagram with the remainder plotting essentially within field C. Interpretation of this distribution of data points would be for a calc-alkaline basaltic origin (Pearce and Cann, op.cit) or a continental tholeiitic origin (Holm, op.cit.).

On the Ti-Sr-Zr diagram (Pearce and Cann, 1973), the western NMC metabasites show a relatively broad scatter, (Fig. 9.10b) possibly due to the mobile nature of Sr during metamorphism, with the majority of samples plotting within the fields of ocean floor and calc-alkaline basalts. Continental tholeiites are not displayed on this diagram. It is worth noting that in the plots of the incompatible elements, the western NMC metabasites do not fall within the fields designated for low-K island-arc tholeiites, in contrast to their classification using Pearce's (1976) major cation discriminant functions.

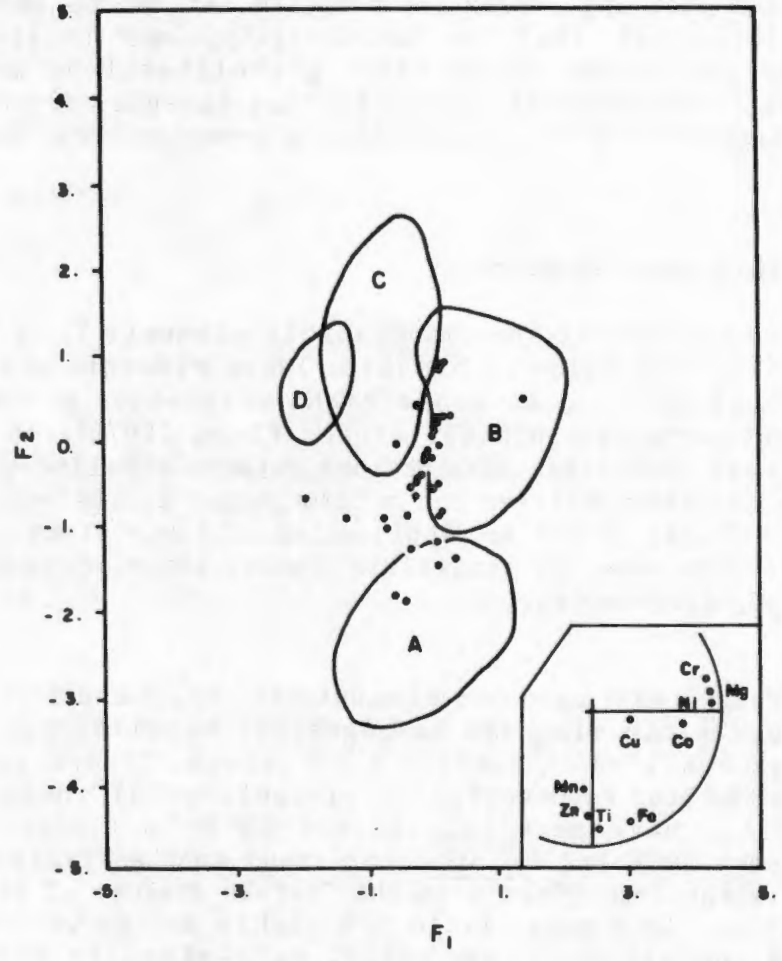

Fig. 9.11 F1-F2 diagram (after Nicollet and Andriambololona, 1980) for transition elements, showing the relative positions of metabasites from the western NMC (dots) relative to the fields of alkali basalts (A), extrusive continental and island arc tholeiites (B), abyssal tholeiites (C) and orogenic volcanic rocks (D). Data from this study and Moore (1977).

9.3.5 Distribution of transition elements

Nicollet and Andriambololona (1980) have studied the distribution of the transition elements Ti, V, Ni, Cr, Co, Cu, Zn, Fe, Mn and Mg in metabasic rocks including basic granulites and amphibolites, and have concluded that they are "not specially affected by medium- and high-grade metamorphism". Application of principal components factor analysis by Nicollet and Andriambololona (op.cit.) has resulted in the formulation of two discriminant functions, F1 and F2, which segregate the basaltic suite of volcanic rocks into various fields depending on their tectonic environment of emplacement in a similar manner to the studies of Pearce and others. Identification of abyssal tholeiitic origins for certain European amphibolites, granulites and eclogites has been demonstrated using the F1-F2 diagram.

Comparison of the western NMC metabasite data with various defined fields on the discriminant plot (Fig. 9.11) reveals that these basic granulites and amphibolites bear closest resemblence to extrusive continental and arc tholeiites in their transition element composition. Compared to this field, however, they have relatively low F1 values and normal F2 values. Factor F1 is dominated by Ni, Cr, Mg and Co and factor F2 by Fe, Ti, Zn and Mn (see inset to Fig. 9.11). The western NMC metabasites, therefore, are apparently depleted in either some or all of the elements Ni, Cr, Mg and Co compared to typical continental and arc tholeiites. Nicollet and Andriambololona (1980) indicate that low Ni, Cr and Cu contents could be related to depletions during low-grade metamorphism or to sea-water alteration. Mg, Ni, Cr and Co, however, are known to show marked depletions during fractional crystallisation of primitive basaltic magmas (Gunn,1971; Miyashiro and Shido,1975) and so low contents of these elements may be due to magmatic differentiation.

9.4 Comparisons between the two "basaltic" types

The Namiesberg-type amphibolites from the extreme northern portions of the study area have distinctly different compositions to the rest of the amphibolites and basic granulites of the western NMC. This is typified by a markedly higher MgO/(MgO + FeO) ratio, high Ni and Cr values and low TiO_2, FeO, V, Y, Na_2O and K_2O as revealed in plots of these elements and oxides against MgO/(MgO + FeO) (Fig. 9.12). MnO, P_2O_5, Zr, Co and Zn show relatively little difference between the two groupings in similar plots. Ba and Sr show equivocal depletions with increasing MgO/(MgO + FeO).

Within the tholeiitic series of volcanic rocks, fractional crystallisation of the parental magma initially results in trends of increasing Fe, Ti and V, reaching a maximum in the field of tholeiites themselves and then decreasing with the crystallisation of more acidic rocks (Miyashiro and Shido,1975). Ni and Cr, however, do not show this initial increase, but simply decrease with advancing fractional crystallisation (Miyashiro and Shido, op.cit.). Gunn (1971), furthermore, has demonstrated, using Hawaiian basalts, that olivine and Cr spinel fractionation partitions Ni, Cr and Mg with lesser Co into the early-crystallising olivine and spinel

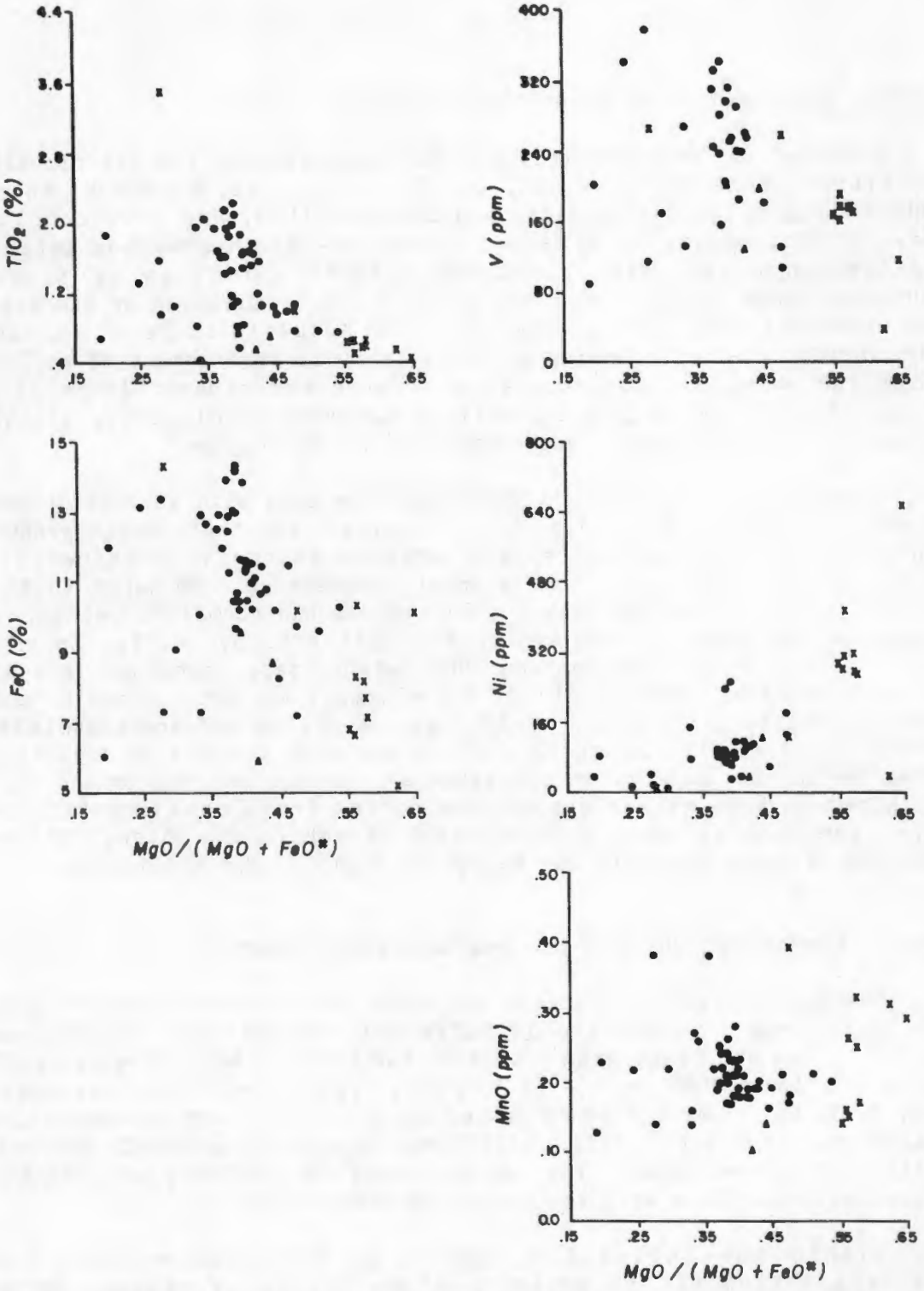

Fig. 9.12 Plots of various major element oxides and trace elements against MgO/(MgO + FeO*). Namiesberg-type amphibolites are represented by crosses and other metabasites from the western NMC by dots. Data from this study and Moore (1977). * total Fe as FeO.

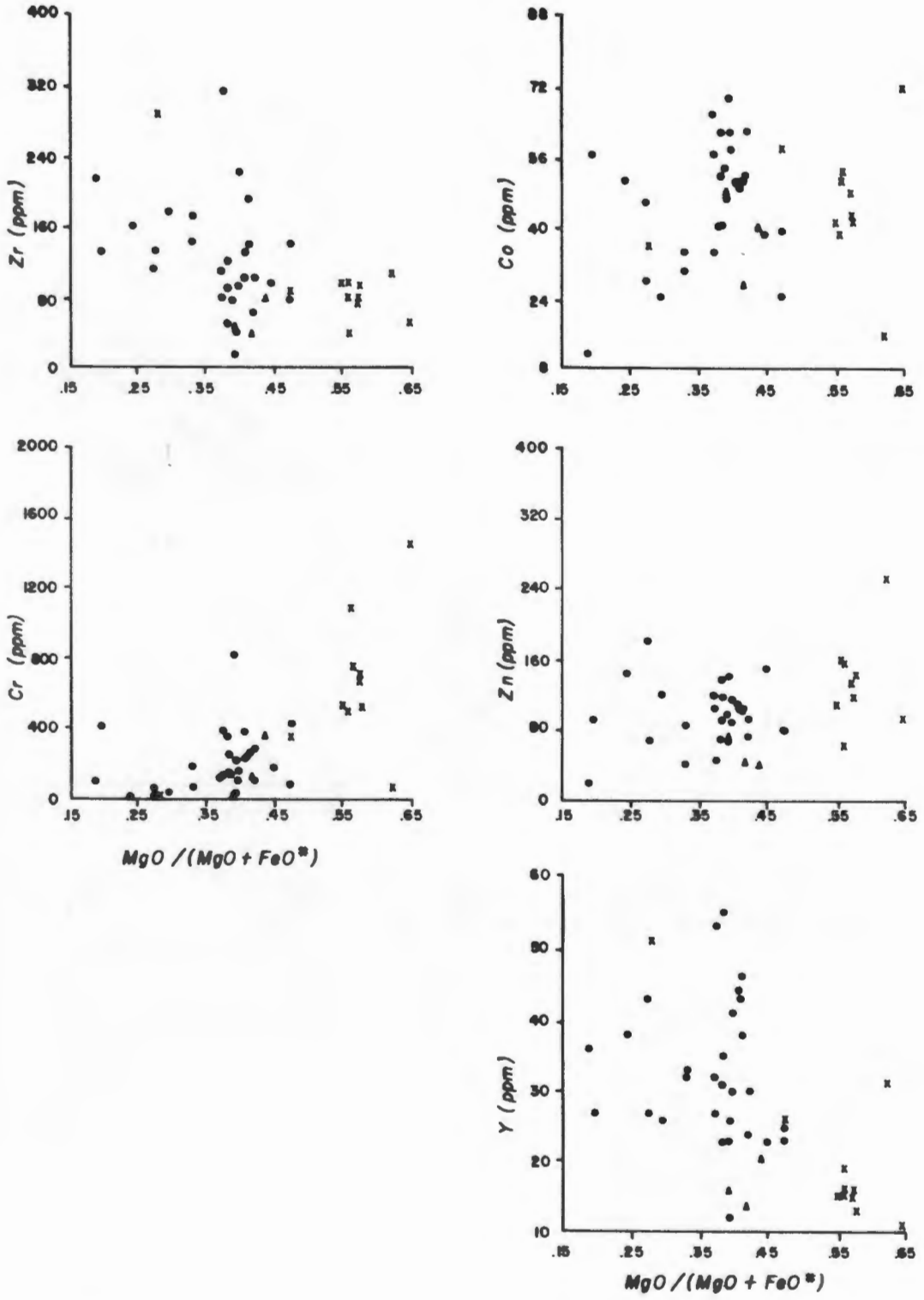

Fig. 9.12 (continued)

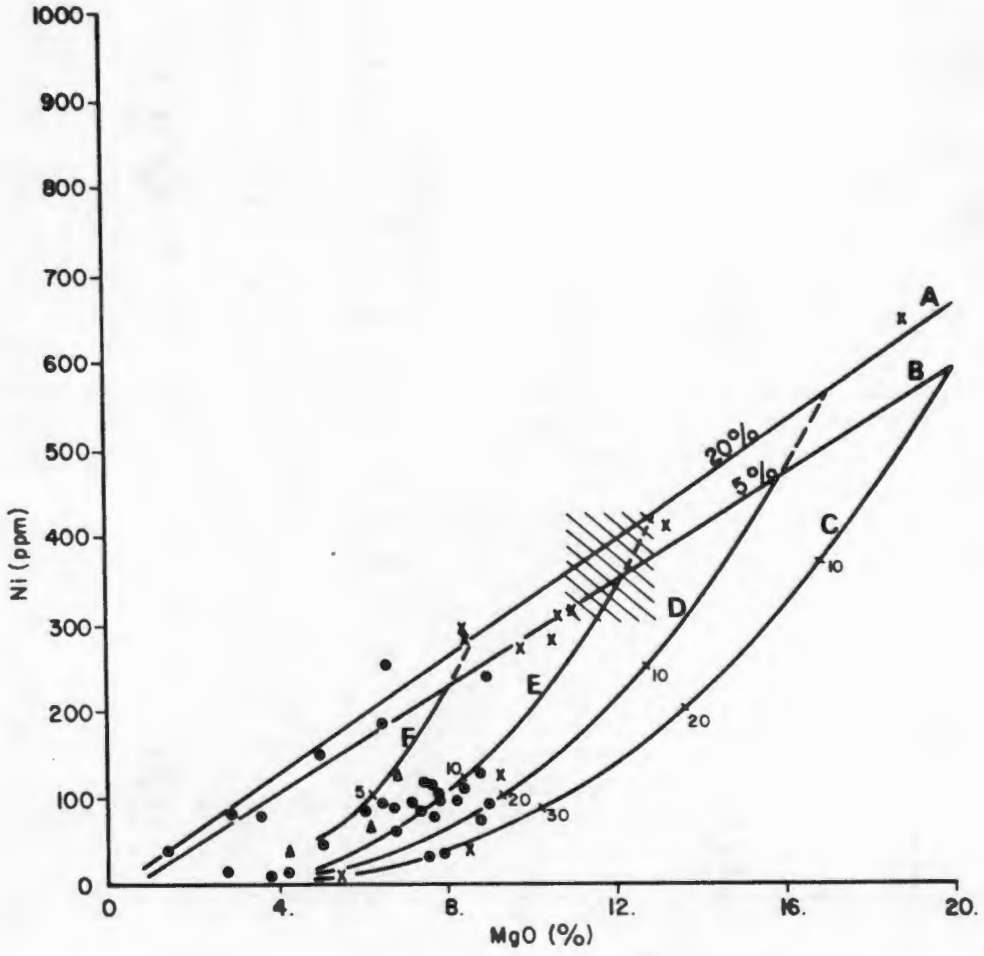

Fig. 9.13 Bivariate plot of Ni vs MgO showing relationships for partial melting - fractional crystallisation models of basaltic rocks (after Hart and Davis, 1978). Partial melting curves of model mantle peridotite are shown for partial melts of 20% (A) and 5% (B). The field of primitive basalt compositions derived from partial melting of mantle peridotites as calculated by Sato (1977) is also shown (hatching). Fractional crystallisation curves are shown for liquids with MgO contents of 20% (C), 16% (D), 12% (E) and 8% (F). Numbers at cross-ties on these curves indicate the amount of olivine crystallised. Data points for Namiesberg-type amphibolites (crosses) and other metabasites from the western NMC (dots) are shown. Data from this study and Moore (1977).

phases and Sc, Cu, Ga, Rb, Sr, Y, Zr and Ba together with "other felsic elements" (presumably K_2O and Na_2O) into the residual liquid. Zn, Fe and Mn have an equable distribution between the olivine and liquid. Rock types such as the Namiesberg-type amphibolites, with higher Mg, Ni and Cr, lower Ti, Fe, V, Y, Na and K and equivalent Mn, Zn, Co and Zr contents compared to the other western NMC metabasites, apparently represent a markedly more primitive, less fractionated or crustal-contaminated magma source.

Using data from Sato (1977) for Ni contents of olivine, orthopyroxene and clinopyroxene, Hart and Davis (1978) have produced partial melting - fractional crystallisation models using a mantle peridotite composition of 70% olivine, 20% orthopyroxene and 10% clinopyroxene as a starting material. When applied to the western NMC metabasites, it can be seen that the Namiesberg-type amphibolites fall on the partial melt curves (5% to 20%), whereas the bulk of the other basic granulites and amphibolites plot within the fields of basalts subjected to varying degrees of fractional crystallisation (Fig. 9.13). The Namiesberg-type amphibolites also lie close to the field of primitive basalt compositions derived from partial melting of mantle peridotites as calculated by Sato (op.cit.), namely 11-13% MgO and 300-425 ppm Ni (Garrison,1981). Despite the fact that two samples show high MgO (>13%) and Ni contents, there is a linear relationship between MgO and Ni within the Namiesberg-type suite. This characteristic is typical of olivine accumulation trends, and the high MgO samples probably represent accumulative basalts and not primitive source magmas, particularly as parental liquids with MgO contents greater than 13% are considered as unlikely to occur from peridotite fractionation (Hart and Davis, op. cit.).

The bulk of the western NMC basic granulites and amphibolites plot within the field of basalts derived from fractional crystallisation of primitive basaltic magmas that have MgO contents between 8 and 13% (Fig. 9.13). This includes the primitive melts defined by the Namiesberg-type amphibolites, and it is possible, but not necessarily imperative, that the latter represent the primitive source magma of these more evolved metabasaltic rocks. The evidence of Cr depletion and Fe, Ti, V, Y, Na and K enrichment in the bulk of the metabasites compared to the Namiesberg-type, supports these contentions. Using the model of Hart and Davis (1978), it is estimated that between 5 and 20% olivine has fractionally crystallised to form these magmas. This is in accordance with the data of Sato (1977) who demonstrates that the NiO content of the magma will decrease by approximately 50% after fractional crystallisation of 6 to 12% of olivine. The Namiesberg-type amphibolites have Ni values of 300 ppm whereas the rest of the NMC metabasites average approximately 100 ppm, representing a 67% decrease in Ni content.

The relatively high SiO_2 values of the Namiesberg-type amphibolites (52-58%) suggest that these rocks do not represent the parental magma from which the bulk of the western NMC metabasites (with average SiO_2 content of 49%) were derived as reductions in SiO_2 content during differentiation by fractional crystallisation are unlikely. High SiO_2 values associated with high MgO and low TiO_2 are typical of the boninite series of volcanic rocks (Hickey and Frey, 1982) and related high-Mg andesites (Jenner,1981). Boninites are virtually plagioclase-free, orthopyroxene-rich mafic volcanics -

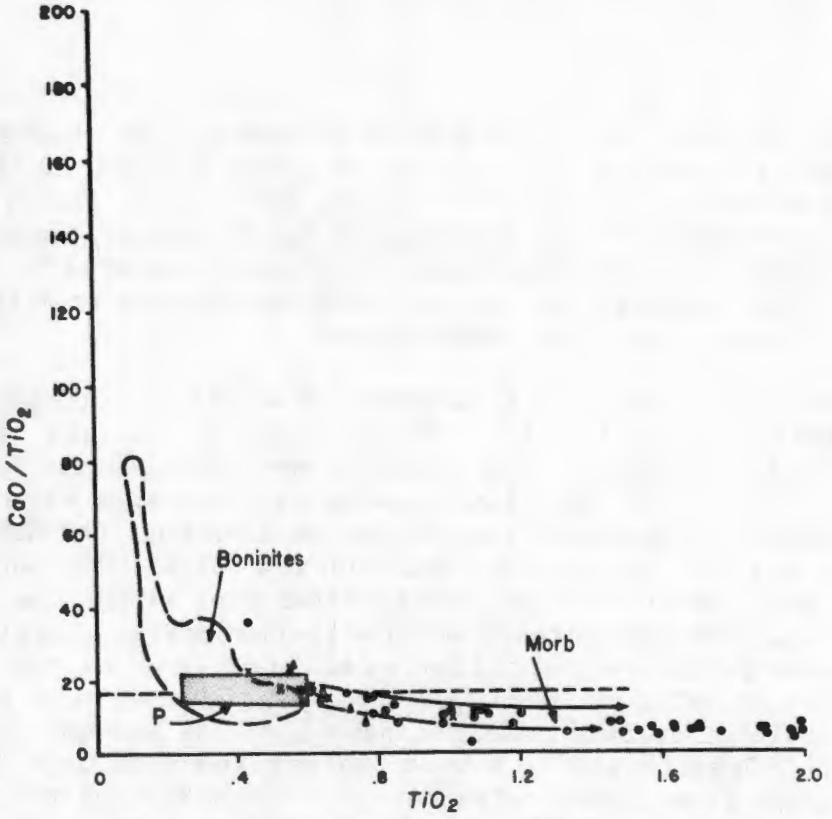

Fig. 9.14a Bivariate plot (after Hickey and Frey, 1982) showing the variation of CaO/TiO_2 ratio with TiO_2 contents in the boninite series of rocks, MORB and model pyrolite mantle source (P). Data points for Namiesberg-type amphibolites (crosses) and other metabasites from the western NMC (dots) are superimposed. Data taken from this study, Zelt (1980) and Moore (1977).

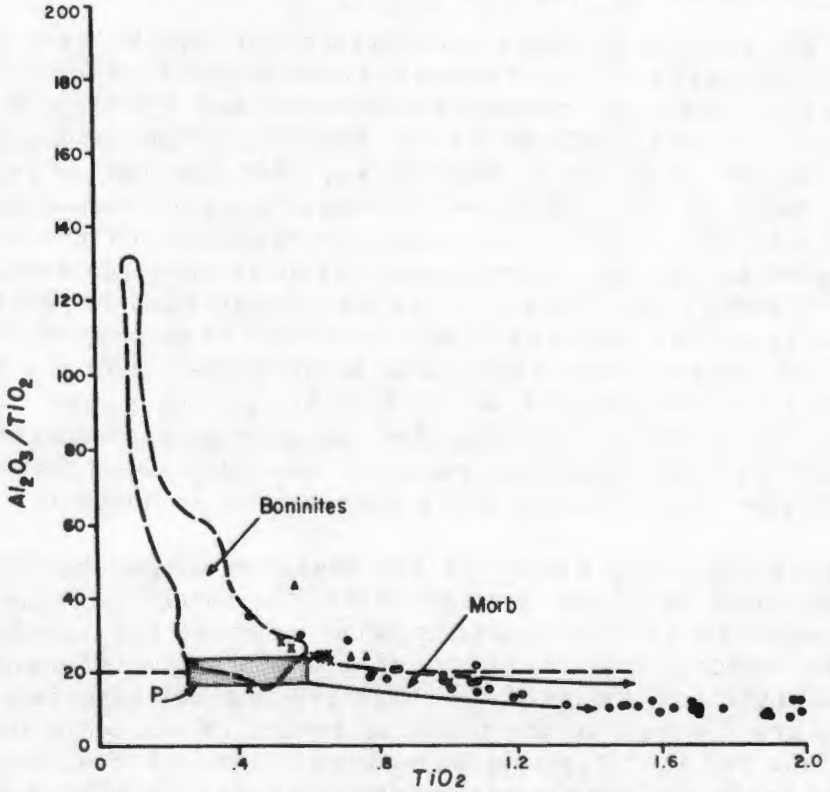

Fig. 9.14b Similar plot showing the variation of Al_2O_3/TiO_2 ratio with TiO_2, using the same data set.

characteristics which, together with high SiO_2 values, would explain the anomalous positions occupied by the Namiesberg-type amphibolites on many of the discriminant diagrams, particularly the R1-R2 and F-E-D-A group. The high SiO_2 contents distinguish boninites from island arc tholeiites and calc-alkaline volcanics, and their high MgO/(MgO + FeO), Ni and Cr values indicate "primary magmas in equilibrium with mantle peridotites" (Hickey and Frey, (op.cit.). Boninites and high-Mg andesites have very high CaO/TiO_2 and Al_2O_3/TiO_2 ratios when compared to other fractionated basaltic rocks such as MORB - a similarity they share with low-Ti basalts from ophiolite complexes (Sun and Nesbitt,1978).

In Fig. 9.14, the CaO/TiO_2 and Al_2O_3/TiO_2 ratios for the western NMC metabasites are plotted against TiO_2 content and compared to fields for MORB, boninites and high-Mg andesites, and model pyrolite mantle source. The bulk of the western NMC metabasites have CaO/TiO_2 and Al_2O_3/TiO_2 ratios and TiO_2 contents similar to basalts, such as MORB, that are derived by fractionation. The Namiesberg-type amphibolites, however, show higher ratios and lower TiO_2 contents at the extreme primitive end of the fractionation trend and just within the fields of both model pyrolite and boninites. There can thus be little doubt that the latter amphibolites represent extremely primitive magma material similar to the boninite series. These low TiO_2, high MgO volcanics are restricted to ophiolite complexes, island arcs and interarc basins in Palaeozoic and modern-day environments (Sun and Nesbitt,1978) and can be derived from remelting of a depleted peridotite residue of earlier arc tholeiite generation (Sun and Nesbitt, op.cit.; Hickey and Frey,1982).

9.5 Summary

The geographic position of the unusual Si-, Mg-rich, Ti-poor Namiesberg-type amphibolites in the extreme northern portions of the study area, and in close proximity to the calc-alkaline volcanics of the Orange River Group is perhaps significant. It is possible that subsequent to the calc-alkaline volcanism, during extensional rifting of relatively thin, attenuated continental crust in a fore-arc or back-arc environment, a depleted peridotite source was melted and tapped by major rift fractures, resulting in the local eruption of these unusual primitive lavas of relatively minor volume and extent within the volcano-sedimentary basin.

The evidence provided by discriminant functions and comparative plots with typical basalt suites in the above sections, predominantly indicates that the bulk of the western NMC metabasites are the metamorphosed equivalents of typical tholeiites derived by fractional crystallisation from a normal "fertile" mantle peridotite source. From the Harker diagrams and the Pearce (1976) major element discriminant plots, it can be seen that the tholeiites are somewhat depleted in alkalis, similar to low-K tholeiites from Palaeozoic and recent island arc environments and unlike "within plate" continental or ocean island tholeiites. Similarities to low-K tholeiites are also observed on the K_2O-TiO_2-P_2O_5 plot whilst the incompatible element data imply tholeiitic, perhaps continental tholeiitic origins (on the Pearce and Cann (1973) Ti-Y-Zr plot, sensu Holm,1982). These metatholeiites form a relatively minor component

of supracrustal sequences dominated by assumed metarhyolite (leucogneiss) and metarhyodacite (biotite gneiss), indicating the presence of bimodal volcanism as opposed to the calc-alkaline volcanism observed within the Orange River Group to the north of the study area (Reid,1977). Tholeiitic mafic volcanics associated with a bimodal suite of volcanic rocks dominated by a felsic component are most typical of continental rift systems including back-arc basins produced by rifting of continental crust (Condie,1982c; Ewart,1979).

Chapter 10

GEOCHEMISTRY OF THE MG-RICH CORDIERITE ROCKS

10.1 Introduction

In the western NMC, cordierite-hypersthene/anthophyllite-phlogopite rocks occur as rare minor constituents of the supracrustal sequences. They are sufficiently unique in their mineralogy and geochemistry to warrant separate classification as a distinct group of lithologies (see Section 3.8), although they are aluminous-rich rocks having both close field associations with, and geochemical similarities to, the metapelitic rocks. Their compositions show considerable variability, being commonly enriched in MgO, FeO, Al_2O_3 and sometimes K_2O, whilst strongly depleted in CaO and Na_2O. These unusual compositions place restrictions on the precursor models that can be applied to explain the Mg-rich lithologies, but this has not prevented a certain degree of argument and controversy arising in this regard. Several sedimentary, volcanic, hydrothermal and partial-melt/restite models have been proposed for similar lithologies in the NMC (Clifford et al., 1975b,1981) and elsewhere. The compositions of the NMC rocks are discussed in the light of these models in the following sections.

10.2 Previous studies

Cordierite-anthophyllite and cordierite-hypersthene rocks have been widely studied in a number of metamorphic terranes, commonly of Proterzoic age, although they are also reported from Archaean and Palaeozoic metamorphic belts. They generally comprise various combinations of the minerals cordierite, anthophyllite, gedrite, orthopyroxene (hypersthene or bronzite), phlogopite/biotite, spinel/hercynite, garnet, quartz, sillimanite, corundum, sapphirine, plagioclase, magnetite and rarer kornerupine, tourmaline and sulphides (commonly pyrite, pyrrhotite, chalcopyrite and/or sphalerite). They are associated with metapelitic rocks (commonly with cordierite-garnet-sillimanite parageneses), mafic rocks (amphibolites or orthopyroxene-bearing basic granulites) and metacarbonate rocks (commonly forsterite marbles and diopside-rich calc-silicate rocks).

Two main theories have been proposed that attempt to explain the formation of these lithologies either by premetamorphic or metamorphic processes. The various metamorphic processes invoked to explain the origins of the magnesian gneisses involve: 1) Mg-metasomatism with introduction of Mg and Fe from intruding granites; 2) redistribution of Fe, Mg and Ca between and within certain lithologies being metamorphosed; and 3) partial melting resulting in the formation of Mg-rich restites after removal of granitic melts. Premetamorphic origins proposed for the Mg-rich cordierite gneisses include: 1) sediments - either lateritic, evaporitic or Mg-rich pelitic rocks;

2) degraded mafic volcanic rocks - formed either by weathering, diagenetic processes or regional low-temperature thermal alteration within a hot volcanic pile; and 3) hydrothermal alteration, generally associated with the formation of submarine exhalative sulphide deposits - either as an altered stockwork or as a Mg-rich exhalite deposit.

Mg-, Fe-metasomatism resulting in the formation of cordierite-anthophyllite rocks observed within the contact metamorphic haloes of intrusive granites was proposed by Eskola (1914) and Tilley (1935). This model requires the formation of Mg- and Fe-rich liquids during the late stages of granitic magma crystallisation which subsequently alter the pre-existing host lithologies along "granitisation fronts" with removal of Ca, Na and K and their replacement by Mg and Fe. Such models are not currently accepted due to difficulties in conceiving the presence of Mg- and Fe-rich solutions in late-stage granitic processes, lack of alteration of this nature in other lithologies closely associated with the cordierite-anthophyllite rocks (e.g. metapelitic and calc-silicate rocks) at most localities, and depletion of Ni and Co in many cordierite-anthophyllite rocks when enrichment in these elements would be expected during the metasomatic process (Chinner and Fox,1974; Floyd,1975). A modification of this model proposed by Floyd (1965), whereby the metasomatism was regarded as being restricted to within the (hornblende-rich) hornfelses themselves with removal of Ca creating Mg- and Fe-rich hornfelses (i.e. cordierite-anthophyllite rocks), and addition of Ca with removal of Si, Al, K, Na, Mg and Fe elsewhere resulting in Ca-rich hornfelses containing diopside and grossularite (i.e. calc-silicate rocks). This model also has difficulty in explaining many of the above objections. Metasomatic models, therefore, are seldom proposed in current genetic modelling of these rocks.

Partial melting models whereby cordierite-hypersthene/anthophyllite assemblages form as restites of certain metasedimentary and metavolcanic rocks after extraction of a granitic melt, have a sound theoretical base (Grant,1968) and have been proposed for a variety of metamorphic terranes including the western NMC (Lal and Moorhouse,1969; Lal *et al.*, 1978; Clifford *et al.*, 1975b,1981). At several localities where cordierite-anthophyllite lithologies occur, however, the P-T conditions of metamorphism were insufficient to produce large-scale partial melting, particularly of Mg-rich premetamorphic rocks (Deb,1980) and so this model becomes inapplicable. In certain higher-grade metamorphic terranes such as the granulite-facies domain of the western NMC, the associated cordierite-garnet-sillimanite metapelitic rocks have chemical compositions which indicate that no, or extremely minimal, partial melting has occurred and in these instances the partial melting model is also suspect. Reasons for rejecting a metamorphic origin for the Mg-rich gneisses of the western NMC were outlined in more detail in Section 6.4.

Isochemical metamorphism of unusual pre-metamorphic Mg- and Fe-rich rock types is by far the most commonly ascribed origin for these lithologies. Metamorphism of metasedimentary precursors has been proposed by a number of authors. Moine *et al.*, (1981) have demonstrated how cordierite-, phlogopite-, anthophyllite-rich rocks may form from the metamorphism of certain impure evaporitic sediments (Table 10.1), and magnesite- and sepiolite-bearing rocks

TABLE 10.1 Chemical analyses of magnesium-rich sediments and altered basalts with compositions similar to those of the Mg-rich cordierite gneisses of the study area.

	1.	2.	3.	4.	5.	6.	7.	8.	9.
SiO_2	45.44	48.09	50.6	47.10	64.00	31.24	40.07	51.05	57.95
TiO_2	0.60	0.71	1.1	0.14		3.38	2.41	3.05	0.59
Al_2O_3	5.32	15.36	18.5	10.89	5.66	15.82	17.01	16.36	13.09
FeO*	4.90	5.25	6.67	6.45	8.14	25.19	24.87	15.93	12.35
MnO	0.04	0.06		0.05		0.38	0.14		
MgO	14.19	11.70	21.15	6.36	9.70	9.64	5.78	4.26	7.24
CaO	0.34	2.30	0.04	0.49	0.50	1.30	0.84	0.62	0.66
Na_2O	1.04	0.31	0.0	3.83	0.30	-	1.24	0.23	0.04
K_2O	4.43	3.65	0.6	5.75	0.90	1.03	1.25	6.73	0.69
H_2O LOI	11.70	10.54	8.2	15.18	9.98	10.35	5.83	8.91	6.57

* total Fe as FeO

1. argillite, Aquitaine Basin, France (Moine et al., 1981).
2. argillite, Canning Basin, Australia (Moine et al., 1981).
3. evaporite mudstone, Sahara Atlas, NW Africa (Schreyer, 1977).
4. green clay, Tukai Beds, Amboseli, Kenya (Stoessell and Hay, 1978).
5. "palaeosol" marly clay,Lebrija, Southern Spain (Galan and Ferrero, 1982).
6. chloritized basalt, Yalwal, New South Wales (Vallance, 1967).
7. cordierite-anthophyllite hornfels derived from altered basalt, Yalwal, New South Wales (Vallance, 1967).
8. illite-montmorillonite weathering product of diabase, King Mountain, Oklahoma (Nichols, 1970).
9. chloritized footwall zone, La Zarza sulphide orebody, Spain (Strauss et al., 1981).

have been proposed as potential precursors to these lithologies (Warren,1979; Deb,1980). Many other authors simply refer to Mg-rich pelitic protoliths or chlorite-rich sediments (Kamineni, 1979; Rao, 1974; Sarkar et al., 1980; Woodford and Wilson, 1976; Wilson, 1978a; Ellis et al., 1980; Stewart and Warren, 1977; Hermans et al., 1976; Kitsul et al., 1972; Sheraton et al., 1982). Iron-rich shales (Nixon et al., 1973; Lal and Shukla,1975) and laterites (Herd,1973; Meng and Moore,1972) have also been proposed to explain the enrichments in Fe and Al within many of these lithologies.

The metamorphism of mafic volcanic rocks, previously altered by hydrothermal or diagenetic processes to chlorite-rich lithologies with leaching of Ca, has been demonstrated by Vallance (1967) to be a feasible mechanism for the formation of cordierite-anthophyllite rocks (Table 10.1). This mode of formation is commonly applied to cordierite-hypersthene/anthophyllite rocks found in close association with hornblende hornfelses, amphibolites or orthopyroxene-bearing basic granulites (Chinner and Fox,1974; Floyd,1975; Davidson and Mathison,1974; James et al.,1978, Wilson,1971; Warren,1979). A chemical study of the weathering of diabase under temperate climatic conditions (Nichols, 1970) indicates that metamorphism of weathered diabase material will commonly also form cordierite-hypersthene/anthophyllite-phlogopite parageneses (Table 10.1).

Hydrothermal alteration within volcanic piles, generally associated with the formation of sulphide deposits, commonly results in the formation of highly chloritic stockworks (e.g. Strauss et al., 1981) and exhalative sediments hosting, or in close proximity to, the mineralisation. Metamorphism of such chloritic zones will also result in the formation of cordierite-, phlogopite-, anthophyllite-rich rocks (de Rozen-Spence, 1969; Pollard, 1981; Treloar et al., 1981; Sheraton et al., 1982, Schermerhorn, 1978). Not all cordierite-anthophyllite/hypersthene rocks associated with sulphide deposits have been interpreted as hydrothermally-altered rocks. Due to their stratiform textures and lateral persistency within mixed metasedimentary/metavolcanic sequences, they are instead described as metasediments or metamorphosed tuffaceous mafic volcanics (Deb, 1980; Raymond et al., 1980; Stewart and Warren, 1977; Wennevirta and Rouhunkoski, 1970). The associated sulphide deposits are commonly dominated by pyrite, pyrrhotite, chalcopyrite and/or sphalerite.

It is apparent from the above resume of previous studies of Mg-rich cordierite rocks, that the majority of these lithologies were derived by pre-metamorphic processes involving the formation of concentrations of chlorite-rich material, either by sedimentation, diagenesis, degradation of mafic volcanics or hydrothermal alteration. In certain instances where the Al_2O_3 content of the rocks is high, kaolinite might also become an important component of the pre-metamorphic parageneses (Ellis et al., 1980). The major elements that dominate the compositions of these lithologies - Si, Al, Mg and Fe - do not provide any critical evidence as to the specific origins of cordierite-hypersthene/anthophyllite lithologies within these four options. Certain other elements of minor and trace concentrations, however, may provide significant evidence in the selection of a specific protolith for the Mg-rich cordierite gneisses of the western NMC and elsewhere. This hypothesis is

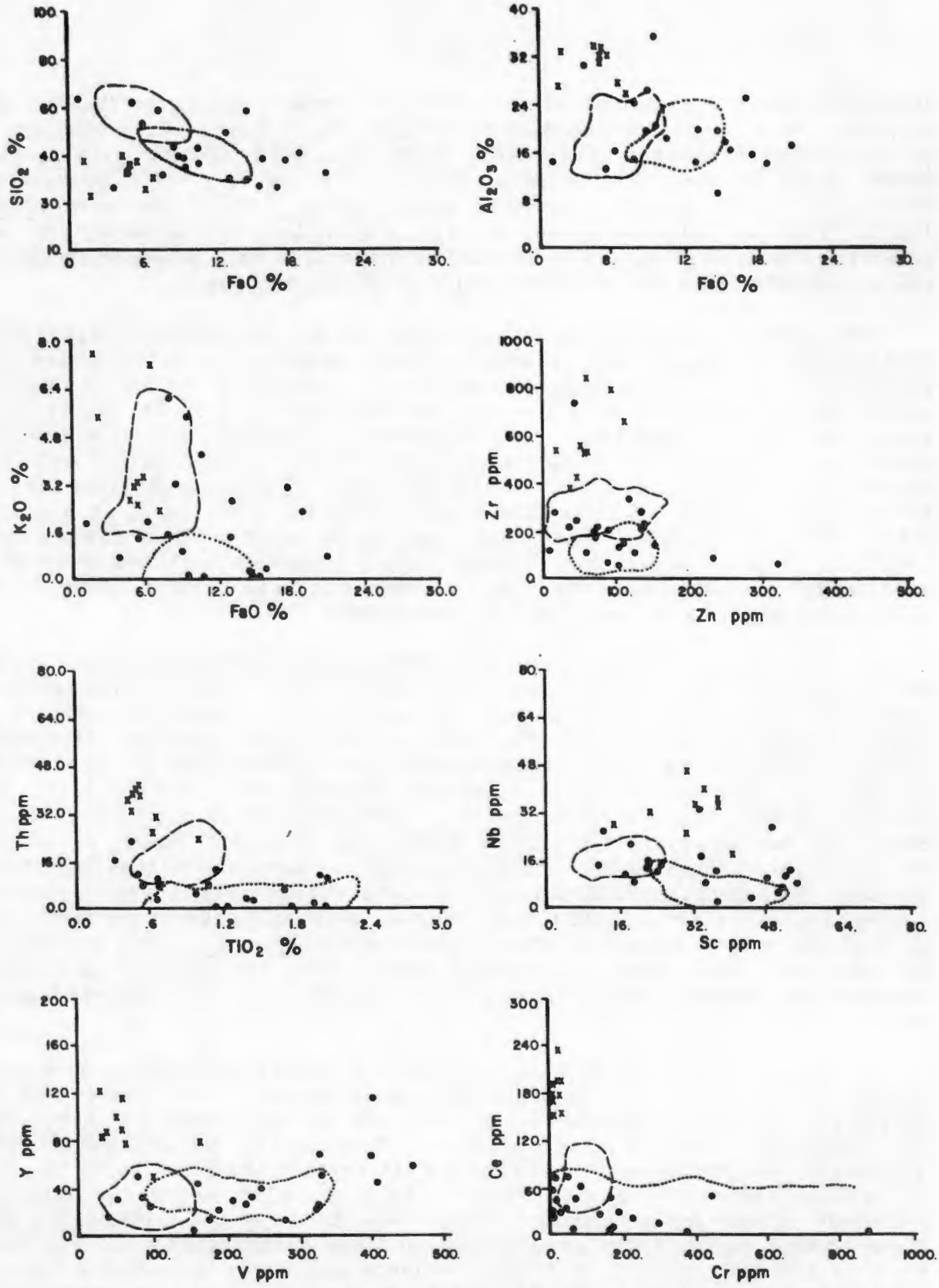

Fig. 10.1 Bivariate plots of various major element oxides (%) and trace elements (ppm) for data from cordierite-phlogopite-quartz and cordierite-hypersthene/anthophyllite rocks (dots) and cordierite-phlogopite rocks (crosses) from the study area. The fields for metapelitic rocks (dotted) and metabasites (dashed) from the study area are also outlined.

examined in the succeeding sections.

10.3 Chemical comparisons with the metapelitic and mafic rocks

Bivariate scatter plots of certain major element oxides (SiO_2, TiO_2, Al_2O_3, FeO and K_2O) and trace elements (Th, Zr, Nb, Cr, V, Sc, Zn, Y and Ce) are displayed for the Mg-rich cordierite gneisses, together with the fields occupied by the bulk of the metapelitic rocks and basic granulites/amphibolites from the study area (Fig. 10.1). The majority of the Mg-rich cordierite gneisses have values and trends similar to the mafic metamorphic rocks. This is particularly apparent in the Th:TiO_2, Y:V and Nb:Sc plots. Cordierite-hypersthene/anthophyllite rocks comprise the bulk of the lithologies showing these trends. There is also a degree of overlap displayed by some samples into the field of the metapelitic rocks. Lithologies showing this type of element distribution are commonly cordierite-phlogopite-quartz rocks. These element distributions suggest that the genesis of the Mg-rich cordierite gneisses may be related in some way to the precursors of the basic granulites and amphibolites, together with a possible minor pelitic component.

One subgroup of Mg-rich cordierite gneisses, however, consistently plots with anomalous values when compared to these two fields. This group is made up essentially of cordierite-phlogopite±sillimanite rocks. The compositions of these lithologies are commonly separated from the basic granulite/amphibolite field by the metapelite field on the scatter plots, showing anomalous enrichment in immobile oxides and elements such as Al_2O_3, Zr, Th, Nb, Sc, Y, Ce as well as K_2O in some samples, and depletions in SiO_2, TiO_2, Cr, V, Ni, Co, Zn and, to a lesser extent, FeO (Fig. 10.1). In this respect their compositions show similarities to the sillimanite-rich rocks in the Pofadder area (Moore,1977,1980b) from which they differ essentially by their high MgO contents and depletion in TiO_2. This subgroup is best segregated from the cordierite-hypersthene/anthophyllite and cordierite-phlogopite-quartz rocks by their high Ce contents (>120ppm) and to a lesser extent by their high Zr (>400ppm) and Th (>20ppm) contents. The Ce:Cr plot was used to define these two different geochemical groups (Fig. 10.1).

10.4 Comparisons between the two different Mg-rich gneiss groups

The two groups defined on the Ce:Cr bivariate plot were subjected to stepwise discriminant analysis using the same group of 27 major and minor elements and oxides that were employed in previous analyses of the metapelitic rocks (see Section 7.5).The compositions of the two groups were found to be significantly different and were segregated by a single canonical variable which used the oxides and trace elements Al_2O_3, CaO, Zn and Ce (Fig. 10.2 and Table 10.2).

Comparison of the mean compositions of the two groups (Table 10.3) reveals that most elements, with the exception of MgO, CaO, Na_2O, Sc and Pb, have significantly different concentrations. The distribution of the oxide and trace element contents of the two groups can be compared in histograms in Fig.

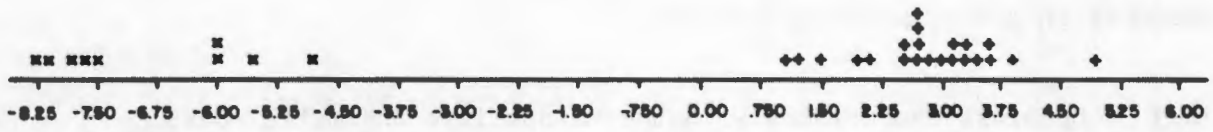

Fig. 10.2 Plot showing the separation of the two groups of Mg-rich cordierite gneisses - cordierite-phlogopite-quartz and cordierite-hypersthene/anthophyllite rocks (+) and cordierite-phlogopite rocks (x) - using the canonical variable from Table 10.2.

TABLE 10.2 Coefficients for the canonical variable and the U-statistic from the stepwise discriminant analysis of Mg-rich cordierite gneisses from the study area.

Variable	Coefficient for canonical variable	U-statistic (Wilks' Lambda)
Al_2O_3	- 0.192	0.075
CaO	1.447	0.059
Zn	- 0.011	0.046
Ce	- 0.057	0.107
Constant	8.788	

TABLE 10.3 Mean compositions of the two groups of Mg-rich cordierite gneisses from the study area. Major element oxides are expressed as percentages and trace elements in ppm.

	1.		2.	
	mean	standard deviation	mean	standard deviation
SiO_2	48.63	11.51	41.36	5.51
TiO_2	1.32	0.85	0.58	0.18
Al_2O_3	20.16	5.54	30.34	3.11
FeO*	10.54	4.85	4.72	1.84
MnO	0.18	0.13	0.09	0.03
MgO	12.92	5.16	13.85	6.01
CaO	0.45	0.29	0.63	0.88
Na_2O	0.70	0.70	0.68	0.59
K_2O	1.88	1.78	4.11	2.01
P_2O_5	0.17	0.17	0.08	0.01
Rb	126	136	230	164
Ba	259	297	796	578
Sr	18	16	126	201
Th	8	6	33	6
Zr	193	137	573	150
Nb	14	8	33	8
Cr	207	303	16	8
V	234	121	69	43
Sc	33	15	32	8
Ni	86	103	13	5
Co	36	18	7	3
Pb	7	9	9	6
Zn	94	64	61	29
Y	35	24	89	22
La	11	12	93	23
Ce	31	24	177	25
Nd	17	13	79	14

* total Fe as FeO

1. cordierite-hypersthene/anthophyllite and cordierite-phlogopite-quartz rocks (22 samples).

2. cordierite-phlogopite $\pm$ sillimanite rocks (9 samples).

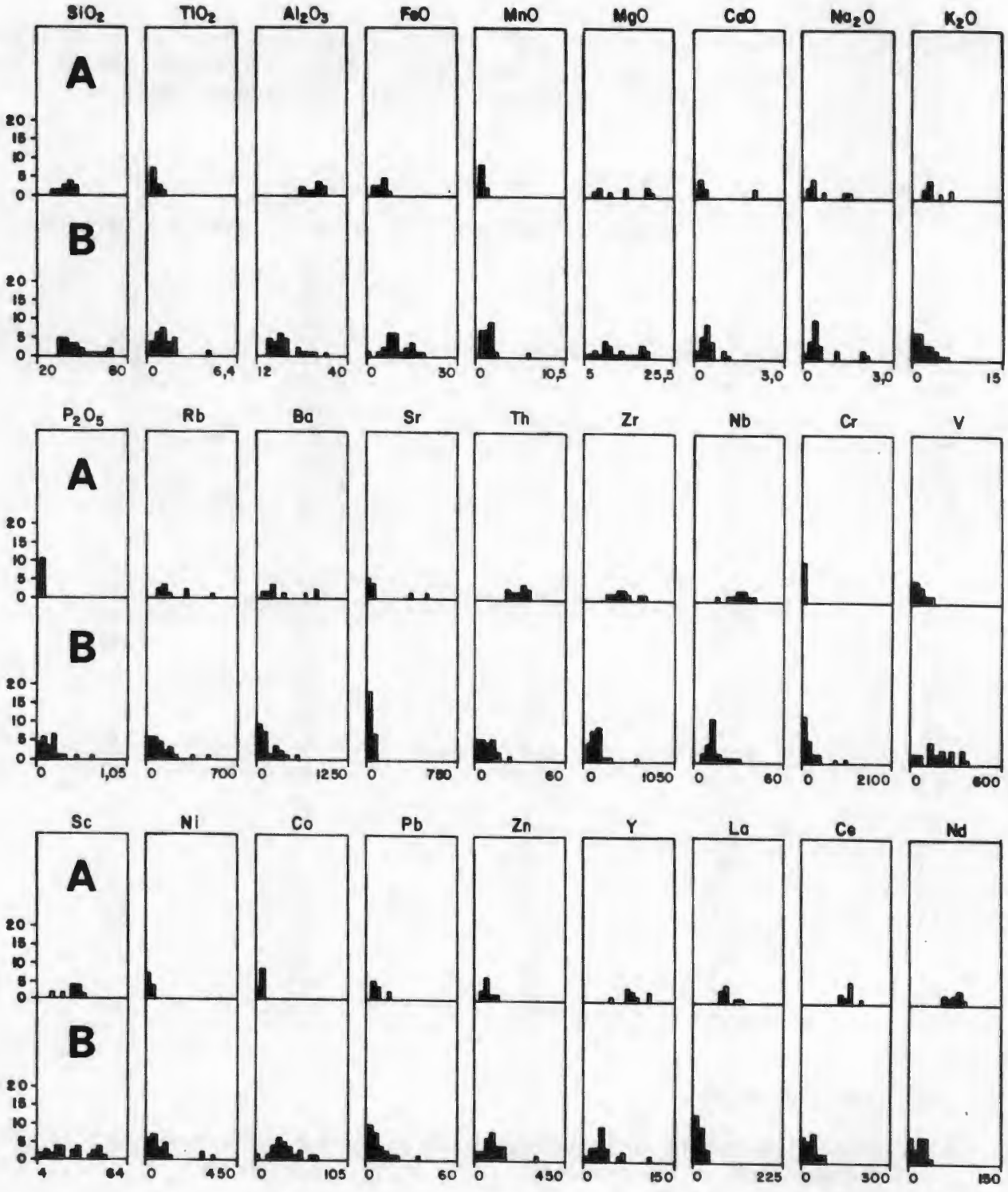

Fig. 10.3 Histograms showing the ranges in composition for major and trace elements of the cordierite-phlogopite rocks (A) and cordierite-phlogopite-quartz and cordierite-hypersthene/anthophyllite rocks (B) from the study area.

10.3. Differences in CaO and Na_2O contents between the two groups are also apparent when the two cordierite-phlogopite-sillimanite-plagioclase gneisses with high CaO and Na_2O contents are excluded from the minor sample set.

The major group comprising cordierite-phlogopite-quartz and cordierite-hypersthene/anthophyllite rocks shows relative enrichments over the cordierite-phlogopite-sillimanite group in SiO_2, TiO_2, FeO, MnO, P_2O_5, Cr, V, Ni, Co and Zn, and relative depletions in Al_2O_3, K_2O, Rb, Ba, Sr, Th, Zr, Nb, Y, La, Ce and Nd. These differences indicate that the major group contains a dominant mafic component and the minor group a dominant pelitic component relative to each other. Although all samples of the minor "phlogopite" group were collected from three adjacent localities on the farms Dabeeb and Hytkoras in the Buffels River paragneiss belt, they occur in association with samples of the major "hypersthene/anthophyllite" group (Fig. 10.4). All other localities where Mg-rich cordierite gneisses were sampled, fall within the major "hypersthene/anthophyllite" group. Sample DRL169 from the farm Houniams on the Orange River is a phlogopite-rich rock of similar mineral paragenesis to those of the minor "phlogopite" group although its composition indicates that it belongs to the "hypersthene/anthophyllite" group.

10.5 Estimations of the precursor mineral assemblages

Employing the same approach that was applied to the metapelitic rocks (see Section 7.6), the compositions of the Mg-rich cordierite gneisses were initially subjected to principal components analysis to determine the dominant element associations within this group of rocks and thus to interpret which premetamorphic mineral constituents might have been present. Because the total sample population of the Mg-rich gneisses is relatively small (31 samples), they were grouped together for this exercise. The number of variables comprised the same 27 major element oxides and trace elements that were used in the discriminant function analysis.

Six varimax rotated factors were calculated which cumulatively accounted for 84.0% of the variance within the sample population (Fig. 10.5). Factor 1 had high positive loadings for Nd, Ce, Th, La, Y, Zr and Nb and moderately positive loadings for Al_2O_3 and Ba as well as low negative loadings for Co, V, Cr, Ni and FeO. This factor accounted for approximately 45% of the variance contained in the six factors, and is interpreted as representing detrital zircon and kaolinite clay in a weakly inverse relationship with iron oxide. Factor 2 has significant positive loadings for Zn, MnO, FeO, Ni, Co, Cr and Sc and very low negative loadings for Al_2O_3 and Nb, and can be interpreted as the inverse of factor 1 with Fe-, Mn-oxides having a weakly antithetic relationship with kaolinite. Factor 3 has positive factor loadings for MgO, Sc, V, TiO_2 and FeO and a strong negative loading for SiO_2, and is thought to represent the inverse relationship between detrital quartz and Mg-rich clay minerals such as chlorite (or sepiolite, palygorskite, magnesite) as well as ilmenite. The fourth factor represents plagioclase or its breakdown products (analcite, calcite) with significant positive factor loadings for CaO, Na_2O and Sr. The fifth factor represents potassic minerals - either K-feldspar, muscovite or illite - with positive factor loadings for K_2O, Rb and Pb. Factor

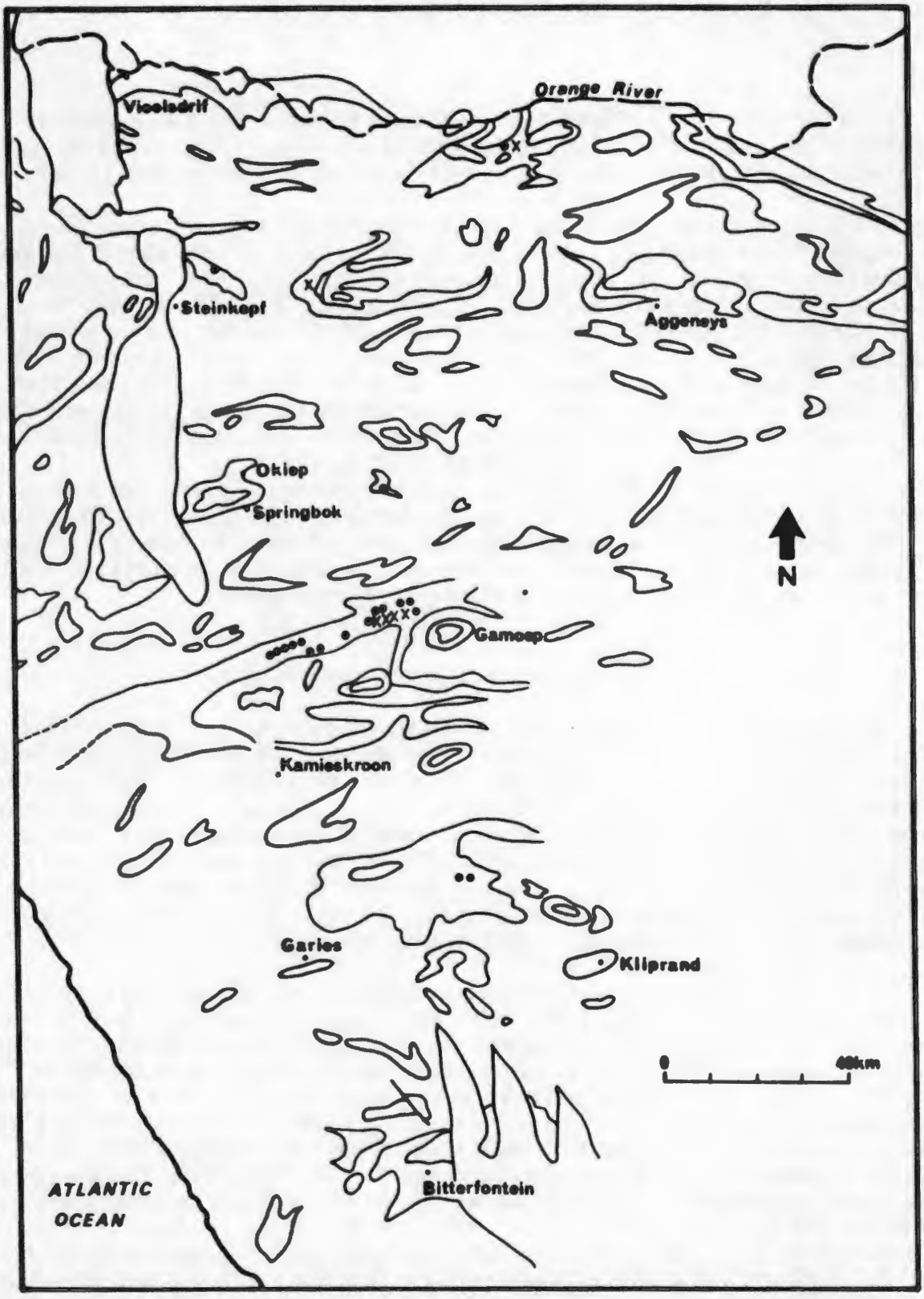

Fig. 10.4 Regional map showing the geographical distribution of samples of cordierite-phlogopite-quartz and cordierite-hypersthene/anthophyllite rocks ( ) and cordierite-phlogopite rocks (x) analysed in this study, compared to major outcrops of supracrustal rocks.

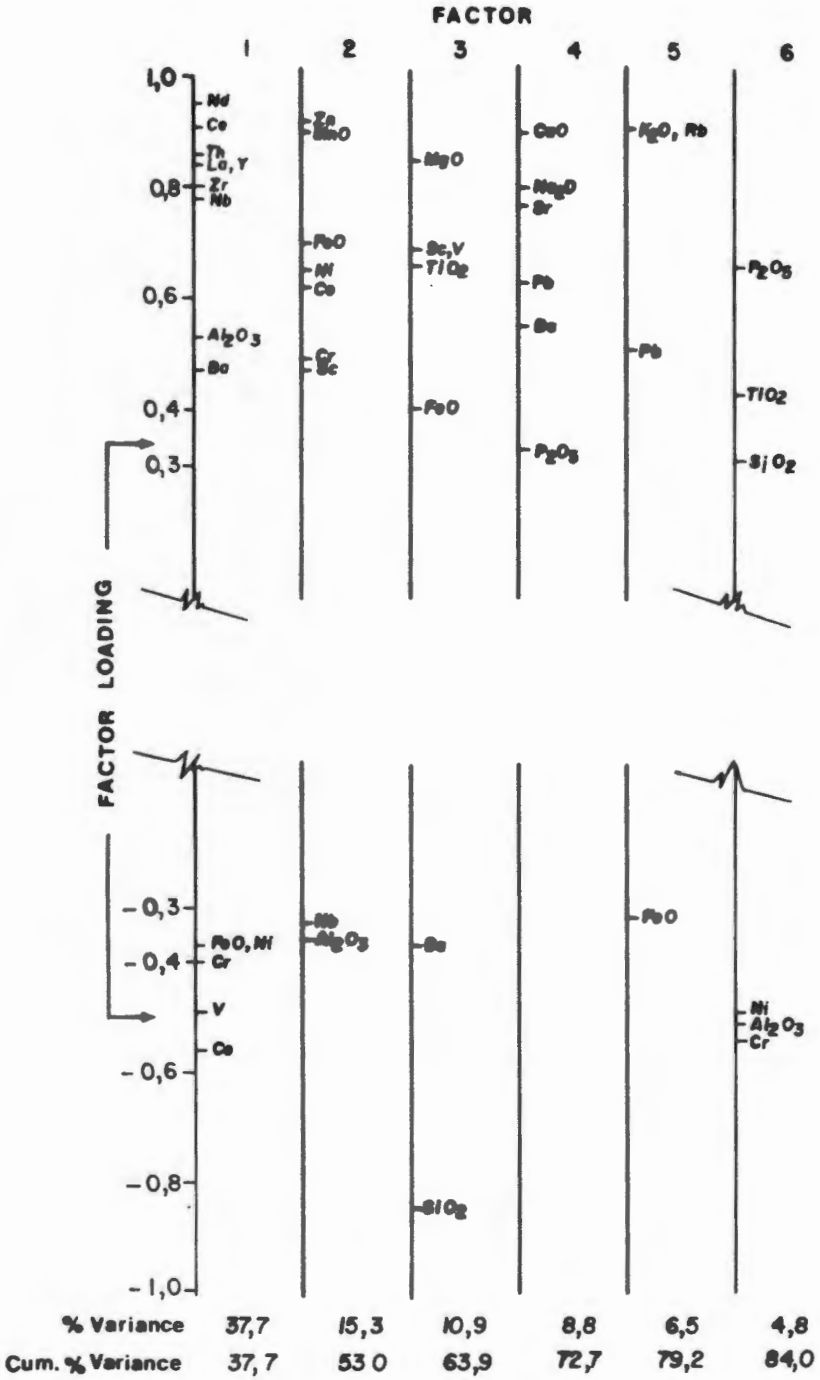

Fig. 10.5 The six major factors, together with the factor loadings of the variables and their cumulative variance, obtained in the principal components analysis of the Mg-rich cordierite gneisses from the study area.

TABLE 10.4 Two estimates, with or without Fe oxide, of the proportions of premetamorphic constituents in the Mg-rich cordierite gneisses, based on least squares approximations.

Mineral constituent	(+ Fe oxide ; n = 32)		(- Fe oxide ; n = 32)	
	mean	range	mean	range
quartz	11	0–50	11	0–50
K-feldspar illite muscovite	23	0–52	24	0–54
kaolinite	18	0–70	11	0–63
chlorite	30	12–52	42	20–70
plagioclase	5	0–30	4	0–21
Fe oxide	7	0–19	-	
montmorillonite	-		3	0–24
ilmenite	3	0–14	1	0–8
magnesite	1	0–14	1	0–17
gibbsite	2	0–21	2	0–14
Sum of squares of differences	0.36	0.01–3.12	0.18	0.01–1.07

6 is interpreted as apatite (P_2O_5), showing an inverse relationship to kaolinite (Al_2O_3) and also possibly to detrital chromite (Ni, Cr).

From the principal components analysis, therefore, it could be deduced that the pre-metamorphic mineral assemblages of the Mg-rich gneisses comprised mixtures of kaolinite, Fe oxides (magnetite and ilmenite), Mg-rich chlorite, quartz, plagioclase and K-rich minerals (either illite, muscovite or K-feldspar), together with lesser apatite and zircon. Many of the factors are similar to those obtained in the principal components analysis of the metapelitic rocks (e.g. "chlorite" elements opposed to SiO_2, the K_2O-Rb factor and the association of Nd, Ce, La, Th and Zr). As a result, the deduced premetamorphic constituents are virtually identical to those proposed for the metapelitic rocks. The most obvious differences between the two types are the dominant Fe-, Mn-oxide component and the association of the zircon-related elements with Al_2O_3 in the Mg-rich gneisses. Although the same premetamorphic "sedimentary" constituents appear to be present in both the metapelitic and Mg-rich gneisses, it is obvious from their differing compositions that they are present in markedly different proportions in the two lithologies.

Using the mineral constituents predicted by the principal components analysis, namely kaolinite, magnetite, chlorite, ilmenite, quartz, plagioclase, and illite/muscovite/K-feldspar, a least-squares mixing exercise similar to that applied to the metapelitic rocks (see Section 7.6) was undertaken to approximate the major element whole-rock compositions of the magnesian gneisses. The components again comprised the eight major element oxides SiO_2, TiO_2, Al_2O_3, total Fe as FeO, MgO, CaO, Na_2O and K_2O. In the majority of samples the results of this exercise were satisfactory with sums of squares of differences totalling less than 0.30. In the case of six samples, excess Al_2O_3 was present that could only be balanced by the introduction of a gibbsite constituent as well as kaolinite, and in three samples, excess MgO existed that could only be explained by the presence of a non-silicate magnesium mineral phase such as magnesite.

The premetamorphic constituent modelling of the magnesian gneisses was not unambiguous, and two different suites of constituents gave similar best fit solutions. The major difference between the two model solutions was in the choice of the major Fe mineral present. The principal components analysis exercise indicated that the association of Fe and Mg was not particularly strong and that FeO and Al_2O_3 showed inverse relationships to one another in two factors. Thus the preferred interpretation of the major Fe-bearing mineral was iron oxide. There was, however, a weak association of MgO and FeO in factor 3, indicating that a portion of the Fe was probably incorporated into chlorite in the precursor assemblage. The compositions of the Mg-rich cordierite gneisses were therefore modelled assuming that all Fe was either in Fe oxides or in chlorite (Table 10.4), whereas the most realistic situation is that both Fe-bearing chlorite and Fe oxides were present in these lithologies prior to metamorphism. In most examples, the Fe-chlorite model gave slightly better solutions (smaller sums of squares of differences) indicating that more Fe was probably present as chlorite than as oxides.

The various model mineral constituents showed wide ranges in

concentration, compatible with the equally wide range displayed by the compositions of the magnesian gneisses (Table 10.3). Approximate mean compositions of these rocks have 30-40% chlorite, 10-20% kaolinite, 20-25% potassic minerals, 10-15% quartz, 0-7% Fe oxides, 5% plagioclase and 2-3% ilmenite. These percentages are markedly different from those obtained for the metapelitic rocks, being enriched in chlorite, Fe oxides and slightly in kaolinite, and depleted in quartz and potassium minerals.

Within the suite of Mg-rich gneisses themselves, certain groupings and trends were noticeable. With the exception of samples RW-4, HY-7 and 7-SI, there was apparent incompatibility between plagioclase and potassic minerals, particularly phlogopite, with the one constituent appearing to the exclusion of the other. The rocks with model plagioclase constituents also contained higher Fe oxide contents. Within the K-rich samples it was observed that, with decreasing quartz content, illite was generally replaced by muscovite and finally by K-feldspar in the modelling exercise. This was required to account for the high K_2O values recorded in many of the low-SiO_2 lithologies.

Silicification, kaolinisation, chloritisation, feldspathisation and Fe-enrichment are all common forms of alteration related to hydrothermal processes, generally occurring as broad transgressive zones around centres of hydrothermal activity that may contain associated sulphide mineralisation. In contrast, the NMC Mg-rich gneisses commonly appear as thin, conformable horizons interbanded within the supracrustal succession. Whilst extremely thin and commonly lenticular in outcrop, they can be traced in certain areas for many kilometres along strike (e.g. in the Dabeeb-Hytkoras-Nuwedam area) and are widespread in their regional distribution. They have, in all of these aspects, an identical appearance to the associated metasedimentary and metavolcanic rocks (e.g. marbles and basic granulites). Mixtures of chlorite, kaolinite, quartz, Fe oxides and feldspars (or their degraded products - analcite, muscovite or illite), in the proportions estimated in the above calculations, would not be unexpected in sediments derived from the weathering of mafic rocks. The presence of gibbsite and magnesite constituents in a few samples could indicate relatively intense weathering or diagenetic processes being operative. These aspects are covered in more detail in the succeeding two sections.

10.6 Comparisons with hypersaline continental-basin sediments

Magnesium-rich sediments are not uncommonly located within continental basins of a hypersaline nature, where the minerals chlorite, montmorillonite/smectite, corrensite, palygorskite, sepiolite, magnesite and huntite occur either as direct weathering products (Lesko,1972) or, more commonly, as neoformed products of early-stage diagenetic processes (Fisher and Jeans,1982; Wetzenstein,1975; Irion and Muller,1968; Galan and Ferrero,1982; Stoessell and Hay,1978). Many of these magnesian clay sediments have compositions that are comparable to those of the Mg-rich gneisses from the study area (Table 10.1). The source of Mg in these sediments, either within the detrital fraction or as Mg-HCO_3-rich waters, is commonly ascribed to the

weathering or degradation of adjacent or underlying mafic volcanic rocks (Lesko, op.cit.; Wetzenstein, op.cit.; Stoessell and Hay, op.cit.; Galan and Ferrero, op.cit.); or to the diagenetic alteration of fine mafic volcanic ash bands (Bradshaw,1975). Illite is also a common constituent of certain Mg-rich sediments (Wetzenstein, op.cit.; Galan and Ferrero, op.cit.) and participated as the detrital material in the neoformational and transformational reactions that resulted in the magnesium minerals.

In the Roodewal area of the Platbakkies-Witwater paragneiss belt, and the Dabeeb/Hytkoras section of the Buffels River belt, the Mg-rich gneisses are commonly found in association with metapelitic gneisses and basic granulites in successions which comprise basal basic granulites overlain sequentially by cordierite-hypersthene/gedrite rocks, cordierite-phlogopite rocks and garnet-cordierite-sillimanite metapelitic gneisses. The basic granulites represent basaltic-to-tholeiitic lavas (see Section 9.2 and Zelt, 1980) and the metapelitic gneisses illite-rich shales (see Section 7.6). The Mg-rich cordierite gneisses were probably formed subsequent to basaltic volcanism within a shallow platform sedimentary basin. Weathering of subaerially-exposed portions of the mafic rocks or in situ degradation, resulted in the deposition or formation of chlorite-quartz-kaolinite rocks directly overlying the mafic lavas (cordierite-hypersthene/gedrite rocks). Resumption of illite-rich sedimentation resulted in mixing of potassic and magnesian sedimentary components which during subsequent diagenesis resulted in neoformed clay mineral assemblages containing Mg-rich constituents such as magnesite and sepiolite (cordierite-phlogopite rocks) under shallow-water hypersaline conditions.

The presence of kornerupine and tourmaline within several samples of these lithologies in the Dabeeb/Hytkoras area, indicates relatively high levels of boron - possibly reaching as much as 0.1% in certain samples. An association of boron with illite is well established in clay-rich sediments (Harder, 1959; Reynolds, 1965) due to chemical adsorption of the $B(OH)^{4-}$ anion to illite flakes and subsequent diffusion of these anions into the clay mineral (Couch and Grim,1968). The boron content of illites has been related to increasing K_2O content of clay-rich sediments (Walker and Price,1963), and also with increasing salinity (Couch and Grim, op.cit.), reaching levels of 1500 ppm in evaporitic environments (Harder, op.cit.). Several authigenic boro-silicates such as searlesite ($NaBSi_2O_6.H_2O$), reedmergnerite ($NaBSi_3O_8$), garrelsite and leucosphenite are also known to occur in saline lacustrine sediments such as the Green River Formation (Milton et al., 1960; Eugster,1980) where they replace clays such as montmorillonite within tuffaceous horizons. Under hypersaline conditions, therefore, boron concentrations of the order of magnitude required to form the minor amounts of tourmaline and kornerupine observed in the Mg-rich cordierite gneisses could be expected, particularly in the K_2O-rich cordierite-phlogopite rocks.

10.7 Comparisons with residual weathering products of mafic rocks

In the Eenriet area, cordierite-anthophyllite rocks are intimately associated with an unusual suite of minor lithologies comprising biotite-

TABLE 10.5 The chemistries of some unusual lithologies associated with the Mg-rich cordierite gneisses.

	1.	2.	3.	4.	5.	6.
SiO_2	30.71	69.15	36.05	79.69	47.91	47.80
TiO_2	6.18	4.51	3.40	0.16	0.13	0.63
Al_2O_3	16.22	2.49	7.83	13.55	35.04	29.28
FeO*	23.49	18.08	35.88	0.83	4.20	4.95
MnO	0.24	0.10	0.13	0.01	0.03	0.11
MgO	6.01	0.44	13.43	0.04	0.60	2.61
CaO	0.33	0.04	0.28	0.02	1.30	0.53
Na_2O	0.38	0.10	-	0.16	1.06	1.51
K_2O	5.79	0.49	0.05	3.78	8.85	9.54
P_2O_5	0.23	0.27	0.03	0.02	0.03	0.18
ZrO_2	0.53	0.41		0.02	0.02	0.04
CuO	2.63	0.08		-	-	-

* total Fe as FeO

1. ER-3, biotite-muscovite-ilmenite schist from Eenriet area.
2. ER-4, quartz-ilmenite-zircon rock from Eenriet area.
3. Sample 40, cordierite-orthopyroxene-magnetite rock, Nababeep (Clifford et al., 1981).
4. ER-6, quartz-muscovite-sillimanite rock from Eenriet area.
5. RFN-4, K-feldspar-sillimanite-corundum-plagioclase rock, Silverfontein-Rietfontein paragneiss belt.
6. HY-24, K-feldspar-biotite-corundum rock, Hytkoras, Buffels River paragneiss belt.

muscovite-ilmenite schist, an ilmenite-zircon-rich iron formation and a quartz-muscovite-sillimanite rock (Table 10.5). The two former associates are both strongly enriched in FeO, TiO_2, Zr, Th, Nb, Y and Ce, and the lattermost is relatively enriched in Al_2O_3 and K_2O and depleted in FeO, MgO, CaO and Na_2O. The biotite-muscovite-ilmenite schist, furthermore, has chemical similarities to the Mg-rich cordierite rocks, being enriched in MgO and K_2O (at the 6% level) and strongly depleted in CaO and Na_2O (<0.5%). The schist also contains significant concentrations of Cu mineralisation (chalcopyrite - now mainly altered to malachite). Clifford *et al.* (1981) describe a chemically similar cordierite-orthopyroxene-magnetite rock, associated with paragneisses within the Nababeep Mine, in which "zircon attains the status of a minor constituent" and Cu-sulphides are present. These enrichments in residual elements Al, Ti and Zr are best explained as concentrations resulting from intense weathering and/or sedimentary sorting, and perhaps mark a hiatus in the depositional cycle at this stage. An ilmenite-zircon heavy mineral sand would seem a plausible precursor for the iron formation lithology (see Section 13.3).

By analogy, the Al_2O_3-, Zr-rich magnesian gneisses in the Dabeeb/Hytkoras area could represent similar, less FeO-, TiO_2-rich equivalents, marking a break between underlying mafic rocks and their degraded equivalents, and overlying normal pelitic rocks. The high concentrations of MgO in these lithologies, which required the presence of magnesite in the least-squares mixing exercise, could be the result of diagenetic processes operating at this "erosional" level during subsequent burial, with the Mg-rich fluids being derived from the underlying mafic rocks in a similar manner to that demonstrated for the recent analogues of the previous section.

Eruptions of basaltic/tholeiitic lava into the sedimentary basin apparently resulted in interruptions in the depositional cycle, causing anomalous concentrations of residual elements Al, Ti and Zr, and also in the degradation of portions of the lavas themselves into chlorite-kaolinite-quartz assemblages with subsequent redistribution of Mg during diagenesis. Isochemical metamorphism of this package of lithologies resulted in the unusual cordierite-phlogopite-hypersthene/anthophyllite rocks and their associates.

A K-feldspar-biotite-corundum rock (sample HY-24) occurs sporadically in association with the Mg-rich cordierite gneisses on the farm Hytkoras, and a similar K-feldspar-sillimanite-corundum-plagioclase lithology (sample RFN-4) was sampled on the adjacent farm Rietfontein, although no direct association with magnesian gneisses was noted here. Geochemically, these two rocks are dominated by SiO_2 ($\pm$ 50%), Al_2O_3 (30 to 35%) and K_2O ($\pm$ 9%), showing slight depletion in the foremost and enrichment in the latter two major element oxides compared to typical metapelitic rocks from the western NMC (Table 10.5).

Least-squares approximations using the compositions of these two lithologies indicate, not unexpectedly, that their premetamorphic mineralogy was dominated by potassic minerals - K-feldspar (25%) and muscovite (50%) in the mixing exercise - with minor chlorite (10-15%), plagioclase (or analcite

plus calcite) (10%), possible gibbsite (0-5%) and ilmenite (1%). The absence of quartz or kaolinite in the modelling is interesting, and it is felt that these rocks could have been extremely illite-rich clay horizons which may have experienced subsequent K-feldspar authigenesis during a diagenetic episode, in similar manner to the post-depositional alterations invoked for some of the magnesian gneisses. Degraded fine potassic tuff horizons within sedimentary sequences such as the Green River Formation (Surdam and Parker, 1972) are commonly "almost entirely replaced by authigenic alumino-silicate minerals" within hypersaline facies conditions and may explain the unusual compositions of these two corundum-rich lithologies.

These two lithologies are also useful in countering arguments for restite models proposed for this unusual suite of Al-, Mg- and sometimes K-rich rocks, as enrichments in Al_2O_3 and K_2O only after removal of partial melt granite material is unlikely and contradictory because Al_2O_3 and K_2O should show opposite trends of enrichment and depletion respectively (see Section 6.7).

Chapter 11

GEOCHEMISTRY OF THE MARBLES AND CALC-SILICATE ROCKS

11.1 Introduction

The calc-silicate rocks and marbles of the supracrustal sequences of the western NMC are extremely diverse in their mineral and chemical compositions, making them one of the more difficult groups to discriminate and evaluate. Based on mineral content (see Section 3.6), these lithologies were divided into five main groups - plagioclase-diopside rocks, plagioclase-garnet rocks, diopside-rich rocks, forsterite marbles and wollastonite/calcite rocks. Although the compositions of these groups show a certain degree of overlap, these subdivisions have been found to be sufficiently significant chemically to be retained in the proceeding sections (Table 11.1).

Sedimentary carbonate rocks are dominated by the minerals calcite and dolomite which can only incorporate very minor amounts of a few elements, notably Mn and Sr, into their crystal structures in significant quantities. The abundances of elements besides Ca, Mg, Mn and Sr, therefore, are generally dependent on the amount and type of detrital or diagenetic material present (Graf,1962). Elements such as Al, Ti, K, Cr, Ni, Rb, Ba and Zr are almost exclusively confined to the clastic detrital fraction, whereas other elements including Si, Fe, Mn, Na and Y occur both within the minor detrital fraction and the major chemical precipitate fraction (McLennan et al., 1979).

A number of metamorphic reactions, outlined in Section 3.6, explain the variety of mineral parageneses observed in the calc-silicate and metacarbonate rocks of the study area. All involve decarbonation processes whereby large volumes of CO_2 are lost from the original rocks, considerably altering the bulk compositions of the newly-formed lithologies compared to their precursors. The metamorphic minerals formed during the prograde reactions, however, are stable to high temperatures and pressures with the result that no partial melting occurs as observed in high-grade metamorphism of metapelitic and metapsammitic rocks. The loss from the original sedimentary rocks, therefore, is primarily restricted to CO_2 and H_2O, and is thus relatively accurately quantifiable if the assumption is made that the CaO and MgO contents of the metamorphic rocks were predominantly incorporated in calcite and dolomite in the unmetamorphosed precursors.

11.2 Chemical comparisons between the five metacarbonate groups

The extreme range of chemical compositions displayed by the metacarbonate rocks of the western NMC is apparent from the distribution of major element oxides on Harker diagrams (Fig. 11.1), typified by SiO_2 which shows a range from 10 to 75%. Another obvious feature, well displayed on the Al_2O_3:SiO_2 plot, is the bimodal nature of the trends (excluding the CaO:SiO_2 plot). Rocks

TABLE 11.1 Mean major element compositions of the various categories of metacarbonate rocks in the study area.

	1.		2.		3.		4.		5.	
SiO_2	61.39	(8.20)+	56.99	(11.37)	50.89	(9.77)	13.75	(4.81)	41.53	(17.27)
TiO_2	0.75	(0.35)	0.46	(0.20)	0.41	(0.39)	0.10	(0.06)	0.16	(0.11)
Al_2O_3	15.60	(3.98)	16.71	(5.68)	9.00	(5.94)	2.08	(1.14)	4.97	(2.01)
FeO*	6.15	(2.95)	5.73	(2.36)	5.07	(2.65)	1.05	(0.71)	1.42	(0.92)
MnO	0.14	(0.06)	0.14	(0.05)	0.16	(0.11)	0.06	(0.09)	0.21	(0.23)
MgO	1.98	(1.46)	0.67	(0.61)	11.23	(3.96)	17.21	(1.09)	1.06	(0.90)
CaO	10.25	(3.60)	15.33	(6.10)	19.73	(5.96)	33.15	(1.83)	38.87	(8.51)
Na_2O	1.91	(1.15)	0.62	(0.27)	0.54	(0.49)	0.02	(0.05)	0.10	(0.10)
K_2O	0.65	(0.70)	1.40	(3.15)	0.63	(0.86)	0.05	(0.11)	0.70	(0.88)
P_2O_5	0.23	(0.10)	0.12	(0.06)	0.76	(1.55)	0.06	(0.10)	0.18	(0.34)
no. of samples	25		8		11		7		7	

* total Fe as FeO + standard deviation

1. plagioclase-diopside calc-silicate rocks
2. plagioclase-garnet calc-silicate rocks
3. diopside-rich calc-silicate rocks
4. forsterite marbles
5. calcite/wollastonite-rich rocks

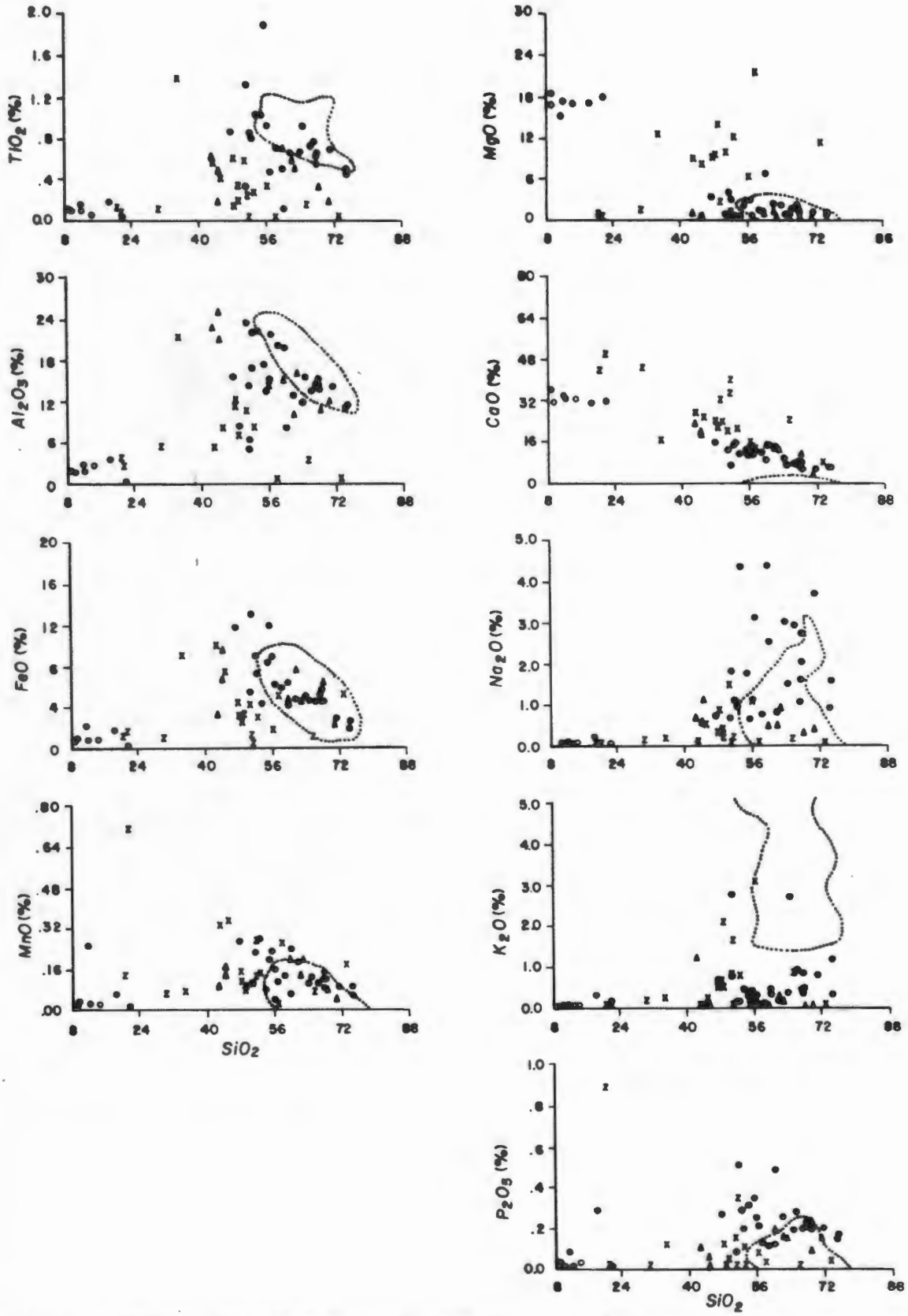

Fig. 11.1 Harker diagrams showing the distribution of major element oxide contents of metacarbonate rocks compared to the field for the metapelitic rocks (stippled line). Forsterite marbles (o), calcite/wollastonite rocks (z), diopside-rich rocks (x), plagioclase-garnet rocks (▲) and plagioclase-diopside rocks (•).

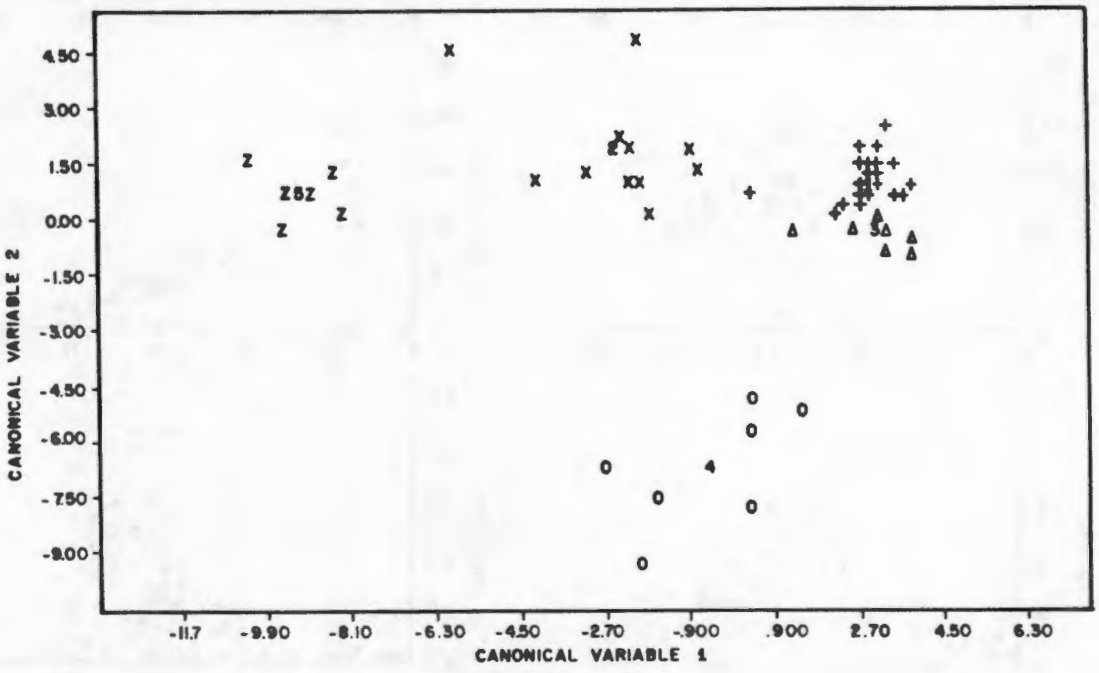

Fig. 11.2 Plot of the two canonical variables calculated in the stepwise discriminant analysis to separate the five categories of metacarbonate rocks. These are plagioclase-diopside calc-silicate rocks (+ with mean value at 1), diopside-rich rocks (x with mean value at 2), plagioclase-garnet calc-silicate rocks (△ with mean value at 3), calcite/wollastonite rocks (0 with mean value at 4) and forsterite marbles (z with mean value at 5).

containing less than 50-55% SiO_2 show positive trends in relation to SiO_2 for the major elements, whereas those with SiO_2 greater than 50-55% generally show negative trends. Positive trends are displayed by the forsterite marbles, wollastonite/calcite rocks and diopside-rich rocks, whilst negative trends are shown by the plagioclase-diopside and, to a lesser degree, by the plagioclase-garnet rocks.

The negative trends of the plagioclase-rich calc-silicate rocks are very similar to those shown by the metapelitic rocks (Fig. 11.1) with the exception of marked enrichment in CaO and depletion in K_2O. Al_2O_3 and TiO_2 are perhaps slightly depleted compared to the metapelitic trend, and P_2O_5 and Na_2O slightly enriched. It is apparent that the compositions of these calc-silicate rocks are dominated by SiO_2 and Al_2O_3 rather than CaO and MgO, and that they represent metamorphosed carbonate-bearing alumino-silicate rocks rather than true carbonate sediments. The MgO contents and trends of these rocks are similar to those of the normal metapelitic rocks, as are their FeO contents, whilst their CaO contents are greatly enriched (Fig. 11.1). This suggests that the MgO content of these rocks is probably located within a clay component (chlorite) and not within dolomite, and that the carbonate constituent of these "metapelitic" rocks was predominantly calcite, despite the relatively low Ca/Mg ratio of the rocks. This applies particularly to the plagioclase-diopside rocks as the plagioclase-garnet rocks generally have extremely low MgO contents and the presence of dolomite in these rocks was not anticipated.

In contrast, the positive trends for the major element oxides (with the exception of CaO and MgO) with increasing SiO_2 content shown by the forsterite marbles, wollastonite/calcite rocks and diopside-rich rocks, indicate that all the major elements, aside from CaO and MgO are essentially dilutants within rocks originally dominated by carbonates. Here it must be borne in mind that the actual values of the major element oxides are generally exaggerated due to considerable loss of CO_2 during metamorphic reactions (see Section 3.6). On the MgO:SiO_2 plot, the MgO-poor nature of the wollastonite/calcite rocks (and the plagioclase-garnet rocks) compared to the forsterite marbles and diopside-rich rocks is apparent, indicating their calcitic and dolomitic natures respectively. The MgO:SiO_2 plot thus successfully discriminates between limestones, dolomites and carbonate-rich pelitic rocks. Within these CaO-, MgO-dominated lithologies, particularly the diopside-rich rocks, there are a few samples which show high values for FeO, MnO and P_2O_5 relative to the normal trends, indicating possible chemogenic (as opposed to detrital) enrichments in these constituents.

The metacarbonate rocks of the study area were subjected to stepwise discriminant analysis in a similar procedure to that described for the metapelitic rocks (see Section 7.5). In this exercise, the five metacarbonate groups were successfully separated from each other by two canonical variables which made use of the variables SiO_2, Al_2O_3, FeO, MgO, CaO and P_2O_5 (Fig. 11.2 and Table 11.2). These variables represent the major chemical constituents of the metacarbonate rocks besides Na_2O, indicating that differences between the groups are significant, being controlled by the major element chemistry, and are not subtle differences defined essentially by minor and trace elements as

TABLE 11.2 Coefficients for the canonical variables and the U-statistic from the stepwise discriminant analysis of the five categories of metacarbonate rocks from the western NMC.

Variable	Coefficients for canonical variable 1	Coefficients for canonical variable 2	U-statistic (Wilks' Lambda)
SiO_2	0.083	-0.038	0.009
Al_2O_3	0.067	0.163	0.003
FeO	0.315	-0.041	0.005
MgO	-0.375	0.339	0.103
CaO	0.004	-0.229	0.021
P_2O_5	-0.382	0.911	0.002
Constant	-4.452	2.507	

in the case of the metapelitic rocks.

11.3 Comparison with amphibolites and basic granulites

The trends displayed by the plagioclase-diopside calc-silicate rocks on Harker diagrams raise certain questions as to their precise origins. It would appear that they represent metamorphosed silicate-rich rocks, either shale-carbonate mixtures or else perhaps degraded mafic volcanic rocks enriched in CaO. In this section, the metacarbonate group of lithologies is compared chemically to the basic granulites and amphibolites of presumed basaltic/tholeiitic origin. Particular emphasis is placed on the precise status of the plagioclase-diopside rocks.

Discrimination between ortho- and para-amphibolites by geochemical means was undertaken by Leake (1964) and van de Kamp (1969) using various Niggli values (al,alk,c,mg) and trace elements, such as Cr and Ni, which generally have relatively high concentrations in mafic igneous rocks and much lower values in carbonate rocks. Leake (op.cit.) used the plot Niggli c vs mg to demonstrate differences between pelitic rocks (with low c and mg values), mafic volcanic rocks (with intermediate c and mg values) and pure and impure carbonate rocks (with high c and mg values). Although the igneous rocks plot between the fields of shales and carbonates on the diagram, and thus overlap with the field of shale-carbonate mixtures, they have a narrow horizontal trend compared to the more scattered vertical trends of the latter, and thus suites of metamorphosed rocks can be discriminated using this diagram.

On the Niggli c vs mg diagram (Fig. 11.3a) the metapelitic rocks from the western NMC plot within the field of shales, the metabasites closely follow the igneous trend defined by the Karroo dolerites, and "true" metacarbonates (excluding the two plagioclase-rich rock types) plot in the fields of limestones and dolomites. The plagioclase-rich calc-silicate rocks have a more scattered distribution with mg values similar to the metapelitic rocks (and lower than the metabasites) but with higher, more variable c values. They plot above the igneous trend line, and thus could be interpreted as shale-limestone mixtures (but not shale-dolomite mixtures). The metapelites, metabasalts, metacarbonates and these proposed metamorphosed shale-limestone mixtures have relatively well defined fields, segregated from one another, and so the Niggli c vs mg plot can be used to discriminate, with minimal overlap, between various supracrustal rock types from the western NMC.

The Niggli al-alk vs c plot utilized by van der Kamp (1969) is similar in many respects to the Niggli c vs mg plot, with the igneous field lying between the shale and carbonate fields and thus theoretically within the region of shale-carbonate mixtures. When the supracrustal rocks from the western NMC are superimposed on this diagram (Fig. 11.3b), the metapelites plot in the field of shales, the metabasites within the igneous field and the "true" metacarbonates within the fields of dolomites and limestones. The plagioclase-rich calc-silicate rocks lie in an intermediate area between the fields of shales and limestones with considerably higher al-alk values than the metabasites, although with similar values to the metapelites. Once again

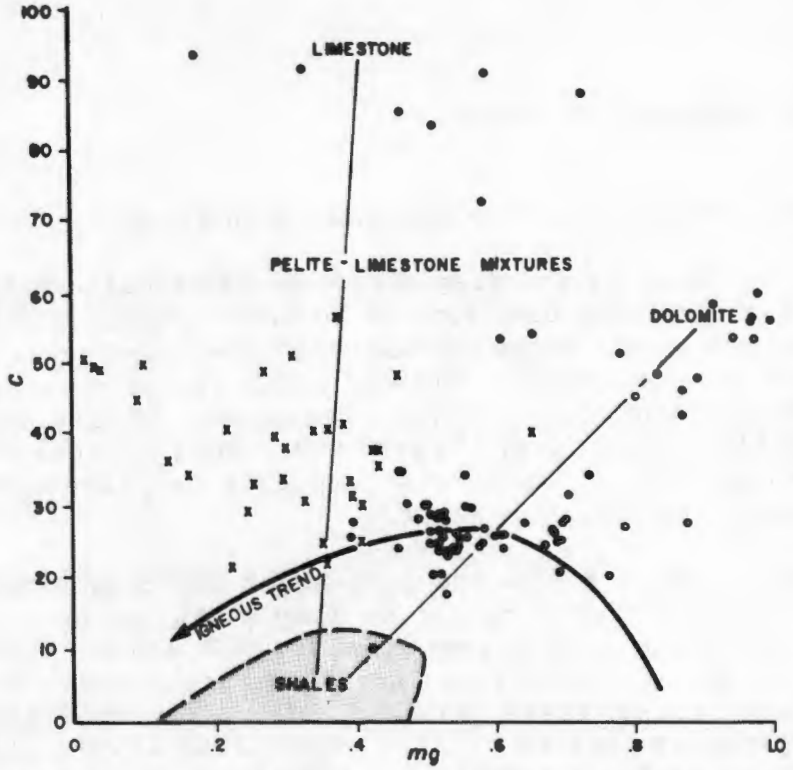

Fig. 11.3a Niggli c:mg plot showing the fields of shales, dolomites, limestones and pelite-limestone mixtures as well as the igneous trend defined by the Karroo basalts (after Leake, 1964). Superimposed on this diagram are data for metapelitic rocks (shaded area), metabasites (•), "true" metacarbonates (o) and plagioclase-rich calc-silicate rocks (x) from the study area.

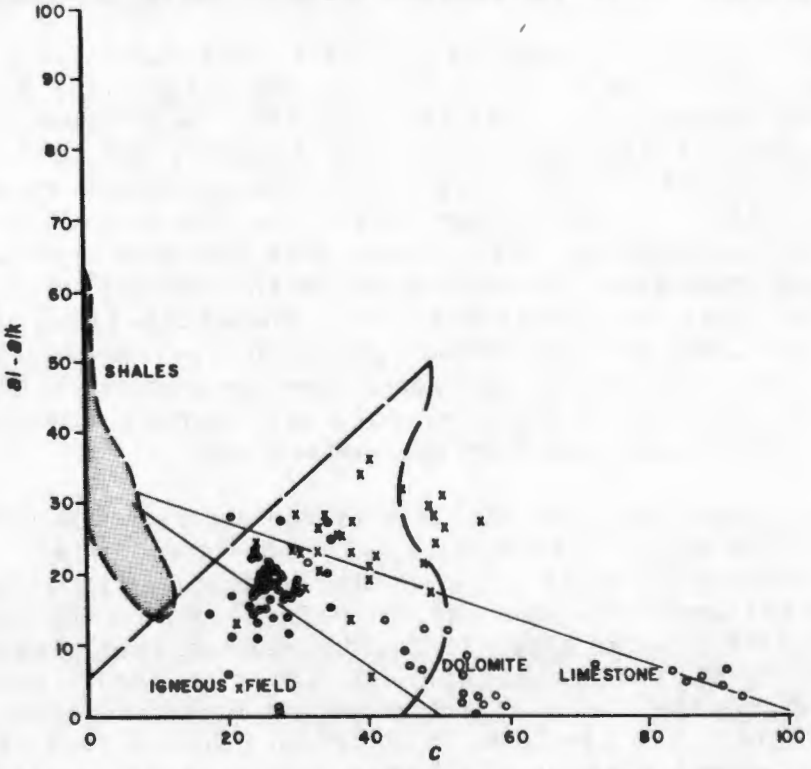

Fig. 11.3b Niggli al-alk:c plot showing the fields of shales, dolomites, limestones and the igneous field (after van de Kamp, 1969). Superimposed data on this diagram are identical to those for Fig. 11.3a.

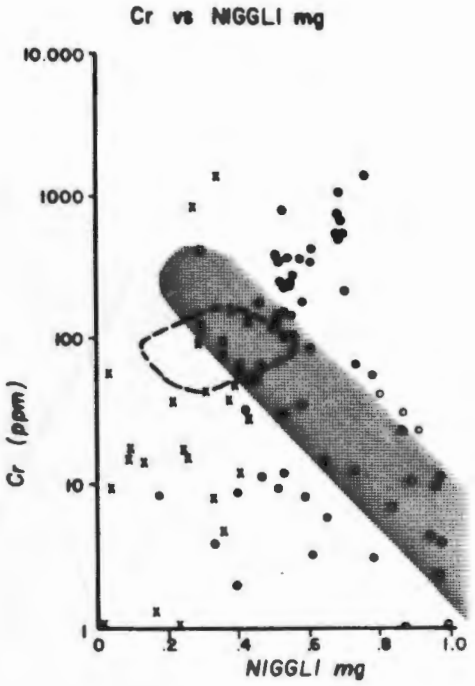

Fig. 11.4a Bivariate plot of Cr vs Niggli mg showing the area of shale-carbonate mixtures (shaded area) as defined by van de Kamp (1969). Data from the study area, including the field of metapelitic rocks (dashed line), metabasites (•), "true" metacarbonates (o) and plagioclase-rich calc-silicate rocks (x), are superimposed.

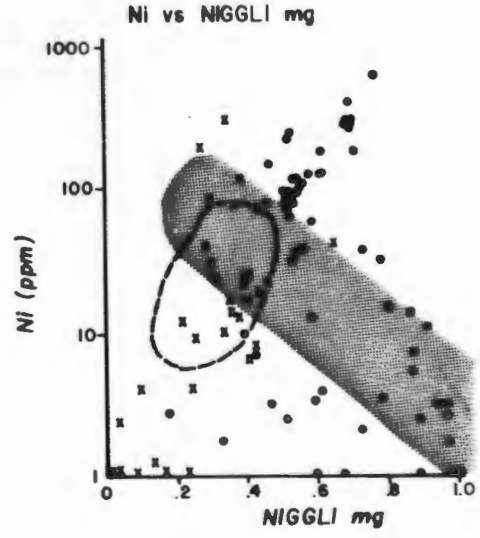

Fig. 11.4b Bivariate plot of Ni vs Niggli mg showing the area of shale-carbonate mixtures (shaded area) as defined by van de Kamp (1969). Data as for Fig. 11.4a.

Fig. 11.5 ACF diagram showing the fields of clays and shales with up to 35% carbonate (I), greywackes (II), marls (arrowed lines), ultramafic rocks (1) and tholeiites and andesites (2) (after Winkler, 1976). Data for metabasites (•), "true" metacarbonates (o) and plagioclase-rich calc-silicate rocks (x) from the study area are superimposed.

mixtures of pelitic components and calcite would best explain this distribution although it must be borne in mind that the alk value may be considerably reduced due to metamorphic processes (see Section 11.4.1).

On both the above diagrams, the metabasites lie in an intermediate position between the metapelitic and dolomitic rocks, indicating that these plots cannot be used exclusively to discriminate between mafic volcanic rocks and shale-dolomite mixtures. Additional plots using trace elements such as Cr and Ni are therefore required to separate metabasalts from metamorphosed shale-dolomite mixtures.

In Niggli mg vs Cr and mg vs Ni plots devised by van de Kamp (1969) (Fig. 11.4), it is apparent that the western NMC metabasites have well-defined positive trends at relatively high Cr and Ni values (as would be expected from mafic volcanic rocks), whereas the "true" metacarbonates have broader scattered distributions at lower Cr and Ni concentrations. The plagioclase-rich calc-silicate rocks, however, have more ambiguous distributions on these diagrams. They show positive trends similar to the metabasites and indeed appear to plot as extensions of the metabasite trends towards the origin on both diagrams, possibly implying that their precursors contained a mafic igneous component. The bulk of the plagioclase-rich calc-silicate rocks also plot in a similar position to the metapelitic rocks of the western NMC with slightly lower Cr and Ni values and as extensions from the metapelitic fields towards the origin in both diagrams. They could thus equally easily be interpreted as shale-carbonate mixtures (calcite, not dolomite). There is a slight compositional gap between the metabasites and the calc-silicate rocks which also show slightly lower mg values than the mafic metavolcanic trends, particularly on the mg vs Cr diagram. An origin as calcite-bearing pelitic rocks, possibly derived from degradation of mafic volcanic rocks is thus favoured as the most satisfactory interpretation of these diagrams. Classification of individual samples from the study area as representing either metavolcanic or metasedimentary rocks using Niggli mg vs Cr or mg vs Ni diagrams is not possible although the broad differences between the three major groups are readily apparent.

The ACF diagram is also an effective means of discriminating between ortho- and para-mafic metamorphic rocks (Winkler,1976). Mafic volcanic rocks plot on the ACF diagram in a relatively narrow belt extending from the F apex towards the mid-point of the A-C tie-line (i.e. the anorthite position), whereas marls and carbonate rocks plot in a broad belt extending from the field of pelitic rocks in the middle of the A-F tie-line towards the C-F tie-line within the range C=50% (dolomite) and C=100% (calcite). These two trends are approximately at right angles to one another and so igneous or sedimentary precursors to suites of metamorphosed mafic rocks should be relatively easy to distinguish.

The western NMC metabasites plot as a relatively tight cluster within the field of tholeiites and andesites as defined by Winkler (1976) (Fig. 11.5). Approximately 50% of the samples, however, fall within the area of overlap between mafic volcanic rocks and dolomite-rich marls, although relatively few of the western NMC metacarbonate rocks plot within this area. A few samples

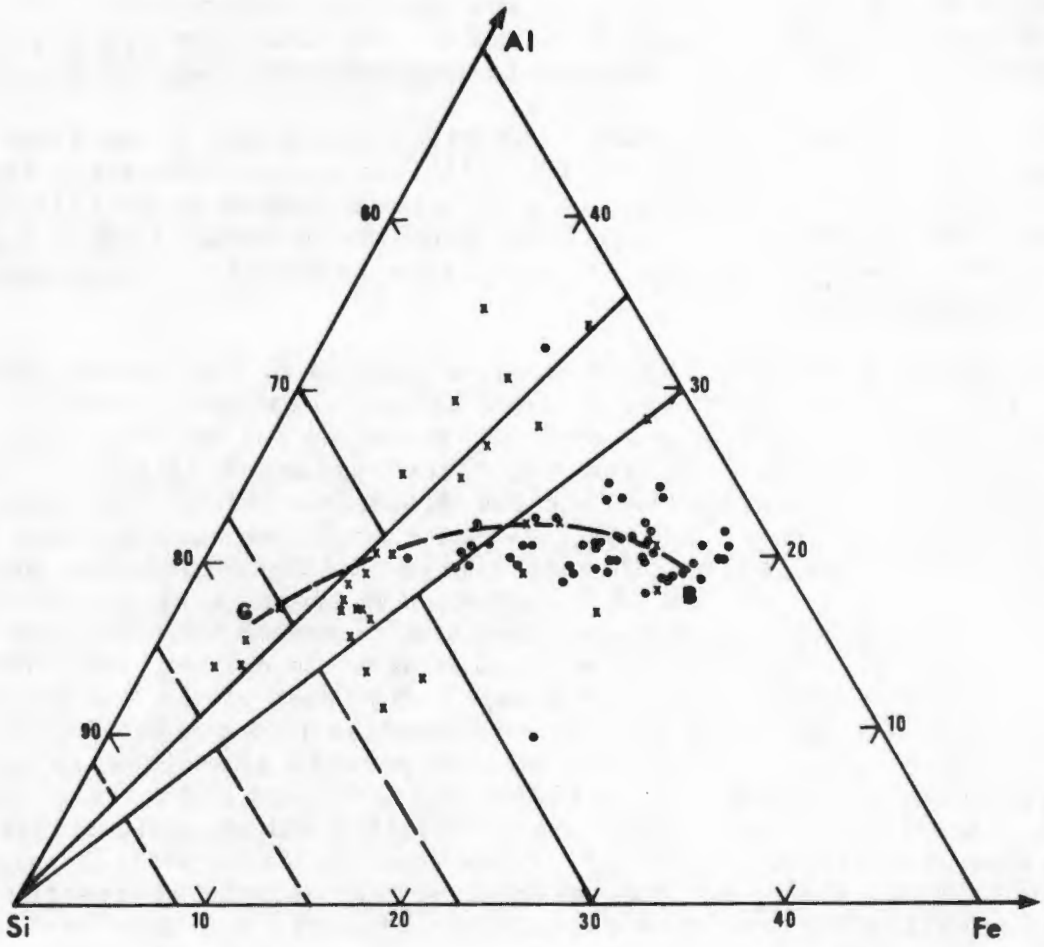

Fig. 11.6 Si-Al-Fe triangular diagram showing the igneous trend from granitic (G) to basaltic (B) rocks and the narrow sedimentary corridor (solid lines from Si apex to Al-Fe tie-line) as defined by Moore and Dennen (1970). Data for metabasites (•) and plagioclase-rich calc-silicate rocks (x) from the study area are superimposed.

TABLE 11.3 Coefficients for the canonical variables and the U-statistic from the stepwise discriminant analysis of the metacarbonate rocks, plagioclase-dominated calc-silicate rocks and metabasites from the western NMC.

Variable	Coefficients for canonical variable 1	Coefficients for canonical variable 2	U-statistic (Wilks' Lambda)
SiO_2	-0.111	-0.001	0.075
MgO	-0.347	-0.142	0.100
CaO	-0.299	-0.037	0.360
K_2O	-0.285	-0.137	0.055
Ni	0.006	0.001	0.061
Co	0.007	-0.060	0.168
Constant	11.989	3.072	

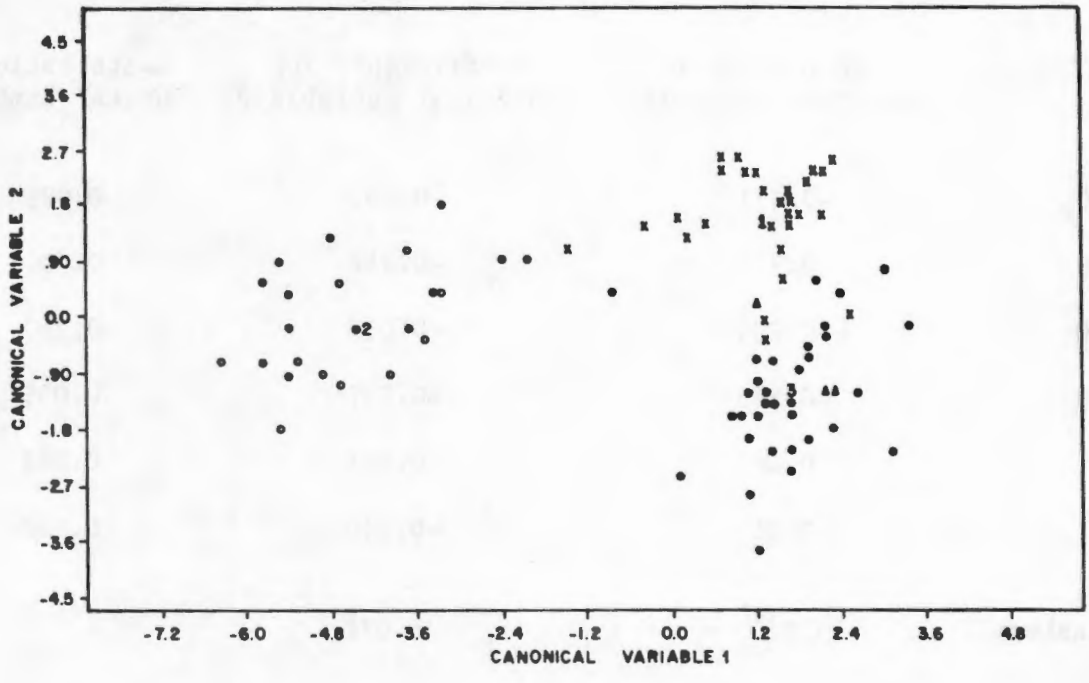

Fig. 11.7 Plot of the two canonical variables calculated in the stepwise discriminant analysis to separate the metabasites (• with mean value at 3) from the plagioclase-rich calc-silicate rocks (x with mean value at 1) and "true" metacarbonates (o with mean value at 2).

plot outside the tholeiite/andesite field and within the field of greywackes. The plagioclase-rich calc-silicate rocks from the western NMC, with the exception of two samples, plot outside the range of tholeiites and andesites towards the A-C tie-line. The majority fall within the field of calcite-rich marls although several have extremely low F values and fall on the A-C tie-line side of the field of common marl compositions. The plagioclase-rich calc-silicate rocks, however, plot in an ambiguous position on the ACF diagram where they can be interpreted either as mixtures of pelitic rocks and a C (calcite) component or as mafic volcanic rocks with an accentuated anorthite component. The calcite/wollastonite rocks plot close to the C apex and the diopside-rich rocks and forsterite marbles close to the mid-point of the C-F tie-line (dolomite) outside the fields of marls and mafic volcanic rocks, indicating their true carbonate character.

The Si-Al-Fe triangular diagram (Moore and Dennen,1970) can also be used to display differences between the distributions of the metavolcanic amphibolites and basic granulites and the plagioclase-rich calc-silicate rocks (Fig. 11.6). The vast majority of mafic metavolcanic rocks plot outside the narrow "sedimentary" corridor towards the basaltic end of the igneous trend-line. The plagioclase-rich calc-silicate rocks on the other hand, show considerable scatter, but mostly plot within the sedimentary corridor, with several samples showing relatively high Al values similar to Al-rich pelitic rocks. Some six calc-silicate samples, however, plot within the field of metabasites, indicating that significant overlap between para- and ortho-mafic metamorphic rocks is possible on the Si-Al-Fe diagram, although their broad trends may differ.

Stepwise discriminant analysis was undertaken to test for separation of the metavolcanic amphibolites and basic granulites from the plagioclase-rich calc-silicate rocks and the "true" metacarbonates based on their chemical compositions (Fig. 11.7 and Table 11.3). The "true" metacarbonates were clearly separated from the other two groups, but there is a certain degree of overlap between the fields of amphibolites/basic granulites and plagioclase-rich calc-silicate rocks. Two discriminant functions were calculated using SiO_2, CaO, MgO, K_2O, Ni and Co. One discriminant function was dominated by MgO, CaO and SiO_2 (carbonates vs silicates ?) and the other by Co and lesser MgO (igneous vs sedimentary ?). The majority of samples in the area of overlap of the two groups came from areas where "true" metacarbonates were not observed (the Bitterfontein paragneiss belt and the eastern portions of the Witwater belt). Three banded amphibolites from the northern portions of the study area, whose field relationships suggested possible sedimentary origins, plotted in positions on the discriminant diagram suggesting that they are in fact derived from mafic volcanic rocks and are not of sedimentary origin.

11.4 Estimations of precursor mineral assemblages

11.4.1 Logarithmic scatter diagrams

In sedimentary carbonate rocks, the elements Ti, Fe, K and Na show strong positive correlations with Al and Si, indicating that they occur predominantly

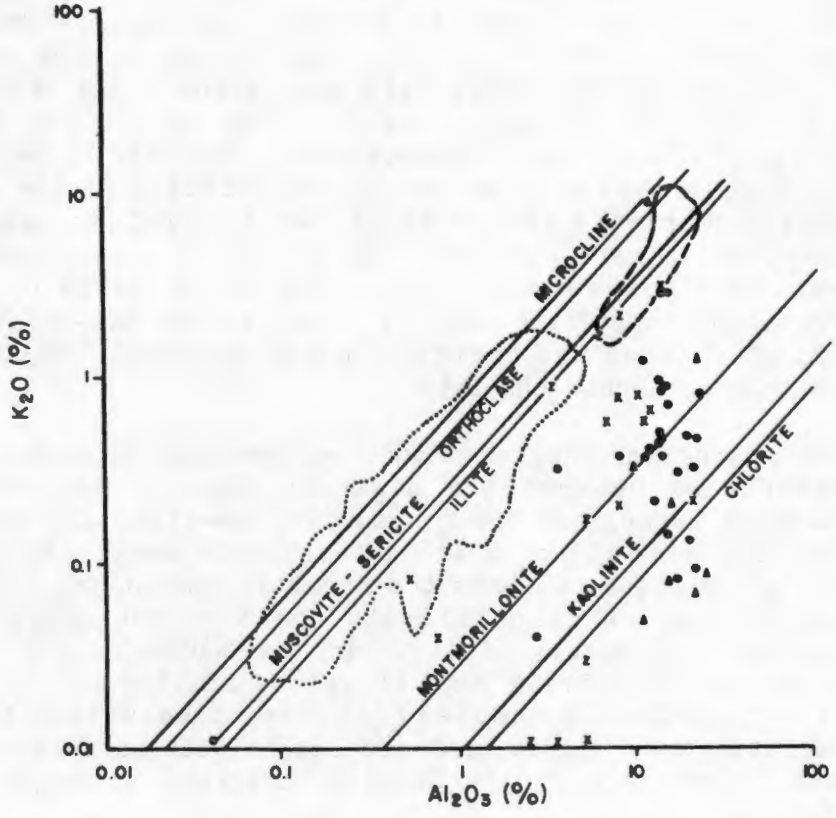

Fig. 11.8 Logarithmic scatter diagram of K_2O vs Al_2O_3 showing regression lines for certain detrital minerals and the fields of carbonate rocks (dotted line) and calcareous mudstones and siltstones (dashed line) as defined by Veizer et al. (1977). Data for plagioclase-diopside calc-silicate rocks (•), plagioclase-garnet calc-silicate rocks (▲), diopside-rich rocks (x), forsterite-marbles (z) and calcite/wollastonite rocks (o) from the study area are superimposed.

in close association with the alumino-silicate minerals (clays) present in these rocks. The dominant mineral constituents that control the distribution of these elements in sedimentary carbonate rocks are: illite > authigenic feldspars (K-feldspar and albite) > chlorite > other clay minerals, as deduced from studies of insoluble residues and as displayed on various logarithmic scatter diagrams (Veizer and Garrett,1978; Veizer,1978).

Caution must be exercised when interpreting data from metamorphosed carbonate rocks, such as the western NMC lithologies, on scatter diagrams, as the actual plotted positions can be misleading, particularly for the diopside-rich and wollastonite-rich rocks. This is due to major loss of CO_2 during metamorphism (representing up to 30% weight loss of the original carbonate rock). This causes a marked enrichment in other major elements with the result that the diopside-rich rocks, for example, have measured concentrations of approximately 9% Al_2O_3 and 50% SiO_2 instead of estimated original contents of approximately 6% and 35% respectively. This is sufficient to displace the data points of these lithologies from the fields of carbonate rocks into the fields of calcareous mudstones and siltstones on certain diagrams. The relative positions of the samples viz-a-viz regression lines representing various alumino-silicate minerals, however, will not change with CO_2 loss, allowing for qualitative comparisons to be made with unmetamorphosed carbonate rocks and their non-carbonate constituents. This latter feature is significant when attempting to predict premetamorphic mineral constituents for the metacarbonate rocks.

On the K_2O:Al_2O_3 scatter diagram (Fig. 11.8), the western NMC metacarbonate rocks show a markedly different distribution compared to typical carbonate rocks, being too depleted in K_2O at relatively high Al_2O_3 levels to be explained by illite-K-feldspar-dominated constituents. Instead their premetamorphic mineralogy is best explained by illite-chlorite mixtures or perhaps a montmorillonite-dominated clay component.

On Na_2O:Al_2O_3 diagrams, a greater dispersion than that displayed by K_2O:Al_2O_3 is generally observed within sedimentary carbonate rocks. This is explained as being due to the presence of non-silicate Na within the lattices of Ca-Mg carbonates and sulphates (Veizer et al., 1977) which would have the effect of displacing Na_2O:Al_2O_3 ratios above the field of clays such as illite. It is, however, apparent that this displacement is most pronounced in the more alumina-rich carbonate rocks (Fig. 11.9), and so can also be accounted for by the presence of an albite/analcite constituent. The western NMC metacarbonates show distributions on the Na_2O:Al_2O_3 diagram (Fig. 11.9) which indicate that mixtures of illite and albite (or analcite) provide a feasible explanation of the Na_2O contents of these rocks, with albite/analcite predominating in the more aluminous plagioclase-rich calc-silicate rocks, and illite in the alumina-poor "true" metacarbonates. The distribution pattern is not widely diffuse but relatively well-defined, and this characteristic, taken together with negative correlations between Na and Sr (see Section 11.4.2), indicates that evaporitic concentrations of Na within carbonate and/or sulphate phases were probably absent. As in the case of the K_2O:Al_2O_3 distribution, the Na_2O contents of the western NMC metacarbonates are displaced towards chlorite relative to the typical field of sedimentary

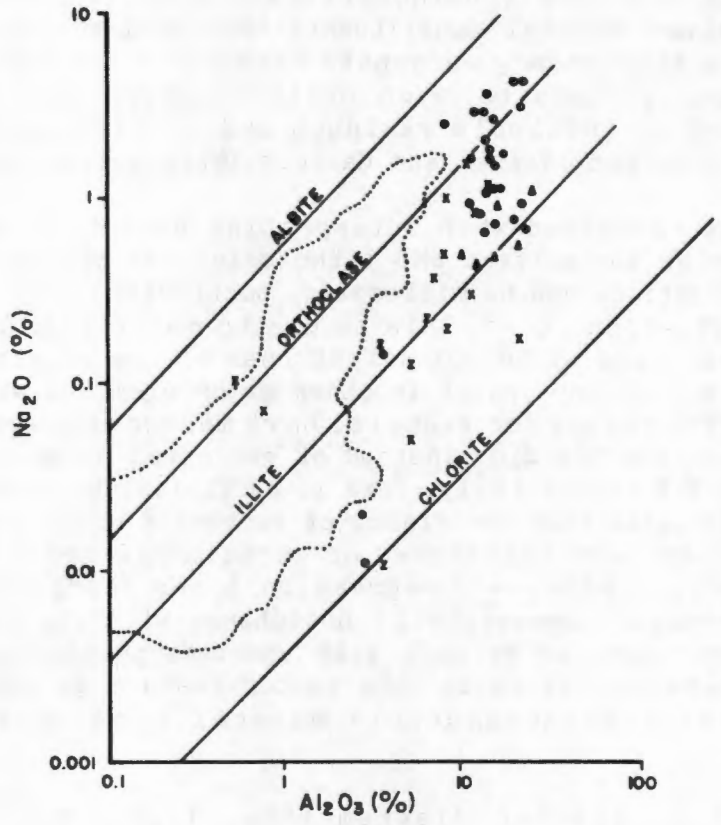

Fig. 11.9 Logarithmic scatter diagram of Na_2O vs Al_2O_3 showing regression lines for certain detrital minerals and the fields of carbonate rocks (dotted line) as defined by Veizer et al. (1977). Superimposed data from the study area as for Fig. 11.8.

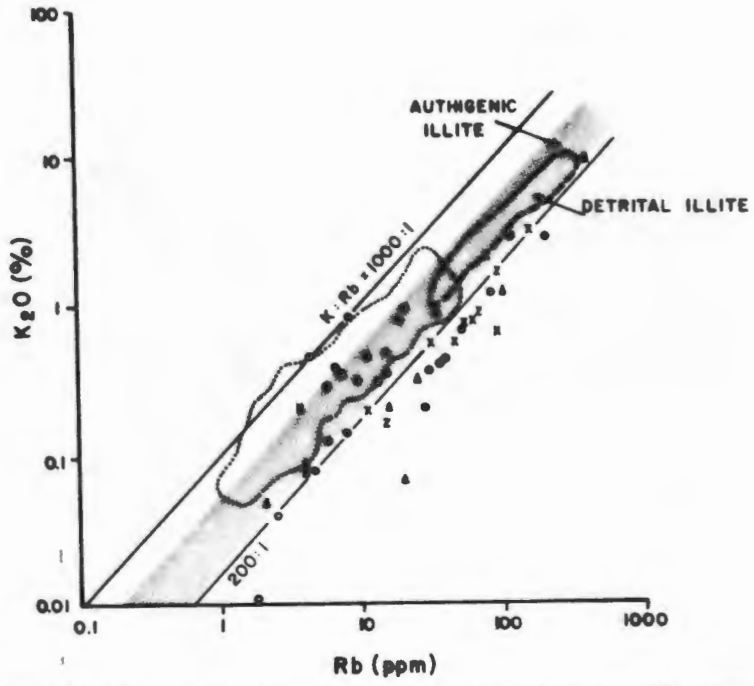

Fig. 11.10a Logarithmic scatter diagram of K_2O vs Rb showing regression lines for various K:Rb ratios and the broad field of authigenic and detrital illites as well as the fields of carbonate rocks (dotted line) and calcareous mudstones and siltstones (dashed line) (after Veizer et al., 1977). Superimposed data from the study area as for Fig. 11.8.

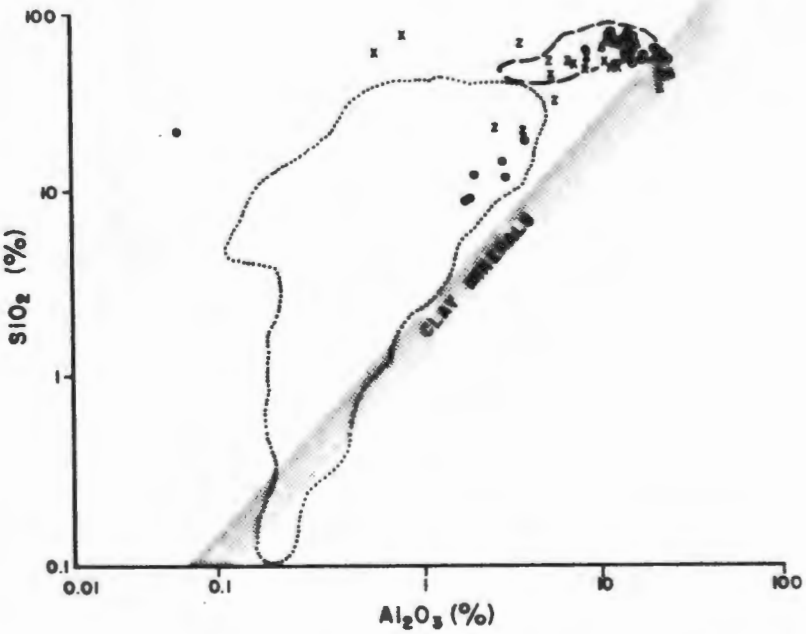

Fig. 11.10b Logarithmic scatter diagram of SiO_2 vs Al_2O_3 showing the regression field for common clay minerals and the fields of carbonate rocks (dotted line) and calcareous mudstones and siltstones (dashed line) as defined by Veizer et al. (1977). Superimposed data from the study area as for Fig. 11.8.

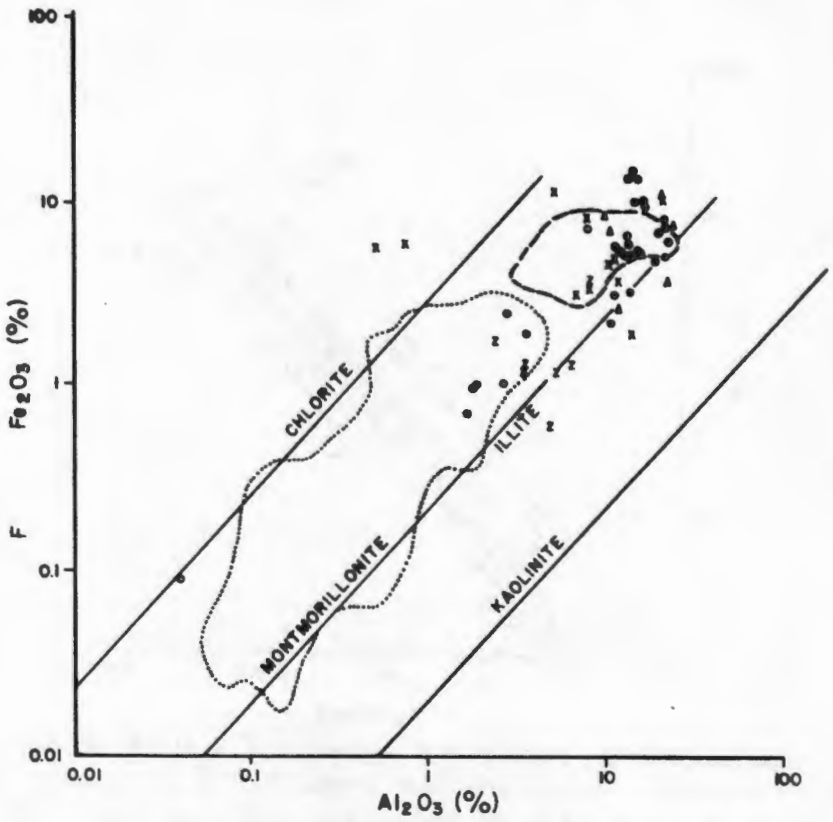

Fig. 11.11a Logarithmic scatter diagram of total Fe as Fe_2O_3 vs Al_2O_3 showing regression lines for certain detrital minerals and the fields of carbonate rocks (dotted line) and calcareous mudstones and siltstones (dashed line) as defined by Veizer (1978). Superimposed data from the study area as for Fig. 11.8.

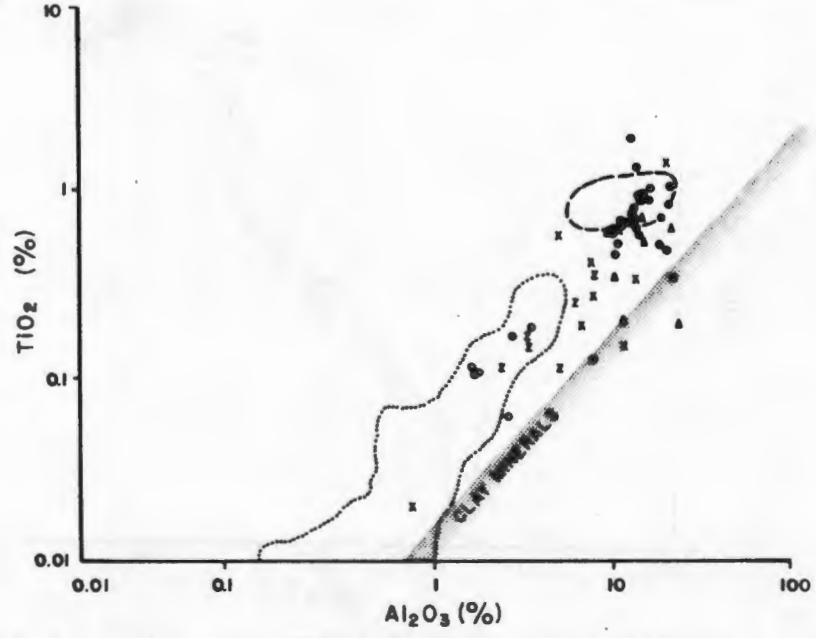

Fig. 11.11b Logarithmic scatter diagram of TiO_2 vs Al_2O_3 showing the regression field for common clay minerals and the fields of carbonate rocks (dotted line) and calcareous mudstones and siltstones (dashed line) as defined by Veizer (1978). Superimposed data from the study area as for Fig. 11.8.

carbonate rocks.

The Rb contents of the metacarbonate rocks are essentially controlled by the K_2O-bearing phases such as biotite and K-feldspar (see Section 6.6), and the distribution on the K_2O:Rb scatter diagram (Fig. 11.10a) probably reflects this, with the samples having low K/Rb ratios ($\pm$200) indicating biotite control, and those of higher ratios (predominantly the plagioclase-diopside calc-silicate rocks) having K-feldspar control of K/Rb ratio. It is noticeable, however, that samples over a very wide range of K_2O and Rb values, including extremely low K_2O (<0.1%) and Rb (<10ppm) contents, show persistent K/Rb ratios in the region of 200. It is possible, therefore, that this reflects the relative premetamorphic proportions of these elements, in which case an origin for the K-, Rb-bearing constituent as detrital illite is indicated for the bulk of the samples.

On the SiO_2:Al_2O_3 diagram, sedimentary carbonate rocks show positive correlations between SiO_2 and Al_2O_3 (less obvious in calcareous mudstones and siltstones). SiO_2 contents are generally in excess of that required by alumino-silicate minerals, indicating that free silica is present. This free silica commonly occurs as detrital quartz in limestones and chalcedony in dolostones (Veizer,1978). The relative positions of the western NMC metacarbonates compared to the sedimentary groups are likely to be markedly displaced on this diagram due to CO_2 loss during metamorphism. They do, however, indicate, in most instances, excess SiO_2 similar to their sedimentary counterparts (Fig. 11.10b). The "true" metacarbonates have positive SiO_2:Al_2O_3 trends whereas the plagioclase-rich calc-silicate rocks show neutral to negative trends similar to calcareous mudstones and siltstones.

Veizer (1978) has demonstrated that the Fe contents of sedimentary carbonate rocks are higher than can be expected from common clay minerals (except for chlorite which is described as being a rare constituent of these rocks - Veizer and Garrett,1978). He (op.cit.) explains this phenomenon, together with the positive correlation of Fe and Al_2O_3, as being due to "coatings of Fe oxides on clays". The western NMC metacarbonate rocks also show this characteristic of relative Fe enrichment compared to illite, montmorillonite and kaolinite, to a certain degree, although a number of samples lie close to or on the illite/montmorillonite line (Fig. 11.11a). Trends of relative Fe enrichment, particularly in the plagioclase-rich calc-silicate rocks, however, may well represent the presence of chlorite in the precursor lithologies, particularly in the light of the low K_2O contents which also indicated trends of this nature. The Fe and Al contents of the plagioclase-rich calc-silicate rocks are similar to those displayed by calcareous mudstones and siltstones, and the Fe and Al contents of the forsterite marbles and calcite-rich to those of dolostones and limestones. The diopside-rich rocks have displaced positions on the diagram as explained, and corrected carbonate compositions for these lithologies appear to fall within the field of dolostones and limestones. The forsterite marbles generally show slightly higher Fe/Al ratios than the calcite/wollastonite rocks, indicating greater Fe accommodation within dolomite than calcite. However, the levels of Fe do not reach the order of magnitude (1-3%) observed in Lower Proterozoic

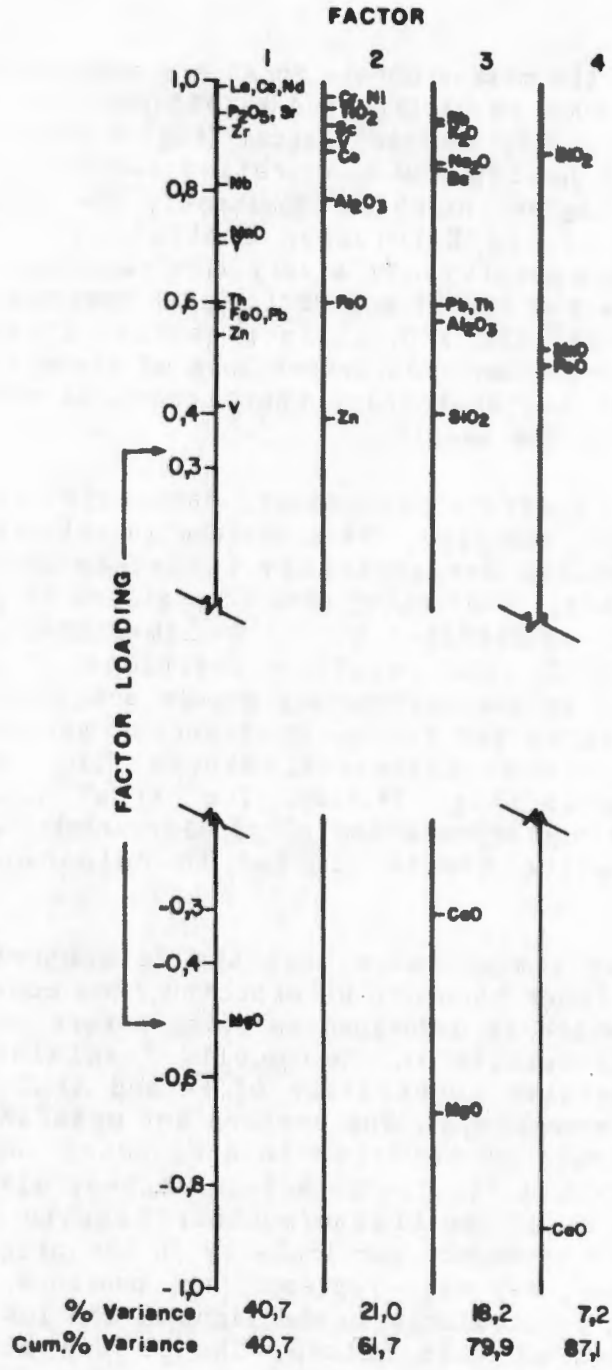

Fig. 11.12 The four principal factors showing the factor loadings of the variables and their cumulative variance obtained in the principal components analysis of the forsterite marbles and diopside-rich calc-silicate rocks from the study area.

carbonate rocks such as those of the Transvaal Sequence (Erikson et al., 1975). This indicates that some Fe was probably present in carbonate form and would also explain deviations from clays observed on the scatter diagram.

The distribution of Ti values in sedimentary carbonate rocks is similar to that of Fe - showing higher contents than can be anticipated from its presence in common clays. Taken in conjunction with positive correlations with Al content, Ti distribution is interpreted as being controlled by detrital minerals such as ilmenite, rutile, brookite or anatase (Veizer,1978). The western NMC metacarbonates also display this characteristic (Fig. 11.11b) with the plagioclase-rich rocks again plotting within the field of calcareous mudstones and siltstones, and the forsterite marbles and calcite/wollastonite rocks within the fields of dolostones and limestones.

On logarithmic scatter diagrams of major element oxides (excluding the carbonate phases CaO and MgO), the metacarbonate rocks of the western NMC show similarities to dolostones and limestones (forsterite marbles and calcite/wollastonite rocks respectively) and calcareous mudstones and siltstones (plagioclase-rich calc-silicate rocks), with the exception that both K_2O and, to a lesser extent, Na_2O appear to be depleted relative to sedimentary rocks. Tanner and Miller (1980) have demonstrated that considerable K and Na loss can occur within calc-silicate rocks during prograde metamorphism. Reactions such as the breakdown of calcite and zoisite in the presence of sodic plagioclase to form anorthite can result in Na leaving the local calc-silicate system in the intergranular fluid. The breakdown of K-bearing phases such as biotite and hornblende during prograde clinopyroxene-forming reactions can similarly result in the expulsion of K in the fluid phase. This may explain the apparent trends towards chlorite on the scatter diagrams. Loss of K_2O content from the NMC carbonate rocks during metamorphism would have to have been on a major scale, however, as K_2O contents of between 0.1 and 1% observed in the plagioclase-rich calc-silicate rocks, should have been an order of magnitude greater (1 to 10%) according to the plots of calcareous mudstones and siltstones (Veizer and Garrett,1978). At these levels of K_2O and Al_2O_3 concentration, it could be expected that K-bearing minerals such as K-feldspars would form during metamorphism rather than radical K loss by fluid migration. The low K and Na values, therefore, may still represent original premetamorphic depletions in the rocks from the study area.

11.4.2 Principal components analysis

In order to assist further in the prediction of potential precursor minerals within the metacarbonate rocks of the study area prior to metamorphism, principal components analysis was undertaken using 27 major and trace elements, in a similar manner to that outlined for the metapelitic rocks (see Section 7.6). The metacarbonate rocks were divided into three groups for this exercise, namely 25 diopside-plagioclase calc-silicate rocks; 15 calcite/wollastonite rocks and garnet-plagioclase calc-silicate rocks (metalimestones); and 18 forsterite marbles and diopside-rich rocks (metadolomites).

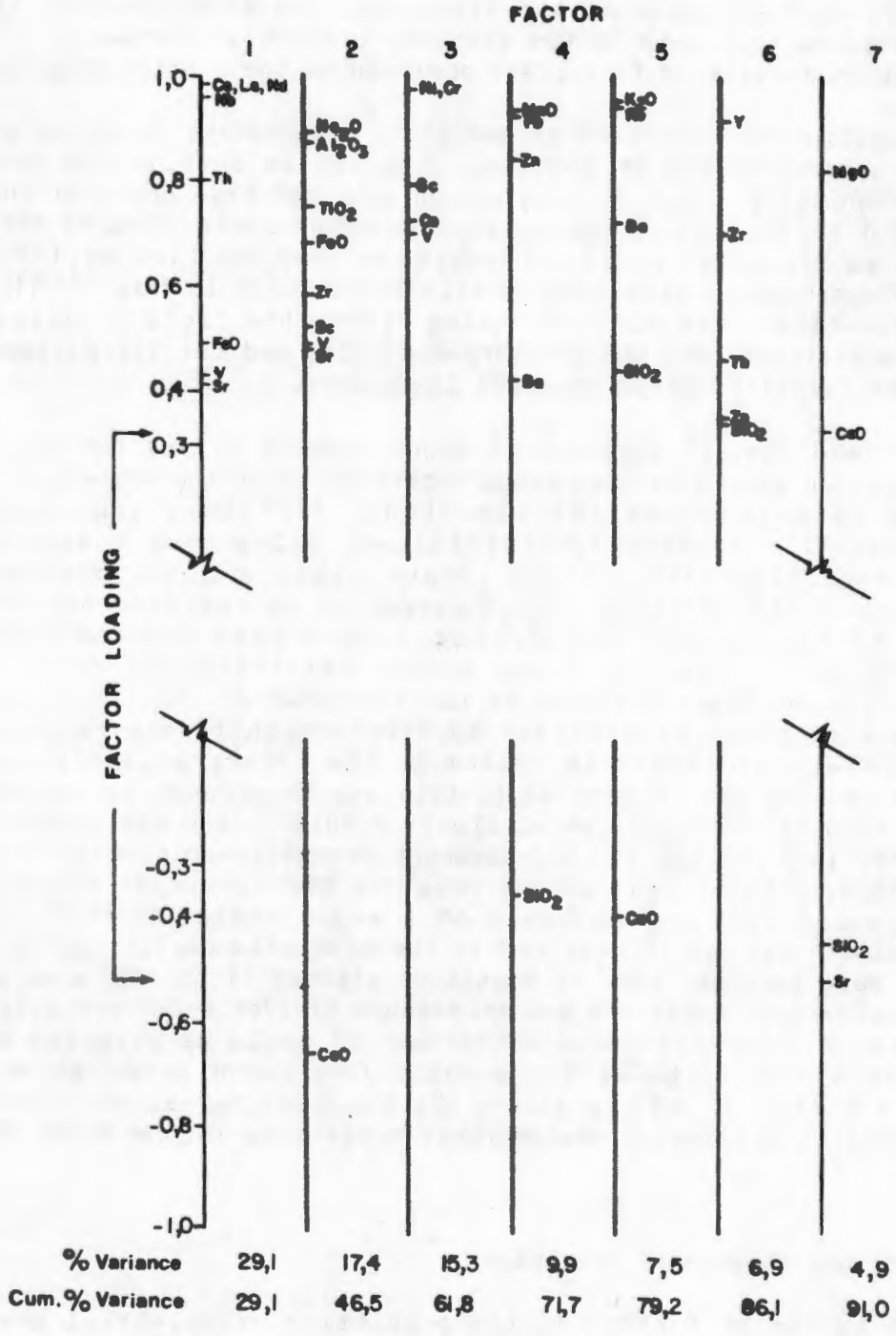

Fig. 11.13 The seven principal factors showing the factor loadings of the variables and their cumulative variance obtained in the principal components analysis of the calcite/wollastonite rocks and plagioclase-garnet calc-silicate rocks from the study area.

The suite of forsterite marbles and diopside-rich rocks provided the simplest solution to the principal components analysis with only four varimax rotated factors cumulatively accounting for 87.1% of the variance in the sample set (Fig. 11.12). Factor 1 has positive factor loadings for La, Ce, Nd, P_2O_5, Sr, Zr, Nb, MnO, Y, Th, FeO, Pb, Zn and V (in order of decreasing significance) and a negative loading for MgO. This is interpreted as a heavy-mineral component (zircon, apatite, Fe-,Mn-oxide) having an inverse concentration to that of dolomite. Factor 2 contains positive factor loadings for Cr, Ni, TiO_2, Sc, V, Co, Al_2O_3, FeO and Zn (in order of decreasing significance) and is interpreted as a chlorite/ilmenite factor. Factor 3 has Rb, K_2O, Na_2O, Ba, Pb, Th, Al_2O_3 and SiO_2 with positive factor loadings, and MgO and weak CaO with negative loadings. Here the interpretation is that of illite and albite/analcite components showing an inverse relationship with dolomite. Finally, factor 4 comprises a positive SiO_2 factor loading and a negative CaO factor loading, representing an antithetical relationship between quartz and calcite. Thus the potential mineral phases identified in the Mg-rich metacarbonate rocks are dolomite, calcite, quartz, illite, albite/analcite, chlorite and lesser zircon, apatite, ilmenite and Fe-,Mn-oxides. With the exception of the chlorite factor, these factors reveal the inverse relationship displayed between carbonate minerals (dolomite and calcite) and quartz plus alumino-silicates.

In the analysis of the calcite/wollastonite and garnet-plagioclase calc-silicate group, seven factors that cumulatively accounted for 91.0% of the variance within the sample set, were calculated (Fig. 11.13). Ce, La, Nd, Nb, Th, FeO, V, and Sr have positive factor loadings in factor 1. The lack of association of rare earth elements with Zr (zircon) and P_2O_5 (monazite), and their association with Th and FeO indicate that this factor may represent a mineral phase such as allanite (as observed in sample SS-4). The second factor contains positive loadings for Na_2O, Al_2O_3, TiO_2, FeO, Zr, Sc, V and Sr and a negative loading for CaO. This is interpreted as the inverse relationship between concentrations of detrital minerals (albite/analcite, kaolinite, ilmenite, zircon) and calcite. Factor 3 comprises the trace elements Ni, Cr, Sc, Co and V and possibly represents a minor chromite phase (or chlorite?). The fourth factor has positive factor loadings for MnO, Pb, Zn and Ba and, as in the case of the northern metapelites, represents the "Aggeneys" mineralisation factor. This is most noticeable in sample SYN-1 from the Aggeneysberge (Table 11.5). Factor 5 has positive factor loadings for K_2O, Rb, Ba and SiO_2 and a negative loading for CaO, representing antithetic concentrations of illite or K-feldspar and calcite. Factor 6 comprises Y, Zr and Th representing zircon, and factor 7 has a positive loading for MgO opposed by a negative loading for SiO2 and Sr, and represents inverse concentrations of dolomite and quartz in the precursor rocks. Thus the precursors to the Ca-rich metacarbonate rocks are thought to have comprised calcite and lesser dolomite and the detrital minerals quartz, illite/K-feldspar, albite/analcite and kaolinite with trace amounts of allanite, ilmenite, zircon, chromite, Zn-,Pb-sulphides and barite.

For the plagioclase-diopside calc-silicate rock suite, seven factors were calculated that cumulatively accounted for 89.3% of the variance (Fig. 11.14).

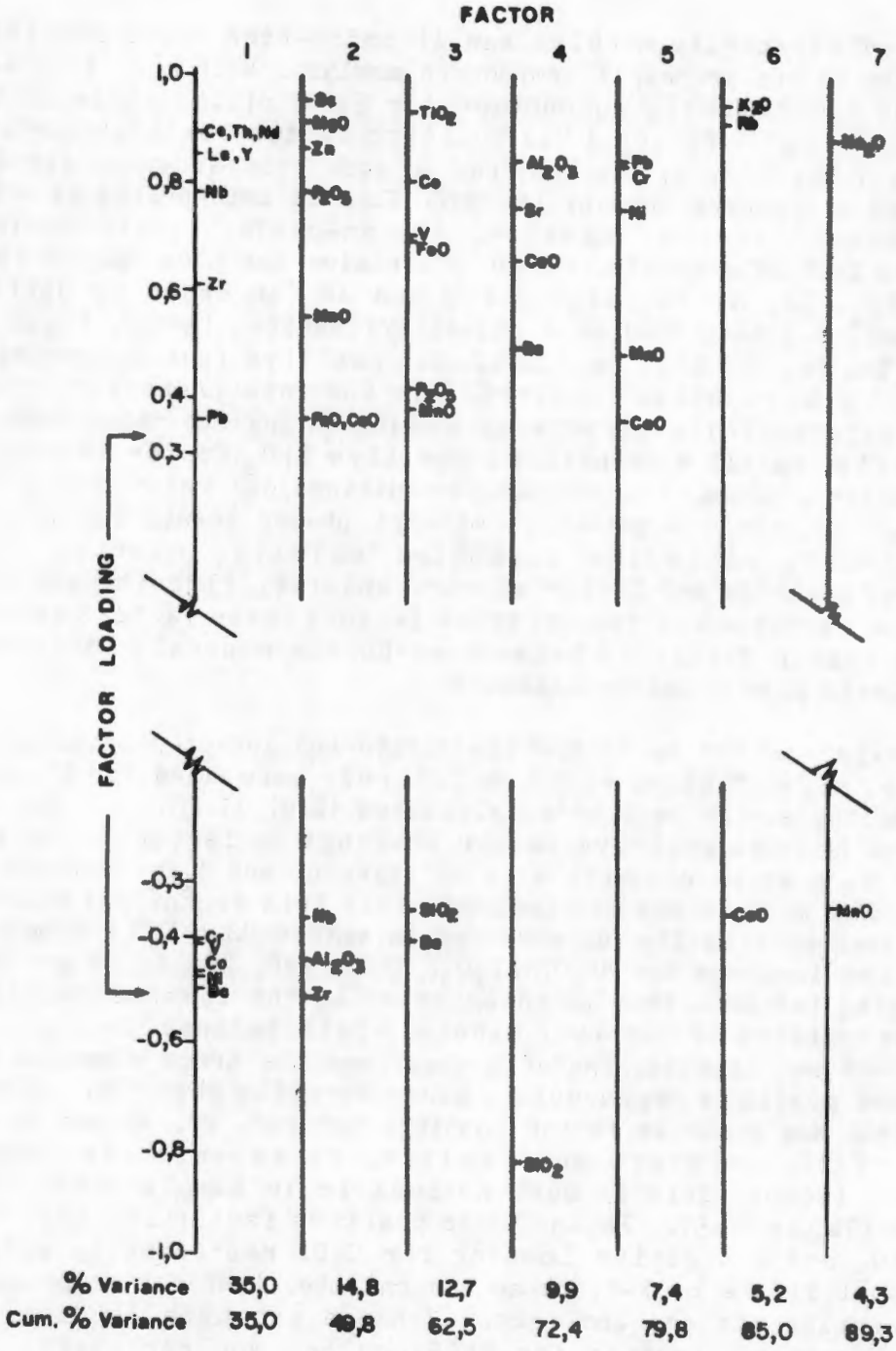

Fig. 11.14 The seven principal factors showing the factor loadings of the variables and their cumulative variance obtained in the principal components analysis of the plagioclase-diopside calc-silicate rocks from the study area.

Factor 1 has positive factor loadings for Ce, Th, Nd, La, Y, Nb, Zr and Pb, interpreted as detrital zircon, and negative factor loadings for Cr, V, Co, Ni and Ba, interpreted as chromite/chlorite. Factor 2 has positive loadings for Sc, MgO, Zn, P_2O_5, MnO, FeO and weak CaO, interpreted as representing Mg-Fe-Ca mineral constituents such as chlorite/montmorillonite/dolomite, and negative loadings for Nb, Al_2O_3 and Zr, interpreted as kaolinite and zircon. Factor 3 has positive loadings for TiO_2, Co, V, FeO, P_2O_5 and MnO and represents the sympathetic association of minor detrital phases ilmenite, apatite and Fe-, Mn-oxides. The fourth factor has positive loadings for Al_2O_3, Sr, CaO and Ba and a negative loading for SiO_2. This is interpreted as an inverse relationship between concentrations of quartz and kaolinite plus calcite (or plagioclase ?). The fifth factor with positive loadings for Pb, Ni and Cr is not readily identifiable but may again represent chromite. Factor 6 with positive factor loadings for K_2O and Rb and a weak negative loading for CaO represents detrital illite/K-feldspar and calcite respectively, and factor 7 with a positive loading for Na_2O is interpreted as albite or analcite. Interpretation of the above seven factors indicates that quartz, kaolinite, illite, chlorite/montmorillonite/dolomite, albite/analcite and calcite (or Ca-rich plagioclase) are present together with minor zircon, chromite, ilmenite, apatite and Fe-, Mn-oxides. Factors 1 and 2 and, to a lesser degree, factors 3, 4 and 6 bear similarities to the first 5 factors in the analysis of the magnesian gneisses (Fig. 10.5). This may indicate that, like the magnesian gneisses, the plagioclase-diopside rocks result from degradation and weathering of mafic igneous rocks.

11. 4.3 Premetamorphic constituent models

Employing the potential major sedimentary constituents deduced from the logarithmic scatter diagrams and principal components analysis, namely quartz, kaolinite, illite, chlorite, montmorillonite, analcite, calcite, dolomite, and ilmenite, the bulkcompositions of the western NMC metacarbonate rocks were quantitatively modelled as precursor quartz/clay/carbonate mixtures. A similar procedure was used to that undertaken with the metapelitic rocks, employing mixing techniques involving least-squares approximations (see Section 7.6). The metacarbonate rocks were grouped according to the five mineralogical categories for this exercise (Table 11.4).

The forsterite marbles were, not unexpectedly, the simplest to model, comprising on average 70% dolomite, 15% calcite, 8% quartz and 7% montmorillonite. The diopside-rich calc-silicate rocks contained considerably less dolomite (30%) and increased quartz (20%) with approximately 15% calcite, 15% montmorillonite, 10% illite and 10% chlorite. Two lithologies with somewhat differing mineralogies to typical diopside-rich rocks, namely a quartz-diopside-hypersthene rock (sample GN-4 from the Oranjefontein outlier) and a quartz-tremolite rock (sample GB-1 from the Geselskapbank area), both enriched in SiO_2 and MgO and strongly depleted in Al_2O_3, were modelled as quartz (60%) - dolomite (30%) - Fe oxide (5%) - magnesite (5%) assemblages. The Oranjefontein rock was closely associated with other Mg-rich lithologies (cordierite-hypersthene gneisses). The calcite/wollastonite rocks were dominated by calcite (55%) and quartz (25%) with 20% clay minerals, mostly

TABLE 11.4 Estimated mean percentages of model premetamorphic constituents for the various categories of metacarbonate rocks using least-squares approximations.

	1.		2.		3.		4.		5.	
quartz	28	(10-46)*	20	(0-28)	8	(4-18)	27	(9-49)	26	(11-50)
illite	4	(0-43)	8	(0-34)	0	(0-4)	2	(0-15)	8	(0-24)
kaolinite	10	(0-40)	2	(0-21)	0		27	(0-42)	1	(0-7)
montmorillonite	20	(0-50)	15	(0-37)	7	(0-11)	4	(0-29)	6	(0-20)
chlorite	10	(2-25)	8	(3-16)	2	(0-4)	10	(5-16)	1	(0-3)
analcite	10	(4-29)	3	(0-10)	0		4	(2-6)	0	
calcite	15	(8-25)	14	(2-22)	15	(9-21)	25	(19-34)	56	(38-76)
dolomite	1		29	(5-44)	68	(61-78)	0		2	(0-6)
ilmenite	1		1		0		1		0	
sum of squares of differences	0.20	(0.00-0.52)	0.22	(0.00-0.59)	0.01	(0.00-0.04)	0.15	(0.02-0.34)	0.03	(0.00-0.09)
no. of samples	23		9		7		7		7	

* range of composition

1. plagioclase-diopside calc-silicate rocks
2. diopside-rich calc-silicate rocks
3. forsterite marbles
4. plagioclase-garnet calc-silicate rocks
5. calcite/wollastonite-rich rocks

illite and montmorillonite. The "true" metacarbonate rocks, therefore, contained between 45 and 85% carbonate minerals, 8 and 25% quartz and 7 and 35% clay minerals (mostly montmorillonite, illite and chlorite).

Model solutions for the garnet-bearing calc-silicate rocks indicated that approximately equal amounts (25%) of quartz, kaolinite and calcite were present together with lesser chlorite, montmorillonite, analcite and ilmenite. Possible alternative solutions to this model, with similar low sums of squares of differences ($\pm$0.15), contained Ca-rich plagioclase instead of kaolinite plus calcite (see also discussion on ACF diagram, Section 11.3). This alternative was not favoured due to opposite factor loadings of Al_2O_3 and CaO in factor 2 of the principal components analysis of these lithologies, whereas sympathetic CaO and Al_2O_3 behaviour would be anticipated in lithologies with large ($\pm$40%) plagioclase contents. In most instances, excess CaO that had to be accommodated in an additional calcite constituent, was also present in the plagioclase model.

The plagioclase-diopside calc-silicate rocks were estimated to contain, on average, 30% quartz, 15% calcite and 55% clay minerals, predominantly montmorillonite, kaolinite, analcite and chlorite. Based on the relative proportions of the clay minerals, they could be subdivided in two distinct groups. One group, predominantly from the northern part of the study area, was dominated by kaolinite (30%) and the other group, almost exclusively from the Bitterfontein and Witwater areas, by montmorillonite (35%). This characteristic is represented by factor 2 of the principal components analysis of the plagioclase-diopside rocks (Fig. 11.14), where MgO, FeO and CaO have opposite factor loadings to Al_2O_3. The restriction of calc-silicate rocks with large model kaolinite contents to the northern parts of the study area coincides with the distribution of metapelitic rocks with high model kaolinite contents (see Section 7.6). Dolomite is virtually entirely absent in all models of the constituents of the plagioclase-bearing calc-silicate rocks.

11.5 Anomalous concentrations of minor and trace elements.

11.5.1 Phosphate concentrations

Certain minor and trace elements are present in extremely high concentrations in a few of the metacarbonate samples collected from the western NMC. The commonest minor element to show anomalous concentration is phosphorus, occurring as apatite in the metamorphic parageneses. Relatively P_2O_5-rich metacarbonate rocks were sampled in the Witwater-Platbakkies paragneiss belt (samples WW-6, WW-14, PH-14) and also occur in the Namiesberg area (sample A-41; Moore,1977) (Table 11.5). In both areas they occur in supracrustal sequences which also contain MnO- and P_2O_5-rich iron formations (see Section 13.3). The P_2O_5-rich metacarbonate rocks also show slight enrichments in MnO, U, Zr, Nb, Zn, Y and light rare earth elements.

Small amounts of phosphate (approximately 0.07%) are known to co-precipitate with calcium carbonate during the formation of limestones from sea-water (Gulbrandson and Cremer,1970), although direct precipitation of

TABLE 11.5 Major element compositions and certain trace element contents (in ppm) of metacarbonate rocks enriched in P, Ba, Pb and light rare earth elements.

	1.	2.	3.	4.	5.	6.
SiO_2	45.21	43.15	64.37	44.54	21.74	50.82
TiO_2	0.41	0.56	0.22	0.48	0.11	0.34
Al_2O_3	8.05	5.20	7.29	21.19	2.48	23.43
FeO*	7.26	9.96	3.45	9.67	1.55	5.50
MnO	0.34	0.33	0.20	0.17	0.71	0.10
MgO	8.09	9.15	6.35	0.19	0.30	0.89
CaO	25.89	27.21	14.51	19.81	50.14	13.34
Na_2O	0.50	0.05	0.54	0.56	0.00	0.68
K_2O	0.20	0.01	0.61	0.07	0.01	0.80
P_2O_5	3.40	4.34	2.13	0.00	0.00	0.08
Ba	26	31	95	4	803	1.85%
Sr	894	617	102	1442	466	1026
Th	11	14		61	10	
U	8	8		-	6	
Zr	351	497	136	213	38	159
Nb	60	11	5	99	-	6
Pb	29	18	31	163	6273	
Zn	200	159	223	72	162	30
Y	71	64	33	31	4	15
La	177	162		4787	-	6
Ce	449	427		8092	23	23
Nd	274	269		1937	8	27

* total Fe as FeO

1. WW-6, diopside-rich calc-silicate rock, Witwater-Platbakkies paragneiss belt.
2. WW-14, diopside-rich calc-silicate rock, Witwater-Platbakkies paragneiss belt.
3. A-41, diopside-plagioclase quartz calc-silicate rock, Namiesberg (Moore, 1977).
4. SS-4, plagioclase-garnet-allanite calc-silicate rock, Kangnas-Smorgen Schaduwe paragneiss belt.
5. SYN-1, calcite-wollastonite-garnet marble, Aggeneysberge.
6. HY-6, plagioclase-garnet calc-silicate rock, Buffels River paragneiss belt.

apatite can be inhibited by the presence of magnesium ions (Martens and Harriss,1970). For concentrations of apatite in the percent range to form within carbonate rocks, however, additional processes such as diagenetic replacement of calcite or organic concentration induced either by nutrient-rich oceanic upwelling (Sheldon,1963; Cook and McElhinny,1979) or by hypophosphite transformation in restricted shallow-water environments (Youssef,1965; Banerjee et al., 1980) are necessary.

Associated enrichments of U, Zn, Y and light rare earth elements within the P_2O_5-rich metacarbonate rocks of the western NMC are similar to enrichments found in bedded phosphorite deposits (Tooms et al., 1969; Gulbrandson,1966). The presence of P_2O_5-rich iron formations within sequences containing P_2O_5-rich metacarbonate rocks indicates that the phosphates were probably precipitated under shallow-water conditions and not within deeper-water environments required by the upwelling model. The depositional environment could have been similar to that proposed for the late Precambrian phosphorites of the Aravalli Supergroup, India (Banerjee et al., 1980), namely restricted, shallow-water, tidal to intertidal flats where stromatolitic assemblages played a vital role in the transformation of sea water phosphorus concentrations into apatite, and its subsequent entrapment within the algal mats.

The P_2O_5-rich metacarbonate rocks are loosely associated with the calcite/wollastonite metacarbonates (metalimestones) and iron formations in their distribution in the western NMC, and are generally restricted to the Witwater-Platbakkies paragneiss belt and the paragneiss belts from Kangnas-Smorgen Schaduwe to Aggeneys and the Namiesberg. (Fig. 11.15). The P_2O_5-poor forsterite marbles and diopside-rich calc-silicate rocks (metadolomites) commonly occur within the paragneiss belts that lie between these two areas, as well as within the "exotic" supracrustal sequence in the Geselskapbank area. Although, on a regional scale, dolomites are typical of platform environments and limestones of deeper-water shelf areas, the reverse association is commonly observed in the shallow-water environment with limestones and dolomitic limestones occurring in the intertidal zone and dolomites in the subtidal zone (Eriksson et al., 1975). It is possible, therefore, that the metalimestones, phosphatic carbonate rocks and iron formations indicate extremely shallow-water conditions of deposition in certain portions of the western NMC, and the metadolomites slightly deeper-water platform environments in other areas.

Mansfield (1940) has pointed out the important role that fluorine can play in the precipitation of phosphate and has suggested that an association could exist between fluorine-rich volcanic eruptive activity and phosphate deposition. Thin fluorite bands have been observed in diopside-rich calc-silicate rocks at Swartkoppies (pers observ.; W. Schreyer,pers.comm.) in the same horizon as the phosphate-rich sample A-41 from the Namiesberg (Moore,1977). Rooney and Kerr (1967) deduced from the presence of clinoptilolite concentrations in the North Carolina phosphorites that volcanic ashfalls played an important role in the formation of these deposits, causing mass mortality of marine organisms and subsequent organic phosphate concentrations. Berner (1973) has demonstrated how P_2O_5 concentrations in

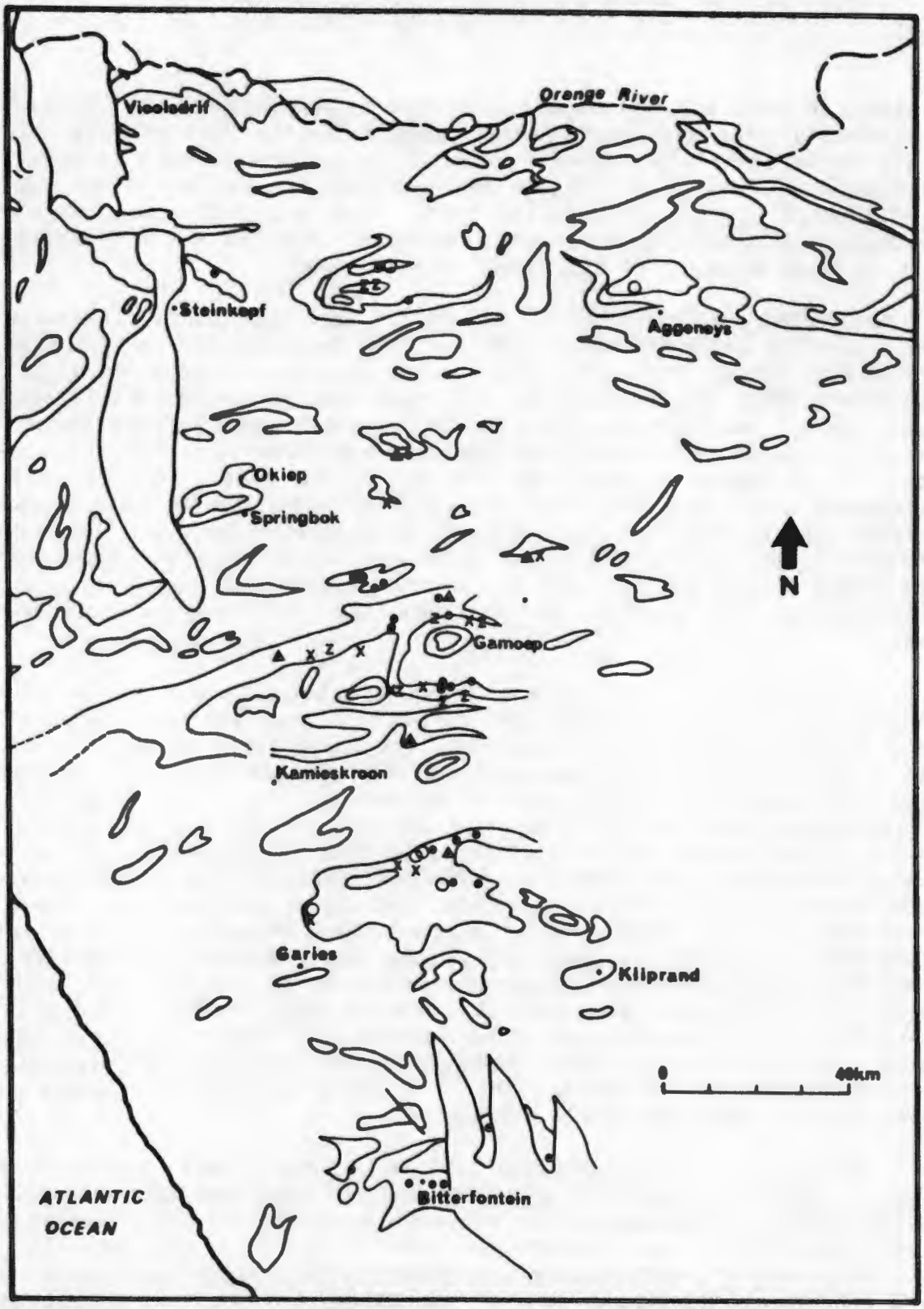

Fig. 11.15 Regional map showing the geographical distribution of the metacarbonate rocks sampled during this study. Plagioclase-diopside calc-silicate rocks (•), plagioclase-garnet calc-silicate rocks (▲), diopside-rich rocks (x), forsterite marbles (z) and calcite/wollastonite rocks (o) are distinguished. Outcrops of paragneiss are marked by finely dashed line.

iron-rich volcanogenic sediments can occur by phosphate extraction from sea water through adsorption onto volcanogenic ferric oxides or as ferric phosphate. It is conceivable, therefore, that phosphate concentrations observed in association with carbonates (in more oxidising conditions) and iron formations (in more reducing conditions) in the western NMC, were derived indirectly from subaerial volcanic activity.

11.5.2 Rare earth element concentrations

At Smorgen Schaduwe, a garnet-plagioclase-allanite calc-silicate rock (sample SS-4; Table 11.5) with minor diopside, quartz, scapolite and sphene occurs in association with plagioclase-diopside-quartz calc-silicate rocks at the base of a supracrustal sequence that consists predominantly of quartz-biotite-sillimanite schists and glassy quartzites. The allanite concentration in the calc-silicate rock is of sufficient magnitude (±20%) that the whole rock averages approximately 5000 ppm La, 8000 ppm Ce, 2000 ppm Nd and 150 ppm Sm. Aside from the light rare earth elements, the calc-silicate rock is also somewhat enriched in Sr, Th, Nb, Mo and Pb as well as Al_2O_3 and total Fe as FeO. No enrichments in P_2O_5, U or Y are observed. Whilst allanite is a relatively common trace constituent of certain calc-silicate rocks (e.g. Rao et al., 1979), concentrations of this magnitude of rare earth elements in metacarbonate rocks are extremely rare. One such occurrence is that of the Mary Kathleen uranium deposit in Queensland, Australia. Here uraninite-allanite-apatite mineralisation is associated with garnet-rich skarn assemblages in calcareous and dolomitic metasediments of similar Mid-Proterozoic age to the NMC paragneisses (Derrick,1977).

Rare earth elements (REE's) are generally found at low concentrations in carbonate rocks (Goldberg et al., 1963; Balashov et al., 1964) and studies of REE distributions in limestones (Parekh et al.,1977) indicate that they are present in both the non-carbonate and calcite phases. Marked depletions of Ce are found in certain limestones, similar to that observed in sea-water, and were deduced to have formed by the rapid removal from sea-water of Ce as Ce^{4+} compared to other light REE's which do not exist in a 4+ ionic state (Parekh et al., op.cit.). In contradiction to these findings, leaching studies of the carbonate-rich Proterozoic Espanola Formation (McLennan et al., 1979) indicate that the absolute abundances of REE's in carbonate minerals are relatively high, that the REE distribution pattern in carbonate minerals is similar to that of associated terrigenous material, and that Ce is not anomalously depleted in comparison to other light REE's.

At increased temperatures and pressures in carbonate-rich environments such as occur during the intrusion of carbonatite complexes (Balashov and Pozharitskaya,1968), during hydrothermal alteration (McLennan and Taylor,1979) and during metamorphism and partial melting (Collerson and Fryer,1978), as well as during diagenesis (Fryer,1977), there is evidence of mobility of rare earth elements, particularly heavy REE's, as soluble carbonate complexes with the form $[REE(CO_3)_3]^{3-}$ which may be removed in a fluid phase resulting in residual concentrations of light REE's. This is particularly obvious in certain lower-temperature (200-300 °C) ankerite-rich stages of carbonatite intrusions. These latter ankeritic carbonatites can also contain REE

concentrations of the order of magnitude observed in sample SS-4, either as perovskite, pyrochlore or one of the many rare earth carbonates, including burbankite, parisite and bastnasite (Balashov and Pozharitskaya, op.cit.).

Whilst it is not suggested that the Smorgen Schaduwe calc-silicate rock represents a metamorphosed carbonatite lens due to its paragneiss associations, the above comparison serves to indicate that concentrations and relative enrichments of light REE`s are distinctly possible during metamorphism of carbonate-rich rocks. Selective enrichment of metacarbonate rocks in Fe, Ca, CO_2, H_2O, uranium and rare earth elements during a metasomatic/metamorphic event has been proposed to explain the late-stage U-REE mineralisation at the Mary Kathleen deposit (Derrick,1977).

Although decarbonisation and loss of heavy REE`s during metamorphism would enhance the concentration of light REE`s in calc-silicate rocks, their original concentration prior to metamorphism must still have been extremely high for this process to produce lithologies such as SS-4 - exceptionally so for carbonate sediments. In this regard, Balashov and Pozharitskaya (1968) demonstrate that ankerite and dolomite have rare earth contents 4 to 5 times lower than calcite, and thus during diagenetic processes such as dolomitization, it is possible that rare earth elements can be concentrated in residual limestone pockets. Sample SS-4, the garnet-plagioclase-allanite calc-silicate rock, has a limestone chemistry, whereas sample SS-3, a diopside-plagioclase rock closely associated with SS-4, has a dolomitic chemistry, indicating that partial dolomitization of carbonate rocks could have taken place at the Smorgen Schaduwe locality. A more intensive study of the REE-rich calc-silicate rock is required to resolve this intriquing concentration.

11.5.3 Barium concentration

In addition to P and light rare earth element enrichments in the metacarbonate rocks, one plagioclase-rich calc-silicate rock from the Buffels River paragneiss belt (sample HY-6; Table 11.5) contains anomalous amounts of barium (1.85%). Barite was not observed in a thin section of this rock and it is possible that a Ba-rich feldspar may have been present. As the mode of occurrence of Ba in this calc-silicate rock is unknown, further discussion on the causes of this concentration (synsedimentary or replacement?) is not warranted.

11.6 Summary

The metacarbonate rocks of the western portions of the NMC are diverse in nature, with forsterite marbles and diopside-rich calc-silicate rocks representing metamorphosed dolomitic rocks of varying purity and calcite/wollastonite rocks metamorphosed limestones. Plagioclase-garnet calc-silicate rocks appear to represent calcite-rich, dolomite-poor marls, perhaps impure equivalents of the calcite/wollastonite rocks. The metalimestone lithologies are restricted to the Witwater-Platbakkies paragneiss belt and the Aggeneys and Geselskapbank areas with the metadolomites occurring in the intervening area, predominantly in the Dikmatje-Stofkraal and Buffels River paragneiss belts. This distribution may represent differing shallow-water

facies conditions, although the metacarbonate occurrences do not represent a single stratigraphic horizon. Rarer phosphate-rich metacarbonate rocks have a similar distribution to the metalimestones. Both these rock types are taken as representing extremely shallow-water chemical sediments although, judging from the uniform, relatively low Na_2O contents and normal-to-low Sr contents of the rocks, evaporitic sediments are not present.

Plagioclase-diopside calc-silicate rocks have a more widespread distribution in the western NMC occurring throughout the study area from Bitterfontein to Geselskapbank in the north. Their premetamorphic origins are less obvious and perhaps more diverse than the other metacarbonate rocks. There is a considerable weight of chemical evidence to suggest that mafic volcanic rocks, degraded by sedimentary and/or diagenetic processes to quartz-montmorillonite-calcite and quartz-kaolinite-chlorite-calcite assemblages are the precursors to these calc-silicate rocks. Similar origins have been proposed for slightly lower-grade amphibolitic rocks in the Dalradian Supergroup of Scotland (van de Kamp,1970). Mixtures of K-poor pelitic material and calcite to produce marly sediments also provide a plausible model for these lithologies.

In general, the metacarbonate rocks of the western NMC are highly depleted in K_2O and also slightly in Na_2O compared to typical carbonate sediments. This is somewhat unexpected, as the supracrustal sequences are dominated by K-rich quartzo-feldspathic and metapelitic lithologies, and cannot be entirely explained as depletion during high-grade metamorphic processes, particularly in the plagioclase-bearing rocks. The metabasites of the study area were also found to have distinctly low K_2O contents (see Section 9.2) comparable with low-K tholeiites. If many of the metacarbonates from the western part of the NMC were derived by degradation of mafic rocks of similar composition to the metabasites, this might explain their K-depleted compositions.

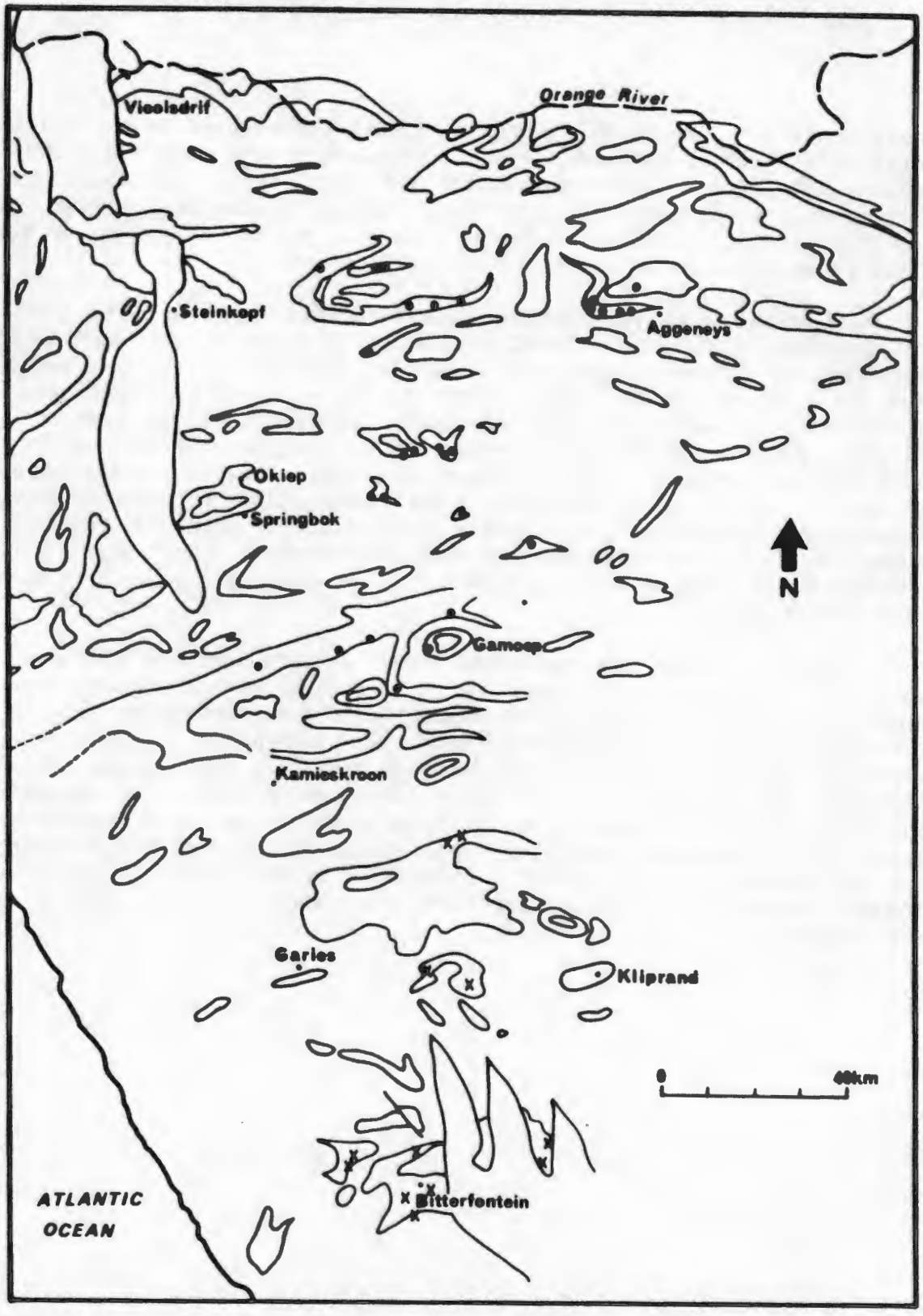

Fig. 12.1 Regional map showing the distribution of paragneiss belts in the western Namaqualand Metamorphic Complex as well as the relative positions of feldspathic quartzite (x) and glassy quartzite (•) samples analysed in this study.

Chapter 12

GEOCHEMISTRY OF THE QUARTZITIC ROCKS

12.1 Introduction

The compositions of quartzitic rocks in general, and those from the western NMC in particular, are dominated to such an extent by Si that all the other major elements invariably show strong negative correlations with silica and have positive correlations with one another. This makes chemical discrimination between quartzitic rocks of different provenance and mode of origin extremely difficult. Virtually all the quartzitic rocks from the western NMC contain greater than 92% SiO_2 and the only other major elements that occur in any significant amounts within these rocks are Al, Fe and K. In several samples, the trace elements Sr, Th, U, Nb, Mo, Cr, V, Sc, Ni, Co, Pb, Zn, Cu, Y, La, Ce and Nd occur at concentration levels below the detection limit of the analytical procedures, effectively leaving only Rb, Ba and Zr present at sufficient concentrations to be utilised quantitatively. Of the six elements besides Si that are present in the western NMC metaquartzites in significant quantities, Al, K, Rb and, in most instances, Ba represent the presence of detrital feldspar and/or clays, Zr represents detrital zircon and Fe (plus Ba in a few cases) represents either detrital iron oxides and Fe-rich clays or a chemogenic component of the iron formation genre. It may thus be possible, using this limited suite of elements, to distinguish within the quartzites of the western NMC, those which originated as detrital quartz sands and those which originated by chemical precipitation - i.e. cherts.

As described in Section 3.4, the metaquartzites of the study area can be divided geographically and petrologically into two suites - feldspathic quartzites which are particularly prevalent in the southern portions of the area, and various glassy quartzites which predominate in the north (Fig. 12.1). The southern feldspathic quartzites contain thin intercalated bands of schist comprising quartz-muscovite-sillimanite-iron oxide in the Bitterfontein area, and, although no primary sedimentary structures were observed during this or previous studies (Joubert,1971; Albat,1984), their origin as quartz-rich sandy sediments is suspected. The glassy quartzites in the north contain a variety of minor constituents, including thin micaceous bands (commonly muscovite-rich) as well as magnetite-, pyrite- and garnet-rich zones, and more rarely tourmaline-, gahnite- and diopside-bearing bands. The Fe-rich zones occasionally attain concentrations of iron similar to the iron formations (see Section 13.2), and further association with B, Zn and Ca, together with extremely high SiO_2 concentrations (the majority of glassy quartzites have SiO_2 contents >98%) suggests that many of these northern quartzitic rocks may have had an origin as cherts. The following sections discuss the chemical differences between these two groups and their possible modes of origin as either clastic or chemical siliceous sediments.

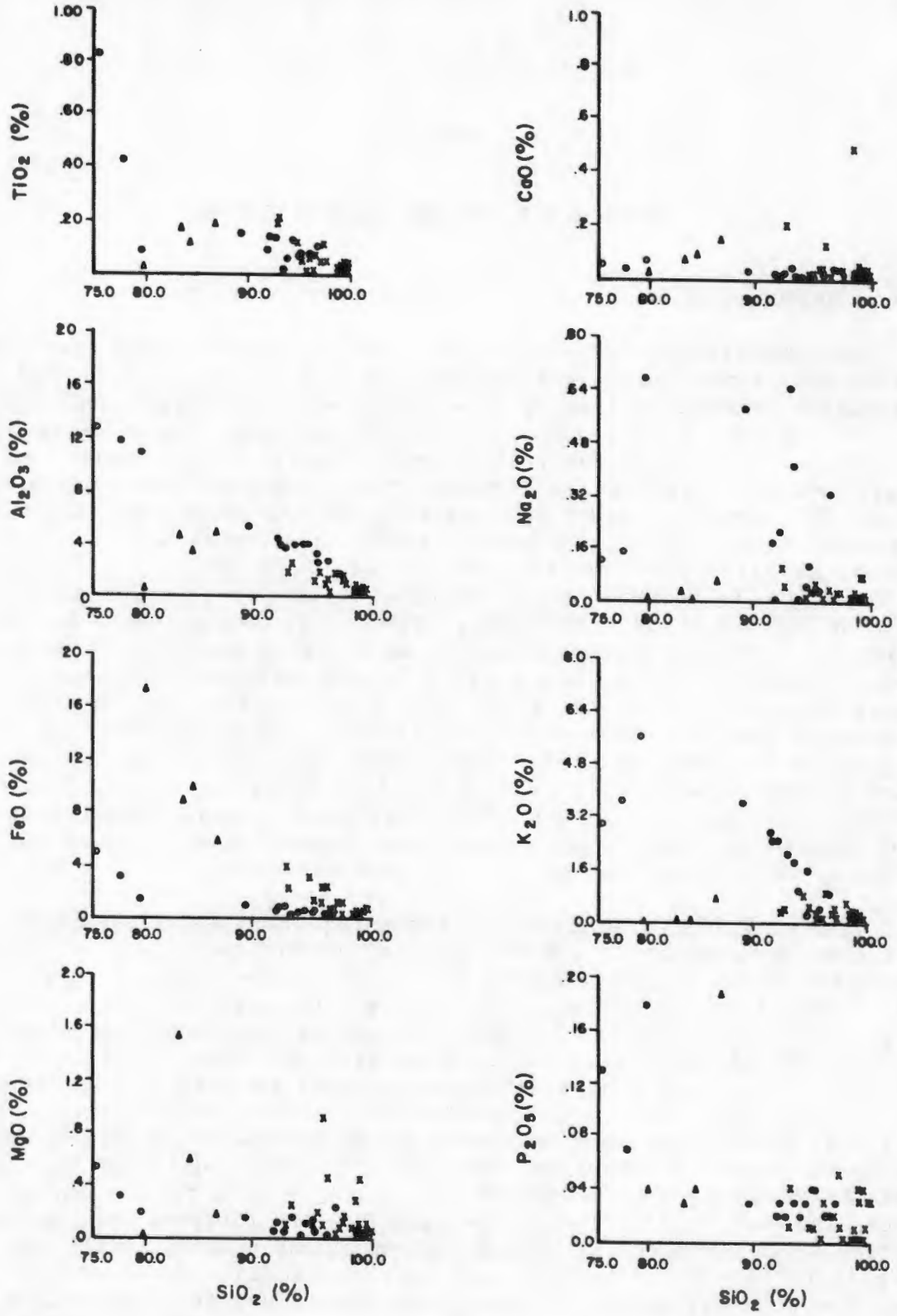

Fig. 12.2 Comparison on Harker diagrams of the major element oxide data for feldspathic quartzites (•), muscovite-sillimanite schists (o), glassy quartzites (x) and garnetiferous/magnetite-rich quartzites (▲) from the study area.

TABLE 12.1 Mean major (%) and trace element (ppm) compositions of the two metaquartzite varieties from the study area together with the chemistries of certain intercalated minor units.

	1.		2.		3.	4.
SiO_2	93.69	(2.19)+	97.74	(2.08)	76.44	79.80
TiO_2	0.10	(0.04)	0.05	(0.05)	0.63	0.03
Al_2O_3	3.47	(0.97)	0.69	(0.58)	12.26	0.38
FeO*	0.44	(0.27)	0.79	(1.02)	4.08	17.21
MnO	0.00	(0.01)	0.04	(0.13)	0.02	0.38
MgO	0.10	(0.07)	0.14	(0.20)	0.43	0.01
CaO	0.02	(0.01)	0.13	(0.45)	0.05	0.02
Na_2O	0.23	(0.23)	0.03	(0.03)	0.14	0.01
K_2O	1.77	(1.06)	0.23	(0.24)	3.33	0.01
P_2O_5	0.03	(0.01)	0.02	(0.02)	0.10	0.04
Rb	62	(35)	9	(8)	188	-
Ba	250	(267)	48	(65)	1285	1440
Sr	46	(38)	2	(3)	113	6
Zr	86	(21)	65	(46)	591	38
Ce	13	(18)	7	(9)	148	8

* total Fe as FeO + standard deviation

1. feldspathic quartzites (11 samples)
2. glassy quartzites (26 samples)
3. quartz-muscovite-sillimanite-Fe oxide schist, Bitterfontein area (2 samples)
4. Fe oxide-rich quartzite, Kouberg

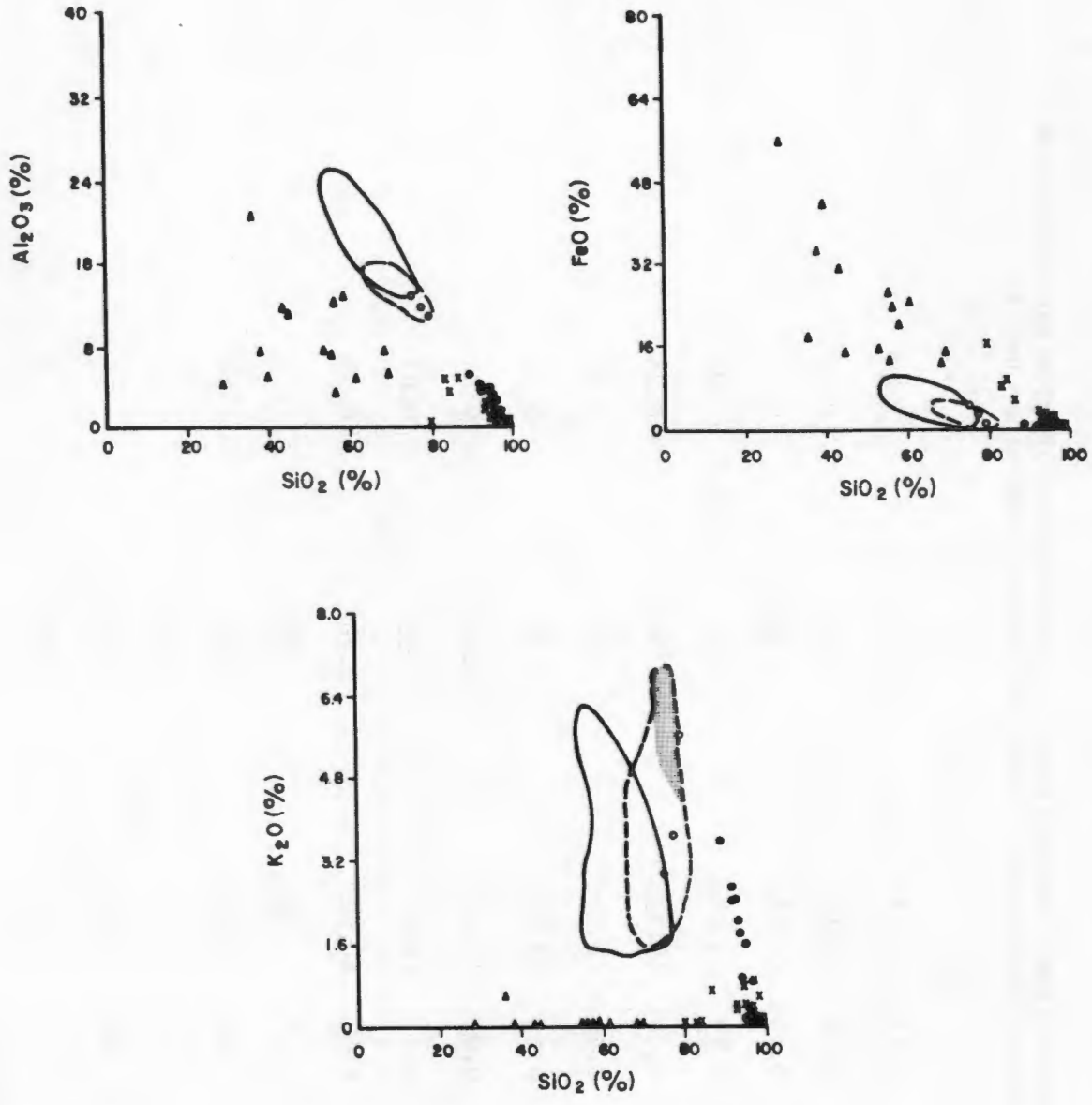

Fig. 12.3 Harker plots for Al_2O_3, FeO total and K_2O of glassy quartzites (x), feldspathic quartzites (•) and muscovite-sillimanite schists (o) compared to iron formations (▲) and the fields for metapelitic (solid line) and metapsammitic (dashed line) gneisses from the study area. The specific field of leucogneisses (stipple) is emphasized in the K_2O:SiO_2 plot.

12.2 Comparisons between the two types of quartzite

12.2.1 Harker diagrams

Although the majority of glassy quartzite samples are so enriched in SiO_2 (>98%) that no trends are discernible for the other major element oxides, nevertheless the remainder of the quartzite samples (with SiO_2 contents between 89% and 98%) show distinct trends on the Harker diagrams (Fig. 12.2). Minor units intercalated within the quartzitic rocks such as muscovite-sillimanite schists in the feldspathic quartzites and garnetiferous and magnetite-rich quartzites in the glassy quartzites are also plotted on the diagrams for comparison.

It is apparent from Fig. 12.2 that the associated minor units generally occur as extensions to the two quartzite trends. This indicates that they are probably present within the quartzites themselves as a distinct component controlling the distribution of the elements apart from Si. It is also noticeable that the two quartzite types have markedly different trends for certain major elements. This is particularly obvious for Al_2O_3 and K_2O, with the feldspathic quartzites showing a distinctly steeper trend, and for total Fe as FeO, with the glassy quartzites showing a more prominent trend (see also Table 12.1). Na_2O is also relatively enriched in the feldspathic quartzites and MgO, although widely scattered, in the glassy quartzites. TiO_2, P_2O_5 and CaO show similar distributions for both quartzite groups, although a few glassy quartzite samples show some CaO enrichment.

Using the distinct trends observed for Al_2O_3, K_2O and total Fe as FeO, the comparison can be extended further by superimposing the fields for metapelitic and metapsammitic rocks and the iron formation suite on similar diagrams (Fig. 12.3). On both the Al_2O_3 vs SiO_2 and total Fe as FeO vs SiO_2 plots, the feldspathic quartzites lie on extensions of the metapelitic and metapsammitic trends towards 100% SiO_2, whereas the garnetiferous and glassy quartzites fall on extensions of the more scattered trends of the iron formations. The scatter on the total Fe as FeO vs SiO_2 diagram is considerably reduced when replaced by (FeO + MnO). On the K_2O vs SiO_2 plot, however, the feldspathic quartzites fall more specifically on extensions of the field of leucogneisses towards 100% SiO_2 rather than the broader field of metapsammitic and metapelitic rocks. Whilst the garnetiferous quartzites show negligible K_2O contents similar to the iron formations, the glassy quartzites show a certain degree of K_2O enrichment relative to these latter rocks, partially overlapping with the feldspathic quartzite trend at extremely high SiO_2 values and possibly lying on extensions to the metapelitic trend towards 100% SiO_2. This is no doubt due to disseminations and rarer fine bands of muscovite and lesser biotite present in the glassy quartzites.

12.2.2 The $(Na_2O + K_2O):SiO_2:(FeO + MgO)$ diagram

Hickman and Wright (1983) have demonstrated the effective use of the $(Na_2O + K_2O)$ vs $(0.05 \times SiO_2)$ vs (FeO + MgO) plot in discriminating between

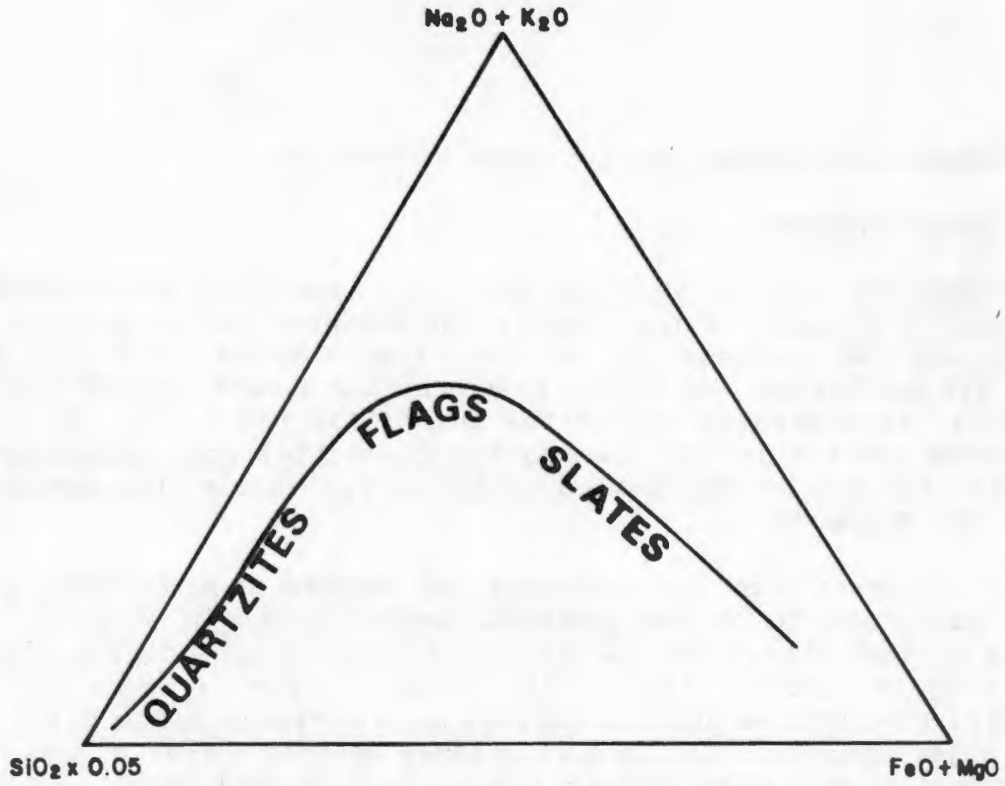

Fig. 12.4a Triangular plot of (SiO_2 x 0.05) : (Na_2O + K_2O) : (FeO + MgO) showing the relative fields of certain clastic sedimentary rocks (after Hickman and Wright, 1983).

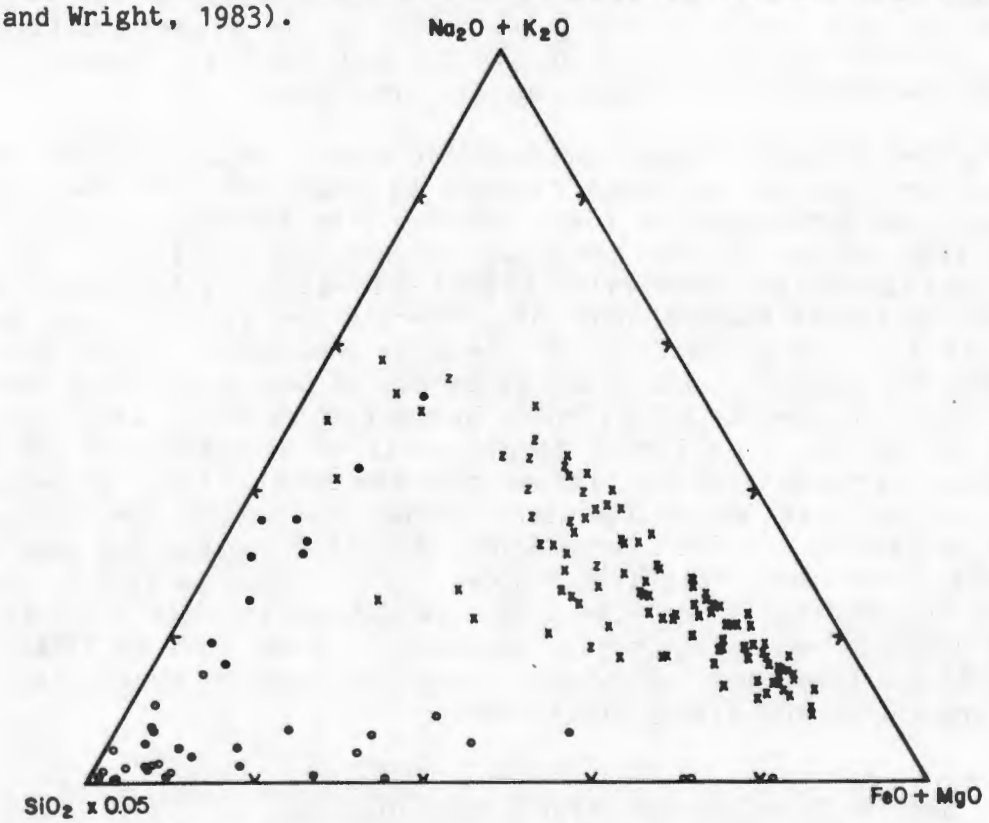

Fig. 12.4b Similar triangular plot showing the distribution of feldspathic quartzites (•), glassy quartzites (o), cordierite-bearing metapsammitic gneisses (z) and metapelitic gneisses and schists (x) from the study area.

immature sediments, quartzites and shales/slates. During chemical weathering, there is a rapid decrease in the relative amounts of K_2O and Na_2O in the formation of both quartzitic and pelitic rocks compared to SiO_2 (dominant in quartzites) and FeO and MgO (dominant in shales) (Fig. 12.4). The relative positions of different quartzite populations on this diagram also give an indication as to their relative maturities - i.e. quartzites clustering close to the SiO_2 apex are likely to be extremely mature quartz sands, whereas those plotting towards the centre of the diagram are likely to represent more immature, flaggy rocks.

When plotted on the $(Na_2O + K_2O):SiO_2:(FeO + MgO)$ diagram, the feldspathic quartzites from the southern portions of the western NMC show a relatively broad scatter along the SiO_2-$(Na_2O + K_2O)$ tie-line, indicating a range from relatively immature flaggy rocks to purer quartzites (Fig. 12.4). Their proximity to the latter tie-line and lack of (FeO + MgO) component "suggests a lack of clays, a rather granitic source and a high energy environment" (Hickman and Wright,1983). The field occupied by metapsammitic cordierite gneisses and metapelitic rocks from the western NMC is plotted for comparative purposes and delineates the distinct trend towards the (FeO + MgO) apex anticipated for pelitic rocks. The glassy and garnetiferous quartzites from the northern parts of the study area, however, have a markedly different distribution, concentrated at the SiO_2 apex and stretching out along the SiO_2-(FeO + MgO) tie-line. Although the lithologies plotting close to the SiO_2 apex could be interpreted as extremely pure quartz sands, the overall distribution trend along the latter tie-line is extremely unusual for a mature clastic sediment and can be interpreted as further evidence in support of a chemogenic origin for the glassy quartzites and an association with iron formations.

12.2.3 The Zr content of the quartzites

Zr is generally restricted to the detrital mineral zircon in sedimentary rocks, and commonly occurs at low concentrations in chemogenic sediments (18 ppm Zr on average in carbonate rocks, Erlank *et al.*, 1978; 23 ppm in cherts, Sugisaki *et al.*, 1982) and much higher concentrations in clastic sediments (197 ppm on average in shales, 188 ppm in sandstones, Erlank *et al.*, *op.cit.*). Comparison of the Zr contents of the two metaquartzite types from the study area (Fig. 12.5) reveals that the feldspathic quartzites have fairly uniform Zr contents with a mean of approximately 90 ppm Zr, whereas the glassy quartzites have a broader Zr distribution with a major cluster at approximately 50 ppm and more scattered values ranging up to 175 ppm. The Zr distribution within the glassy quartzites is very similar to that of the iron formations which are concentrated within the 0-70 ppm Zr range but also include several samples with higher values (up to 220 ppm), and to that of the "true" metacarbonate rocks (forsterite marbles, calcite/wollastonite rocks, diopside-rich rocks) which contain isolated samples reaching concentrations of 500 ppm (Fig. 12.5). The levels of Zr concentration within the glassy quartzites are, therefore, not incompatible with a chemogenic origin as cherts.

The sporadic samples with relatively high Zr concentrations within the

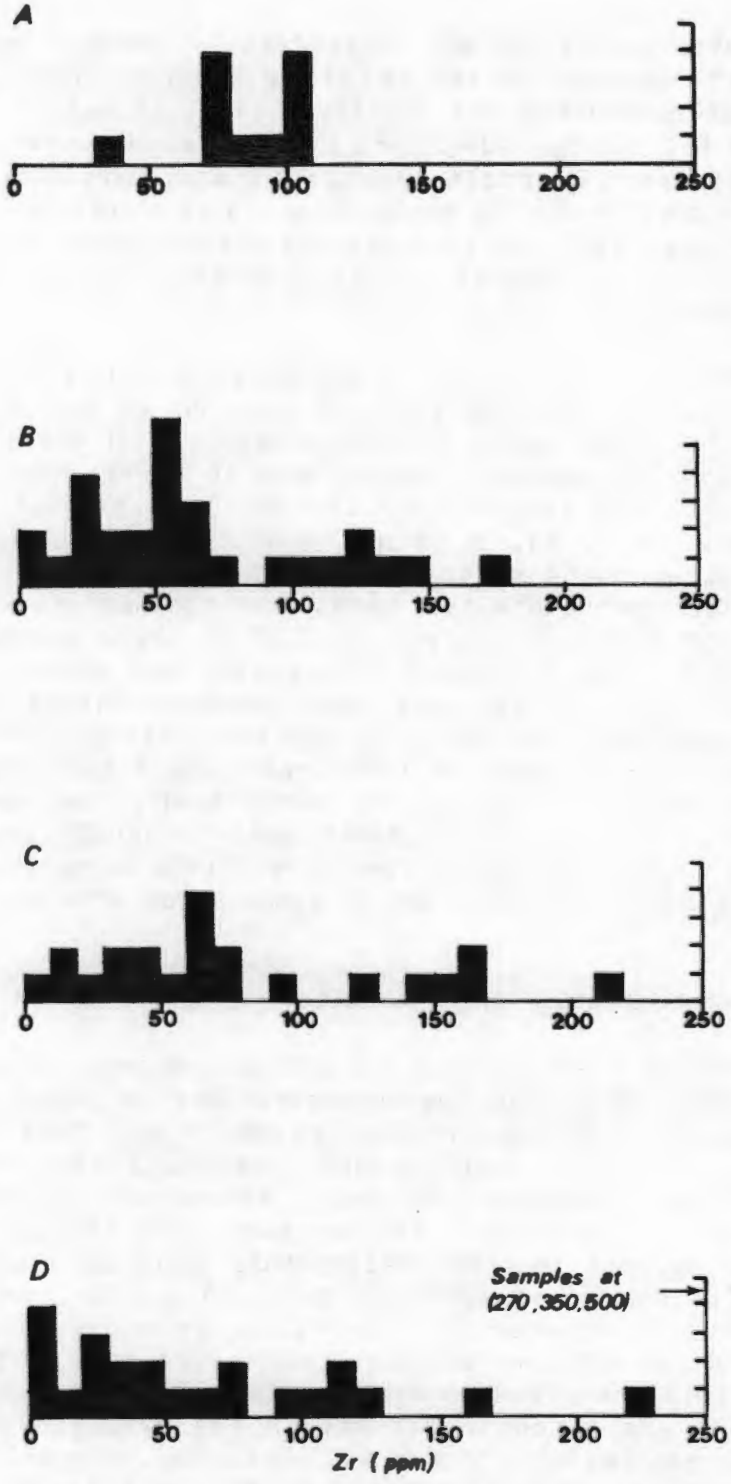

Fig. 12.5 Histograms showing the distribution of Zr contents in feldspathic quartzites (A), glassy quartzites (B), iron formations (C) and metacarbonate rocks (D) (excluding plagioclase-rich varieties) from the study area.

glassy quartzites, iron formations and diopside-rich calc-silicate rocks deserve further comment. At Kangnas, Aggeneys and in the Namiesberg, certain fine dark horizons within the basal portions of the glassy quartzites contain low-level concentrations of detrital minerals such as ilmenite and zircon (J.Hobbs, R.Lipson, pers. comm.). At Hosabees in the Anegas-Boesmanplaat paragneiss belt and in the Eenriet mountains, calc-silicate rocks are closely associated with ilmenite-zircon-rich iron formations (see Section 13.2) thought to be heavy-mineral detrital accumulations. In the Buffels River belt, Zr and rare earth element concentrations are associated with cordierite-phlogopite rocks and are believed to represent heavy-mineral accumulations during weathering of mafic volcanic rocks (see Section 10.7). It would appear that concentrations of heavy minerals regularly occur within the supracrustal rocks of the western NMC, perhaps indicating minor breaks in the rate of sedimentation. Judging by the variety of lithologies within which these heavy-mineral accumulations are observed - sillimanite-rich rocks (Moore,1977), cordierite-phlogopite rocks, iron formations, calc-silicate rocks, quartzites, leucogneisses (in the Kenhardt area, Frick and Wheelock, 1983) - it would appear that these concentrations are independant of other volcano-sedimentary processes taking place and can occur in both clastic and chemogenic sediments.

Within the glassy quartzites, the presence of thin bands containing either concentrations of minerals such as zircon, or micas such as muscovite and biotite, need not preclude a chemical origin for the silica. Thick sequences of Palaeozoic and Miocene cherts commonly contain fine partings comprised of shale or acid tuffaceous material (Bramlette, 1946; Sugisaki et al., 1982; McBride and Folk, 1977) as well as minor shale bands, chert pebble conglomerates, sandstones, manganiferous and jasperitic beds and carbonate bands (McBride and Folk, op.cit.) and acidic vitric tuff and bentonite beds (Iijima and Tada,1981; Bramlette, op.cit.). The fine shale partings are enriched in Zr (164 ppm) and TiO_2 (0.77%) compared to the cherts themselves (23 ppm Zr and 0.08% TiO_2) (Sugisaki et al., op.cit. (Table 12.2). Sedimentary features such as minor graded bedding, ripple-marks, intraformational unconformities and tidal channel conglomerates are also observed in shallow-water cherts or novaculites (Folk,1973; McBride and Folk, op.cit.; Sugisaki et al., op.cit.). Such minor "clastic" components to chemical sediments could well include low-order concentrations of detrital zircon along individual bedding planes.

12.3 Models of the depositional environment of the quartzites

12.3.1 Major element discriminatory plots

Bhatia (1983) has shown by the use of bivariate plots of selected geochemical parameters (notably Fe_2O_3 + MgO, TiO_2, Al_2O_3/SiO_2, K_2O/Na_2O and $Al_2O_3/(CaO + Na_2O)$) and of discriminant functions based on major element analyses, that sandstones of different sedimentary provenance and tectonic setting can be characterized geochemically. Sandstones from oceanic and continental island arc environments are typified by relatively high (Fe_2O_3 + MgO) contents and low Al_2O_3/SiO_2 and K_2O/Na_2O ratios, whereas sandstones from

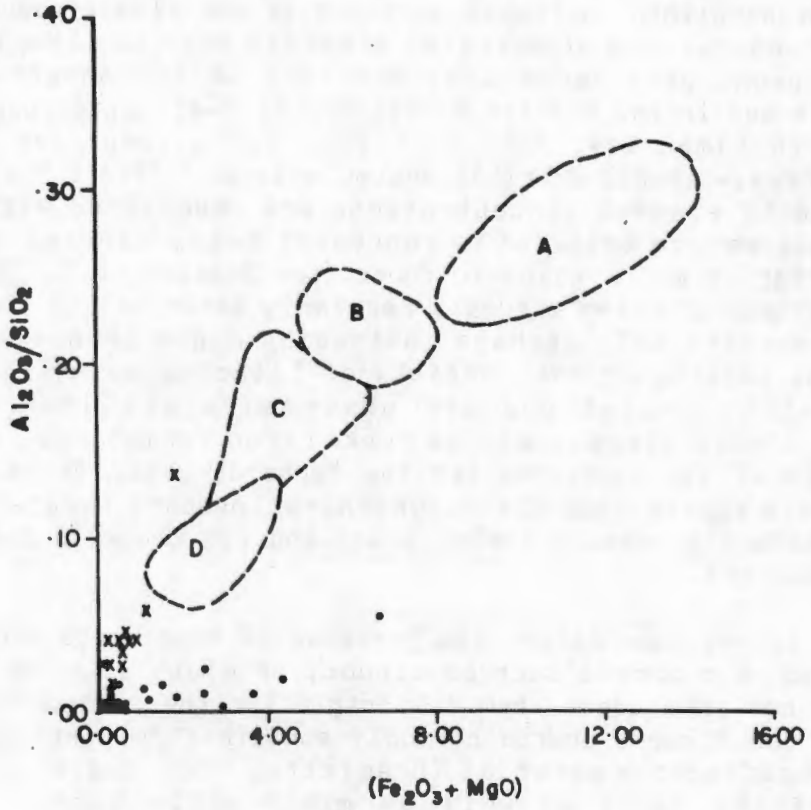

Fig. 12.6 Bivariate plot of Al_2O_3/SiO_2 : (Fe_2O_3 total + MgO) showing the distribution of data for feldspathic quartzites (x) and glassy quartzites (•) from the study area in comparison to fields for sandstones from oceanic island arcs (A), continental island arcs (B), active continental margins (C) and passive continental margins (D) (after Bhatia, 1983).

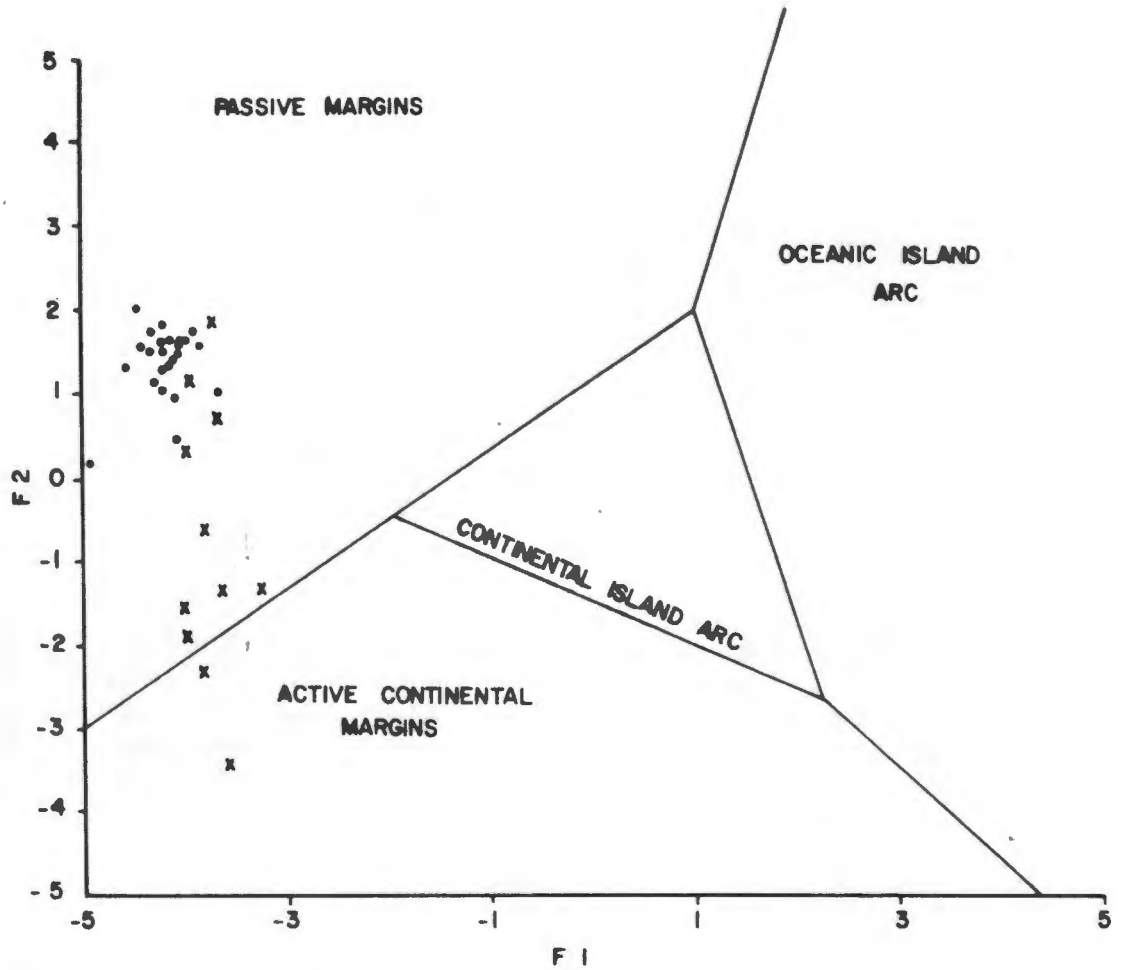

Fig. 12.7 Bivariate plot of discriminant functions F_1 and F_2 (as calculated by Bhatia, 1983) showing the position of feldspathic quartzites (x) and glassy quartzites (•) from the study area relative to the fields of sandstones from various tectonic regions.

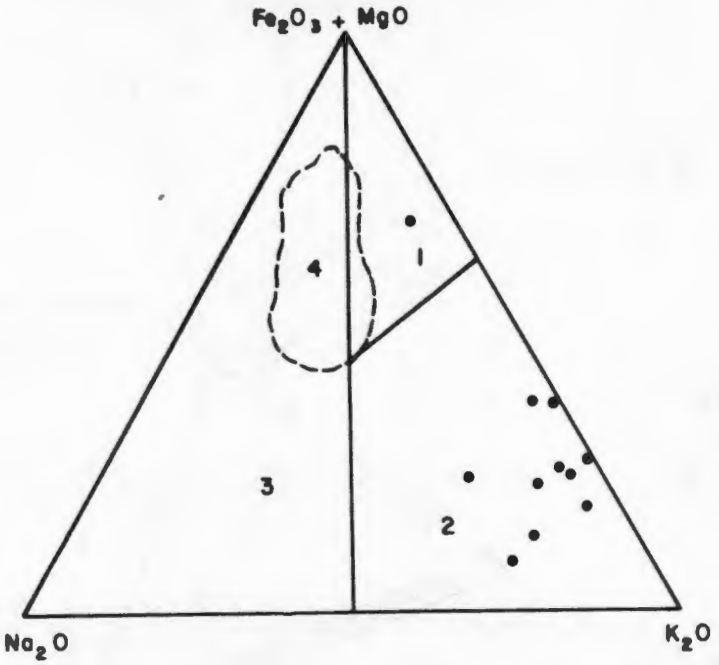

Fig. 12.8a Triangular plot of Na_2O : (Fe_2O_3 total + MgO) : K_2O showing the distribution of feldspathic quartzites from the study area relative to the fields for sandstones from exogeosynclinal "clastic-wedge" environments (1), taphrogeosynclinal "faulted basin" environments (2) and eugeosynclinal environments (3) (after Blatt et al., 1980). The field of greywackes (4) is further outlined (dashed line).

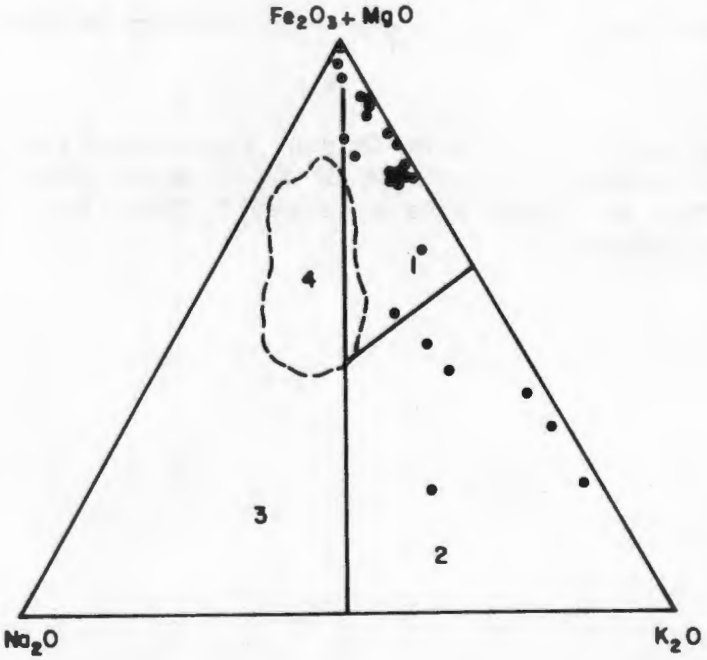

Fig. 12.8b Similar triangular plot showing the distribution of glassy quartzites from the study area relative to these fields.

continental margin environments are typified by enrichments in SiO_2 and depletions in (Fe_2O_3 + MgO), Na_2O, CaO and TiO_2, "suggesting their highly recycled and matured nature" (Bhatia, op.cit.).

When compared to the sandstones used in Bhatia's (1983) study, the quartzites of the western NMC can be seen to be highly enriched in SiO_2 and, as a result, depleted in all other major elements. This results in the western NMC quartzites consistently plotting on the various diagrams in domains most closely related to passive continental margins and least related to oceanic or continental island arc environments (i.e. as extremely mature quartz sands). In this regard, the Al_2O_3/SiO_2 : (Fe_2O_3 + MgO) plot is perhaps the most informative, with the feldspathic quartzites from the south/central portions of the study area plotting as natural extensions of the fields for sandstones from oceanic island arcs through continental island arcs, active continental margins and passive continental margins towards the origin, indicating a definite sandstone affinity and extremely mature nature (Fig. 12.6). The glassy quartzites from the northern parts of the study area, however, define a trend of (Fe_2O_3 + MgO) enrichment at very low Al_2O_3/SiO_2 ratios, quite atypical of common sandstones, but not unexpected for rocks of chemogenic origin. A passive margin environment of deposition is also indicated for both types of quartzite by the F1-F2 discriminant function plot (Fig. 12.7).

A similar triangular diagram comparing the relative concentrations of Na_2O, K_2O and (Fe_2O_3 + MgO) has been used by Blatt et al. (1980) to separate sandstones deposited in various geosynclinal environments. Eugeosynclinal sandstones (greywackes) are separated from sandstones deposited in faulted cratonic basins (mostly arkoses) and sandstones deposited in craton-edge clastic wedges (lithic arenites). The feldspathic quartzites of the study area have typical arkosic signatures (Fig. 12.8) whereas the glassy quartzites display Fe + Mg enrichment with varying dilution by K-rich detrital material. There appears, therefore, to be little doubt that the metaquartzites of the western NMC were deposited in a cratonic or continental environment.

12.3.2 TiO_2-normalisation techniques

Sugisaki et al. (1982) noted that Al, Ti and Zr tend to concentrate in the resistates during the sedimentation process and that the relative abundances of these elements, therefore, remain stationary during the sedimentary cycle. By normalising other major element oxides such as Al_2O_3, total Fe as Fe_2O_3 and MnO to TiO_2, they observed various distribution patterns for marine argillaceous and siliceous (cherty) sediments from continental shelf to deep ocean floor environments (Figs. 12.9a, b and c). The Al_2O_3/TiO_2 ratio of argillaceous sediments remains essentially constant as expected, whereas the Fe_2O_3/TiO_2 ratio increases slightly from continental to deep ocean environments. The most dramatic change, however, is in the MnO/TiO_2 ratio which shows a marked increase from shallow-water to pelagic environments. This is due to the precipitation of Mn from ocean water, creating enrichments in Mn in deep ocean sediments that receive relatively minor terrestrial clastic input.

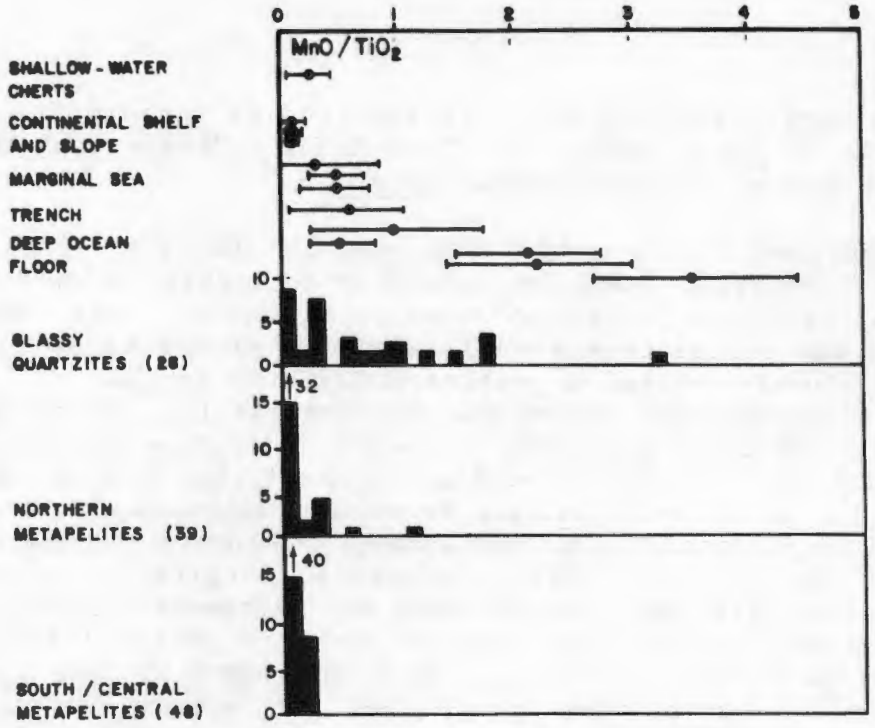

Fig. 12.9a Histogram showing the distribution of MnO/TiO_2 ratios for glassy quartzites and metapelitic rocks from the study area compared to ratios for cherts from various marine environments (after Sugisaki et al., 1982).

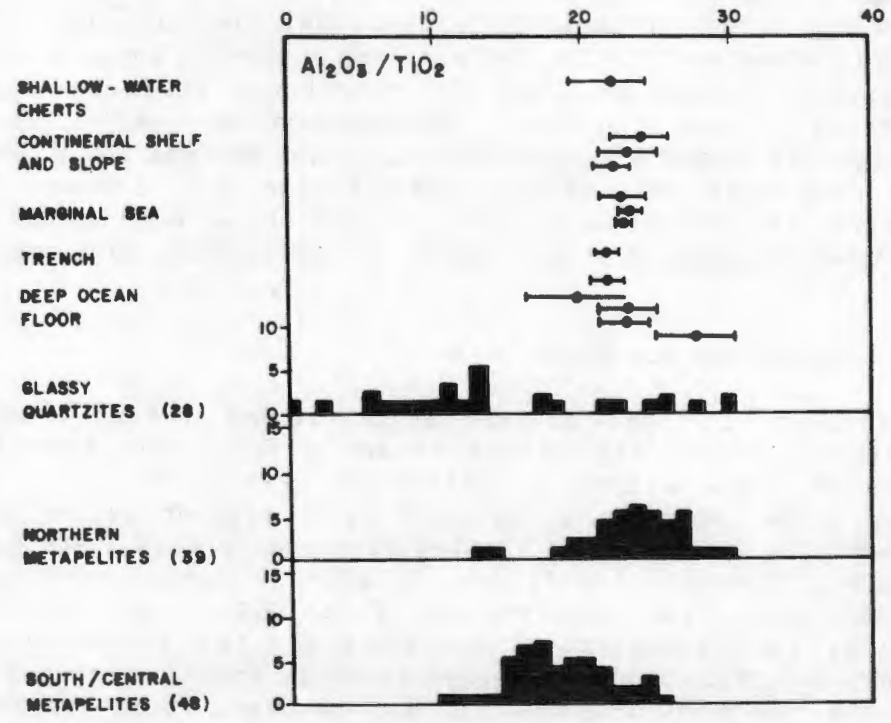

Fig. 12.9b Similar histogram showing the distribution of Al_2O_3/TiO_2 ratios.

In Figs. 12.9a, b and c the TiO_2-normalised ranges of MnO, Al_2O_3 and total Fe as Fe_2O_3 for the glassy and garnetiferous quartzites (potential metacherts) from the northern parts of the study area and the northern and south/central metapelitic rocks are compared to the ranges for Japanese argillaceous and siliceous rocks from various marine environments. The data for the south/central metapelites are the best constrained and indicate TiO_2-normalised MnO and total Fe ranges similar to continental shelf argillaceous rocks and Al_2O_3 values slightly lower than average Japanese argillaceous rocks. The northern metapelitic rocks have slightly higher Al_2O_3 values similar to the Japanese argillaceous rocks, and the bulk of their MnO values indicate a shallow marine depositional environment similar to that for the south/central rocks. A slight tail towards higher MnO values (similar to marginal sea sediments) is observed. Although the majority of Fe_2O_3 values for the northern metapelites fall within a similar range to that of the south/central metapelites, there is considerably greater scatter than observed for the latter rocks and the Japanese argillites. This lack of correlation of total Fe with TiO_2 is thought to indicate that a certain proportion of the iron in the northern metapelites is not detrital but chemogenic in origin.

The TiO_2-normalised ranges of Al_2O_3, total Fe as Fe_2O_3 and MnO for the glassy and garnetiferous quartzites are by far the most scattered, indicating little correlation between TiO_2 and the other three major element oxides. This may be partly the result of analytical error due to the extremely low levels of concentration of some of these oxides, particularly MnO and TiO_2. The Al_2O_3 values show two crude clusters, one with similar values to Japanese argillaceous rocks and shallow-water cherts as well as the closely-associated northern metapelites, and the other at considerably lower Al_2O_3 values than any other lithologies. These are felt to represent glassy quartzites with a detrital component (thin micaceous bands) and those that are entirely chemogenic, respectively. The Fe_2O_3 values of the quartzites show an even greater range than the northern metapelites with several samples plotting outside the range shown on the diagram (Fig. 12.9c). One group of glassy quartzites has similar Fe_2O_3 values to the northern and south/central metapelites, whereas several other samples show various degrees of Fe_2O_3 enrichment. A few samples with extremely low Fe_2O_3 values may again be due to analytical error as their concentrations of both total Fe and TiO_2 are extremely low. The enrichment trend in Fe relative to Ti is thought to represent non-detrital chemogenic iron within these siliceous rocks. The MnO values of the quartzites are clustered chiefly in the range of shallow-water cherts although several samples show considerably higher values in the field of deep-ocean-floor sediments.

It would therefore appear that the pelitic and siliceous rocks of the western NMC have all been deposited in a relatively shallow-water environment similar to recent continental shelf/slope environments. Enrichments in Fe and Mn relative to Ti occur in certain pelitic and siliceous rocks from the northern portions of the study area, similar to deeper-water modern-day environments. This is interpreted as representing chemically-precipitated Fe and Mn but does not necessarily imply a deep-water depositional site, as iron

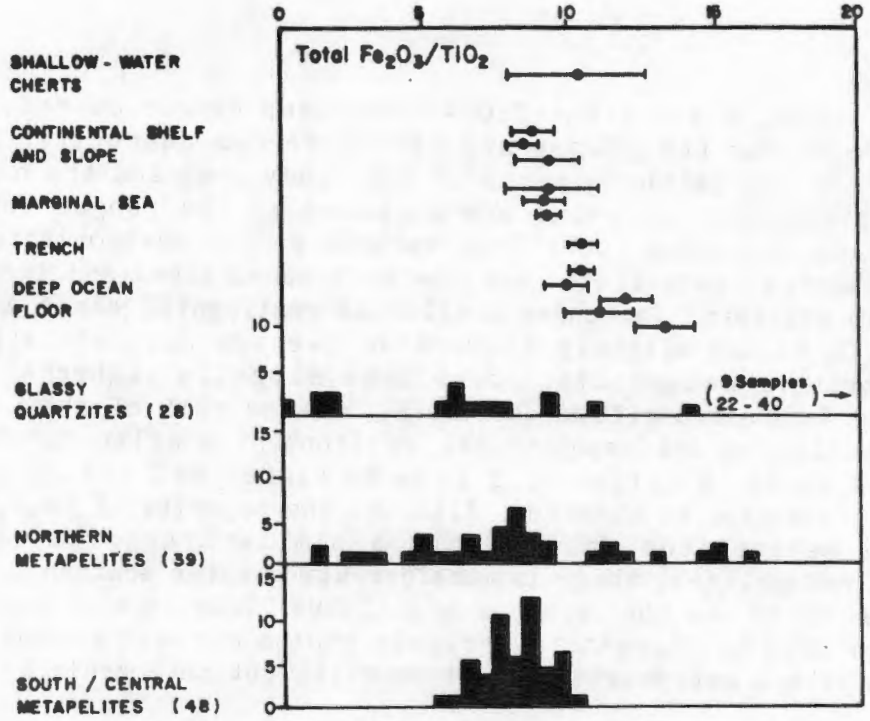

Fig. 12.9c Similar histogram showing the distribution of Fe_2O_3 total/TiO_2 ratios.

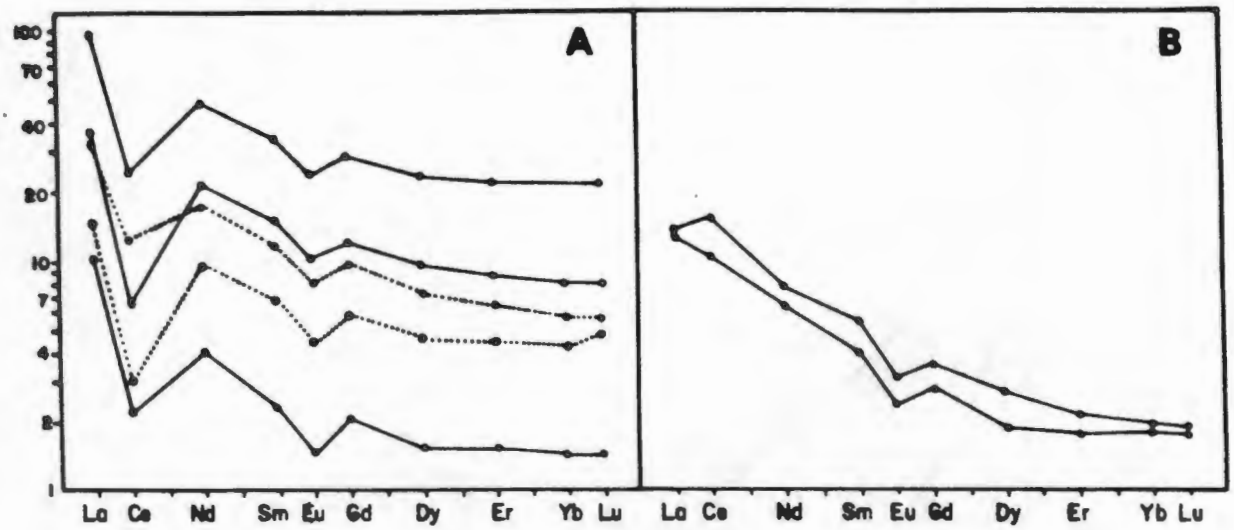

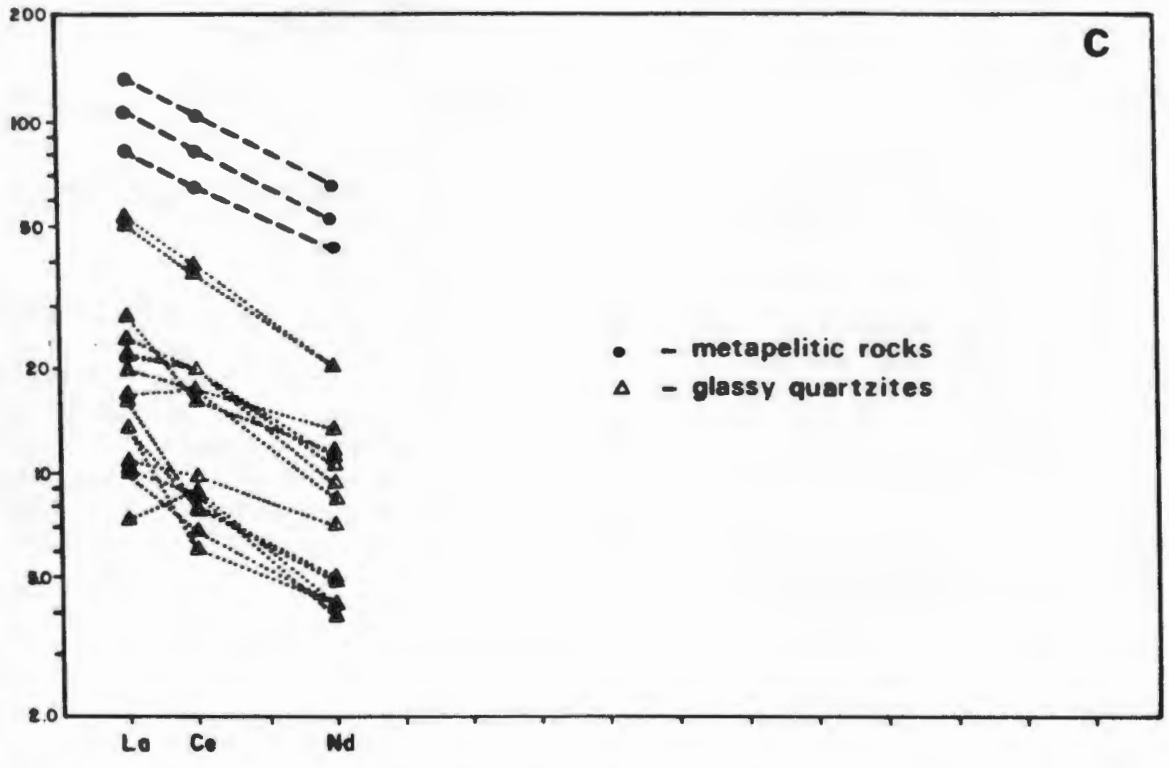

Fig. 12.10 Chondrite-normalised REE patterns for deep-sea cherts (A) and shallow-water cherts (B) (after Shimuzu and Masuda, 1977) and the light REE pattern for glassy quartzites and metapelitic rocks from the study area.

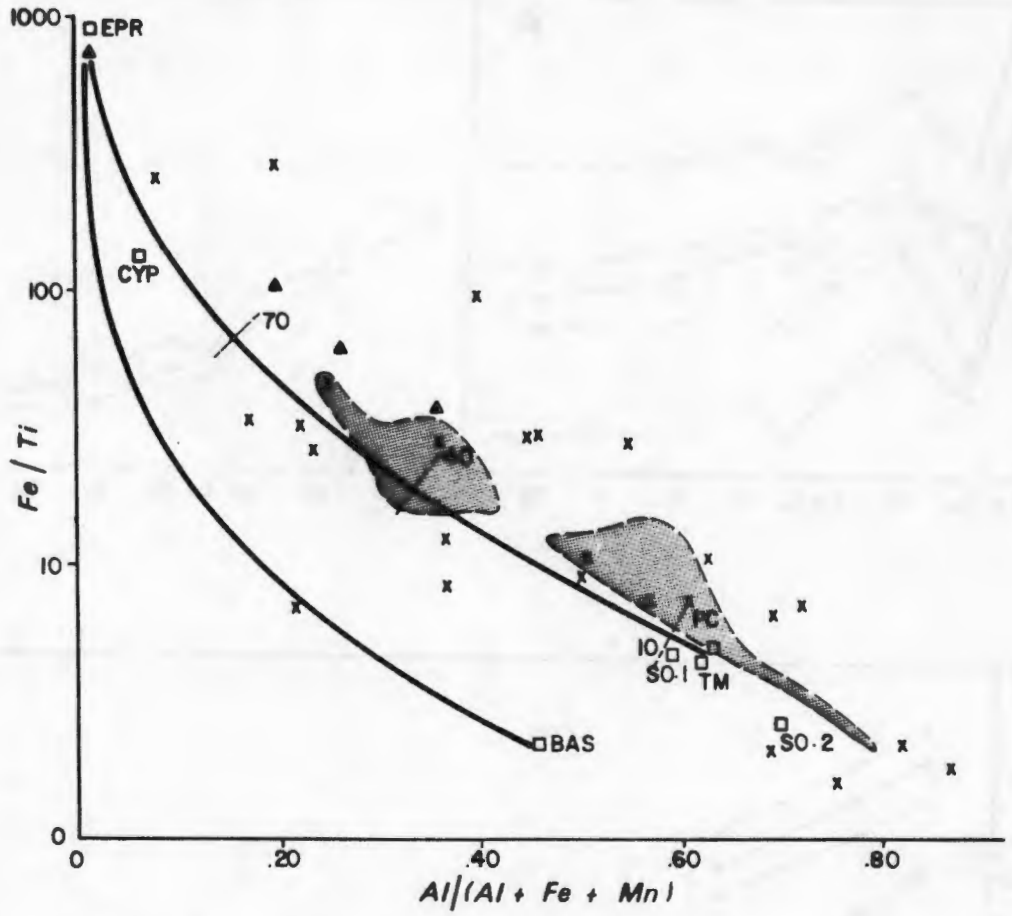

Fig. 12.11 Plot of Fe/Ti : Al/(Al + Fe + Mn) showing the positions of glassy quartzites (+) and garnetiferous quartzites (▲) relative to mixing curves between metalliferous sediment and terrigenous matter/pelagic clay (upper curve) between metalliferous sediment and oceanic tholeiite (lower curve) (from Barrett, 1981). The relative positions of East Pacific Rise metalliferous sediment (EPR), umber from the Troodos Complex, Cyprus (CYP), pelagic clay (PC), terrigenous matter (TM), siliceous ooze (SO.1 and SO.2), oceanic tholeiite (BAS) and Jurassic bedded chert from the Apennines, Italy (stipple) are also shown.

formations commonly occur in shallow-water, near-shore environments that were not included in the study of Sugisaki et al. (1982).

12.3.3 Cerium anomalies

The behaviour of cerium differs from the other light rare earth elements in the marine environment where it is commonly depleted compared to adjacent REE's in both sea water and certain marine carbonate sediments (see Section 11.5). A similar phenomenon has been observed in deep-sea cherts (Shimuzu and Masuda,1977), which show large negative Ce anomalies in their chondrite-normalised REE patterns (Fig. 12.10). This is in contrast to other ancient cherts exposed on land that generally show small positive Ce anomalies and which are thought to have formed in shallow-water environments. Thus "the presence or absence of a Ce anomaly and its extent and direction of deviation can be good indicators of aquaeous (perhaps marine) environment of formation for cherty rocks" (Shimuzu and Masuda, op.cit.).

When comparing the light REE distributions of the glassy quartzites of the northern portions of the study area with the data for cherts, it must be borne in mind that only three of the light REE's have been analysed (La, Ce and Nd). This is, however, sufficient to observe within a reasonable population of samples any prominent Ce anomaly - i.e. divergence from a line joining the La and Nd values. It is also apparent that many of the quartzite samples (±50%) have light REE values below the detection limit of the XRF technique employed (±3-5 ppm) and that the other samples are only just above this limit. Conclusions based on this data, therefore, must be guarded.

The fifteen garnetiferous and glassy quartzites plotted on the chondrite-normalised diagram show either no Ce anomaly or relatively minor positive or negative anomalies (Fig. 12.10). No prominent negative Ce anomalies were observed. They also indicate a relatively strong degree of fractionation from Nd through Ce to La, similar to that observed in post-Archaean sedimentary rocks (Taylor and McLennan, 1981; Haskin et al., 1966) and also of similar slope to that observed in the metapelitic rocks from the western NMC. Tentative conclusions to be derived from this data are that the glassy quartzites of the northern portions of the study area were not deposited in a deep-sea environment and that the light REE`s present in these quartzites were derived from minor suspended clay particles of terrestrial source and were not chemically precipitated from seawater during some marine chert-forming process.

12.3.4 The Bostrom diagram

In a study of bedded cherts in the North Appenines, Italy, Barrett (1981) deduced that the radiolarites and siliceous mudstones that made up the bedded chert unit were derived from "mixing between biogenic radiolarian ooze and terrigenous clays", and also demonstrated the presence of a "hydrothermal" Fe-Mn component in certain basal parts of the deposit. A plot has been developed by Bostrom (1973) that presents an ideal mixing curve between

component" (Fe, Mn) represented by East Pacific Rise metalliferous sediment, and a similar mixing curve between oceanic tholeiite and metalliferous sediment. This plot has been utilised to demonstrate both a terrigenous sedimentary source as opposed to a basaltic volcanic origin for the Italian cherts, and the amount of "hydrothermal" component present in the various chert beds. The interpretation of excess Fe and Mn over normal detrital amounts as being specifically from a hydrothermal source is, however, not justified. The diagram essentially plots potential chemogenic Fe and Mn (high Fe/Ti and low Al/(Al + Fe + Mn) values) against clastic Al and Ti (relatively low Fe/Ti and high Al/(Al + Fe + Mn) values) and need not imply a hydrothermal source for the chemogenic components.

When the glassy and garnetiferous quartzites and iron formations from the western NMC are plotted on the Bostrom (1973) diagram (Fig. 12.11), several observations can be made. Firstly, all these lithologies follow the mixing line between terrigenous material and metalliferous sediment and not the mixing line from oceanic tholeiite. Secondly, the glassy quartzites show an extreme range of values, similar to the Italian cherts, from typical siliceous oozes with no "hydrothermal" component to lithologies with approximately 90% metalliferous sediment component, and thirdly the garnetiferous quartzites and iron formations all appear to contain a major metalliferous component (>50%). As in the case of the Italian cherts, the glassy quartzites appear to consist of two groups - those which are simply siliceous ooze/terrigenous material (clays) mixtures and those with an additional (Fe + Mn) chemogenic component. The diagram thus provides additional evidence for a possible chemogenic origin for the glassy and garnetiferous quartzites, similar to the iron formations, and their association with terrigenous material indicates a possible shallow-water, near-shore depositional environment.

12.4 Summary

The feldspathic quartzites of the southern and central portions of the western NMC contain a significant minor K-Al component which is interpreted as having been derived from weathering of K-rich quartzo-feldspathic rocks. Their stratigraphic position between underlying quartzo-feldspathic gneisses, some of which represent basement rocks, and overlying metapelitic rocks as well as their progressive enrichment in SiO_2 from base to top, also suggests that they represent metamorphosed clastic quartz-rich sandstones. Thin (<10 cm) bands enriched in Al, Fe and Zr occur sporadically within the feldspathic quartzites representing concentrations of heavy minerals perhaps during breaks in sedimentation.

The glassy quartzites of the northern portions of the western NMC have compositions dominated by SiO_2 ($\pm$98%) making chemical evaluation of potential precursors, to say the least, hazardous. They do show certain trends of Fe and Mn enrichment (oxides, garnet), and commonly contain minor ferruginous units (with up to 17% total Fe as FeO), suggesting similar origins to the closely-associated iron formations. As well as Fe and Mn, they contain widespread units enriched in S (pyrite) and more localized units enriched in B (tourmaline) and Zn and Pb (gahnite, galena). At Geselskapbank, Ca-, Mg-rich

TABLE 12.2 Mean major element compositions of various chert formations, interlayered shale partings and orthoquartzites for comparison with the glassy metaquartzites of the study area (Table 12.1).

	1.		2.	3.	4.	5.	6.	7.
SiO_2	96.22	(2.23)	63.60	98.30	95.45	92.80	92.52	95.4
TiO_2	0.08	(0.04)	0.77	0.07	tr	0.13	0.08	0.2
Al_2O_3	1.74	(0.86)	16.98	0.92	0.75	3.01	2.77	1.1
FeO*	0.69	(0.34)	5.73	0.17	0.61	1.32	1.59	0.5
MnO	0.02	(0.01)	0.13	0.004	0.58	0.15	0.09	-
MgO	0.44	(0.30)	2.48	<0.07	0.74	0.78	0.73	0.1
CaO	0.35	(0.02)	0.19	0.00	0.65	0.25	0.05	1.6
Na_2O	0.08	(0.02)	0.17	0.29	0.10	0.35	0.04	0.1
K_2O	0.40	(0.23)	4.81	0.18	0.34	0.48	0.53	0.2
P_2O_5	0.04	(0.02)	0.24	0.07	0.04	0.03	0.04	-
Zr (ppm)	23	(23)	164				21	
no. of samples	69		37	1	2	5	?	26

* total Fe as FeO
standard deviation

1. chert, Kamiaso, central Japan (Sugisaki et al., 1982).
2. shale partings, Kamiaso, central Japan (Sugisaki et al., 1982).
3. layered chert, Miocene Monterey Shale, California (Murata and Larson, 1975). Calculated H_2O free.
4. massive chert, Noda-Tamagawa Mn mine, Japan (Watanabe et al., 1970).
5. thin-bedded chert, Noda-Tamagawa Mn mine, Japan (Watanabe et al., 1970).
6. radiolarite beds, North Appenines, Italy (Barrett,1981).
7. orthoquartzites (Pettijohn, 1975).

bands occur in the quartzites (diopside, wollastonite). All these features suggest that chemical origins for the glassy quartzites as cherts are not unrealistic. Stratigraphically, the glassy quartzites do not occur between the quartzo-feldspathic gneisses and the metapelitic rocks as do the feldspathic quartzites, but instead overlie the latter. They may represent siliceous chemical sedimentation at the end of a cycle of major subaerial acid volcanism similar to many circum-Pacific chert formations of Miocene age (Bramlette,1946; Iijima and Tada,1981) (Table 12.2).

Apart from the Fe-, Mn-component to their compositions the glassy quartzites also contain minor quantities of K and Al manifest as disseminations and thin bands of muscovite and biotite. These K-rich metapelite bands become increasingly more common and thicker within the upper portions of the quartzite formations and probably represent shale or acid tuff partings in these rocks. In addition, fine heavy-mineral partings are observed in the lower portions of the quartzite formations at most localities. Although it would appear that such features suggest a detrital origin for the glassy metaquartzites, many shallow-water chert formations contain similar clastic characteristics as a result of localized reworking. The origins of the glassy quartzites are, therefore, somewhat equivocal although the preference in this study is for their consisting predominantly of shallow-marine chemical sediments.

The presence of major units of chert in association with lithologies interpreted as distal rhyolitic volcanic rocks (leucogneisses) and their weathering products (mica-sillimanite schists) is not unexpected. Chert bands are known to be commonly associated with degraded acid volcanic rocks which contain relatively high levels of easily-leached, soluble SiO_2 generally in the form of volcanic glass (Bramlette,1946; Gibson and Towe,1971; Hughes,1976). In addition, soluble silica is released in reactions whereby certain clay minerals break down during weathering to form kaolinite (e.g. montmorillonite + H_2O -> kaolinite + SiO_2 + Fe_2O_3, MgO, K_2O....; Altschuler et al., 1963). Kaolinite is thought to have been a prominent component of the metapelitic rocks of the northern parts of the study area prior to metamorphism. Thus extremely high levels of dissolved silica were distinctly possible in the northern portions of the western NMC. Under evaporitic conditions (indicated by the tourmaline-rich bands?) in a restricted-basin environment, this silica could be precipitated in shallow water as widespread chert formations.

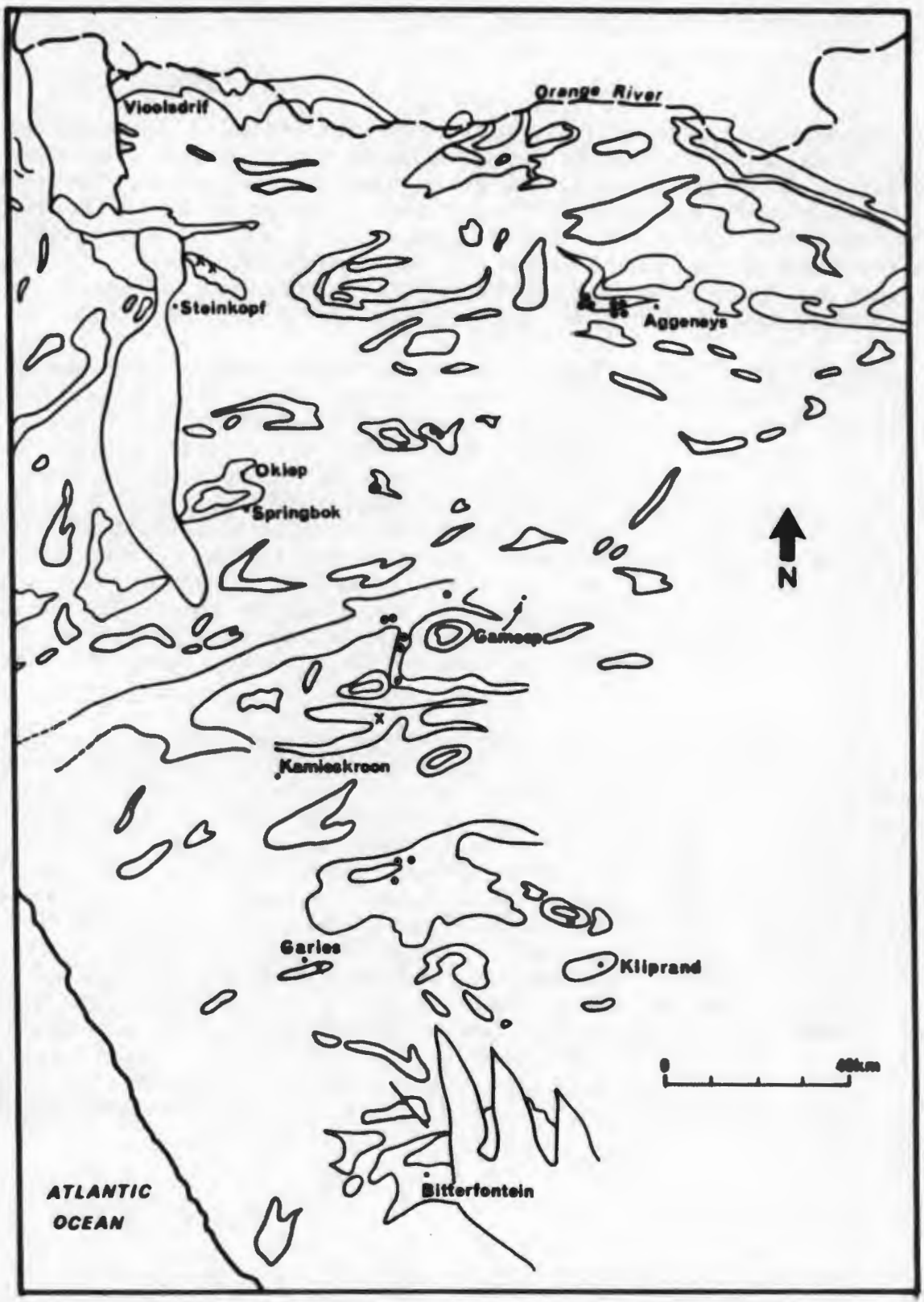

Fig. 13.1 Regional map showing the distribution of paragneiss belts in the western Namaqualand Metamorphic Complex and the relative positions of the iron formations (•) and Zr-Ti-rich "heavy mineral" rocks (x) sampled for this study.

Chapter 13

GEOCHEMISTRY OF THE IRON FORMATIONS

13.1 Introduction

A detailed petrological and geochemical study of iron formations within the Bushmanland and Okiep Groups has been undertaken by Rozendaal (1982) covering most of the northern portion of the study area, with particular emphasis on the Gamsberg Zn deposit. The iron formations are interpreted as the metamorphosed equivalents of oxide, silicate, carbonate and lesser sulphide facies chemical sediments derived from fumarolic exhalative sources, generally along growth faults, and precipitated in a shallow-water platform environment. Variations in Eh and pH due to complexities and changes in this depositional environment are presumed to have accounted for the variety of facies types present. Away from the Aggeneys-Gamsberg area, the iron formations generally have low base metal (Cu, Pb, Zn, Co) and barium concentrations and these lithologies are interpreted by Rozendaal (op.cit.) as representing "low-temperature, base-metal-depleted precursors parasitic to the main fumarolic system that produced the base metal deposits".

In the present study, samples of iron formation have been collected from the Witwater-Platbakkies paragneiss belt northwards to the Smorgen Schaduwe-Kangnas paragneiss belt (Fig. 13.1) as a south-westward extension to the area covered by Rozendaal's (1982) study and geographically further away from the Aggeneys-Gamsberg "fumarolic" centre. A few samples were also analysed from the base-metal-rich Broken Hill, Black Mountain and Big Syncline iron formations at Aggeneys for comparative purposes. The majority of iron formations comprise quartz, garnet and Fe oxides in varying proportions with rarer samples containing Fe-rich amphiboles, pyroxenes and sulphides. A minor suite of iron-rich rocks containing concentrations of ilmenite, zircon and monazite are found at widely scattered localities in the Garies area (Joubert,1971), the Anegas-Boesmanplaat paragneiss belt and in the Eenriet mountains. The latter rocks are thought to represent clastic heavy-mineral concentrations whereas the former represent either clastic or chemical sediments with or without a hydrothermal "exhalative" component. In this section, compositions of the ferruginous rocks are examined with the aim of defining more precisely the likely precursors to these rocks and the presence or absence of an exhalative source for the iron, silica and base metals.

Ferruginous sedimentary rocks (sediments with greater than 15 wt % Fe) are commonly subdivided into two major groups termed iron formations and ironstones. The former result from the chemical precipitation of chert and iron minerals, and the latter comprise mixtures of Fe carbonates and hydroxides with clays and other detrital constituents (James,1969). Iron formations predominate in Archaean and Proterozoic sequences and ironstones in those of Phanerozoic age. Iron formations have been subdivided further into two major classes, the Lake Superior type, deposited in association with

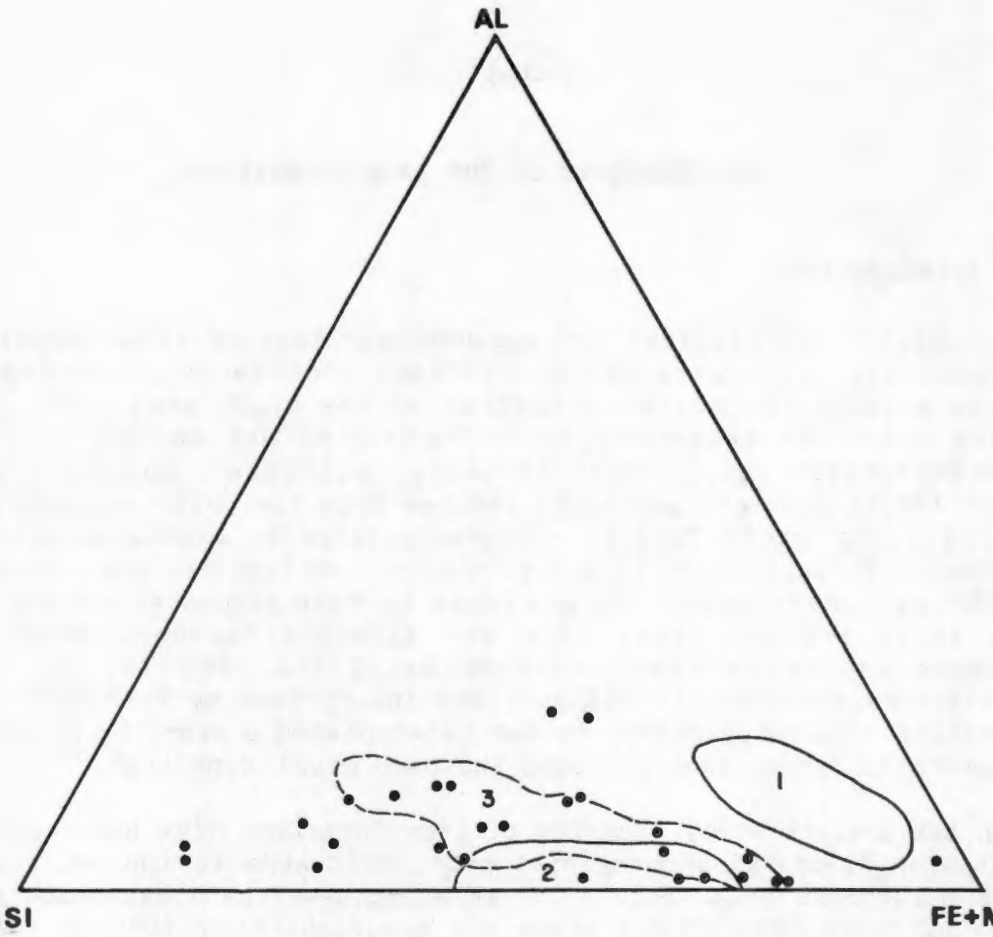

Fig. 13.2 Triangular diagram of Si : Al : Fe + Mn showing the fields defined for ironstones (1) and iron formations (2) by James (1969). Also plotted is the field of iron formations from the Bushmanland Group (3) (modified from Rozendaal, 1982). Data for iron formations from the present study (dots) are superimposed.

mature sediments in continental-shelf environments, and the Algoma type, associated with volcanic rocks and greywackes in arc and rift environments (Gross,1980) and several other minor categories (Kimberley,1978). Both major classes of iron formation display considerable facies variation ranging from oxide through carbonate and silicate to sulphide. Chemical distinctions between ironstones, Lake Superior-type and Algoma-type iron formations have been proposed based on major and trace element data sets (James,1969; Kimberley,1979; Gross and McLeod,1980). Gole and Klein (1981), however, have demonstrated that compositional similarities between the two different iron formation classes are generally more significant than their differences.

The analysis of iron- and manganese-rich rocks by X-ray fluorescence techniques is somewhat problematical due to the difficulty in dissolving these metals in high concentrations for the preparation of Norrish fusion discs (see Section 1.5). To avoid this problem, the samples are diluted in a 50:50 mixture with pure quartz prior to fusion. A consequence of this dilution is that the inherent level of error in the major element analysis is at least doubled. A further problem arises with the presence of Ba, Zn, Cu and Pb in relatively high concentrations in certain samples, particularly from the Aggeneys area. As a result of this, problems occur in trace element analysis due to absorbtion and enhancement effects related to the absorbtion edges of these elements. This may affect the apparent concentrations of other trace elements by up to 25%, either positively or negatively, at the concentration levels of the metals present in the samples. In addition, the concentrations of Ba, Zn, Cu and Pb in these samples are extrapolated from standards with considerably lower concentrations and are therefore themselves subject to increased inaccuracies. The estimated concentrations of major and trace elements in the iron formations, therefore, are not nearly as accurate in this study as they are for other lithologies.

13.2 Chemical distinction between ironstones and iron formations

Chemical distinction between ironstones and iron formations can be made using the Si:Al:Fe(+Mn) triangular diagram (James,1969). Iron formations are relatively Si-rich compared to ironstones which are, in turn, more Al-rich. This reflects the relative significance of silica and clays respectively in the compositions of these two ferruginous sediments. Data for Fe-rich rocks from the study area, superimposed on this plot, indicate that lithologies equivalent to Phanerozoic ironstones are not present (Fig. 13.2). The majority of samples have compositions similar to iron formations, but somewhat Si- and Al-enriched relative to the field defined by James (op.cit.). Similar results were obtained by Rozendaal (1982) for iron formations from Gamsberg and elsewhere in the Bushmanland Group.

On a bivariate Si:Al plot, the iron formations from the study area can be seen to have Si/Al ratios comparable with iron formations rather than ironstones (as defined by Kimberley,1979) (Fig. 13.3). They are also similar to modern-day hydrothermal deposits, displaying higher Si/Al ratios than hydrogenous ferromanganese nodules and detrital ironstones (Crerar et al., 1982). These two diagrams establish a probable chemogenic origin for the

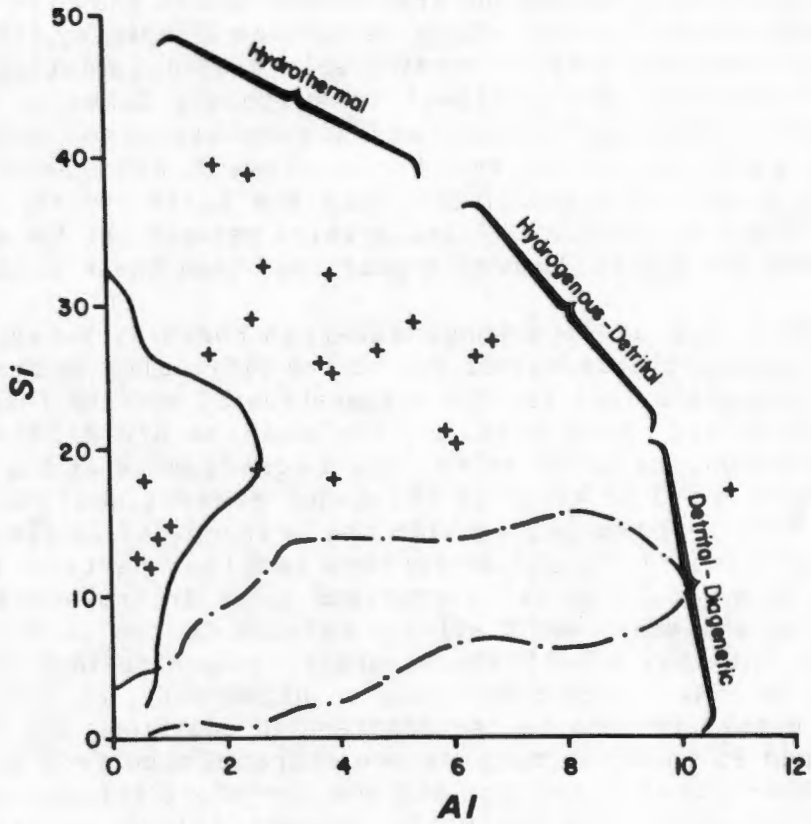

Fig. 13.3 Plot of Si vs Al (wt %) for iron formations from the study area (+) compared to the fields for Lake Superior-type iron formations (solid line, after Gross and McLeod, 1980) and ironstones (broken line, after Kimberley, 1979) and various types of Fe-Mn deposits (after Crerar et al., 1982).

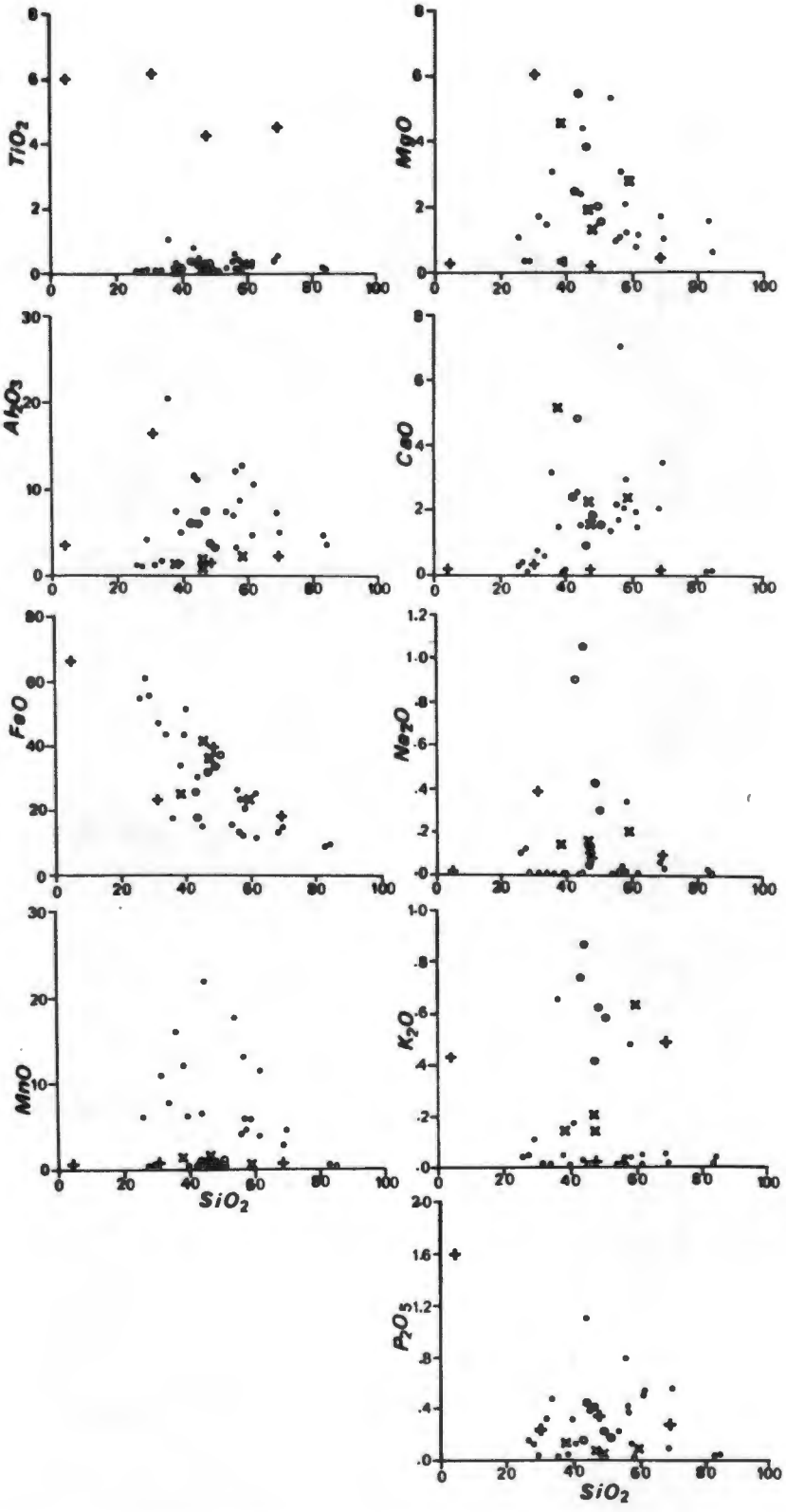

Fig. 13.4 Comparison on Harker diagrams of the major element oxide data for iron formations and Zr-Ti-rich "heavy mineral" rocks (+) with average values for various facies of Lake Superior-type (x) and Algoma-type (o) (after Gross and McLeod, 1980).

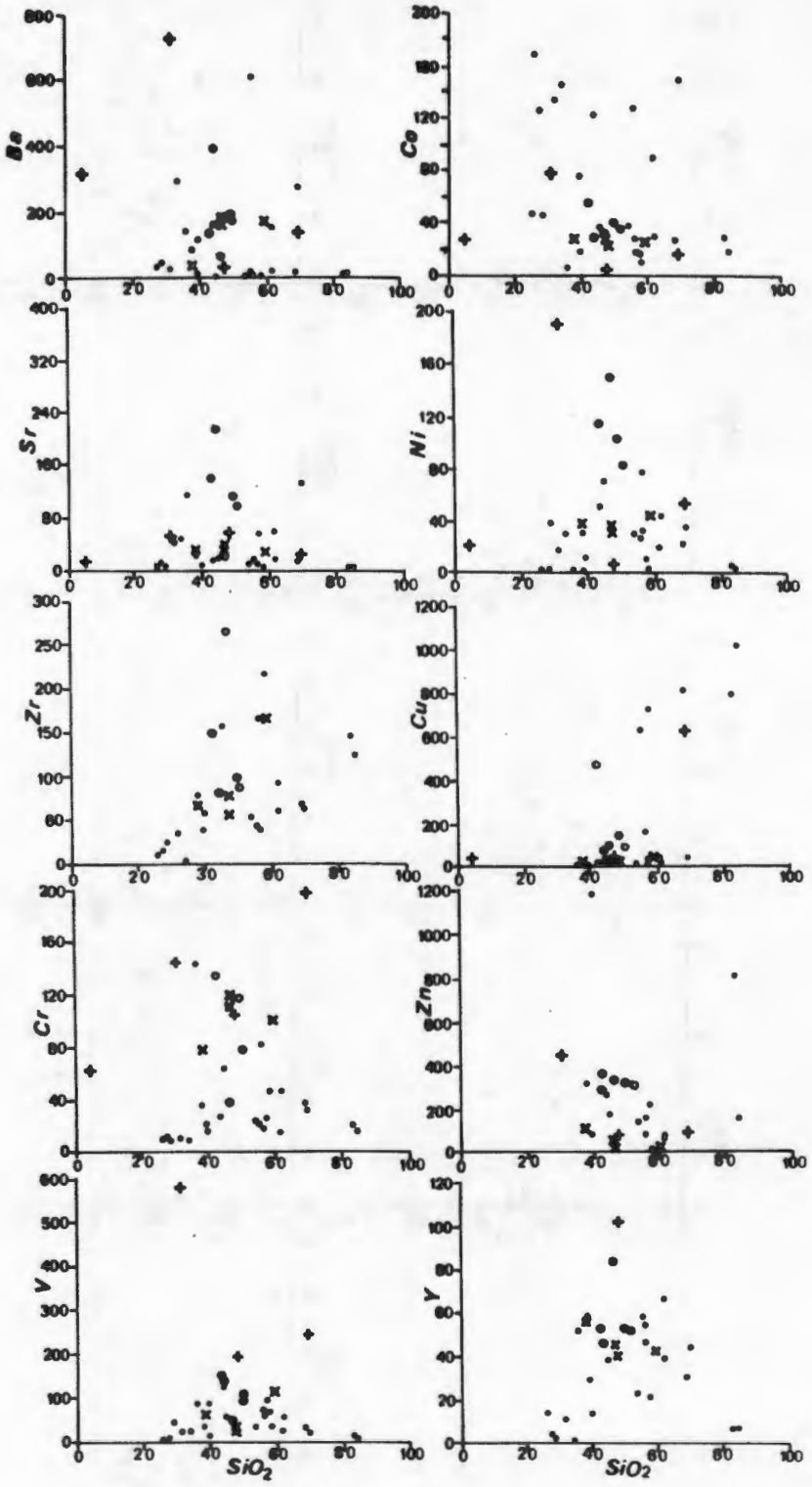

Fig. 13.5 Comparison on Harker diagrams of trace element data for iron formations (•) and Zr-Ti-rich "heavy mineral" rocks (+) from the study area with average values for various facies of Lake Superior-type (x) and Algoma-type (o) iron formations (after Gross and McLeod, 1980).

majority of iron formations of the western NMC as opposed to a detrital source.

13.3 Distinction between iron formation types

The major element compositions of the iron formations of the study area are extremely variable with ranges of 10-80% SiO2 and 10-70% total Fe as FeO. When they are compared to average Lake Superior-type and Algoma-type iron formations on the Harker diagrams (Fig. 13.4), several distinctive trends are noticeable. With regard to TiO_2, Al_2O_3, FeO, CaO and P_2O_5 contents, the iron formations from the study area have similar concentrations to the two classes, particularly to silicate facies rocks. The majority of iron formations from the study area , however, are considerably enriched in MnO and depleted in K_2O, Na_2O and, to a lesser extent, MgO. As far as trace elements are concerned, the iron formations have similar Zr, Ba, V, Co, Y and Zn contents to the two classes of iron formation, markedly depleted Cr contents, and relatively low Ni and Sr concentrations similar to Lake Superior-type iron formations (Fig. 13.5 and Table 13.1). There are two populations of Cu values with approximately half the samples having very low Cu contents (<50 ppm) similar to Lake Superior-type iron formations whilst the others have anomalously-enriched Cu concentrations (>600 ppm).

The four ilmenite-zircon-rich rocks are easily discriminated from the other iron formations on the TiO_2:SiO_2 and Zr:SiO_2 plots by their exceptionally high TiO_2 and Zr contents. These ferruginous metasediments are interpreted as representing heavy-mineral concentrations. Sample GA-BIF from the Garies area contains appreciable amounts of monazite indicated by anomalously high P_2O_5 (1.59%) and Ce (1.10%) contents. These clastic Fe-rich rocks can also be distinguished from the other iron formations on the V:Ti logarithmic plot. On this diagram, the ilmenite-zircon-rich rocks plot in a similar position to the field defined for titaniferous magmatic iron ores, being enriched in both V and Ti, whereas the other iron formations are depleted in these two elements and plot in the sedimentary iron ore field (as defined by Loberg and Horndahl,1983) (Fig. 13.6). Significantly, virtually no samples are located in the volcano-sedimentary iron ore field.

It would appear from the high MnO contents, low Na_2O, K_2O, Cr, V, Ni and Sr contents and V/Ti ratios of iron formations from the study area that they are not particularly representative of Algoma-type iron formations. This is in contradiction to the findings of Rozendaal (1982) who noted similarities in the Al, K, P, Cu, Ni, Sr, Ti and V contents of the Bushmanland Group iron formations, particularly those at Gamsberg, and Algoma-type iron formations. The iron formations from the study area and those at Gamsberg are enriched in Al_2O_3 and P_2O_5 compared to the oxide facies-dominated mean contents for Algoma- and Lake Superior-type iron formations (Gross and McLeod,1980) (Table 13.2). The A and B members of the Gams Iron Formation contain relatively high Al_2O_3, K_2O and TiO_2 contents reflecting the presence of a detrital component (illite, kaolinite, ilmenite?). The A member also contains a prominent CaO-rich carbonate subunit and the B member is extremely enriched in S and C. Comparison of the compositions of the A and B members of the Gams Iron Formation with those of oxide-facies iron formations is therefore probably

TABLE 13.1 Selected trace element contents of iron formations from the study area compared to those of Algoma-type and Lake Superior-type iron formations.

	1.		2.	3.
Ba	101*	(168)+	190	160
Sr	48	(107)	116	37
Zr	80	(59)	98	81
Cr	28	(19)	118	112
V	46	(32)	109	42
Sc	8	(10)	8	18
Co	55*	(46)	41	28
Ni	26	(22)	103	37
Zn	160*	(120)	330	40
Y	44	(51)	54	47
no. of samples	22		447	201

* taken from a subset of 14 samples excluding those from the Aggeneys area.
\+ standard deviation

1. iron formations from the present study.

2. Algoa-type iron formations, all facies (Gross and McLeod, 1980).

3. Lake Superior-type iron formations, all facies (Gross and McLeod, 1980).

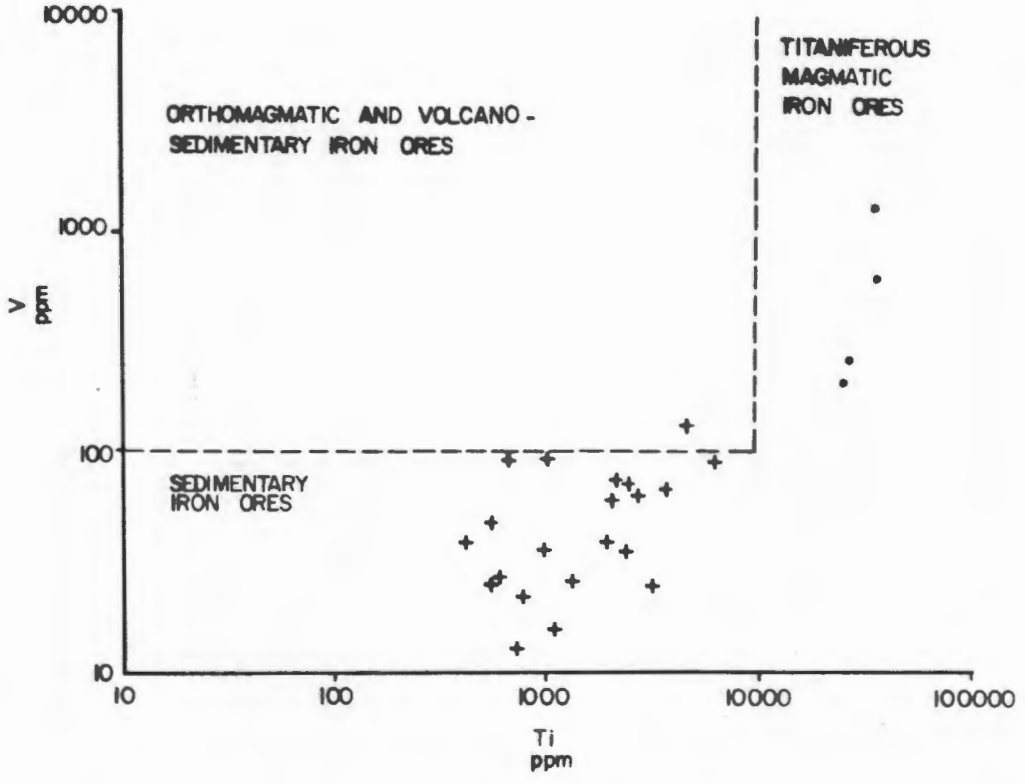

Fig. 13.6 Logarithmic plot of V : Ti showing the relative positions of iron formations (+) and Zr-Ti-rich "heavy mineral" rocks (•) from the study area compared to the fields of various magmatic and sedimentary iron ores (as defined by Loberg and Horndahl, 1983).

TABLE 13.2 Comparison of the mean major element composition of iron formations from the study area, the Gams Iron Formation and Algoma-type and Lake Superior-type iron formations.

	1.		2.	3.	4.	5.	6.
SiO_2	50.91	(16.98)+	55.32	38.03	48.24	48.9	47.1
TiO_2	0.26	(0.20)	0.53	0.40	0.33	0.21	0.07
Al_2O_3	6.08	(3.83)	9.43	6.14	5.33	3.70	1.50
FeO*	28.64	(17.15)	12.49	27.79	27.11	33.9	36.1
MnO	6.60	(5.77)	6.46	1.53	8.11	0.25	0.63
MgO	1.49	(1.32)	2.08	0.64	1.20	2.00	1.93
CaO	1.53	(1.57)	6.40	0.72	2.63	1.87	2.24
Na_2O	0.04	(0.08)	0.20	0.28	0.14	0.43	0.13
K_2O	0.06	(0.10)	1.18	1.06	0.29	0.62	0.20
P_2O_5	0.31	(0.28)	0.34	0.41	0.52	0.23	0.08
No. of samples	22		19	38	32	447	201

* total Fe as FeO + standard deviation

1. iron formations from the present study.
2. A member, Gams Iron Formation (Rozendaal, 1982).
3. B member, Gams Iron Formation (Rozendaal, 1982).
4. C member, Gams Iron Formation (Rozendaal, 1982).
5. Algoma-type iron formations, all facies (Gross and McLeod, 1980).
6. Lake Superior-type iron formations, all facies (Gross and McLeod, 1980).

inappropriate. These characteristics are essentially restricted to the Aggeneys-Gamsberg area, although S-rich iron formations are also found locally in the Haramoep-Koeris-Lemoenpoort area to the immediate north (Rozendaal, op.cit.).

The bulk of iron formations from the study area are similar in their compositions to the C member of the Gams Iron Formation containing, on average, 50% SiO_2 and 35% (FeO + MnO), similar proportions to mean Algoma- and Lake Superior-type iron formations. The C member, like the iron formations of the study area, has low K, Na and Sr, although V and Ni are apparently present in distinctly greater amounts (Rozendaal,1982) (Table 13.1). Ba, Cu, Pb, Zn and Co are significantly enriched in samples from the Aggeneys-Gamsberg area, resulting in large standard deviations and high mean concentrations for these elements in the data set. A smaller subset of iron formations (14 samples) excluding the Aggeneys rocks has mean Ba (101 ppm), Zn (160 ppm) and Co (55 ppm) values of a similar order of magnitude to the two major classes of iron formation, but not specifically definitive of either type.

In summary, it can be said that the iron formations of the western NMC have compositions that differ from typical Precambrian iron formations in their relatively high MnO, Al_2O_3 and P_2O_5 contents. Outside the Aggeneys-Gamsberg area, the iron formations are generally depleted in trace elements (Sr, Zr, Cr, V, Sc, Ni, Y, Zn, Ba) with the possible exception of Co and Cu, and in this regard can be compared to sediment-associated iron formations of the Lake Superior-type rather than volcanic-associated Algoma-type rocks.

13.4 Comparison with hydrothermal and hydrogenous marine sediments

In the marine environment, metalliferous (Fe-, Mn-rich) sediments form by two markedly different processes, either from hydrothermal discharge generally associated with mid-ocean ridge rift systems and rapid subsequent precipitation, or by hydrogenous enrichment of ocean-floor sediments during slow precipitation of iron and manganese hydroxides from seawater (Bonatti et al., 1972; Toth,1980; Marchig et al., 1982). Both types of metalliferous sediment are enriched in Fe, Mn and other transition metals such as Cu, Co and Ni and depleted in various detrital components such as Al, Ti and K compared to normal pelitic sediments. Within the hydrothermal environment there is usually strong fractionation between iron and manganese as a result of the lower solubility of iron species during oxidation processes as well as an association of iron and silica resulting from co-precipitation of SiO_2 and iron oxyhydroxides (Toth, op.cit.). The hydrogenous Fe-Mn sediments contain roughly equal amounts of both Fe and Mn (Fe/Mn ratios between 0.5 and 5) and relatively high concentrations of the minor elements Co, Ni, Cu, Pb, Cr and Ba scavenged from seawater by Fe and Mn oxyhydroxides during slow precipitation (Bonatti et al., op.cit.). This contrasts with the lower minor metal contents of hydrothermal sediments which formed during a more rapid process of deposition.

These chemical characteristics are emphasized on two triangular diagrams devised by Bonatti et al., (1972) and modified by Toth (1980). The first

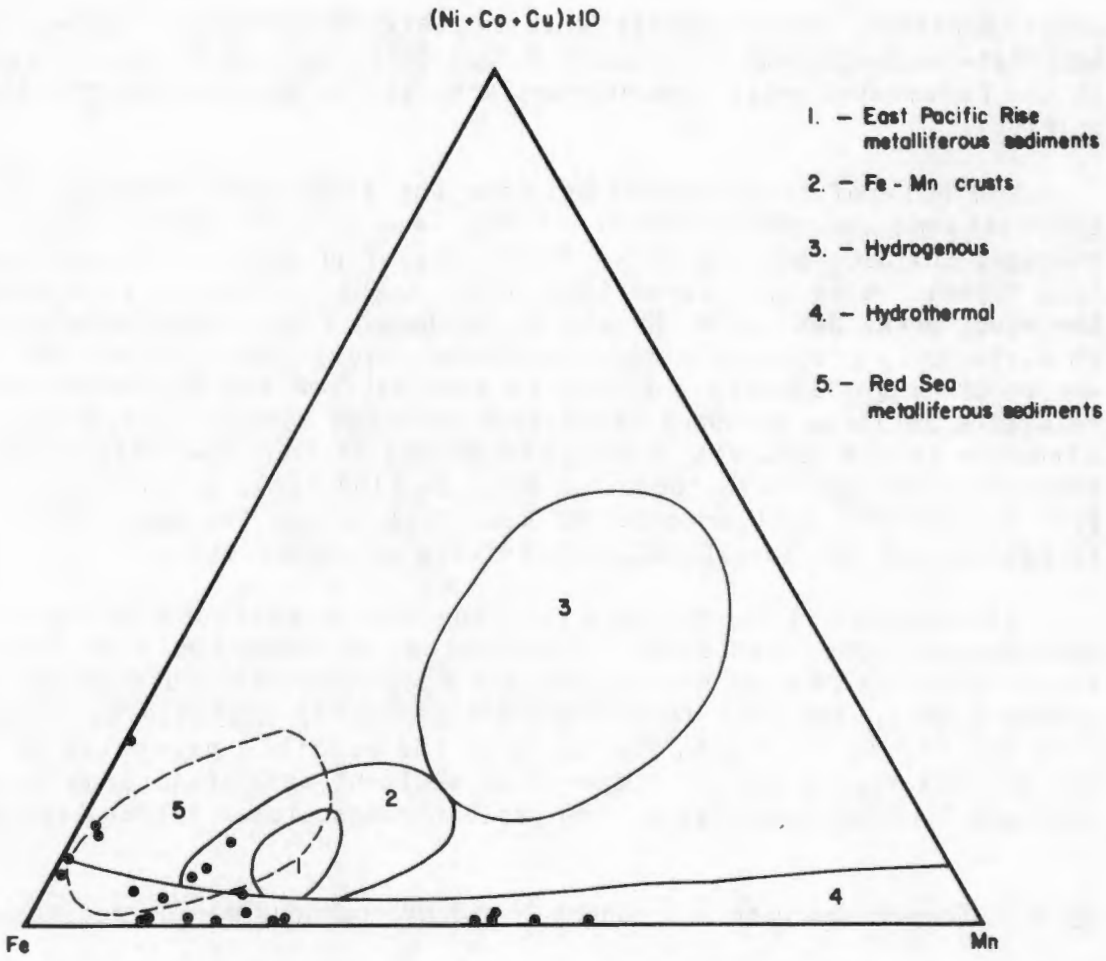

Fig. 13.7 Triangular plot of Fe : (Ni + Co + Cu) x 10 : Mn showing the positions of iron formations from the study area relative to the fields of various marine sediments (after Bonatti et al., 1972; Toth, 1980).

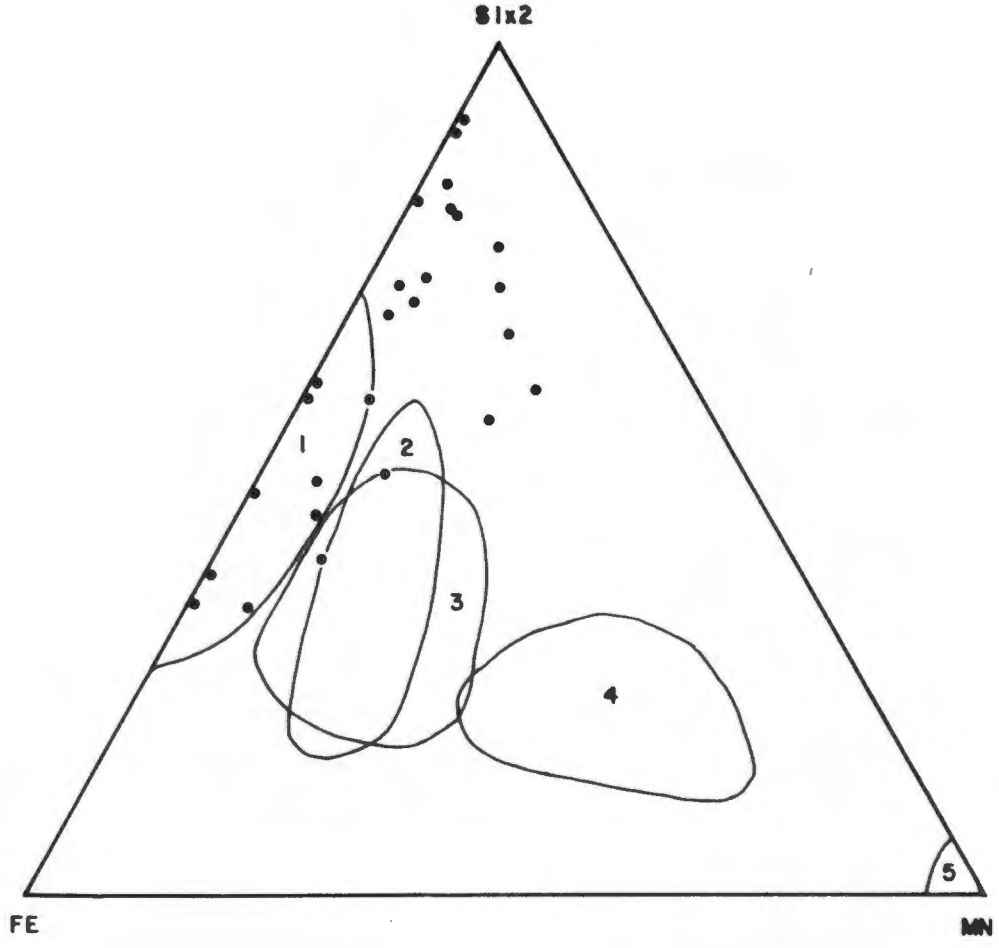

Fig. 13.8 Triangular plot of Fe : Si x 2 : Mn showing the positions of iron formations from the study area relative to the fields of hydrothermal Fe-rich crusts (1), East Pacific Rise metalliferous sediments (2), hydrogenous Fe-Mn crusts (3), Mn nodules (4) and hydrothermal Mn-rich crusts (5).

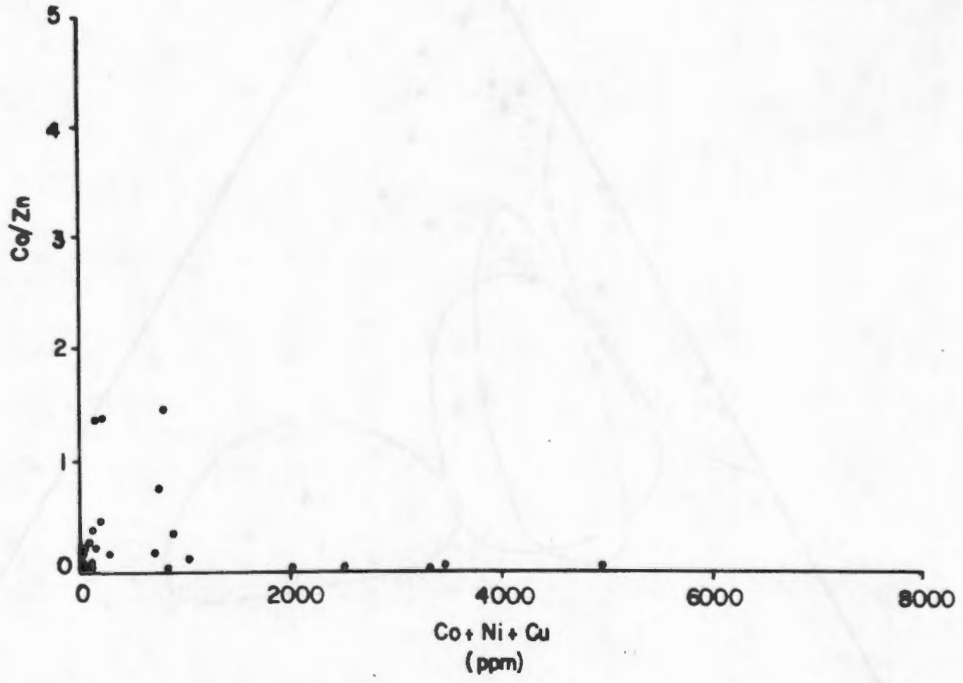

Fig. 13.9 Bivariate plot of Co/Zn ratio versus (Co + Ni + Cu) using data from iron formations from the study area.

diagram (Fig. 13.7) is a relative comparison of Fe, Mn and the minor metals (Co + Ni + Cu) with hydrothermal sediments such as the Red Sea deposits tending to concentrate at the Fe and Mn apices whilst Fe-Mn crusts, manganese nodules and hydrogenous sediments occupy more central fields. When data for iron formations from the study area are superimposed on this diagram, the majority of samples plot within the hydrothermal field due to low minor element contents. The more Fe-rich rocks contain, in general, slightly higher concentrations of minor elements, particularly Cu. The broad scatter in Fe/Mn ratios displayed by the study area rocks is not typical of hydrothermal deposits but comparable to the range displayed by hydrogenous sediments. The majority of samples do, however, have similar Fe/Mn ratios to the Red Sea and East Pacific Rise metalliferous sediments (Bonatti et al., op.cit.; Toth, op.cit.).

The second diagram compares the relative concentrations of the major components Fe, Mn and Si. Hydrothermal deposits concentrate at the Mn apex and along the Fe-Si tie-line, and hydrogenous rocks again occupy more central fields (Fig. 13.8). The majority of samples from the study area plot relatively close to the Fe-Si tie-line indicating probable "hydrothermal" rapid precipitation. A few samples have Mn components equivalent to Fe-Mn crusts and East Pacific Rise metalliferous sediments. A large proportion of the samples (±50%) are distinctly enriched in Si compared to typical marine sediments.

Whilst hydrothermal sediments might be depleted in Co, Ni, Cu and Pb, they are commonly enriched in Zn relative to hydrogenous sediments (Toth,1980). Zinc does not have as strong a chalcophile nature as Co, Ni, Cu and Pb and therefore tends to show greater dispersal away from hydrothermal centres than these metals which concentrate in sulphide precipitates within or close to the vent systems. Thus low Co/Zn ratios and (Co + Ni + Cu) contents indicate probable hydrothermal origins for Fe-Mn-rich sediments. Iron formations from the study area generally have low Co/Zn ratios and also relatively low (Co + Ni + Cu) contents (Fig. 13.9). Those samples with relatively high Cu contents also have very low Co/Zn ratios excluding a hydrogenous source for these base metals.

Bostrom (1973) devised a diagram for estimating the relative amounts of mixing between hydrothermal metalliferous sediments and terrigenous or deep-sea sediments using the Fe/Ti ratio and Al contents of the various rock types (Fig. 13.10). This diagram has also been used to infer chemogenic components for precursors of the glassy quartzites (see Section 12.3.4). Iron formations from the study area display a relatively wide range from virtually 100% metalliferous sediment to 40:60 mixtures of metalliferous and detrital sediments on this diagram. This apparently high percentage of detrital dilution is unusual for true hydrothermal deposits and more typical of hydrogenous sediments.

Certain trace elements such as Zr, Y, La and Ce are also concentrated in relatively greater amounts in hydrogenous metalliferous sediments than in hydrothermal equivalents, either as detrital components or during diagenetic alteration of apatite. Bivariate plots comparing Zr/Cr and Y/P_2O_5 ratios have

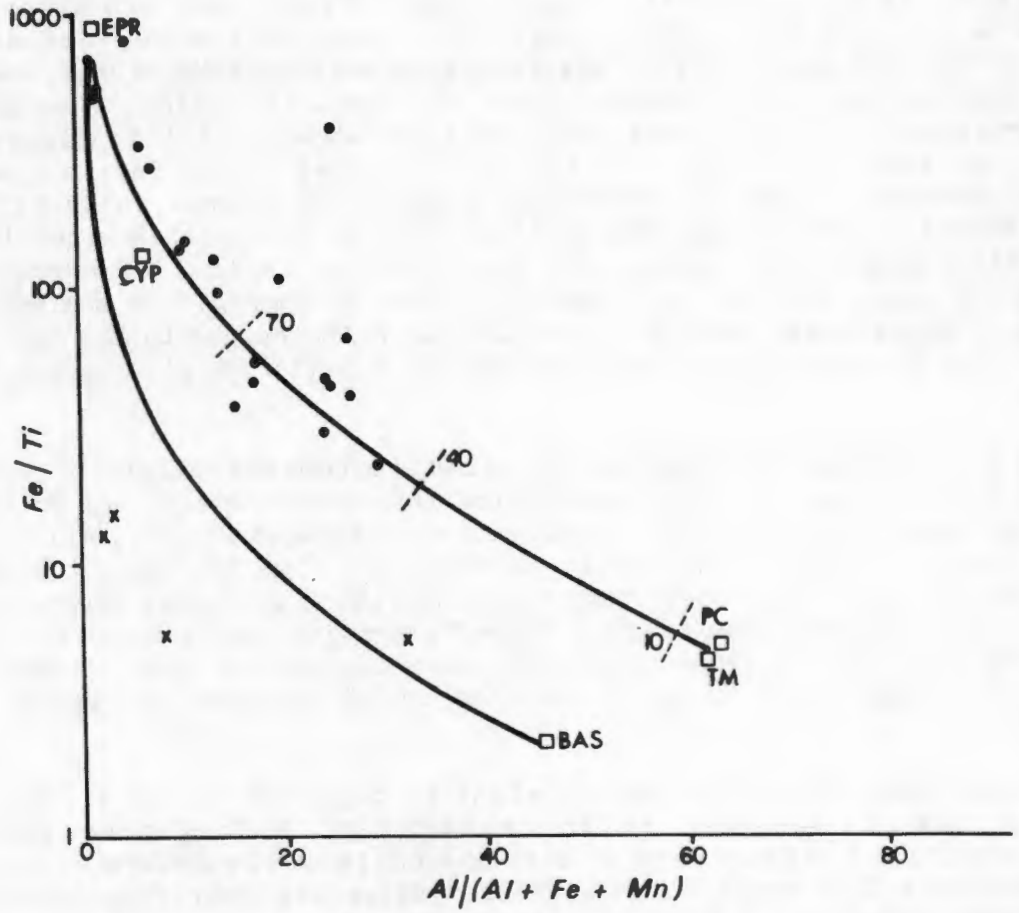

Fig. 13.10 Plot of Fe/Ti ratio versus Al/(Al + Fe + Mn) showing the positions of iron formations (•) and Zr-Ti-rich "heavy mineral" rocks relative to mixing curves between metalliferous sediment and terrigenous matter (upper curve), and metalliferous sediment and oceanic tholeiite (lower curve) (modified from Barrett, 1981). The relative positions of East Pacific Rise metalliferous sediment (EPR), umber from the Troodos Complex, Cyprus (CYP), pelagic clay (PC), terrigenous matter (TM) and oceanic tholeiite (BAS) are also shown.

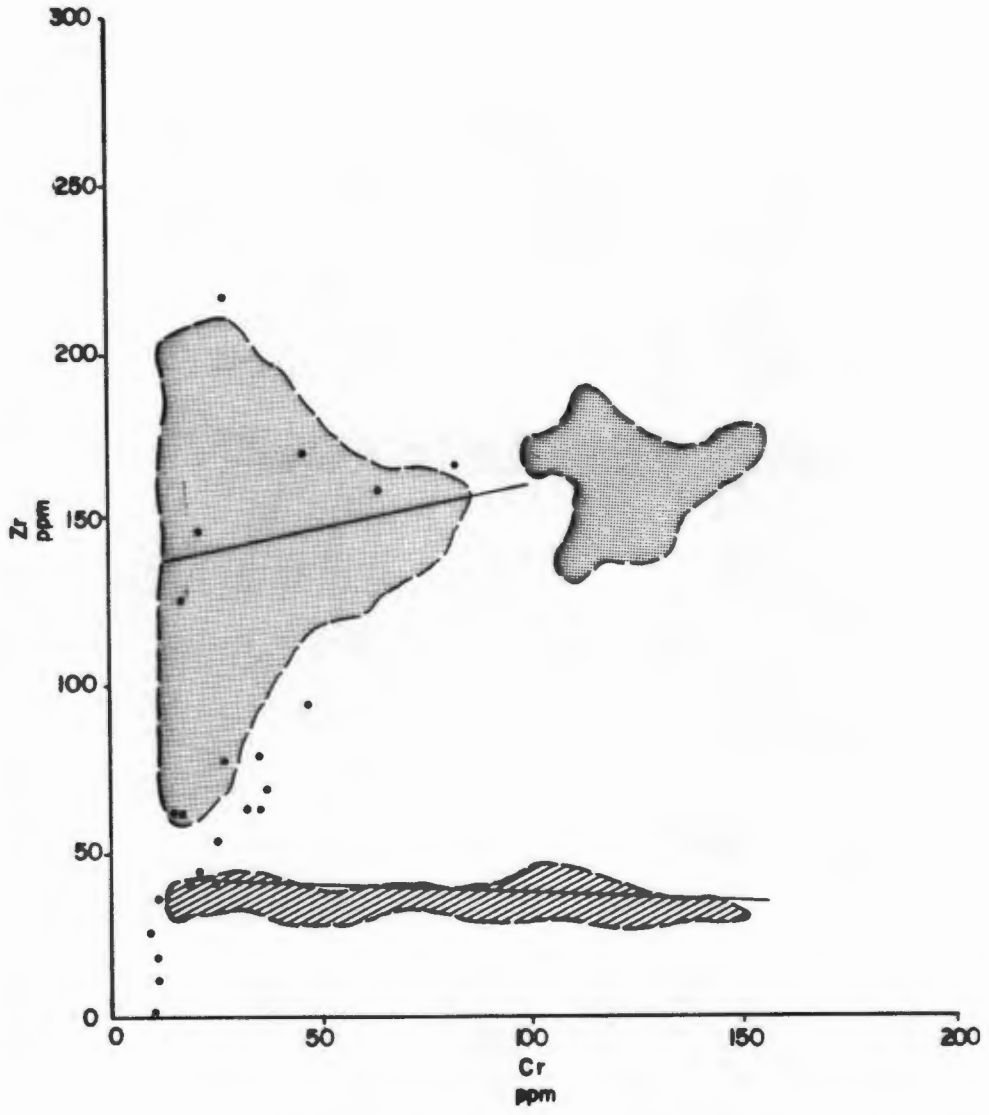

Fig. 13.11 Bivariate plot of Zr : Cr for iron formations from the study area compared to fields and regression lines for hydrogenous (stipple) and hydrothermal (cross-hatch) metalliferous sediments (after Marchig et al., 1982).

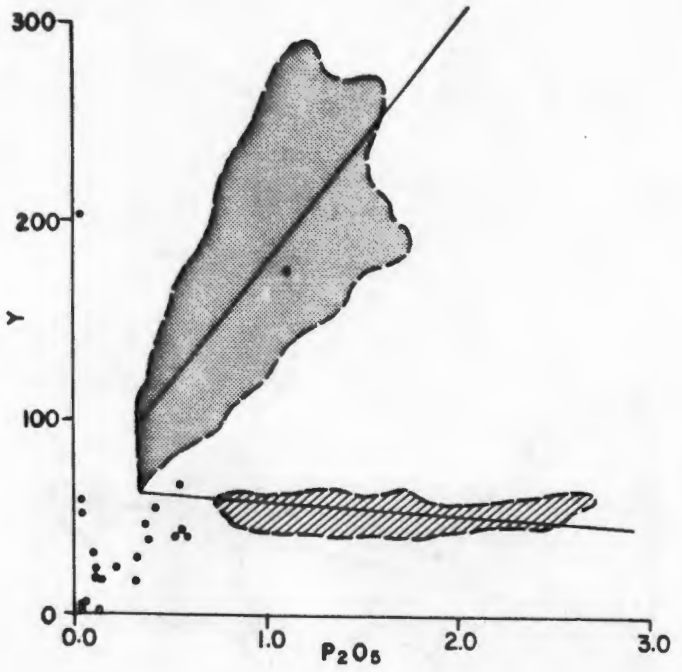

Fig. 13.12 Bivariate plot of Y : P_2O_5 for iron formations from the study area compared to fields and regression lines for hydrogenous (stipple) and hydrothermal (cross-hatch) metalliferous sediments (after Marchig et al., 1982).

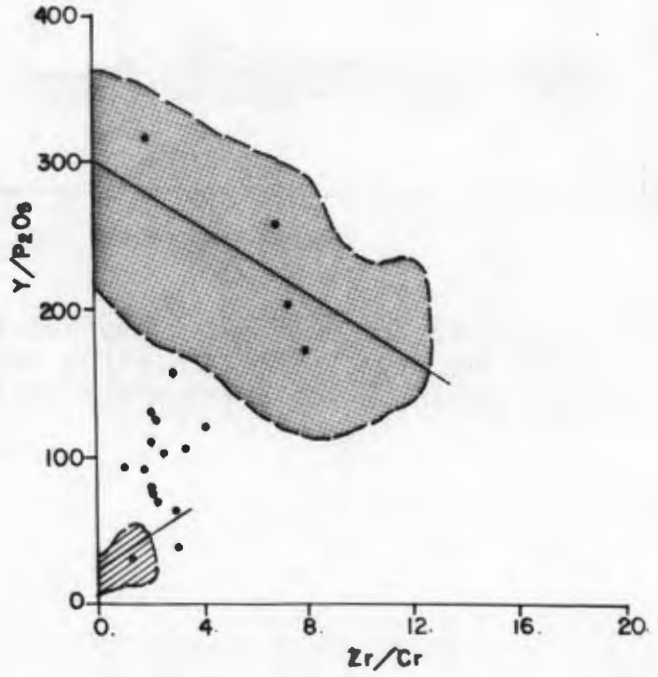

Fig. 13.13 Bivariate plot of Y/P_2O_5 : Zr/Cr for iron formations from the study area compared to fields and regression lines for hydrogenous (stipple) and hydrothermal (cross-hatch) metalliferous sediments (after Marchig et al., 1982).

been devised by Marchig et al., (1982) to distinguish between the two types of sediment. Iron formations from the study area have low Cr and Zr values, the latter occurring in concentrations comparable to the glassy metaquartzites and metacarbonate rocks of the western NMC (Fig. 12.5). The majority of samples resemble hydrothermal deposits rather than hydrogenous sediments on the Zr:Cr plot (Fig. 13.11), although they show considerable scatter compared to the former. Likewise on the $Y:P_2O_5$ plot (Fig. 13.12), the western NMC rocks have low Y contents similar to hydrothermal sediments. On the Y/P_2O_5 vs Zr/Cr plot (Fig. 13.13), the majority of iron formations plot in an entirely ambiguous position between the fields of the two sediment types.

La/Ce ratios can be used to distinguish deep-water hydrothermal sediments which have low absolute rare earth element (REE) concentrations and depleted Ce contents from hydrogenous sediments with variable, usually enriched, REE concentrations and relative Ce enrichment due to rapid precipitation of Ce from seawater (see Section 11.5) (Toth,1980). Iron formations from the study area have La/Ce ratios (mean 0.43) considerably lower than hydrothermal sediments (similar to seawater, approximately 2.8) but at low concentration levels which are generally atypical of hydrogenous sediments (Fig. 13.14).

Direct comparisons between modern-day deep-ocean sediments and Proterozoic manganiferous iron formations from the western NMC are probably not directly applicable, particularly as a shallow-marine environment is envisaged for the latter metasediments. Nevertheless the above plots indicate that the western NMC rocks have a dominant "hydrothermal" chemogenic component together with a not-inconsiderable minor "hydrogenous", possibly detrital, component. This minor component is revealed by distinctive Ti and Al contents whilst the hydrothermal component is deduced from relatively high Si contents, low minor transition metals (Co + Ni + Cu), low Co/Zn ratios and low Y, Zr and rare earth contents. Furthermore, the Fe/Mn ratios of the iron formations are somewhat atypical of hydrothermal deposits which generally show greater separation of Fe and Mn (Zantop, 1981; Crerar et al., 1982).

13.5 Comparison with ancient manganese deposits

The high mean MnO content of the iron formations of the western NMC (6.60%) makes comparisons with manganese deposits perhaps more appropriate than those with Lake Superior-type and Algoma-type iron formations. Like the Precambrian iron formations, ancient manganese deposits are subdivided into two groups - nonvolcanogenic and volcanogenic-sedimentary - depending on whether the source of the manganese is from weathering processes or directly related to volcanism, including exhalative sources (Roy,1976).

During periods of major acid volcanism, such as are proposed for the western NMC, magmatic volatiles, either associated with the erupted volcanics (phreatic) or with associated exhalations (fumarolic), are highly acidic, and as a result leach out Fe, Mn and other minor metals such as Zn, Pb and Cu from the volcanic rocks. On mixing with seawater, these acidified waters become progressively more alkaline and oxidised resulting in precipitation of the metals. If the rate of seawater mixing is rapid, then Fe and Mn precipitate

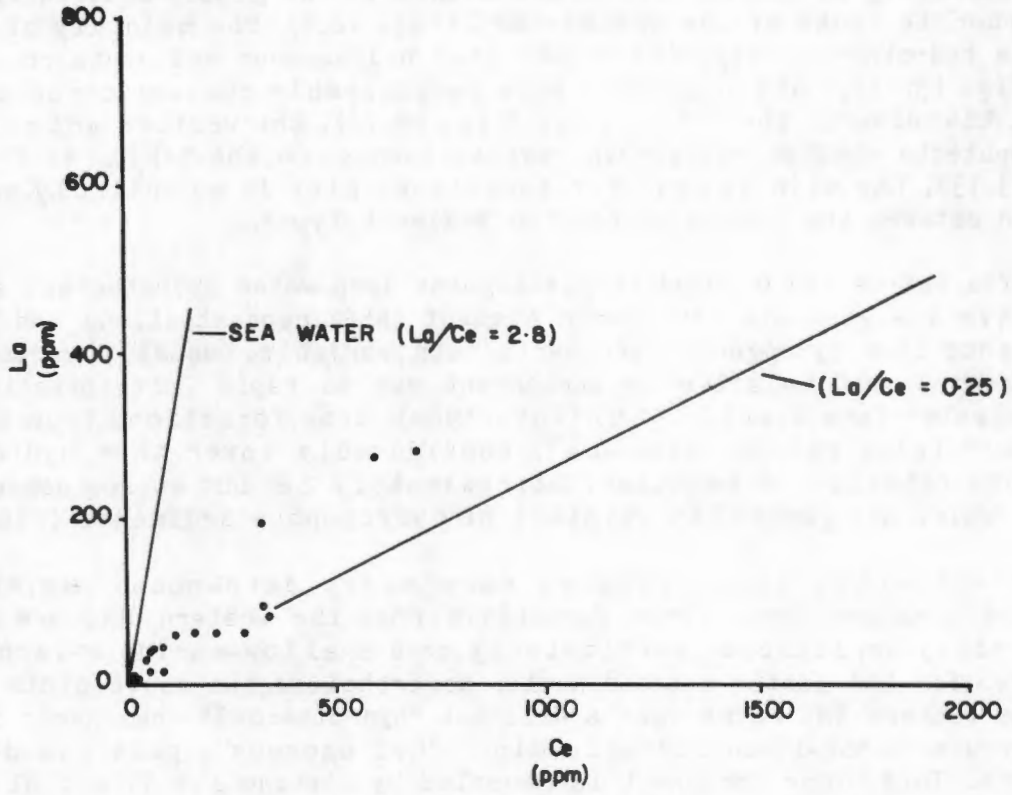

Fig. 13.14 Bivariate plot of La : Ce for iron formations from the study area compared to sea-water ratios and the lower limit of hydrogenous marine sediments (La/Ce = 0.25) (after Toth, 1980).

together, but if the rate is slow, then Fe is the first to be deposited (at lower Eh and pH conditions) followed by Mn either stratigraphically higher or more distal. Silica also suffers the same fate, being removed in solution from the volcanic rocks and reprecipitated in the marine environment together with Fe and Mn, forming iron and manganese formations and cherts.

The group of volcanogenic-sedimentary manganese deposits formed by this process has been termed the "porphyry-siliceous" group, being associated with acidic volcanic lavas and tuffs (quartz porphyry, rhyolite, dacite, andesite) and with associated jaspers, siliceous rocks and shales (Roy,1976). Distal cherty iron formations formed in association with acidic volcanism are also described by Mel'nik (1982). The volume of these manganese and iron formations within the enclosing sequences is extremely low compared to their sedimentary counterparts in nonvolcanogenic sequences such as the Sishen iron ore deposit (van Wyk and Beukes,1982) and the Kalahari manganese field (Kleyenstuber,1982). The manganese deposits form at variable distances from volcanic centres with larger deposits tending to be more distal. They are associated with iron formations in either mixed or differentiated sequences as oxide, carbonate, silicate and rarer sulphide facies. In the sulphide facies, Fe, Zn and Pb sulphides and barite are sometimes present.

One specific type of "porphyry-siliceous" volcanogenic-sedimentary manganese deposit (the Noda-Tamagawa type, Roy,1976) is commonly associated with a dominant chert member together with slates, greywackes and rarer tuffs and carbonate rocks. At the Noda-Tamagawa mine, Japan, the manganese deposits consist of lenses up to 200 metres long and 1.5 metres thick interbedded in massive and thinly-bedded metachert (92-97% SiO_2, Table 12.2) (Watanabe et al., 1970). The ores range from pyrochroite-rich lenses (53% Mn, 5% SiO_2) to manganiferous hornfelses (10% Mn, 60% SiO_2). Other ancient examples of chert-associated manganese concentrations include the late Jurassic Franciscan assemblage of California (Crerar et al., 1982) and the Arkansas Novaculite Formation of west-central Arkansas (Wagner et al., 1979). The latter formation is an equivalent of the Caballos Novaculite of Texas described by Folk (1973) and McBride and Folk (1977) to which the glassy quartzites of the northern parts of the study area were compared in Section 12.2. Two other types of volcanogenic-sedimentary manganese deposit (the Langban type and Karadzhal type, Roy, op.cit.) show associations with distal acidic volcanic rocks (tuffs, porphyries, keratophyres), carbonate rocks and stratiform, lenticular-to-sheetlike polymetallic sulphide bodies (commonly Pb, Zn, Fe, Cu) together with barite. Similarities between these sequences and the supracrustal sequences of the western NMC are readily apparent.

13.6 Summary

From the above discussion it would appear that one potential model for the genesis of the western NMC manganiferous iron formations involves widespread subaerial acid volcanism. Such a model would be compatible with models proposed for the genesis of the majority of other lithologies within the paragneiss belts of the area. In this model, leaching of Fe, Mn, Si and base metals from volcanic ash and pyroclastics by acidic magmatic-dominated

waters occurs during eruptive episodes and initial weathering processes. Mixing of these acidic waters with saline-to-alkaline waters in a sedimentary basin follows resulting in the relatively rapid precipitation of Fe-, Mn- and Si-rich deposits in shallow-water oxide-silicate-dominated facies environments. Precipitation of base metal-rich sulphides, carbonates and barite is essentially restricted to localised deeper sub-basins where anaerobic conditions exist. This model explains the association with the host paragneisses, the widespread distribution of these lithologies and their repetitive occurrence at more than one stratigraphic level (see Section 5.3), the relatively poorly-segregated nature of the bulk of the Fe-Mn deposits and the paucity of carbonate-sulphide facies rocks. It also explains some of the ambiguity in the findings concerning hydrothermal and hydrogenous sources and Lake Superior-type and Algoma-type iron formations as being due to a volcanogenic source for the metals but a subsequent sedimentary history of transport and deposition. These latter processes may involve dilution by detrital material, hence the relatively high Al and Ti contents of the rocks.

The Aggeneys-Gamsberg Fe-Mn-base metal-barite deposits occur in close association with glassy quartzites at similar stratigraphic positions to many of the other manganiferous iron formations (see Section 5.3 and Rozendaal,1982) from which they differ in several ways. These include increased thickness (<5 metres increasing to 10-50 metres), a greater range in Fe/Mn ratios, the presence of sulphide and carbonate facies lithologies and concentrations of barite, Zn, Pb, Cu and lesser Co. The sulphide facies rocks also contain a minor detrital component (muscovite, biotite and sillimanite) at the Broken Hill orebody and Big Syncline, Aggeneys (Ryan et al., 1982) and at Gamsberg (Rozendaal,1980).

The currently-favoured model for the genesis of these deposits is that of the sedimentary-exhalative type (sensu Large,1981 and Russell et al., 1981). This involves the leaching of Fe, Mn, Si and base metals from underlying volcanic/sedimentary rocks by hot fluids driven by convective processes above a magmatic heat source. The hot metal-rich fluids rise along growth faults associated with the formation of a second-order basin in the Aggeneys-Gamsberg area. Exhalation of these fluids occurs as well as precipitation of zoned sulphide and sulphate ore deposits on the adjacent basin floor due to mixing with cold, oxidised, saline basin water. The more widespread, thinner, base-metal-poor, manganiferous iron formations could represent transport of exhalative fluids related to the major Aggeneys-Gamsberg centre to more distal parts of the sedimentary basin. This would be particularly applicable to iron formations at the same approximate stratigraphic level (e.g. at Kangnas). An alternative suggestion is that these iron formations represent precipitation of chemical sediments derived from other exhalative sources within the basin (Rozendaal,1982). There is, however, no direct evidence for an exhalative source in the Aggeneys-Gamsberg area such as discordant feeder or sulphide-stringer zones. Nor is there evidence for growth faulting aside perhaps from the presence of metaconglomerate and metadiamictite ("psuedoconglomerate", Lipson,1978) units that generally overlie the iron formations.

There are thus two models for the genesis of the manganiferous iron formations of the western NMC and associated base metal concentrations. They

formed either as a result of dominantly extra-basinal or intra-basinal metal-leaching processes and were subsequently concentrated by chemical precipitation in a basin containing restricted anoxic zones. Both processes are compatible with the volcanic, sedimentary and tectonic environment thought to have existed during deposition of the supracrustal lithologies of the western NMC and deposits of both types may well be present in the area. Resolution of this genetic paradox will not be easy and requires additional studies and techniques beyond the scope of this project.

Chapter 14

SYNTHESIS

14.1 Introduction

In terms of crustal evolution, the Proterozoic (2500 to 500 Ma) is recognized as a transitional period between Archaean granite-greenstone terranes and Phanerozoic continental/oceanic crustal regimes controlled by Wilson-Cycle plate tectonics (Windley,1981). During the Archaean, high heat flows resulted in a buoyant lithosphere which inhibited subduction processes, and sialic "proto-continents" grew by aggregation, underplating and vertical accretion (Kroner,1981). In Proterozoic times, heat flows were considerably lower, the lithosphere thicker and some modified form of subduction commenced. Proterozoic plate tectonics are thought initially not to have involved the formation of large ocean basins, but rather the deformation of thinner, weaker, sialic crust against more rigid cratonic "cores" resulting in the formation of mobile belts by collision, underthrusting and subduction of continental crust (Kroner, op. cit.). Evidence that Proterozoic mobile-belt tectonism developed on pre-existing continental crust is provided by relicts of older lithologies within the mobile belts, the matching of Archaean/early Proterozoic crustal provinces across mobile belts, the absence of ophiolites and true arc volcanic and sedimentary rocks and the absence of high-pressure blueschist-facies metamorphic zones (Condie, 1982b). Only in late Proterozoic terranes (younger than 1000 Ma) do unequivocal ophiolite/deep-sea sediment sequences first appear, signifying the presence of negatively-buoyant oceanic crust and the onset of subduction, plate-margin volcanism and orogeny that typify present-day Wilson-Cycle tectonics. Within the timespan of the formation of the western NMC (approximately 2000 to 1000 Ma), therefore, some form of plate tectonics, modified to a greater or lesser degree compared to modern-day counterparts, was probably the operative force, controlling the type of volcanicity, sedimentation and tectonism.

Early to middle Proterozoic (2500 to 1300 Ma) supracrustal rocks have been classified into three major lithological assemblages by Condie (1982a). The assemblages are: (1) quartzite-carbonate-shale; (2) bimodal volcanics-quartzite-arkose; and (3) calc-alkaline volcanics-greywacke, and these may grade both laterally and vertically into one another. The quartzite-carbonate-shale assemblages are the most commonly recorded sequences (>60%), dominated by quartzites and sandstones with lesser dolomites, shales, limestones, cherts and iron formations and attaining thicknesses up to 10 km. The bimodal volcanics-quartzite-arkose assemblages are less frequently reported (20%), thinner (5-10 km thick) and contain both tholeiitic basalts and rhyolites, with either type predominating, in association with feldspathic sandstones, quartzites, arkoses, shales, conglomerates and rarer evaporites. The calc-alkaline volcanics-greywacke assemblages are the least common (<20%) comprising continuous volcanic suites in association with turbiditic

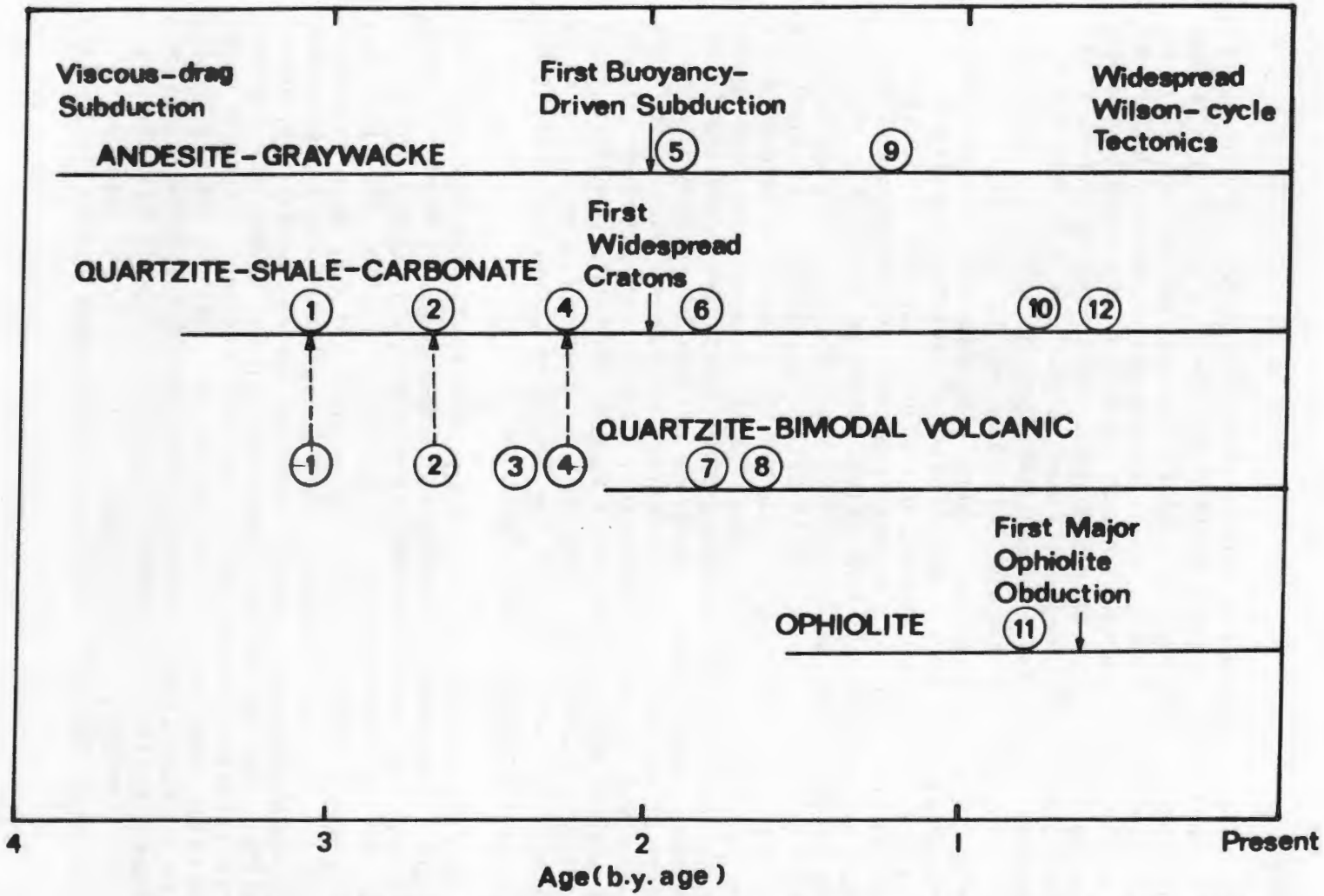

Table 14.1 A summary of the distribution of supracrustal assemblages with geologic time (after Condie, 1982b) together with the superimposition of major assemblages from southern Africa.
(1) Pongola Sequence; (2) Witwatersrand Supergroup; (3) Ventersdorp Supergroup; (4) Transvaal Sequence; (5) Orange River Group ; (6) Waterberg Group; (7) Soutpansberg Group; (8) supracrustal rocks of the study area; (9) Sinclair Sequence; (10) Damara Sequence; (11) Matchless Member, Damara Sequence; (12) Nama Group.

greywackes and argillites.

The three different supracrustal assemblages reflect the major tectonic settings that occurred in early-to-middle Proterozoic times. As interpreted by Condie (1982a), assemblage (1) (quartzite-carbonate-shale) is indicative of sedimentation on stable craton margins or within the interiors of stable Archaean cratons; assemblage (2) (bimodal volcanics-quartzite-arkose) formed in lithosphere-activated continental rifts either above subduction zones or associated with continent-collision boundaries; and assemblage (3) (calc-alkaline volcanics-greywacke) is thought to reflect mantle-activated rifting either within cratonic areas (in the early Proterozoic) or at convergent plate boundaries. Assemblage (3) is recorded from Archaean terranes (±3800 Ma) as well as throughout the Proterozoic and Phanerozoic whereas assemblage (1) only attained widespread distribution about 2000 million years ago (Condie,1982b) when most cratons became sufficiently stable to accomodate the deposition of platform sediments. The proliferation of assemblage (2) at about 1700 Ma is interpreted as indicating the onset of lithospheric rifting and the initiation of buoyancy-driven subduction (Condie, op. cit.) (Table 14.1).

14.2 Regional aspects

In southern Africa, particularly in the relatively stable cratonic areas, there appears to be a distinct association of assemblage (1) and assemblage (2), with the lowermost portions of the major Proterozoic lithological subdivisions containing bimodal volcanics and the upper portions platform sediments (Table 14.1). This is characteristic of the Pongola Sequence (3050 Ma), the Witwatersrand Supergroup (2500 Ma) and the Transvaal Sequence (2200 Ma). In the early Proterozoic assemblages (including the Ventersdorp Supergroup at 2300 Ma), basic volcanics (tholeiite, Mg-rich tholeiite, "andesite") generally predominate, although rhyolitic rocks, quartz porphyry and acid tuffs are also present. Volcanic rocks account for some 5200 m in the Insuzi Subgroup of the Pongola Sequence, 2600 m in the Dominion Group of the Witwatersrand Supergroup, 4000 m in the Ventersdorp Supergroup and less than 2000 m in the basal Wolkberg Group of the Transvaal Sequence (Button et al.,1981).

At the end of the depositional cycle of the Transvaal Sequence, major thicknesses of acid volcanics were extruded as the Rooiberg Felsites (3000 m) and in the time-equivalent Griqualand West Sequence, mafic volcanics in the form of the Ongeluk Lavas. The Rooiberg Felsites represent the first major thicknesses of acid volcanics (at approximately 2100 Ma, just prior to the intrusion of the Bushveld Complex) related to the initiation of lithospheric rifting as opposed to mantle-activated rifting (Condie,1982b). The younger Waterberg-Matsap-Soutpansberg basins (2000-1300 Ma) consist either of clastic arenaceous sediments with comparatively minor volcanicity (Waterberg) or of similar sediments associated with major thicknesses of basaltic, andesitic and trachytic lavas (Soutpansberg) in a deeper trough interpreted as an aulacogen (Jansen,1974).

Post-Archaean tectono-sedimentary cycles in the cratonic environments of

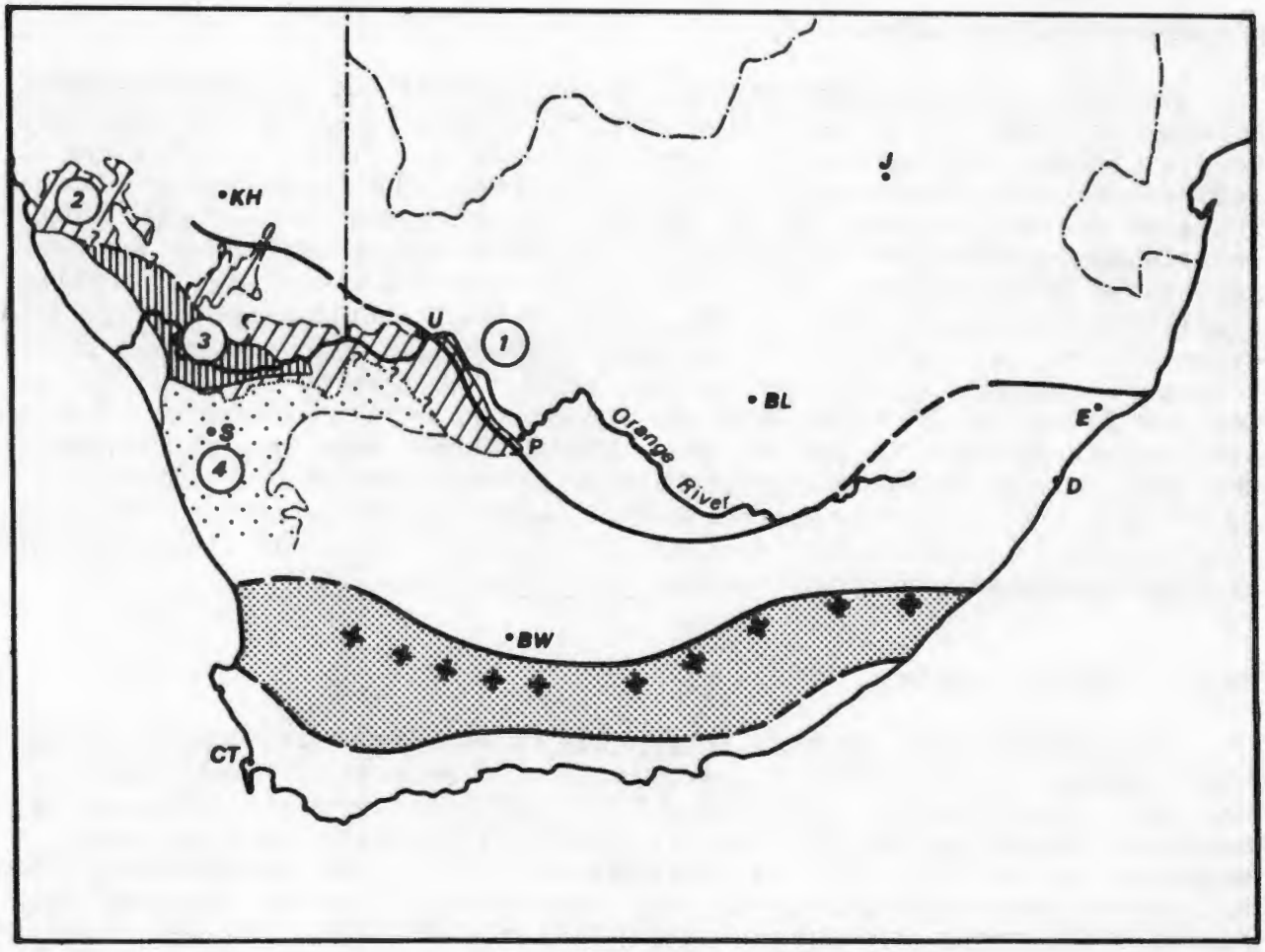

Fig. 14.1 Regional map showing the southern boundary of the Kaapvaal Craton as inferred from gravity data, the Southern Cape Conductive Belt (stipple) and the Beattie magnetic anomaly (+) (from de Beer and Meyer, 1983) as well as the distribution of the three major supracrustal groups within the western NMC, namely the Grunau Sequence (2), the Orange River Group (3) and the Bushmanland/Okiep Group of the study area (4). KH - Keetmanshoop, S - Springbok, CT - Cape Town, U - Upington, P - Prieska, BW - Beaufort West, BL - Bloemfontein, J - Johannesburg, E - Eshowe, D - Durban.

southern Africa appear to have been initiated by vertical tectonics involving rifting and subsidence. This rifting tapped underlying upper-mantle magmatic sources resulting in mafic-dominated volcanism that was succeeded by extensive coarse clastic-dominated sedimentation. Minor acid volcanism resulted from melting of continental crust and widespread carbonate sedimentation occurred during quiescent phases, predominantly in the Transvaal/Griqualand West Sequences. Plutonic activity associated with these events comprised the intrusion of mafic layered complexes (such as the Great Dyke and the Bushveld Complex) and associated granites (such as the Bushveld Granite) that appear to represent plutonic equivalents to the extrusive rocks of the Proterozoic sequences.

In contrast to the supracrustal assemblages of the cratonic area, the metasedimentary and metavolcanic sequences of the Namaqualand Metamorphic Complex - a middle Proterozoic mobile belt bounding the Kaapvaal Craton to the west and south - contain distinctly different assemblages. The oldest lithologies occur within the Vioolsdrif domain (Fig. 14.1) and comprise an intrusive tonalite-granodiorite-granite suite emplaced within cogenetic extrusive calc-alkaline volcanic rocks of the Orange River Group (Reid,1977; Reid and Barton,1983). The calc-alkaline volcanic rocks have an extrusion age of 1996 Ma (Reid,1979) and include a differentiated suite of lavas with compositions ranging from basaltic andesite to rhyolite, dominated by andesites, and a thick sequence of acid volcanics (Hom Formation) which includes ignimbrites and tuffs. Coarse volcaniclastic rocks in the Haib area of southern Namibia indicate proximity to volcanic centres whereas more uniform felsic and mafic metavolcanic and metasedimentary rocks to the south of the Orange River (primarily of the Hom and Guadom Formations) imply a more distal depositional environment (Blignault *et al.*, 1983). Whilst the Hom Formation is reported as being 2000 metres thick in the type area (Blignault *et al., op.cit.*), the Orange River Group does not appear to be very thick (<4000 m) south of the Orange River, and major units that could be interpreted as metamorphosed greywacke successions are absent. Therefore, although the differentiated calc-alkaline affinity of the volcanic rocks implies classification under assemblage (3) of Condie (1982a), these lattermost characteristics are somewhat atypical of calc-alkaline volcanics-greywacke assemblages.

Despite these apparent anomalies, the intrusive rocks of the Vioolsdrif domain have a distinctly I-type chemical signature (Reid and Barton,1983), andesitic volcanic rocks are common, and the Haib porphyry copper deposit represents one of very few Precambrian porphyries directly comparable with Phanerozoic equivalents (Minnitt,1979). There is thus convincing evidence for some form of mantle-tapping subduction process, probably involving the consuming of oceanic crust at a convergent plate boundary, and the creation of new sialic crustal material.

To the east and north of the Vioolsdrif domain, metapelitic gneisses with associated minor metacarbonate and feldspathic quartzite units of uncertain age predominate in supracrustal sequences (Beukes,1973; Geringer,1973; Jackson,1976; Toogood,1976; Blignault,1977) that are grouped together as the Grunau Sequence by Blignault *et al.* (1983) (Fig. 14.1). To the south of the

Vioolsdrif domain, certain banded silicic gneisses in the Steinkopf domain (Marais et al.,1975) and the Aggeneys area (Moore,1977) apparently represent a basement complex yielding Pb-Pb whole rock isochron ages of 1700-1800 Ma (Reid and Barton,1983) and 2000 Ma (Welke and Smith,1984) respectively, on which the supracrustal sequences of this study were deposited. This basement is separated from the adjacent Vioolsdrif lithologies by a major lineament termed the Groothoek Thrust (Theart,1980; Blignault et al., op.cit.) that has been subsequently folded during F3 deformation (sensu Joubert,1971). Although the basement lithologies apparently change across this early lineament, the supracrustal sequences do not, and the schist-quartzite associations typical of the northern portions of the study area occur on both sides of the thrust, most noticeably in the Dabenoris-Pella area.

The supracrustal sequences to the south of the Vioolsdrif domain, incorporating the present study area, belong to Condie's (1982a) assemblage (2) and comprise an older sequence of metamorphosed rhyolite/rhyodacite succeeded by feldspathic quartzites and shales, and a slightly younger sequence of metamorphosed rhyolite, potassic shales, quartzite/chert and tholeiitic basalts. It is exclusively lithologies of this younger sequence that straddle the Groothoek Thrust. The supracrustal sequences of the Namaqua mobile belt differ from their cratonic Proterozoic counterparts and predecessors in having either calc-alkaline or acid-dominant volcanic associations (as opposed to tholeiite-dominant), and in lacking the great thicknesses of either coarse clastic or carbonate sedimentation, containing instead relatively thin shale-sandstone-dominated assemblages.

These differences between supracratonic and circumcratonic assemblages can be explained in terms of models that propose the existence of a supercontinent incorporating the Archaean cratonic "cores" of Australia, India, Antarctica, Africa and South America (i.e. Gondwanaland) from early to middle Proterozoic times (Hurley and Rand,1969; Piper,1976; Condie,1982a). Supracrustal assemblages deposited on this supercontinent formed in areas of rifting and graben-formation, commonly comprising the initial extrusion of flood basalts succeeded by coarse clastic sediments and carbonates as typical trough fillings. Assemblages forming peripheral to the supercontinent occurred either as passive-margin coarse-to-fine clastic sedimentation or as active-margin deposits associated with subduction and/or continent collision as well as either calc-alkaline or acid volcanism. As the lithosphere was still relatively buoyant in early to middle Proterozoic times, mantle-tapping subduction seldom occurred, accounting for the rarity of calc-alkaline assemblages such as the Orange River Group. Instead subduction took the form of shallow underplating of the continental crust at the margins of the supercontinent resulting in thrust-dominated mobile-belt tectonics, high-T, low-P metamorphism and the generation of large amounts of S-type granitic rocks and associated acid volcanism. A further consequence was that deep troughs seldom formed in which major thicknesses of immature sediments could accumulate. Much of the deformation at the plate boundary may have involved relatively thin sialic crust rather than subduction of mafic oceanic material (Kroner,1981). This thinner crust represented either extensions of the supercontinent itself or microcontinents/suspect terranes that accreted to the supercontinent during collision events.

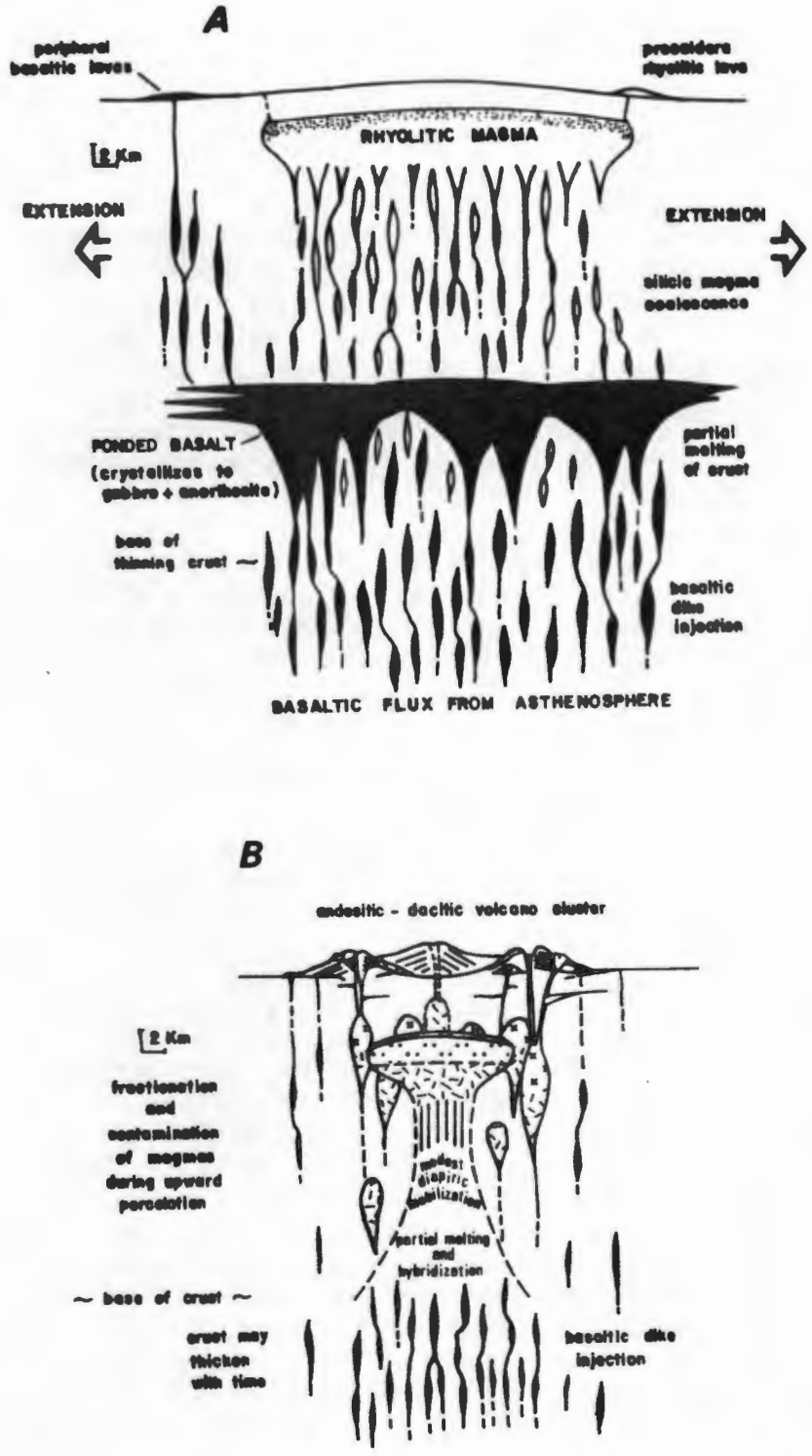

Fig. 14.2 Schematic diagrams of two different styles of lithospheric magmatism (after Hildreth, 1981):
A - extensional stress conditions, resulting in acid-dominated, bimodal volcanism and
B - where extensional conditions are absent, resulting in a continuous suite of calc-alkaline volcanic and intrusive lithologies.

14,3 Volcanic processes

The metavolcanic rocks in the western NMC supracrustal sequences of the study area are predominantly rhyolitic to rhyodacitic in composition with the leucogneiss lithologies resembling high-silica rhyolites and biotite gneisses slightly less extreme acid differentiates. Minor amounts of metabasic lithologies are present, representing tholeiitic intrusive and extrusive rocks derived from partial melting of mantle peridotite and subsequent fractional crystallisation. Bimodal acid-dominated volcanic suites and high-silica rhyolites are restricted to certain specific crustal processes and environments, such as the Basin and Range province of the western U.S.A., that are discussed below.

There are three major processes whereby granitic and rhyolitic magmas are generated. These are (1) partial melting of pre-existing solid rocks; (2) closed-system crystal-liquid fractionation from more basic liquids; and (3) coupled fractionation-melting in which magmas of mafic or intermediate composition incorporate wallrocks and/or roof (Barker,1981). Granitic rocks that have formed from partial melting processes are subdivided into three broad types depending on their source material and tectonic setting. These are S-, I- and A-types which are derived from melting of sedimentary (S) and igneous (I) rocks generally in orogenic environments (Chappell and White,1974), or from residual crustal sources (A) in anorogenic environments (Collins et al.,1982). The granites are intruded as mixtures of both the partial melt and incorporated remnants of the residual restite material. Extrusive equivalents of these granitic rocks have also been reported (Wyborn et al.,1981) containing residual minerals such as cordierite, orthopyroxene and almandine garnet.

Melts of granitic composition can also be separated from a parent basaltic liquid by crystal-liquid fractionation or differentiation (Bowen,1948). However, closed-system processes such as this are probably not capable of generating the extremely large volumes of rhyolites observed in environments such as the Basin and Range province of the western U.S.A. (and the western NMC ?) due to unrealistically large volumes of mafic magma required for their formation. The majority of silicic magmas are probably derived by a combination of the two above processes of partial melting and crystal fractionation (e.g. Barker et al.,1975). The heat that is generated during the partial melting of ultramafic mantle to produce a basaltic magma is transferred, during intrusion of this magma, to the lower crust which is, in turn, partially melted (Barker,1981).

The two principal tectonic regimes, those of extension and compression, are the loci of markedly different behaviour during intrusion of basaltic magma into the lower crust. In extensional tectonic regimes, injection of basaltic magma into the lower crust results in crustal melting and the formation of rhyolitic liquids that rise rapidly along vertical paths of brittle fracture, reducing to a minimum (1) basalt-rhyolite hybridization, (2) the entrainment of residual material and (3) melting extensive enough to generate liquids less silicic than rhyodacite (Hildreth,1981). The rhyolitic

liquids, rising along dyke-like zones, may aggregate or coalesce at shallow levels in large, horizontally-extensive magma chambers within which differentiation is accomplished by gravity-driven liquid-state thermodiffusion, resulting in the concentration of high-silica, volatile-rich magma immediately beneath the roof of the chamber (Hildreth,1979) (Fig. 14-2a).

Roof-collapse of the magma chamber causes the extrusion of vast amounts (up to 3000 km^3) of high-silica rhyolitic and rhyodacitic ignimbrites and ash-flow tuffs from major caldera structures. An example of such an eruption is that of the Blacktail Tuff in the eastern Snake River plain, western U.S.A. where high-silica rhyolitic tuffs erupted from a caldera with dimensions of 100 km x 60 km and cover an area in excess of 12,000 km^2 to an average thickness of 75 metres (ranging from 2 - 200 m thick) (Morgan et al., 1984). The Huckleberry Ridge Tuff in the adjacent Yellowstone Plateau volcanic field has similar dimensions and represents the erupted products of another major caldera (85km x 45 km) only 4 m.y. younger (Morgan et al., op.cit.). Erupted high-silica flows are dominantly crystal-poor (<2%) or aphyric, have SiO_2 contents in the region of 77%, and may show striking major element geochemical homogeneity (Bacon et al., 1981).

All the above-mentioned features have distinct parallels in the widespread, equigranular, chemically-homogeneous leucogneisses of the western NMC. Subsequent to the acid eruption, minor intrusion and extrusion of basaltic rocks from the deeper-seated basaltic magmas may occur. This is observed in the Aggeneys-Gamsberg area where major extrusive mafic units occur at the top of the observed lithological sequence (Joubert, 1974b; Rozendaal, 1975). Extensional tectonic regimes with which acid-dominated volcanism is associated, generally occur in zones of incipient rifting. As rifting progresses, the bimodal volcanism is likely to become more mafic-dominated as observed in the Proterozoic sequences of the cratonic areas (see Section 14-2).

In tectonic environments where extension is generally absent, such as island arcs and continental-margin arcs (i.e. areas of subduction), vertical transport of magma is a slower process of percolation with the result that fractionation and hybridization within and between basaltic magmas and the crustal partial melts occurs on an increasing scale, forming predominantly intermediate magmas (Fig. 14-2b). Extruded volcanic rocks are thus commonly andesitic-to-dacitic in composition, and instead of the magmas rising rapidly along dyke-like conduits, the entire mass rises diapirically, injecting a segregated suite of granodioritic, adamellitic and alaskitic plutons into the upper crust in the form of a major batholith (Hildreth,1981). This scenario adequately explains the compositions and lithological succession observed in the older calc-alkaline Orange River Group and the associated intrusive Vioolsdrif Suite (Reid, 1977,1979) and indicates that compressional forces preceded extensional prior to the formation of the supracrustal rocks in the study area.

14.4 Sedimentary processes

Interpretation of the depositional environments of sedimentary rocks generally involves the identification of various sedimentary facies within the lithological sequence. A sedimentary facies can be defined as "a distinctive rock that forms under certain conditions of sedimentation, reflecting a particular process or environment" (Reading,1978). Facies are distinguished using the criteria of colour, bedding, composition, texture, fossils and sedimentary structures (Reading, op.cit.). In the western NMC, virtually all of these characteristics have been obliterated or strongly modified by the affects of high-grade metamorphism and deformation, however, and it has not been possible to ascribe precise lithofacies to individual rock types during this study. Nevertheless, it is apparent from the vertical lithological sequences described (see Chapter 5) that changes in facies have occurred and, as a result, it is possible to make certain basic statements and generalisations about changes in the environment of deposition of the western NMC lithologies.

Changes in rock types or facies in a vertical sedimentary sequence generally indicate that fluctuations in sea level have occurred, commonly as the result of tectonic activity. Landward migration of the shoreline is described as transgression and seaward migration of the shoreline as regression or progradation. The significant difference between these two depositional sequences is that they are reversed viz-a-viz one another. A facies sequence is defined as "a series of facies which pass gradually from one into the other" (Reading,1978) and is bounded by a sharp, erosional contact either at the top or bottom. Two common sequences exist in clastic sediments, coarsening-upwards sequences where the grain-size coarsens upwards from a sharp base, and fining-upwards sequences where the grain-size becomes finer towards a sharp top. Coarsening-upwards sequences are typical of progradational or regressive sedimentary cycles whereas fining-upwards sequences are more typical of transgressive cycles. These characteristics are the result of the interplay of subsidence or rise in sea-level and sediment supply. Where subsidence is greater than supply (i.e. transgression), less and less clastic material becomes available for deposition resulting in reworking, diagenesis and ultimately in the precipitation of chemical sediments. Where sediment supply is greater than subsidence (i.e. progradation) an increase in proportion of coarse-grained continental clastic facies results (Reading op.cit.).

The supracrustal sequences in the study area can be divided into two basic types (see Section 5.3). The paragneiss belts of south/central parts comprise basal leucogneisses and biotite gneisses interpreted as acid volcanics, overlain by the metamorphic equivalents of feldspathic sandstones, psammitic and pelitic rocks and minor impure carbonates. On large, medium and small scales, facies sequences are observed showing variation from coarse-grained clastic sediments through fine-grained to chemical sediments. On the large scale this is observed as sequences containing basal volcanic detritus and impure sandstones grading via psammitic sediments into pelites containing

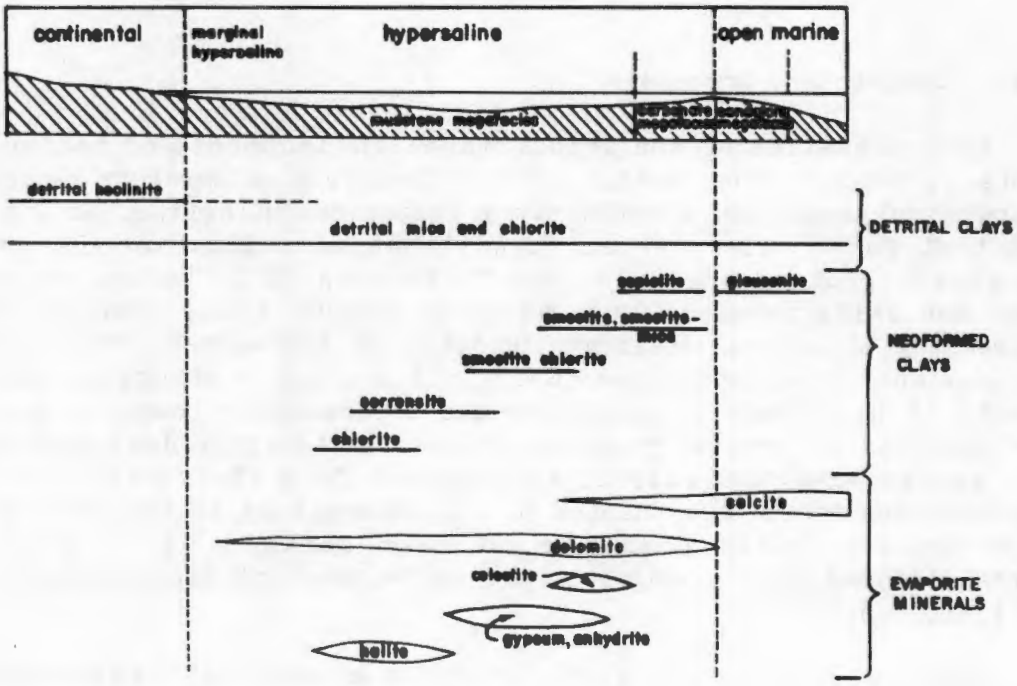

Fig. 14.3 Schematic model showing the distribution of detrital clays, neoformed clays and evaporite minerals in different continental-margin sedimentary environments (after Fisher and Jeans, 1982).

impure carbonate rocks towards the top of the observed stratigraphic section. Similar variations, sometimes with one or more component missing, can be observed on the medium scale. For example, in the Witwater-Platbakkies belt, several cycles comprising volcanic rocks - psammitic sediments (± pelitic sediments) (± iron formation and carbonate rocks) occur in the lower portions of the supracrustal sequence. On the small scale (± one metre), fining-upwards sequences consisting of a psammitic base and pelitic top with sharp upper contact were observed, most convincingly in the Zout Rivier area of the Bitterfontein paragneiss belt.

These lines of evidence indicate that transgressive processes were dominant during the deposition of these particular sediments. Marine transgressions are recognized as being one of the most important mechanisms whereby major blanket sandstone deposits accumulate (Johnson, in Reading,1978). Large sand bodies are deposited during episodes of coastal progradation and subsequently drowned and preserved during major transgressions. This may partly explain the dominance of psammitic and sandstone units within the south/central sequences. Abundant sand supply in a high-energy environment is also implied by the relative lack of fine-grained and chemical sediments.

The supracrustal sequences in the northern parts of the study area contain similar basal leucogneisses, also interpreted as volcanic detritus. These are overlain by pelitic sediments which contain a considerable feldspathic component in their basal parts. The pelites are capped by extremely pure siliceous rocks, either cherts or pure quartz sands or both, lesser manganiferous iron formations and rarer carbonate rocks. Pyritic and graphitic zones occur in both the pelitic and siliceous sediments. A second cycle of pelitic and quartzitic sediments overlies the first. In this cycle, the pelites and siliceous rocks are more interbanded although still strongly segregated from each other. These sharp lithological contacts are in distinct contrast to the gradational contacts observed in the south/central rocks and, as a result, no coarsening-upwards or fining-upwards facies sequences were detected. The supracrustal sequence contains a more restricted upper portion in the Gamsberg - Aggeneys - Koeris area (Lipson,1978; Rozendaal,1982), containing quartz-pebble conglomerates, diamictites, amygdaloidal basaltic volcanics and impure carbonate rocks.

On the large scale, the northern supracrustal sequences are also interpreted initially as having been deposited during a transgressive event. Coarse acid volcanic detritus is somewhat gradationally superceded by finer pelitic sediments and then by siliceous, ferruginous, manganiferous rocks that are interpreted in this study as regional chemical sediments. Apart from the initial volcanic input, sediment supply appears to have been restricted and chemical conditions within the basin somewhat unusual in order to account for the rarity of carbonate rocks and the widespread occurrence of SiO_2, Fe and Mn precipitates instead. Such environments of limited sediment supply and unusual water chemistry generally only occur in highly restricted small pelagic basins such as the depository of the Monterey Formation of California (Jenkyns, in Reading,1978) or non-marine closed basins such as Lake Magadi in the Rift Valley of Kenya (Eugster,1969).

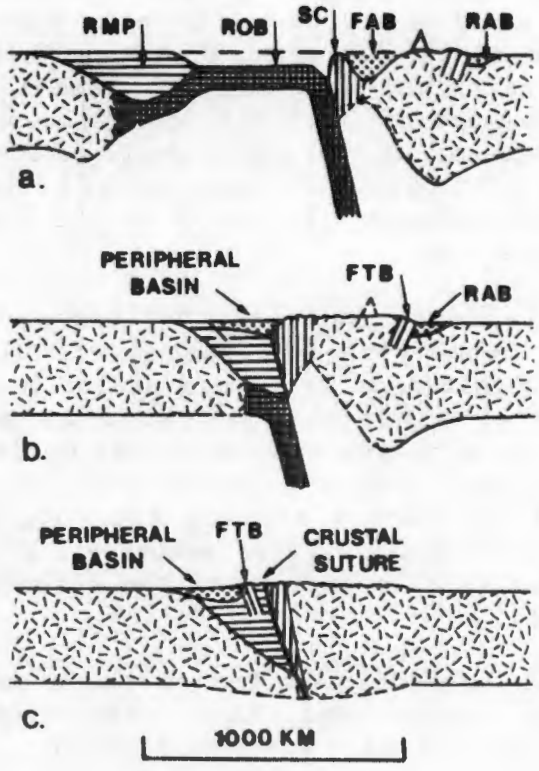

Fig. 14.4 Series of schematic diagrams illustrating the sequence of events during crustal collision and the formation of peripheral sedimentary basins. Oceanic crust is cross-hatched; continental crust jackstrawed. RMP - rifted margin prism; ROB - remnant oceanic basin; SC - subduction complex; FAB - fore-arc basin; RAB - retro-arc basin; FTB - fold-thrust belts (after Dickinson, 1974).

The presence of pyritic and carbonaceous pelites is indicative of a bituminous mud facies which commonly forms in "tranquil basins with a restricted oxygen budget" (Johnson, in Reading,1978). There appears to be a complementary association of extensive cherts, resulting from enhanced production of organic matter (radiolaria ?) and anoxic sediments containing pyrite and graphite, resulting from the removal of oxygen during the intense organic activity. The existence of anoxic enclaves within the northern sedimentary basin created a favourable environment for the precipitation of base metal sulphide concentrations in that specific area.

Within restricted or closed basins, as opposed to the open marine facies, hypersaline conditions can exist, resulting in the association of neoformed clay minerals and evaporite minerals. The neoformed clay assemblages commonly comprise magnesium-rich minerals such as chlorite, smectite, sepiolite and palygorskite (Fisher and Jeans,1982) that form during early diagenesis of the sediments (Fig 14-3). The magnesium-rich cordierite gneisses in the study area could well represent such evaporite-associated diagenetic processes.

In contrast to the neoformed clay constituents, detrital clays such as illite and kaolinite predominated in the precursors of the metapelitic rocks of the study area, indicating that hypersaline conditions were ephemeral and not dominant in the overall history of sedimentation. The marked increase in kaolinite components in the northern metapelitic rocks indicates proximity to source material (Fig. 14.3), more intense weathering and perhaps a more arid or hotter climate (Nesbitt and Young,1982) when compared to the illite-dominated south/central metapelites. All these factors are common features within restricted continental basins.

14.5 Regional model

Based on the above premises, the following 4-stage model is proposed for the formation of the western Namaqualand Metamorphic Complex.

(1) The lithologies of the Grunau Sequence represent metamorphosed equivalents of the Matsap sediments that were deposited in a craton-margin environment. They represent the oldest-recorded lithologies in the Aus (Jackson,1976) and Grunau (Blignault,1977) areas, of unknown thickness and forming on an unknown basement. Rocks of the Grunau Sequence are apparently interbanded with metavolcanic rocks of the Orange River Group in the Onseepkans area (Toogood,1976; Blignault et al.,1983) indicating that they have an age of approximately 2000 Ma. The Orange River Group and associated Vioolsdrif Intrusive Suite constitute a coeval calc-alkaline igneous province representing compressional subduction processes along the margin of this 2000 m. y. old Proterozoic supercontinent (Fig. 14.5a). Subduction at this time involved primarily basaltic oceanic crust and led to the production of widespread andesite-dominated volcanism and granodiorite-dominated plutonism. Remnants of this oceanic crust are thought to be preserved as the well-known "black bodies" to the immediate north of the Groothoek Thrust (Joubert,1974a). There is a noticeable polarity within the metavolcanic rocks of the Orange

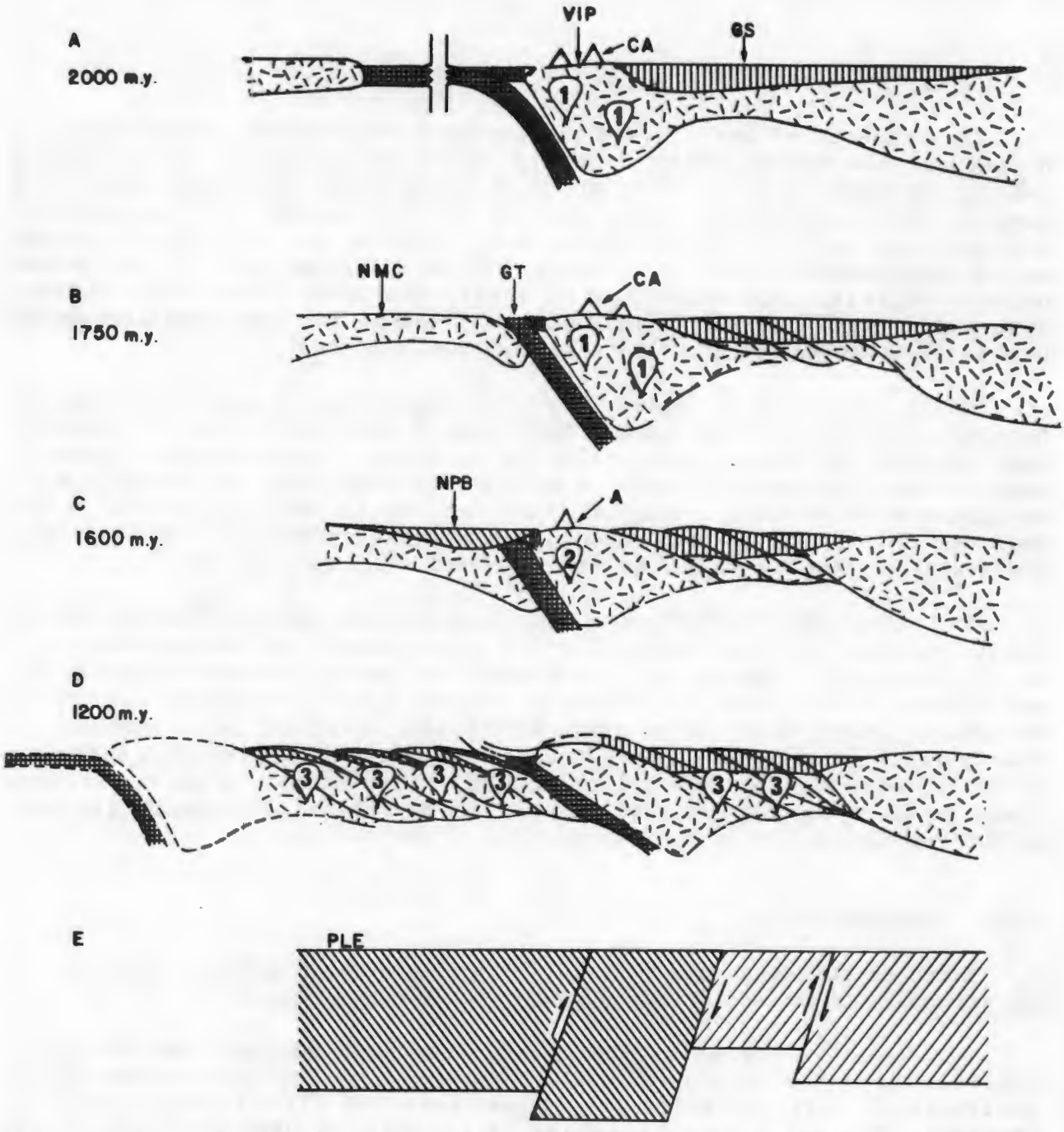

Fig. 14.5 Series of schematic diagrams illustrating a hypothetical sequence of events leading to the present-day configurations of metamorphosed supracrustal and intrusive rocks in the western NMC. VIP - Vioolsdrif Igneous Province; CA - calc-alkaline volcanism; GS - Grunau Sequence; NMC - Namaqualand "microcontinent"; GT - Groothoek thrust zone; A - acid-dominated volcanism; NPB - Namaqualand "peripheral basin"; (1) - calc-alkaline intrusive rocks; (2) - acid plutonism; (3) main stage of intrusion of granitic rocks. Section E is a schematic block diagram showing the interpretation by de Beer and Meyer (1983) of the present crustal tectonic and geophysical situation in the western NMC. Close hatching represents the Namaqua-Natal Mobile Belt and wider hatching the Kaapvaal Craton. PLE - present level of erosion.

River Group with the majority of mafic rocks concentrated on the southern side of the Vioolsdrif domain. Mafic rocks at Groot Swartkop, along this belt, have a whole rock Pb-Pb age of 2000 Ma (Welke,pers. comm.) supporting the above model. The environment probably resembled the present-day Andean margin of South America with limited fore-arc and back-arc development, accounting for the absence of large thicknesses of greywacke assemblages. A similar model was considered by Botha and Grobler (1979) to explain both sedimentation and tectonism in eastern Namaqualand but rejected due to the large time gap between Matsap and Kheis sedimentation (2000 - 1800 Ma) and the Namaqua tectonothermal episode (1400 - 900 Ma).

(2) At approximately 1750 Ma, a micro(?)-continent collided with the supercontinental margin and was partially subducted/consumed in the region where the Groothoek Thrust is now located and along extensions of this lineament into the Kakamas-Kenhardt area (Fig. 14.5b). Continental collision may have led to the early F1 deformation within the Grunau Sequence and Matsap lithologies (sensu Stowe,1983) and the intrusion of G1 granitic rocks (Stowe, op.cit.) in this domain as well as the initiation of the late acid igneous phase of the Vioolsdrif Suite (Reid,1982). It is also conceivable that the northern high-grade metamorphic belt, involving exclusively lithologies of the Grunau Sequence and their south-eastern extensions in the Upington-Prieska area (Fig14.6), formed during this event. Metapelitic rocks of this domain in the Kakamas-Kenhardt area show the imprint of two distinct high-grade events - an early granulite event and a younger amphibolite event (Harris, pers. comm.) whereas metapelitic rocks within the Bushmanland and Okiep Groups (i.e. on the microcontinent) only show one high-grade imprint (Albat,1984; Waters,pers. comm.). The microcontinent comprised primarily newly-formed silicic S-type granitic material (2000 - 1800 m.y. old). Remnants of mafic rocks along the Groothoek Thrust may represent an ophiolite or "proto-ophiolite" belt associated with the collision event. Much of the suture-belt melange may be essentially hidden (i.e. covered by overriding thrust sheets) or cryptic (i.e. squeezed tectonically upward and lost during subsequent erosion) (Dickinson, 1974) and thus not readily observed in the present-day crustal exposures. The boundary of the two proposed continental fragments approximates that defined by Joubert (1976) as separating "Kheis" from "Namaqua" lithologies.

(3) Subsequent to the collision-accretion event, a period of extensional tectonic activity occurred predominantly to the south of the Groothoek Thrust (i.e. on the colliding microcontinent). Lithospheric rifting, subsidence, acid-dominated subaerial volcanism and the deposition of siliclastic sediments comprising a transgressive sequence of feldspathic sandstones, psammitic and pelitic sediments containing fining-upwards cycles occurred in a shallow-marine continental setting (Fig. 14.5c). This was closely followed by a transgressive-regressive cycle of sedimentation within a more restricted basin with no, or extremely limited, access to the open marine environment. This latter basin has present-day (post-tectonic) dimensions of approximately 100 x 300 km and sediment thickness is insubstantial (500 - 1000 m). Bimodal, acid-dominated volcanism persisted and distinctive K-enriched, Na-, Ca-depleted shales and siliceous cherts were deposited. Metals leached from the acid volcanics either by hydrothermal or weathering processes concentrated in highly restricted anaerobic sub-basins where they precipitated as

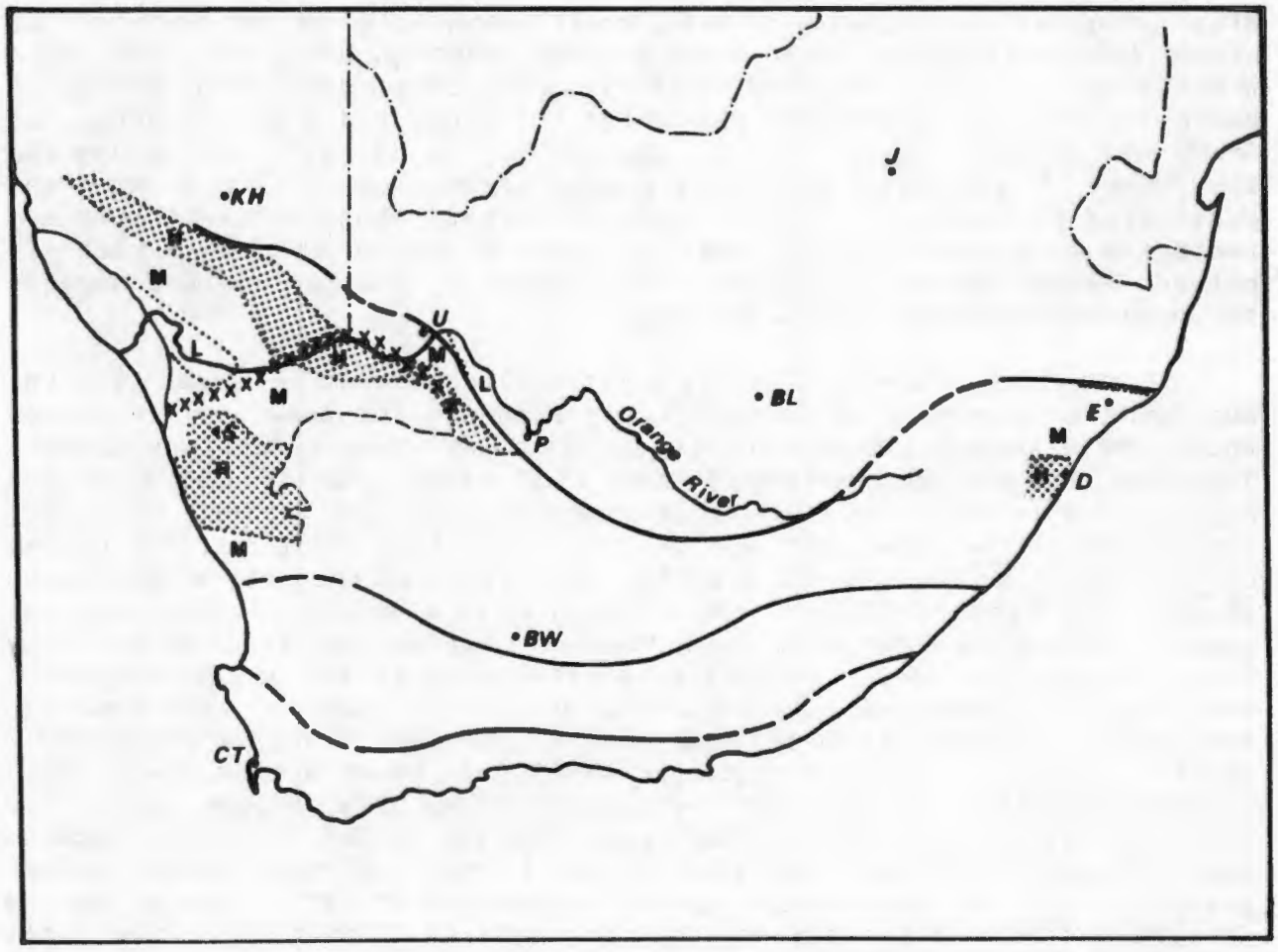

Fig. 14.6 Regional map showing the major metamorphic belts within the NMC. L - low-grade; M - medium-grade; H - high-grade metamorphism. Crosses designate the extent of the major pegmatite belt. For further explanation of localities, see Fig. 14.1.

manganiferous iron formations and base metal sulphide deposits. A whole rock Nd-Sm isochron age for amphibolites at Gamsberg indicates a 1600 Ma age for this continental volcano-sedimentary sequence (Betton,1984). These two sedimentary sequences represent a peripheral basin developed during and/or subsequent to collision between a rifted continental margin (microcontinent) and continental margin arc (supercontinent) (sensu Dickinson,1974; Fig. 14.4). The supracrustal sequences in the western NMC are thus predominantly shallow-water deposits accumulated in an ensialic environment as opposed to eugeosynclinal deep-water sediments deposited partly on oceanic crust as was required in the plate-tectonic model of Botha and Grobler (1979).

(4) A major high-T, low-P tectonothermal event (or events) followed, taking place over a long timespan between 1500 and 900 Ma, probably activated by the resumption of subduction to the north-west (Rehoboth Magmatic Arc, Watters,1976) and perhaps to the south and south-west of the present-day outcrop area of the western NMC (de Beer and Meyer,1983) (Fig. 14.5d). This tectonothermal event affected both the "supercontinent" in the domain containing the Grunau Sequence and the colliding "microcontinent", whereas the intervening calc-alkaline volcano-plutonic Vioolsdrif complex apparently resisted the effects of this event in its central parts. This is possibly due to its thickened batholithic nature (see Section 14.3) and to being surrounded by areas of thinner, more easily deformed crust to the north and south. Rather than involving subduction of oceanic crust and the formation of a calc-alkaline suite of lithologies, the process is thought to have involved underthrusting and subduction of continental crust (sensu Kroner,1981) with the formation of numerous suites of syntectonic and post-tectonic granitic rocks (e.g. the Little Namaqualand and Spektakel Suites). A major high-temperature thermal dome developed in the western NMC (now exposed in the Namaqualand highlands) as a result of the underthrusting process and large-scale partial-melt granite intrusion (Reid and Barton,1983) (Fig. 14.6). Associated deformation, incorporating both supracrustal sequences and augen gneiss basement, was initially thrust- and isoclinal fold-dominated (F2, Joubert,1971) with major reactivation occurring along the collision zone, resulting in the formation of the Groothoek Thrust zone. Subsequent intrusive/deformational episodes involved an increasing component of lateral shear (F3, F4, Joubert,1974) and slightly lower temperatures and pressures. A final "magmatic" episode associated with cooling of the thermal dome between 1000 and 900 Ma, resulted in the formation of the major 500 km long pegmatite belt stretching from the Steinkopf area along the Orange River to Augrabies and south to Kenhardt (Gevers et al.,1937; Hugo,1969) peripheral to the dome.

REFERENCES

Albat, H. M. (1979) Preliminary report on the geology of the Kliprand area Namaqualand. Ann. Rep. Precambr. Res. Unit, Univ. Cape Town, **16**, 47-57.

Albat, H. M. (1980) The Kliprand area - a major charnockite province in Namaqualand. Ann. Rep. Precambr. Res. Unit, Univ. Cape Town, **17**, 49-64.

Albat, H.M. (1984) The Proterozoic granulite facies terrane around Kliprand, Namaqualand Metamorphic Complex. Bull. Precambr. Res. Unit, Univ. Cape Town, **33**, 382p.

Altschuler, Z.S., Dwornik, E.J. and Kramer, H. (1963) Transformation of montmorillonite to kaolinite during weathering. Science, **141**, 148-149.

Anderson, J.L., Cullers, R.L. and Van Schmus, W.R. (1980) Anorogenic metaluminous and peraluminous granite plutonism in the mid-Proterozoic of Wisconsin. Contrib. Mineral. Petrol., **74**, 311-328.

Ashworth, J.R. and Chinner, G.A. (1978) Coexisting garnet and cordierite in migmatites from the Scottish Caledonides. Contrib. Mineral. Petrol., **65**, 379-394.

Bacon, C.R., MacDonald, R., Smith, R.L. and Baedecker, P.A. (1981) Pleistocene high-silica rhyolites of the Coso volcanic field, Inyo County, California. J. Geophys. Res., **86**, B11, 10223-10241.

Balashov, Y.A. and Pozharitskaya, L.K. (1968) Factors governing the behavior of rare-earth elements in the carbonatite process. Geochem. International, **5**, 271-288.

Balashov, Y.A., Ronov, A.B., Migdisov, A.A. and Turanskaya, N.V. (1964) The effect of climate and facies environment on the fractionation of the rare earths during sedimentation. Geochem. International, **1**, 951-969.

Banerjee, D.M., Basu, P.C. and Srivastava, N. (1980) Petrology, mineralogy, geochemistry, and origin of the Precambrian Aravallian phosphate deposits of Udaipur and Jhabua, India. Econ. Geol., **75**, 1181-1199.

Barbey, P. and Cuney, M. (1982) K, Rb, Sr, Ba, U and Th geochemistry of the Lapland granulites (Fennoscandia). LILE fractionation controlling factors. Contrib. Mineral. Petrol., **81**, 304-316.

Barker, F. (1981) Introduction to special issue on granites and rhyolites: a commentary for the nonspecialist. J. Geophys. Res., **86**, B11, 10131-10135.

Barker, F., Wones, D.R., Sharp, W.N. and Desborough, G.A. (1975) The Pikes Peak batholith, Colorado Front Range, and a model for the origin of the gabbro - anorthosite - syenite - potassic granite suite. Precambr. Res., 2, 97-160.

Barrett, T.J. (1981) Chemistry and mineralogy of Jurassic bedded chert overlying ophiolites in the north Appenines, Italy. Chem. Geol., 34, 289-317.

Barton, E.S. (1983) Reconnaissance isotopic investigations in the Namaqua mobile belt and implications for Proterozoic crustal evolution - Namaqualand geotraverse. Spec. Publ. geol. Soc. S. Afr., 10, 45-66.

Beeson, R. (1980) The relationship of siltstone geochemistry to sedimentary environments and uranium mineralisation in the Beaufort Group, Cape Province, South Africa. Chem. Geol., 30, 81-107.

Berner, R.A. (1973) Phosphate removal from sea water by adsorption on volcanogenic ferric oxides. Earth Planet. Sci. Letters, 18, 77-86.

Bertrand, J.M. (1975) Granitoids and deformation sequence in the Goodhouse-Henkries area. A new interpretation between rocks in the Vioolsdrif-Goodhouse area and the Namaqualand and Bushmanland gneisses. Ann. Rep. Precambr. Res. Unit, Univ. Cape Town, 13, 61-70.

Betton, P.J. (1984) Nd and Sr isotopic evidence for the evolution of the Namaqualand Mobile Belt, southern Africa. Abstr., Conf. on Middle to Late Proterozoic Crustal Evolution, Precambr. Res. Unit, Univ. Cape Town, p7.

Beukes, G.J. (1973) 'n Geologiese ondersoek van die gebied suid van Warmbad Suidwes-Afrika, met spesiale verwysing na die metamorf-magmatiese assosiasies van die Voorkambriese gesteentes. Unpubl. D.Sc. thesis, Univ. Orange Free State, 333p.

Bhatia, M.R. (1983) Plate tectonics and geochemical composition of sandstones. J. Geol., 91, 611-627.

Bhatia, M.R. and Taylor, S.R. (1981) Trace-element geochemistry and sedimentary provinces : a study from the Tasman Geosyncline, Australia. Chem. Geol., 33, 115-125.

Blatt, H., Middleton, G.V. and Murray, R.C. (1980) Origin of Sedimentary Rocks. Prentice-Hall Inc., Englewood Cliffs, New Jersey, 782p.

Blignault, H.J. (1977) Structural-metamorphic imprint on part of the Namaqua mobile belt in South West Africa. Bull. Precambr. Res. Unit, Univ. Cape Town, 23, 197p.

Blignault, H.J., Marais, J.A.H., van der Merwe, S.W., van Aswegen, G. and Muller, J.A. (1980) The Namaqualand Geotraverse. Annex. to Spec. Publ. geol. Soc. S. Afr., 10.

Blignault, H.J., van Aswegen, G., van der Merwe, S.W. and Colliston, W.P. (1983) The Namaqua geotraverse and environs: part of the Proterozoic Namaqua mobile belt. Spec. Publ. geol. Soc. S. Afr., 10, 1-30.

Boles, J.R. and Surdam, R.C. (1979) Diagenesis of volcanogenic sediments in a Tertiary saline lake; Wagon Bed Formation, Wyoming. Am. J. Sci., 279, 832-853.

Bonatti, E., Fisher, D.E., Joensuu, O., Rydell, H.S. and Beyth, M. (1972) Iron-manganese-barium deposit from the northern Afar Rift (Ethiopia). Econ. Geol., 67, 717-730.

Bostrom, K. (1973) The origin and fate of ferromanganoan active ridge sediments. Stockholm Contrib. Geol., 27, 149-243.

Botha, B.J.V. and Grobler, N.J. (1979) Models for the geotectonic evolution of the Middle to Late Precambrian Namaqua Mobile Belt in eastern Namaqualand, South Africa. Precambr. Res., 10, 21-41.

Bowen, N.L. (1928) The Evolution of the Igneous Rocks. Princeton University Press, Princeton, New Jersey, 332p.

Bradshaw, M.J. (1975) Origin of montmorillonite bands in the Middle Jurassic of eastern England. Earth Planet. Sci. Letters, 26, 245-252.

Bramlette, M.N. (1946) The Monterey formation of California and the origin of its siliceous rocks. U.S. geol. Surv. Prof. Paper, 212, 57p.

Brink, W.C. (1950) The geology, structure and petrology of the Nuwerus area, Cape Province. Ann. Univ. Stellenbosch, 26, 97-221.

Brown, R.E., Stevens, B.P.J., Willis, I.L., Stroud, W.J., Bradley, G.M. and Barnes, R.G. (1983) Quartzo-feldspathic rocks. Rec. geol. Surv. New S. Wales, 21, part 1, 127-226.

Bryan, W.B., Finger, L.W. and Chayes, F. (1969) Estimating propors in petrographic mixing equations by least-squares approximation. Science, 163, 926-927.

Bultitude, R.J. and Wyborn, L.A.I. (1982) Distribution and geochemistry of volcanic rocks in the Duchess-Urandangi region, Queensland. B.M.R. J. Austr. Geol. Geophys., 7, 99-112.

Burt, D.M., Sheridan, M.F., Bikun, J.V. and Christiansen, E.H. (1982) Topaz rhyolites - distribution, origin, and significance for exploration. Econ. Geol., 77, 1818-1836.

Button, A. (1981) The older sedimentary-volcanic basins. In: Hunter, D.R. (ed.). Developments in Precambrian Geology, 2. Precambrian of the Southern Hemisphere. Elsevier Scientific Publishing Company, Amsterdam, 501-536.

Cameron, E.M. and Garrels, R.M. (1980) Geochemical compositions of some Precambrian shales from the Canadian Shield. Chem. Geol., **28**, 181-197.

Chappell, B.W. and White, A.J.R. (1974) Two contrasting granite types. Pac. Geol., **8**, 173-174.

Chayes, F. (1972) RKFNSYS version 3 of the users guide to the rock information system. Rep. Carnegie Inst., Washington D.C. (unpubl.).

Chinner, G.A. and Fox, J.S. (1974) The origin of cordierite-anthophyllite rocks in the Land's End aureole. Geol. Mag., **111**, 397-408.

Christiansen, E.H., Burt, D.M., Sheridan, M.F. and Wilson, R.T. (1983) The petrogenesis of topaz rhyolites from the western United States. Contrib. Mineral. Petrol. **83**, 16-30.

Clark, M.D. (1979) Geology of the older Precambrian rocks of the Grand Canyon. Part III. Petrology of mafic schists and amphibolites. Precambr. Res., **8**, 277-302.

Clifford, T.N., Gronow, J., Rex, D.C. and Burger, A.J. (1975a) Geochronological and petrogenetic studies of high grade metamorphic rocks intrusives in Namaqualand, South Africa. J. Petrol.,**16**, 154-188.

Clifford, T.N., Stumpfl, E.F. and McIver, J.R. (1975b) A sapphirine-cordierite-bronzite-phlogopite paragenesis from Namaqualand, South Africa. Mineral. Mag., **40**, 347-356.

Clifford, T.N., Stumpfl, E.F., Burger, A.J., McCarthy, T.S. and Rex, D.C. (1981). Mineral-chemical and isotopic studies of Namaqualand granulites, South Africa : a Grenville analogue. Contrib. Miner. Petrol., **77**, 225-250.

Cobbold, P.R. and Quinquis, H. (1980) Development of sheath folds in shear regimes. J. Struct. Geol. **2**, 119-126.

Coetzee, C.B. (1940) Sillimanite-corundum rock : a metamorphosed bauxite in Namaqualand, South Africa. Trans. R. Soc. S. Afr., **28**, 199-205.

Coetzee, C.B. (1941) An anorthite-epidote-garnet hornfels from Namaqualand, South Africa. Mineral. Mag. **26**, 134-139.

Coetzee, C.B. (1942a) The petrology of the Goodhouse - Pella area, Namaqualand, South Africa. Trans. geol. Soc. S. Afr., **44**, 167-206.

Coetzee, C.B. (1942b) Metamorphosed sediments from the Goodhouse - Pella area, Namaqualand, South Africa. Trans. R. Soc. S. Afr., **29**, 91-112.

Coetzee, C.B. (1958) Manganiferous iron ore, haematite, barite and sillimanite on Gams (Portion 1), Namaqualand. Bull. geol. Surv. S. Afr., **28**, 29p.

Collerson, K.D. (1975) Contrasted patterns of K/Rb distribution in Precambrian high grade metamorphic rocks from central Australia. J. geol. Soc. Austr., **22**, 145-158.

Collerson, K.D. and Fryer, B.J. (1978) The role of fluids in the formation and subsequent development of early continental crust. Contrib. Mineral. Petrol., **67**, 151-167.

Collins, W.J., Beams, S.D., White, A.J.R. and Chappell, B.W. (1982) Nature and origin of A-type granites with particular reference to southeastern Australia. Contrib. Mineral. Petrol., **80**, 189-200.

Condie, K.C. (1982a) Early and middle Proterozoic supracrustal successions and their tectonic settings. Am. J. Sci., **282**, 341-357.

Condie, K.C. (1982b) Plate Tectonics and Crustal Evolution. Pergamon Press, New York, 2nd edition, 310p.

Condie, K.C. (1982c) Plate-tectonics model for Proterozoic continental accretion in the southwestern United States. Geology, **10**, 37-42.

Cook, P.J. and McElhinny, M.W. (1979) A reevaluation of the spatial and temporal distribution of sedimentary phosphate deposits in the light of plate tectonics. Econ. Geol., **74**, 315-330.

Couch, E.L. and Grim, R.E. (1968) Boron fixation by illites. Clays and Clay Minerals, **16**, 249-256.

Crerar, D.A., Namson, J., So Chyi, M., Williams, L. and Feigenson, M.D. (1982) Manganiferous cherts of the Franciscan Assemblage: I. General geology, ancient and modern analogues, and implications for hydrothermal convection at oceanic spreading centres. Econ. Geol., **77**, 519-540.

Croxford, N.J.W. (1964) Origin and significance of volcanic potassic-rich rocks from Mount Isa. Trans. Inst. Min. Metall., **74**, 33-43.

Currie, K.L. (1971) The reaction: 3 cordierite = 2 garnet + 4 sillimanite + 5 quartz as a geological thermometer in the Opinicon Lake region, Ontario. Contrib. Mineral. Petrol., **33**, 215-226.

Davidson, L.R. and Mathison, C.I. (1974) Aluminous orthopyroxenes and associated cordierites, garnets and biotites from granulites of the Quairading district, Western Australia. Neues Jahrb. Mineral. Mh., 272-287.

Davis, R.A. (1983) Depositional systems. A genetic approach to sedimentary geology. Prentice-Hall Inc., Englewood Cliffs, New Jersey, 669p.

Deb, M. (1980) Genesis and metamorphism of two stratiform massive sulfide deposits at Ambaji and Deri in the Precambrian of western India. Econ. Geol., 75, 572-591.

de Beer, J.H. and Meyer, R. (1983) Geoelectrical and gravitational characteristics of the Namaqua-Natal mobile belt and its boundaries. Spec. Publ. geol. Soc. S. Afr., 10, 91-100.

Deer, W.A., Howie, R.A. and Zussman, J. (1971) An Introduction to the Rockforming Minerals. Longman, London, 528p.

de Jager, D.H. (1963) Sillimanite in Namaqualand : review of reserves and report on some low-grade deposits. Bull. geol. Surv. S. Afr., 40, 42p.

de Jager, D.H. and Simpson, N. (1962) Wollastonite near Garies, Namaqualand. Ann. geol. Surv. S. Afr., 1, 127-135.

de Jager, D.H. and von Backstrom, J.W. (1961) The sillimanite deposits in Namaqualand near Pofadder. Bull. geol. Surv. S. Afr., 33, 49p.

de la Roche, H. (1966) Sur l'existence de plusieurs facies geochimiques dans les schistes paleozoiques des Pyrenees Luchonnaises. Geol. Rundschau 55, 274-301.

de la Roche, H. (1981) Chemistry of ultramafic and mafic rocks related to their mineral assemblages in the multicationic F-E-D-A tetrahedron and derived diagrams. Chem. Geol., 34, 181-193.

de la Roche, H., Leterrier, J., Grandclaude, P. and Marchal, M. (1980) A classification of volcanic and plutonic rocks using R1-R2- diagram and major-element analyses - its relationships with current nomenclature. Chem. Geol., 33, 183-210.

de Rozen-Spence, A. (1969) Genese des roches a cordierite-anthophyllite des gisements cupro-zinciferes de la region de Rouyn-Noranda, Quebec, Canada. Can. J. Earth Sci., 6, 1339-1344.

Derrick, G.M. (1977) Metasomatic history and origin of uranium mineralization at Mary Kathleen, northwest Queensland. B.M.R. J. Austr. Geol. Geophys. 2, 123-130.

de Villiers, J. and Sohnge, P.G. (1959) The geology of the Richtersveld. Mem. geol. Surv. S. Afr., **48**, 266p.

de Waard, D. (1965) A proposed subdivision of the granulite facies. Am. J. Sci., **263**, 455-461.

Dickinson, W.R. (1974) Plate tectonics and sedimentation. In: Dickinson, W.R. (ed.) Tectonics and Sedimentation. Spec. Publ. Soc. Econ. Paleontologists and Mineralogists, 22, 1-27.

Dixon, W.J. (ed.) (1981) BMDP Statistical Software 1981. Univ. California Press, Berkeley, 726p.

Drury, S.A. (1973) The geochemistry of Precambrian granulite facies rocks from the Lewisian complex of Tiree, Inner Hebrides, Scotland. Chem. Geol., **11**, 167-188.

Ellis, D.J., Sheraton, J.W., England, R.N. and Dallwitz, W.B. (1980) Osumilite-sapphirine-quartz granulites from Enderby Land Antarctica - mineral assemblages and reactions. Contrib. Mineral. Petrol., 72, 123-143.

Eriksson, K.A., McCarthy, T.S. and Truswell, J.F. (1975) Limestone formation and dolomitization in a Lower Proterozoic succession from South Africa. J. Sedim. Petrol., 45, 604-614.

Erlank, A.J., Smith, H.S., Marchant, J.W., Cardoso, M.P. and Ahrens, L.H. (1978) Zirconium B-O. In: Wedepohl, K.H. (ed.). Handbook of Geochemistry, **II/5**, Springer-Verlag Publishing Company, Berlin.

Eskola, P. (1914) On the petrology of Orijarvi region, southwest Finland. Bull. Comm. Geol. Finlande, **44**, 109-143.

Eugster, H.P. (1969) Inorganic bedded cherts from the Magadi area, Kenya. Contrib. Mineral. Petrol., **22**, 1-31.

Eugster, H.P. (1980) Geochemistry of evaporitic lacustrine deposits. Ann. Rev. Earth Planet. Sci., **8**, 35-63.

Ewart, A.A. (1979) A review of the mineralogy and chemistry of Tertiary-Recent dacitic, latitic, rhyolitic and related salic volcanic rocks. In: Barker, F. (ed.) Trondhjemites, Dacites and Related Rocks. Elsevier Scientific Publishing Company, Amsterdam, 13-121.

Ferry, J.M. and Spear, F.S. (1978) Experimental calibration of the partitioning of Fe and Mg between biotite and garnet. Contrib. Mineral. Petrol., **66**, 113-117.

Fisher, M.J. and Jeans, C.V. (1982) Clay mineral stratigraphy in the Permo-Triassic red bed sequences of BNOC 72/10-1A, Western Approaches, and the South Devon coast. Clay Minerals, **17**, 79-89.

Flood, R.H. and Shaw, S.E. (1975) A cordierite-bearing granite suite from the New England batholith, N.S.W., Australia. Contrib. Mineral. Petrol., **52**, 157-164.

Floyd, P.A. (1965) Metasomatic hornfelses of the Land's End aureole at Tater-du, Cornwall. J. Petrol., **6**, 223-245.

Floyd, P.A. (1975) Exotic hornfelses from the Land's End aureole. Geol. Mag., **112**, 315-319.

Floyd, P.A. and Winchester, J.A. (1975) Magma type and tectonic setting discrimination using immobile elements. Earth Planet. Sci. Letters, **27**, 211-218.

Folk, R.L. (1973) Evidence for peritidal deposition of Devonian Caballos Novaculite, Marathon Basin, Texas. Bull. Am. Assoc. Petroleum Geologists, **57**, 702-725.

Frick, C. and Coetzee, C.B. (1974) The mineralogy and petrology of the sillimanite deposits west of Pofadder, Namaqualand. Trans. geol. Soc. S. Afr., **77**, 169-184.

Frick, C. and Wheelock, G. (1983) Evidence for a sedimentary origin of the pink gneisses of the Kokerberg Formation, Korannaland. Trans. geol. Soc. S. Afr., **86**, 81-86.

Fromberg, E.D. (1980) Origin of ultrapotassic rhyolite. Dokl. Akad. Nauk SSSR, **253**, 684-687.

Fryer, B.J. (1977) Rare earth evidence in iron-formations for changing Precambrian oxidation states. Geochim. Cosmochim. Acta, **41**, 361-367.

Galan, E. and Ferrero, A. (1982) Palygorskite-sepiolite clays of Lebrija, southern Spain. Clays and Clay Minerals, **30**, 191-199.

Garrels, R.M. and MacKenzie, F.T. (1971) Evolution of Sedimentary Rocks. Norton, New York, 397p.

Garrison, J.R. (1981) Metabasalts and metagabbros from the Llano Uplift, Texas: petrologic and geochemical characterization with emphasis on tectonic setting. Contrib. Mineral. Petrol., **78**, 459-475.

Geringer, G.J. (1973) Die geologie van die Argiese gesteentes en jongere formasies in die gebied wes van Upington met spesiale verwysing na die verskillende granietvoorkomstes. Unpubl. D.Sc. thesis, Univ. Orange Free State, 203p.

Gevers, T.W., Partridge, F.C. and Joubert, G.K. (1937) The pegmatite area south of the Orange River in Namaqualand. Mem. geol. Surv. S. Afr., **31**, 180p.

Ghent, E.D. (1976) Plagioclase-garnet-Al_2SiO_5-quartz: a potential geobarometer-geothermometer. Amer. Mineral., **61**, 710-714.

Gibson, T.G. and Towe, K.M. (1971) Eocene volcanism and the origin of horizon A. Science, **172**, 152-154.

Glen, R.A. and Laing, W.P. (1975) The significance of sedimentary structures in the Willyama Complex. Proc. Austr. Inst. Min. Metall., **256**, 15-20.

Goldberg, E.D., Koide, M., Schmitt, R.A. and Smith, H. (1963) Rare-earth distribution in the marine environment. J. Geophys. Res., **68**, 4209-4217.

Gole, M.J. and Klein, C. (1981) Banded iron-formations through much of Precambrian time. J. Geol., **89**, 169-183.

Gordon, T.M. and Greenwood, H.J. (1971) The stability of grossularite in H2O-CO2 mixtures. Am. Mineral., **56**, 1674-1688.

Graf, D.L. (1962) Minor element distribution in sedimentary carbonate rocks. Geochim. Cosmochim. Acta, **26**, 849-856.

Grant, J.A. (1968) Partial melting of common rocks as a possible source of cordierite-anthophyllite bearing assemblages. Am. J. Sci., **266**, 908-931.

Grant, J.A. (1973) Phase equilibria in high-grade metamorphism and partial melting of pelitic rocks. Am. J. Sci., **273**, 289-317.

Gray, C.M. (1977) The geochemistry of central Australian granulites in relation to the chemical and isotopic effects of granulite facies metamorphism. Contrib. Mineral. Petrol., **65**, 79-89.

Green, T.H. (1976) Experimental generation of cordierite- or garnet-bearing granitic liquids from a pelitic composition. Geology, **4**, 85-88.

Green, T.H. (1977) Garnet in silicic liquids and its possible use as a P-T indicator. Contrib. Mineral. Petrol., **65**, 59-67.

Greenwood, H.J. (1976) Metamorphism at moderate temperatures and pressures. In: Bailey, D.K. and MacDonald, R. (eds.). The Evolution of the Crystalline Rocks. Academic Press, London, 261-332.

Gross, G.A. (1980) A classification of iron formations based on depositional environments. Can. Mineral., **18**, 215-222.

Gross, G.A. and McLeod, C.R., (1980) A preliminary assessment of the chemical composition of iron formations in Canada. Can. Mineral., **18**, 223-229.

Gulbrandsen, R.A. (1966) Chemical composition of phosphorites of the Phosphoria formation. Geochim. Cosmochim. Acta, **30**, 769-778.

Gulbrandsen, R.A. and Cremer, M. (1970) Coprecipitation of carbonate and phosphate from sea water. U.S. geol. Surv. Prof. Paper, **700-C**, C125-C126.

Gunn, B.M. (1971) Trace element partition during olivine fractionation of Hawaiian basalts. Chem. Geol., **8**, 1-13.

Halbich, I.W. (1978) Minor structures in gneiss and the origin of steep structures in the Okiep Copper District. In: Verwoerd, W.J. (ed.). Mineralization in metamorphic terranes. Spec. Publ. geol. Soc. S. Afr., **4**, 297-322.

Harder, H. (1959) Contribution to the geochemistry of boron: II Boron in sediments. Nachr. Akad. Wiss. Gottingen: II Math-Physik, **6**, 123-183.

Hart, S.R. and Davis, K.E. (1978) Nickel partitioning between olivine and silicate melt. Earth Planet. Sci. Letters, **40**, 203-219.

Haskin, L.A., Wildeman, T.R., Frey, F.A., Collins, K.A., Keedy, C.R. and Haskin, M.A. (1966) Rare earths in sediments. J. Geophys. Res., **71**, 6091-6105.

Heier, K.S. (1978) The distribution and redistribution of heat producing elements in the continents. Phil. Trans. R. Soc. London, **A288**, 393-400.

Hensen, B.J. and Green, D.H. (1971) Experimental study of the stability of cordierite and garnet in pelitic compositions at high pressures and temperatures. I. Compositions with excess alumina-silicate. Contrib. Mineral. Petrol., **35**, 331-354.

Herd, R.K. (1973) Sapphirine and kornerupine occurrences within the Fiskenaesset Complex. Gronlandse Geol. Undersogelse Rapp., **51**, 65-71.

Hermans, G.A.E.M., Hakstege, A.L., Jansen, J.B.H. and Poorter, R.P.E. (1976) Sapphirine occurrence near Vikesa in Rogaland, southwestern Norway. Norsk Geologisk Tidsskrift, **56**, 397-412.

Hickey, R.L. and Frey, F.A. (1982) Geochemical characteristics of boninite series volcanics: implications for their source. Geochim. Cosmochim. Acta, **6**, 2099-2115.

Hickman, A.H. and Wright, A.E. (1983) Geochemistry and chemostratigraphical correlation of slates, marbles and quartzites of the Appin Group, Argyll, Scotland. Trans. R. Soc. Edinburgh: Earth Sci., **73**, 251-278.

Hicks, J.A. (1983) A mineralogical study of gahnite from Namaqualand, South Africa. Unpubl. B.Sc(Hons). thesis, Univ. Cape Town, 113p.

Hildreth, W. (1979) The Bishop Tuff: evidence for the origin of compositional zonation in silicic magma chambers. Spec. Paper geol. Soc. Am., **180**, 43-74.

Hildreth, W. (1981) Gradients in silicic magma chambers: implications for lithospheric magmatism. J. Geophys. Res., **86**, B11, 10153-10192.

Holdaway, M.J. and Lee, S.M. (1977) Fe-Mg cordierite stability in high-grade pelitic rocks based on experimental, theoretical and natural observations. Contrib. Mineral. Petrol., **63**, 175-198.

Holm, P.E. (1982) Non-recognition of continental tholeiites using the Ti-Y-Zr diagram. Contrib. Mineral. Petrol., **79**, 308-310.

Hughes, C.J. (1976) Volcanogenic cherts in the late Precambrian Conception Group, Avalon Peninsula, Newfoundland. Can. J. Earth Sci., **13**, 512-519.

Hugo, P.J. (1969) The pegmatites of the Kenhardt and Gordonia Districts, Cape Province. Mem. geol. Surv. S. Afr., **58**, 94p.

Hunter, D. R. (ed.) (1981) Developments in Precambrian geology, vol.2. Precambrian of the southern hemisphere. Elsevier Scientific Publishing Company, Amsterdam, 882p.

Hurley, P.M. and Rand, J.R. (1969) Pre-drift continental nucleii. Science, **164**, 1229-1232.

Iijima, A. and Tada, R. (1981) Silica diagenesis of Neogene diatomaceous and volcaniclastic sediments in northern Japan. Sedimentology, **28**, 185-200.

Irion, G. and Muller, G. (1968) Huntite, dolomite, magnesite and polyhalite of Recent age from Tuz Golu, Turkey. Nature, **220**, 1309-1310.

Irving, A.J. (1974) Geochemical and high pressure experimental studies of garnet pyroxenite and pyroxene granulite xenoliths from the Delegate basaltic pipes, Australia. J. Petrol., **15**, 1-40.

Jack, A.M. (1980) The geology of western Namaqualand. Bull. Precambr. Res. Unit, Univ. Cape Town, **29**, 173p.

Jackson, M.P.A. (1976) High grade metamorphism and migmatization of the Namaqua Metamorphic Complex around Aus in the southern Namib Desert, South West Africa. Bull. Precambr. Res. Unit, Univ. Cape Town, **18**, 299p.

James, H.L. (1969) Comparison between Red Sea deposits and older ironstone and iron formation. In: Degens, E.T. and Ross, D.A. (eds.) Hot Brines and Recent Heavy Metal Deposits in the Red Sea. Springer-Verlag, Berlin, 525-532.

James, R.S., Grieve, R.A.F. and Pauk, L. (1978) The petrology of cordierite-anthophyllite gneisses and associated mafic and pelitic gneisses at Manitouwadge, Ontario. Am. J. Sci., **278**, 41-63.

Jansen, H. (1960) The geology of the Bitterfontein area, Cape Province. Geol. Surv. S. Afr., Expl. of sheet 253 (Bitterfontein).

Jansen, H. (1974) The Soutpansberg trough - an aulacogen. Trans. geol. Soc. S. Afr., **78**, 129-136.

Jenner, G.A. (1981) Geochemistry of high-Mg andesites from Cape Vogel, Papua New Guinea. Chem. Geol., **33**, 307-332.

Joubert, P. (1971) The regional tectonism of the gneisses of part of Namaqualand. Bull. Precambr. Res. Unit, Univ. Cape Town, **10**, 220p.

Joubert, P. (1974a) 1:100,000 maps of the Pofadder and Aggeneys sheets. Precambr. Res. Unit, Univ. Cape Town.

Joubert, P. (1974b) Wrench-fault tectonics in the Namaqualand Metamorphic Complex. Bull. Precambr. Res. Unit, Univ. Cape Town, **15**, 17-23.

Joubert, P. (1976) The relationship between the Namaqualand Metamorphic Complex and the Kheis Group. S. Afr. J. Sci., **72**, 312-313.

Joubert, P. (1981) The Namaqualand Metamorphic Complex. In: Hunter, D.R. (ed.). Developments in Precambrian Geology, 2. Precambrian of the Southern Hemisphere. Elsevier Publishing Company, Amsterdam, 671-705.

Kaiser, H.F. (1958) The varimax criteria for analytical relation in factor analysis. Psychology, **23**, 187-200.

Kamineni, D.C. (1979) Metasedimentary cordierite-gedrite rocks of Archaean age near Yellowknife, Canada. Precambr. Res., **9**, 289-301.

Kerrick, D.M. (1972) Experimental determination of muscovite and quartz stability with $PH_2O < PTOTAL$. Am. J. Sci., **272**, 946-958.

Kimberley, M.M. (1978) Palaeoenvironmental classification of iron formations. Econ. Geol., **73**, 215-229.

Kimberley, M.M. (1979) Geochemical distinctions among environmental types of iron formations. Chem. Geol., **25**, 185-212.

Kitsul, V.I., Brovkin, A.A., Lutts, B.G., Parinova, Z.K. and Kuznetskova, I.K. (1972) A find of kornerupine on the Aldan Shield. Dokl. Akad. Nauk SSSR, **206**, 146-149.

Kleyenstuber, A.S.E. (1982) A review of the geology and mining of the Kalahari manganese field. Proc. 12th CMMI Congress, S. Afr. Inst. Min. Metall., 213-220.

Koeppel, V. (1980) Lead isotope studies of stratiform ore deposits of Namaqualand, NW Cape Province, South Africa, and their implications on the age of the Bushmanland Sequence. Proc. 5th IAGOD Symp., **1**, 195-207.

Kroner, A. (1968) The gneiss-sediment relationships northwest of Vanrhynsdorp, Cape Province. Bull. Precambr. Res. Unit, Univ. Cape Town, **3**, 233p.

Kroner, A. (1981) Precambrian plate tectonics. In: Kroner, A. (ed.). Developments in Precambrian Geology, 4. Precambrian Plate Tectonics. Elsevier Scientific Publishing Company, Amsterdam, 57-90.

Lal, R.K. and Moorhouse, W.W. (1969) Cordierite-gedrite rocks and associated gneisses of Fishtail Lake, Harcourt Township, Ontario. Can. J. Earth Sci., **6**, 145-165.

Lal, R.K. and Shukla, R.S. (1975) Low-pressure regional metamorphism in the northern portion of the Khetri Copper Belt of Rajasthan, India. Neues Jahrb. Miner. Abh., **124**, 294-325.

Lal, R.K., Ackermand, D., Seifert, F. and Haldar, S.K. (1978) Chemographic relationships in sapphirine-bearing rocks from Sonapahar, Assam, India. Contrib. Mineral. Petrol., **67**, 169-187.

Lambert, I.B. and Heier, K.S. (1967) The vertical distribution of uranium, thorium, and potassium in the continental crust. Geochim. Cosmochim. Acta, **31**, 377-390.

Lambert, I.B. and Heier, K.S. (1968) Geochemical investigations of deep-seated rocks in the Australian Shield. Lithos, **1**, 30-53.

Lambert, R.St.J., Holland, J.G. and Winchester J.A. (1982) A geochemical comparison of the Dalradian Leven schists and the Grampian Division Monadliath schists of Scotland. J. geol. Soc. London, **139**, 71-84.

Lambert, R.St.J., Winchester, J.A. and Holland, J.G. (1981) Comparative geochemistry of pelites from the Moinian and Appin Group (Dalradian) of Scotland. Geol. Mag., **118**, 477-490.

Lamont, G.T. (1947) The geology of part of the Vanrhynsdorp division, Cape Province. Ph.D thesis, Univ. Cape Town.

Large, D.E. (1981) Sediment-hosted submarine exhalative lead-zinc deposits - a review of their geological characteristics and genesis. In: K.H. Wolf (ed.). Handbook of Strata-bound and Stratiform Ore Deposits, 9, Elsevier Publishing Company, Amsterdam, 469-507.

Leake, B.E. (1964) The chemical distinction between ortho- and para-amphibolites. J. Petrol., **5**, 238-254.

le Maitre, R.W. (1976) The chemical variability of some common igneous rocks. J. Petrol., **17**, 589-598.

le Maitre, R.W. (1982) Numerical Petrology. Statistical interpretation of geochemical data. Developments in Petrology, 8. Elsevier Scientific Publishing Company, Amsterdam, 281p.

Lesko, I. (1972) Uber die bildung von magnesitlagerstatten. Mineral. Deposita, **7**, 61-72.

Lewis, J.D. and Spooner, C.M. (1973) K/Rb ratios in Precambrian granulite terranes. Geochim. Cosmochim. Acta, **37**, 1111-1118.

Lipson, R.D. (1978) Some aspects of the geology of part of the Aggeneysberge and surrounding gneisses, Namaqualand. Unpubl. M.Sc. thesis, Univ. Witwatersrand, 100p.

Lipson, R.D. (1980) The granitic rocks surrounding the Aggeneysberge, a metamorphosed rapakivi suite. Trans geol. Soc. S. Afr., **83**, 179-192.

Lipson, R.D. and McCarthy, T.S. (1977) Geochemical correlation between some rock-types of the Namaqualand granite-gneiss complex. Trans. geol. Soc. S. Afr., **80**, 177-181.

Loberg, B.E.H. and Horndahl, A-K. (1983) Ferride geochemistry of Swedish Precambrian iron ores. Mineral. Deposita, **18**, 487-504.

Macrae, N.D. and Nesbitt, H.W. (1980) Partial melting of common metasedimentary rocks : a mass balance approach. Contrib. Mineral. Petrol., **75**, 21-26.

Mansfield, G.R. (1940) The role of fluorine in phosphate deposition. Am. J. Sci., **238**, 863-879.

Marais, J.A.H., Packham, B. de V. and Schreuder, F.J.G. (1975) Regional geology of the O'okiep Copper District. Abstracts 16th Congress geol. Soc. S. Afr., 88-89.

Marchig, V., Gundlach, H., Moller, P. and Schley, F. (1982) Some geochemical indicators for discrimination between diagenetic and hydrothermal metalliferous sediments. Marine Geol., **50**, 241-256.

Marriott, F.H.C. (1974) The Interpretation of Multiple Observations. Academic Press, London, 117p.

Martens, C.S. and Harriss, R.C. (1970) Inhibition of apatite precipitation in the marine environment by magnesium ions. Geochim. Cosmochim. Acta, **34**, 621-625.

Mathias, M. (1940a) The occurrence of barite in an iron ore deposit in Namaqualand. Trans. R. Soc. S. Afr., **28**, 207-217.

Mathias, M. (1940b) A comparative study of the Namaqualand granites. Trans. geol. Soc. S. Afr., **43**, 175-203.

Mathias, M. (1952) An unusual cordierite-rock from Upington, Cape Province. Mineral. Mag., **29**, 936-945.

McBride, E.F. and Folk, R..L. (1977) The Caballos Novaculite revisited: Part II: chert and shale members and synthesis. J. Sedim. Petrol., **47**, 1261-1286.

McCarthy, T.S. (1976) Chemical interrelationships in a low-pressure granulite terrain in Namaqualand, South Africa, and their bearing on granite genesis and the composition of the lower crust. Geochim. Cosmochim. Acta, **40**, 1057-1068.

McCarthy, T.S. (1978) A geochemical study of the gneisses of the Nababeep district, Namaqualand. Spec. Publ. geol. Soc. S. Afr., **4**, 351-354.

McLennan, S.M. and Taylor, S.R. (1979) Rare earth element mobility associated with uranium mineralisation. Nature, **282**, 247-250.

McLennan, S.M., Fryer, B.J. and Young, G.M. (1979) The geochemistry of the carbonate-rich Espanola Formation (Huronian) with emphasis on the rare earth elements. Can. J. Earth Sci., **16**, 230-239.

McLennan, S.M., Nance, W.B. and Taylor, S.R. (1980) Rare earth element-thorium correlations in sedimentary rocks, and the composition of the continental crust. Geochim. Cosmochim. Acta, **44**, 1833-1839.

Mehnert, K.R. (1968) Migmatites and the origin of granitic rocks. Elsevier Scientific Publishing Company, Amsterdam, 405p.

Mel'nik, Y.P. (1982) Developments in Precambrian Geology, 5. Precambrian Banded Iron-formations. Elsevier Scientific Publishing Company, Amsterdam, 310p.

Meng, L.K. and Moore, J.M. (1972) Sapphirine-bearing rocks from Wilson Lake, Labrador. Can. Mineral., **11**, 777-790.

Milton, C., Chao, E.C.T., Exelrod, J.M. and Grimaldi, F.S. (1960) Reedmergnerite, the boron analog of albite, from the Green River Formation, Utah. Amer. Mineral., **45**, 188-199.

Minnitt, R.C.A. (1979) The geological setting of porphyry-type copper mineralization in the Haib River area, South West Africa. Unpubl. Ph.D thesis, Univ. Witwatersrand, 366p.

Miyashiro, A. and Shido, F. (1975) Tholeiitic and calc-alkalic series in relation to the behaviors of titanium, vanadium, chromium and nickel. Am. J. Sci., **275**, 265-277.

Moine, B., Sauvan, P. and Jarousse, J. (1981) Geochemistry of evaporite-bearing series : a tentative guide for the identification of metaevaporites. Contrib. Mineral. Petrol., **76**, 401-412.

Moore, B.R. and Dennen, W.H. (1970) A geochemical trend in silicon-aluminum-iron ratios and the classification of clastic sediments. J. Sedim. Petrol., **40**, 1147-1152.

Moore, J.M. (1977) The geology of Namiesberg, Northern Cape. Bull. Precambr. Res. Unit, Univ. Cape Town, **20**, 69p.

Moore, J.M. (1980a) A study of certain paragneiss associations and their metallogenic characteristics in Namaqualand and Bushmanland. Ann. Rep. Precambr. Res. Unit, Univ. Cape Town, **17**, 65-73.

Moore, J.M. (1980b) Palaeo-environmental implications of the origin of sillimanite-rich rocks in the north-west Cape, South Africa, and their relation to the sulfide deposits of the area. Proc. 5th Quad. IAGOD Symp., **1**, 209-215.

Moore, J.M. (1983) Investigations of and for "Aggeneys-type" Zn-Pb-Cu-Ag ore deposits in Namaqualand, South Africa - past and present. SME-AIME Ann. Meeting, 1983, Preprint 83-12, 6p.

Morgan, L.A., Doherty, D.J. and Leeman, W.P. (1984) Ignimbrites of the eastern Snake River Plain: evidence for major caldera-forming eruptions. J. Geophys. Res., **89**, B10, 8665-8678.

Murata, K.J. and Larson, R.R. (1975) Diagenesis of Miocene siliceous shales, Temblor Range, California. J. Res. U.S. geol. Surv., **3**, 553-566.

Mutschler, F.E., Rougon, D.J. and Lavin, O.R. (1976) PETROS, a data bank of major element chemical analyses of igneous rocks for research and teaching. Comput. Geosci., **2**, 51-57.

Nanz, R.H. (1953) Chemical composition of Precambrian slates with notes on the geochemical evolution of lutites. J. Geol., **61**, 51-64.

Nesbitt, H.W. (1980) Genesis of the New Quebec and Adirondack granulites : evidence for their production by partial melting. Contrib. Mineral. Petrol., **72**, 303-310.

Nesbitt, H.W. and Young, G.M. (1982) Early Proterozoic climates and plate motions inferred from major element chemistry of lutites. Nature, **299**, 715-717.

Nichols, C.R. (1970) Diabase argillation at King Mountain, Kiowa County, Oklahoma. J. Sedim. Petrol., **40**, 848-854.

Nicolaysen, L.O. and Burger, A.J. (1965) Note on an extensive zone of 1000 million-year-old metamorphic and igneous rocks in Southern Africa. Sci. de la Terre, **10**, 497-518.

Nicollet, C. and Andriambololona, D.R. (1980) Distribution of transition elements in crustal metabasic igneous rocks. Chem. Geol., **28**, 79-90.

Nixon, P.H., Reedman, A.J. and Burns, L.K. (1973) Sapphirine-bearing granulites from Labwor, Uganda. Mineral. Mag., **39**, 420-428.

Norrish, K. and Hutton, J.T. (1969) An accurate X-ray spectrographic method for the analysis of a wide range of geological samples. Geochim. Cosmochim. Acta, **33**, 431-453.

Odling, N.E. (1983) The structure of Gamsberg, Namaqualand, N.W. Cape - an intermediate report. Ann. Rep. Precambr. Res. Unit, Univ. Cape Town, **18-20**, 76-104.

Paizes, P.E. (1975) The geology of an area in the vicinity of Pofadder. Unpubl. M.Sc. thesis, Univ. Witwatersrand, 220p.

Parekh, P.P., Moller, P., Dulski, P. and Bausch, W.M. (1977) Distribution of trace elements between carbonate and non-carbonate phases of limestone. Earth Planet. Sci. Letters, **34**, 39-50.

Pearce, J.A. (1976) Statistical analysis of major element patterns in basalts. J. Petrol., **17**, 15-43.

Pearce, J.A. and Cann, J.R. (1973) Tectonic setting of basic volcanic rocks determined using trace element anomalies. Earth Planet. Sci. Letters, **19**, 290-300.

Pearce, J.A., Gorman, B.E. and Birkett, T.C. (1975) The TiO_2-K_2O-P_2O_5 diagram: a method of discriminating between oceanic and non-oceanic basalts. Earth Planet. Sci. Letters, **24**, 419-426.

Pearce, J.A., Gorman, B.E. and Birkett, T.C. (1977) The relationship between major element chemistry and tectonic environment of basic and intermediate volcanic rocks. Earth Planet. Sci. Letters, **36**, 121-132.

Pettijohn, E.J. (1975) Sedimentary Rocks. Harper and Row, New York, 3rd edition, 628p.

Piper, J.D.A. (1976) Palaeomagnetic evidence for a supercontinent. Phil. Trans. R. Soc. London, **A280**, 469-490.

Pollard, P.J. (1981) Hydrothermal tin-tungsten mineralisation and origin of associated cordierite-anthophyllite rocks at Tommy Burns mine, north Queensland,Australia. Trans. Inst. Min. Metall. (Sect. B), **90**, B65-B69.

Quinquis, H., Audren, C., Brun, J.P. and Cobbold P.R. (1978) Intense progressive shear in Ile de Groix blueschists and compatibility with subduction or obduction. Nature, **273**, 43-45.

Rao, T.R. (1974) A bedded deposit of anthophyllite schist in the Precambrian belt of Nellore, south India. Geol. Mag., **111**, 221-228.

Rao, A.T., Rao, A.G. and Rao, P.P. (1979) Fluorian allanite from calc-granulite and pegmatite contacts at Garividi, Andhra Pradesh, India. Mineral. Mag., **43**, 312.

Raymond, W.H., Leiggi, P.A. and Sheridan, D.M. (1980) Sapphirine in Precambrian rocks associated with stratabound sulfide deposits, Custer County, Colorado. Bull. U.S. geol. Surv., **1513**, 22p.

Reading, H.G. (1978) Sedimentary Environments and Facies. Elsevier Scientific Publishing Company, New York, 557p.

Reid, D.L. (1977) Geochemistry of Precambrian igneous rocks in the lower Orange River region. Bull. Precambr. Res. Unit, Univ. Cape Town, **23**, 397p.

Reid, D.L. (1979) Total rock Rb-Sr and U-Th-Pb isotopic study of Precambrian metavolcanic rocks in the lower Orange River region, southern Africa. Earth Planet. Sci. Lett., **42**, 368-378.

Reid, D.L. (1982) Age relationships within the Vioolsdrif batholith, lower Orange River region II. A two stage emplacement history and the extent of Kibaran overprinting. Trans. geol. Soc. S. Afr., **85**, 105-110.

Reid, D.L. and Barton, E.S. (1983) Geochemical characterization of granitoids in the Namaqualand Geotraverse. Spec. Publ. geol. Soc. S. Afr., **10**, 67-82.

Reynolds, R.C. (1965) The concentration of boron in Precambrian seas. Geochim. Cosmochim. Acta, **29**, 1-16.

Ritter, U. (1980) The Precambrian evolution of the eastern Richtersveld. Bull. Precambr. Res. Unit, Univ. Cape Town, **26**, 276p.

Robinson, D. and Leake, B.E. (1975) Sedimentary and igneous trends on AFM diagrams. Geol. Mag., **112**, 305-307.

Rollinson, H.R. and Windley, B.F. (1980) Selective elemental depletion during metamorphism of Archaean granulites, Scourie, NW Scotland. Contrib. Mineral. Petrol., **72**, 257-263.

Rooney, R.T. and Kerr, P.F. (1967) Mineralogical nature and origin of phosphorite, Beaufort County, North Carolina. Bull. geol. Soc. Am., **78**, 731-741.

Roy, S. (1976) Ancient manganese deposits. In: Wolf K.H. (ed.). Handbook of Strata-bound and Stratiform Ore Deposits, 7. Elsevier Scientific Publishing Company, Amsterdam, 395-476.

Rozendaal, A. (1975) The geology of Gamsberg, Namaqualand, South Africa. Unpubl. M.Sc. thesis, Univ. Stellenbosch.

Rozendaal, A. (1978) The Gamsberg zinc deposit, Namaqualand. In: Verwoerd, W.J. (ed.). Mineralization in metamorphic terrains. Spec. Publ. geol. Soc. S. Afr., **4**, 235-265.

Rozendaal, A. (1980) The Gamsberg zinc deposit, South Africa : a banded stratiform base-metal sulfide ore deposit. Proc. 5th Quad. IAGOD Symp., **1**, 619-634.

Rozendaal, A. (1982) The petrology of the Gamsberg zinc deposit and the Bushmanland iron formations with special reference to their relationships and genesis. Unpubl. Ph.D thesis, Univ. Stellenbosch, 349p.

Russell, M.J., Solomon, M. and Walshe, J.L. (1981) The genesis of sediment-hosted, exhalative zinc + lead deposits. Mineral. Deposita, **16**, 113-127.

Ryan, P.J., Lawrence, A.L., Lipson, R.D., Moore, J.M., Paterson, A., Stedman, D.P. and van Zyl, D. (1982) The Aggeneys base metal sulphide deposits, Namaqualand, South Africa. Econ. Geol. Res. Unit, Univ. Witwatersrand, Inf. Circ., **160**, 33p.

SACS (South African Committee for Stratigraphy) (1980) Stratigraphy of South Africa. Part 1 (comp. L.E. Kent). Lithostratigraphy of the Republic of South Africa, South West Africa/Namibia, and the Republics of Bophuthatswana, Transkei and Venda. Handb. geol. Surv. S. Afr., **8**, 690p.

Sarkar, S.C., Bhattacharyya, P.K. and Mukherjee, A.D. (1980) Evolution of the sulfide ores of Saladipura, Rajasthan, India. Econ. Geol., **75**, 1152-1167.

Sato, H. (1977) Nickel content of basaltic magmas: identification of primary magmas and a measure of the degree of olivine fractionation. Lithos, **10**, 113-120.

Saxena, S.K. (1976) Two pyroxene geothermometer: a model with an approximate solution. Amer. Mineral., **61**, 643-652.

Schermerhorn, L.J.G. (1978) Epigenetic magnesium metasomatism or syngenetic chloritite metamorphism at Falun and Orijarvi. Trans. Inst. Min. Metall. (Sect. B), **87**, B162-B166.

Schreyer, W. (1977) Whiteschists: their compositions and pressure-temperature regimes based on experimental, field and petrographic evidence. Tectonophysics, **43**, 127-144.

Senior, A. and Leake, B.E. (1978) Regional metasomatism and the geochemistry of the Dalradian metasediments of Connemara, western Ireland. J. Petrol., **19**, 585-625.

Sheldon, R.P. (1963) Physical stratigraphy and mineral resources of Permian rocks of western Wyoming. U.S. geol. Surv. Prof. Paper, **313-B**, 49-273.

Sheraton, J.W., England, R.N. and Ellis, D.J. (1982) Metasomatic zoning in sapphirine-bearing granulites from Antarctica. B.M.R. J. Austr. Geol. Geophys., **7**, 269-273.

Shimuzu, H. and Masuda, A. (1977) Cerium in chert as an indicator of marine environment of its formation. Nature, **266**, 346-348.

Sighinolfi, G.P. (1971) Investigations into deep crustal levels : Fractionating effects and geochemical trends related to high-grade metamorphism. Geochim. Cosmochim. Acta, **35**, 1005-1021.

Smith, E.I. (1978) Precambrian rhyolites and granites in south-central Wisconsin: field relations and geochemistry. Bull. geol. Soc. Am., **89**, 875-890.

Smith, R.L. (1979) Ash-flow magmatism. Spec. Paper Geol. Soc. Am., **180**, 5-27.

Smithson, S.B., Fikkan, P.R. and Houston, R.S. (1971) Amphibolitization of calc-silicate metasedimentary rocks. Contrib. Mineral. Petrol., **31**, 228-237.

Sparks, R.S.J. and Walker, G.P.L. (1977) The significance of vitric-enriched air-fall ashes associated with crystal-enriched ignimbrites. J. Volcanol. Geotherm. Res., **2**, 329-341.

Stedman, D.P. (1980) The structural geology and metamorphic petrology of Black Mountain, Namaqualand. Unpubl. M.Sc. thesis, Univ. Witwatersrand.

Stevens, B.P.J. and Willis, I.L. (1983) Systematic classification of rock units: a key to mapping and interpretation of the Willyama Complex. Rec. geol. Surv. New S. Wales, **21**, part 1, 1-56.

Stewart, A.J. and Warren, R.G. (1977) The mineral potential of the Arunta Block, central Australia. B.M.R. J. Austr. Geol. Geophys., **2**, 21-34.

Stoessell, R.K. and Hay, R.L. (1978) The geochemical origin of sepiolite and kerolite at Amboseli, Kenya. Contrib. Mineral. Petrol., **65**, 255-267.

Stowe, C.W. (1983) The Upington geotraverse and its implications for craton margin tectonics. Spec. Publ. geol. Soc. S.Afr., **10**, 147-172.

Strauss, G.K., Roger, G., Lecolle, M. and Lopera, E. (1981) Geochemical and geologic study of the volcano-sedimentary sulfide orebody of La Zarza, Huelva Province, Spain. Econ. Geol., **76**, 1975-2000.

Sugisaki, R., Yamamoto, K. and Adachi, M. (1982) Triassic bedded cherts in central Japan are not pelagic. Nature, **298**, 644-647.

Sun, S-S. and Nesbitt, R.W. (1978) Geochemical regularities and genetic significance of ophiolite basalts. Geology, **6**, 689-693.

Surdam, R.C. and Parker, R.D. (1972) Authigenic aluminosilicate minerals in the tuffaceous rocks of the Green River formation, Wyoming. Bull. geol. Soc. Am., **83**, 689-700.

Tankard, A.J., Jackson, M.P.A., Eriksson, K.A., Hobday, D.K., Hunter, D.R. and Minter, W.E.L. (1982) Crustal Evolution of Southern Africa. 3.8 billion years of earth history. Springer-Verlag, New York, 523p.

Tanner, P.W.G. and Miller, R.G. (1980) Geochemical evidence for loss of Na and K from Moinian calc-silicate pods during prograde metamorphism. Geol. Mag., **117**, 267-275.

Taylor, S.R. and McLennan, S.M. (1981) The composition and evolution of the continental crust: rare earth element evidence for sedimentary rocks. Phil. Trans. R. Soc. London, **A301**, 381-399.

Theart, H.F.J. (1980) The geology of the Precambrian terrane in parts of Western Namaqualand. Bull. Precambr. Res. Unit, Univ. Cape Town, **30**, 103p.

Thompson, A.B. (1975) Calc-silicate diffusion zones between marble and pelitic schist. J. Petrol., **16**, 314-346.

Tilley, C.E. (1935) Metasomatism associated with the greenstone hornfelses of Kenidjack and Botallack, Cornwall. Mineral. Mag., **24**, 181-202.

Toogood, D.J. (1976) Structural and metamorphic evolution of a gneiss terrain in the Namaqua Belt near Onseepkans, South West Africa. Bull. Precambr. Res. Unit, Univ. Cape Town, **19**, 189p.

Tooms, J.S., Summerhayes, C.P. and Cronan, D.S.L. (1969) Geochemistry of marine phosphate and manganese deposits. Ann. Rev. Oceanogr. Mar. Biol., **7**, 49-100.

Toth, J.R. (1980) Deposition of submarine crusts rich in manganese and iron. Bull. geol. Soc. Am., **91**, 44-54.

Treloar, P.J., Koistinen, T.J. and Bowes, D.R. (1981) Metamorphic development of cordierite-amphibole rocks and mica schists in the vicinity of the Outokumpu ore deposit, Finland. Trans. R. Soc. Edinburgh : Earth Sciences, **72**, 201-215.

Tuttle, O.F. and Bowen, N.L. (1958) Origin of granite in the light of experimental studies in the system $NaAlSi_3O_8$ - $KAlSi_3O_8$ - SiO_2 - H_2O. Mem. geol. Soc. Am., **74**, 153p.

Vallance, T.G. (1967) Mafic rock alteration and isochemical development of some cordierite-anthophyllite rocks. J. Petrol., **8**, 84-96.

van de Kamp, P.C. (1969) Origin of amphibolites in the Beartooth Mountains - new data and interpretation. Bull. geol. Soc. Am., **80**, 1127-1136.

van de Kamp, P.C. (1970) The Green Beds of the Scottish Dalradian series: geochemistry, origin, and metamorphism of mafic sediments. J. Geol., **78**, 281-303.

van Wyk, J.P. and Beukes, N.J. (1982) The geology of the Sishen iron ore deposit. Proc. 12th CMMI Congress, S.Afr. Inst. Min. Metall., 203-211.

Veizer, J. (1978) Secular variations in the composition of sedimentary carbonate rocks, II. Fe, Mn, Ca, Mg, Si and minor constituents. Precambr. Res., **6**, 381-413.

Veizer, J. and Garrett, D.E. (1978) Secular variations in the composition of sedimentary carbonate rocks, I. Alkali metals. Precambr. Res., **6**, 367-380.

Veizer, J., Lemieux, J., Jones, B., Gibling, M.R. and Savelle, J. (1977) Sodium : palaeosalinity indicator in ancient carbonate rocks. Geology, **5**, 177-179.

Viljoen, R.P., Viljoen, M.J., Grootenboer, J. and Longshaw, T.G. (1975) ERTS-1 imagery : an appraisal of applications in geology and mineral exploration. Minerals Sci. Engng., **7**, 132-168.

von Backstrom, J.W. (1964) The geology of an area around Keimoes, Cape Province, with special reference to phacoliths of charnockitic adamellite- porphyry. Mem. geol. Surv. S. Afr., **53**, 218p.

von Backstrom, J.W. and de Villiers, J. (1972) The geology along the Orange River between Onseepkans and the Richtersveld. Explan. Sheets 2817D (Vioolsdrif), 2818C and D (Goodhouse) and 2819C (Onseepkans), geol. Surv. S. Afr., 101p.

Wagner, G.H., Konig, R.H., Vogelpohl, S. and Jones, M.D. (1979) Base metals and other minor elements in the manganese deposits of west-central Arkansas. Chem. Geol., **27**, 309-327.

Walker, C.T. and Price, N.B. (1963) Departure curves for computing paleosalinity from boron in illites and shales. Bull. Am. Assoc. Petroleum Geologists, **47**, 833-841.

Warren, R.G. (1979) Sapphirine-bearing rocks with sedimentary and volcanogenic protoliths from the Arunta Block. Nature, **278**, 159-161.

Watanabe, T., Yui, S. and Kato, A. (1970) Metamorphosed bedded manganese deposits of the Noda-Tamagawa mine. In: Watanabe T. (ed.). Volcanism and Ore Genesis. Univ. Tokyo Press, Tokyo, 143-152.

Waters, D.J., Joubert, P. and Moore, J.M. (1983) A suggested re-interpretation of Namaqua basement and cover rocks south and west of Bitterfontein. Trans. geol. Soc. S. Afr., **86**, 293-300.

Watters, B.R. (1976) Possible late Precambrian subduction zone in South West Africa. Nature, **259**, 471-473.

Welke, H.J. and Smith, C.B. (1984) Lead isotope characterization of the Aggeneys-Gamsberg ore bodies in relation to possible source rocks, with implications for Bushmanland metallogenesis. Abs., Conf. on Middle to Late Proterozoic Crustal Evolution, Precambr. Res. Unit, Univ. Cape Town, 8-9.

Wells, R.A. (1977) Pyroxene thermometry in simple and complex systems. Contrib. Mineral. Petrol., **62**, 129-139.

Wennervirta, H. and Rouhunkoski, P. (1970) Lithogeochemical aspects of the Vihanti zinc ore deposit, Finland. Econ. Geol., **65**, 564-578.

Wetzenstein, W. (1975) Limnische huntit-hydromagnesit-magnesit lagerstatten in Mazedonien/Nordgriechenland. Mineral. Deposita, **10**, 129-140.

White, A.J.R. and Chappell, B.W. (1977) Ultrametamorphism and granitoid genesis. Tectonophysics, **43**, 7-22.

Willis, I.L. (1982) Description and interpretation of a useful leucogneiss marker in the Willyama Complex, Broken Hill Block, N.S.W. J. and Proc. R. Soc. New S. Wales, **115**, 21-32.

Willis, I.L., Stevens, B.P.J., Stroud, W.J., Brown, R.E., Bradley, G.M. and Barnes, R.G. (1983) Metasediments, composite gneisses, and migmatites. Rec. geol. Surv. New S. Wales, **21**, part 1, 57-126.

Wilson, A.F. (1971) Some geochemical aspects of the sapphirine-bearing pyroxenites and related highly metamorphosed rocks from the Archaean ultramafic belt of South Quairading, Western Australia. Spec. Publ. geol. Soc. Austr., 3, 401-411

Wilson, A.F. (1978a) Large crystals of kornerupine from a new locality in the granulites of the Strangways Range, central Australia. Neues Jahrb. Mineral. Mh., 249-256.

Wilson, I.H. (1978b) Volcanism on a Proterozoic continental margin in northwestern Queensland. Precambr. Res., **7**, 205-235.

Winchester, J.A. and Floyd, P.A. (1976) Geochemical magma type discrimination: application to altered and metamorphosed basic igneous rocks. Earth Planet. Sci. Letters, **28**, 459-469.

Winchester, J.A., Lambert, R.St.J. and Holland, J.G. (1981) Geochemistry of the western part of the Moinian assemblage. Scott. J. Geol., **17**, 281-294.

Windley, B.F. (1981) Precambrian rocks in the light of the plate tectonic concept. In: Kroner, A. (ed.). Developments in Precambrian Geology, 4. Precambrian Plate Tectonics. Elsevier Scientific Publishing Company, Amsterdam, 1-20.

Winkler, H.G.F. (1976) Petrogenesis of Metamorphic Rocks. Springer-Verlag, Berlin, 334p.

Wood, B.J. (1977) The activities of components in clinopyroxene and garnet solid solutions and their applications to rocks. Phil. Trans. R. Soc. London, **A286**, 331-342.

Wood, B.J. (1979) Activity-composition relationships in $Ca(Mg,Fe)Si_2O_6$ - $CaAl_2SiO_6$ clinopyroxene solid solutions. Am. J. Sci., **279**, 854-875.

Wood, B.J. and Banno, S. (1973) Garnet-orthopyroxene and orthopyroxene-clinopyroxene relationships in simple and complex systems. Contrib. Mineral. Petrol., **42**, 109-124.

Wood, D.A., Joron, J-L. and Treuil, M. (1979) A re-appraisal of the use of trace elements to classify and discriminate between magma series erupted in different tectonic settings. Earth Planet. Sci. Letters, **45**, 326-336.

Woodford, P.J. and Wilson, A.F. (1976) Sapphirine, hogbomite, kornerupine, and surinamite from aluminous granulites, north-eastern Strangways Range, central Australia. Neues Jahrb. Mineral. Mh., 15-35.

Wyborn, D., Chappell, B.W. and Johnston, R.M. (1981) Three S-type volcanic suites from the Lachlan Fold Belt, southeast Australia. J. Geophys. Res., **86**, B11, 10335-10348.

Youssef, M.I. (1965) Genesis of bedded phosphates. Econ. Geol., **60**, 590-600.

Zantop, H. (1981) Trace elements in volcanogenic manganese oxides and iron oxides: the San Francisco manganese deposit, Jalisco, Mexico. Econ. Geol., **76**, 545-555.

Zelt, G.A.D. (1980) Granulite-facies metamorphism in Namaqualand, South Africa. Precambr. Res., **13**, 253-274.

Table A.1 Routine instrumental conditions adopted for XRF spectrometers in the Department of Geochemistry, University of Cape Town and used in this study.

ELEMENT	LINE	SPECTRO-METER	TUBE	KV	MA	CRYSTAL	COLLI-MATOR	DETECTOR		TIME PK	TIME BK	SAMPLE TYPE
Si	Ka	SRS-1	Cr	60	45	PET	C	F	V	100		F
Ti	Ka	SRS-1	Cr	60	45	LiF(200)	F	F	V	40		F
Al	Ka	SRS-1	Cr	60	45	PET	C	F	V	100		F
Fe	Ka	SRS-1	Cr	60	45	LiF(220)	F	F	V	100		F
Mn	Ka	SRS-1	Cr+Al	60	45	LiF(220)	F	F	V	100		F
Mg	Ka	SRS-1	Cr	60	45	TLAP	F	F	V	200		F
Ca	Ka	SRS-1	Cr	60	45	LiF(200)	F	F	V	40		F
K	Ka	SRS-1	Cr	60	45	LiF(200)	C	F	V	40		F
P	Ka	SRS-1	Cr	60	45	Ge	C	F	V	100		F
Na	Ka	SRS-1	Cr	60	45	TLAP	C	F	V	200	100	B
S	Ka	PW1400	Cr	50	55	Ge	C	F	V	80	40	B
Ba	La	SRS-1	Cr	60	45	LiF(200)	F	F	V	100	40	B
Sc	Ka	SRS-1	Cr	60	45	LiF(200)	F	F	V	100	40	B
Rb	Ka	PW1400	W	50	55	LiF(200)	F	S		80	40	B
Sr	Ka	PW1400	W	50	55	LiF(200)	F	S		80	40	B
Y	Ka	PW1400	W	50	55	LiF(200)	F	S		80	40	B
Zr	Ka	PW1400	W	50	55	LiF(200)	F	S		80	40	B
Nb	Ka	PW1400	W	50	55	LiF(200)	F	S		80	40	B
Mo	Ka	SRS-1	W	60	45	LiF(220)	F	S		100	40	B
Co	Ka	PW1400	W	50	55	LiF(220)	F	S	V	80	40	B
Cr	Ka	PW1400	W	50	55	LiF(220)	F	S	V	80	40	B
V	Ka	PW1400	W	50	55	LiF(220)	F	S	V	80	40	B
Zn	Ka	PW1400	Au	50	55	LiF(220)	F	FS	V	80	40	B
Cu	Ka	PW1400	Au	50	55	LiF(220)	F	FS	V	80	40	B
Ni	Ka	PW1400	Au	50	55	LiF(220)	F	FS	V	80	40	B
U	La	PW1400	W	50	55	LiF(200)	F	FS		80	40	B
Th	La	PW1400	W	50	55	LiF(200)	F	FS		80	40	B
Pb	Lb	PW1400	W	50	55	LiF(200)	F	FS		80	40	B
La	La	PW1400	W	50	55	LiF(220)	F	FS	V	160	80	B
Ce	Lb	PW1400	W	50	55	LiF(220)	F	FS	V	160	80	B
Nd	La	PW1400	W	50	55	LiF(220)	F	FS	V	160	80	B
MU	Mo KaC	PW1220	Mo	70	28	LiF(220)	F	S				B
MU	Mo KaC	PW1400	Mo	50	55	LiF(220)	F	S				B
MU	Mo KaC	SRS-1	Mo	60	45	LiF(220)	F	S				B

V = run under vacuum; F (sample) = fusion disc; B = powder briquette; C = coarse, F = fine (collimator).
MU = mass absorption coefficient for Mo Ka Compton for 4×10^5 counts

Table A.2 The lower limits of detection and absolute errors (standard deviation) for major element oxides in the X-ray fluorescence spectroscopic analysis of samples from this study.

	lower limits of detection (%)	absolute error (%)
SiO_2	0.03	0.21
TiO_2	0.008	0.01
Al_2O_3	0.02	0.09
Fe_2O_3	0.02	0.11
MnO	0.03	0.01
MgO	0.08	0.08
CaO	0.01	0.03
Na_2O	0.08	0.09
K_2O	0.005	0.02

Table A.3 The lower limits of detection and absolute errors (standard deviation) for trace elements in the X-ray fluorescence spectroscopic analysis of samples from this study. The concentration levels quoted below are typical values for metapelitic rocks. Detection limits and errors will vary with variations in the mass absorption coefficients of different lithologies.

	Concentration (ppm)	lower limit of detection (ppm)	absolute error (ppm)
Rb	181	1.5	0.7
Ba	824	1.8	2.1
Sr	100	1.5	0.6
Th	23	2.4	0.8
U	6.3	3.3	1.1
Zr	270	2.1	0.9
Nb	17	1.5	0.5
Mo	2.4	1.4	0.5
Cr	118	1.5	0.8
V	102	2.6	1.1
Sc	16	1.0	0.4
Ni	30	1.1	0.4
Co	19	1.9	0.7
Pb	30	4.1	1.4
Zn	72	0.9	0.4
Cu	13	1.3	0.5
S	79	5.5	2.1
Y	33	1.7	0.6
La	36	3.9	1.4
Ce	62	4.1	1.5
Nd	32	3.9	1.4

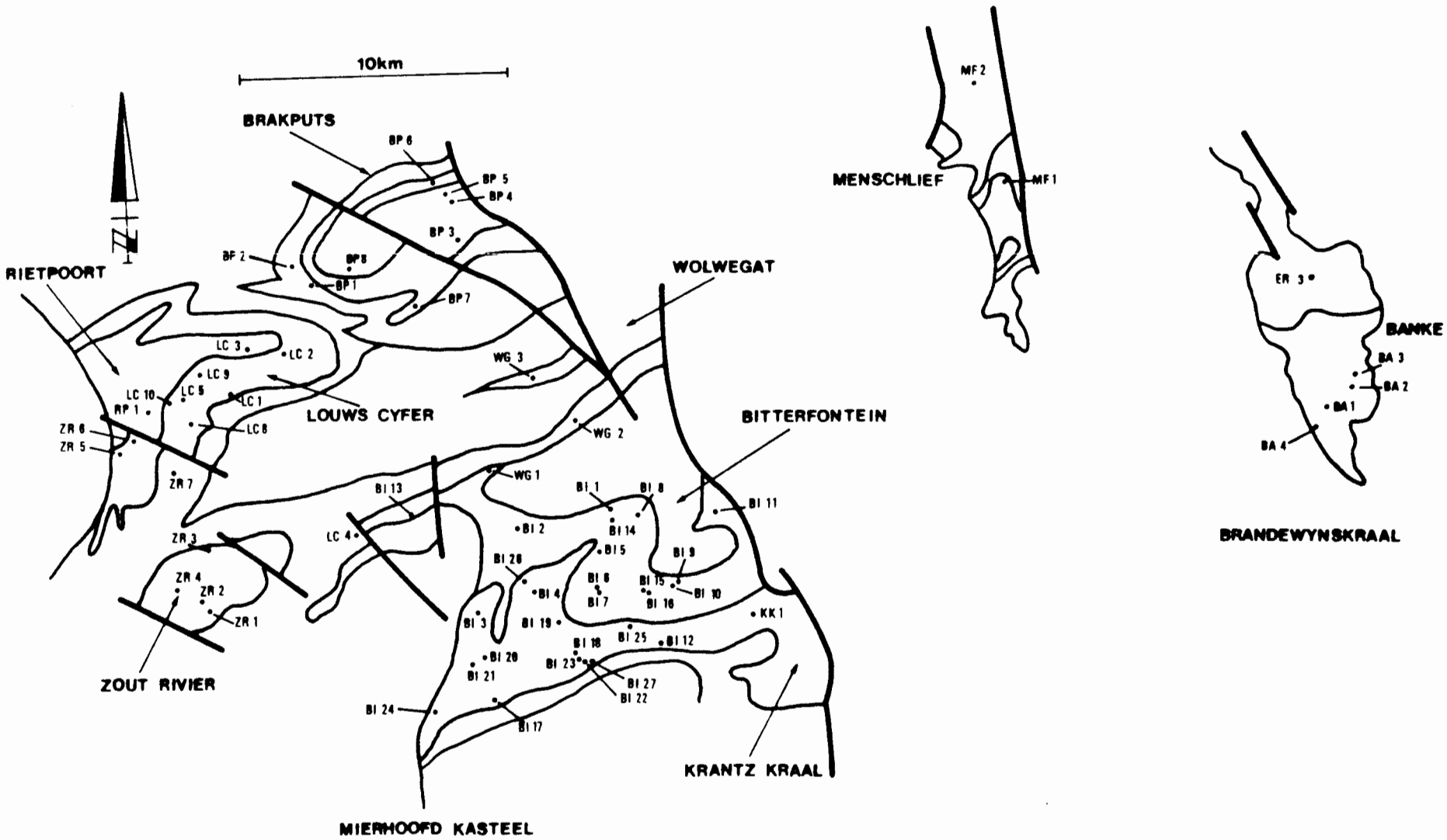

Fig. A.1. Sample locality map for the Bitterfontein paragneiss belt. For geological explanation see Fig. 4.2.

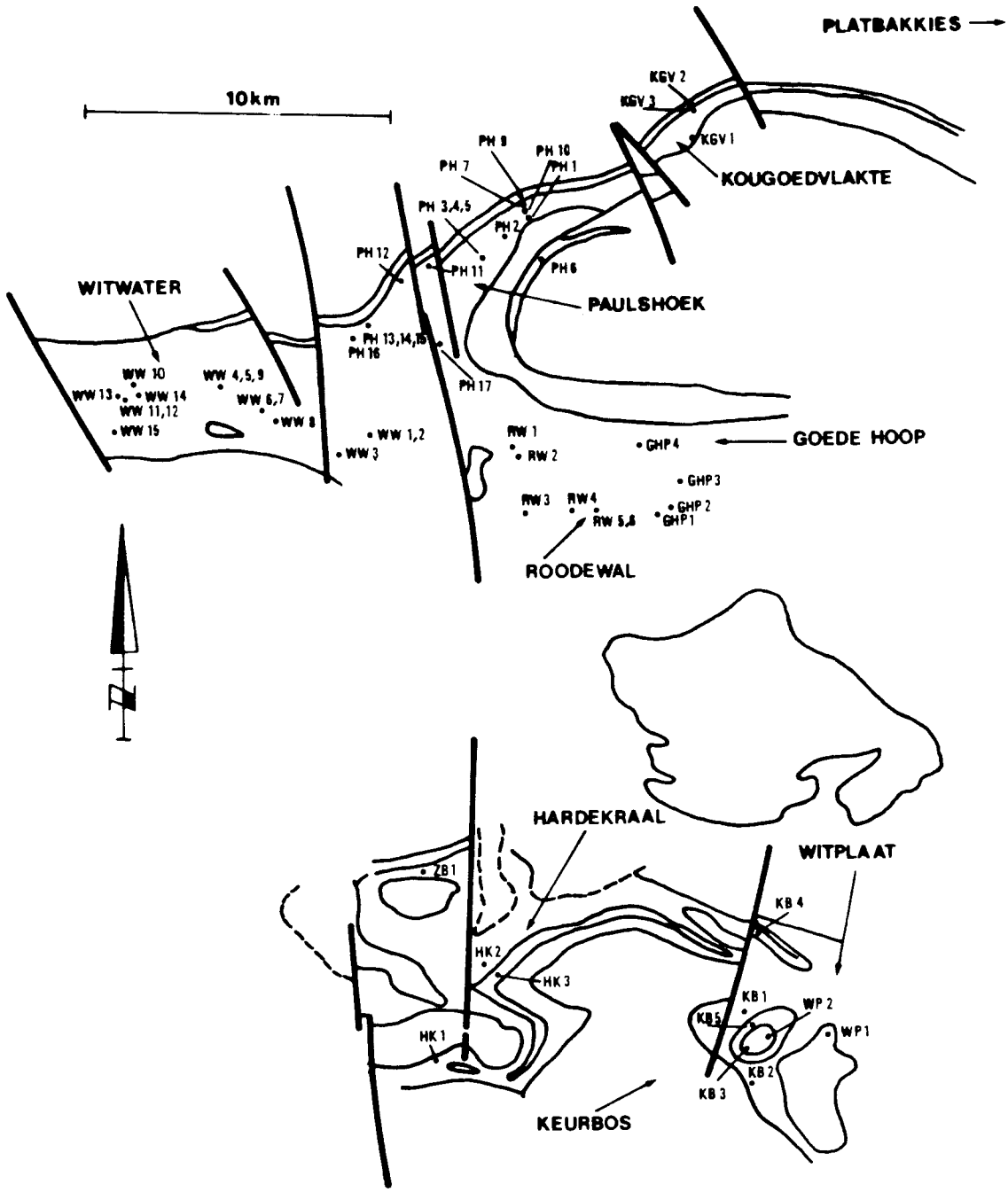

Fig. A.2. Sample locality map for the Witwater-Platbakkies paragneiss belt. For geological explanation see Fig. 4.5.

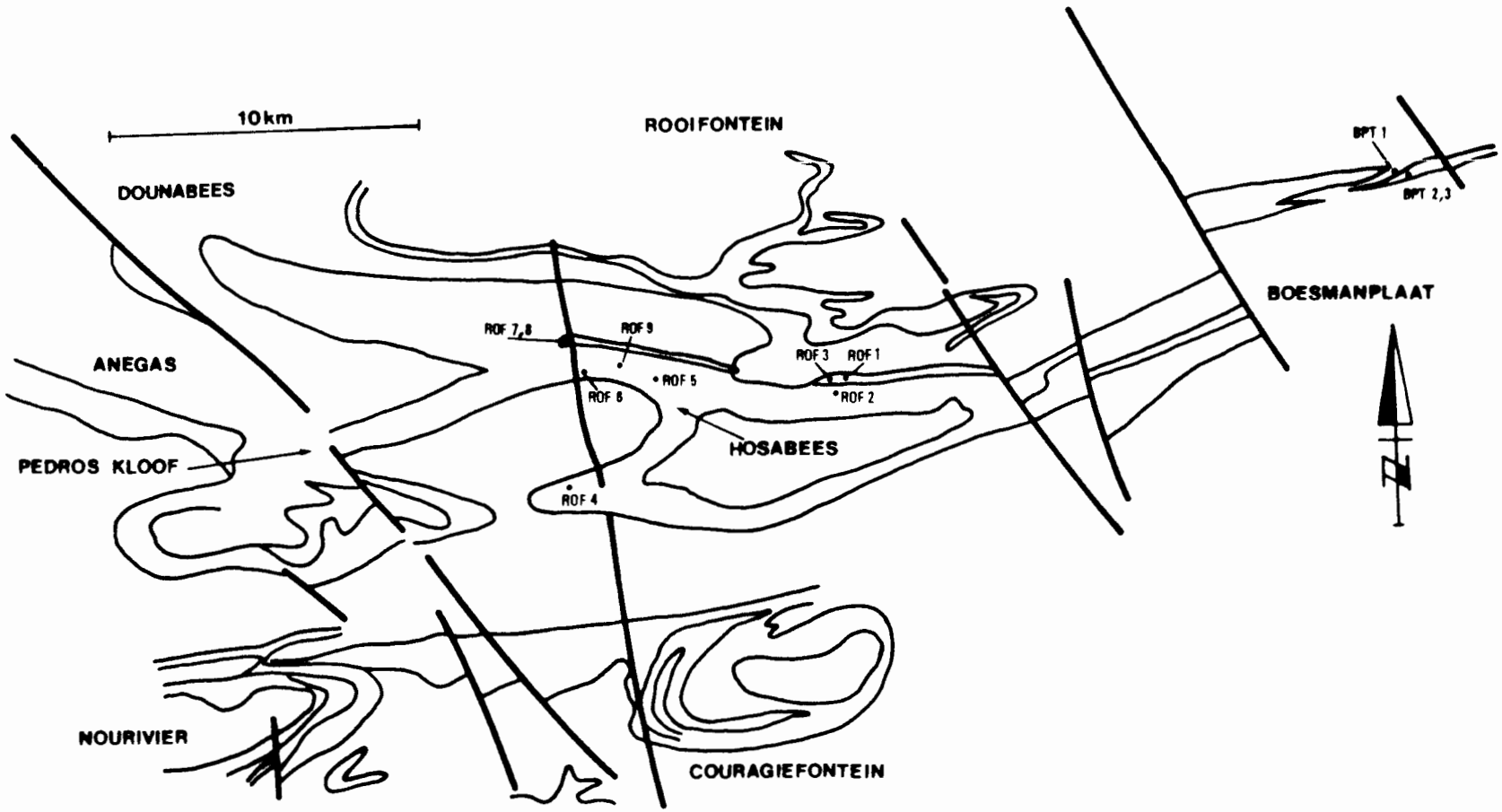

Fig. A.3. Sample locality map for the Anegas-Boesmanplaat paragneiss belt. For geological explanation see Fig. 4.8.

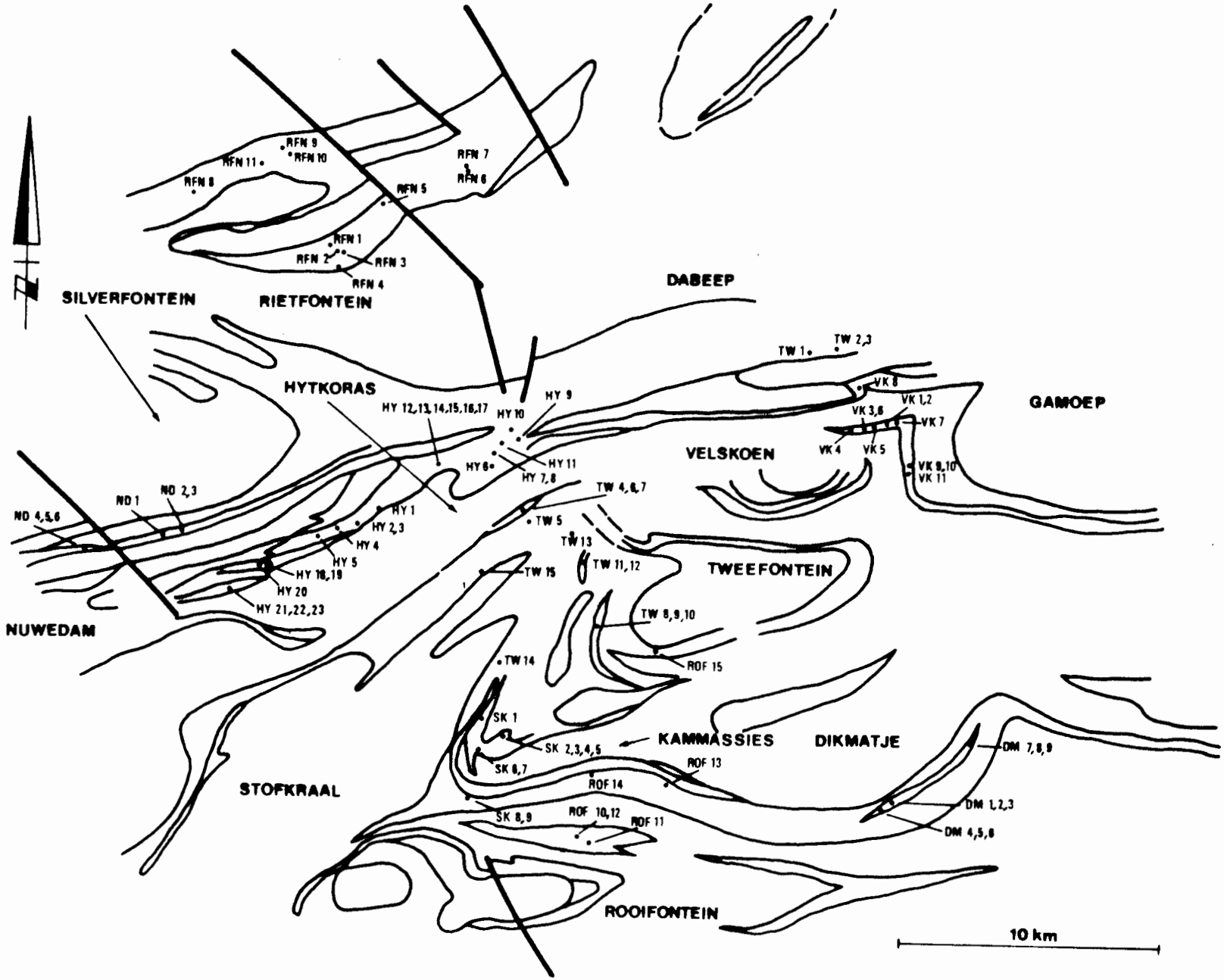

Fig. A.4. Sample locality map for the Silverfontein-Rietfontein, Buffels River and Stofkraal-Dikmatje paragneiss belts. For geological explanation see Fig. 4.10.

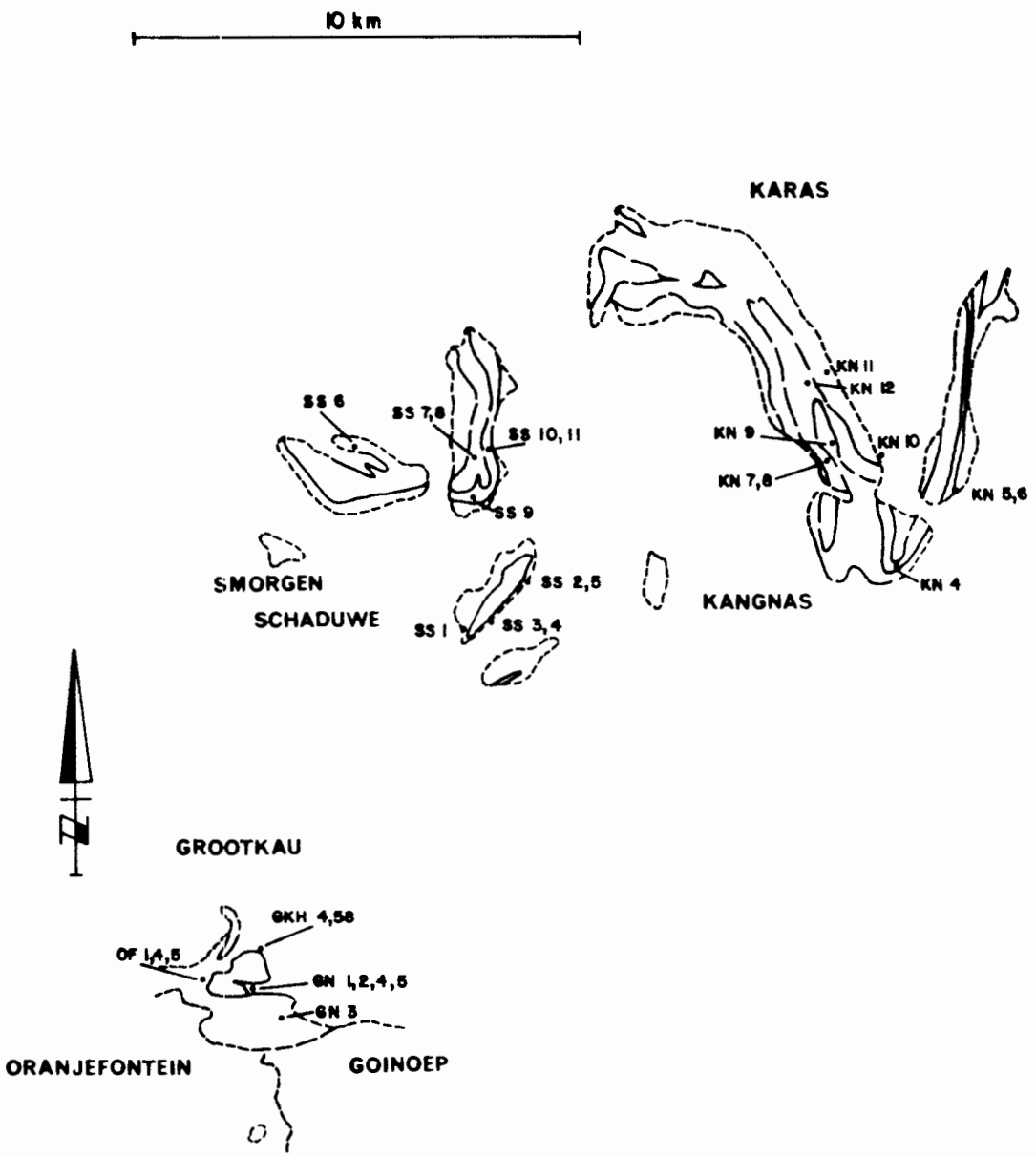

Fig. A.5. Sample locality map for the Smorgen Schaduwe-Kangnas paragneiss belt. For geological explanation see Fig. 4.13.

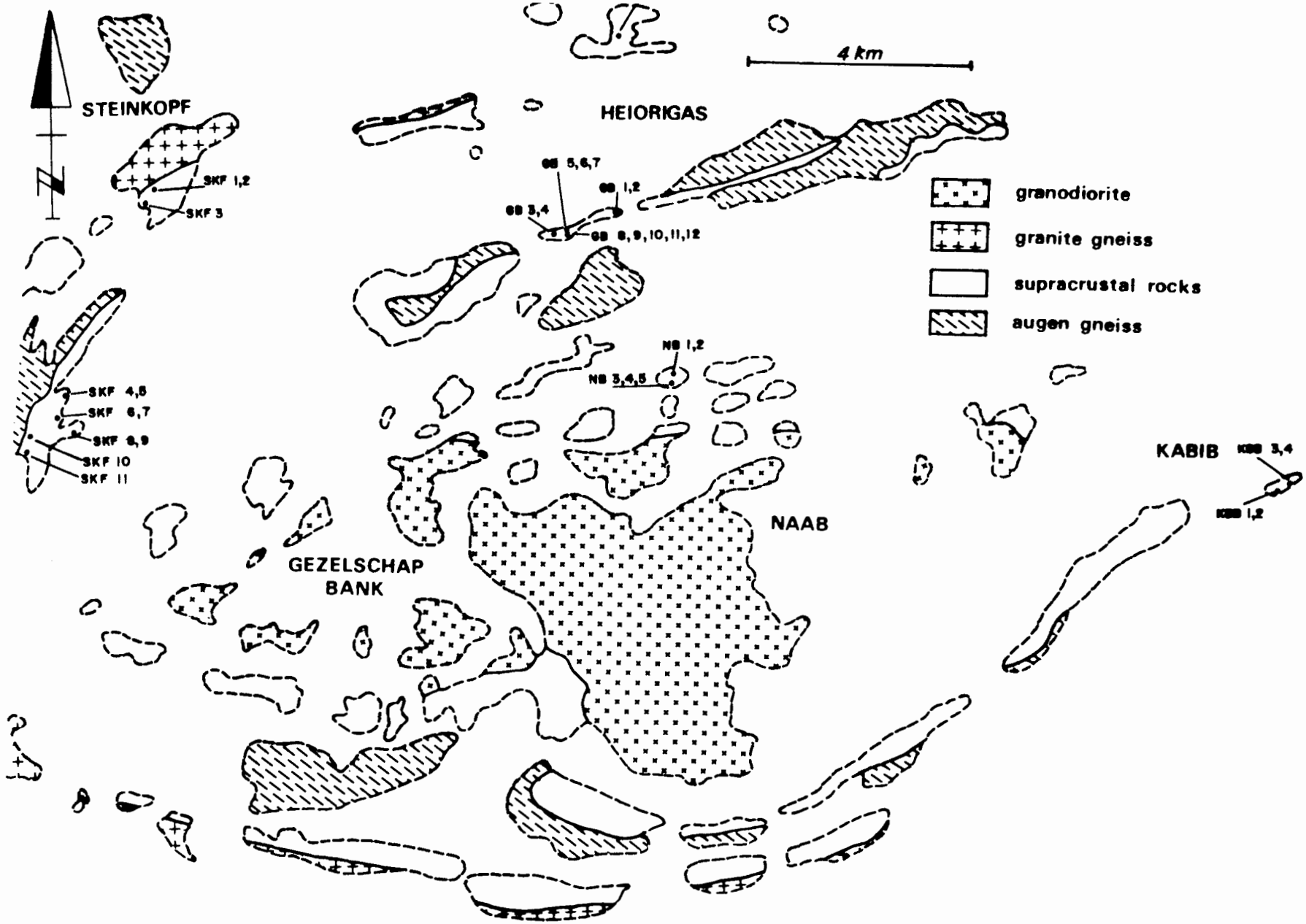

Fig. A.6. Sample locality map for the Geselskapbank area. Geological data simplified from D. Strydom (Ph.D thesis, in prep., U.O.F.S.).

Additional samples, not included on the above maps, are :-

WF-1,2 - Wilgenhoutfontein farm, north-east of Garies

DBD-1 - Dabidas farm, north of Kliprand

LB-1,2 - Luisberg, Brakdam farm, north of Gamoep

KO-1,3,4,5,6,7,8 - Kouberg, north-east of Gamoep

EK2-35,130,180,210 - Eendop se Kop, south of Geselskapbank

BB-1,2,3,4,5,6,7,8,9,10 - Beenbreek farm, east of Kabib, Geselskapbank

ER-1,2,3,4,6 - Eenriet mountains, north-east of Steinkopf

BH156-1,2,3,4,5,6,7,8, BHU-148,213,302,424, BH114-32, BH126-35 - borehole core samples from Broken Hill, Aggeneys

AG56, AG56-100,115,240, AG51-145,215, AG80-195 - borehole core samples from Swartberg (Black Mountain), Aggeneys

SW26, SW26-85,145,175, SW22-155 - borehole core samples from Big Syncline, Aggeneysberge

SYN-1, FU - Zuurwater farm, Aggeneys.

METAPELITIC ROCKS

	LC-2	WG-1	BA-1	WP-2	BI-23	BI-5	BP-8	KB-4	BI-11	RP-1	ZR-1	BP-5
SIO2	61.18	60.68	60.51	65.68	62.35	67.11	68.30	61.99	64.07	63.17	60.11	66.08
TIO2	1.13	1.16	1.13	1.09	1.10	.90	.81	1.14	.79	.86	1.16	.93
AL2O3	18.28	18.20	18.02	18.11	17.99	16.64	16.61	19.38	18.25	18.59	17.90	16.98
FEO	7.99	8.74	8.95	7.28	8.44	6.01	5.62	7.71	6.53	6.57	8.86	6.46
MNO	.14	.15	.14	.11	.15	.09	.09	.13	.09	.07	.10	.09
MGO	2.62	2.65	2.64	2.29	2.69	1.73	1.87	2.50	2.16	2.53	2.83	1.99
CAO	1.35	1.12	1.18	1.35	1.39	.86	.99	.86	1.06	.51	1.60	.90
NA2O	1.48	1.53	1.72	1.20	1.40	1.63	1.64	1.18	1.73	.93	1.80	1.39
K2O	3.40	3.38	3.25	1.42	2.98	4.10	3.99	4.02	3.98	4.40	3.26	3.77
P2O5	.18	.10	.11	.06	.13	.10	.05	.09	.10	.10	.11	.08
LOI	1.42	1.33	1.25	1.13	1.07	.63	.27	.82	.83	1.18	1.58	.69
H2O-	.13	.14	.11	.12	.15	.11	.09	.09	.15	.13	.11	.21
TOTAL	99.34	99.23	99.07	99.87	99.84	99.96	100.40	99.94	99.78	99.05	99.49	99.60
RB	102	108	80	66	101	176	147	166	175	176	255	169
BA	914	1090	1105	488	877	810	853	1290	718	907	1045	892
SR	142	152	166	127	128	127	147	127	147	123	151	125
TH	19	24	21	22	22	17	17	20	17	23	22	18
U				3.4						2.8		
ZR	328	340	317	263	362	241	239	297	197	234	330	355
NB	16	16	14	18	16	15	17	21	14	17	17	19
CR	98	110	132	88	101	70	66	103	77	82	121	80
V	122	113	131	108	119	108	89	115	114	104	131	115
SC	22	22	20	24	19	15	15	19	16	15	25	16
NI	45	51	57	45	48	53	26	52	33	35	66	35
CO	26	27	28	25	27	24	19	26	19	21	26	18
PB	23	28	29	16	23	34	28	32	28	30	20	25
ZN	112	128	131	114	130	116	97	118	127	116	149	125
CU		12		48	27				13			
Y	53	49	47	52	50	46	49	66	42	46	49	50
LA	42	49	48	45	50	31	40	53	32	43	51	35
CE	94	99	93	92	101	88	84	101	80	90	107	85
ND	46	49	46	46	50	39	43	45	37	43	54	40

METAPELITIC ROCKS

	ZR-4	BI-13	KB-1	BI-2	BI-6	BI-4	LC-5	ZR-2	KB-3	BP-4	HY-2	HY-3
SIO2	63.43	59.52	60.79	63.02	69.69	65.44	60.85	59.94	56.97	64.09	65.64	58.92
TIO2	.98	1.00	.86	.85	.80	1.02	1.08	1.20	1.10	.86	.78	1.16
AL2O3	19.03	20.93	17.52	18.16	13.50	16.18	18.53	18.55	21.55	17.14	16.09	24.75
FEO	7.14	8.04	7.39	7.25	4.11	6.74	8.20	8.99	9.66	6.81	6.43	8.77
MNO	.09	.11	.12	.11	.05	.10	.14	.13	.12	.10	.10	.14
MGO	2.47	2.63	3.77	2.16	1.47	1.90	2.52	2.48	2.58	2.26	3.54	2.18
CAO	.93	.87	2.37	1.12	2.08	1.92	1.22	.90	.07	.92	2.46	.49
NA2O	1.22	1.04	1.56	1.84	2.15	1.87	1.67	1.64	1.32	1.34	2.19	.73
K2O	3.45	4.53	3.80	4.10	4.61	2.88	3.48	2.69	3.29	4.64	1.97	2.74
P2O5	.08	.07	.14	.09	.17	.26	.11	.09	.08	.08	.07	.02
LOI	.87	.81	.97	.68	.69	1.15	1.09	2.00	1.31	1.76	.43	< .06
H2O-	.17	.10	.11	.16	.21	.23	.13	.13	.12	.04	.06	
TOTAL	99.89	99.71	99.47	99.58	99.56	99.71	99.07	98.77	99.13	100.10	99.78	99.91
RB	136	173	251	166	186	93	113	99	114	201	125	152
BA	1045	1145	1395	770	972	780	1040	1120	244	841	722	767
SR	132	162	222	130	215	164	166	191	188	113	158	48
TH	17	18	14	13	10	20	19	17	20	16	16	22
U												
ZR	238	206	228	164	284	394	294	343	264	221	215	317
NB	17	19	11	16	15	16	15	16	17	15	17	23
CR	117	97	139	82	60	82	104	124	130	74	99	117
V	120	117	108	128	83	102	106	139	135	117	99	101
SC	16	18	21	20	12	18	20	20	22	19	16	23
NI	63	45	62	42	25	43	45	58	52	34	40	41
CO	24	25	24	20	13	19	27	27	29	17	22	28
PB	25	26	29	28	24	26	28	23	31	21	11	11
ZN	96	110	106	124	90	77	114	116	146	123	95	88
CU										3.1	7.3	
Y	49	46	53	47	23	57	49	43	43	50	36	56
LA	43	42	29	38	34	40	42	45	44	43	39	57
CE	79	86	64	79	70	98	93	96	95	88	77	109
ND	40	41	38		39	53	45	48	46	42	35	46

METAPELITIC ROCKS

	TW-4	DM-3	DM-9	SK-1	SK-7	HY-20	VK-4	SK-6	TW-10	BPT-3	ROF-7	KGV-1
SIO2	70.56	70.21	62.99	73.46	72.00	64.57	69.40	70.36	65.38	64.56	71.20	64.37
TIO2	.76	1.06	.97	.67	1.19	.78	.81	1.09	1.08	.80	1.01	1.08
AL2O3	18.76	15.36	18.66	12.75	13.03	18.03	14.19	12.88	19.97	16.66	14.11	16.10
FEO	5.28	6.29	7.85	5.09	6.89	5.22	5.28	6.49	6.38	6.85	6.01	8.30
MNO	.03	.03	.07	.04	.03	.06	.04	.04	.06	.16	.10	.18
MGO	1.03	1.94	3.01	1.20	1.39	1.25	1.68	1.37	1.99	2.15	2.34	2.59
CAO	.14	.15	.18	1.21	1.40	1.36	.24	1.25	.23	1.43	1.18	1.23
NA2O	.47	.74	.49	2.10	.97	2.36	3.15	1.82	.64	1.20	.96	1.33
K2O	2.56	3.16	3.18	2.90	1.79	4.69	4.10	2.50	2.45	3.08	1.73	3.45
P2O5	.03	.05	.04	.04	.03	.08	.05	.07	.04	.08	.06	.11
LOI	.31	1.07	1.92	.66	.06	.98	.25	.85	.85	1.13	.93	.97
H2O-	.14	.22	.14	.13	.09	.11	.11	.10	.12	.08	.09	.10
TOTAL	100.10	100.30	99.53	100.30	98.91	99.53	99.33	98.85	99.20	98.21	99.71	99.79
RB	87	121	116	118	75	142	149	114	98	146	91	117
BA	307	711	596	738	1215	2045	543	564	581	959	480	1030
SR	69	66	54	154	182	167	34	151	37	100	58	121
TH	24	6.6	17	15	14	19	15	13	10	14	29	15
U								1.8				
ZR	305	351	247	233	476	306	281	360	397	199	330	233
NB	15	16	16	10	14	16	18	13	22	15	16	12
CR	122	102	114	44	80	50	91	123	114	89	95	107
V	79	102	111	67	114	64	69	99	115	98	90	112
SC	22	16	13	10	20	9.6	8.3	16	16	20	15	19
NI	27	37	51	23	32	15	30	40	41	35	35	55
CO	19	19	28	12	20	16	19	19	23	19	23	28
PB	7.1	16	8.0	23	16	48	16	16	13	24	12	14
ZN	19	79	93	81	116	84	49	85	80	82	92	114
CU	12	3.1	15	31	2.0	13	1.0	3.0	22	11	10	60
Y	55	4.6	20	27	45	22	14	44	23	47	35	34
LA	55	25	40	38	54	54	45	36	30	43	51	40
CE	110	51	73	72	90	99	87	76	55	76	99	73
ND	45	20	31	32	40	43	33	39	22	35	44	33

METAPELITIC ROCKS

	GN-5	PH-1	RW-3	WW-3	WW-4	WW-8	WW-10	WW-13	ZR-5	BA-3	SS-2	SS-5
SIO2	64.47	68.52	56.47	63.03	70.48	69.55	61.80	68.24	55.90	58.51	66.24	69.76
TIO2	1.14	.75	1.11	.83	.84	.68	.76	.73	1.22	1.02	.68	.66
AL2O3	14.74	10.73	21.50	17.65	15.18	15.76	18.69	17.50	20.64	17.34	20.55	16.99
FEO	6.45	5.99	9.87	7.12	5.24	5.64	6.92	5.18	9.78	8.60	1.60	3.23
MNO	.11	.08	.18	.09	.05	.10	.09	.08	.12	.14		
MGO	2.19	1.65	2.70	2.94	1.79	1.67	2.46	1.60	2.56	3.85	.62	1.40
CAO	.81	.24	.20	.73	1.02	1.03	.89	.70	.86	2.23	.12	.09
NA2O	.13	1.46	.75	1.45	1.03	1.69	1.09	1.71	1.32	1.39	.07	.05
K2O	3.77	2.39	2.64	5.17	3.34	3.15	4.33	3.91	1.63	3.90	4.73	2.00
P2O5	.10	.04	.07	.11	.08	.06	.11	.07	.10	.16	.02	.01
LOI	3.93	.39	1.15	.80	1.12	.77	2.63	.59	2.50	1.78	4.95	5.43
H2O-	.63	.11	3.16	.10	.09	.16	.15	.15	.18	.11	.84	.81
TOTAL	98.46	101.40	99.79	100.00	100.20	100.30	99.92	100.40	98.81	99.03	100.40	100.40
RB	133	189	123	255	245	99	257	185	113	154	328	114
BA	757	911	1120	881	522	817	753	778	1145	1240	447	331
SR	38	90	78	76	60	151	64	107	183	211	27	13
TH	12	16	21	19	18	13	19	16	21	17	13	15
U							2.8					
ZR	210	283	247	200	289	248	194	231	301	247	152	175
NB	11	16	17	14	16	16	13	17	17	12	11	12
CR	111	106	133	89	75	71	80	59	132	144	106	105
V	84	117	139	97	57	66	110	65	151	126	90	69
SC	13	16	20	18	16	15	20	14	25	22	11	20
NI	25	51	53	39	30	23	34	17	68	67	8.1	20
CO	14	24	30	23	15	17	14	14	27	26	4.0	12
PB	22	17	26	33	27	33	33	36	31	21	11	
ZN	49	91	128	113	93	70	125	81	135	144	18	50
CU	42	2.1	2.9		1.8	4.4	73	5.5			17	27
Y	26	32	39	47	41	40	42	38	40	27	18	23
LA	29	36	46	40	43	52	45	58	23	39	55	23
CE	46	73	88	93	80	92	84	104	43	79	46	47
ND	20	32	41	40	38	38	38	45	20	41	61	23

METAPELITIC ROCKS

	SS-8	SS-9	SKF-1	SKF-2	SKF-4	SKF-9	NB-3	NB-5	NB-6	KN-11	BB-1	BB-6
SIO2	69.69	55.76	67.00	66.62	53.39	57.24	67.17	66.00	65.48	57.40	75.59	72.87
TIO2	.88	.89	.66	.75	.90	.86	.96	1.07	.89	1.08	.56	.52
AL2O3	17.16	23.72	19.39	20.20	24.49	22.75	16.27	15.84	13.97	22.60	12.75	12.56
FEO	3.80	6.16	.86	1.98	9.46	8.58	7.79	7.96	7.52	4.55	3.98	5.36
MNO		.01	.01	.01	.10	.20	.11	.11	.10	.02	.03	.05
MGO	.75	1.11	.73	.32	2.70	2.28	2.50	2.29	3.06	1.20	.70	1.76
CAO	.06	.04	.16	.06	.20	.21	1.12	1.11	2.81	.10	.04	.11
NA2O	.04	.09	.15	.08	.93	.88	.99	1.22	1.94	.05	.07	.10
K2O	1.78	6.21	5.20	2.70	4.97	5.80	2.29	2.32	1.83	2.18	2.26	3.81
P2O5	.01	.01	.03	.05	.08	.08	.02	.04	.01	.04	.02	.08
LOI	6.03	5.27	5.48	6.39	1.25	.84	1.03	1.37	.97	7.15	3.34	2.53
H2O-	.82	1.19	.42	.56	.12	.09	.08	.26	.24	2.95	.39	.29
TOTAL	101.00	100.50	100.10	99.71	98.59	99.80	100.30	99.58	98.83	99.32	99.73	100.00
LI	156	303	279	155	183	172	67	58	84	160	170	215
BA	210	596	412	192	952	825	1005	1435	712	370	628	500
SR	11	50	20	13	118	106	160	144	200	30	14	7.8
TH	15	13	17	18	14	23	15	18	9.0	24	11	16
U			4.8	6.7		4.5					3.0	
ZR	250	168	199	205	181	174	290	307	256	310	314	314
NB	16	15	13	17	16	12	11	11	8.5	18	15	16
CR	120	124	87	119	120	107	142	113	134	157	86	65
V	72	86	200	214	112	101	113	111	126	102	48	60
SC	19	26	18	18	25	22	20	19	22	22	14	14
NI	13	41	4.5	5.4	65	61	53	45	65	78	9.4	14
CO	12	34	1.5	3.1	33	35	29	27	31	18	5.7	6.0
PB		5.5	16	3.2	30	32	16	22	12	25	27	
ZN	54	100	5.5	32	39	121	88	94	89	66	163	12
CU	60	5.2	8.4	18			6.6	3.1	34	12	30	2.4
Y	13	24	21	25	40	32	9.8	7.0	12	27	16	43
LA	25	26	23	25	40	43	30	33	24	47	14	12
CE	62	51	51	58	86	86	59	67	41	74	36	31
ND	35	30	24	26	41	41	27	32	17	31	16	14

METAPELITIC ROCKS

	BB-8	BB-9	AG51-215	AG56-115	BH156-1	BH156-2	BH156-3	BH156-4	BH156-5	BH156-7	HS4-55	BH114-32
SIO2	77.05	75.95	70.90	76.58	71.18	69.88	67.86	65.52	56.77	62.29	62.52	63.27
TIO2	.50	.58	.66	.48	.65	.67	.65	.76	.94	.75	.66	.82
AL2O3	13.02	13.82	14.64	10.08	14.75	16.84	16.28	17.94	20.42	19.68	16.47	19.19
FEO	2.96	.81	4.76	6.56	4.49	4.98	4.72	5.25	9.22	9.96	6.76	6.22
MNO	.03	.01	.05	.16	.03	.03	.04	.04	.33	.46	.04	.26
MGO	.55	.45	1.12	1.16	1.14	1.13	1.34	1.44	1.29	.85	1.97	1.23
CAO	.07	.15	.17	.07	.14	.11	.16	.15	.07	.11	.35	.28
NA2O	.10	.25	.10	.06	.41	.18	.30	.26	.06	.07	.62	.15
K2O	1.71	3.74	3.52	2.30	2.66	2.77	3.24	4.03	5.51	2.33	5.75	5.18
P2O5	.02	.04	.11	.03	.06	.04	.03	.04	.04	.07	.06	.12
LOI	3.70	3.60	2.75	1.54	3.58	2.84	3.79	2.72	4.17	2.11	5.04	2.14
H2O-	.41	.38	.34	.14	.29	.31	1.02	.03	.36	.30	.28	.28
TOTAL	100.10	99.78	99.11	99.16	99.36	99.77	99.42	98.18	99.16	98.98	100.50	99.14
RB	124	226	180	125	157	177	184	218	285	163	375	277
BA	349	536	509	536	455	260	423	468	683	3325	615	1535
SR	6.6	22	8.7	7.5	56	25	41	32	13	24	31	48
TH	14	16	15	13	18	17	15	16	19	21	19	18
U					4.8		3.7		4.4	4.6	7.0	
ZR	315	226	357	524	365	343	300	285	271	273	171	322
NB	12	18	15	15	15	15	14	16	24	18	18	18
CR	71	67	89	94	93	94	98	114	116	97	120	75
V	41	71	42	27	73	56	124	98	89	72	245	85
SC	12	13	11	5.7	15	16	15	18	17	15	17	17
NI	5.5	3.3	18	10	19	23	25	20	31	11	60	20
CO	3.6		12	22	11	12	12	14	22	30	24	13
PB	12	29	9.3	36	18	4.5	20	26	42	85	52	45
ZN	104	7.3	117	280	73	34	81	114	824	535	359	99
CU	42	32		2220	24	12	29	25	81	25	217	
Y	17	21	31	30	19	22	22	22	30	37	41	37
LA	15	20	25	34	22	20	22	22	29	42	48	33
CE	34	43	58	82	51	49	44	54	70	83	109	69
ND	16	19	29	42	23	20	20	24	33	35	55	34

METAPELITIC ROCKS

	SW22-155	SW26-145	AG80-195	GK4-58	BH126-35	EK2-35	EK2-130	EK2-210	LB-1	9-PEL	ROF-3	ROF-12
SIO2	64.95	65.34	63.41	60.20	64.74	57.99	61.90	63.78	61.20	60.60	68.77	70.62
TIO2	.70	.59	.84	.87	.83	.74	.71	.66	.91	.73	.96	.89
AL2O3	19.55	12.50	18.18	20.37	18.78	19.57	18.73	16.17	22.36	18.61	14.50	14.92
FEO	5.90	7.57	5.69	7.00	5.48	8.75	7.71	9.47	7.11	5.71	6.56	4.96
MNO	.03	.65	.17	.07	.31	.08	.06	.05	.10	.08	.15	.08
MGO	.86	1.10	1.54	1.92	1.10	1.48	1.28	1.05	.98	1.70	2.19	.31
CAO	.05	.85	.11	.24	.22	.07	.05	.04	.12	.91	1.75	1.29
NA2O	.08	.18	.19	.15	.19	.08	.07	.08	1.10	.88	1.47	1.11
K2O	3.69	3.75	5.62	5.45	5.02	4.65	3.79	3.71	4.92	5.58	2.46	4.01
P2O5	.04	.13	.04	.02	.10	.06	.07	.04	.14	.13	.04	.20
LOI	2.68	3.54	3.24	3.04	1.63	4.00	3.97	3.31	1.68	2.66	1.66	1.30
H2O-	.26	.23	.47	.46	.11	.29	.29	.23	.17	.16	.08	.16
TOTAL	98.79	96.42	99.50	99.80	98.50	97.78	98.64	98.59	100.80	97.73	100.60	99.85
RB	202	225	253	251	267	328	258	224	188	215	154	168
BA	661	847	646	967	2945	595	535	563	491	1085	489	1505
SR	47	50	19	21	46	18	13	10	24	112	95	127
TH	15	9.1	17	10	18	20	17	45	15	16	9.5	19
U	4.6	4.6	3.6		5.2	4.4						
ZR	205	233	277	198	326	204	256	237	263	226	241	378
NB	16	11	21	14	20	20	20	15	16	14	19	21
CR	102	63	105	132	52	66	49	69	95	162	110	12
V	160	63	78	99	63	88	57	69	91	114	107	68
SC	17	11	18	17	16	20	16	17	21	21	19	17
NI	23	19	26	35	11	23	17	19	26	39	35	5.4
CO	8.5	9.5	14	21	10	16	22	18	19	19	22	12
PB	15	6290	89	11	62	6.7	5.2	41	14	13	9.4	23
ZN	290	11930	236	74	269	107	80	96	83	72	78	68
CU	2.9	130		17	49	167	373	1890	24		6.9	45
Y	21	28	29	34	31	34	38	27	49	32	44	33
LA	20	20	24	17	30	29	34	25	35	30	32	39
CE	49	51	60	35	73	63	77	54	68	58	68	80
ND	23	22	28	18	37	31	36	26	29	27	38	36

	METAPELITIC ROCKS				METAPSAMMITIC ROCKS							
	TW-13	KO-5	HK-1	TW-14	KN-9	KN-10	BI-20	BI-24	BI-1	BI-19	BP-3	WG-2
SIO2	68.48	55.94	66.20	66.21	74.03	75.91	67.45	67.52	74.47	69.72	68.91	82.37
TIO2	.79	1.08	.93	1.10	.73	.65	.74	.76	.55	.61	.74	.46
AL2O3	14.29	25.02	15.91	15.05	12.78	11.56	14.40	14.38	12.16	13.93	14.60	8.40
FEO	4.79	4.62	5.52	7.98	4.35	2.44	5.20	5.15	3.69	4.21	4.83	1.76
MNO	.08	.02	.08	.07	.02		.10	.09	.06	.07	.08	.04
MGO	1.45	.86	1.94	2.07	.30	.83	2.42	2.42	1.17	2.06	1.62	.66
CAO	2.61	.05	1.28	1.39	.34	.04	3.81	3.39	1.62	2.33	1.33	1.41
NA2O	2.50	.18	1.89	2.02			2.95	2.58	1.70	2.12	2.29	1.21
K2O	3.56	3.04	5.24	3.34	1.27	4.24	2.01	2.33	2.43	3.28	4.25	3.19
P2O5	.18	.07	.08	.05	.07	.07	.18	.18	.07	.17	.09	.13
LOI	1.30	7.52		.21	5.28	3.07	.50	1.04	1.34	.97	.67	.59
H2O-	.17	.41	.10	.21	.71	.18	.06	.09	.08	.11	.05	.07
TOTAL	100.20	98.82	99.95	99.74	99.86	99.01	99.85	99.97	99.34	99.63	99.49	100.20
RB	150	191	255	192	56	183	133	143	104	143	167	109
BA	1095	846	988	899	874	526	574	487	674	879	1285	738
SR	262	18	163	165	63	52	189	222	160	202	211	121
TH	18	12	21	15	41	11	13	14	12	11	14	9.0
U					3.6		3.9					
ZR	194	291	258	306	227	301	224	226	220	203	268	293
NB	15	20	18	16	14	13	15	12	10	11	16	8.0
CR	26	118	72	102	94	132	94	90	42	76	59	19
V	79	138	81	113	112	69	90	93	46	76	83	29
SC	11	9.9	15	18	10	15	18	15	11	14	14	5.9
NI	13	28	28	49	17	22	49	52	19	37	24	9.5
CO	14	12	17	22	7.8	17	20	21	12	17	13	4.5
PB	29	12	26	21	24	18	17	18	21	21	27	15
ZN	79	72	84	100	47	22	92	96	68	79	89	24
CU		3.6	16	3.1	11		2.9	28		4.1		
Y	27	8.4	54	55	99	11	36	39	36	32	59	36
LA	17	16	44	42	44	16	24	37	24	23	39	23
CE	41	35	95	87	90	37	61	71	63	46	91	50
ND	20	17	46	41	48	17	31	36	36	28	43	33

METAPSAMMITIC ROCKS

	BI-9	BI-14	LC-3	BI-15	KB-2	VK-11	TW-1	KO-3	PH-6	PH-11	PH-16	BPT-2
SIO2	70.97	74.18	71.80	70.32	75.76	70.13	71.58	71.23	70.76	65.95	68.21	66.50
TIO2	.77	.35	.46	.62	.67	.59	.46	.13	.51	.59	.56	.69
AL2O3	12.50	13.19	14.31	14.61	12.02	14.85	13.98	10.42	14.47	13.43	14.80	15.65
FEO	4.68	2.75	3.60	3.46	3.75	3.22	2.47	5.87	3.34	4.79	3.39	3.92
MNO	.06	.05	.07	.04	.05	.05	.07	.23	.05	.10	.05	.07
MGO	1.28	.93	.89	1.18	.89	1.11	.70	.83	1.01	4.23	.92	.78
CAO	1.68	.78	1.21	1.11	.61	1.79	2.15	.15	2.57	4.60	2.43	3.33
NA2O	2.18	1.46	1.83	2.69	1.28	2.78	3.24	.47	1.92	2.11	3.02	2.68
K2O	5.10	4.45	4.51	4.48	3.54	5.42	4.37	6.36	3.30	1.25	4.68	4.28
P2O5	.18	.09	.06	.11	.08	.17	.16	.06	.15	.19	.17	.23
LOI	.50	1.07	.73	.53	1.27	.49	.28	1.43	.92	.77	.49	.36
H2O-	.20	.31	.09	.14	.08	.07	.07	.44	.12	.09	.08	.05
TOTAL	100.10	99.63	99.59	99.32	100.00	100.20	99.53	97.61	99.14	98.19	98.82	98.55
RB	184	185	169	169	156	179	189	311	196	106	181	214
BA	769	1000	1100	1035	762	1600	850	2465	961	397	967	1505
SR	167	161	154	181	91	308	226		312	564	268	377
TH	7.3	9.0	13	15	18	28	15	11	18	13	56	10
U							1.9					
ZR	311	227	166	318	262	384	207	192	221	161	282	324
NB	12	8.0	13	14	12	14	17	11	11	10	13	12
CR	56	22	33	47	31	3.8	3.2	1.6	14	305	10	12
V	71	45	38	67	59	37	21	8.1	46	72	61	55
SC	15	6.1	10	10	11	4.7	7.9	4.6	11	16	9.0	13
NI	24	11	11	19	18	5.6	1.1	13	5.7	127	5.1	6.0
CO	13	6.7	8.2	8.7	11	8.3	4.4	11	6.5	24	7.3	9.2
PB	20	23	26	26	13	36	22	54	30	22	36	40
ZN	86	50	53	81	53	54	45	142	59	66	49	64
CU						2.3	2.0	12000	6.7			
Y	30	28	49	42	34	21	36	23	31	30	23	33
LA	30	20	38	36	33	96	55	22	47	40	73	44
CE	67	50	73	73	77	162	102	37	85	76	128	83
ND	35	28	36	35	32	55	44	19	37	37	52	41

METAPSAMMITIC ROCKS

	ROF-1	ROF-2	ROF-6	ROF-10	PH-2	GHP-1	WW-1	WW-5	ZR-6	SS-7	RFN-6	RFN-7
SIO2	66.09	65.73	66.13	66.22	63.38	74.16	70.20	71.88	66.54	84.99	71.55	74.48
TIO2	.91	.75	.70	.73	.82	.25	.56	.75	.79	.47	.58	.26
AL2O3	15.76	13.92	14.01	15.72	15.26	14.20	14.73	13.83	14.54	7.54	13.98	13.48
FEO	4.29	9.11	8.05	4.50	5.01	1.51	4.45	4.32	5.51	2.39	3.37	1.49
MNO	.04	.18	.18	.10	.10	.03	.04	.06	.10		.04	.02
MGO	1.14	.58	.62	1.43	2.85	.54	1.49	1.50	2.39	1.08	.81	.56
CAO	2.42	4.10	3.08	3.31	4.08	1.80	1.80	1.33	2.87	.02	2.18	1.07
NA2O	2.73	2.00	2.25	2.34	2.40	2.35	1.81	1.63	1.99	.03	3.00	3.46
K2O	5.61	2.28	3.74	4.67	4.64	4.61	3.93	3.57	3.07	1.34	4.85	5.32
P2O5	.27	.27	.28	.20	.34	.06	.07	.92	.19	.02	.15	.06
LOI	.58	.33	.24	.38	.74	.77	1.08	1.27	1.38	2.04	.25	.73
H2O-	.10	.06	.06	.06	.07	.10	.09	.11	.08	.23	.05	.08
TOTAL	99.93	99.32	99.32	99.66	99.68	100.40	100.30	100.40	99.45	100.10	100.80	101.00
RB	291	96	143	223	219	179	190	150	118	87	212	239
BA	1040	1520	1535	2290	1125	1270	792	812	708	225	1030	896
SR	184	270	226	401	370	202	104	123	223	2.0	152	153
TH	35	12	13	11	45	15	20	19	14	8.9	22	33
U												3.7
ZR	812	386	340	278	409	243	273	365	247	327	265	168
NB	16	12	12	13	15	8.1	12	13	13	7.9	20	17
CR	5.9			12	89	3.0	49	48	102	57	8.4	5.0
V	41	3.3	5.0	61	92	8.8	49	41	94	38	35	15
SC	8.9	22	24	15	13	5.2	10	11	15	8.9	12	5.5
NI	2.5			7.0	39		17	14	52	7.0	6.6	4.2
CO	8.3	4.5	7.1	9.1	17	2.2	10	12	20	10	9.9	3.7
PB	27	25	25	32	51	41	32	28	29		24	25
ZN	76	114	111	62	69	28	99	66	97	20	38	9.5
CU	6.5				2.2		8.2		4.4	4.7	4.5	
Y	32	65	67	33	27	23	47	43	35	4.8	53	30
LA	147	40	44	37	66	78	42	46	39	17	66	50
CE	294	89	84	70	135	135	89	90	80	38	127	94
ND	117	50	48	36	61	51	42	39	39	18	62	40

METAPSAMMITIC ROCKS

	RFN-8	SKF-8	ER-6	BB-3	BB-4	SW26-175	HY-5	ROF-5	ROF-11
SIO2	69.96	71.35	79.69	75.17	86.82	77.49	78.22	75.15	70.71
TIO2	.77	.76	.16	.16	.60	.54	.33	.27	.40
AL2O3	14.19	13.74	13.55	6.76	6.77	10.51	10.19	12.88	14.05
FEO	4.10	5.42	.83	4.09	.69	4.19	3.61	2.44	3.45
MNO	.03	.10	.01	.08	.01	.18	.04	.11	.09
MGO	1.13	1.39	.04	5.18	.20	.80	2.89	.26	2.24
CAO	2.52	1.36	.02	1.64	.54	.96	.26	.99	3.88
NA2O	2.80	1.92	.16	.15	3.39	.15	.41	1.69	2.77
K2O	4.95	2.49	3.78	3.05	.85	3.33	1.95	5.71	1.60
P2O5	.19	.07	.02	1.31	.05	.08	.06	.04	.11
LOI	.28	.97	1.77	.95	.28	1.49	2.06	.78	.78
H2O-	.07	.12	.18	.11	.11	.07	.03	.05	.11
TOTAL	101.00	99.68	100.20	98.59	100.30	99.79	100.00	100.40	100.20
RB	225	60	185	279	34	196	92	234	183
BA	953	826	486	144	160	972	375	1060	641
SR	158	169	12	7.6	50	50	21	160	257
TH	21	14	11	8.2	17	12	13	24	16
U					3.6				4.8
ZR	281	203	113	251	920	266	174	178	137
NB	19	9.7	8.7	6.6	19	12	11	8.0	12
CR	14	71	2.1	35	174	50	21		125
V	59	70	2.7	51	21	48	34	9.0	48
SC	15	14	4.8	9.0	6.1	9.3	6.6	5.0	12
NI	9.5	30		38	1.9	17	9.7	1.6	53
CO	9.9	18		7.5	1.7	12	7.7	3.4	14
PB	17	20	2.9		6.7	49	8.4	41	17
ZN	21	71	2.0	44	2.8	126	48	53	54
CU		98	5.2		1.1				
Y	50	25	11	38	56	28	23	38	33
LA	59	26	17	5.1	16	28	22	43	32
CE	115	54	34	18	37	60	42	84	62
ND	58	27	18	13	18	29	20	45	31

MAGNESIAN GNEISSES

	HY-4	HY-7	HY-9	HY-12	HY-13	HY-17	HY-22	HY-10	HY-15	ND-6	GN-1	ND-2
SIO2	52.39	43.73	31.35	47.68	34.72	47.67	70.62	71.68	62.23	35.37	46.50	45.02
TIO2	.98	.53	1.01	.32	1.14	.51	.50	.44	1.05	4.26	1.95	2.00
AL2O3	19.83	33.34	32.57	25.87	24.06	33.34	13.54	14.70	16.08	17.81	16.04	18.72
FEO	8.54	5.18	1.93	9.05	16.93	4.60	5.32	1.00	6.16	15.35	15.75	10.62
MNO	.12	.09	.04	.19	.24	.14	.10	.05	.08	.14	.14	.19
MGO	9.79	7.91	20.53	13.31	17.51	7.99	6.61	7.61	9.70	19.99	16.80	19.72
CAO	.40	2.17	.12	.10	.26	.20	.15	.07	.20	1.01	.48	.53
NA2O	.40	1.59	.24	.32	.70	.86	.11	.40	.16	.65	.34	1.21
K2O	3.24	2.45	5.33	.94	.03	2.61	1.37	1.87	1.95	.13	.38	.10
P2O5	.12	.08	.08	.02	.06	.07	.12	.03	.15	.48	.22	.04
LOI	3.00	1.67	6.16	1.37	1.17	1.57	1.18	2.26	1.12	1.59	.71	1.10
H2O-	.33	.09	.15	.12	.12	.11	.10	.14	.11	.13	.19	.12
TOTAL	99.15	98.83	99.51	99.31	97.93	99.67	99.74	100.30	98.99	96.94	99.50	99.37
RB	188	132	347	69	2.2	83	99	151	97	9.0	26	8.4
BA	647	1375	275	106	2.6	1590	348	122	99	4.3	19	8.9
SR	33	557	63	5.3	6.1	29	6.1	6.3	4.2	7.4	4.9	7.4
TH	5.7	37	23	17	1.0	40	12	23	8.5		2.5	12
U		4.9	4.0	2.9	1.9	5.0	2.5	3.6				3.9
ZR	137	544	525	216	53	520	198	273	236	324	142	208
NB	8.4	36	32	14	3.8	40	15	26	14	28	11	14
CR	45	20	18	62	302	26	16	8.0	70	83	228	
V	191	38	102	85	332	55	51	38	162	403	327	456
SC	20	38	23	23	45	35	12	13	26	50	49	54
NI	30	8.5	18	36	315	12	13	5.4	37	95	78	8.7
CO	25	5.6	7.6	25	75	9.9	15	2.6	22	59	56	39
PB		18	8.7	4.6	3.0	10	1.8	5.8			5.3	10
ZN	103	53	19	35	102	57	70	15	45	118	150	74
CU											3.4	
Y	21	86	48	34	67	100	32	16	44	66	25	58
LA	13	135	123		4.5	90	37	29	18	12		6.6
CE	34	230	189	8.5	13	172	72	56	47	63	22	31
ND	17	99	59	4.9	6.6	82	34	23	26	45	18	16

MAGNESIAN GNEISSES

	ND-3	ND-4	RW-4	RW-5	SKF-10	ER-1	9-CD	7-K	7-CD	7-S	7-SI
SIO2	38.02	57.69	51.30	46.33	44.66	45.81	46.64	34.43	41.84	42.04	45.39
TIO2	2.05	1.69	1.16	.68	1.44	.66	.65	.46	.43	.46	.49
AL2O3	19.53	14.46	18.95	20.19	34.63	15.34	26.65	27.02	30.77	31.92	32.08
FEO	13.04	12.80	10.60	9.33	9.36	17.58	1.59	6.39	5.00	5.07	5.64
MNO	.26	.22	.23	.13	.19	.67	.08	.10	.08	.08	.09
MGO	21.55	9.81	8.99	12.93	6.72	10.90	10.44	20.33	14.36	14.26	6.69
CAO	.36	.41	1.16	.19	.38	.56	.15	.02	.31	.40	2.16
NA2O	.26	.42	2.31	.37	.60	.29	.28	.31	.38	.35	1.74
K2O	2.65	1.43	4.20	5.49	.04	3.09	7.48	7.10	3.23	3.20	3.36
P2O5	.04	.26	.70	.06	.01	.07	.08	.05	.08	.10	.08
LOI	1.44	.23	.62	3.35	2.53	2.30	5.75	2.87	3.31	3.24	1.80
H2O-	.17	.07	.11	.31	.09	.24	.22	.12	.24	.24	.13
TOTAL	99.38	99.49	99.71	99.34	100.70	97.52	100.00	99.21	100.00	101.30	99.65
RB	183	96	205	423	3.0	244	585	340	156	160	178
BA	50	71	791	1025	4.5	496	694	403	478	492	1650
SR	8.9	8.2	63	22	24	32	36	9.9	21	21	387
TH	11	6.6	13	8.9	3.7	3.6	30	32	36	38	39
U				3.3			7.8	9.3	9.0	10	5.7
ZR	216	199	211	59	722	57	377	646	775	824	526
NB	11	13	18	9.2	22	2.3	28	35	25	46	34
CR		164	40	137	383	874	9.8	8.2	7.3	6.1	16
V	410	248	209	281	156	178	63	61	35	32	66
SC	53	38	34	35	19	38	15	33	31	31	38
NI	11	73	15	49	116	362	8.0	22	12	11	7.7
CO	52	32	30	45	44	73	3.2		9.7	8.7	8.1
PB	12	5.8	38	21	7.9	14	7.3	4.2	4.8	4.3	18
ZN	140	88	136	89	47	321	38	114	95	62	60
CU			7.8		486						
Y	44	39	30	15	4.4	13	117	89	84	122	76
LA	6.5	15	35	14			96	68	77	85	93
CE	23	46	74	27			167	148	172	180	188
ND	14	29	32	13			62	78	88	92	87

MAGNESIAN GNEISSES							HORNBLENDE/EPIDOTE ROCKS				
	HY-21	K3-S	K3-K	9-GG	9-ANT	9-SG	KK-1	BI-12	BI-3	BI-18	BI-21
SIO2	67.25	39.19	40.00	39.84	37.80	34.91	59.88	60.78	58.36	61.43	61.76
TIO2	.66	.64	1.39	2.00	1.25	1.74	.73	.78	.79	.78	.72
AL2O3	14.91	25.41	24.02	17.29	19.93	30.31	13.25	14.12	14.28	14.03	12.87
FEO	7.69	7.04	7.84	20.75	14.46	3.79	5.22	5.61	6.05	5.43	4.97
MNO	.15	.11	.18	.22	.14	.06	.10	.16	.11	.10	.09
MGO	5.24	22.17	15.50	9.61	20.11	20.43	3.79	3.41	4.39	3.12	3.62
CAO	.26	.17	.33	.99	.56	.50	8.38	5.31	6.08	5.76	8.35
NA2O		.40	.37	2.27	2.18	1.25	4.76	4.52	3.74	5.06	4.48
K2O	1.53	2.28	6.02	.73	.23	.76	2.87	4.25	4.52	3.03	2.36
P2O5	.20	.08	.18	.18	.20	.03	.19	.20	.22	.19	.19
LOI	2.25	2.32	2.95	2.76	2.96	3.73	.65	.68	.62	.69	.61
H2O-	.15	.13	.17	.12	.12	.15	.10	.08	.05	.13	.05
TOTAL	100.30	99.95	98.95	96.74	99.94	97.67	99.95	99.94	99.25	99.78	100.10
RB	95	94	534	40	15	53	95	151	167	105	
BA	605	206	442	126	3.9	171	677	767	707	636	
SR	7.9	8.4	25	36	6.8	41	472	369	432	420	
TH	11	25	3.9				14	12	1.2	12	
U						4.6					
ZR	147	418	164	105	108	116	191	215	196	206	
NB	11	18	34	9.3	7.3	13	13	13	12	14	
CR	14	29	447	191	1215	162	78	88	97	87	
V	93	168	228	406	328	235	100	117	117	100	
SC	18	41	34	55	52	25	17	18	20	17	
NI	22	18	101	90	300	63	46	71	54	51	
CO	25	9.1	38	33	37	21	24	21	25	22	
PB		4.3	4.4				17	20	14	21	
ZN	110	48	73	127	57	7.9	111	105	119	96	
CU				2.6				15	.6	16	
Y	26	79	26	116	27	31	56	38	45	38	
LA	17	70	19		15		49	26	31	30	
CE	43	149	50	29	32	6.8	91	57	69	71	
ND	21	66	31	26	19	4.1	44	31	40	36	

CALC-SILICATE ROCKS/MARBLES

	ZR-7	BA-2	BI-7	LC-4	BI-10	BI-16	VK-6	DM-5	SK-8	TW-2	HY-6	HY-19
SIO2	56.32	74.87	67.49	52.14	66.49	67.80	42.87	56.24	49.12	62.92	50.82	52.76
TIO2	.93	.51	.78	.87	.74	.63	.63	.33	.18	.53	.34	.27
AL2O3	15.17	11.37	14.07	16.98	13.62	14.43	22.83	14.21	6.98	16.06	23.43	8.17
FEO	8.96	2.76	5.32	9.10	4.58	4.67	3.35	1.68	2.77	4.73	5.50	3.00
MNO	.16	.09	.12	.14	.11	.12	.09	.03	.07	.20	.10	.14
MGO	2.96	1.20	2.13	3.26	1.76	1.79	1.15	6.52	13.84	.10	.89	12.02
CAO	14.05	6.52	6.90	15.50	7.66	7.84	23.41	15.56	23.58	13.23	13.34	21.07
NA2O	1.13	1.61	1.06	1.10	2.94	1.62	.68	1.14	.36	.92	.68	.98
K2O	.14	.36	.45	.08	.95	.37	1.24	3.08	.56	.21	.80	.77
P2O5	.21	.17	.23	.29	.20	.21	.11	.07	.04	.15	.08	.10
LOI	.17	.60	.95	.24	.33	.11	2.83	.85	1.86	.57	.33	.86
H2O-	.06	.06	.08	.07	.02	.07	.10	.06	.07	.11	.11	.08
TOTAL	100.30	100.10	99.59	99.83	99.45	99.68	99.31	99.79	99.45	99.75	96.44	100.30
RB	7.9	7.2	39	4.7	20	30	101	153	46	16	19	5.8
BA	20	169	922	92	458	568	166	1555	154	57	18500	73
SR	546	310	296	1535	233	245	294	166	103	1025	1025	107
TH	5.3	19	6.3	11	13	16	16	14	2.1	18	< 16	9.8
U		4.2		2.6		4.0	8.8	3.1		2.5	< 18	
ZR	95	293	335	75	278	268	314	119	115	273	159	92
NB	3.3	9.8	12	3.3	15	13	13	6.8	1.5	12	5.8	8.1
CR	77	51	64	160	55	47	38	31	10	9.2	36	23
V	197	59	84	148	68	63	65	31	28	39	102	22
SC	28	9.7	16	30	14	14	9.9	2.4	9.1	11	13	8.1
NI	77	19	25	113	24	22	13	5.4	2.5		12	14
CO	36	9.0	15	42	11	10	8.4	2.7	4.2		4.0	10
PB	6.1	11	13	14	17	20	39	26		14	< 15	
ZN	62	61	104	59	81	84	40	17	71	3.7	30	111
CU	74		23					6.8				
Y	26	36	37	24	61	44	25	14	50	28	15	19
LA	6.3	32	33		47	40	31	5.8	41	56	6.2	22
CE	27	69	72	24	92	81	64	22	118	97	23	37
ND	17	35	34	18	46	43	30	11	65	40	27	17

CALC-SILICATE ROCKS/MARBLES

	VK-10	TW-15	DM-7	RFN-1	RFN-2	RFN-5	ROF-4	ROF-15	KGV-3	ND-1	PH-10	GHP-4
SIO2	34.82	50.76	48.13	59.88	44.44	64.82	70.88	48.37	61.98	68.44	68.01	68.12
TIO2	1.37	.59	.60	.50	.19	.93	.20	.14	.66	.34	.56	.66
AL2O3	21.17	10.50	11.34	19.84	25.00	15.48	12.06	12.10	12.84	11.01	15.31	13.74
FEO	9.04	4.14	4.38	4.23	6.78	4.84	2.38	3.22	4.81	6.40	4.59	5.01
MNO	.07	.10	.15	.06	.14	.13	.05	.11	.19	.09	.09	.15
MGO	12.52	9.84	9.20	1.21	.08	.94	.42	9.58	2.43	.42	1.47	1.18
CAO	16.83	20.20	24.27	8.86	20.81	6.93	4.07	21.93	14.11	11.91	5.46	7.84
NA2O	.17	1.47	.30	4.38	1.12	1.52	.43	.83	.82	.31	2.74	2.05
K2O	.21	.80	.56	.47	.09	2.72	9.14	.65	.21	.05	.88	.49
P2O5	.11	.15	.12	.12	.06	.28	.16	.01	.26	.10	.20	.23
LOI	2.98	1.67	1.61	.13	.37	.47	.29	2.73	1.42	1.14	.37	.20
H2O-	.07	.14	.09	.06	.07	.08	.07	.08	.14	.10	.09	.06
TOTAL	99.78	100.40	100.80	99.74	99.19	99.18	100.10	99.73	99.86	100.30	99.77	100.50
RB	3.7	61	31	4.4	4.0	205	403	91	28	2.1	34	15
BA	36	914	1220	212	58	613	824	73	387	19	959	171
SR	192	357	137	498	940	451	87	171	482	1545	562	674
TH		14	8.9	12	11	30	19	3.2	17	20	15	16
U		6.3	3.5		3.3	3.5	3.4		3.2			3.9
ZR	80	221	161	302	98	342	315	101	236	161	157	136
NB		12	12	11	1.0	24	16		13	9.9	8.2	6.6
CR	219	42	56	8.2		17		6.8	53	17	94	15
V	206	60	107	41	78	30		27	61	50	84	84
SC	43	23	14	12	6.8	15	5.6	7.6	14	7.5	18	17
NI	181	15	32	10		4.1			22	4.0	17	9.3
CO	56	7.1	15	2.9		5.4		6.7	16		14	17
PB		22	15	15	14	49	19	16	12	23	39	17
ZN	151	59	103	7.2		19	54	120	97	13	65	48
CU	102					1.9		63	14	2.3		
Y	29	99	27	41	30	65	41	7.9	46	24	32	28
LA		76	31	90	26	83	19	17	44	33	57	38
CE	16	134	60	141	51	158	55	28	88	67	100	64
ND	14	61	29	55	23	71	39	10	41	27	44	32

CALC-SILICATE ROCKS/MARBLES

	KO-6	KO-7	GN-4	PH-4	PH-13	PH-15	SS-3	SS-4	RFN-10	RFN-11	ER-2	WF-1
SIO2	47.55	62.03	73.38	59.83	74.70	51.49	60.14	44.54	71.30	52.48	55.56	49.13
TIO2	.87	.59	.02	.71	.45	.25	.12	.48	.70	.82	1.89	.35
AL2O3	15.64	10.10	.75	15.44	11.13	6.52	8.11	21.19	14.09	22.01	13.63	8.35
FEO	11.80	7.61	5.23	4.95	1.95	1.17	6.51	9.67	2.91	7.32	11.97	3.39
MNO	.27	.14	.18	.20	.06	.13	.24	.17	.09	.28	.23	.09
MGO	3.55	1.64	11.38	1.33	.86	.76	7.10	.19	1.16	.43	2.93	2.76
CAO	16.20	13.98	7.64	15.45	6.36	34.64	15.04	19.81	5.14	15.94	11.02	32.87
NA2O	.73	.49	.07	.48	.92	.22	2.53	.56	3.72	.95	.67	.20
K2O	.69	.33	.04	.08	1.21	1.67	.36	.07	.83	.09	.42	2.12
P2O5	.27	.16	.04	.19	.15	.35	.49		.20	.20	.25	
LOI	.39	2.05	.37	.25	1.37	2.94	.13	.43	1.12	.22	.29	.60
H2O-	.13	.09	.15	.09	.06	.03	.09	.04	.05	.07	.14	.12
TOTAL	98.38	99.41	99.23	99.04	99.22	100.20	100.90	97.16	101.30	100.80	99.02	99.97
RB	51	24		4.0	83	90	15	20	8.3		35	78
BA	196	76	110	31	960	420	55	3.6	131	39	46	831
SR	540	672	5.9	191	271	537	228	1440	222	609	287	51
TH			5.8	27	12	17	13	61	27	33	3.7	
U				6.3					2.9	9.1		
ZR	70	47	47	671	355	270	78	213	288	321	135	128
NB	3.8			11	12	8.4	3.2	99	19	23	11	4.8
CR	1365	839	3.0	43	28	9.1	14	58	12	15	420	35
V	258	177	2.9	68	31	20	44	145	55	105	205	37
SC	35	24	1.8	10	10	7.0	188	11	15	16	28	3.4
NI	310	196	3.4	23	8.2	2.5	41	2.4	6.4		84	13
CO	37	23	3.7	13	3.9	3.4	6.6		5.4	1.5	57	8.8
PB	79	31		6.3	16	16	16	163	16	89	15	16
ZN	93	51	28	155	27	19	255	72	37	37	93	36
CU	2.1				5.2							
Y	16	14	4.3	72	36	68	40	31	55	60	27	17
LA	7.3	6.1	5.3	30	45	34	42	4785	60	59	7.4	
CE	18	14	12	70	81	116	107	8090	121	115	27	11
ND	9.0	9.7	4.8	39	38	41	56	1935	61	57	21	7.0

CALC-SILICATE ROCKS/MARBLES

	WW-6	WW-14	DM-1	GB-1	GB-2	GB-12	SK-9	VK-1	DM-8	HY-18	PH-14	NB-1
SIO2	45.21	43.15	56.80	57.86	51.51	58.54	8.78	9.19	14.38	11.66	20.59	21.77
TIO2	.41	.56	.48			.71	.11	.10	.06	.16	.14	
AL2O3	8.05	5.20	21.67	.52	5.07	20.05	1.67	1.77	2.72	2.84	3.59	.04
FEO	7.26	9.96	6.32	5.08	.55	6.01	.63	.85	.91	2.24	1.16	.08
MNO	.34	.33	.11	.26	.27	.13	.02	.03	.02	.25	.13	.01
MGO	8.09	9.15	.73	21.37	.26	1.40	16.86	18.73	17.09	15.24	1.03	18.09
CAO	25.89	27.21	10.87	12.90	40.14	12.01	36.72	31.60	32.75	34.08	43.87	32.15
NA2O	.50	.05	3.14	.10		.77			.02	.01	.01	
K2O	.20	.01	.32	.08	.03	.13			.04		.01	.01
P2O5	3.40	4.34	.13	.03		.11		.03	.03	.08	.89	.01
LOI	.44	< .01	.12	1.87	1.26	.36	35.49	37.35	30.14	33.32	28.63	27.82
H2O-	.06	.10	.18	.13	.05	.06	.10	.10	.17	.14	.05	.12
TOTAL	99.84	100.10	100.80	100.20	99.14	100.30	100.40	99.80	98.38	100.10	100.20	100.10
RB	11		9.3			5.8		.7	2.5			1.8
BA	26	31	23	29		29	17	11	18	4.5		
SR	894	617	482	6.2	21	1470	286	94	111	161	229	150
TH	11	14	9.2		34	37		1.0	3.4	7.5	4.7	5.3
U	7.9	8.1						2.7	3.7	5.8	6.8	3.6
ZR	351	497	271		5.4	216	12	26	26	38	65	
NB	60	11	8.0		35	15		.5	.4	4.0	4.7	
CR	5.5	3.1	1.3	1.0	3.9	93	3.9	11	9.4	23	8.0	
V	90	130	60	3.5	6.8	91	9.4	12	12	12	14	2.9
SC	13	14	17	5.1	3.4	24						
NI		3.8		7.1	1.8	39		3.1	2.6	11	3.4	
CO	22	27	3.2	21	16	12		2.6	2.5	11	3.3	
PB	29	18	44			16	14	3.8	20		11	6.8
ZN	200	159	66	17	63	21	16	10	21	272	34	1.7
CU			3.3	3.3		1.1		13				
Y	71	64	27	22	67	36	8.3	4.0	4.5	12	19	
LA	177	162	57			76	33			8.1	8.3	
CE	449	427	121			148	60	7.3	10	23	31	
ND	274	269	57	4.7	4.9	75	21	6.5	7.8	13	20	3.1

CALC-SILICATE ROCKS/MARBLES

	RW-1	RW-2	KBB-1	VK-5	TW-3	VK-9	NB-2	SYN-1	WF-2
SIO2	65.68	54.97	51.35	64.12	53.63	12.09	18.40	21.74	30.57
TIO2	.16	1.03	1.33	.67	1.04	.10	.18	.11	.11
AL2O3	3.48	17.38	14.44	11.88	22.41	1.88	3.63	2.48	5.33
FEO	1.08	8.45	13.14	5.11	4.42	.89	1.74	1.55	1.06
MNO	.07	.20	.22	.10	.08	.02	.06	.71	.06
MGO	.60	2.15	4.25	2.21	.42	17.35	17.12	.30	1.73
CAO	25.21	12.87	7.59	10.10	11.70	33.30	31.43	50.14	45.25
NA2O	.16	1.76	1.81	3.01	4.39		.14		.13
K2O	.89	.30	2.80	.40	.46		.31	.01	.17
P2O5	.01	.35	.51	.19	.31		.29		
LOI	2.51	.19	.55	.70	.26	34.46	26.98	23.79	16.88
H2O-	.13	.15	.09	.11	.08	.19	.12	.20	.15
TOTAL	99.97	99.80	98.07	98.62	99.22	100.30	100.40	101.00	101.40
RB	67	5.6	118	6.7	11		13		15
BA	128	252	831	186	108	8.5	652	803	313
SR	330	876	574	92	639	128	165	466	175
TH	4.0	19		14	21		2.2	9.8	
U		4.4		3.7	5.2			5.5	
ZR	76	188	164	191	423	21	50	38	56
NB	3.0	7.3	9.8	14	25		3.0		
CR	11	124	4.8	136	14	2.3	4.2	8.2	12
V	8.3	205	341	263	61	12	10	11	9.9
SC		36	42	18	18	2.0			
NI	3.2	30	14	72	1.2	1.7	3.1	2.7	2.1
CO	3.0	27	51	16			4.8	14	3.7
PB	9.1	21	15	22	14		7.7	6270	39
ZN	17	79	145	166	5.4	41	45	162	23
CU				30	1.8	6.0		235	
Y	15	38	38	32	50	5.2	11	3.9	7.8
LA	9.5	41	28	38	79		7.9		12
CE	22	84	72	72	128	11	15	23	14
ND	10	50	38	36	56	7.1	10	8.2	8.7

FELDSPATHIC QUARTZITES

	LC-1	BI-22	KGV-2	PH-9	WG-3	KB-5	LC-10	BA-4
SIO2	75.30	77.58	96.92	93.33	95.04	89.24	96.08	91.85
TIO2	.82	.44	.10	.03	.07	.16	.08	.10
AL2O3	12.83	11.68	1.57	3.73	3.21	5.21	2.63	4.26
FEO	4.94	3.22	.12	.08	.33	.93	.20	.52
MNO	.03	.01				.01		
MGO	.53	.33	.24	.16	.15	.14	.02	.06
CAO	.05	.04	.04	.04		.03	.01	.02
NA2O	.12	.15	.33	.64	.05	.58	.03	.18
K2O	2.96	3.69	.91	2.10	.20	3.63	.40	2.73
P2O5	.13	.07	.03	.03	.04	.03	.02	.02
LOI	1.82	1.81	.04	.19	1.15	.27	.87	.43
H2O-	.18	.11		.03	.11	.10	.09	.06
TOTAL	99.72	99.13	100.30	100.40	100.40	100.30	100.50	100.20
RB	178	197	37	73	10	114	16	112
BA	1570	997	282	325	161		228	749
SR	150	75	25	47	15	71	26	53
TH	25	29			3.6	3.9	3.7	3.8
U								
ZR	656	526	103	78	88	93	75	75
NB	36	20	3.9		1.4	2.4	2.1	1.1
CR	24	9.0		4.3	4.4			
V	39	22	2.6		2.4		3.1	3.6
SC	15	13			1.1		.6	1.6
NI	8.6	1.9	2.4					.9
CO	7.0	3.6			1.2			
PB	12	19	5.5	22	8.6	15	3.8	11
ZN	77	29				2.4		1.9
CU								
Y	74	89	2.9		6.9	10	9.7	5.4
LA	49	83		3.8	25		13	9.7
CE	120	176	4.9	4.9	55		28	19
ND	60	85			29		21	14

	FELDSPATHIC QUARTZITES					GLASSY QUARTZITES					
	BI-26	BI-27	EX-3	LC-9	HK-3	BI-25	VK-3	HY-1	TW-7	SK-2	TW-9	KO-4
SIO2	92.10	79.49	92.55	94.36	93.90	95.18	99.35	99.04	99.94	99.71	99.29	79.80
TIO2	.15	.10	.14	.13	.07	.08	.04	.03	.04	.03	.03	.03
AL2O3	3.78	10.82	3.59	3.87	3.84	2.49	.47	.39	.23	.20	.39	.38
FEO	.71	1.45	.77	.41	.30	.43	.23	.17	.05	.05	.05	17.21
MGO	.01	.02	.01	.02			.01			.01	.01	.38
MGO	.10	.21	.03	.12	.01	.06	.01	.46	.01	.01	.01	.01
CAO	.01	.07	.02	.01	.01		.01	.02	.01	.02	.02	.02
NA2O	.01	.67	.21	.01	.41	.11	.08	.01	.01	.01	.08	.01
K2O	2.47	5.65	2.48	1.01	1.85	1.64	.22	.19	.07	.04	.16	.01
P2O5	.03	.18	.02	.03	.02	.04				.03	.04	.04
LOI	.41	1.09	.32	.67	.45	.32	.11	.20	< .07	.09	.09	2.29
H2O-	.09	.23	.09	.11	.10	.08	.03	.01	.05	.02	.03	.06
TOTAL	99.84	99.98	100.20	100.80	101.00	100.40	100.60	100.80	100.30	100.20	100.20	100.24
RB	63	204	82	39	84	49	7.5	16	4.2	3.1	7.7	
BA	708	295	656	94	318	689	83	11	3.6	24	46	1440
SR	47	28	51	9.2	18	146	2.8			1.4	1.9	5.9
TH	7.0	11		5.0	1.1	2.5				2.5	1.2	
U										1.8		
ZR	108	203	106	104	35	77	41	29	54	31	56	38
NB	2.7	14	3.1	5.2	2.9	.4				.6		2.1
CR	6.0	3.5	4.4	5.9						1.6	1.9	3.8
V	7.2	7.0	8.0	5.8		3.1		1.5				8.9
SC	1.4	1.8	1.5	1.2	.5	1.0		.8				.9
NI	1.2			1.3		.3						3.5
CO	1.7			2.2								9.3
PB	8.3	30	17	5.4	9.4	3.7				6.3		
ZN	3.1	81		4.4			2.3	3.5	2.1	1.6		20
CU							5.2					18
Y	17	13	3.0	6.0	2.2	14		2.8		.8	.9	1.9
LA	25	4.1	15	31	3.4	11						3.4
CE	63	7.1	36	68	1.4	27		11	8.2	5.2	3.8	7.9
ND	22		15	30	5.9	22		4.1	2.5	2.2		4.2

GLASSY QUARTZITES

	KN-8	SKF-3	FU	BB-2	BB-7	BB-10	ND-5	GN-2	GB-3	GB-4	SS-10	SS-11
SIO2	86.61	99.72	97.42	99.57	96.68	94.77	98.85	96.28	95.82	98.62	97.61	99.56
TIO2	.20	.04	.10	.02	.07	.12	.03	.01	.01		.04	.03
AL2O3	4.86	.43	1.31	.21	1.52	.96	.32	.28	.81	.08	.73	.38
FEO	5.82	.28	.14	.49	.39	3.15	.38	2.19	.81	.22	.88	.25
MNO	.12	.01	.01	.01	.01	.01	.01	.02	.02			
MGO	.18	.04	.10	.03	.01	.12	.03	.46	.92	.30	.15	.12
CAO	.15	.01	.03	.01	.01	.01	.01	.13	2.30	.50		
NA2O	.06	.02	.02	.01	.03	.01	.03	.01	.05	.01	.02	.01
K2O	.73	.10	.39	.07	.90	.81	.12	.01	.03	.01	.13	.10
P2O5	.19		.01	.03	.02	.01	.03	.02				.01
LOI	1.29	.20	.24	.27	.44	.34	.16	.22	.15	.11	.32	.17
H2O-	.14	.03	.09	.04	.06	.06	.04	.05	.02	.02	.04	.01
TOTAL	100.40	100.90	99.87	100.80	100.10	100.40	99.99	99.66	100.90	99.84	99.91	100.60
RB	23	7.0	20	3.2	15	18	5.2				8.8	6.0
BA	675	6.0	258	76	126	43	31	13	32	13	7.8	6.4
SR	119	1.1	6.9		10		1.8		10			
TH	6.3				5.4							
U								3.4				
ZR	50	57	150	58	180	61	94	29	3.8		56	125
NB		1.7	1.8		1.4						2.1	
CR	74	5.3	83	2.6	6.6	5.0	2.1	2.7	1.1	.4	5.3	2.6
V	36	2.5	17	1.7	4.4	12	2.9	2.0	3.8		1.7	1.2
SC	4.4		2.1	.7	1.1	1.0	.6		.9		.7	
NI	3.2							1.8	3.0		1.3	
CO	5.9			1.3		2.2			23	18		
PB	4.9		22	5.5	31	8.3		3.4				
ZN	10	1.0	1.5	57	12	67	2.1	2.3	7.0	1.3	2.2	1.2
CU	2.6			110		3.5	1.8		5.8	23		
Y	26	2.2	2.3	1.8	11		3.4	2.2	4.1		6.0	2.5
LA	18	3.3	4.2	2.3	6.8			5.4			8.8	5.0
CE	41		6.4	7.2	16		3.6				13	6.5
ND	25		2.9	2.5	5.5		2.7				6.8	3.0

GLASSY QUARTZITES

	KN-4	KN-6	OF-4	LB-2	KBB-3	AG56-100	BH156-6	BH156-8	SW26-85	EK2-180
SIO2	98.94	99.41	98.91	98.94	98.55	95.30	97.25	95.98	92.99	92.75
TIO2	.03	.02	.01	.03	.01	.05	.04	.06	.21	.19
AL2O3	.53	.12	.45	.07	.25	1.52	1.13	1.07	2.29	1.72
FEO	.15	.13	.24	.16	.09	1.16	.91	2.13	2.02	3.79
MNO	.01	.01	.01	.01	.01	.06	.03	.05	.68	.02
MGO	.04	.05	.10	.01	.08	.18	.04	.07	.24	.12
CAO			.01		.01	.03	.03	.03	.21	.02
NA2O	.01	.01	.01	.01	.01	.03	.01	.03	.04	.10
K2O	.10	.03	.09	.02	.60	.44	.28	.26	.45	.38
P2O5	.04				.01	.01	.05	.03	.04	.01
LOI	.23	.16	.20	.07	.54	.42	.28	.25	.52	.39
H2O-	.01		.02	.07	.02	.06	.05	.04	.05	.06
TOTAL	100.10	99.93	100.10	99.38	100.20	99.26	100.10	100.00	99.74	99.56
RB	5.9	2.6	6.5	1.2	2.4	27	18	12	26	22
BA	31	6.5	14	2.4	14	175	59		161	63
SR			2.0		1.9		2.1		4.3	2.3
TH		3.9				5.2	4.9	2.9	3.1	9.3
U										
ZR	61	24	20	68	24	70	58	114	135	102
NB						3.4	1.5		2.3	4.0
CR	2.5	2.0	1.6	10	3.1	4.7	3.8	7.7	9.1	15
V	1.5	1.2	2.2	2.1	1.2	1.8	3.1	3.3	16	17
SC						1.6			1.8	1.6
NI									1.9	1.6
CO						3.3	4.7	7.6	3.2	16
PB		11	3.5		7.5	59	8.6	7.1	180	5.3
ZN			8.5	.9		93	66	195	1035	17
CU	1.4					1495	104	376	17	188
Y	2.0	1.4			1.4	11	6.8	9.4	10	5.9
LA	4.2	3.2	1.8		3.1	6.9	16	17	5.2	7.6
CE	4.9	7.0			5.5	16	30	32	14	16
ND	2.5	2.3			2.5	6.2	12	12	5.0	6.6

IRON FORMATIONS

	VK-8	TW-6	TW-11	TW-12	SK-3	TW-8	ER-3	ER-4	KN-12	AG51-145	AG56-240	KN-7
SIO2	69.42	44.93	56.12	53.69	58.32	68.46	30.71	69.15	38.08	84.38	83.22	39.65
TIO2	.53	.45	.60	.16	.07	.39	6.18	4.51	.32	.12	.18	.17
AL2O3	5.17	11.13	12.19	7.44	12.78	7.40	16.22	2.49	7.39	3.61	4.73	4.90
FEO	15.11	15.02	13.35	15.41	20.33	13.10	23.49	18.08	34.34	9.72	8.78	43.52
MNO	4.48	21.64	12.97	17.60	5.73	2.72	.24	.10	12.11	.21	.28	6.07
MGO	1.05	4.39	1.03	5.33	1.18	1.67	6.01	.44	.30	.62	1.53	.20
CAO	3.45	1.51	1.69	1.33	2.92	2.02	.33	.04	1.43	.09	.07	.10
NA2O	.03	.01	.02		.02	.06	.38	.10			.03	
K2O	.02	.02		.01	.04	.06	5.79	.49	.05	.05	.02	
P2O5	.56	.38	.42	.22	.03	.10	.23	.27	.04	.04	.03	.33
LOI	.14	.38	.06	.92	.74	3.41	5.53	2.81	4.54	1.19	1.13	4.82
H2O-	.39	.29	.36	.17	.36	.25	.70	.23	.26	.03	.05	.08
TOTAL	100.40	100.15	98.81	102.28	102.52	98.21	95.81	98.71	98.85	99.83	99.73	99.85
RB						.7	629	45		3.5		
BA	275		10			21	717	142	89	15	11	17
SR	131	20	11	9.5	4.6	15	52	24	25	3.0		37
TH	7.1	19	18	19	105	9.3	197	336		8.1	15	
U		2.3			7.8	2.1	20	26				
ZR	63	158	165	53	169	69	3895	3000	79	125	146	41
NB	5.5	17	17	2.8	1.6	9.7	254	146	7.0	1.7	3.3	7.4
CR	32	64	82	25	46	37	145	199	35	17	21	24
V	25	62	66	37	38	36	587	254	39	13	16	94
SC	8.5	10	13	5.9	40	9.5	91	35	11	2.2	3.0	3.5
NI	36	70	78	31	2.8	23	192	54	31	3.1	5.2	12
CO	149	39	28	38	9.8	27	78	17	33	19	29	19
PB			8.1	3.6	8.3	1.6	36	33	15	4.5	141	
ZN	108	172	165	141	13	76	445	89	317	151	806	83
CU	36	1.0	162	9.2	721	814	21000	631	1.0	1005	789	1.0
Y	44	39	55	24	202	32	129	289	59	8.2	7.8	30
LA	61	44	59	7.9	194	27	282	769	14	6.2		7.2
CE	213	84	112	17	321	44	689	1615	56	14	7.4	26
ND	53	27	42	4.4	136	18	326	755	29	7.9		9.1

IRON FORMATIONS

	KO-8	ROF-9	DBD-1	WW-7	WW-11	WW-15	BHU-213	BHU-302	BHU-424
SIO2	28.79	47.76	56.61	61.45	55.45	43.56	33.84	39.85	27.57
TIO2	.09	4.23	.11	.22	.36	.78	.10	.13	.04
AL2O3	4.18	1.45	3.36	4.79	7.04	11.51	1.71	1.44	.97
FEO	55.77	39.81	23.42	24.82	26.52	30.86	42.70	51.62	60.61
MNO	.32	.27	5.87	3.68	4.15	6.38	7.75	.30	.33
MGO	.32	.15	3.07	.78	.95	2.35	1.43	.36	.32
CAO	.10	.01	6.96	1.90	2.15	2.51	.56	.16	.34
NA2O		.08	.05						.12
K2O	.11	.01	.04	.01	.02	.03	.01	.17	.05
P2O5	.04	.34	.37	.55	.80	1.11	.46	.13	.13
LOI	7.93	4.92	3.67	2.86	3.07	4.63	3.31	4.46	5.81
H2O-	.70	.11	.11	.13	.15	.12	.05	.12	.21
TOTAL	98.34	99.14	101.51	100.98	100.65	101.44	92.54	99.33	98.33
RB	6.9					3.7		29	6.0
BA	47	28	3.4	158	607	164	291	115	28
SR	5.5	59	56	58	18	17	48	7.0	10
TH	21	120	7.7	10	9.0	30		23	21
U		9.6					66		
ZR	26	4290	40	62	44	77		61	18
NB	15	50	3.4	4.6	6.2	7.4			
CR	9.0	105	19	15	21	27	10	17	11
V	47	200	94	26	74	132	27	22	9.0
SC	4.1	21	5.3	5.9	6.6	30	1.0	2.0	1.0
NI	39	6.2	33	18	27	51	30		
CO	46	1.0	18	90	128	122	147	76	125
PB	27	21	20	14	23	23	836	1330	3830
ZN	460	82	219	66	88	262	3920	1180	11300
CU	12000	36	1.0	39	631	1.0	2335	3385	3195
Y	2.6	102	47	67	59	175		14	4.0
LA		273	42	82	62	94			
CE	12	589	63	335	280	323	26	28	23
ND	8.8	285	36	73	59	96	12	13	12

	IRON FORMATIONS					METABASITES						
	OF-1	SS-6	GA BIF	SW-26	AG56	BHU-148	BP-1	ZB-1	BI-8	BP-2	WP-1	HK-2
SIO2	35.92	61.66	4.40	57.48	25.85	31.71	50.84	51.02	47.02	48.51	48.50	46.96
TIO2	1.05	.34	6.01	.41	.06	.09	1.77	1.53	2.00	1.68	1.07	1.57
AL2O3	20.59	10.69	3.46	8.83	1.21	1.34	16.60	15.72	15.74	16.17	17.70	18.18
FEO	17.79	11.67	65.97	12.30	54.29	46.93	11.16	10.32	14.19	11.05	9.77	11.49
MNO	15.80	11.18	.40	4.52	6.11	10.87	.19	.18	.26	.18	.18	.19
MGO	3.06	1.10	.24	2.08	1.05	1.71	7.82	7.17	8.80	7.61	8.77	8.40
CAO	3.15	1.41	.17	2.06	.27	.71	10.19	9.30	10.94	10.21	10.22	11.07
NA2O		.01		.34	.10		.88	2.82	.81	2.59	2.35	1.19
K2O	.65	.05	.44	.48	.04	.01	.55	.81	.07	.75	.69	.41
P2O5	.04	.53	1.59	.13	.15	.33	.21	.24	.16	.22	.10	.19
LOI	2.01	.28	8.85	4.05	4.71	2.93	-.40	.17	-.85	.47	.09	-.32
H2O-	.07	.10	.25	.12	.23	.08	.10	.09	.06	.10	.07	.12
TOTAL	100.10	99.01	91.78	98.49	95.58	97.80	99.97	99.44	99.27	99.62	99.58	99.51
RB	32		25	31			37	27	2.8	12	21	12
BA	143	20	319	32536	4035	29	159	224	10	103	40	61
SR	115	19	16	507	4.0	42	167	195	328	193	238	763
TH	38	8.0	4430			36	4.6	1.9	4.0	4.2	4.8	5.4
U			155									
ZR	1025	94	564	216	11	36	143	193	95	134	80	106
NB	29	8.2	54	5.0			4.3	5.5	1.6	5.1	1.7	3.4
CR	144	47	64	27	11	11	254	243	154	240	88	109
V	89	60	1195	72	7.0	25	239	186	341	241	108	255
SC	23	7.5	38			2.0	37	32	48	40	34	42
NI	1.0	44	22	11		18	101	95	72	115	129	110
CO	7.0	29	27	17	169	134	51	50	52	51	25	62
PB	212		247	9955	4150	5465	10	10	13	7.8	6.1	9.6
ZN	2280	75	1875	24400	4995	3930	104	101	138	103	79	92
CU	1.0	19	33	31	1870	4785	14	39	23	58	4.6	
Y	52	40	1320	22	14	12	38	46	35	43	23	30
LA	61	36	4960	6.0	15		12	18	9.5	13	130	2.5
CE	158	53	11000	32	87	16	31	36	69	43	27	24
ND	48	32	5790	37	40	5.0	25	26	13	26	38	19

METABASITES

	HY-23	RFN-3	HY-8	HY-16	PH-17	ROF-8	BP-7	VK-7	TW-5	DM-2	SK-5	HY-14
SIO2	45.05	40.85	53.16	37.29	57.35	53.27	48.05	47.00	49.57	46.05	56.05	40.66
TIO2	1.89	1.99	.82	1.07	.78	.98	1.70	1.45	1.20	2.17	1.18	1.97
AL2O3	15.08	22.50	14.84	22.90	15.13	17.26	16.54	14.18	16.28	16.89	15.04	23.44
FEO	13.84	10.11	10.27	14.34	7.22	8.34	11.58	12.47	10.73	13.93	10.52	11.31
MNO	.28	.14	.21	.20	.17	.19	.21	.20	.19	.25	.17	.24
MGO	8.98	4.98	6.56	8.92	6.48	6.78	7.90	7.43	7.77	8.22	6.51	6.77
CAO	12.71	15.43	9.67	11.72	8.47	10.06	11.13	12.41	12.65	10.73	9.57	8.48
NA2O	.86	1.16	2.41	1.12	.73	1.53	1.95	2.36	1.31	.54	.84	1.45
K2O	.17	.50	.54	.16	.88	.49	.53	.91	.42	.67	.20	.11
P2O5	.16	.40	.27	.18	.21	.19	.13	.12	.08	.26	.27	.20
LOI	-.49	.45	.10	.16	1.11	.24	-.25	.27	-.34	-.07	-.27	4.19
H2O-	.07	.07	.11	.07	.07	.07	.15		.10	.12	.08	.08
TOTAL	98.68	98.65	99.13	98.22	98.73	99.41	99.74	99.01	100.00	99.83	100.30	99.00
RB	3.0	7.9	5.3		51	4.8	4.8	30	18	34	7.3	4.6
BA	38	21	209	2.5	342	226	99	67	50	123	22	24
SR	162	1370	401	460	363	406	209	198	154	264	586	526
TH	2.7	5.1			7.9	1.5	1.4					23
U	2.1											4.4
ZR	42	146	80	53	144	100	104	82	65	113	124	315
NB	6.4		7.6		5.5	3.6	5.0	6.3	4.9	4.5	7.8	24
CR	228	184	824	259	430	180	383	138	290	124	365	392
V	311	268	206	282	132	183	291	245	260	309	237	331
SC	52	42	36	49	27	36	53	41	44	42	31	46
NI	92	150	255	239	186	60	37	84	106	98	95	88
CO	70	35	54	62	40	39	51	57	52	66	41	35
PB	8.3	17	8.4		8.9	14	2.9		5.4	6.9	5.0	11
ZN	142	42	98	92	80	151	109	105	72	121	70	45
CU	8.2							5.7	3.6		49	1.7
Y	26	32	23	23	25	23	44	27	24	32	31	53
LA		15	11		27	11					27	59
CE	20	52	31	12	58	32	34	22	12	24	65	123
ND	17	30	19	12	31	21	23	16	10	17	32	55

METABASITES

	SKF-5	SKF-11	NB-4	MF-1	PH-3	GN-3	RW-6	GHP-2	GHP-3	WW-2	GB-11
SIO2	51.61	50.09	47.94	59.49	59.96	46.82	59.19	51.43	49.74	48.27	51.74
TIO2	.72	.52	.76	.85	.98	1.49	1.06	2.26	.58	1.68	.43
AL2O3	17.03	14.45	18.47	16.79	18.29	14.47	17.40	14.73	17.44	19.27	6.53
FEO	8.76	10.35	9.63	7.33	7.33	11.32	9.14	9.70	11.65	11.62	10.16
MNO	.14	.15	.23	.16	.14	.19	.22	.17	.21	.22	.29
MGO	6.84	13.22	6.18	3.63	2.79	7.48	3.85	6.05	7.52	7.65	18.82
CAO	9.13	9.11	6.61	7.30	8.28	8.80	3.13	7.35	9.78	9.68	9.73
NA2O	2.18	.50	1.61	2.42	1.72	1.56	5.05	2.30	2.52	.86	.59
K2O	1.04	.19	5.39	.66	.37	1.17	1.35	3.49	.27	.78	.07
P2O5	.19	.15	.37	.22	.21	.36	.08	1.14	.07	.18	.17
LOI	1.50	.79	2.89	.46	.08	4.93	-.01	.43	-.04	.15	1.18
H2O-	.10	.08	.06	.07	.05	.27	.08	.19	.08	.72	.07
TOTAL	99.08	99.59	100.10	99.42	100.20	98.86	100.50	99.23	99.81	100.40	99.77
RB	67	8.2	159	18	6.9	83	13	135		37	
BA	309	24	1945	611	82	471	723	2545	135	158	25
SR	415	247	855	709	510	146	150	898	181	215	22
TH	3.8	4.4	6.3	4.7	5.8		62	9.4		3.2	
U											
ZR	82	43	51	175	136	225	180	629	18	96	55
NB	5.2	1.8	59	9.2	5.1	9.9	10	14			5.4
CR	377	1080	12	66	8.5	161	33	148	31	104	1435
V	200	177	204	135	117	255	171	159	295	251	116
SC	32	36	19	26	22	43	29	28	47	42	35
NI	126	413	66	79	17	118	6.9	84	31	78	649
CO	41	53	49	31	29	58	25	41	47	62	72
PB	5.8	7.1	11	19	17	29	42	47	7.6	21	
ZN	42	62	71	86	68	114	121	117	69	88	92
CU	124	6.5	8.3			103	5.8	27		4.3	
Y	21	19	16	33	27	41	26	55	12	30	11
LA	20	11	82	25	18	25	37	112			12
CE	43	28	162	63	38	66	76	245	7.0	11	34
ND	25	18	70	37	21	39	34	125		15	22

	BIOTITE/HORNBLENDE ROCKS				LEUCOGNEISSES					
	GB-5	GB-7	SKF-6	SKF-7	HY-24	RFN-4	HY-11	KO-1	PH-12	BPT-1
SIO2	60.46	61.32	61.86	60.07	47.80	47.91	74.32	73.45	77.07	77.23
TIO2	1.23	1.08	.57	.60	.63	.13	.01	.16	.14	.13
AL2O3	16.16	15.52	15.24	15.77	29.28	35.04	14.01	12.16	11.46	11.45
FEO	5.51	6.08	6.60	7.23	4.95	4.20	.93	3.82	1.23	1.42
MNO	.09	.10	.18	.14	.11	.03	.01	.33	.01	.02
MGO	2.77	3.06	5.04	5.39	2.61	.60	.10	.59	.12	.04
CAO	3.88	4.29	4.83	5.65	.53	1.30	.72	.18	.24	.54
NA2O	2.32	2.27	1.70	1.79	1.51	1.06	3.80	.87	1.79	2.49
K2O	5.62	4.52	2.33	2.11	9.54	8.85	5.50	6.94	6.96	5.90
P2O5	.64	.56	.10	.12	.18	.03	.04	.05	.05	.06
LOI	.73	1.11	.92	.81	1.43	.44	.29	.63	.47	.24
H2O-	.07	.09	.07	.07	.08	.09	.11	.17	.09	.05
TOTAL	99.48	100.00	99.44	99.73	98.67	99.69	99.85	99.36	99.64	99.57
RB	203	173	127	106	378	417	239	301	284	284
BA	1880	1725	629	435	1635	1115	68	2240	271	150
SR	1155	930	230	259	134	115	25	74	73	31
TH	22	17	7.5	9.0	30	58	6.1	6.1	33	38
U					1.9	3.5				2.8
ZR	330	289	108	116	361	180	102	206	186	226
NB	23	21	6.9	7.0	30	16	6.9	11	8.4	17
CR	37	79	193	199	18	9.8		1.5	2.1	
V	181	175	135	142	83	15		9.5		
SC	14	16	22	24	14	6.1	1.2	5.8	2.7	2.4
NI	42	54	66	73	15	8.8		2.7		
CO	24	28	29	33	9.0	11		10		1.5
PB	37	35	12	11	56	11	61	117	47	39
ZN	70	78	90	72	93	9.8	78	148	11	41
CU	141	179	5.8	13	1.4	2.0	4.8	470		
Y	18	19	12	16	52	66	6.4	47	14	43
LA	87	78	17	22	93	49	5.3	31	69	106
CE	166	144	35	49	167	105	19	50	133	187
ND	72	62	15	24	74	62	9.0	20	55	85

LEUCOGNEISSES

	GB-8	RFN-9	BB-5	KBB-2	ROF-13	PH-5	PH-7	WW-9	WW-12	GB-6
SIO2	74.31	78.54	91.58	84.11	77.17	79.00	74.22	74.98	76.69	76.51
TIO2	.48	.13	.27	.29	.17	.09	.28	.10	.14	.08
AL2O3	15.20	12.13	4.23	5.60	11.62	12.08	13.51	14.23	12.89	13.81
FEO	1.29	.60	.62	4.47	1.33	1.36	1.37	.64	1.14	.70
MNO			.01	.32	.04	.01	.04	.02	.05	.01
MGO	.73	.18	.54	.47	.23	.18	.38	.48	.18	.16
CAO	.15	.50	.21	.73	.43	.09	.76	1.04	.51	.44
NA2O	.99	3.01	.91	.06	2.40	.75	3.32	2.33	2.64	3.05
K2O	4.87	6.05	.90	2.81	6.20	5.49	5.60	6.58	6.11	5.98
P2O5	.02		.01	.21	.06	.05	.05	.11	.04	.11
LOI	2.45	.43	.43	.71	.28	.74	.36	.40	.40	.68
H2O-	.26	.11	.11	.10	.06	.12	.07	.11	.16	.07
TOTAL	100.70	101.70	99.81	99.87	99.98	99.96	99.97	101.00	100.90	101.60
RB	262	401	64	179	300	199	171	306	230	295
BA	1115	89	187	723	248	418	1465	586	153	272
SR	64	30	14	42	33	91	165	119	29	61
TH	10	81	11	4.7	46	17	16	27	28	4.9
U		12			5.4			4.1	3.6	3.2
ZR	213	131	600	124	193	100	256	137	204	41
NB	13	25	8.4	5.6	15		9.9	2.6	9.1	13
CR	42		35	18				3.2		3.3
V	51		12	97		3.9	4.1	5.9		4.2
SC	14	5.4	2.7	6.7	1.8	1.7	6.2	4.3	4.8	6.7
NI	7.6	6.2	2.2	30						1.7
CO	2.0		1.4	16		2.5		2.7		1.5
PB		30		100	37	33	40	58	59	36
ZN	8.4	6.6	3.4	201	28	25	37	4.2	29	7.0
CU	19			3.4				2.4	5.1	155
Y	26	80	15	21	70	5.2	24	48	28	23
LA	17	50	5.9	15	84	36	46	49	55	6.5
CE	31	98	16	38	164	62	86	89	87	16
ND	20	43	7.5	19	74	22	37	37	31	6.7